

Special Issue Reprint

Glutathione

Chemistry and Biochemistry

Edited by
Pál Perjési

www.mdpi.com/journal/molecules

Glutathione: Chemistry and Biochemistry

Glutathione: Chemistry and Biochemistry

Editor

Pál Perjési



Basel • Beijing • Wuhan • Barcelona • Belgrade • Novi Sad • Cluj • Manchester

Editor

Pál Perjési

Institute of Pharmaceutical Chemistry

University of Pécs

Pécs

Hungary

Editorial Office

MDPI

St. Alban-Anlage 66

4052 Basel, Switzerland

This is a reprint of articles from the Special Issue published online in the open access journal *Molecules* (ISSN 1420-3049) (available at: www.mdpi.com/journal/molecules/special_issues/glutathione_biochemistry).

For citation purposes, cite each article independently as indicated on the article page online and as indicated below:

Lastname, A.A.; Lastname, B.B. Article Title. <i>Journal Name</i> Year , Volume Number, Page Range.
--

ISBN 978-3-0365-8667-0 (Hbk)

ISBN 978-3-0365-8666-3 (PDF)

doi.org/10.3390/books978-3-0365-8666-3

© 2023 by the authors. Articles in this book are Open Access and distributed under the Creative Commons Attribution (CC BY) license. The book as a whole is distributed by MDPI under the terms and conditions of the Creative Commons Attribution-NonCommercial-NoDerivs (CC BY-NC-ND) license.

Contents

About the Editor	vii
Pál Perjési	
Preface to the Special Issue “Glutathione: Chemistry and Biochemistry” Reprinted from: <i>Molecules</i> 2023 , <i>28</i> , 5993, doi:10.3390/molecules28165993	1
Janka Vašková, Ladislav Kočan, Ladislav Vaško and Pál Perjési	
Glutathione-Related Enzymes and Proteins: A Review Reprinted from: <i>Molecules</i> 2023 , <i>28</i> , 1447, doi:10.3390/molecules28031447	4
Elena Kalinina and Maria Novichkova	
Glutathione in Protein Redox Modulation through S-Glutathionylation and S-Nitrosylation Reprinted from: <i>Molecules</i> 2021 , <i>26</i> , 435, doi:10.3390/molecules26020435	26
Trnka Daniel, Hossain Md Faruq, Jordt Laura Magdalena, Gellert Manuela and Lillig Christopher Horst	
Role of GSH and Iron-Sulfur Glutaredoxins in Iron Metabolism—Review Reprinted from: <i>Molecules</i> 2020 , <i>25</i> , 3860, doi:10.3390/molecules25173860	45
George Jitcă, Erzsébet Fogarasi, Bianca-Eugenia Ősz, Camil Eugen Vari, Ibolya Fülöp and Mircea Dumitru Croitoru et al.	
Profiling the Concentration of Reduced and Oxidized Glutathione in Rat Brain Using HPLC/DAD Chromatographic System Reprinted from: <i>Molecules</i> 2021 , <i>26</i> , 6590, doi:10.3390/molecules26216590	71
Siyu Zhang, Cuina Wang, Weigang Zhong, Alyssa H. Kemp, Mingruo Guo and Adam Killpartrick	
Polymerized Whey Protein Concentrate-Based Glutathione Delivery System: Physicochemical Characterization, Bioavailability and Sub-Chronic Toxicity Evaluation Reprinted from: <i>Molecules</i> 2021 , <i>26</i> , 1824, doi:10.3390/molecules26071824	81
Klaudia Bontor and Bożena Gabryel	
Sulodexide Increases Glutathione Synthesis and Causes Pro-Reducing Shift in Glutathione-Redox State in HUVECs Exposed to Oxygen–Glucose Deprivation: Implication for Protection of Endothelium against Ischemic Injury Reprinted from: <i>Molecules</i> 2022 , <i>27</i> , 5465, doi:10.3390/molecules27175465	94
Jan Čapek and Tomáš Roušar	
Detection of Oxidative Stress Induced by Nanomaterials in Cells—The Roles of Reactive Oxygen Species and Glutathione Reprinted from: <i>Molecules</i> 2021 , <i>26</i> , 4710, doi:10.3390/molecules26164710	109
Agnieszka Potęga	
Glutathione-Mediated Conjugation of Anticancer Drugs: An Overview of Reaction Mechanisms and Biological Significance for Drug Detoxification and Bioactivation Reprinted from: <i>Molecules</i> 2022 , <i>27</i> , 5252, doi:10.3390/molecules27165252	129
Péter Hajdinák, Melinda Szabó, Emese Kiss, Lili Veress, Lívius Wunderlich and András Szarka	
Genetic Polymorphism of GSTP-1 Affects Cyclophosphamide Treatment of Autoimmune Diseases Reprinted from: <i>Molecules</i> 2020 , <i>25</i> , 1542, doi:10.3390/molecules25071542	158

Fatemeh Kenari, Szilárd Molnár and Pál Perjési

Reaction of Chalcones with Cellular Thiols. The Effect of the 4-Substitution of Chalcones and Protonation State of the Thiols on the Addition Process. Diastereoselective Thiol Addition

Reprinted from: *Molecules* **2021**, *26*, 4332, doi:10.3390/molecules26144332 **170**

Antônio S. N. Aguiar, Igor D. Borges, Leonardo L. Borges, Lucas D. Dias, Ademir J. Camargo and Pál Perjési et al.

New Insights on Glutathione's Supramolecular Arrangement and Its In Silico Analysis as an Angiotensin-Converting Enzyme Inhibitor

Reprinted from: *Molecules* **2022**, *27*, 7958, doi:10.3390/molecules27227958 **183**

About the Editor

Pál Perjési

Pál Perjési received a master's degree in pharmacy from the Albert Szent-Györgyi University (Szeged, Hungary). After spending two years at the Department of Pharmaceutical Chemistry of Albert Szent-Györgyi University, he was appointed Assistant Professor of Medical Chemistry at the Department of Medical Chemistry at the University of Pécs (Pécs, Hungary). He is currently a professor of pharmaceutical chemistry at the Institute of Pharmaceutical Chemistry at the University of Pécs. He received his doctorate from Albert Szent-Györgyi University in 1983. Later, he received a Candidate of Science degree from the Hungarian Academy of Sciences in 1994. This degree was acknowledged as a Ph.D. degree by Albert Szent-Györgyi University in 1996. He earned a habilitation from the University of Pécs in chemistry in 2000. He has a pharmacy specialization in preparative chemical laboratory investigations and toxicology. His general research interests are focused on the investigation of the regio- and stereochemistry of intestinal and hepatic metabolic transformations of chalcones, capsaicinoids, and selected non-steroid anti-inflammatory drugs (NSAIDs), the mechanism and stereochemistry of nucleophilic addition of thiols onto unsaturated carbonyl compounds, and the effect of oxidative stress (hyperglycemia) on intestinal and hepatic biotransformations of the three classes of compounds. He has published over 100 peer-reviewed papers, several books, book chapters, and patents.

Editorial

Preface to the Special Issue “Glutathione: Chemistry and Biochemistry”

Pál Perjési 

Institute of Pharmaceutical Chemistry, University of Pécs, H-7624 Pécs, Hungary; pal.perjesi@gytk.pte.hu

This year we celebrate the 135th anniversary of the discovery of glutathione (L- γ -glutamyl-L-cysteinyl-glycine). The major intracellular thiol compound was first described in the literature in 1888 by J. De-Rey Pailhade [1]. He named the substance *phylothion*, the Greek expression for sulfur-loving. Since then, chemists, biochemists, and medical professionals accumulated a wide range of information about this molecule's cellular and organizational functions. The broad interest in glutathione-related topics is reflected by several recent reviews [2–4].

It has been known that endogenous glutathione content and its speciation plays a role, among others, in redox homeostasis, cell cycle control, immunological defense, and pathological abnormalities. Among the latter, hemolytic anemia, cardiovascular diseases, neurological disorders, and distinct types of cancer can be mentioned [5]. Furthermore, it plays a significant role in the biotransformation of drugs and other endogenous or exogenous electrophilic species. In most cases, such transformations protect cellular nucleophilic sites and eliminate the target molecules [6]. Most of these cellular functions are related to the thiol (SH) function of the cysteine moiety.

Due to the redox characteristics of the thiol function, the reduced form of glutathione (GSH) is not only a powerful nucleophile but an antioxidant as well. Because of the high cellular level, the GSSG/2GSH couple is the most abundant redox couple in the cells. Changes in the half-cell reduction potential (E_{hc}) of the GSSG/2GSH couple appear to correlate with the biological status of the cells: proliferation $E_{hc} \sim -240$ mV differentiation; $E_{hc} \sim -200$ mV; or apoptosis $E_{hc} \sim -170$ mV [7]. Although it does not mean that the actual redox potential of the GSSG/2GSH system is a determining factor of the cells' fate [8], the correlations are remarkable and worth further investigation.

Recent clinical trials indicated that oral GSH supplements can elevate body stores of glutathione and markers of immune function [9,10]. The increased demand for pharmaceutical grade glutathione signals the importance of new, economical biotechnology-based technologies for the production and pharmaceutical qualification of glutathione preparations [11]. Additionally, drug delivery systems enhancing the bioavailability of oral glutathione are becoming an important issue. Besides using qualified glutathione (GSH) products as a pharmakon, it can be successfully applied in various other industries where the compound's reversible redox and antioxidant properties can be utilized.

This book presents the publications that appeared in the Special Issue of Molecules, “Glutathione: Chemistry and Biochemistry”. The contributions provide current information on three fields of glutathione research. The first three contributions [12–14] review the present-day knowledge of the GSH/GSSG system and the essential GSH-related proteins involved in controlling various cellular events.

The following four contributions [15–18] present selected interventions which modulate the GSH/GSSG system. One of the contributions of this session [15] describes a new HPLC/DAD method to quantify the reduced glutathione (GSH) and oxidized glutathione (GSSG) levels in rat brain.

The third session involves three [19–21] contributions demonstrating the role of GSH in the metabolism of different candidate and clinically used anticancer drugs. One of the

Citation: Perjési, P. Preface to the Special Issue “Glutathione: Chemistry and Biochemistry”. *Molecules* **2023**, *28*, 5993. <https://doi.org/10.3390/molecules28165993>

Received: 8 August 2023

Accepted: 9 August 2023

Published: 10 August 2023



Copyright: © 2023 by the author. Licensee MDPI, Basel, Switzerland. This article is an open access article distributed under the terms and conditions of the Creative Commons Attribution (CC BY) license (<https://creativecommons.org/licenses/by/4.0/>).

contributions [22] a theoretical work, provides valuable information for developing GSH analogs with high ACE inhibitor activity.

By purpose and content, this Special Issue is addressed to the vast number of life science researchers (academic and industrial) and medical professionals who are interested or already engaged in research that involves glutathione.

Conflicts of Interest: The author declares no conflict of interest.

References



- Lillig, C.H.; Berndt, C. Preface. Cellular Functions of Glutathione. *Biochim. Biophys. Acta* **2013**, *1830*, 3137–3138. [CrossRef] [PubMed]
- Lou, M.F. Glutathione and Glutaredoxin in Redox Regulation and Cell Signaling of the Lens. *Antioxidants* **2022**, *11*, 1973. [CrossRef] [PubMed]
- Dwivedi, D.; Megha, K.; Mishra, R.; Mandal, P.K. Glutathione in Brain: Overview of its Conformations, Functions, Biochemical Characteristics, Quantitation and Potential Therapeutic Role in Brain Disorders. *Neurochem. Res.* **2020**, *45*, 1461–1480. [CrossRef] [PubMed]
- Kalinina, E.V.; Chernov, N.N.; Novichkova, M.D. Glutathione and Glutathione Dependent Enzymes in Redox Regulation of Cellular Processes. In *Glutathione: Biosynthesis, Functions and Biological Implications*; Perjési, P., Ed.; Nova Science Publishers: New York, NY, USA, 2019; pp. 131–167.
- Ballatori, N.; Krance, S.M.; Notenboom, S.; Shi, S.; Tieu, K.; Hammond, C.L. Glutathione Dysregulation and the Etiology and Progression of Human Diseases. *Biol. Chem.* **2009**, *390*, 191–214. [CrossRef] [PubMed]
- Chasseaud, L.F. The Role of Glutathione and Glutathione S-Transferases in the Metabolism of Chemical Carcinogens and other Electrophilic Agents. In *Advances in Cancer Research*; Klein, G., Weinhouse, S., Eds.; Academic Press: San Diego, CA, USA, 1979; pp. 175–274.
- Schafer, F.Q.; Buettner, G.R. Redox Environment of the Cell as Viewed through the Redox State of the Glutathione Disulfide/Glutathione Couple. *Free Radic. Biol. Med.* **2001**, *30*, 1191–1212. [CrossRef]
- Flohé, L. The Fairytale of the GSSG/GSH Redox Potential. *Biochem. Biophys. Acta* **2013**, *1830*, 3139–3142. [CrossRef] [PubMed]
- Richie, J.P., Jr.; Nichenametla, S.; Neidig, W.; Calcagnotto, A.; Haley, J.S.; Schell, T.D.; Muscat, J.E. Randomized Controlled Trial of Oral Glutathione Supplementation on Body Stores of Glutathione. *Eur. J. Nutr.* **2015**, *54*, 251–263. [CrossRef]
- Sinha, R.; Sinha, I.; Calcagnotto, A.; Trushin, N.; Haley, J.S.; Schell, T.D.; Richie, J.P., Jr. Oral Supplementation with Liposomal Glutathione Elevates Body Stores of Glutathione and Markers of Immune Function. *Eur. J. Clin. Nutr.* **2018**, *72*, 105–111. [CrossRef]
- Kobayashi, J.; Sasaki, D.; Hara, K.Y.; Kondo, A. Genetic Engineering of Microorganisms for High Glutathione Production. In *Glutathione: Biosynthesis, Functions and Biological Implications*; Perjési, P., Ed.; Nova Science Publishers: New York, NY, USA, 2019; pp. 83–104.
- Vaskova, J.; Kocan, L.; Vasko, L.; Perjési, P. Glutathione-Related Enzymes and Proteins: A Review. *Molecules* **2023**, *28*, 1447. [CrossRef]
- Kalinina, E.; Novichkova, M. Glutathione in Protein Redox Modulation through S-Glutathionylation and S-Nitrosylation. *Molecules* **2021**, *26*, 435. [CrossRef]
- Daniel, T.; Faruq, H.M.; Laura Magdalena, J.; Manuela, G.; Christopher Horst, L. Role of GSH and Iron-Sulfur Glutaredoxins in Iron Metabolism—Review. *Molecules* **2020**, *25*, 3860. [CrossRef] [PubMed]
- Jitca, G.; Fogarasi, E.; Ósz, B.-E.; Vari, C.E.; Fülöp, I.; Croitoru, M.D.; Rusz, C.M.; Dogaru, M.T. Profiling the Concentration of Reduced and Oxidized Glutathione in Rat Brain Using HPLC/DAD Chromatographic System. *Molecules* **2021**, *26*, 6590. [CrossRef] [PubMed]
- Zhang, S.; Wang, C.; Zhong, W.; Kemp, A.H.; Guo, M.; Killpartrick, A. Polymerized Whey Protein Concentrate-Based Glutathione Delivery System: Physicochemical Characterization, Bioavailability and Sub-Chronic Toxicity Evaluation. *Molecules* **2021**, *26*, 1824. [CrossRef] [PubMed]
- Bontor, K.; Gabryel, B. Sulodexide Increases Glutathione Synthesis and Causes Pro-Reducing Shift in Glutathione-Redox State in HUVECs Exposed to Oxygen–Glucose Deprivation: Implication for Protection of Endothelium against Ischemic Injury. *Molecules* **2022**, *27*, 5465. [CrossRef] [PubMed]
- Capek, J.; Rousar, T. Detection of Oxidative Stress Induced by Nanomaterials in Cells—The Roles of Reactive Oxygen Species and Glutathione. *Molecules* **2021**, *26*, 4710. [CrossRef] [PubMed]
- Potega, A. Glutathione-Mediated Conjugation of Anticancer Drugs: An Overview of Reaction Mechanisms and Biological Significance for Drug Detoxification and Bioactivation. *Molecules* **2022**, *27*, 5252. [CrossRef] [PubMed]
- Hajdinák, P.; Szabó, M.; Kiss, E.; Veress, L.; Wunderlich, L.; Szarka, A. Genetic Polymorphism of GSTP-1 Affects Cyclophosphamide Treatment of Autoimmune Diseases. *Molecules* **2020**, *25*, 1542. [CrossRef] [PubMed]

21. Kenari, F.; Molnár, S.; Perjési, P. Reaction of Chalcones with Cellular Thiols. The Effect of the 4-Substitution of Chalcones and Protonation State of the Thiols on the Addition Process. Diastereoselective Thiol Addition. *Molecules* **2021**, *26*, 4332. [CrossRef] [PubMed]
22. Aguiar, A.S.N.; Borges, I.D.; Borges, L.L.; Dias, L.D.; Camargo, A.J.; Perjési, P.; Napolitano, H.B. New Insights on Glutathione's Supramolecular Arrangement and Its In Silico Analysis as an Angiotensin-Converting Enzyme Inhibitor. *Molecules* **2022**, *27*, 7958. [CrossRef] [PubMed]

Disclaimer/Publisher's Note: The statements, opinions and data contained in all publications are solely those of the individual author(s) and contributor(s) and not of MDPI and/or the editor(s). MDPI and/or the editor(s) disclaim responsibility for any injury to people or property resulting from any ideas, methods, instructions or products referred to in the content.

Review

Glutathione-Related Enzymes and Proteins: A Review

Janka Vašková^{1,*} , Ladislav Kočan², Ladislav Vaško¹ and Pál Perjési^{3,*} 

¹ Department of Medical and Clinical Biochemistry, Faculty of Medicine, Pavol Jozef Šafárik University in Košice, 040 11 Košice, Slovakia

² Clinic of Anaesthesiology and Intensive Care Medicine, East Slovak Institute of Cardiovascular Disease, 040 11 Košice, Slovakia

³ Institute of Pharmaceutical Chemistry, University of Pécs, 7600 Pécs, Hungary

* Correspondence: janka.vaskova@upjs.sk (J.V.); pal.perjesi@gytk.pte.hu (P.P.); Tel.: +42-155-234-3232 (J.V.)

Abstract: The tripeptide glutathione is found in all eukaryotic cells, and due to the compartmentalization of biochemical processes, its synthesis takes place exclusively in the cytosol. At the same time, its functions depend on its transport to/from organelles and interorgan transport, in which the liver plays a central role. Glutathione is determined as a marker of the redox state in many diseases, aging processes, and cell death resulting from its properties and reactivity. It also uses other enzymes and proteins, which enables it to engage and regulate various cell functions. This paper approximates the role of these systems in redox and detoxification reactions such as conjugation reactions of glutathione-S-transferases, glyoxylases, reduction of peroxides through thiol peroxidases (glutathione peroxidases, peroxiredoxins) and thiol–disulfide exchange reactions catalyzed by glutaredoxins.

Keywords: cell; redox homeostasis; glutathione; glutathionylation; glutathione system; glutathione enzyme

1. Introduction

Glutathione (GSH) was first isolated in 1888 by De-Rey-Pailhade. He named the substance *phylothion*, the Greek expression for sulfur loving [1]. Its structure was controversial for several years. Initially, it was described as a sulfur-containing dipeptide [2]. Later the structure was refined, demonstrating that the substance is a tripeptide, γ -Glu-Cys-Gly [3–5]. Other related compounds, such as γ -Glu-Cys-Gly-spermidine and $(\gamma$ -Glu-Cys)_n-Gly in *E. coli* and plants, were also described [6]. The thiol group of the cysteine residue enables GSH to function as both a reducing agent and a nucleophilic center [7]. Glutathione occurs in two free forms: the reduced (GSH) thiol and the oxidized (GSSG) disulfide forms (Figure 1). In addition, it can be bound to proteins and other thiols, affecting their activity. In its reduced and oxidized forms (GSH, GSSG), glutathione is ubiquitous in mammalian cells ranging in 1–10 mM concentrations [8]. Under physiological conditions, more than 98% of total GSH occurs in the reduced form [9,10]. It is an essential antioxidant against reactive oxygen and nitrogen species [11]. The compound plays a critical role in maintaining the redox homeostasis of the cells and in cell cycle regulation, apoptosis, immunological defense, and pathological abnormalities [8]. Furthermore, it is one of the endogenous substances involved in the metabolism of endogenous (e.g., estrogens, leukotrienes, prostaglandins) and exogenous compounds (e.g., drugs, non-energy-producing xenobiotics) [12]. These latter transformations could be the molecular basis for eliminating foreign substances from the body. In this review, the role of glutathione and glutathione-dependent enzymes in the maintenance of redox homeostasis is summarized.

Citation: Vašková, J.; Kočan, L.; Vaško, L.; Perjési, P. Glutathione-Related Enzymes and Proteins: A Review. *Molecules* **2023**, *28*, 1447. <https://doi.org/10.3390/molecules28031447>

Academic Editor: Hyun-Ock Pae

Received: 15 January 2023

Revised: 30 January 2023

Accepted: 31 January 2023

Published: 2 February 2023



Copyright: © 2023 by the authors. Licensee MDPI, Basel, Switzerland. This article is an open access article distributed under the terms and conditions of the Creative Commons Attribution (CC BY) license (<https://creativecommons.org/licenses/by/4.0/>).

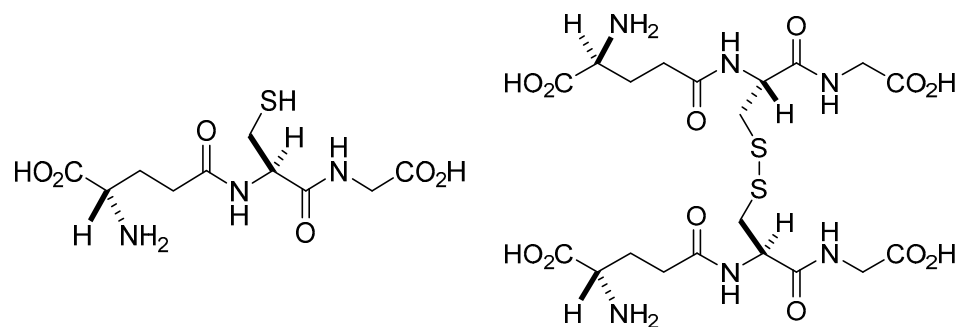


Figure 1. Structure of reduced (GSH) and oxidized (GSSG) forms of glutathione.

2. Glutathione

Together with glutaredoxins (Grx), GSH acts to reduce disulfide bonds and is, in turn, oxidized to glutathione disulfide (GSSG), which is reduced by NADPH-dependent glutathione reductase. The GSH/GSSG, NADPH/NADP⁺, Grx-SH/Grx-SS, and Trx-SH/Trx-SS are the most important redox couples in maintaining cellular redox homeostasis [13]. The standard apparent redox potential (E°) of GSH is -288 mV (pH 7, 298.15 K, 0.25 M ionic strength), which is well between the most negative H^+/H_2 (-423 mV) and the most positive, O_2/H_2O ($+849$ mV) redox couples [14]. Accordingly, the GSH/GSSG redox couple can readily interact with most physiologically relevant redox couples, undergoing reversible oxidation or reduction [7].

Given the availability of glutathione in the cells, the reactions of protein thiols are mediated by multiple enzymes and enzyme systems, thus allowing it to participate in the abovementioned functions and regulatory pathways. Among them are glutaredoxins, which are central in the response against oxidative stress as the biological activity of many proteins are modified by the formation of GSH-mixed disulfides. Furthermore, other redox-maintaining enzymes such as glutathione peroxidases, and detoxification enzymes, glyoxylases, are closely related to carbohydrate metabolism [15,16]. Thus, the involvement of glutathione and its activity in the cell represents a wide range of biological and biochemical processes. The consequence of its deficiency results in increased stress conditions, which is the basis of the pathophysiology of many organ or tissue-specific diseases such as inflammation, virus infections (HIV), sickle cell anemia, cancer, diabetes, heart attack, stroke, liver disease, cystic fibrosis, Alzheimer's, and Parkinson's disease [17,18].

2.1. The Role of the Liver in Glutathione Synthesis and Distribution

Synthesis of GSH occurs in the cytoplasm in all cells in two subsequent ATP-dependent reactions catalyzed by glutamate-cysteine ligase and GSH synthetase, from where it is transported to other organelles and extracellular space [8,19]. Glycine, glutamate, and cysteine as nonessential amino acids can be obtained from dietary sources or synthesis.

The liver removes a significant amount of resorbed cysteine from the portal vein [20]. However, cysteine can be synthesized by methionine transsulfuration in the liver [21]. The liver is responsible for the metabolism of up to half of the daily methionine intake, predisposing the liver to almost exclusive transsulfuration activity and being the most important in interorgan GSH homeostasis [22]. Thus, a considerable amount of GSH is produced by the liver and released into plasma and bile [22]. Rat liver cytosolic GSH has a half-life of 2–3 h [8], and the daily turnover for GSH is estimated to be higher than cysteine turnover in the body protein pool, around 40 mmol per day [21]. Transsulfuration is not present in the fetus, newborn infants, or patients with cirrhosis [23]. Cirrhosis causes a decrease in methionine adenosyltransferase activity following a reduction in S-adenosylmethionine production and lower effectivity of the transsulfuration pathway [24]. Glutathione concentration within extracellular fluids and blood plasma reaches only several μ M; however, in some extracellular fluids, such as lung lining fluid, 100–400 μ M levels have been detected [25,26].

2.2. Cell Uptake and Metabolism of Glutathione

To date, two mechanisms of glutathione uptake into mammalian cells are known [19]. The most common one is primarily associated with the activity of γ -glutamyl transpeptidase (GGT) (Figure 2). GGT is localized to the cell surface and cleaves only extracellular substrates, GSH, and oxidized GSH (GSSG), its most abundant ones. The amide bond between the glutamine γ -carboxyl and the cysteine amino units does not allow cleavage of GSH by cellular and circulating serum peptidases [27]. It is hydrolyzed by the γ -glutamyltranspeptidase (GGT) to glutamate and Cys-Gly. Cys-Gly can be cleaved by membrane-bound dipeptidases (MDBs) or intracellular Cys-Gly peptidases. Cellular uptake of Cys-Gly or the individual Cys, Gly, and glutamate units serve as precursors for intracellular GSH synthesis. GGT is expressed on the luminal surface of excretive and absorptive cells that line glands and ducts throughout the body, with the highest level of GGT activity in the kidney and pancreas ducts [28]. It is nearly absent, however, from the hepatocytes and cardiac myocytes [7]. The absence of GGT activity on the apical surface of the kidney's proximal tubules by genetic disorder results in glutathionuria [29,30].

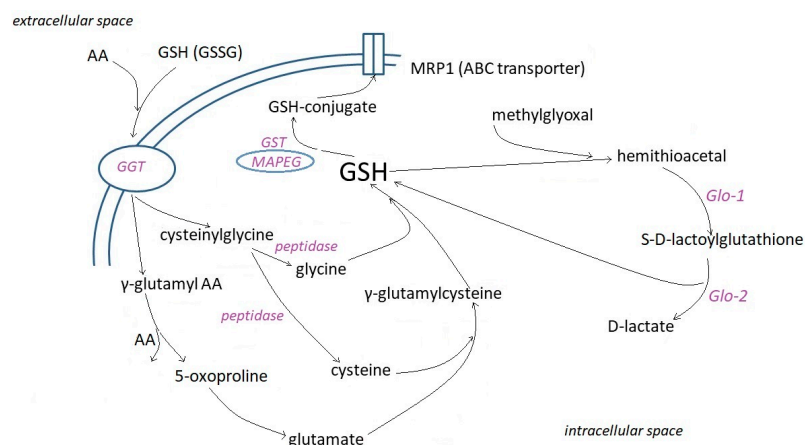


Figure 2. Involvement of γ -glutamyl transpeptidase (GGT), glutathione-S-transferases (GST), their subfamily of Membrane Associated Proteins in Eicosanoid and Glutathione metabolism (MAPEG), and glyoxylases (Glo) in the intracellular metabolism of GSH. MRP1 (multidrug resistance-associated protein 1) transporter facilitates the unidirectional transport of conjugates.

GGT has multiple functions, including catalytic transfer of γ -glutamyl groups to amino acids and short peptides, hydrolysis of GSH to glutamyl moiety and cysteinyl glycine, and catabolism of GSH conjugates [31]. GGT allows hydrolysis of a broad range of γ -glutamyl amides and transpeptidation of amino acids or dipeptides [32]. So GSH, its *S*-conjugates, GSSG, γ -glutamyl di- or tripeptides, glutamine, *l*- α -methyl derivatives of γ -glutamyl amides, various lipid-derived mediators (e.g., leukotriene C4), geranylgeranyl, poly- γ -glutamyl derivatives serve as substrates of GGT [33–36]. Many tumor cells express GGT on their entire cell surface and can therefore cleave GSH not only in the ductal but also in interstitial fluid and blood [37]. GGT expression provides tumor cells with an additional source of cysteine and cystine from the breakdown of extracellular GSH and GSSG [38].

Besides the GGT pathway, there is evidence of Na^+ -dependent and Na^+ -independent glutathione transport systems for glutathione cell uptake expressed in the renal basolateral membrane [38,39], the small intestine [40], and the brain [41]. In the renal basolateral membrane, two Na^+ -independent Organic Anion Transport systems (OAT1 and OAT3) [42] and the Na^+ -dependent dicarboxylate carriers are the most important organizations [43,44]. On the other hand, the plasma membrane glutathione efflux can be facilitated by specifically or ubiquitously expressed membrane proteins and anion channels such as multidrug resistance-associated proteins (MRP1-5), Cystic Fibrosis Transmembrane Conductance Regulator (CFTR), Arginine/Ornithine Transport ATP-binding Proteins (OATP 1,2), and ATP-Binding Cassette superfamily G member 2 (ABCG2) [19].

2.3. Intracellular Distribution and Functions of GSH

Within the cell, there are three main glutathione pools. The cytosol (80–85%), the mitochondria (10–15%), and the endoplasmic reticulum [45–47]. Studies by Birk et al. and Montero et al. [48,49] pointed out that the total glutathione content in the lumen of the endoplasmic reticulum even exceeds the entire cellular glutathione content. GSH and GSSG concentrations depend on the subcellular compartment, the cell type, and the organism. Accordingly, the redox potential of the GSSG/2GSH system varies from tissue to tissue, from organism to organism. This relies on the proportion of GSH and GSSG and the total concentration of glutathione, which is quite challenging to estimate their actual concentration and ratio in vivo [50,51]. For example, taking the local pH and GSSG/2GSH ratios into consideration, cytosolic $E_{pH7.0} = -289$ mV (or even lower), mitochondrial matrix $E_{pH7.0} = -296$ mV (or even lower), and human plasma $E_{pH7.4} = -118$ mV half-cell reduction potentials (E_{hc}) have been estimated [52]. Furthermore, a correlation has been found between the cell cycle, the condition of the cell (stressed, apoptotic, etc.), and the GSSG/2GSH ratio. For instance, in cell proliferation ($E_{hc} = \sim -240$ mV), in cell differentiation ($E_{hc} = \sim -200$ mV), and in apoptosis ($E_{hc} = \sim -170$ mV), which can be applicable for a better understanding of oxidative stress [13,53]. Van't Erve et al. [54] found that GSSG/2GSH levels and reduction potential in erythrocytes reflect genetic differences between individuals.

Cytoplasmic glutathione levels impact glutathione diffusion through nuclear pore complexes [55], playing a role in oxidative signaling during proliferation, epigenetic control of histone activity, and the cell cycle control, mainly in the S + G₂/M phase [56,57]. ATP-dependent transporters have also been reported to import glutathione into the nucleus [58].

Glutathione synthesis occurs only in the cytosol; thus, the mitochondrial pool is supplied by GSH transport and maintained by reducing its oxidized form via the activity of glutathione reductase. Glutathione passes the mitochondrial outer membrane through the mitochondrial porin, a voltage-dependent anion channel (VDAC). As a negatively charged molecule, glutathione cannot diffuse through the mitochondrial inner membrane. Its transport into the mitochondrial matrix is either active or provided in exchange for another anion [7]. Six of the eight anion carriers have the potential for GSH import through the inner membrane into mitochondria. Monocarboxylate, dicarboxylate (DIC), 2-oxoglutarate (OGC), tricarboxylate (or citrate), glutamate-hydroxide, glutamate-aspartate transporters involved in the transport of GSH also provide intermediates of the Krebs cycle and the gluconeogenesis pathway [59]. DIC and OGC were identified as major GSH transporters, although at the expense of Krebs cycle intermediates [60]. Around 70–80% of GSH transport could be associated with DIC and OGC activity in the kidney, but only about 45–50% of liver mitochondria [61]. DIC imparts malate (malonate or succinate) in exchange for phosphate, sulfate, and thiosulfate. Malate conversion into oxalacetate, followed by the formation of phosphoenolpyruvate, is limited for gluconeogenesis in the cytosol. Reduction in DIC expression leads to decreased glutathione levels and impaired complex I activity [62]. OGC transfers 2-oxoglutarate substituting dicarboxylate [63], thus regulating respiration and glycolysis. While succinate from the matrix side increases the affinity of OGC to malate, substrates such as phenyl succinate, pyridoxal phosphate, retinoic acid, and ethanol cause inhibition of OGC. Reduced activity of OGC leads to lower energy production, increased oxidative stress, and it could be the basis of liver or nervous tissue diseases [64–66]. GSSG is not transported out from mitochondria [67].

The endoplasmic reticulum offers a unique setting concerning GSH homeostasis. It contains the thiol oxidase Ero1, which catalyzes the formation of disulfides transmitted to folding substrates via protein disulfide isomerase (Pdi1). Both reduced and oxidized forms of glutathione are transported into the endoplasmic reticulum at different rates, with a preference for the reduced form [68]. Since GSH is oxidized but not reduced in the ER, GSH must be imported into the ER, while GSSG is exported to the cytosol [69]. A study by Ponsoero et al. [70] brought up the finding of facilitated diffusion of GSH through the Sec61 protein translocation complex. In the sarcoplasmic reticulum, ryanodine receptor

calcium channel type 1 (RyR1) was suggested to play an important role [71]. However, Bachhawat et al. [19] pointed out that this might result from the S-glutathionylation of several cysteine residues within the RyR1 molecule. To maintain GSH homeostasis, part of GSSG is transported to the cytosol through vesicular transport [72]. Most GSSG reacts with proteins or protein disulfide isomerase involved in oxidative protein folding [64]. A lower GSH:GSSG ratio results in more oxidizing conditions (−240 mV) [70] in the endoplasmic reticulum allowing protein disulfide formation.

GSH plays an essential role not only in the peripheral tissues but in the central nervous system (CNS) as well. Brain tissues are rich in unsaturated fatty acids. Due to their relatively low levels of antioxidants or antioxidant enzymes, they are rather sensitive to oxidative damage. The most important small molecular CNS antioxidants are GSH, ascorbic acid (vitamin C), and α -tocopherol (vitamin E) [73]. Among these antioxidants, GSH seems to be the determining agent because it is selectively decreased in the brains of patients with these neurodegenerative diseases (e.g., Parkinson's disease, Alzheimer's disease, and Amyotrophic lateral sclerosis) [74]. Therefore, regulating the redox state by intracellular GSH is crucial for maintaining cellular functions under physiological and pathological conditions.

In the central nervous system, besides the functional neurons, there are several other types of cells for the nervous system to function properly. This is where a set of glial cells intervene, which make up 25–50% of the nerve mass [75]. The most common type of glial cells in the CNS are the astrocytes and the microglia. Synthesis of GSH occurs both in the neurons and the glial cells. In an early work by Rice and Russo-Menna (1998) [76], GSH levels of glutathione in neurons and glia were reported to be 2.5 nM and 3.8 mM, respectively. The authors found that ascorbate predominates in neurons (10 mM), whereas GSH is slightly predominant in glia. According to the above, GSH supplementation seems promising for treating patients with neurodegenerative diseases.

2.4. Acid–Base Properties

The acid–base properties of glutathione (GSH) have long been the focus of scientific interest. It has three acidic (thiol, glyciny carboxyl, glutamyl carboxyl) and one basic (amino) functional group. Accordingly, in an aqueous solution, glutathione can exist in four different macroscopic protonation states:



where L^{3-} is the fully deprotonated, H_4L^{+} is the fully protonated GSH molecule.

Since the HL^{2-} and the H_3L forms have four protonation isomers (microspecies) each, and the H_2L^{-} form has six microspecies, the molecule has sixteen different protonation states (microspecies) altogether [77].

The micro and sub-micro protonation constants characterize the acid–base properties at the submolecular level [78]. These constants allow quantification of the proton binding capacity of submolecular basic units when the protonation states of all other sites are defined in the molecule [79]. Group constants are special micro constants when the rest of the groups in the molecule are far enough apart, and their protonation does not affect the basicity of the group [80]. The rotational state of the flexible parts of the molecules is defined by the sub-micro constants when protonation occurs [81]. The correct characterization of the basicity of the sites of protonation of multidentate ligands can be conducted using the micro and sub-micro constants. In addition, this group of constants is used to measure the concentration of different protonation forms, of which the principal form is not always the reactive form in chemical and biological processes. [82–86]. The macroscopic protonation constants (K_1 – K_4) determined by 1H NMR–pH titrations were as follows: $\log K_1$ 9.65; $\log K_2$ 8.78; $\log K_3$ 3.52; and $\log K_4$ 2.22 [77].

The obtained values were found to be very similar to those determined in earlier works of Pirie and Pinhey [87] (9.62, 8.66, 3.53, 2.12), Li et al. [88] (9.65, 8.75, 3.59), and

Martin and Edsall [89] (9.62, 8.74). The results demonstrated that the first and the second protonation constants were predominated by the overlapping protonation of the amino and the thiolate site, the amino being typically more favored. The carboxylate groups also protonated in an overlapping fashion, the glyciny carboxylate being more basic. It is worth mentioning that the protonated amino group makes the inherently more basic glutamyl carboxylate more acidic [77].

It is important to note that the physico-chemical properties (e.g., complex formation, nucleophilic reactivity, redox properties) and biological functions of glutathione could be significantly different at different protonation states (i.e., in solutions with different pH values) [90–93] and its redox behavior [94,95]. Furthermore, ionic strength and the nature of ionic media also affect the acid–base characteristics of glutathione [96].

2.5. Antioxidant Properties

The pKa value of GSH (ranging from 8.6 to 8.8 [87–89]) results in low thiol reactivity in the cellular environment [97]. Still, high GSH concentrations enable some reducing activities against oxidizing agents in the cell [98]. GSH, for example, can reduce H_2O_2 , resulting in GSSG and water [99]. The rate of reaction depends on the cellular GSH level and the ratio of GSH to H_2O_2 concentrations [100]. Recently, Zinatullina et al. [101] confirmed that the oxidation of GSH is accompanied by radical formation. GSH reacts with the majority of free radicals generating thiyl radicals. Consecutive reactions of the radicals with a thiolate anion and molecular oxygen lead to disulfide and superoxide radicals formation [102]. Furthermore, γ -glutamylcysteine, a GSH precursor, was found to decompose H_2O_2 similarly to glutathione peroxidase-1 [103].

Glutathione exists in 100 μ M concentrations as glutathione persulfide (GSSH) [104], the latter exhibiting higher activities due to its higher nucleophilic power than GSH [105]. Under specific conditions, GSSH reacts with H_2O_2 , while GSH does not [106]. Furthermore, its reactions with one-electron oxidants are faster than similar reactions of thiols [107]. GSSH are intermediates in the synthesis of iron-sulfur clusters and mitochondrial H_2S oxidation [108–110]. GSH can react with HS^- catalyzed by sulfide quinone oxidoreductase or thiosulfate sulfurtransferase, forming GSSH, which can reduce oxidized thioredoxin. Single-domain sulfurtransferase (TSTD1, known as rhodanese) and mercapto pyruvate sulfurtransferase can also directly transfer sulfides to GSH and the thioredoxin antioxidant systems [111]. Mutations in persulfite dioxygenase, oxidizing GSSH to sulfite and GSH, are bases for autosomal-recessive inherited ethylmalonic encephalopathy [112].

2.6. Redox Signaling Properties

Signaling is the process that makes cells capable of reacting to the change in their environment (intercellular signaling) or their homeostasis (intracellular). The initial step of the process is the interaction of the signaling particles (ligands) with the target molecule (receptor). The well-known signaling mechanisms involve protein–protein interactions, allosteric changes induced by the binding of ligands, proteolytic processing, and chemical modifications such as acylation, acetylation, alkylation, and phosphorylation of proteins. On the contrary, redox signaling is the transduction of signals based on the transfer of electrons. Redox signaling involves a broad spectrum of pathways involving free radicals, redox-active metals (e.g., iron, copper), or reductive equivalents [74]. Here only those pathways are mentioned that are based on a modification of signaling proteins through the modification of one amino acid, cysteine.

The physiological level of hydrogen peroxide (H_2O_2) and nitric oxide ($\cdot NO$) can selectively react with the thiol function of the cysteinyl residues at the active site of the proteins (receptors, enzymes, transporters, etc.). Accordingly, the receptor-mediated stimulation of the H_2O_2 and $\cdot NO$ production are part of normal physiology; this is especially true for the longer-lived H_2O_2 . [113]. However, overproduction of these and related species (ROS and RNS) lead to irreversible oxidation of the thiol residues and impairs cellular protein functions [114,115]. The GSSG/2GSH redox system is fundamental in the cells and, together

with other redox-active couples (including NADPH/NADP⁺, Trx-SH/Trx-SS), regulates and maintains the appropriate cellular redox status. For example, the GSSG/2GSH half-cell reduction potential differed in cell proliferation, differentiation, and apoptosis [13,53]. Thus, changes in the GSSG/2GSH ratio are fundamental in controlling signal transduction that supports cell cycle regulation and other cellular processes [55].

The functions and activities of GSH as the main regulator of cellular redox status and redox signal transduction have been reviewed [17,116–119]. GSH acts protectively against oxidative stress by reacting directly with [•]NO, superoxide anion radical (O₂^{•-}), H₂O₂, hydroxyl radical ([•]OH), peroxynitrite anion (ONOO⁻), and the lipid peroxidation product 4-hydroxy-2-nonenal (4-HNE) [116,117]. Such reactions directly modify the cellular GSSG/2GSH half-cell potential, a physiological signaling event. Furthermore, changing the GSH level results in a selective change in the activity of the thioredoxin/glutathione systems [118], the glutaredoxin/glutathione system [119], and the activity of some GST isoforms. The latter protein family is involved not only in the metabolism of xenobiotics but also of endogenous compounds which play critical roles in regulating signaling pathways [120–122].

2.7. Reactions with Electrophilic Xenobiotics

Glutathione-S-transferases (GST) lower the pK_a of GSH thiol under 6, enhancing rates of nucleophilic addition and substitution reactions with electrophilic xenobiotics (Figure 2). These reactions are examples of Phase II bioconjugation reactions, most of which result in reduced toxic effects of the parent compounds or their metabolites [98,123]. Other enzymes/enzyme systems, e.g., selenium-containing glutathione peroxidases (GPx) or peroxiredoxins (Prdx), use GSH to reduce various peroxides and hydroperoxides. Glyoxalase (Glo) performs conjugation of GSH with the glycolysis byproduct methylglyoxal to form (S)-lactoylglutathione (Figure 2). Moreover, glyoxalase II (Glo-2) catalyzes S-glutathionylation using (S)-lactoylglutathione [124].

3. The Glutathione Peroxidase System

The glutathione or glutathione peroxidase system consists of glutathione peroxidase (GPx) and glutathione reductase (GR). In the decomposition reaction of H₂O₂ or other organic peroxides (HOOR), two molecules of GSH reduce the substrate to H₂O or the corresponding alcohol (HOR) and restore the enzyme forming GSSG with concomitant formation of GSSG and H₂O.



GSSG can be excreted from the cell or recycled by GR using the reducing power of NADPH (Figure 3). NADPH arises in two reactions of the pentose phosphate pathway, which is the most potent source of it. However, NADPH can also be formed directly in the mitochondria by NAD(P)⁺ transhydrogenase, mitochondrial/cytosolic NADP-dependent isocitrate dehydrogenase, or cytosolic malate dehydrogenase [125].

GR is a homodimeric flavoprotein consisting of 52 kD monomers. Except for synthesis, the activity of GR represents a second source of GSH in the cytosol and some organelles, such as mitochondria. Although inhibition of GR has been reported to cause a depletion of GSH and accumulation of GSSG [126], a comprehensive study of the GR and the cellular thiol redox system is missing [127]. Inhibition of the enzyme has also been related to the toxicity of various chemicals and metals [128,129].

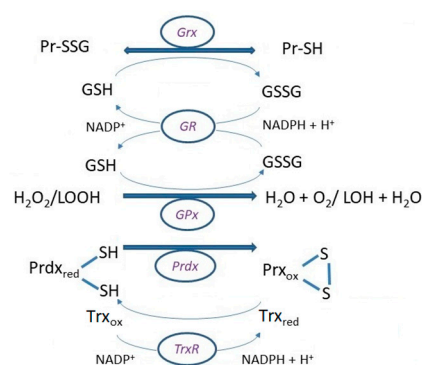
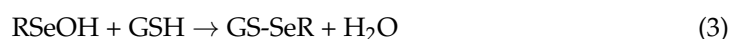
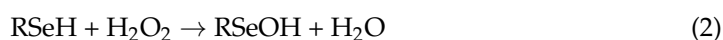


Figure 3. Basic reaction mechanisms of glutathione peroxidase (GPx), and glutaredoxin in (de)glutathionylation using (GSH)GSSG, respectively, and reduction of GSSG by the activity of glutathione reductase (GR) with reducing the power of NADPH + H⁺. Reduction of peroxidoredoxin (Prdx) after disposal of peroxides is ensured by thioredoxin (Trx), which is reduced by consumption of NADPH + H⁺ in catalytic efficiency of thioredoxin reductase (TrxR).

The term glutathione peroxidase (GPx) describes only a small subgroup of the peroxidases [130], which belong to a group of phylogenetically related enzymes. GPx 1–4 are selenoproteins with selenocysteine (SeCys) in the catalytic center. GPx6 is a human selenoprotein [131]. Their important antioxidant function was shown in various places and cell structures: GPx1 is ubiquitous in the cytosol and mitochondria, GPx2 in the intestinal epithelium, and GPx3 in the plasma; all three work in the aqueous phase reducing H₂O₂ and free fatty acid peroxides [131]. GPx4 protects mainly membranes by reducing phospholipid and cholesterol peroxides [131,132]. Gpx5, which contains cysteine instead of Se in the active center, is a secretory enzyme of the epididymis. GPx6 is a human selenoprotein and is formed by the olfactory epithelium. GPx7 and GPx8 are also CysGPx with low peroxidase activity. GPx1, 2, 3, 4, 5, and 6 are homotetramers, which could determine their specificity for hydrogen peroxide. GPx4, 7, and 8 are monomers. This structure probably enables the reaction with more complex lipid hydroperoxides, but this has been proven only for GPx4 [132]. The catalytic center of GPx was first characterized as a triad consisting of SeCys or Cys, Gln, and Trp. It was later found to be a tetrad with Asn. A conservative feature for these GPx is the presence of a second or even a third cysteine residue.

The reaction mechanism differs between individual GPx isoforms, whose activity requires GSH. In general, they do not form a ternary complex between the enzyme, hydroperoxide, and GSH, but the reaction has a concomitant oxidation and a reduction part. In the oxidation part, deprotonation takes place in the same way. The side chains of the Glu, Try, and Asp residues form a highly nucleophilic region in the enzyme's active center, where oxidation of the active site selenocysteine (RSeH) or cysteine (RSH) occurs after binding the peroxide. This reaction results in the formation of a selenenic acid (RSeOH) derivative. The selenenic acid is then converted back to the selenol (RSeH) by a two-step process that begins with a reaction with GSH to form the GS-SeR and water. A second GSH molecule reduces the GS-SeR intermediate back to the selenol, releasing GS-SG as the byproduct [52,132]. A simplified representation (with H₂O₂ as a substrate) is shown below:



Glutathione reductase then reduces the oxidized glutathione to complete the cycle:



Selenium deficiency results in increased GSH synthesis in the liver with accompanying release to the plasma [133]. Increased plasma GSH led to cysteine depletion, impaired protein synthesis, decreased GPx, and increased GST activities [134]. Usually, GPx requires GSH in millimolar concentrations in the intracellular space, and plasma GSH reaches micromolar concentrations, which questions GPx's antioxidant function [135]. However, within the cell, in the cytosol and mitochondria, the GPx system appears to be very efficient in the elimination of H₂O₂ due to the low (100–200 μM) K_m value of the enzyme [136] and the range of substrates [137]. Mimicking GSH, γ-glutamylcysteine can be used by GPx1 as a cofactor [103].

4. Glutaredoxins (Grx)

The thiol oxidoreductase glutaredoxins (Grx) are small proteins reducing various protein disulfides (PrSSPr) and GSH-protein mixed disulfides (PrSSG), where the electron donor is glutathione [138]. Grxs catalyze glutathionylation, post-transcriptional modifications, and the disulfide exchange between GSSG and protein thiols (PrSH) [139] (Figure 3). Grx-catalyzed (de)glutathionylation is an important event in signal transductions and serves as the primary protective mechanism against the irreversible oxidation of cysteine residues [115]. As mentioned above, the standard cell potential changes depending on the environment and the cell itself. Cell proliferation occurs at approximately −240 mV, differentiation at about −200 mV, and apoptosis at around −170 mV [55]. Changes in the GSH/GSSG redox potential can be sensed by Grxs, which operate as GSH-dependent reductases at about −240 mV and GSSG-dependent oxidases at about −170 mV [140].

Grxs are characterized by their active site motif. Dithiol-type Grx (class I) enzymes have a Cys-Pro-Tyr-Cys active site, while monothiol Grx (class II) enzymes do not contain a thiol at the C-terminus of the active site (Cys-Gly-Phe-Ser). Dithiol Grxs and monothiol Grxs with one Grx domain are found in all living organisms. Multi-domain monothiol Grxs (PICOTs, PKC-interacting cousin of thioredoxin) are present in eukaryotic cells. These contain an N-terminal Trx-like domain and three C-terminal monothiol Grxs domains [141]. Two other regions were recognized near the active site, the Grx characteristic motif GG and the TVP, which are involved in binding GSH [142].

4.1. Glutathionylation

Glutathionylation involves the reversible attachment of glutathione to cysteine residues in target proteins. Conditions of elevated oxidative stress increase the levels of protein glutathionylation. The glutathionylation/deglutathionylation cycle is viewed as a process that acts primarily against ROS/RNS via reducing aberrant cysteine modifications and thereby preventing the formation of damaging irreversible cysteine modifications.

There are three pathways of glutathionylation. (a) The thiol-disulfide exchange between GSSG and PrSH is accomplished at a low GSH:GSSH ratio. The reactivity of PrSH depends on the thiol pKa [143]. (b) The oxidation of the PrSH yields a thiyl radical (RS[•]), which reacts with the deprotonated form of glutathione (GS[−]), forming a mixed disulfide radical (RSSG^{•−}). After the loss of an electron, a mixed disulfide (RSSG) and a superoxide anion radical (O₂^{•−}) are formed [144]. (c) Mixed disulfides can also be formed with low molecular weight thiols with indistinct biological relevance. As Lushchak [60] discussed, inhibition of glutathione reductase, phosphofructokinase, fatty acid synthase, or activation of fructose-1,6-bisphosphatase by CoASSG was shown.

Cysteine residues of proteins with a low pKa are targets for redox modulation under oxidative or nitrosative stress conditions. The primary products of these oxidative transformations are the respective thiyl radicals (PrS[•]). These reactive intermediates can react with glutathione (GSH) to form stable glutathionylated protein disulfides (PrSSG) to prevent their further oxidation with molecular oxygen. The protected protein thiol can be regenerated by the deglutathionylation process (e.g., through a reaction with another GSH molecule). Under oxidative stress, the thiyl radical can be further oxidized to form sulfenic (RSOH), sulfinic (RSO₂H), or sulfonic acid (RSO₃H) derivatives of the

proteins. Both sulfenic and sulfinic acids of proteins can be reduced by Trx and sulfiredoxin, respectively [145–147]. In contrast, sulfonic acid cannot be reduced. Both sulfenic and sulfinic acids of proteins can be conjugated to GSH to form S-glutathionylated proteins via glutathione S-transferases (GSTs), Grx, or nonenzymatically. Glutathionylation was referenced to cytoskeletal proteins, metabolic, redox enzymes, cyclophilin, stress proteins, nucleophosmin, transgelin, galectin, and fatty acid binding protein [148], affecting their activity either in activation or decrease.

4.2. Deglutathionylation

Deglutathionylation undergoes cleavage of the disulfide linkage of the glutathionylated protein with another GSH molecule (Figure 3). The reaction can proceed (a) either in a mixed disulfide intermediate with an N-terminal thiol active site; (b) in a mixed disulfide intermediate by the attack of a second GSH molecule; or (c) by non-covalent binding of the thiol function of both an N-terminal thiol active site and GSH-coordinating metal cofactor in the [Fe-S] binding Grx subgroup [142]. The motif in the active site and the type of disulfide bond in the target protein are decisive for the reaction mechanism [149]. In the reaction mechanism of monothiol Grxs, the reduction of glutathionylated proteins (PrSSG) begins with a nucleophilic attack of the N-terminal cysteine. As a result, glutathionylated Grx and reduced substrate protein are released. The Grx-SG intermediate is cleaved by a GSH molecule, resulting in reduced Grx and GSSG, which is subsequently reduced by GR [150] (Figure 3). In the mechanism of dithiol Grxs, the reduction of PSSG and mixed disulfides begins with a nucleophilic attack of the N-terminal cysteine, but GSH is released. The Grx-protein intermediate is reduced by the second C-terminal active cysteine of Grx, forming oxidized Grx and reduced protein [151,152]. Dithiol Grx can also use monothiol mechanisms. However, both mechanisms are critically dependent on the availability of reduced GSH [153].

Apart from oxidoreductase activity, both classes of Grx proteins can bind [Fe-S] clusters. Class II enzymes are essential in the processes of regulation of Fe metabolism. Their function depends on the [Fe-S] binding capacity and not on the reductase activity [154]. In addition, Grxs have dehydroascorbate reductase and transhydrogenase activity, catalyzing denitrosylation and partial cystine conversion [155].

Monothiol Grxs (Grx3 and Grx5) form an iron–sulfur complex. Both isoforms can transfer iron to specific proteins. However, monothiol Grxs cannot deglutathionylate target proteins [156]. Grx3, localized in the cytosol, has a unique domain structure consisting of an N-terminal Trx-homology domain [141,157]. The first discovered function of Grx3 was related to that of protein kinase C theta, and in T-cells, Grx3 colocalizes with it, hence the name PICOT [157]. Since Grx3 is expressed in a wide variety of organs and tissues, it has been proposed as a redox sensor in signal transduction in response to reactive oxygen and nitrogen species [158]. Nuclear Grx3 has a role in the epigenetic regulation of chromatin by regulating the methylation of myelin transcription factor 1 and cell proliferation [159,160]. Grx5 participates in the biogenesis of [4Fe–4S] clusters by interacting with ISCA1 of the mitochondrial homolog of the iron–sulfur cluster assembly and ISCA2 of the cytosolic iron cluster [161,162]. Grx5 forms a cluster in the cytosol with a family of BolA-like proteins (regulatory DNA-binding proteins) for the maturation of iron–sulfur proteins [163].

Grx1 and Grx2 are dithiol Grxs. Most human Grx1 is found in the cytosol, less in the nucleus [164] and the mitochondrial intermembrane space [165]. Grx1, unlike Trx, is not an essential protein [98]. Grx1 activity depends on the redox state of the cells, especially the GSH/GSSG ratio [166]. In addition to deglutathionylation activity, Grx1 has also been able to denitrosylate protein Cys-NOs and prevent the pro-apoptotic effect of nitric oxide in tumor cell lines and cardiomyocytes [167,168]. Grx2 is about 20 times less abundant than Grx1 [169]. Depending on gene splicing, it is localized in mitochondria, cytosol, or nucleus [170]. Like Grx1, it catalyzes the reduction of disulfides mixed with GSH with a higher affinity but with a lower turnover rate [171]. However, these two proteins behave differently in response to an oxidative environment. While Grx1 is inhibited

when other structural cysteine residues are oxidatively modified [154], Grx2 is activated. The different response to oxidative conditions is due to the ability of Grx2 to form [Fe–S] clusters [172]. The [Fe–S] clusters act as sensors for Grx2 activity under oxidative conditions [154]. Outside the active site, two cysteines form a [2Fe–2S]-bridged dimer that is enzymatically inactive. Oxidative stress increases GSSG concentration and reduces the availability of GSH for coordination of the [Fe–S] complex, leading to cluster degradation and formation of enzymatically active Grx2 monomers [154]. Grx2 can cycle and accept electrons from thioredoxin reductase1 (TrxR1) [171]. In mitochondria, Grx2 has been shown to efficiently catalyze (de)glutathionylation of complex I and SOD1 [173,174].

5. Peroxiredoxins (Prdx)

Peroxiredoxins (Prdxs) are cysteine-dependent peroxidase enzymes [132,175], whose low K_m for H_2O_2 (10 μM) and their ubiquity, comprising up to 0.8% of total protein in some animal cells predispose them for reduction H_2O_2 [176]. However, they can also reduce peroxynitrite, peroxynitrous acid, and lipid peroxides [177,178]. Their peroxidatic functions overlap with GPx and catalase, and their catalytic efficiency is lower ($\sim 10^5 M^{-1} s^{-1}$) compared to GPx ($\sim 10^8 M^{-1} s^{-1}$) and catalase ($\sim 10^6 M^{-1} s^{-1}$) [179]. Furthermore, comparing Prdx K_m for H_2O_2 with that of GPx and catalase exceeding even the millimolar range [180] suggests that the role of Prdx is rather as a sensor of H_2O_2 [178] than oxidative stress condition reversal.

Prdxs are divided into the subgroups Prdx1/AhpC, Prdx5, Prdx6, Tpx (thiol peroxidase), PrdxQ/BCP, and AhpE. Human Prdxs can be posttranscriptionally modified by glutathionylation, acetylation, ubiquitination, oxidation (RSOH, RSSR, RSO₂, RSO₃), S-nitrosylation, phosphorylation [181] or tyrosine nitration [182]. Prdxs proceed the same catalytic cycle, where the active site cysteine (peroxidatic cysteine, Cys_P) reduces peroxides and forms Cys_P-sulfenic acid (RSOH), releasing water or the corresponding alcohol. Some Prdxs contain a second, so-called resolving cysteine (Cys_R), which reacts with RSOH forming disulfide (Cys_P-S-S-Cys_R) and water [183]. Cys_R can originate from the adjacent monomer, the same monomer, glutathione, or a redox-relay binding partner [184]. Accordingly, six human Prdxs isoforms are diversified into three subgroups.

In general, the Prdx1 subfamily enzymes are the most highly expressed, making up 0.1–1% of the soluble protein in the cell. The “typical 2-Cys” Prdxs are homodimers with two active sites (having both a Cys_P and Cys_R). The disulfide bond is formed between the two subunits in the reaction of RSOH and Cys_R of the other subunit. Reduction of disulfide bond is catalyzed by Trx (Figure 3), trypanredoxin, or alkyl hydroperoxide reductase [179,185]. In the reduced state, PrdxI, II, and IV form decamers or dodecamers such as PrdxIII [186]. Reduced decamers show efficient peroxidase activity and, depending on other posttranslational modifications, form high molecular weight oligomers associated with cell cycle checkpoints, chaperones, and various intracellular processes [187–189]. The “atypical 2-Cys” Prdxs (Prdx5) are monomers forming intramolecular disulfide since both Cys_R and Cys_P are within the same molecule; their reduction is achieved by Trx. The “atypical 2-Cys” Prdxs can form dimers independently of the redox state [179]. The “1-Cys” Prdxs (Prdx6) contains only Cys_P in the N-terminus [190]. The resolving electron donor thiol can be glutathione, allowing the formation of a mixed disulfide, while the second donor thiol enables the reduction of the formed disulfide bonding. Ascorbate, lipoic acid, and cyclophilin, but most commonly GSH, can serve as electron donors for disulfide reduction [179,185,191]. Prdx6 reduces phospholipid hydroperoxides using GSH, and also the GST P1-1 class showed the ability to act as phospholipase A₂ [192]. Hyperoxidation, formation of RSO₂H or RSO₃H, and phosphorylation regulate the activity of Prdxs [181]. The “1-Cys” Prdxs are resistant to hyperoxidation. Hyperoxidation can be repaired by sulfiredoxin, but not in human Prdx6 [193].

6. Glutathione-S-Transferases (GST)

GSTs belong to the Phase II biotransformation enzymes catalyzing the GSH-mediated peroxide reduction [194] and conjugation of GSH with a variety of reactive electrophiles, most commonly generated by cytochrome P450 metabolism [195]. GSTs expressed ubiquitously, but tissue-specific distribution is probably an adaptive response against endo- and exogenous metabolites [196]. GSTs comprise two distinct superfamilies, membrane-bound microsomal and soluble cytosolic. In humans, cytosolic GSTs are encoded by 16 genes, while the microsomal, at least by six genes, in addition to significant genetic polymorphisms [197]. According to the degree of sequence identity and localization, the cytosolic GSTs (cGSTs) are divided into alpha, mu, pi, omega, theta, delta, sigma, and zeta (A, M, P, O, T, D, S, Z) classes. Mitochondrial GSTs (mGSTs) are divided into A, M, P, and kappa (K) classes. A novel superfamily designated MAPEG (Membrane Associated Proteins in Eicosanoid and Glutathione metabolism) includes members of widespread origin with diversified biological functions. Members of this family are leukotriene C-4 synthase, 5-lipoxygenase activating protein, prostaglandin E synthase, and microsomal glutathione S-transferases (MGST) 1, 2 and 3 [198,199].

Due to polymorphisms, gene duplication, and genetic recombination, GSTs have multiple isoenzymes with overlapping substrate specificity and diversity [200]. In humans, the highest cytosolic GST activity level is present in the liver, whereas the kidney, lung, and intestine show lower activity levels than that of the liver at 22, 66, and 63%, respectively [201]. Intracellularly, some specific GST activities also were detected in the plasma membrane, outer mitochondrial membrane, and nucleus [198].

In mammals, GSTs exist as homodimers with analogous tertiary structures [202]. All GSTs have a basic protein fold comprising two subunits with C-terminal and N-terminal domains. The N-terminal domain includes a thioredoxin-like fold, β - α - β - α - β - α , where β - β - α motif, known as G-site, serves as the binding site for GSH through the γ -glutamyl unit. The C-terminal domain is diverging [202–204]. The conserved proline residue at the N-terminal β 3 strand ensures catalytic function and stability of thioredoxin-like proteins [205]. The G-site sequence similarity divides GST into two subgroups. Tyrosine-type GSTs contain Tyr residue (T- or P-class), which activates GSH [206]. Replacement of Tyr by Phe reduces the catalytic activity [207]. The Ser/Cys-type GSTs (O-class) used Ser or Cys to form mixed disulfides with GSH. These GSTs are more involved in redox reactions [208]. Selectivity for the substrates is determined by high variations in hydrophobic amino acid residues in the cleft between domains, called the H-site [208].

GSTs transfer GSH to several various electrophilic compounds [209]. The reactions with some compounds, such as benzyl and phenethyl isothiocyanates and alkyl dihalides, can be reversible, increasing their toxicity [210]. Some classes conjugate GSH with epoxides and catalyze isomerization or reduction of harmful peroxides [52]. It was shown that the physiological function of Z-class GSTs is the cis-trans isomerization of 4-maleylacetoacetate to 4-fumarylacetoacetate [211]. The A-class GSTs display selenium-independent GPx activity, thereby reducing phospholipid peroxides and cholesterol hydroperoxides within the membrane without phospholipase A₂-mediated release [212]. Anionic A-class GSTs also efficiently conjugate 4-hydroxynonenal, balancing lipid production and peroxidation [213]. Furthermore, isomerization of the double bond in selected 3-oxo- Δ^5 -steroids releasing 3-oxo- Δ^4 -steroids has been detected in some A-class GSTs [214]. S-class GSTs enable anti-, proinflammatory, and immunomodulatory functions [215]. From this class, prostaglandin-D₂ synthase and prostaglandin-E₂ synthase catalyze the cleavage of prostaglandin H₂, forming prostaglandin-D₂ or E₂ [216]. The enzyme leukotriene-C₄ synthase (MAPEG) catalyzes the conjugation of GSH with epoxide leukotriene A₄ [217]. Unique blood-barrier functions were described for M-class GSTs in the testis and brain [218]. O-class GSTs were able to modulate ryanodine receptor calcium release channels in cardiac muscle due to structural similarities to Chloride Intracellular Channel Proteins (CLIC) [219]. Approximately 15% sequence identity was found between O-class GSTs and CLIC1 [219]. CLIC proteins contain Grx-like active site motif, Cys-Pro-(Phe/Ser)-(Ser/Cys), present also in

O-class GSTs [208,220,221]. CLIC, however, bind GSH covalently creating a mixed disulfide, unlike classical GSTs, which bind GSH in the active site non-covalently but with high affinity [220]. Finally, as indicated by the structural similarity, (de)glutathionylation activity by Menon and Board [222] but also dehydroascorbate reductase, S-(phenylacetyl)glutathione reductase [223,224] activities of GSTO1-1 were confirmed. In P-class GSTs, chaperone functions and the influence of the MAPK pathway through JNK and TRAF2 modulation in response to oxidative/nitrosative stress were also detected [225]. One of the unwanted consequences and the subject of intensive ongoing research is resistance to drugs owing to increased GSTs activities [226].

7. Glyoxylases (Glo)

The glyoxalase system is a ubiquitous enzymatic network present in the cytoplasm, and some of them are also in the nucleus. It consists of glyoxalase 1 (Glo-1), glyoxalase 2 (Glo-2), and reduced glutathione (GSH) (Figure 2), which perform an essential metabolic function in cells by detoxifying methylglyoxal (MG) and other endogenous harmful metabolites into non-toxic D-lactate [227,228]. As discussed in Rabbani et al. [229], in mammals, methylglyoxal arises in 0.05–0.1% as a minor product from (a) glyceraldehyde-3-phosphate and dihydroxyacetone phosphate degradation in glycolysis, (b) oxidation of acetone by cytochrome P450, (c) oxidation of aminoacetone by semicarbazide amine oxidase, and (d) degradation of glycated proteins and monosaccharides. Methylglyoxal, whose formation can reach 3 mg/kg body weight/day [230], is a glycating agent, forming mainly arginine-derived hydroimidazolone adducts, DNA adducts, and isomeric imidazopurinones [231]. In the glyoxalase system, the rate-limiting enzyme is glyoxalase 1 (Glo-1, lactoylglutathione lyase). Methylglyoxal undergoes spontaneous thiolation with GSH, followed by the Glo-1 catalyzed conversion of methylglyoxal thioacetal to (S)-lactoylglutathione [232,233]. Studies have revealed that Glo-1 is a dimeric metal ion-dependent isomerase converting various glutathione-hemithioacetals to glutathione thioesters [234]. The activity of Glo-1 can be modified by phosphorylation or nitrosylation. While acetylation and oxidation have no effect, acylation of GSH inhibits Glo-1 activity [235]. Glo-2 is a thioesterase catalyzing the hydrolysis of (S)-lactoylglutathione to D-lactate and GSH. Glo-2 predominantly interacts with glutathione moieties allowing hydrolysis of a variety of glutathione substrates [234,236,237]. Glo-3, found in bacteria, catalyzes the conversion of methylglyoxal to D-lactate without the participation of GSH. DJ-1 and its homologs may display this function in humans [232].

Dicarbonyl stress causes protein modification and misfolding, affecting their structure and function, increasing the importance of Glo-1 in detoxification and its implication in the pathophysiology of diseases [238]. Moreover, there is evidence that the Glo-1 gene is a hotspot for copy-number variation associated with multidrug resistance in tumor chemotherapy [239].

8. Conclusions

Glutathione reaches the highest concentration in cells, with the predominant component being the reduced form. An electrochemical potential of a redox couple GSH/GSSG at different pH within cell compartments allows reversibility of oxidation or reduction reactions, thereby mediating a cell redox signaling mechanism. Several enzymes use glutathione in reaction mechanisms and fulfill a variety of protective, defensive, synthetic, or signaling roles in cellular metabolism. Either it can be through redox reaction in reduction of peroxides by thiol peroxidases or most common reversible modification, S-glutathionylation by thiol transferases or in conjugation reactions of toxic metabolites through glyoxalase or a variety of other compounds by glutathione-S-transferases. It also raises the question of the suggested genetic basis for differences in glutathione levels. Glutathione is undoubtedly part of a vast complex of cellular machinery processes. Therefore, monitoring it as a marker of specific conditions and dynamic changes in its concentration but also in some systems of which it is a part has a significant value.

Author Contributions: Conceptualization, J.V. and L.V.; writing—original draft preparation, J.V., L.V., L.K. and P.P.; writing—review and editing, J.V. and P.P.; visualization, L.K. and P.P. All authors have read and agreed to the published version of the manuscript.

Funding: This research received no external funding.

Institutional Review Board Statement: Not applicable.

Informed Consent Statement: Not applicable.

Data Availability Statement: No new data were created or analyzed in this study. Data sharing is not applicable to this article.

Conflicts of Interest: The authors declare no conflict of interest.

References

- Lillig, C.H.; Berndt, C. Preface. Cellular functions of glutathione. *Biochim. Biophys. Acta* **2013**, *1830*, 3137–3138. [CrossRef] [PubMed]
- Hopkins, F.G. On an autoxidizable constituent of the cell. *Biochem. J.* **1921**, *15*, 286–305. [CrossRef] [PubMed]
- Hopkins, F.G. On glutathione, a reinvestigation. *J. Biol. Chem.* **1929**, *84*, 269–320. [CrossRef]
- Hunter, G.; Eagles, B.A. Glutathione. A critical study. *J. Biol. Chem.* **1927**, *72*, 147–166. [CrossRef]
- Simoni, R.D.; Hill, R.L.; Vaughan, M. The discovery of glutathione by F. Gowland Hopkins and the beginning of biochemistry at Cambridge University. *J. Biol. Chem.* **2002**, *277*, 27–28. [CrossRef]
- Alanazi, A.M.; Mostafa, G.A.E.; Al-Badr, A.A. Glutathione. *Profiles Drug Subst. Excip. Relat. Methodol.* **2015**, *40*, 43–158.
- Lash, L.H. Mitochondrial glutathione transport: Physiological, pathological and toxicological implications. *Chem. Biol. Interact.* **2006**, *163*, 54–67. [CrossRef]
- Lu, S.C. Glutathione synthesis. *Biochim. Biophys. Acta* **2013**, *1830*, 3143–3153. [CrossRef]
- Ballatori, N.; Krance, S.M.; Notenboom, S.; Shi, S.; Tieu, K.; Hammond, C.L. Glutathione dysregulation and the etiology and progression of human diseases. *Biol. Chem.* **2009**, *390*, 191–214. [CrossRef]
- Forman, H.J.; Zhang, H.; Rinna, A. Glutathione: Overview of its protective roles, measurement, and biosynthesis. *Mol. Asp. Med.* **2009**, *30*, 1–12. [CrossRef]
- Jozefczak, M.; Remans, T.; Vangronsveld, J.; Cuypers, A. Glutathione is a key player in metal-induced oxidative stress defenses. *Int. J. Mol. Sci.* **2012**, *13*, 3145–3175.
- Dickinson, D.A.; Forman, H.J. Cellular glutathione and thiols metabolism. *Biochem. Pharmacol.* **2002**, *64*, 1019–1026. [CrossRef] [PubMed]
- Jones, D.P. Redox potential of GSH/GSSG couple: Assay and biological significance. *Methods Enzymol.* **2002**, *348*, 93–112. [PubMed]
- Alberty, R.A. Standard apparent reduction potentials of biochemical half reactions and thermodynamic data on the species involved. *Biophys. Chem.* **2004**, *111*, 115–122. [CrossRef] [PubMed]
- López-Lázaro, M. A new view of carcinogenesis and an alternative approach to cancer therapy. *Mol. Med.* **2010**, *16*, 144–153.
- Xue, M.; Weickert, M.O.; Qureshi, S.; Kandala, N.B.; Anwar, A.; Waldron, M.; Shafie, A.; Messenger, D.; Fowler, M.; Jenkins, G.; et al. Improved Glycemic Control and Vascular Function in Overweight and Obese Subjects by Glyoxalase 1 Inducer Formulation. *Diabetes* **2016**, *65*, 2282–2294. [CrossRef]
- Aquilano, K.; Baldelli, S.; Ciriolo, M.R. Glutathione: New roles in redox signaling for an old antioxidant. *Front. Pharmacol.* **2014**, *5*, 196.
- Townsend, D.M.; Tew, K.D.; Tapiero, H. The importance of glutathione in human disease. *Biomed. Pharmacother.* **2003**, *57*, 145–155. [CrossRef]
- Bachhawat, A.K.; Thakur, A.; Kaur, J.; Zulkifli, M. Glutathione transporters. *Biochim. Biophys. Acta* **2013**, *1830*, 3154–3164. [CrossRef]
- Garcia, R.A.; Stipanuk, M.H. The splanchnic organs, liver and kidney have unique roles in the metabolism of sulfur amino acids and their metabolites in rats. *J. Nutr.* **1992**, *122*, 1693–1701. [CrossRef]
- Stipanuk, M.H.; Dominy, J.E., Jr.; Lee, J.I.; Coloso, R.M. Mammalian cysteine metabolism: New insights into regulation of cysteine metabolism. *J. Nutr.* **2006**, *136*, 1652S–1659S. [CrossRef] [PubMed]
- Ookhtens, M.; Kaplowitz, N. Role of the liver in interorgan homeostasis of glutathione and cyst(e)ine. *Semin. Liver Dis.* **1998**, *18*, 313–329. [CrossRef]
- Lu, S.C. Regulation of glutathione synthesis. *Mol. Asp. Med.* **2009**, *30*, 42–59. [CrossRef] [PubMed]
- Lu, S.C.; Mato, J.M. S-adenosylmethionine in liver health, injury, and cancer. *Physiol. Rev.* **2012**, *92*, 1515–1542. [CrossRef] [PubMed]
- Cantin, A.M.; North, S.L.; Hubbard, R.C.; Crystal, R.G. Normal alveolar epithelial lining fluid contains high levels of glutathione. *J. Appl. Physiol.* **1987**, *63*, 152–157. [CrossRef] [PubMed]

26. van der Vliet, A.; O'Neill, C.A.; Cross, C.E.; Koostra, J.M.; Volz, W.G.; Halliwell, B.; Louie, S. Determination of low-molecular-mass antioxidant concentrations in human respiratory tract lining fluids. *Am. J. Physiol.* **1999**, *276*, L289–L296. [CrossRef]
27. Lieberman, M.W.; Wiseman, A.L.; Shi, Z.Z.; Carter, B.Z.; Barrios, R.; Ou, C.N.; Che'vez-Barrios, P.; Wang, Y.; Habib, G.M.; Goodman, J.C.; et al. Growth retardation and cysteine deficiency in gammaglutamyl transpeptidase-deficient mice. *Proc. Natl. Acad. Sci. USA* **1996**, *93*, 7923–7926. [CrossRef]
28. Kiba, N. Enzymes in physiological samples. In *Encyclopedia of Analytical Science*, 2nd ed.; Worsfold, P., Poole, C.F., Eds.; Elsevier: Amsterdam, The Netherlands, 2005; pp. 536–544.
29. Griffith, O.W.; Meister, A. Translocation of intracellular glutathione to membrane-bound γ -glutamyl transpeptidase as a discrete step in the γ -glutamyl cycle: Glutathionuria after inhibition of transpeptidase. *Proc. Natl. Acad. Sci. USA* **1979**, *76*, 268–272. [CrossRef] [PubMed]
30. Njalsson, R.; Norgren, S. Physiological and pathological aspects of GSH metabolism. *Acta Paediatr.* **2005**, *94*, 132–137. [CrossRef]
31. Csanaky, I.; Gregus, Z. Role of glutathione in reduction of arsenate and of gamma-glutamyltranspeptidase in disposition of arsenite in rats. *Toxicology* **2005**, *207*, 91–104. [CrossRef]
32. Calvio, C.; Romagnuolo, F.; Vulcano, F.; Speranza, G.; Morelli, C.F. Evidences on the role of the lid loop of γ -glutamyltransferases (GGT) in substrate selection. *Enzym. Microb. Technol.* **2018**, *114*, 55–62. [CrossRef] [PubMed]
33. Allison, D. γ -Glutamyl transpeptidase: Kinetics and mechanism. *Methods Enzymol.* **1985**, *113*, 419–437. [PubMed]
34. Lam, B.K.; Austen, K.F. Leukotriene C4 synthase: A pivotal enzyme in cellular biosynthesis of the cysteinyl leukotrienes. *Prostag. Other Lipid Mediat.* **2002**, *68–69*, 511–520. [CrossRef]
35. Lu, E.; Wolfreys, F.D.; Muppidi, J.R.; Xu, Y.; Cyster, J.G. S-Geranylgeranyl-L-glutathione is a ligand for human B cell-confinement receptor P2RY8. *Nature* **2019**, *567*, 244–248. [CrossRef] [PubMed]
36. Tate, S.S.; Meister, A. Interaction of γ -glutamyl transpeptidase with amino acids, dipeptides and derivatives and analogs of glutathione. *J. Biol. Chem.* **1974**, *249*, 7593–7602. [CrossRef]
37. Hanigan, M.H.; Frierson, H.F., Jr.; Swanson, P.E.; De Young, B.R. Altered expression of gamma-glutamyl transpeptidase in human tumors. *Hum. Pathol.* **1999**, *30*, 300–305. [CrossRef]
38. Hanigan, M.H. Gamma-glutamyl transpeptidase: Redox regulation and drug resistance. *Adv. Cancer Res.* **2014**, *122*, 103–141.
39. Lash, L.H.; Jones, D.P. Transport of glutathione by renal basal-lateral membrane vesicles. *Biochem. Biophys. Res. Commun.* **1983**, *112*, 55–60. [CrossRef]
40. Lash, L.H. Renal glutathione transport: Identification of carriers, physiological functions, and controversies. *Biofactors* **2009**, *35*, 500–508. [CrossRef]
41. Iantomasi, T.; Favilli, F.; Marraccini, P.; Magaldi, T.; Bruni, P.; Vincenzini, M.T. Glutathione transport system in human small intestine epithelial cells. *Biochim. Biophys. Acta* **1997**, *1330*, 274–283. [CrossRef]
42. Kannan, R.; Mittur, A.; Bao, Y.; Tsuruo, T.; Kaplowitz, N. GSH transport in immortalized mouse brain endothelial cells: Evidence for apical localization of a sodium-dependent GSH transporter. *J. Neurochem.* **1999**, *73*, 390–399. [CrossRef] [PubMed]
43. Lash, L.H.; Putt, D.A. Renal cellular transport of exogenous glutathione: Heterogeneity at physiological and pharmacological concentrations. *Biochem. Pharmacol.* **1999**, *58*, 897–907. [CrossRef] [PubMed]
44. Lash, L.H. Role of glutathione transport processes in kidney function. *Toxicol. Appl. Pharmacol.* **2005**, *204*, 329–342. [CrossRef] [PubMed]
45. Giustarini, D.; Galvagni, F.; Tesei, A.; Farolfi, A.; Zanoni, M.; Pignatta, S.; Milzani, A.; Marone, I.M.; Dalle-Donne, I.; Nassini, R.; et al. Glutathione, glutathione disulfide, and S-glutathionylated proteins in cell cultures. *Free Radic. Biol. Med.* **2015**, *89*, 972–981. [CrossRef] [PubMed]
46. Hwang, C.; Sinsky, A.J.; Lodish, H.F. Oxidized redox state of glutathione in the endoplasmic reticulum. *Science* **1992**, *257*, 1496–1502. [CrossRef]
47. Yuan, L.; Kaplowitz, N. Glutathione in liver diseases and hepatotoxicity. *Mol. Asp. Med.* **2009**, *30*, 29–41. [CrossRef]
48. Birk, J.; Meyer, M.; Aller, I.; Hansen, H.G.; Odermatt, A.; Dick, T.P.; Meyer, A.J.; Appenzeller-Herzog, C. Endoplasmic reticulum: Reduced and oxidized glutathione revisited. *J. Cell Sci.* **2013**, *126*, 1604–1617. [CrossRef]
49. Montero, D.; Tachibana, C.; Rahr Winther, J.; Appenzeller-Herzog, C. Intracellular glutathione pools are heterogeneously concentrated. *Redox Biol.* **2013**, *1*, 508–513. [CrossRef]
50. Kojer, K.; Bien, M.; Gangel, H.; Morgan, B.; Dick, T.P.; Riemer, J. Glutathione redox potential in the mitochondrial intermembrane space is linked to the cytosol and impacts the Mia40 redox state. *EMBO J.* **2012**, *31*, 3169–3182. [CrossRef]
51. López-Mirabal, H.R.; Winther, J.R. Redox characteristics of the eukaryotic cytosol. *Biochim. Biophys. Acta* **2008**, *1783*, 629–640.
52. Deponte, M. Glutathione catalysis and the reaction mechanisms of glutathione-dependent enzymes. *Biochim. Biophys. Acta* **2013**, *1830*, 3217–3266. [PubMed]
53. Aw, T.Y. Cellular redox: A modulator of intestinal epithelial cell proliferation. *News Physiol. Sci.* **2003**, *18*, 201–204. [CrossRef] [PubMed]
54. Van 't Erve, T.J.; Wagner, B.A.; Ryckman, K.K.; Raife, T.J.; Buettner, G.R. The concentration of glutathione in human erythrocytes is a heritable trait. *Free Radic. Biol. Med.* **2013**, *65*, 742–749. [CrossRef] [PubMed]
55. Schafer, F.Q.; Buettner, G.R. Redox environment of the cell as viewed through the redox state of the glutathione disulfide/glutathione couple. *Free Radic. Biol. Med.* **2001**, *30*, 1191–1212.

56. Bellomo, G.; Palladini, G.; Vairetti, M. Intranuclear distribution, function and fate of glutathione and glutathione-S-conjugate in living rat hepatocytes studied by fluorescence microscopy. *Microsc. Res. Tech.* **1997**, *36*, 243–252. [CrossRef]
57. Markovic, J.; Borrás, C.; Ortega, A.; Sastre, J.; Viña, J.; Pallardó, F.V. Glutathione is recruited into the nucleus in early phases of cell proliferation. *J. Biol. Chem.* **2007**, *282*, 20416–20424. [CrossRef]
58. Pallardó, F.V.; Markovic, J.; García, J.L.; Viña, J. Role of nuclear glutathione as a key regulator of cell proliferation. *Mol. Asp. Med.* **2009**, *30*, 77–85. [CrossRef]
59. Palmieri, F. The mitochondrial transporter family (SLC25): Physiological and pathological implications. *Pflügers Arch.* **2004**, *447*, 689–709. [CrossRef]
60. Lushchak, V.I. Glutathione homeostasis and functions: Potential targets for medical intervention. *J. Amino Acids* **2012**, *2012*, 736837. [CrossRef]
61. Zhong, Q.; Putt, D.A.; Xu, F.; Lash, L.H. Hepatic mitochondrial transport of glutathione: Studies in isolated rat liver mitochondria and H4IIE rat hepatoma cells. *Arch. Biochem. Biophys.* **2008**, *474*, 119–127. [CrossRef]
62. Kamga, C.K.; Zhang, S.X.; Wang, Y. Dicarboxylate carrier-mediated glutathione transport is essential for reactive oxygen species homeostasis and normal respiration in rat brain mitochondria. *Am. J. Physiol. Cell Physiol.* **2010**, *299*, C497–C505. [CrossRef]
63. Booty, L.M.; King, M.S.; Thangaratnarah, C.; Majd, H.; James, A.M.; Kunji, E.R.S.; Murphy, M.P. The mitochondrial dicarboxylate and 2-oxoglutarate carriers do not transport glutathione. *FEBS Lett.* **2015**, *589*, 621–628. [CrossRef] [PubMed]
64. Cione, E.; Pingitore, A.; Perri, M.; Genchi, G. Influence of all-trans-retinoic acid on oxoglutarate carrier via retinoylation reaction. *Biochim. Biophys. Acta* **2009**, *1791*, 3–7. [CrossRef] [PubMed]
65. Coll, O.; Colell, A.; García-Ruiz, C.; Kaplowitz, N.; Fernández-Checa, J.C. Sensitivity of the 2-oxoglutarate carrier to alcohol intake contributes to mitochondrial glutathione depletion. *Hepatology* **2003**, *38*, 692–702. [CrossRef] [PubMed]
66. Ribas, V.; García-Ruiz, C.; Fernández-Checa, J.C. Glutathione and mitochondria. *Front. Pharmacol.* **2014**, *5*, 151. [PubMed]
67. Yin, F.; Sancheti, H.; Cadenas, E. Mitochondrial thiols in the regulation of cell death pathways. *Antioxid. Redox Signal.* **2012**, *17*, 1714–1727. [CrossRef]
68. Bánhegyi, G.; Lusini, L.; Puskás, F.; Rossi, R.; Fulceri, R.; Braun, L.; Mile, V.; di Simplicio, P.; Mandl, J.; Benedetti, A. Preferential transport of glutathione versus glutathione disulfide in rat liver microsomal vesicles. *J. Biol. Chem.* **1999**, *274*, 12213–12216. [CrossRef]
69. Bulleid, N.J.; Ellgaard, L. Multiple ways to make disulfides. *Trends Biochem. Sci.* **2011**, *36*, 485–492. [CrossRef]
70. Ponsoero, A.J.; Igarria, A.; Darch, M.A.; Miled, S.; Outten, C.E.; Winther, J.R.; Palais, G.; D'autreaux, B.; Delaunay-Moisan, A.; Toledano, M.B. Endoplasmic Reticulum Transport of Glutathione by Sec61 Is Regulated by Ero1 and Bip. *Mol. Cell* **2017**, *67*, 962–973. [CrossRef]
71. Csala, M.; Fulceri, R.; Mandl, J.; Benedetti, A.; Bánhegyi, G. Ryanodine receptor channel dependent glutathione transport in the sarcoplasmic reticulum of skeletal muscle. *Biochem. Biophys. Res. Commun.* **2001**, *287*, 696–700. [CrossRef] [PubMed]
72. Appenzeller-Herzog, C.; Riemer, J.; Zito, E.; Chin, K.-T.; Ron, D.; Spiess, M.; Ellgaard, L. Disulphide production by Ero1 alpha-PDI relay is rapid and effectively regulated. *EMBO J.* **2010**, *29*, 3318–3329. [CrossRef]
73. Aoyama, K. Glutathione in the Brain. *Int. J. Mol. Sci.* **2021**, *22*, 5010. [CrossRef]
74. Aoyama, K.; Nakaki, T. Impaired glutathione synthesis in neurodegeneration. *Int. J. Mol. Sci.* **2013**, *14*, 21021–21044. [PubMed]
75. von Bartheld, C.S.; Bahney, J.;erculano-Houzel, S. The search for true numbers of neurons and glial cells in the human brain: A review of 150 years of cell counting. *J. Comp. Neurol.* **2016**, *524*, 3865–3895.
76. Rice, M.E.; Russo-Menna, I. Differential compartmentalization of brain ascorbate and glutathione between neurons and glia. *Neuroscience* **1998**, *82*, 1213–1223. [CrossRef] [PubMed]
77. Mirzahosseini, A.; Somlyay, M.; Noszál, B. The comprehensive acid–base characterization of glutathione. *Chem. Phys. Lett.* **2015**, *622*, 50–56. [CrossRef]
78. Mazák, K.; Noszál, B. Advances in microspeciation of drugs and biomolecules: Species-specific concentrations, acid-base properties and related parameters. *J. Pharm. Biomed. Anal.* **2016**, *130*, 390–403. [CrossRef]
79. Bjerrum, N. Dissociation constants of polybasic acids and their application to the calculation of molecular dimensions. *Z. Phys. Chem.* **1923**, *106*, 219–242. [CrossRef]
80. Noszál, B. Group constant: A measure of submolecular basicity. *J. Phys. Chem.* **1986**, *90*, 4104–4110. [CrossRef]
81. Fujiwara, S.; Ishizuka, H.; Fudano, S. NMR study of amino acids and their derivatives. *Chem. Lett.* **1974**, *3*, 1281–1284. [CrossRef]
82. Noszál, B.; Scheller-Krattiger, V.; Martin, R.B. A unified view of carbon bound hydrogen exchange of H(2) in imidazoles and H(8) in purine nucleosides and their metal ion complexes. *J. Am. Chem. Soc.* **1982**, *104*, 1078–1081. [CrossRef]
83. Noszál, B.; Rabenstein, D.L. Nitrogen-protonation microequilibria and C(2)-deprotonation microkinetics of histidine, histamine, and related compounds. *J. Phys. Chem.* **1991**, *95*, 4761–4765. [CrossRef]
84. Szakács, Z.; Noszál, B. Determination of dissociation constants of folic acid, methotrexate, and other photolabile pteridines by pressure-assisted capillary electrophoresis. *Electrophoresis* **2006**, *27*, 3399–3409. [CrossRef] [PubMed]
85. Orgován, G.; Tihanyi, K.; Noszál, B. NMR analysis, protonation equilibria and decomposition kinetics of tolperisone. *J. Pharm. Biomed. Anal.* **2009**, *50*, 718–723. [CrossRef] [PubMed]
86. Tóth, G.; Baska, F.; Schretner, A.; Rácz, Á.; Noszál, B. Site-specific basicities regulate molecular recognition in receptor binding: In silico docking of thyroid hormones. *Eur. Biophys. J.* **2013**, *42*, 721–730. [CrossRef]
87. Pirie, N.W.; Pinhey, K.G. The titration curve of glutathione. *J. Biol. Chem.* **1929**, *84*, 321–333. [CrossRef]

88. Li, N.C.; Gawron, O.; Bascuas, G. Stability of zinc complexes with glutathione and oxidized glutathione. *J. Am. Chem. Soc.* **1954**, *76*, 225–229. [CrossRef]
89. Martin, R.B.; Edsall, J.T. Glutathione: Ionization in basic solutions and molecular rearrangement in strongly acid solution. *Bull. Soc. Chim. Biol.* **1958**, *40*, 1763–1771.
90. Dorcák, V.; Krezel, A. Correlation of acid–base chemistry of phytochelatin PC2 with its coordination properties towards the toxic metal ion Cd(II). *Dalton Trans.* **2003**, *11*, 2253–2259. [CrossRef]
91. Mah, V.; Jalilehvand, F. Mercury(II) complex formation with glutathione in alkaline aqueous solution. *J. Biol. Inorg. Chem.* **2008**, *13*, 541–553. [CrossRef]
92. Noszál, B.; Szakács, Z. Microscopic protonation equilibria of oxidized glutathione. *J. Phys. Chem. B* **2003**, *107*, 5074–5080. [CrossRef]
93. Wang, X.; Li, K.; Yang, X.D.; Wang, L.L.; Shen, R.F. Complexation of Al(III) with reduced glutathione in acidic aqueous solutions. *J. Inorg. Biochem.* **2009**, *103*, 657–666. [CrossRef]
94. Gough, J.D.; Lees, W.J. Effects of redox buffer properties on the folding of a disulfide-containing protein: Dependence upon pH, thiol pK_a, and thiol concentration. *J. Biotechnol.* **2005**, *115*, 279–290. [CrossRef]
95. Madej, E.; Wardman, P. The oxidizing power of the glutathione thiyl radical as measured by its electrode potential at physiological pH. *Arch. Biochem. Biophys.* **2007**, *462*, 94–102. [CrossRef]
96. Cigala, R.M.; Crea, F.; De Stefano, C.; Lando, G.; Milea, D.; Sammartano, S. Modeling the acid–base properties of glutathione in different ionic media, with particular reference to natural waters and biological fluids. *Amino Acids.* **2012**, *43*, 629–648. [CrossRef]
97. Harris, T.K.; Turner, G.J. Structural basis of perturbed pK_a values of catalytic groups in enzyme active sites. *IUBMB Life* **2002**, *53*, 85–98. [CrossRef]
98. Matsui, R.; Ferran, B.; Oh, A.; Croteau, D.; Shao, D.; Han, J.; Pimentel, D.R.; Bachschmid, M.M. Redox Regulation via Glutaredoxin-1 and Protein S-Glutathionylation. *Antioxid. Redox Signal.* **2020**, *32*, 677–700. [CrossRef]
99. Chatgililoglu, C.; Bowry, V.W. Why Not Trans? Inhibited Radical Isomerization Cycles and Coupling Chains of Lipids and Alkenes with Alkane-thiols. *J. Org. Chem.* **2018**, *83*, 9178–9189. [CrossRef]
100. Abedinzadeh, Z.; Gardes-Albert, M.; Ferradini, C. Kinetic study of the oxidation mechanism of glutathione by hydrogen peroxide in neutral aqueous medium. *Can. J. Chem.* **1989**, *67*, 1247–1255. [CrossRef]
101. Zinatullina, K.M.; Kasaikina, O.T.; Kuz'min, V.A.; Khrameeva, N.P. Interaction of Glutathione with Hydrogen Peroxide: A Kinetic Model. *Kinet. Catal.* **2019**, *60*, 266–272. [CrossRef]
102. Winterbourn, C.C. Radical Scavenging by Thiols and the Fate of Thiyl Radicals. In *Oxidative Stress and Redox Regulation*; Jakob, U., Reichmann, D., Eds.; Springer: Dordrecht, The Netherlands, 2013; pp. 43–58.
103. Quintana-Cabrera, R.; Bolaños, J.P. Glutathione and γ -glutamylcysteine in hydrogen peroxide detoxification. *Methods Enzymol.* **2013**, *527*, 129–144.
104. Kasamatsu, S.; Nishimura, A.; Morita, M.; Matsunaga, T.; Abdul Hamid, H.; Akaike, T. Redox signaling regulated by cysteine persulfide and protein polysulfidation. *Molecules* **2016**, *21*, 1712. [CrossRef]
105. Sawa, T.; Ono, K.; Tsutsuki, H.; Zhang, T.; Ida, T.; Nishida, M.; Akaike, T. Reactive cysteine persulphides: Occurrence, biosynthesis, antioxidant activity, methodologies, and bacterial persulphide signalling. *Adv. Microb. Physiol.* **2018**, *72*, 1–28.
106. Ida, T.; Sawa, T.; Ihara, H.; Tsuchiya, Y.; Watanabe, Y.; Kumagai, Y.; Suematsu, M.; Motohashi, H.; Fujii, S.; Matsunaga, T.; et al. Reactive cysteine persulfides and S-polythiolation regulate oxidative stress and redox signaling. *Proc. Natl. Acad. Sci. USA* **2014**, *111*, 7606–7611. [CrossRef]
107. Chauvin, J.-P.R.; Griesser, M.; Pratt, D.A. Hydropersulfides: H-atom transfer agents par excellence. *J. Am. Chem. Soc.* **2017**, *139*, 6484–6493. [CrossRef]
108. Libiad, M.; Motl, N.; Akey, D.L.; Sakamoto, N.; Fearon, E.R.; Smith, J.L.; Banerjee, R. Thiosulfate sulfurtransferase-like domain-containing 1 protein interacts with thioredoxin. *J. Biol. Chem.* **2018**, *293*, 2675–2686. [CrossRef]
109. Filipovic, M.R.; Zivanovic, J.; Alvarez, B.; Banerjee, V. Chemical biology of H₂S signaling through persulfidation. *Chem. Rev.* **2018**, *118*, 1253–1337.
110. Mueller, E.G. Trafficking in persulfides: Delivering sulfur in biosynthetic pathways. *Nat. Chem. Biol.* **2006**, *2*, 185–194. [CrossRef]
111. Kruihof, P.D.; Lunev, S.; Aguilar Lozano, S.P.; de Assis Batista, F.; Al-Dahmani, Z.M.; Joles, J.A.; Dolga, A.M.; Groves, M.R.; van Goor, H. Unraveling the role of thiosulfate sulfurtransferase in metabolic diseases. *Biochim. Biophys. Acta Mol. Basis Dis.* **2020**, *1866*, 165716. [CrossRef] [PubMed]
112. Kabil, O.; Motl, N.; Strack, M.; Seravalli, J.; Metzler-Nolte, N.; Banerjee, R. Mechanism-based inhibition of human persulfide dioxygenase by γ -glutamyl-homocysteinyl-glycine. *J. Biol. Chem.* **2018**, *293*, 12429–12439. [CrossRef]
113. Sies, H.; Jones, D.P. Reactive oxygen species (ROS) as pleiotropic physiological signalling agents. *Nat. Rev. Mol. Cell Biol.* **2020**, *21*, 363–383.
114. Giustarini, D.; Rossi, R.; Milzani, A.; Colombo, R.; Dalle-Donne, I. S-glutathionylation: From redox regulation of protein functions to human diseases. *J. Cell. Mol. Med.* **2004**, *8*, 201–212. [CrossRef]
115. Mieyal, J.J.; Chock, P.B. Posttranslational modification of cysteine in redox signaling and oxidative stress: Focus on s-glutathionylation. *Antioxid. Redox Signal.* **2012**, *16*, 471–475. [CrossRef]
116. Forman, H.J.; Fukuto, J.M.; Miller, T.; Zhang, H.; Rinna, A.; Levy, S. The chemistry of cell signaling by reactive oxygen and nitrogen species and 4-hydroxynonenal. *Arch. Biochem. Biophys.* **2008**, *477*, 183–195. [CrossRef]

117. Forman, H.J.; Ursini, F.; Maiorino, M. An overview of mechanisms of redox signaling. *J. Mol. Cell. Cardiol.* **2014**, *73*, 2–9. [CrossRef]
118. Ren, X.; Zou, L.; Zhang, X.; Branco, V.; Wang, J.; Carvalho, C.; Holmgren, A.; Lu, J. Redox Signaling Mediated by Thioredoxin and Glutathione Systems in the Central Nervous System. *Antioxid. Redox Signal.* **2017**, *27*, 989–1010. [CrossRef]
119. Lou, M.F. Glutathione and Glutaredoxin in Redox Regulation and Cell Signaling of the Lens. *Antioxidants* **2022**, *11*, 1973. [CrossRef]
120. Pajaud, J.; Kumar, S.; Rauch, C.; Morel, F.; Aninat, C. Regulation of signal transduction by glutathione transferases. *Int. J. Hepatol.* **2012**, *2012*, 137676. [CrossRef]
121. Laborde, E. Glutathione transferases as mediators of signaling pathways involved in cell proliferation and cell death. *Cell Death Differ.* **2010**, *17*, 1373–1380. [CrossRef]
122. Singh, R.R.; Reindl, K.M. Glutathione S-transferases in cancer. *Antioxidants* **2021**, *10*, 701. [CrossRef]
123. Wang, J.Q.; Yang, Y.; Cai, C.Y.; Teng, Q.X.; Cui, Q.; Lin, J.; Assaraf, Y.G.; Chen, Z.S. Multidrug resistance proteins (MRPs): Structure, function and the overcoming of cancer multidrug resistance. *Drug Resist. Updat.* **2021**, *54*, 100743. [PubMed]
124. Ercolani, L.; Scirè, A.; Galeazzi, R.; Massaccesi, L.; Cianfruglia, L.; Amici, A.; Piva, F.; Urbanelli, L.; Emiliani, C.; Principato, G.; et al. A possible S-glutathionylation of specific proteins by glyoxalase II: An in vitro and in silico study. *Cell Biochem. Funct.* **2016**, *34*, 620–627. [CrossRef] [PubMed]
125. Rydström, J. Mitochondrial NADPH, transhydrogenase and disease. *Biochim. Biophys. Acta.* **2006**, *1757*, 721–726. [CrossRef] [PubMed]
126. Cereser, C.; Boget, S.; Parvaz, P.; Revol, A. Thiram-induced cytotoxicity is accompanied by a rapid and drastic oxidation of reduced glutathione with consecutive lipid peroxidation and cell death. *Toxicology* **2001**, *163*, 153–162. [CrossRef]
127. Zhao, Y.; Seefeldt, T.; Chen, W.; Wang, X.; Matthees, D.; Hu, Y.; Guan, X. Effects of glutathione reductase inhibition on cellular thiol redox state and related systems. *Arch. Biochem. Biophys.* **2009**, *485*, 56–62. [CrossRef]
128. Arning, J.; Dringen, R.; Schmidt, M.; Thiessen, A.; Stolte, S.; Matzke, M.; Bottin-Weber, U.; Caesar-Geertz, B.; Jastorff, B.; Ranke, J. Structure-activity relationships for the impact of selected isothiazol-3-one biocides on glutathione metabolism and glutathione reductase of the human liver cell line Hep G2. *Toxicology* **2008**, *246*, 203–212. [CrossRef]
129. Franco, J.L.; Posser, T.; Mattos, J.J.; Sánchez-Chardi, A.; Trevisan, R.; Oliveira, C.S.; Carvalho, P.S.; Leal, R.B.; Marques, M.R.; Bairy, A.C.; et al. Biochemical alterations in juvenile carp (*Cyprinus carpio*) exposed to zinc: Glutathione reductase as a target. *Environ. Res.* **2008**, *66*, 88–89. [CrossRef]
130. Maiorino, M.; Ursini, F.; Bosello, V.; Toppo, S.; Tosatto, S.C.; Mauri, P.; Becker, K.; Roveri, A.; Bulato, C.; Benazzi, L.; et al. The thioredoxin specificity of Drosophila GPx: A paradigm for a peroxiredoxin-like mechanism of many glutathione peroxidases. *J. Mol. Biol.* **2007**, *365*, 1033–1046. [CrossRef]
131. Toppo, S.; Flohé, L.; Ursini, F.; Vanin, S.; Maiorino, M. Catalytic mechanisms and specificities of glutathione peroxidases: Variations of a basic scheme. *Biochim. Biophys. Acta* **2009**, *1790*, 1486–1500. [CrossRef]
132. Flohé, L.; Toppo, S.; Cozza, G.; Ursini, F. A comparison of thiol peroxidase mechanisms. *Antioxid Redox Signal.* **2011**, *15*, 763–780. [CrossRef]
133. Hill, K.E.; Burk, R.F.; Lane, J.M. Effect of selenium depletion and repletion on plasma glutathione and glutathione-dependent enzymes in the rat. *J. Nutr.* **1987**, *117*, 99–104. [CrossRef] [PubMed]
134. Burk, R.F.; Hill, K.E.; Awad, J.A.; Morrow, J.D.; Lyons, P.R. Liver and kidney necrosis in selenium-deficient rats depleted of glutathione. *Lab. Investig.* **1995**, *72*, 723–730. [PubMed]
135. Hatfield, D.L.; Gladyshev, V.N. How selenium has altered our understanding of the genetic code. *Mol. Cell. Biol.* **2002**, *22*, 3565–3576. [CrossRef]
136. Woo, H.A.; Yim, S.H.; Shin, D.H.; Kang, D.; Yu, D.Y.; Rhee, S.G. Inactivation of peroxiredoxin I by phosphorylation allows localized H₂O₂ accumulation for cell signaling. *Cell* **2010**, *140*, 517–528. [CrossRef]
137. Seiler, A.; Schneider, M.; Förster, H.; Roth, S.; Wirth, E.K.; Culmsee, C.; Plesnila, N.; Kremmer, E.; Rådmark, O.; Wurst, W.; et al. Glutathione peroxidase 4 senses and translates oxidative stress into 12/15-lipoxygenase dependent- and AIF-mediated cell death. *Cell Metab.* **2008**, *8*, 237–248. [CrossRef]
138. Gallogly, M.M.; Starke, D.W.; Mieyal, J.J. Mechanistic and kinetic details of catalysis of thiol-disulfide exchange by glutaredoxins and potential mechanisms of regulation. *Antioxid. Redox Signal.* **2009**, *11*, 1059–1081. [CrossRef] [PubMed]
139. Hurd, T.R.; Filipovska, A.; Costa, N.J.; Dahm, C.C.; Murphy, M.P. Disulfide formation on mitochondrial protein thiols. *Biochem. Soc. Trans.* **2005**, *33*, 1390–1393. [CrossRef]
140. Aslund, F.; Berndt, K.D.; Holmgren, A. Redox potentials of glutaredoxins and other thiol-disulfide oxidoreductases of the thioredoxin superfamily determined by direct protein-protein redox equilibria. *J. Biol. Chem.* **1997**, *272*, 30780–30786. [CrossRef]
141. Isakov, N.; Witte, S.; Altman, A. PICOT-HD: A highly conserved protein domain that is often associated with thioredoxin and glutaredoxin modules. *Trends Biochem. Sci.* **2000**, *25*, 537–539. [CrossRef]
142. Lillig, C.H.; Berndt, C.; Holmgren, A. Glutaredoxin systems. *Biochim. Biophys. Acta* **2008**, *1780*, 1304–1317.
143. Di Simplicio, P.; Cacace, M.G.; Lusini, L.; Giannerini, F.; Giustarini, D.; Rossi, R. Role of protein -SH groups in redox homeostasis—the erythrocyte as a model system. *Arch. Biochem. Biophys.* **1998**, *355*, 145–152. [CrossRef] [PubMed]
144. Jung, C.H.; Thomas, J.A. S-glutathiolated hepatocyte proteins and insulin disulfides as substrates for reduction by glutaredoxin, thioredoxin, protein disulfide isomerase, and glutathione. *Arch. Biochem. Biophys.* **1996**, *335*, 61–72. [CrossRef] [PubMed]

145. Cooper, J.L.; Pinto, J.T.; Callery, P.S. Reversible and irreversible protein glutathionylation: Biological and clinical aspects. *Expert Opin. Drug Metab. Toxicol.* **2011**, *7*, 891–910. [CrossRef] [PubMed]
146. Findlay, V.J.; Townsend, D.M.; Morris, T.E.; Fraser, J.P.; He, L.; Tew, K.D. A novel role for human sulfiredoxin in the reversal of glutathionylation. *Cancer Res.* **2006**, *66*, 6800–6806. [CrossRef] [PubMed]
147. Holmgren, A.; Lu, J. Thioredoxin and thioredoxin reductase: Current research with special reference to human disease. *Biochem. Biophys. Res. Commun.* **2010**, *396*, 120–124. [CrossRef]
148. Fratelli, M.; Demol, H.; Puype, M.; Casagrande, S.; Eberini, I.; Salmons, M.; Bonetto, V.; Mengozzi, M.; Duffieux, F.; Miclet, E.; et al. Identification by redox proteomics of glutathionylated proteins in oxidatively stressed human T lymphocytes. *Proc. Natl. Acad. Sci. USA* **2002**, *99*, 3505–3510. [CrossRef]
149. Rouhier, N.; Lemaire, S.D.; Jacquot, J.P. The role of glutathione in photosynthetic organisms: Emerging functions for glutaredoxins and glutathionylation. *Annu. Rev. Plant Biol.* **2008**, *59*, 143–166. [CrossRef]
150. Nordstrand, K.; Sandström, A.; Aslund, F.; Holmgren, A.; Otting, G.; Berndt, K.D. NMR structure of oxidized glutaredoxin 3 from *Escherichia coli*. *J. Mol. Biol.* **2000**, *303*, 423–432. [CrossRef]
151. Begas, P.; Liedgens, L.; Moseler, A.; Meyer, A.J.; Deponte, M. Glutaredoxin catalysis requires two distinct glutathione interaction sites. *Nat. Commun.* **2017**, *8*, 14835. [CrossRef]
152. Ukuwela, A.A.; Bush, A.I.; Wedd, A.G.; Xiao, Z. Reduction potentials of protein disulfides and catalysis of glutathionylation and deglutathionylation by glutaredoxin enzymes. *Biochem. J.* **2017**, *474*, 3799–3815. [CrossRef]
153. Ogata, F.T.; Branco, V.; Vale, F.F.; Coppo, L. Glutaredoxin: Discovery, redox defense and much more. *Redox Biol.* **2021**, *43*, 101975. [PubMed]
154. Lillig, C.H.; Berndt, C.; Vergnolle, O.; Lönn, M.E.; Hudemann, C.; Bill, E.; Holmgren, A. Characterization of human glutaredoxin 2 as iron-sulfur protein: A possible role as red ox sensor. *Proc. Natl. Acad. Sci. USA* **2005**, *102*, 8168–8173. [CrossRef]
155. Prigge, J.R.; Coppo, L.; Martin, S.S.; Ogata, F.; Miller, C.G.; Bruschiwein, M.D.; Orlicky, D.J.; Shearn, C.T.; Kundert, J.A.; Lytchier, J.; et al. Hepatocyte Hyperproliferation upon Liver-Specific Co-disruption of Thioredoxin-1, Thioredoxin Reductase-1, and Glutathione Reductase. *Cell Rep.* **2017**, *19*, 2771–2781. [CrossRef] [PubMed]
156. Tamarit, J.; Bellí, G.; Cabisco, E.; Herrero, E.; Ros, J. Biochemical characterization of yeast mitochondrial Grx5 monothiol glutaredoxin. *J. Biol. Chem.* **2003**, *278*, 25745–25751. [CrossRef] [PubMed]
157. Witte, S.; Villalba, M.; Bi, K.; Liu, Y.; Isakov, N.; Altman, A. Inhibition of the c-Jun N-terminal kinase/AP-1 and NF- κ B pathways by PICOT, a novel protein kinase C-interacting protein with a thioredoxin homology domain. *J. Biol. Chem.* **2000**, *275*, 1902–1909. [CrossRef] [PubMed]
158. Haunhorst, P.; Hanschmann, E.M.; Bräutigam, L.; Stehling, O.; Hoffmann, B.; Mühlenhoff, U.; Lill, R.; Berndt, C.; Lillig, C.H. Crucial function of vertebrate glutaredoxin 3 (PICOT) in iron homeostasis and hemoglobin maturation. *Mol. Biol. Cell* **2013**, *24*, 1895–1903. [CrossRef] [PubMed]
159. Pandya, P.; Pasvolsky, R.; Babichev, Y.; Braiman, A.; Witte, S.; Altman, A.; Isakov, N. PICOT binding to the polycomb group protein, EED, alters H3K27 methylation at the MYT1 PRC2 target gene. *Biochem. Biophys. Res. Commun.* **2019**, *509*, 469–475. [CrossRef]
160. Pandya, P.; Isakov, N. PICOT promotes T lymphocyte proliferation by down-regulating cyclin D2 expression. *World J. Immunol.* **2020**, *10*, 1–12. [CrossRef]
161. Brancaccio, D.; Gallo, A.; Mikolajczyk, M.; Zovo, K.; Palumaa, P.; Novellino, E.; Piccioli, M.; Ciofi-Baffoni, S.; Banci, L. Formation of [4Fe-4S] clusters in the mitochondrial iron-sulfur cluster assembly machinery. *J. Am. Chem. Soc.* **2014**, *136*, 16240–16250. [CrossRef]
162. Banci, L.; Brancaccio, D.; Ciofi-Baffoni, S.; Del Conte, R.; Gadepalli, R.; Mikolajczyk, M.; Neri, S.; Piccioli, M.; Winkelmann, J. [2Fe-2S] cluster transfer in iron-sulfur protein biogenesis. *Proc. Natl. Acad. Sci. USA* **2014**, *111*, 6203–6208. [CrossRef]
163. Nasta, V.; Giachetti, A.; Ciofi-Baffoni, S.; Banci, L. Structural insights into the molecular function of human [2Fe-2S] BOLA1-GRX5 and [2Fe-2S] BOLA3-GRX5 complexes. *Biochim. Biophys. Acta Gen. Subj.* **2017**, *1861*, 2119–2131. [CrossRef] [PubMed]
164. Rozell, B.; Barcena, J.A.; Martinez-Galisteo, E.; Padilla, C.A.; Holmgren, A. Immunochemical characterization and tissue distribution of glutaredoxin (thioltransferase) from calf. *Eur. J. Cell Biol.* **1993**, *62*, 314–323.
165. Pai, H.V.; Starke, D.W.; Lesnefsky, E.J.; Hoppel, C.L.; Mieyal, J.J. What is the functional significance of the unique location of glutaredoxin 1 (GRx1) in the intermembrane space of mitochondria? *Antioxid. Redox Signal.* **2007**, *9*, 2027–2033. [CrossRef] [PubMed]
166. Ukuwela, A.A.; Bush, A.I.; Wedd, A.G.; Xiao, Z. Glutaredoxins employ parallel monothiol-dithiol mechanisms to catalyze thiol-disulfide exchanges with protein disulfides. *Chem. Sci.* **2017**, *9*, 1173–1183. [CrossRef] [PubMed]
167. González, R.; López-Grueso, M.J.; Muntané, J.; Barcena, J.A.; Padilla, C.A. Redox regulation of metabolic and signaling pathways by thioredoxin and glutaredoxin in NOS-3 overexpressing hepatoblastoma cells. *Redox Biol.* **2015**, *6*, 122–134. [CrossRef]
168. Inadomi, C.; Murata, H.; Ihara, Y.; Goto, S.; Urata, Y.; Yodoi, J.; Kondo, T.; Sumikawa, K. Overexpression of glutaredoxin protects cardiomyocytes against nitric oxide-induced apoptosis with suppressing the S-nitrosylation of proteins and nuclear translocation of GAPDH. *Biochem. Biophys. Res. Commun.* **2012**, *425*, 656–661. [CrossRef]
169. Lundberg, M.; Fernandes, A.P.; Kumar, S.; Holmgren, A. Cellular and plasma levels of human glutaredoxin 1 and 2 detected by sensitive ELISA systems. *Biochem. Biophys. Res. Commun.* **2004**, *319*, 801–809. [CrossRef]

170. Lundberg, M.; Johansson, C.; Chandra, J.; Enoksson, M.; Jacobsson, G.; Ljung, J.; Johansson, M.; Holmgren, A. Cloning and expression of a novel human glutaredoxin (Grx2) with mitochondrial and nuclear isoforms. *J. Biol. Chem.* **2001**, *276*, 26269–26275. [CrossRef]
171. Johansson, C.; Lillig, C.H.; Holmgren, A. Human mitochondrial glutaredoxin reduces S-glutathionylated proteins with high affinity accepting electrons from either glutathione or thioredoxin reductase. *J. Biol. Chem.* **2004**, *279*, 7537–7543. [CrossRef]
172. Hashemy, S.I.; Johansson, C.; Berndt, C.; Lillig, C.H.; Holmgren, A. Oxidation and S-nitrosylation of cysteines in human cytosolic and mitochondrial glutaredoxins: Effects on structure and activity. *J. Biol. Chem.* **2007**, *282*, 14428–14436. [CrossRef]
173. Wu, H.; Xing, K.; Lou, M.F. Glutaredoxin 2 prevents H₂O₂-induced cell apoptosis by protecting complex I activity in the mitochondria. *Biochim. Biophys. Acta Bioenerg.* **2010**, *1797*, 1705–1715. [CrossRef] [PubMed]
174. Ferri, A.; Fiorenzo, P.; Nencini, M.; Cozzolino, M.; Pesaresi, M.G.; Valle, C.; Sepe, S.; Moreno, S.; Carri, M.T. Glutaredoxin 2 prevents aggregation of mutant SOD1 in mitochondria and abolishes its toxicity. *Hum. Mol. Genet.* **2010**, *19*, 4529–4542. [CrossRef]
175. Rhee, S.G.; Woo, H.A. Multiple functions of peroxiredoxins: Peroxidases, sensors and regulators of the intracellular messenger H₂O₂, and protein chaperones. *Antioxid. Redox Signal.* **2011**, *15*, 781–794. [CrossRef] [PubMed]
176. Georgiou, G.; Masip, L. Biochemistry. An overoxidation journey with a return ticket. *Science* **2003**, *300*, 592–594. [CrossRef] [PubMed]
177. Bryk, R.; Griffin, P.; Nathan, C. Peroxynitrite reductase activity of bacterial peroxiredoxins. *Nature* **2000**, *407*, 211–215. [CrossRef] [PubMed]
178. Rhee, S.G.; Woo, H.A.; Kil, I.S.; Bae, S.H. Peroxiredoxin functions as a peroxidase and a regulator and sensor of local peroxides. *J. Biol. Chem.* **2012**, *287*, 4403–4410. [CrossRef]
179. Wood, Z.A.; Schröder, E.; Robin Harris, J.; Poole, L.B. Structure, mechanism and regulation of peroxiredoxins. *Trends Biochem. Sci.* **2003**, *28*, 32–40. [CrossRef]
180. Nadeem, M.S.; Khan, J.A.; Murtaza, B.N.; Muhammad, K.; Rauf, A. Purification and properties of liver catalase from water buffalo (*Bubalus bubalis*). *South Asian J. Life Sci.* **2015**, *3*, 51–55. [CrossRef]
181. Rhee, S.G.; Woo, H.A. Multiple functions of 2-Cys peroxiredoxins, I and II, and their regulations via posttranslational modifications. *Free Radic. Biol. Med.* **2020**, *152*, 107–115. [CrossRef]
182. Randall, L.; Manta, B.; Nelson, K.J.; Santos, J.; Poole, L.B.; Denicola, A. Structural changes upon peroxynitrite-mediated nitration of peroxiredoxin 2; nitrated Prx2 resembles its disulfide-oxidized form. *Arch. Biochem. Biophys.* **2016**, *590*, 101–108. [CrossRef]
183. Nelson, K.J.; Perkins, A.; Van Swearingen, A.E.D.; Hartman, S.; Brereton, A.E.; Parsonage, D.; Salisbury, F.R., Jr.; Karplus, P.A.; Poole, L.B. Experimentally dissecting the origins of peroxiredoxin catalysis. *Antioxid. Redox Signal.* **2018**, *28*, 521–536. [CrossRef] [PubMed]
184. Bolduc, J.; Koruza, K.; Luo, T.; Malo Pueyo, J.; Nghia Vo, T.; Ezeriņa, D.; Messens, J. Peroxiredoxins wear many hats: Factors that fashion their peroxide sensing personalities. *Redox Biol.* **2021**, *42*, 101959.
185. Monteiro, G.; Horta, B.B.; Pimenta, D.C.; Augusto, O.; Netto, L.E. Reduction of 1-Cys peroxiredoxins by ascorbate changes the thiol-specific antioxidant paradigm, revealing another function of vitamin C. *Proc. Natl. Acad. Sci. USA* **2007**, *104*, 4886–4891. [CrossRef] [PubMed]
186. Phillips, A.J.; Littlejohn, J.; Yewdall, N.A.; Zhu, T.; Valéry, C.; Pearce, F.G.; Mitra, A.K.; Radjainia, M.; Gerrard, J.A. Peroxiredoxin is a Versatile Self-Assembling Tecton for Protein Nanotechnology. *Biomacromolecules* **2014**, *15*, 1871–1881. [CrossRef] [PubMed]
187. Kim, Y.; Jang, H.H. Role of Cytosolic 2-Cys Prx1 and Prx2 in Redox Signaling. *Antioxidants* **2019**, *8*, 169. [CrossRef]
188. Phalen, T.J.; Weirather, K.; Deming, P.B.; Anathy, V.; Howe, A.K.; van der Vliet, A.; Jonsson, T.J.; Poole, L.B.; Heintz, N.H. Oxidation state governs structural transitions in peroxiredoxin II that correlate with cell cycle arrest and recovery. *J. Cell Biol.* **2006**, *175*, 779–789. [CrossRef]
189. Saccoccia, F.; Di Micco, P.; Boumis, G.; Brunori, M.; Koutris, I.; Miele, A.E.; Morea, V.; Sriratana, P.; Williams, D.L.; Bellelli, A.; et al. Moonlighting by different stressors: Crystal structure of the chaperone species of a 2-Cys peroxiredoxin. *Structure* **2012**, *20*, 429–439. [CrossRef]
190. Rhee, S.G.; Chae, H.Z.; Kim, K. Peroxiredoxins: A historical overview and speculative preview of novel mechanisms and emerging concepts in cell signaling. *Free Radic. Biol. Med.* **2005**, *38*, 1543–1552. [CrossRef]
191. Manevich, Y.; Feinstein, S.I.; Fisher, A.B. Activation of the antioxidant enzyme 1-CYS peroxiredoxin requires glutathionylation mediated by heterodimerization with pi GST. *Proc. Natl. Acad. Sci. USA* **2004**, *101*, 3780–3785. [CrossRef]
192. Schremmer, B.; Manevich, Y.; Feinstein, S.I.; Fisher, A.B. Peroxiredoxins in the lung with emphasis on peroxiredoxin VI. *Subcell. Biochem.* **2007**, *44*, 317–344.
193. Poole, L.B.; Nelson, K.J. Distribution and features of the six classes of peroxiredoxins. *Mol. Cells* **2016**, *39*, 53–59. [PubMed]
194. Aniya, Y.; Imaizumi, N. Mitochondrial glutathione transferases involving a new function for membrane permeability transition pore regulation. *Drug Metab. Rev.* **2011**, *43*, 292–299. [CrossRef] [PubMed]
195. Kural, C.; Kocdogan, A.K.; Şimşek, G.G.; Oguztuzun, S.; Kaygın, P.; Yılmaz, I.; Bayram, T.; Izci, Y. Glutathione S-transferases and cytochrome P450 enzyme expression in patients with intracranial tumors: Preliminary report of 55 patients. *Med. Princ. Pract.* **2018**, *28*, 56–62. [CrossRef] [PubMed]
196. Raza, H. Dual localization of glutathione S-transferase in the cytosol and mitochondria: Implications in oxidative stress, toxicity and disease. *FEBS J.* **2011**, *278*, 4243–4251. [CrossRef]

197. Hayes, J.D.; Strange, R.C. Glutathione S-transferase polymorphisms and their biological consequences. *Pharmacology* **2000**, *61*, 154–166. [CrossRef]
198. Hayes, J.D.; Flanagan, J.U.; Jowsey, I.R. Glutathione transferases. *Annu. Rev. Pharmacol. Toxicol.* **2005**, *45*, 51–88. [CrossRef]
199. Chatterjee, A.; Gupta, S. The multifaceted role of glutathione S-transferases in cancer. *Cancer Lett.* **2018**, *433*, 33–42. [CrossRef]
200. Townsend, D.; Tew, K. The role of glutathione-S-transferase in anti-cancer drug resistance. *Oncogene* **2003**, *22*, 7369–7375. [CrossRef]
201. Pacifici, G.; Franchi, M.; Bencini, C.; Repetti, F.; Di Lascio, N.; Muraro, G. Tissue distribution of drug-metabolizing enzymes in humans. *Xenobiotica* **1988**, *18*, 849–856. [CrossRef]
202. Oakley, A. Glutathione transferases: A structural perspective. *Drug Metab. Rev.* **2011**, *43*, 138–151. [CrossRef]
203. Ladner, J.E.; Parsons, J.F.; Rife, C.L.; Gilliland, G.L.; Armstrong, R.N. Parallel evolutionary pathways for glutathione transferases: Structure and mechanism of the mitochondrial class kappa enzyme rGSTK1-1. *Biochemistry* **2004**, *43*, 352–361. [CrossRef] [PubMed]
204. Li, J.; Xia, Z.; Ding, J. Thioredoxin-like domain of human kappa class glutathione transferase reveals sequence homology and structure similarity to the theta class enzyme. *Protein Sci.* **2005**, *14*, 2361–2369. [CrossRef] [PubMed]
205. Nathaniel, C.; Wallace, L.A.; Burke, J.; Dirr, H.W. The role of an evolutionarily conserved cis-proline in the thioredoxin-like domain of human class Alpha glutathione transferase A1-1. *Biochem. J.* **2003**, *372*, 241–246. [CrossRef] [PubMed]
206. Atkinson, H.J.; Babbitt, P.C. Glutathione transferases are structural and functional outliers in the thioredoxin fold. *Biochemistry* **2009**, *48*, 11108–11116. [CrossRef]
207. Stenberg, G.; Board, P.G.; Mannervik, B. Mutation of an evolutionarily conserved tyrosine residue in the active-site of a human class alpha-glutathione transferase. *FEBS Lett.* **1991**, *293*, 153–155. [CrossRef]
208. Board, P.G.; Coggan, M.; Chelvanayagam, G.; Easteal, S.; Jermini, L.S.; Schulte, G.K.; Danley, D.E.; Hoth, L.R.; Griffor, M.C.; Kamath, A.V.; et al. Identification, characterization, and crystal structure of the omega class glutathione transferases. *J. Biol. Chem.* **2000**, *275*, 24798–24806. [CrossRef]
209. Mannervik, B.; Board, P.G.; Hayes, J.D.; Listowsky, I.; Pearson, W.R. Nomenclature for mammalian soluble glutathione transferases. *Methods Enzymol.* **2005**, *401*, 1–8.
210. Hayes, J.D.; Pulford, D.J. The glutathione S-transferase gene family: Regulation of GST and the contribution of the isoenzymes to cancer chemoprotection and drug resistance. *Crit. Rev. Biochem. Mol. Biol.* **1995**, *30*, 445–600.
211. Fernández-Cañón, J.M.; Peñalva, M.A. Characterization of a fungal maleylacetoacetate isomerase gene and identification of its human homologue. *J. Biol. Chem.* **1998**, *273*, 329–337. [CrossRef]
212. Yang, Y.; Sharma, R.; Zimniak, P.; Awasthi, Y.C. Role of α class glutathione S-transferases as antioxidant enzymes in rodent tissues. *Toxicol. Appl. Pharmacol.* **2002**, *182*, 105–115. [CrossRef]
213. Yang, J.Y.; Sharma, R.; Sharma, A.; Awasthi, S.; Awasthi, Y.C. Lipid peroxidation and cell cycle signaling: 4-hydroxynonenal, a key molecule in stress mediated signaling. *Acta Biochim. Pol.* **2003**, *50*, 319–336. [CrossRef]
214. Johansson, A.S.; Mannervik, B. Human glutathione transferase A3-3, a highly efficient catalyst of double-bond isomerization in the biosynthetic pathway of steroid hormones. *J. Biol. Chem.* **2001**, *276*, 33061–33065. [CrossRef]
215. Flanagan, J.U.; Smythe, M.L. Sigma-class glutathione transferases. *Drug Metab. Rev.* **2011**, *43*, 194–214. [CrossRef]
216. Kanaoka, Y.; Ago, H.; Inagaki, E.; Nanayama, T.; Miyano, M.; Kikuno, R.; Fujii, Y.; Eguchi, N.; Toh, H.; Urade, Y.; et al. Cloning and crystal structure of hematopoietic prostaglandin D synthase. *Cell* **1997**, *90*, 1085–1095. [CrossRef]
217. Welsch, D.J.; Creely, D.P.; Hauser, S.D.; Mathis, K.J.; Krivi, G.G.; Isakson, P.C. Molecular cloning and expression of human leukotriene-C4 synthase. *Proc. Natl. Acad. Sci. USA* **1994**, *91*, 9745–9749. [CrossRef]
218. Campbell, E.; Takahashi, Y.; Abramovitz, M.; Peretz, M.; Listowsky, I. A distinct human testis and brain mu-class glutathione S-transferase. Molecular cloning and characterization of a form present even in individuals lacking hepatic type mu isoenzymes. *J. Biol. Chem.* **1990**, *265*, 9188–9193. [CrossRef] [PubMed]
219. Dulhunty, A.; Gage, P.; Curtis, S.; Chelvanayagam, G.; Board, P. The glutathione structural family includes a nuclear chloride channel and a ryanodine receptor calcium release channel modulator. *J. Biol. Chem.* **2001**, *276*, 3319–3323. [CrossRef]
220. Harrop, S.J.; DeMaere, M.Z.; Fairlie, W.D.; Reztsova, T.; Valenzuela, S.M.; Mazzanti, M.; Tonini, R.; Qiu, M.R.; Jankova, L.; Warton, K.; et al. Crystal structure of a soluble form of the intracellular chloride ion channel CLIC1 (NCC27) at 1.4-Å resolution. *J. Biol. Chem.* **2001**, *276*, 44993–45000. [CrossRef] [PubMed]
221. Wilce, M.C.; Parker, M.W. Structure and function of glutathione S-transferases. *Biochim. Biophys. Acta* **1994**, *1205*, 1–18. [CrossRef] [PubMed]
222. Menon, D.; Board, P.G. A role for glutathione transferase Omega 1 (GSTO1-1) in the glutathionylation cycle. *J. Biol. Chem.* **2013**, *288*, 25769–25779. [CrossRef]
223. Board, P.G.; Anders, M.W. Glutathione transferase omega 1 catalyzes the reduction of S-(phenacyl)glutathiones to acetophenones. *Chem. Res. Toxicol.* **2007**, *20*, 149–154. [CrossRef]
224. Schmuck, E.M.; Bard, P.G.; Whibread, A.K.; Tetlow, N.; Cavanaugh, J.A.; Blackburn, A.C.; Masoumi, A. Characterization of the monomethylarsonate reductase and dehydroascorbate reductase activities of omega class glutathione transferase variants. Implications for arsenic metabolism and the age-at-onset of Alzheimer’s and Parkinson’s diseases. *Pharmacogenet. Genom.* **2005**, *15*, 493–501. [CrossRef]

225. Dong, S.; Sha, H.; Xu, X.; Hu, T.; Lou, R.; Li, H.; Wu, J.; Dan, C.; Feng, J. Glutathione S-transferase π : A potential role in antitumor therapy. *Drug Des. Dev. Ther.* **2018**, *12*, 3535–3547. [CrossRef]
226. Townsend, D.M.; Findlay, V.L.; Tew, K.D. Glutathione S-transferases as regulators of kinase pathways and anticancer drug targets. *Methods Enzymol.* **2005**, *401*, 287–307.
227. Antognelli, C.; Ferri, I.; Bellezza, G.; Siccu, P.; Love, H.D.; Talesa, V.N.; Sidoni, A. Glyoxalase 2 drives tumorigenesis in human prostate cells in a mechanism involving androgen receptor and p53-p21 axis. *Mol. Carcinog.* **2017**, *56*, 2112–2126. [CrossRef]
228. Sousa Silva, M.; Gomes, R.A.; Ferreira, A.E.; Ponces Freire, A.; Cordeiro, C. The glyoxalase pathway: The first hundred years . . . and beyond. *Biochem. J.* **2013**, *453*, 1–15. [CrossRef]
229. Rabbani, N.; Xue, M.; Thornalley, P.J. Dicarbonyls and glyoxalase in disease mechanisms and clinical therapeutics. *Glycoconj. J.* **2016**, *33*, 513–525. [CrossRef]
230. Ellis, K.J. Human body composition: In vivo methods. *Physiol. Rev.* **2000**, *80*, 649–680.
231. Thornalley, P.J.; Waris, S.; Fleming, T.; Santarius, T.; Larkin, S.J.; Winklhofer-Roob, B.M.; Stratton, M.R.; Rabbani, N. Imidazopurines are markers of physiological genomic damage linked to DNA instability and glyoxalase 1-associated tumour multidrug resistance. *Nucleic Acids Res.* **2010**, *38*, 5432–5442. [CrossRef]
232. He, Y.; Zhou, C.; Huang, M.; Tang, C.; Liu, X.; Yue, Y.; Diao, Q.; Zheng, Z.; Liu, D. Glyoxalase system: A systematic review of its biological activity, related-diseases, screening methods and small molecule regulators. *Biomed. Pharmacother.* **2020**, *131*, 110663. [CrossRef]
233. Sarker, M.K.; Lee, J.H.; Lee, D.H.; Chun, K.H.; Jun, H.S. Attenuation of diabetic kidney injury in DPP4-deficient rats; role of GLP-1 on the suppression of AGE formation by inducing glyoxalase 1. *Aging* **2020**, *12*, 593–610. [PubMed]
234. Thornalley, P.J. The glyoxalase system in health and disease. *Mol. Asp. Med.* **1993**, *14*, 287–371.
235. Birkenmeier, G.; Stegemann, C.; Hoffmann, R.; Gunther, R.; Huse, K.; Birkemeyer, C. Posttranslational modification of human glyoxalase 1 indicates redox-dependent regulation. *PLoS ONE* **2010**, *5*, e10399.
236. Limphong, P.; Nimako, G.; Thomas, P.W.; Fast, W.; Makaroff, C.A.; Crowde, M.W. *Arabidopsis thaliana* mitochondrial glyoxalase 2–1 exhibits beta-lactamase activity. *Biochemistry* **2009**, *48*, 8491–8493. [PubMed]
237. Wendler, A.; Irsch, T.; Rabbani, N.; Thornalley, P.J.; Krauth-Siegel, R.L. Glyoxalase II does not support methylglyoxal detoxification but serves as a general trypanothione thioesterase in African trypanosomes. *Mol. Biochem. Parasitol.* **2009**, *163*, 19–27. [PubMed]
238. Hara, T.; Toyoshima, M.; Hisano, Y.; Balan, S.; Iwayama, Y.; Aono, H.; Fatamura, Y.; Osada, H.; Owada, Y.; Yoshikawa, T. Glyoxalase I disruption and external carbonyl stress impair mitochondrial function in human induced pluripotent stem cells and derived neurons. *Transl. Psychiatry* **2021**, *11*, 275.
239. Xue, M.; Shafie, A.; Qaiser, T.; Rajpoot, N.M.; Kaltsas, G.; James, S.; Gopalakrishnan, K.; Fisk, A.; Dimitriadis, G.K.; Grammatopoulos, D.K.; et al. Glyoxalase 1 copy number variation in patients with well differentiated gastro-entero-pancreatic neuroendocrine tumours (GEP-NET). *Oncotarget* **2017**, *8*, 76961–76973. [PubMed]

Disclaimer/Publisher’s Note: The statements, opinions and data contained in all publications are solely those of the individual author(s) and contributor(s) and not of MDPI and/or the editor(s). MDPI and/or the editor(s) disclaim responsibility for any injury to people or property resulting from any ideas, methods, instructions or products referred to in the content.

Review

Glutathione in Protein Redox Modulation through S-Glutathionylation and S-Nitrosylation

Elena Kalinina * and Maria Novichkova 

T.T. Berezov Department of Biochemistry, Peoples' Friendship University of Russia (RUDN University),
6 Miklukho-Maklaya Street, 117198 Moscow, Russia; novichkova-md@rudn.ru

* Correspondence: kalinina-ev@rudn.ru

Abstract: S-glutathionylation and S-nitrosylation are reversible post-translational modifications on the cysteine thiol groups of proteins, which occur in cells under physiological conditions and oxidative/nitrosative stress both spontaneously and enzymatically. They are important for the regulation of the functional activity of proteins and intracellular processes. Connecting link and “switch” functions between S-glutathionylation and S-nitrosylation may be performed by GSNO, the generation of which depends on the GSH content, the GSH/GSSG ratio, and the cellular redox state. An important role in the regulation of these processes is played by Trx family enzymes (Trx, Grx, PDI), the activity of which is determined by the cellular redox status and depends on the GSH/GSSG ratio. In this review, we analyze data concerning the role of GSH/GSSG in the modulation of S-glutathionylation and S-nitrosylation and their relationship for the maintenance of cell viability.

Keywords: S-glutathionylation; S-nitrosylation; GSH; nitrosoglutathione; redox-regulation

Citation: Kalinina, E.; Novichkova, M. Glutathione in Protein Redox Modulation through S-Glutathionylation and S-Nitrosylation. *Molecules* **2021**, *26*, 435. <https://doi.org/10.3390/molecules26020435>

Received: 12 November 2020

Accepted: 12 January 2021

Published: 15 January 2021

Publisher's Note: MDPI stays neutral with regard to jurisdictional claims in published maps and institutional affiliations.



Copyright: © 2021 by the authors. Licensee MDPI, Basel, Switzerland. This article is an open access article distributed under the terms and conditions of the Creative Commons Attribution (CC BY) license (<https://creativecommons.org/licenses/by/4.0/>).

1. Introduction

Redox-dependent processes largely determine cell viability, participating in the regulation of division, bioenergetics, and programmed death. The cellular redox status is characterized by low-molecular-weight indicators (GSH, NADH). The change in their oxidized/reduced form ratio occurs as a reaction to changes in reactive oxygen and nitrogen species (RONS) levels and, so, they can play the role of a trigger in the redox-dependent regulation of cellular processes. Undoubtedly, such an important trigger role is played by glutathione (γ -glutamyl-L-cysteinylglycine, GSH), a water-soluble tripeptide consisting of the amino acids L-glutamate, L-cysteine, and glycine, which is widely present in both eukaryotes and prokaryotes [1–3]. GSH is less susceptible to oxidation than Cys, which makes it the most suitable for maintaining intracellular redox status [1]. The presence of a γ -peptide bond at the Glu residue protects GSH from the action of peptidases, while the SH group at the Cys residue makes GSH a good electron donor, allowing it to participate in reactions with strong electrophiles.

Normally, the ratio of reduced glutathione (GSH) to oxidized glutathione (GSSG), GSH/GSSG—which characterizes the cellular redox status—is 100/1 in the cytoplasm, 10/1 in mitochondria, and 3/1 to 1 in the endoplasmic reticulum [4]. This ratio varies depending on the physiological state of cells, such as proliferation, differentiation, or apoptosis, and the consequences of its disturbance are significant changes in cellular signaling reactions. This role of GSH/GSSG is largely due to its regulatory effect on the functional activities of protein thiols [5–7].

Although Cys residues in mammalian proteins do not exceed 3% [6], they are highly sensitive to oxidative modification, which significantly affects the functioning of proteins, as thiol groups play a significant role in the formation of protein tertiary and quaternary structures and enzyme active sites. The pKa value of most SH groups of cellular proteins is more than 8.0, which keeps thiol groups predominantly protonated at physiological pH values (pH 7.0–7.4) [8,9]. However, in proteins, in the immediate vicinity of the basic

amino acid residues (histidine, lysine, and arginine), the pKa of the SH groups decreases (usually to 5.0–7.0) and these thiols dissociate at physiological pH. The resulting thiolate anions (Pr-S^-) are effective nucleophiles and have high activity with respect to electrophilic targets [10–12]. The reactivity of SH groups and the functional activity of proteins are largely regulated by S-glutathionylation and S-nitrosylation [6,13–16].

Under S-glutathionylation, GSH can bind to the cysteinyl residues of proteins through the creation of reversible disulfide bonds, depending on the cysteine position and redox potential [12,13]. This post-translational modification to the protein can lead to enhanced or suppressed activity, may prevent protein degradation by proteolysis or sulfhydryl overoxidation, and plays an important role in cellular signaling. At present, the dual role of S-glutathionylation in maintaining cellular homeostasis and participating in various pathological processes may be indicated [14,17].

Under S-nitrosylation, NO is covalently attached to the SH group of a cysteine residue and, as a consequence, can cause alterations in the cellular function of a variety of proteins [18,19]. S-nitrosoglutathione, formed as the result of GSH S-nitrosylation, serves as a NO reservoir and can transfer NO groups to new cysteine residues in transnitrosylation reactions [20,21].

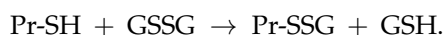
The GSH/GSSG ratio can be considered a key redox sensor, which determines the redox-dependent alteration of the protein functional activity through such significant post-translational modifications as S-glutathionylation and S-nitrosylation. The modulation of the activity of these reactions in response to a change in the GSH/GSSG ratio, as a result of an increase or decrease in RONS levels, provides a significant contribution to cell functional adaptation to redox changes of the environment [22–25].

In this review, we analyze data concerning the roles of GSH and GSH/GSSG in the redox modulation of S-glutathionylation and S-nitrosylation and their relationship for the maintenance of cell viability.

2. Glutathione and Protein S-Glutathionylation

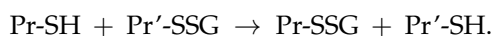
A widespread form of cysteine modification is S-glutathionylation—the reversible formation of protein mixed disulfides with GSH (Pr-SSG)—which occurs in the cell under physiological conditions and oxidative stress, both spontaneously and enzymatically. The S-glutathionylation of proteins suggests the possible involvement of this post-translational modification in cellular signaling and the redox regulation of protein functions [6,13,24]. In addition to the potential regulatory role, S-glutathionylation can serve as a means of GSH storage, as well as protection from the irreversible oxidation of protein thiol groups under stress conditions [26], often due to a temporary loss of primary protein activity as, if the modified sulfhydryl group of a protein is functionally critical, S-glutathionylation can render the protein inactive or alter its activity, ultimately disrupting cellular functions [27]. In addition, this reaction can affect a change in conformation and/or charge, which can modify the function of the protein, as the attachment of GSH introduces an additional negative charge at the expense of the glutamic acid residue.

Non-enzymatic S-glutathionylation reactions can occur during thiol-disulfide exchange, through the participation of protein thiol (Pr-SH) and oxidized glutathione GSSG:

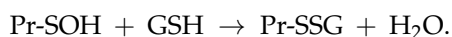


The equilibrium constant of the reaction K_{mix} is expressed by the ratio $[\text{Pr-SSG}] \cdot [\text{GSH}] / [\text{Pr-SH}] \cdot [\text{GSSG}]$, where the extent of S-glutathionylated proteins ($[\text{Pr-SSG}] / [\text{Pr-SH}]$) strongly depends on the local ratio $[\text{GSH}] / [\text{GSSG}]$ [28,29]. The S-glutathionylation of most proteins with typical redox potential ($K_{\text{mix}} \sim 1$) by about 50% can occur when this ratio drops very dramatically (i.e., from 100:1 to 1:1). These extreme conditions are rare in vivo. Therefore, for most proteins, the spontaneous formation of Pr-SSG—as a result of the exchange of Pr-SH and GSSG—is not common and, as a rule, takes place under pathological condi-

tions [30]. In addition, a variant of thiol-disulfide exchange between Pr-SH and a protein which is already S-glutathionylated (Pr'-SSG) is possible:

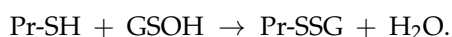


S-glutathionylation can occur when Pr-SH or GSH reacts with an oxidized derivative of the protein cysteine residue; for example, sulfenic acid (-SOH), thiyl radical (-S[•]), or S-nitrosyl (-SNO) group. Thus, when Pr-SH is oxidized with, for example, H₂O₂, sulfenic acid (Pr-SOH) is formed and then quickly reacts with GSH to form Pr-SSG:



Sulfenic acid is unstable and can undergo further oxidation to sulfinic acid (Pr-SO₂H) and eventually to sulfonic acid (Pr-SO₃H), the formation of which, as a rule, leads to the irreversible deactivation of the protein. Thus, the S-glutathionylation of sulfenic acid can prevent the oxidation of protein cysteine residues [6,25]. Under physiological conditions, the intracellular level of H₂O₂ is in the sub-micromolar range (10⁻⁹–10⁻⁷ M) [31]. Therefore, *in vivo* spontaneous S-glutathionylation proceeds rather slowly by this mechanism.

The formation of S-glutathionylated protein is also possible, due to its interaction with GSSG in the form of sulfenic acid (GSOH):



Thus, it is obvious that the S-glutathionylation of proteins can occur spontaneously; however, the rate and extent of this process increases with the participation of enzymes, among which glutathione transferase isoform P1-1 (GSTP1-1) plays the greatest role [32,33]. GSTP1-1 has been shown to facilitate S-glutathionylation for a number of proteins, including peroxiredoxin 6 (Prx6) [34,35], aldose reductase [36], actin [37], histone H3 [38], 5'AMP-activated protein kinase (AMPK) [32], estrogen receptor α [39], heat shock protein BiP, protein disulfide isomerase (PDI), calnexin, calreticulin, and sarcoplasmic reticulum Ca²⁺-ATPase (SERCA) [33].

During the reaction, GSTP1-1 binds GSH in the active center and decreases the pK_a of the GSH cysteine residue from 9.2 to 6.3 [40], deprotonates it with the participation of Tyr7, forming a thiolate anion (GS⁻), which is transferred to the cysteine residue in the substrate. In cells with the Tyr7 GSTP1-1 mutation, a decrease in the total content of S-glutathionylated proteins has been observed upon treatment with GSSG, the mimetic of oxidized glutathione NOV-002 and diazeniumdiolate-based NO-donor prodrug PABA/NO [36]. An example is the S-glutathionylation of Prx6 from the 1-Cys groups of peroxiredoxins. As a result of human Prx6 peroxidase activity, the Cys47 in the active center is oxidized to sulfenic acid; this deprives it of activity; as for the reduction of which, a second thiol is required to form a mixed disulfide, then a sulfhydryl group. However, the availability of the sulfenic group is low, due to the peculiarities of the globular structure of Prx6. Prx6 activation occurs during the formation of a heterodimer with GSTP1-1, which promotes the S-glutathionylation of Cys47 Prx6. The conformational changes of the heterodimer occur, providing the formation of a disulfide bond between Cys47 GSTP1-1 and Cys47 Prx6, followed by the reduction of disulfide with the participation of GSH and the regeneration of Cys47 Prx6 [34].

The enzymatic S-glutathionylation of AMP-activated protein kinase (AMPK) occurs not only with the participation of GSTP1-1, but also GSTM1-1 in the absence of strong oxidants (i.e., under conditions which are similar to physiological oxidation). S-glutathionylation occurs at the Cys299 and Cys304 residues and causes conformational changes that activate the kinase activity of human AMPK [32].

The ability of S-glutathionylation was found in the enzyme glyoxylase 2 (Glo2). Glo2 hydrolyzes S-D-lactoylglutathione to glutathione and lactic acid, while GS⁻ is formed in the active center of Glo2, similar to GSTP1-1 [41]. It has been established that actin and malate dehydrogenase can serve as substrates for S-glutathionylation by Glo2 [42].

S-glutathionylation is a reversible post-translational modification and, as a rule, deglutathionylation proceeds with the participation of enzymes and is more carefully regulated, in comparison with S-glutathionylation. Glutaredoxin (Grx) is one of the most effective and well-studied enzymes, which reduces Pr-SSG. In the traditional classification, they are divided into mono- and dithiol Grx, depending on whether one or two cysteine residues, respectively, are in the active center. The role of dithiol Grxs is mainly considered in the regulation of reversible S-glutathionylation [26,43,44].

Mammalian dithiol Grxs, Grx1 and Grx2, are found in many cellular compartments; however, Grx1 is mainly present in the cytosol ($\sim 1 \mu\text{M}$) and mitochondrial intermembrane space ($\sim 0.1 \mu\text{M}$), while Grx2 is localized mainly in the mitochondrial matrix ($\sim 1 \mu\text{M}$) [45,46]. Being thiol oxidoreductases, Grx1 and Grx2 contain the CXXC motif (Cys^N-XX-Cys^C; CPYC in Grx1 and CSYC in Grx2) in the active site. In addition, they are characterized by the presence of a thioredoxin fold, consisting of four β -sheets surrounded by three α -helices, and a site responsible for stabilizing GSH. Grx uses GSH as a co-substrate for the reduction of Pr-SSG mixed disulfides.

It should be noted that, depending on the value of the GSH/GSSG ratio, Grx can not only carry out deglutathionylation but, on the contrary, may promote S-glutathionylation (Figure 1). Grx2 functions as a glutathionylation enzyme under a decrease of GSH/GSSG and an increase in the level of O_2 (e.g., in relation to the respiratory complex I) whereas, at a high level of GSH/GSSG, and low concentrations of O_2 , Grx2 has a deglutathionylating activity [47]. The putative mechanism of S-glutathionylation proceeds in several stages: first, there is a nucleophilic attack of the disulfide bond GSSG by the thiolate anion Grx-S⁻, along with the formation of the glutathionylated intermediate Grx-SSG, from which the activated cationic radical [GS[•]]⁺ is transferred to the target protein with the formation of Pr-SSG, while Grx is again capable of catalyzing the reaction. For this process, the possibility of the reversible formation of Grx-S₂ from Grx-SSG is also noted [48].

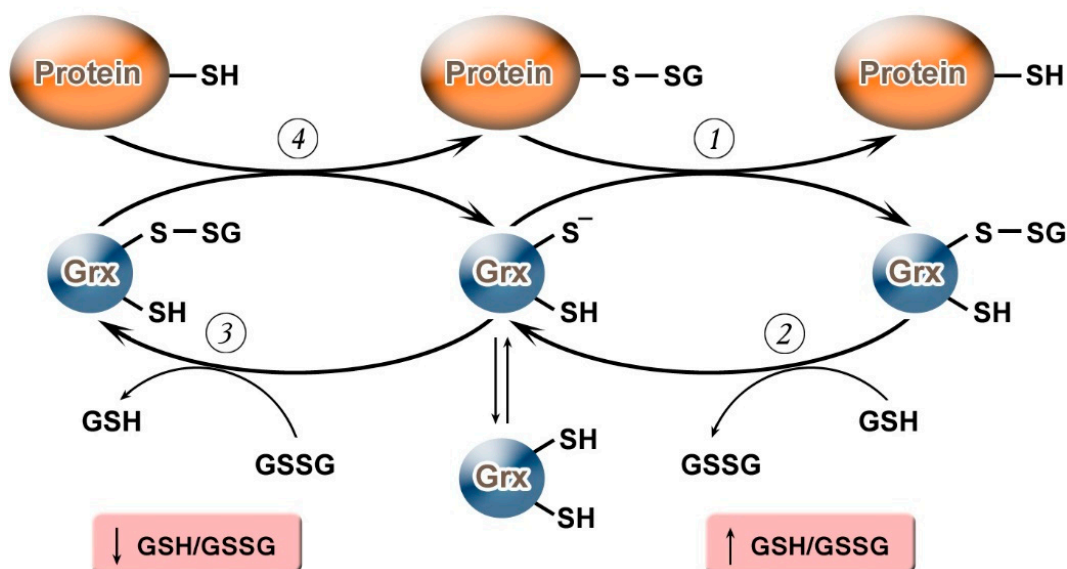


Figure 1. Glutaredoxin catalytic mechanism in dependence of GSH/GSSG ratio. Under an increase in GSH/GSSG, Grx can catalyze the deglutathionylation of proteins. The glutathionylated sulfur moiety of the protein-SSG is attacked by the thiolate anion of the enzyme (Grx-S⁻), forming the covalent enzyme intermediate (Grx-SSG) and releasing the reduced protein-SH as the first product (1). The second rate-determining step involves the reduction of Grx-SSG by GSH to produce glutathione disulfide (GSSG) as the second product, recycling the reduced enzyme (Grx-S⁻) (2). Under conditions of decreased GSH/GSSG ratio, Grx can catalyze S-glutathionylation of proteins. The S-glutathionylated Grx (Grx-SSG), formed in reaction with GSSG (3), reacts with a protein to create S-glutathionylated protein (protein-SSG) (4).

In addition to Grx, the ability to catalyze deglutathionylation has been observed in some other enzymes (Table 1).

Table 1. Enzymes with capacity to catalyze S-glutathionylation and deglutathionylation.

Protein Modification	Enzyme	Reference
S-glutathionylation	GST P1-1	[32–39,49]
	GST M1-1	[32]
	Glo2	[42]
	Grx1	[48]
	Grx2	[47,48]
Deglutathionylation.	Grx1	[48,50,51]
	Grx2	[47,48,50,52]
	GSTO1-1	[53–55]
	Srx	[13,56–58]
	Trx	[59–62]
	PDIs	[63]

The isoform of glutathione transferase, GSTO1-1, has the ability to catalyze protein deglutathionylation [54,55]. The isozyme is structurally similar to Grx, including Trx-like folding and a glutathione binding site, where it can form a disulfide bond with a conserved cysteine residue in the active site [53]. Other GST isoforms, including GSTA, GSTM, GSTP, GSTT, GSTS, and GSTZ, in contrast, have catalytic tyrosine or serine residues. In addition, GSTO1-1 has a relatively accessible pocket in the active site, which can potentially accommodate a protein or peptide as a substrate [54,64]. GSTO1-1 catalyzes Grx-like protein deglutathionylation in two similar stages: in the first, the Cys32 of the active site in human GSTO1-1 interacts with Pr-SSG, resulting in reduced Pr-SH and mixed disulfide GSTO1-1-Cys₃₂S-SG, which is deglutathionylated with the participation of GSH to form GSSG and functional active GSTO1-1, which is capable of catalyzing the deglutathionylation of the next protein substrate [54]. The question of the role that GSTO1-1 plays in the S-glutathionylation of proteins remains open [53,55].

The process of deglutathionylation is also carried out with the participation of the main members of the Trx family, which play essential roles in maintaining cellular redox homeostasis. Thioredoxins (Trx) 1 and 2 restore disulfide bonds in proteins. This process involves two cysteine residues of the Trx active site (Cys-X-X-Cys), where the disulfide bond is transferred from the substrate protein to Trx. Then, the oxidized Trx is reduced by the NADPH-dependent Trx reductase (TrxR) [65]. In addition, using the mechanism of dithiol reduction, Trxs are able to carry out deglutathionylation without the participation of GSH, which has been shown for glyceraldehyde-3-phosphate dehydrogenase, Prx3, 20S proteasome, and NOS3 [59–62]; however, the exact mechanism of deglutathionylation has not yet been determined.

The ability to deglutathionate proteins has also been observed in protein disulfide isomerases (PDIs), which are also included in the Trx family [63]. However, the significance of the PDI contribution to this process is not yet clear, as their main function is the exchange of the disulfide bonds of PDIs and target proteins. PDIs are enzymes of the endoplasmic reticulum, which are specifically responsible for protein folding through the oxidation of newly formed proteins and isomerization of proteins with improperly formed disulfide bonds, achieving the formation of their native structure. Moreover, PDIs can be secreted by the cell or associated with the cell surface to maintain proteins in a reduced state [62].

Sulfiredoxin (Srx), for which the ability to reduce the cysteine residue oxidized to sulfinic acid in the active site of typical 2-Cys periredoxins (2-Cys Prx) was originally established, is also capable of deglutathionylation, in relation to at least the Prx isoforms [13,56,57], actin, and tyrosine protein phosphatase 1B [58]. For example, it has been shown in vitro that human Prx1 can be S-glutathionylated at three out of four cysteine residues—Cys52, Cys173, and Cys83—and deglutathionylation at Cys83 and Cys173 is catalyzed

by Srx, while deglutathionylation at Cys52 is carried out by Grx [56]. The mechanism of Srx-catalyzed deglutathionylation has not yet been fully determined. The data indicate that it proceeds by a mechanism similar to that catalyzed by Grx through the formation of the Srx-SSG intermediate glutathionylated at the conservative Cys99 residue [56]. Srx-catalyzed deglutathionylation appears to have broad substrate specificity. In HEK293 cells transfected with Srx, a decrease in the total content of S-glutathionylated proteins formed under conditions of nitrosative stress after treatment with the nitric oxide donor PABA/NO has been demonstrated [58].

3. Protein S-Nitrosylation and Denitrosylation

S-nitrosylation, as well as S-glutathionylation, serves as a reversible post-translational modification of thiol groups of proteins [15,66,67]. In mammals, nitric oxide (NO) is mainly synthesized by nitric oxide synthase (NOS), for which three isoforms are known: Two constitutive—NOS1 (neuronal, nNOS) and NOS3 (endothelial eNOS)—as well as inducible NOS2 (iNOS), which have approximately 50% homology [68–70]. The activities of constitutive NOS1 and NOS3 are mainly regulated by phosphorylation, S-nitrosylation, protein–protein interactions, and changes in calcium levels, due to which steady-state NO concentrations are largely maintained [71]. On the contrary, inducible NOS2 produces high levels of NO in response to various factors [71]. In addition, the isoform mtNOS, a homolog of NOS1, has been found in the inner mitochondrial membrane and matrix. Its influence on the mitochondrial function has been intensively studied in recent years [72,73].

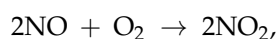
Under conditions of oxidative stress (NOS3 incubated with 2 mM GSSG, molar ratio of NOS3 to GSSG of 1:250), S-glutathionylation causes the decoupling of the NOS3 function and switches its activity from NO synthesis to the generation of $O_2^{\bullet-}$, thereby affecting the regulation of vascular tone [74,75]. In the human NOS3 reductase domain, the sites of S-glutathionylation are Cys689 and Cys908. Their modification in the presence of high concentrations of GSSG led to a noticeable increase in the formation of $O_2^{\bullet-}$, as shown in experiments carried out on the purified enzyme, as well as endothelial cells and intact vessels [75]. In the presence of GSH (1 mM), Grx1 reversed GSSG-mediated S-glutathionylation of NOS3, facilitating restoration of NO-synthase activity [75]. However, an increase in [GSSG]/[GSH] above 0.2, which can be observed in tissues under ischemia-reperfusion, causes S-glutathionylation at the Cys382 in the NOS3 oxygenase domain with the participation of Grx1. On the contrary, a decrease in [GSSG]/[GSH] below 0.1 leads to the deglutathionylation of the site. Thus, the S-glutathionylation of NOS3 by Grx1 at Cys382 is sensitive to fluctuations in the [GSSG]/[GSH] level and provides a unique mechanism for protection of the NOS3 thiol against oxidation.

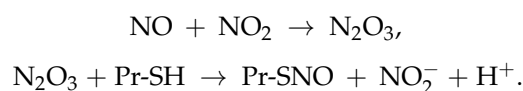
The formed NO is actively involved in signal transduction, either as an activator of guanylate cyclase—which synthesizes cGMP as a secondary messenger—or due to post-translational modifications of biomolecules, which occurs with the participation of NO itself or under the action of NO derivatives and includes the S-nitrosylation of protein thiols, the nitrosylation of transition metal ions, and the oxidative nitration of various molecules, such as tyrosine residues, amines, fatty acids, and guanine [76–78].

As a rule, for the S-nitrosylation of cysteine thiol groups, one-electron oxidation is necessary, which occurs with the participation of O_2 or a transition metal ion (e.g., iron or copper) [76]. The variant of the possible direct addition of NO occurs quite rarely, with the participation of a thiyl radical:

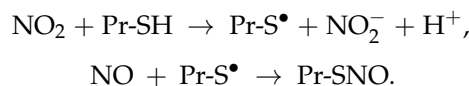


When NO interacts with O_2 , a set of oxides with a higher degree of nitrogen oxidation (so-called auto-oxidation) are formed, among which N_2O_3 is considered as the main nitrosylating agent that promotes the appearance of nitrosothiol and nitrite:



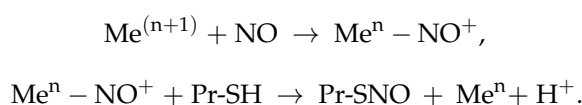


The interaction of NO_2 with thiol to form a thiyl radical and its further reaction with NO is possible:



Both processes are limited by the speed of NO_2 formation and its availability. The formation of GSNO can occur in the same way.

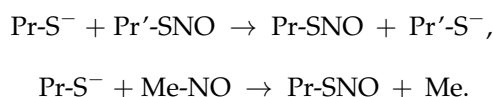
A variant of S-nitrosylation catalyzed by transition metal ions (Fe^{3+} or Cu^{2+}) has been described; in this case, one-electron oxidation of NO occurs and the resulting nitrosonium ion (NO^+) can nitrosylate a thiol located in its immediate vicinity:



This mechanism takes place during the autonitrosylation of hemoglobin and the formation of nitrosogluthione (GSNO), through the participation of ceruloplasmin and cytochrome c [76,79].

The S-nitrosylation of proteins can be accomplished by transnitrosylation, by which a low-molecular-weight nitrosothiol (e.g., GSNO), or a protein nitrosylated at a cysteine residue or containing a nitrosylated metal ion (e.g., in heme), interacts with the protein and transfers NO to the protein cysteine residue. This transfer between thiol-containing compounds promotes the sequential remote transfer of NO from the site of its synthesis, including NO transfer between different sub-cellular structures [80,81].

Trans-nitrosylation can occur between Cys residues (Cys-to-Cys) or between a metal and Cys residues (Me-to-Cys):



The terms “S-nitrosylase” and “trans-nitrosylase” are used to designate the enzymes involved in the transfer of NO groups [79]. In a process with the participation of a transition metal ion (e.g., iron or copper), the NO group can be transported intra- or inter-molecularly. For example, in hemoglobin, the NO group is transferred from the heme iron to neighboring thiols in the same molecule; whereas, in cytochrome *c*, NO is coordinated with the iron atom and transferred to the SH group of glutathione to form GSNO [81]. In Me-to-Cys trans-nitrosylases, the transition metal can perform the redox functions that are necessary for the formation of Pr-SNO without molecular oxygen [82].

During trans-nitrosylation, the thiolate anion of the recipient carries out a nucleophilic attack of the nitrogen in the nitrosyl group of the donor [83]. To date, several trans-nitrosylases have been identified (Table 2), for which only specific cysteines seem to be targets that allow for the selective regulation of certain cellular signaling pathways [80].

The main factor determining the selective transfer of NO is the physical distance between the donor (S-nitrosylase) and recipient thiol group. As a rule, the nitrosylated protein contains the I/L-X-C-X2-D/E motif. Another factor is the redox potential between thiols. Thus, trans-nitrosylation occurs only when two proteins interact directly and have corresponding redox potentials that provide electron transfer with subsequent NO transfer. It is assumed that the physical association of the two proteins causes their conformational change, allowing the recipient thiol to form a thiolate anion, which then attacks the donor’s nitrosyl group [80].

Table 2. Transnitrosylases and their substrates.

Type	Transnitrosylase	Substrate	Reference
Me-to-Cys	Cytochrome <i>c</i>	GSH	[84]
	Ceruloplasmin	GSH	[85]
	Hemoglobin	Glypican-1 Auto-S-nitrosylation	[86] [87]
Cys-to-Cys	GAPDH	SIRT1, HDAC2, DNA-PK	[88]
	Trx1	Hsp60, Acetoacetyl-CoA thiolase, VDAC1	[89]
	Caspase 3	Caspase 3	[90]
		Prx1	[91]
		XIAP	[92]
		Trx1	[93]
		Cyclin-dependent kinase 5	Dynamin-related protein 1
	Protein Deglycase DJ-1	PTEN	[95]
	Hemoglobin	Anion-exchanger 1 protein	[96]

An interesting example of an enzyme involved in trans-nitrosylation is glyceraldehyde-3-phosphate dehydrogenase (GAPDH). Human GAPDH is S-nitrosylated at the catalytic residue Cys152 (in humans) using calcium- and zinc-dependent proteins (participants in the process of inflammation and immune response), nitrosylated in turn under the action of NOS2, which is accompanied by a loss of pro-inflammatory properties. S-nitrosylated GAPDH (GAPDH-SNO) interacts with the E3 ubiquitin-protein ligase Siah1 and moves from cytoplasm to nucleus. In the nucleus, Siah1 initiates ubiquitination and the degradation of nuclear proteins to initiate apoptosis, while GAPDH-SNO binds to p53, which also activates apoptosis. In addition, GAPDH-SNO transnitrosylates proteins involved in DNA transcription and repair. These proteins include SIRT1 and HDAC2 deacetylases, which are inhibited after S-nitrosylation. On the contrary, DNA-activated protein kinase (DNA-PK), which is involved in DNA repair, is activated by S-nitrosylation with the participation of GAPDH-SNO [88,97]. In response to stress, GAPDH is translocated into the mitochondria, where it transnitrosylates Hsp60, acetyl-CoA thiolase, and VDAC1, thus affecting membrane permeability, the regulation of mitochondrial function, and cell death [98,99].

S-nitrosylation is a reversible post-translational modification; hence, the removal of the NO group is an important aspect of signal transduction involved with it. It has generally been accepted that the levels of cellular nitrosothiols are low, due to the high reversibility of the process. Initial information on denitrosylation has indicated that it is an unregulated and spontaneous reaction. Several non-enzymatic mechanisms of denitrosylation that can potentially act *in vivo* have been described. These include reactions involving transition metal ions, nucleophilic compounds, and reducing agents, such as glutathione, ascorbate, bilirubin, and sulfite [100,101].

The most S-nitrosylated proteins are rapidly denitrosylated by reducing agents, such as GSH. However, there are targets for NO that are capable of forming stable S-nitrosothiols *in vivo*, where stable nitrosothiols appear as a result of the protein conformational changes that reduce the availability of the NO group in the solution [102]. Some of these proteins are the generally recognized targets of NO. It has been suggested that physiological signaling involving NO uses exactly stable S-nitrosothiols, for which highly specific enzymatic intracellular denitrosylation pathways are probably used to complete NO-dependent signaling, involving the cysteine residues of proteins. A large amount of data has shown that the denitrosylation process is catalyzed by the several enzymes, both *in vitro* and *in vivo* (see Table 3) [103–105].

The main denitrosylases are S-nitrosogluthathione reductase (GSNOR) and Trx, for which the role has been shown *in vivo* [104,106]. In addition, there are *in vitro* data obtained in cell lysates or isolated systems on the denitrosylase activity of carbonyl reductase, xanthine oxidase, Cu/Zn superoxide dismutase, PDI, glutathione peroxidase, and glutaredoxin [103,105]. The reaction products (depending on the enzyme) are various S-nitrosothiols, NO, peroxynitrite, hydroxylamine, and ammonia.

The most important denitrosylase is GSNOR. Although GSNOR is formally characterized as a class III alcohol dehydrogenase (ADH5) or glutathione-dependent formaldehyde

dehydrogenase (FDH), it is most active against the GSNO substrate as a reductase and does not use other S-nitrosothiols as a substrate [107]. GSNOR is found in most human tissues, but its greatest activity has been observed in the liver [108]. The maximum content of GSNOR has been found in the cytoplasm, but this enzyme was also found in the nucleus [109].

Table 3. The major denitrosylases and their substrates.

Denitrosylase	Substrate	Reference	
GSNO reductase	G-protein-coupled receptor kinase 2	[110]	
	β -arrestin 2	[111]	
	HIF1 α	[112]	
	Ras	[113]	
	Ryanodine receptor 2	[114]	
	Connexin	[115]	
	AGT	[116]	
	Dynammin-related protein 1	[117]	
	Parkin	[117,118]	
	Caspase 3	[93,119,120]	
	Thioredoxin	Caspase 9, PTP-1B, GAPDH	[93]
		NSF	[121]
		Insulin receptor, Akt, PDE3B	[122]
		Actin	[123]
NF- κ B		[124]	
NOS1		[125]	
NOS2, MEK1		[126]	
CD95, NOS3		[127]	
Glutaredoxin 1		L-Cys-SNO, GSNO, Caspase 3, Cathepsin B	[103]
			[128–130]
Protein disulfide isomerase	GSNO	[131]	
Glutathione peroxidase	GSNO	[132]	
Carbonyl reductase	GSNO	[132]	
Ceruloplasmin	Glypican-1	[86]	

GSNOR is active as a homodimer. The recovery of GSNO occurs during an irreversible reaction, the products of which are not involved in the S-nitrosylation of cellular proteins. In the first step, GSNO is reduced to the unstable intermediate *N*-hydroxysulfonamide (GSNHOH), using NADH as a specific co-substrate. At the next stage of the reaction, depending on the local concentration of GSH, *N*-hydroxysulfonamide is either decomposed to hydroxylamine and GSSG under physiological GSH levels in millimolar range or, under low GSH levels, spontaneously converts to glutathione sulfinamide, which can be hydrolyzed to glutathione sulfinic acid and ammonia [132]. This has been shown through in vitro experiments where low concentrations of GSH (0–1 mM) promoted the rearrangement of GSNHOH to glutathione sulfinamide, then into sulfinic acid and ammonia; however, the presence of 5 mM GSH favored yields of hydroxylamine and GSSG [133].

The Trx-dependent system has a wide range of denitrosylation substrates [93,134]. The reaction catalyzed by Trx involves its direct interaction with Pr-SNO (Figure 2). The attack of the more nucleophilic cysteine residue in the active site (i.e., Cys32 of human Trx1) can occur either against the sulfur atom or the nitrogen atom of the S-nitroso group of the nitrosylated protein. In the first case, it leads to the formation of a mixed disulfide between Trx and the S-nitrosylated protein with the release of the nitroxyl anion (NO[−]); then, due to the second cysteine of the Trx active center (i.e., Cys35 of human Trx1), the thiol group of the protein is reduced, while the intermolecular disulfide bond is replaced by the intramolecular bond in the active center of thioredoxin (Trx-S₂). In the second case, at the beginning, a trans-nitrosylation reaction occurs with the formation of denitrosylated protein (Pr-SH) and S-nitrosylated Trx-NO, followed by the release of the nitrosyl group (in the form of NO or NO[−]) and the formation of an intramolecular disulfide bond in thioredoxin, which is reduced by TrxR with the participation of NADPH [93,119]. It is

assumed that the geometry and electronic structure near the ONS group of the substrate protein may be responsible for the choice of the attack site; on the other hand, it is possible that structural elements near the Trx active center play a decisive role [119].

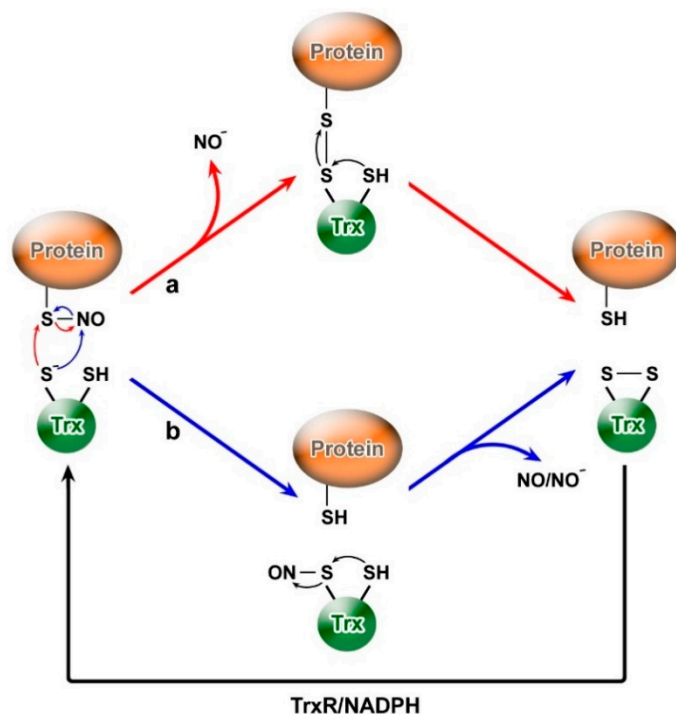


Figure 2. Protein denitrosylation by the Trx/TrxR system. Two thioresoxin-dependent mechanisms of protein denitrosylation are proposed: (a) formation of Trx linkage with substrate protein by a disulfide bridge; (b) trans-nitrosylation due to transient S-nitrosylation of Trx.

A wide range of substrates have been identified for denitrosylation catalyzed by Trx. For example, cytosolic caspase 3 and caspase 8 are activated by the denitrosylation action of Trx1, while mitochondrial caspase 3 is denitrosylated by Trx2 upon activation of Fas-induced apoptosis [93,120,135]. Trx also denitrosylates NF- κ B after stimulation with cytokines, illustrating the importance of denitrosylation for immune signaling [124].

It is likely that Trx catalyzes the denitrosylation of participants in signaling cascades activated by insulin in adipocytes, which is especially important as NOS2 is induced in obesity [122].

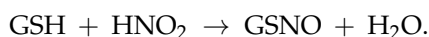
Most cells express various Trx-like proteins; however, there is currently insufficient information on the roles these proteins play in denitrosylation processes. However, it has been found that protein TXNDC17 (TRP14/TXNL5), a representative of a large group of proteins with Trx-like domains, is capable of denitrosylating GSNO [136].

It has recently been found that Grx, which is also a member of the Trx superfamily proteins, may possess denitrosylase activity. It has been shown that the low-molecular-weight S-nitrosothiols L-Cys-SNO and GSNO are substrates of Grx1 while, among the proteins, caspase 3 and cathepsin B are denitrosylated by this cytosolic isoform of glutaredoxin [103]. As caspase 3 and cathepsin B play important roles in the development of apoptosis, the functional activity of Grx1 in the regulation of apoptosis may be carried out through their denitrosylation. As the active centers of Grx dithiol isoforms, similar to Trxs isoforms, contain two cysteine residues CXXC (Cys^N-XX-Cys^C; CPYC in Grx1 and CSYC in Grx2), it has been assumed that denitrosylation, in this case, proceeds in a similar manner as Trx, with the formation of an intramolecular disulfide in the active center of glutaredoxin. The reduced dithiol Grxs catalyze the denitrosylation reaction in the absence of GSH, whereas monothiol Grx only does so in the presence of GSH [103].

Another member of the Trx family, PDI, which is localized on the cytoplasmic membrane, promotes NO transfer from extracellular Pr-SNO to intracellular thiols, suggesting that PDI is involved in NO transfer from the extracellular environment to the cytoplasm [128]. However, it remains unclear whether this function is mediated directly by PDI or by an alternative membrane protein whose redox state is regulated by PDI. It has been found that PDI catalyzes the degradation of GSNO in vitro. This reaction apparently proceeds with the participation of cysteine residues in the active centers of two PDI sub-units through several intermediates with the formation of oxidized PDI and NO [129]. The involvement of PDI in NO transfer from extracellular albumin to intracellular metallothionein has been shown [130].

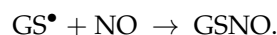
4. Nitrosogluthathione: Its Formation and Role in the Relationship and Control of S-Glutathionylation and S-Nitrosylation

GSNO is the most abundant low-molecular-weight S-nitrosothiol and an important NO donor. It is present in both animals and plants. The efficient and simple chemical synthesis of GSNO can be carried out by the interaction of GSH and nitrous acid [137]:

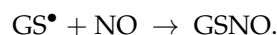
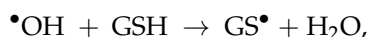
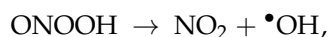
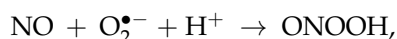


However, it should be noted that the exact mechanisms leading to the formation of GSNO in vivo remain unclear. Apparently, one of the possible mechanisms for the synthesis of GSNO is the interaction of GSH with N_2O_3 , which is formed due to the auto-oxidation of NO [138].

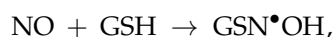
The appearance of GSNO is possible when NO interacts with the thiyl radical of glutathione GS^\bullet , which is formed as another product of NO auto-oxidation [138]:



As a result of the interaction of NO with the superoxide radical anion, peroxyxynitrite is formed; the protonated form of which can decompose, with the formation of nitric oxide (NO_2) and hydroxyl radical ($^\bullet\text{OH}$), leading to the further formation of GS^\bullet :



Despite the fact that many researchers do not believe that there is a direct reaction between thiols and NO, the formation of GSNO from GSH and NO in the presence of an electron acceptor (it may be O_2) has been assumed [139] and was proven for sub-millimolar NO concentrations ($<0.6 \mu\text{M}$) [138]. It has been assumed that, at first, GSH can interact with free NO to form the hydroxyl amino radical ($\text{GSN}^\bullet\text{OH}$); then, an electron acceptor (e.g., O_2) can convert it to GSNO [139]:

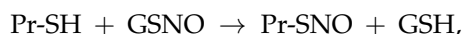
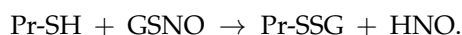


GSNO formed in mitochondria can translocate to various parts of the cell, where it can participate in the transnitrosylation reactions of a number of proteins, such as NF- κ B, STAT3, AKT, EGFR, and IGF-1R, the S-nitrosylation of which significantly affects their activity [79,140].

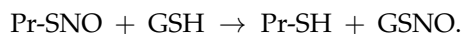
In recent years, interest has increased in the study of nitro derivatives of high unsaturated fatty acids (NO₂-FAs) which, by themselves or as part of complex lipids, exhibit a rather wide range of biological functions in humans, animals, and plants and are considered to be signal transducers. Although the *in vivo* mechanisms of formation of NO₂-FAs are not yet fully understood, it has been shown that they proceed with the participation of NO and its derivatives. On the other hand, NO₂-FAs have been shown to be capable of releasing NO and carrying out post-translational protein modifications through nitroalkylation [141–144], due to which NO₂-FAs (e.g., nitro-oleic and nitro-linoleic acids) are able to provide vasodilating, antioxidant, and anti-inflammatory action, which are important for the physiology of animals and plants, promoting the activation of defense mechanisms in stressful conditions.

For plants—in particular, for *Arabidopsis*—it has been shown that nitrolinolenic acid (NO₂-Ln) can release NO at physiological pH and temperature [142]. This NO may contribute to the generation of intracellular GSNO. It has been assumed that the direct interaction of NO and GSH is possible in *Arabidopsis*, due to the sub-micromolar concentration of NO required for GSNO synthesis [138], which has been demonstrated to be produced from NO₂-Ln (0.21 μM/min) [142,145].

It is important to note that, under interaction with protein thiols, GSNO can lead to the S-glutathionylation of proteins, with the formation of a mixed thiol and nitroxyl [49,76]:



A possible variant is the reaction of trans-nitrosylation with the formation of GSNO during the interaction of Pr-SNO with GSH, while GSH takes on the NO group with the formation of GSNO [146]:



GSH-mediated trans-nitrosylation is more preferable than S-glutathionylation [147], which is possibly due to the fact that the nitrogen atom in the S-N bond is more positive than the sulfur atom and, thus, it is more favorable for the nucleophilic attack of GSH [148].

Due to the change in the GSNO level, the regulation of cell sensitivity to the activation of apoptosis can be carried out. In several HNSCC lines of human head and neck squamous cell carcinoma, it has been shown that the activation of STAT3 by phosphorylation was reversibly inhibited by GSNO, due to the S-nitrosylation of human STAT3 at the Cys259 residue [149]. In addition, GSNO contributed to a decrease in basal and cytokine-stimulated activation of NF-κB in HNSCC cells. The decreases in STAT3 and NF-κB activity upon treatment with GSNO correlated with a decrease in the proliferation and activation of apoptosis of HNSCC cells. Through *in vivo* model experiments in mice with human HNSCC tumor xenografts, tumor growth was reduced by systemic treatment with GSNO and further decreased in combination with cisplatin chemotherapy and radiation therapy. Thus, the potential possibility of using GSNO to block NF-κB and STAT3, which are responsible for cell survival and proliferation, has been suggested to enhance the therapeutic effect of traditional treatment methods [149].

As a NO donor, GSNO can induce apoptosis through the S-nitrosylation of Prx2. For example, in cells of non-small cell lung carcinoma, the S-nitrosylation of human Prx2 at Cys51 and Cys172 caused by GSNO disrupted the formation of the Prx2 dimer and suppressed its antioxidant activity, causing the accumulation of endogenous H₂O₂ and the activation of AMP-activated protein kinase (AMPK), which then activated sirtuin 1 (SIRT1). Phosphorylated SIRT1 loses its deacetylase activity against p53 in A549 cells or FOXO1 in NCI-H1299 cells, which ultimately leads to the apoptosis of tumor cells [150].

In vitro studies have shown that proteins, such as papain, creatine phosphokinase, and glyceraldehyde 3-phosphate dehydrogenase are sensitive to both S-nitrosylation and S-glutathionylation by GSNO, while alcohol dehydrogenase, bovine serum albu-

min, and actin apparently become S-nitrosylated [147]. In addition, the treatment of cells with PABA/NO [*O*²-[2,4-dinitro-5-[4-(*N*-methylamino)benzoyloxy]phenyl] 1-(*N,N*-dimethylamino) diazen-1-ium-1,2-diolate] led to a dose-dependent increase in intracellular NO followed by S-nitrosylation, the level of which was extremely low. However, a very high level of S-glutathionylation was detected for some proteins, including β -lactate dehydrogenase, Rho GDP-dissociation inhibitor β , ATP synthase, elongation factor 2, PDI, nucleophosmin-1, actin, protein tyrosine phosphatase 1B, and glucosidase II [151,152]. These data indicate that there may be two different pools of S-nitrosylated proteins, one of which remains stable, while the other is labile with respect to GSH and is subject to the rapid conversion to S-glutathionylated products. However, the conditions that favor the formation of Pr-SSG, in comparison with Pr-SNO, have not yet been determined [13].

The fact that S-nitrosylation of cysteine residues can serve as a transient intermediate has been evidenced by studies on rat smooth muscle cells treated with CysNO. The total pool of reduced thiols did not change significantly, while the level of reduced non-protein thiols—in particular, GSH—decreased. A decrease in GSH content prior to the use of CysNO by pre-treatment with BSO, which is an inhibitor of gamma-glutamylcysteine synthetase (a key enzyme of GSH de novo synthesis), led to a significant increase in S-nitrosylated proteins, indicating a violation of the ability to reduce Pr-SNO due to S-glutathionylation [148]. In contrast, the increase in cellular GSH by the GSH ethyl ester after CysNO treatment significantly attenuated the S-nitrosylation of proteins. In addition, the treatment of cells with only one selective GSNOR inhibitor N6022 did not change the S-nitrosylation pattern; whereas, in the treatment with CysNO, the inhibition of GSNOR significantly increased the Pr-SNO level. These data illustrate that interventions that lead to a decrease in cellular redox and repair status can lead to imbalances in the levels of S-nitrosylated proteins [153].

5. Conclusions

Cellular redox status, as the state of oxidant/antioxidant balance, largely determines the viability of cells, including the processes of proliferation, differentiation, bioenergetics, and apoptosis. To a large extent, this is facilitated by the redox-dependent post-translational modifications of proteins, which alter their functional activity. Among these reactions, S-glutathionylation and S-nitrosylation are the best studied, although their relationship and regulation are still questionable. The function of a connecting link and a "switch" between S-glutathionylation and S-nitrosylation can be performed by GSNO, the level of which depends on the GSH content, the GSH/GSSG ratio, and RONS levels.

The algorithms that determine the ratio of S-glutathionylation and S-nitrosylation will be the subject of further study; however, we can already say that they are determined, on one hand, by the RONS ratio and, on the other, by GSH/GSSG and largely depend on the conditions that maintain the intracellular level of GSH, including its de novo synthesis and the rate of GSSG recovery. Trx family enzymes (Trx, Grx, PDI) play an important role in the regulation of these processes, the activity of which is determined by the cellular redox status and the GSH/GSSG level.

Taken together, this allows us to emphasize the important role of GSH in protein redox modulation—through S-glutathionylation and S-nitrosylation—in order to determine the contribution of these processes to the maintenance and regulation of cellular redox homeostasis.

Author Contributions: E.K. conceptualized the paper. E.K. and M.N. wrote and approved the final version of the manuscript. The authors have read and agreed to the published version of the manuscript.

Funding: This paper was supported by the RUDN University Strategic Academic Leadership Program.

Institutional Review Board Statement: Not Applicable.

Informed Consent Statement: Not Applicable.

Data Availability Statement: Data is contained within the article.

Conflicts of Interest: The authors declare no conflict of interest.

References

- Dwivedi, D.; Megha, K.; Mishra, R.; Mandal, P.K. Glutathione in Brain: Overview of Its Conformations, Functions, Biochemical Characteristics, Quantitation and Potential Therapeutic Role in Brain Disorders. *Neurochem. Res.* **2020**, *45*, 1461–1480. [CrossRef] [PubMed]
- Lv, H.; Zhen, C.; Liu, J.; Yang, P.; Hu, L.; Shang, P. Unraveling the Potential Role of Glutathione in Multiple Forms of Cell Death in Cancer Therapy. *Oxid. Med. Cell. Longev.* **2019**, *2019*, 3150145. [CrossRef] [PubMed]
- Paul, B.D.; Sbodio, J.I.; Snyder, S.H. Cysteine Metabolism in Neuronal Redox Homeostasis. *Trends Pharmacol. Sci.* **2018**, *39*, 513–524. [CrossRef] [PubMed]
- Moriarty-Craige, S.E.; Jones, D.P. Extracellular thiols and thiol/disulfide redox in metabolism. *Annu. Rev. Nutr.* **2004**, *24*, 481–509. [CrossRef] [PubMed]
- Giustarini, D.; Colombo, G.; Garavaglia, M.L.; Astori, E.; Portinaro, N.M.; Reggiani, F.; Badalamenti, S.; Aloisi, A.M.; Santucci, A.; Rossi, R.; et al. Assessment of glutathione/glutathione disulphide ratio and S-glutathionylated proteins in human blood, solid tissues, and cultured cells. *Free Radic. Biol. Med.* **2017**, *112*, 360–375. [CrossRef] [PubMed]
- Musaogullari, A.; Chai, Y.C. Redox Regulation by Protein S-Glutathionylation: From Molecular Mechanisms to Implications in Health and Disease. *Int. J. Mol. Sci.* **2020**, *21*, 8113. [CrossRef] [PubMed]
- Bjorklund, G.; Tinkov, A.A.; Hosnedlova, B.; Kizek, R.; Ajsuvakova, O.P.; Chirumbolo, S.; Skalnaya, M.G.; Peana, M.; Dadar, M.; El-Ansary, A.; et al. The role of glutathione redox imbalance in autism spectrum disorder: A review. *Free Radic. Biol. Med.* **2020**, *160*, 149–162. [CrossRef]
- Giles, G.I.; Tasker, K.M.; Jacob, C. Hypothesis: The role of reactive sulfur species in oxidative stress. *Free Radic. Biol. Med.* **2001**, *31*, 1279–1283. [CrossRef]
- Shi, Y.; Carroll, K.S. Activity-Based Sensing for Site-Specific Proteomic Analysis of Cysteine Oxidation. *Acc. Chem. Res.* **2020**, *53*, 20–31. [CrossRef]
- Grek, C.L.; Zhang, J.; Manevich, Y.; Townsend, D.M.; Tew, K.D. Causes and consequences of cysteine S-glutathionylation. *J. Biol. Chem.* **2013**, *288*, 26497–26504. [CrossRef]
- Bechtel, T.J.; Weerapana, E. From structure to redox: The diverse functional roles of disulfides and implications in disease. *Proteomics* **2017**, *17*, 1600391. [CrossRef] [PubMed]
- Benhar, M. Oxidants, Antioxidants and Thiol Redox Switches in the Control of Regulated Cell Death Pathways. *Antioxidants* **2020**, *9*, 309. [CrossRef] [PubMed]
- Zhang, J.; Ye, Z.W.; Singh, S.; Townsend, D.M.; Tew, K.D. An evolving understanding of the S-glutathionylation cycle in pathways of redox regulation. *Free Radic. Biol. Med.* **2018**, *120*, 204–216. [CrossRef] [PubMed]
- Mailloux, R.J. Protein S-glutathionylation reactions as a global inhibitor of cell metabolism for the desensitization of hydrogen peroxide signals. *Redox Biol.* **2020**, *32*, 101472. [CrossRef] [PubMed]
- Shi, X.; Qiu, H. Post-Translational S-Nitrosylation of Proteins in Regulating Cardiac Oxidative Stress. *Antioxidants* **2020**, *9*, 1051. [CrossRef] [PubMed]
- Zhang, Y.; Deng, Y.; Yang, X.; Xue, H.; Lang, Y. The Relationship Between Protein S-Nitrosylation and Human Diseases: A Review. *Neurochem. Res.* **2020**, *45*, 2815–2827. [CrossRef]
- Lermant, A.; Murdoch, C.E. Cysteine Glutathionylation Acts as a Redox Switch in Endothelial Cells. *Antioxidants* **2019**, *8*, 315. [CrossRef]
- Mishra, D.; Patel, V.; Banerjee, D. Nitric Oxide and S-Nitrosylation in Cancers: Emphasis on Breast Cancer. *Breast Cancer* **2020**, *14*, 1178223419882688. [CrossRef]
- Begara-Morales, J.C.; Sanchez-Calvo, B.; Chaki, M.; Valderrama, R.; Mata-Perez, C.; Padilla, M.N.; Corpas, F.J.; Barroso, J.B. Antioxidant Systems are Regulated by Nitric Oxide-Mediated Post-translational Modifications (NO-PTMs). *Front. Plant Sci.* **2016**, *7*, 152. [CrossRef]
- Choi, M.S. Pathophysiological Role of S-Nitrosylation and Transnitrosylation Depending on S-Nitrosoglutathione Levels Regulated by S-Nitrosoglutathione Reductase. *Biomol. Ther.* **2018**, *26*, 533–538. [CrossRef]
- Arora, D.; Jain, P.; Singh, N.; Kaur, H.; Bhatla, S.C. Mechanisms of nitric oxide crosstalk with reactive oxygen species scavenging enzymes during abiotic stress tolerance in plants. *Free Radic. Res.* **2016**, *50*, 291–303. [CrossRef] [PubMed]
- Belcastro, E.; Gaucher, C.; Corti, A.; Leroy, P.; Lartaud, I.; Pompella, A. Regulation of protein function by S-nitrosation and S-glutathionylation: Processes and targets in cardiovascular pathophysiology. *Biol. Chem.* **2017**, *398*, 1267–1293. [CrossRef] [PubMed]
- Weise-Cross, L.; Resta, T.C.; Jernigan, N.L. Redox Regulation of Ion Channels and Receptors in Pulmonary Hypertension. *Antioxid. Redox Signal.* **2019**, *31*, 898–915. [CrossRef] [PubMed]
- Dominko, K.; Dikic, D. Glutathionylation: A regulatory role of glutathione in physiological processes. *Arh. Hig. Rada Toksikol.* **2018**, *69*, 1–24. [CrossRef] [PubMed]
- Moldogazieva, N.T.; Mokhosoev, I.M.; Feldman, N.B.; Lutsenko, S.V. ROS and RNS signalling: Adaptive redox switches through oxidative/nitrosative protein modifications. *Free Radic. Res.* **2018**, *52*, 507–543. [CrossRef]

26. Young, A.; Gill, R.; Mailloux, R.J. Protein S-glutathionylation: The linchpin for the transmission of regulatory information on redox buffering capacity in mitochondria. *Chem. Biol. Interact.* **2019**, *299*, 151–162. [CrossRef]
27. Nulton-Persson, A.C.; Starke, D.W.; Mieryl, J.J.; Szveda, L.I. Reversible inactivation of alpha-ketoglutarate dehydrogenase in response to alterations in the mitochondrial glutathione status. *Biochemistry* **2003**, *42*, 4235–4242. [CrossRef]
28. Gilbert, H.F. Thiol/disulfide exchange equilibria and disulfide bond stability. *Methods Enzymol.* **1995**, *251*, 8–28. [CrossRef]
29. Gilbert, H.F. Molecular and cellular aspects of thiol-disulfide exchange. *Adv. Enzymol. Relat. Areas Mol. Biol.* **1990**, *63*, 69–172. [CrossRef]
30. Rashdan, N.A.; Shrestha, B.; Pattillo, C.B. S-glutathionylation, friend or foe in cardiovascular health and disease. *Redox Biol.* **2020**, *37*, 101693. [CrossRef]
31. Arbault, S.; Pantano, P.; Sojic, N.; Amatore, C.; Best-Belpomme, M.; Sarasin, A.; Vuillaume, M. Activation of the NADPH oxidase in human fibroblasts by mechanical intrusion of a single cell with an ultramicroelectrode. *Carcinogenesis* **1997**, *18*, 569–574. [CrossRef] [PubMed]
32. Klaus, A.; Zorman, S.; Berthier, A.; Polge, C.; Ramirez, S.; Michelland, S.; Seve, M.; Vertommen, D.; Rider, M.; Lentze, N.; et al. Glutathione S-transferases interact with AMP-activated protein kinase: Evidence for S-glutathionylation and activation in vitro. *PLoS ONE* **2013**, *8*, e62497. [CrossRef] [PubMed]
33. Ye, Z.W.; Zhang, J.; Ancrum, T.; Manevich, Y.; Townsend, D.M.; Tew, K.D. Glutathione S-Transferase PMediated Protein S-Glutathionylation of Resident Endoplasmic Reticulum Proteins Influences Sensitivity to Drug-Induced Unfolded Protein Response. *Antioxid. Redox Signal.* **2017**, *26*, 247–261. [CrossRef] [PubMed]
34. Ralat, L.A.; Manevich, Y.; Fisher, A.B.; Colman, R.F. Direct evidence for the formation of a complex between 1-cysteine peroxidase and glutathione S-transferase pi with activity changes in both enzymes. *Biochemistry* **2006**, *45*, 360–372. [CrossRef]
35. Zhou, S.; Sorokina, E.M.; Harper, S.; Li, H.; Ralat, L.; Dodia, C.; Speicher, D.W.; Feinstein, S.I.; Fisher, A.B. Peroxiredoxin 6 homodimerization and heterodimerization with glutathione S-transferase pi are required for its peroxidase but not phospholipase A2 activity. *Free Radic. Biol. Med.* **2016**, *94*, 145–156. [CrossRef]
36. Townsend, D.M.; Manevich, Y.; He, L.; Hutchens, S.; Pazoles, C.J.; Tew, K.D. Novel role for glutathione S-transferase pi. Regulator of protein S-Glutathionylation following oxidative and nitrosative stress. *J. Biol. Chem.* **2009**, *284*, 436–445. [CrossRef]
37. Uemura, T.; Tsapralis, G.; Gerner, E.W. GSTT1 stimulates caveolin-1-regulated polyamine uptake via actin remodeling. *Oncotarget* **2019**, *10*, 5713–5723. [CrossRef]
38. Wetzelberger, K.; Baba, S.P.; Thirunavukkarasu, M.; Ho, Y.S.; Maulik, N.; Barski, O.A.; Conklin, D.J.; Bhatnagar, A. Postischemic deactivation of cardiac aldose reductase: Role of glutathione S-transferase P and glutaredoxin in regeneration of reduced thiols from sulfenic acids. *J. Biol. Chem.* **2010**, *285*, 26135–26148. [CrossRef]
39. Zhang, J.; Ye, Z.W.; Chen, W.; Manevich, Y.; Mehrotra, S.; Ball, L.; Janssen-Heininger, Y.; Tew, K.D.; Townsend, D.M. S-Glutathionylation of estrogen receptor α affects dendritic cell function. *J. Biol. Chem.* **2018**, *293*, 4366–4380. [CrossRef]
40. Graminski, G.F.; Kubo, Y.; Armstrong, R.N. Spectroscopic and kinetic evidence for the thiolate anion of glutathione at the active site of glutathione S-transferase. *Biochemistry* **1989**, *28*, 3562–3568. [CrossRef]
41. Deponte, M. Glutathione catalysis and the reaction mechanisms of glutathione-dependent enzymes. *Biochim. Biophys. Acta* **2013**, *1830*, 3217–3266. [CrossRef]
42. Ercolani, L.; Scire, A.; Galeazzi, R.; Massaccesi, L.; Cianfruglia, L.; Amici, A.; Piva, F.; Urbanelli, L.; Emiliani, C.; Principato, G.; et al. A possible S-glutathionylation of specific proteins by glyoxalase II: An in vitro and in silico study. *Cell Biochem. Funct.* **2016**, *34*, 620–627. [CrossRef] [PubMed]
43. Burns, M.; Rizvi, S.H.M.; Tsukahara, Y.; Pimentel, D.R.; Luptak, I.; Hamburg, N.M.; Matsui, R.; Bachschmid, M.M. Role of Glutaredoxin-1 and Glutathionylation in Cardiovascular Diseases. *Int. J. Mol. Sci.* **2020**, *21*, 6803. [CrossRef] [PubMed]
44. Xiao, Z.; La Fontaine, S.; Bush, A.I.; Wedd, A.G. Molecular Mechanisms of Glutaredoxin Enzymes: Versatile Hubs for Thiol-Disulfide Exchange between Protein Thiols and Glutathione. *J. Mol. Biol.* **2019**, *431*, 158–177. [CrossRef] [PubMed]
45. Ren, X.; Zou, L.; Zhang, X.; Branco, V.; Wang, J.; Carvalho, C.; Holmgren, A.; Lu, J. Redox Signaling Mediated by Thioredoxin and Glutathione Systems in the Central Nervous System. *Antioxid. Redox Signal.* **2017**, *27*, 989–1010. [CrossRef]
46. Gallogly, M.M.; Starke, D.W.; Mieryl, J.J. Mechanistic and kinetic details of catalysis of thiol-disulfide exchange by glutaredoxins and potential mechanisms of regulation. *Antioxid. Redox Signal.* **2009**, *11*, 1059–1081. [CrossRef]
47. Beer, S.M.; Taylor, E.R.; Brown, S.E.; Dahm, C.C.; Costa, N.J.; Runswick, M.J.; Murphy, M.P. Glutaredoxin 2 catalyzes the reversible oxidation and glutathionylation of mitochondrial membrane thiol proteins: Implications for mitochondrial redox regulation and antioxidant DEFENSE. *J. Biol. Chem.* **2004**, *279*, 47939–47951. [CrossRef]
48. Ukuwela, A.A.; Bush, A.I.; Wedd, A.G.; Xiao, Z. Reduction Potentials of Protein Disulfides and Catalysis of Glutathionylation and Deglutathionylation by Glutaredoxin Enzymes. *Biochem. J.* **2017**, *474*, 3799–3815. [CrossRef]
49. Zhang, J.; Ye, Z.W.; Chen, W.; Culpepper, J.; Jiang, H.; Ball, L.; Mehrotra, S.; Blumental-Perry, A.; Tew, K.D.; Townsend, D.M. Altered Redox Regulation and S-Glutathionylation of BiP Contribute to Bortezomib Resistance in Multiple Myeloma. *Free Radic. Biol. Med.* **2020**, *160*, 755–767. [CrossRef]
50. Gallogly, M.M.; Mieryl, J.J. Mechanisms of reversible protein glutathionylation in redox signaling and oxidative stress. *Curr. Opin. Pharmacol.* **2007**, *7*, 381–391. [CrossRef]
51. Muronetz, V.I.; Melnikova, A.K.; Saso, L.; Schmalhausen, E.V. Influence of oxidative stress on catalytic and non-glycolytic functions of glyceraldehyde-3-phosphate dehydrogenase. *Curr. Med. Chem.* **2020**, *27*, 2040–2058. [CrossRef]

52. Chalker, J.; Gardiner, D.; Kuksal, N.; Mailloux, R.J. Characterization of the impact of glutaredoxin-2 (GRX2) deficiency on superoxide/hydrogen peroxide release from cardiac and liver mitochondria. *Redox Biol.* **2018**, *15*, 216–227. [CrossRef] [PubMed]
53. Menon, D.; Board, P.G. A role for glutathione transferase Omega 1 (GSTO1-1) in the glutathionylation cycle. *J. Biol. Chem.* **2013**, *288*, 25769–25779. [CrossRef] [PubMed]
54. Board, P.G.; Menon, D. Structure, function and disease relevance of Omega-class glutathione transferases. *Arch. Toxicol.* **2016**, *90*, 1049–1067. [CrossRef] [PubMed]
55. Hughes, M.M.; Hooftman, A.; Angiari, S.; Tummala, P.; Zaslona, Z.; Runtsch, M.C.; McGettrick, A.F.; Sutton, C.E.; Diskin, C.; Rooke, M.; et al. Glutathione Transferase Omega-1 Regulates NLRP3 Inflammasome Activation through NEK7 Deglutathionylation. *Cell Rep.* **2019**, *29*, 151–161. [CrossRef]
56. Park, J.W.; Mieyal, J.J.; Rhee, S.G.; Chock, P.B. Deglutathionylation of 2-Cys peroxiredoxin is specifically catalyzed by sulfiredoxin. *J. Biol. Chem.* **2009**, *284*, 23364–23374. [CrossRef]
57. Calderón, A.; Lázaro-Payo, A.; Iglesias-Baena, I.; Camejo, D.; Lázaro, J.J.; Sevilla, F.; Jiménez, A. Glutathionylation of Pea Chloroplast 2-Cys Prx and Mitochondrial Prx IIF Affects Their Structure and Peroxidase Activity and Sulfiredoxin Deglutathionylates Only the 2-Cys Prx. *Front. Plant Sci.* **2017**, *8*, 118. [CrossRef]
58. Findlay, V.J.; Townsend, D.M.; Morris, T.E.; Fraser, J.P.; He, L.; Tew, K.D. A novel role for human sulfiredoxin in the reversal of glutathionylation. *Cancer Res.* **2006**, *66*, 6800–6806. [CrossRef]
59. Bedhomme, M.; Adamo, M.; Marchand, C.H.; Couturier, J.; Rouhier, N.; Lemaire, S.D.; Zaffagnini, M.; Trost, P. Glutathionylation of cytosolic glyceraldehyde-3-phosphate dehydrogenase from the model plant *Arabidopsis thaliana* is reversed by both glutaredoxins and thioredoxins in vitro. *Biochem. J.* **2012**, *445*, 337–347. [CrossRef]
60. Hanschmann, E.M.; Lonn, M.E.; Schutte, L.D.; Funke, M.; Godoy, J.R.; Eitner, S.; Hudemann, C.; Lillig, C.H. Both thioredoxin 2 and glutaredoxin 2 contribute to the reduction of the mitochondrial 2-Cys peroxiredoxin Prx3. *J. Biol. Chem.* **2010**, *285*, 40699–40705. [CrossRef]
61. Silva, G.M.; Netto, L.E.; Discola, K.F.; Piassa-Filho, G.M.; Pimenta, D.C.; Barcena, J.A.; Demasi, M. Role of glutaredoxin 2 and cytosolic thioredoxins in cysteinyl-based redox modification of the 20S proteasome. *FEBS J.* **2008**, *275*, 2942–2955. [CrossRef]
62. Subramani, J.; Kundumani-Sridharan, V.; Hilgers, R.H.; Owens, C.; Das, K.C. Thioredoxin Uses a GSH-independent Route to Deglutathionylate Endothelial Nitric-oxide Synthase and Protect against Myocardial Infarction. *J. Biol. Chem.* **2016**, *291*, 23374–23389. [CrossRef] [PubMed]
63. Peltoniemi, M.J.; Karala, A.R.; Jurvansuu, J.K.; Kinnula, V.L.; Ruddock, L.W. Insights into deglutathionylation reactions. Different intermediates in the glutaredoxin and protein disulfide isomerase catalyzed reactions are defined by the gamma-linkage present in glutathione. *J. Biol. Chem.* **2006**, *281*, 33107–33114. [CrossRef] [PubMed]
64. Xie, Y.; Dahlin, J.L.; Oakley, A.J.; Casarotto, M.G.; Board, P.G.; Baell, J.B. Reviewing Hit Discovery Literature for Difficult Targets: Glutathione Transferase Omega-1 as an Example. *J. Med. Chem.* **2018**, *61*, 7448–7470. [CrossRef] [PubMed]
65. Lu, J.; Holmgren, A. The thioredoxin antioxidant system. *Free Radic. Biol. Med.* **2014**, *66*, 75–87. [CrossRef] [PubMed]
66. Rossi-George, A.; Gow, A. Nitric Oxide Biochemistry: Pathophysiology of Nitric Oxide-Mediated Protein Modifications. In *Oxidative Neural Injury. Contemporary Clinical Neuroscience*; Veasey, S.C., Ed.; Humana Press: Totowa, NJ, USA, 2009; pp. 29–44. [CrossRef]
67. Bhatia, V.; Elnagary, L.; Dakshinamurti, S. Tracing the path of inhaled nitric oxide: Biological consequences of protein nitrosylation. *Pediatr. Pulmonol.* **2020**. [CrossRef]
68. Stuehr, D.J.; Haque, M.M. Nitric oxide synthase enzymology in the 20 years after the Nobel Prize. *Br. J. Pharmacol.* **2019**, *176*, 177–188. [CrossRef]
69. Anavi, S.; Tirosh, O. iNOS as a metabolic enzyme under stress conditions. *Free Radic. Biol. Med.* **2020**, *146*, 16–35. [CrossRef]
70. Akanji, M.A.; Adeyanju, A.A.; Rotimi, D.; Adeyemi, O.S. Nitric oxide balance in health and diseases: Implications for new treatment strategies. *Open Biochem. J.* **2020**, *14*, 25–32. [CrossRef]
71. Förstermann, U.; Sessa, W.C. Nitric oxide synthases: Regulation and function. *Eur. Heart J.* **2012**, *33*, 829–837. [CrossRef]
72. Sakamuri, S.S.V.P.; Sperling, J.A.; Evans, W.R.; Dholakia, M.H.; Albuck, A.L.; Sure, V.N.; Satou, R.; Mostany, R.; Katakam, P.V.G. Nitric Oxide Synthase Inhibitors Negatively Regulate Respiration in Isolated Rodent Cardiac and Brain Mitochondria. *Am. J. Physiol. Heart Circ. Physiol.* **2020**, *318*, H295–H300. [CrossRef]
73. Gerdes, H.J.; Yang, M.; Heisner, J.S.; Camara, A.K.S.; Stowe, D.F. Modulation of peroxynitrite produced via mitochondrial nitric oxide synthesis during Ca²⁺ and succinate-induced oxidative stress in cardiac isolated mitochondria. *Biochim. Biophys. Acta Bioenerget.* **2020**, *1861*, 148290. [CrossRef] [PubMed]
74. Chen, C.A.; Wang, T.Y.; Varadharaj, S.; Reyes, L.A.; Hemann, C.; Talukder, M.A.; Chen, Y.R.; Druhan, L.J.; Zweier, J.L. S-glutathionylation uncouples eNOS and regulates its cellular and vascular function. *Nature* **2010**, *468*, 1115–1118. [CrossRef] [PubMed]
75. Chen, C.A.; De Pascali, F.; Basye, A.; Hemann, C.; Zweier, J.L. Redox modulation of endothelial nitric oxide synthase by glutaredoxin-1 through reversible oxidative post-translational modification. *Biochemistry* **2013**, *52*, 6712–6723. [CrossRef] [PubMed]
76. Martínez-Ruiz, A.; Araújo, I.M.; Izquierdo-Álvarez, A.; Hernansanz-Agustín, P.; Lamas, S.; Serrador, J. Specificity in S-nitrosylation: A short-range mechanism for NO signaling? *Antioxid. Redox Signal.* **2013**, *19*, 1220–1235. [CrossRef] [PubMed]

77. Reina-Torres, E.; de Ieso, M.; Pasquale, L.R.; Overby, D.R.; Stamer, W.D. The vital role for nitric oxide in intraocular pressure homeostasis. *Prog. Retin. Eye Res.* **2020**, 100922. [CrossRef] [PubMed]
78. López-Sánchez, L.M.; Aranda, E.; Rodríguez-Ariza, A. Nitric oxide and tumor metabolic reprogramming. *Biochem. Pharmacol.* **2020**, *176*, 113769. [CrossRef] [PubMed]
79. Fernando, V.; Zheng, X.; Walia, Y.; Sharma, V.; Letson, J.; Furuta, S. S-Nitrosylation: An Emerging Paradigm of Redox Signaling. *Antioxidants* **2019**, *8*, 404. [CrossRef]
80. Nakamura, T.; Lipton, S.A. Emerging role of protein-protein transnitrosylation in cell signaling pathways. *Antioxid. Redox Signal.* **2013**, *18*, 239–249. [CrossRef]
81. Umanah, G.K.E.; Ghasemi, M.; Yin, X.; Chang, M.; Kim, J.W.; Zhang, J.; Ma, E.; Scarffe, L.A.; Lee, Y.-I.; Chen, R.; et al. AMPA Receptor Surface Expression Is Regulated by S-Nitrosylation of Thorase and Transnitrosylation of NSF. *Cell Rep.* **2020**, *33*, 108329. [CrossRef]
82. Anand, P.; Stamler, J. Enzymatic mechanisms regulating protein S-nitrosylation: Implications in health and disease. *J. Mol. Med.* **2012**, *90*, 233–244. [CrossRef]
83. Broniowska, K.A.; Hogg, N. The chemical biology of S-nitrosothiols. *Antioxid. Redox Signal.* **2012**, *17*, 969–980. [CrossRef] [PubMed]
84. Basu, S.; Keszler, A.; Azarova, N.A.; Nwanze, N.; Perlegas, A.; Shiva, S.; Broniowska, K.A.; Hogg, N.; Kim-Shapiro, D.B. A novel role for cytochrome c: Efficient catalysis of S-nitrosothiol formation. *Free Radic. Biol. Med.* **2010**, *48*, 255–263. [CrossRef] [PubMed]
85. Inoue, K.; Akaike, T.; Miyamoto, Y.; Okamoto, T.; Sawa, T.; Otagiri, M.; Suzuki, S.; Yoshimura, T.; Maeda, H. Nitrosothiol formation catalyzed by ceruloplasmin. Implication for cytoprotective mechanism in vivo. *J. Biol. Chem.* **1999**, *274*, 27069–27075. [CrossRef] [PubMed]
86. Mani, K.; Cheng, F.; Havsmark, B.; David, S.; Fransson, L.A. Involvement of glycosylphosphatidylinositol-linked ceruloplasmin in the copper/zinc-nitric oxide-dependent degradation of glypican-1 heparan sulfate in rat C6 glioma cells. *J. Biol. Chem.* **2004**, *279*, 12918–12923. [CrossRef] [PubMed]
87. Pawloski, J.R.; Hess, D.T.; Stamler, J.S. Export by red blood cells of nitric oxide bioactivity. *Nature* **2001**, *409*, 622–626. [CrossRef] [PubMed]
88. Kornberg, M.D.; Sen, N.; Hara, M.R.; Juluri, K.R.; Nguyen, J.V.; Snowman, A.M.; Law, L.; Hester, L.D.; Snyder, S.H. GAPDH mediates nitrosylation of nuclear proteins. *Nat. Cell Biol.* **2010**, *12*, 1094–1100. [CrossRef]
89. Kohr, M.J.; Murphy, E.; Steenbergen, C. Glyceraldehyde-3-phosphate dehydrogenase acts as a mitochondrial trans-S-nitrosylase in the heart. *PLoS ONE* **2014**, *9*, e111448. [CrossRef] [PubMed]
90. Mitchell, D.A.; Marletta, M.A. Thioredoxin catalyzes the S-nitrosation of the caspase-3 active site cysteine. *Nat. Chem. Biol.* **2005**, *1*, 154–158. [CrossRef]
91. Wu, C.; Liu, T.; Chen, W.; Oka, S.; Fu, C.X.; Jain, M.R.; Parrott, A.M.; Baykal, A.T.; Sadoshima, J.; Li, H. Redox Regulatory Mechanism of Transnitrosylation by Thioredoxin. *Mol. Cell. Proteom.* **2010**, *9*, 2262–2275. [CrossRef]
92. Nakamura, T.; Wang, L.; Wong, C.C.L.; Scott, F.L.; Eckelman, B.P.; Han, X.M.; Tzitzilonis, C.; Meng, F.J.; Gu, Z.Z.; Holland, E.A.; et al. Transnitrosylation of XIAP Regulates Caspase-Dependent Neuronal Cell Death. *Mol. Cell* **2010**, *39*, 184–195. [CrossRef]
93. Benhar, M.; Forrester, M.T.; Hess, D.T.; Stamler, J.S. Regulated protein denitrosylation by cytosolic and mitochondrial thioredoxins. *Science* **2008**, *320*, 1050–1054. [CrossRef] [PubMed]
94. Qu, J.; Nakamura, T.; Cao, G.; Holland, E.A.; McKercher, S.R.; Lipton, S.A. S-Nitrosylation activates Cdk5 and contributes to synaptic spine loss induced by beta-amyloid peptide. *Proc. Natl. Acad. Sci. USA* **2011**, *108*, 14330–14335. [CrossRef] [PubMed]
95. Choi, M.S.; Nakamura, T.; Cho, S.J.; Han, X.M.; Holland, E.A.; Qu, J.; Petsko, G.A.; Yates, J.R.; Liddington, R.C.; Lipton, S.A. Transnitrosylation from DJ-1 to PTEN attenuates neuronal cell death in parkinson's disease models. *J. Neurosci.* **2014**, *34*, 15123–15131. [CrossRef] [PubMed]
96. Pawloski, J.R.; Hess, D.T.; Stamler, J.S. Impaired vasodilation by red blood cells in sickle cell disease. *Proc. Natl. Acad. Sci. USA* **2005**, *102*, 2531–2536. [CrossRef]
97. Hara, M.R.; Agrawal, N.; Kim, S.F.; Cascio, M.B.; Fujimuro, M.; Ozeki, Y.; Takahashi, M.; Cheah, J.H.; Tankou, S.K.; Hester, L.D.; et al. S-nitrosylated GAPDH initiates apoptotic cell death by nuclear translocation following Siah1 binding. *Nat. Cell Biol.* **2005**, *7*, 665–674. [CrossRef]
98. Nakajima, H.; Itakura, M.; Kubo, T.; Kaneshige, A.; Harada, N.; Izawa, T.; Azuma, Y.T.; Kuwamura, M.; Yamaji, R.; Takeuchi, T. Glyceraldehyde-3-phosphate Dehydrogenase (GAPDH) Aggregation Causes Mitochondrial Dysfunction during Oxidative Stress-induced Cell Death. *J. Biol. Chem.* **2017**, *292*, 4727–4742. [CrossRef]
99. Tossounian, M.A.; Zhang, B.; Gout, I. The Writers, Readers, and Erasers in Redox Regulation of GAPDH. *Antioxidants* **2020**, *9*, 1288. [CrossRef]
100. Barone, E.; Trombino, S.; Cassano, R.; Sgambato, A.; De Paola, B.; Di Stasio, E.; Picci, N.; Preziosi, P.; Mancuso, C. Characterization of the S-denitrosylating activity of bilirubin. *J. Cell. Mol. Med.* **2009**, *13*, 2365–2375. [CrossRef]
101. Stamler, J.S.; Toone, E.J. The decomposition of thionitrites. *Curr. Opin. Chem. Biol.* **2002**, *6*, 779–785. [CrossRef]
102. Paige, J.S.; Xu, G.; Stancevic, B.; Jaffrey, S.R. Nitrosothiol reactivity profiling identifies S-nitrosylated proteins with unexpected stability. *Chem. Biol.* **2008**, *15*, 1307–1316. [CrossRef]
103. Ren, X.; Sengupta, R.; Lu, J.; Lundberg, J.O.; Holmgren, A. Characterization of mammalian glutaredoxin isoforms as S-denitrosylases. *FEBS Lett.* **2019**, *593*, 1799–1806. [CrossRef] [PubMed]

104. Stomberski, C.T.; Hess, D.T.; Stamler, J.S. Protein S-Nitrosylation: Determinants of Specificity and Enzymatic Regulation of S-Nitrosothiol-Based Signaling. *Antioxid. Redox Signal.* **2019**, *30*, 1331–1351. [CrossRef] [PubMed]
105. Benhar, M.; Forrester, M.T.; Stamler, J.S. Protein denitrosylation: Enzymatic mechanisms and cellular functions. *Nat. Rev. Mol. Cell Biol.* **2009**, *10*, 721–732. [CrossRef] [PubMed]
106. Barnett, S.D.; Buxton, I.L.O. The role of S-nitrosoglutathione reductase (GSNOR) in human disease and therapy. *Crit. Rev. Biochem. Mol. Biol.* **2017**, *52*, 340–354. [CrossRef] [PubMed]
107. Rizza, S.; Filomeni, G. Chronicles of a reductase: Biochemistry, genetics and physio-pathological role of GSNOR. *Free Radic. Biol. Med.* **2017**, *110*, 19–30. [CrossRef]
108. Liu, L.; Yan, Y.; Zeng, M.; Zhang, J.; Hanes, M.A.; Ahearn, G.; McMahon, T.J.; Dickfeld, T.; Marshall, H.E.; Que, L.G.; et al. Essential roles of S-nitrosothiols in vascular homeostasis and endotoxic shock. *Cell* **2004**, *116*, 617–628. [CrossRef]
109. Fernandez, M.R.; Biosca, J.A.; Pares, X. S-nitrosoglutathione reductase activity of human and yeast glutathione-dependent formaldehyde dehydrogenase and its nuclear and cytoplasmic localisation. *Cell. Mol. Life Sci.* **2003**, *60*, 1013–1018. [CrossRef]
110. Whalen, E.J.; Foster, M.W.; Matsumoto, A.; Ozawa, K.; Violin, J.D.; Que, L.G.; Nelson, C.D.; Benhar, M.; Keys, J.R.; Rockman, H.A.; et al. Regulation of beta-adrenergic receptor signaling by S-nitrosylation of G-protein-coupled receptor kinase 2. *Cell* **2007**, *129*, 511–522. [CrossRef]
111. Ozawa, K.; Whalen, E.J.; Nelson, C.D.; Mu, Y.; Hess, D.T.; Lefkowitz, R.J.; Stamler, J.S. S-nitrosylation of beta-arrestin regulates beta-adrenergic receptor trafficking. *Mol. Cell* **2008**, *31*, 395–405. [CrossRef]
112. Lima, B.; Lam, G.K.W.; Xie, L.; Diesen, D.L.; Villamizar, N.; Nienaber, J.; Messina, E.; Bowles, D.; Kontos, C.D.; Hare, J.M.; et al. Endogenous S-nitrosothiols protect against myocardial injury. *Proc. Natl. Acad. Sci. USA* **2009**, *106*, 6297–6302. [CrossRef]
113. Marozkina, N.V.; Wei, C.; Yemen, S.; Wallrabe, H.; Nagji, A.S.; Liu, L.; Morozkina, T.; Jones, D.R.; Gaston, B. S-nitrosoglutathione reductase in human lung cancer. *Am. J. Respir. Cell Mol. Biol.* **2012**, *46*, 63–70. [CrossRef] [PubMed]
114. Moon, Y.; Cao, Y.; Zhu, J.J.; Xu, Y.Y.; Balkan, W.; Buys, E.S.; Diaz, F.; Kerrick, W.G.; Hare, J.M.; Percival, J.M. GSNOR Deficiency Enhances In Situ Skeletal Muscle Strength, Fatigue Resistance, and RyR1 S-Nitrosylation Without Impacting Mitochondrial Content and Activity. *Antioxid. Redox Signal.* **2017**, *26*, 165–181. [CrossRef] [PubMed]
115. Straub, A.C.; Billaud, M.; Johnstone, S.R.; Best, A.K.; Yemen, S.; Dwyer, S.T.; Looft-Wilson, R.; Lysiak, J.J.; Gaston, B.; Palmer, L.; et al. Compartmentalized connexin 43 s-nitrosylation/denitrosylation regulates heterocellular communication in the vessel wall. *Arterioscler. Thromb. Vasc. Biol.* **2011**, *31*, 399–407. [CrossRef] [PubMed]
116. Wei, W.; Li, B.; Hanes, M.A.; Kakar, S.; Chen, X.; Liu, L. S-nitrosylation from GSNOR deficiency impairs DNA repair and promotes hepatocarcinogenesis. *Sci. Transl. Med.* **2010**, *2*, 19ra13. [CrossRef] [PubMed]
117. Rizza, S.; Cardaci, S.; Montagna, C.; Di Giacomo, G.; De Zio, D.; Bordi, M.; Maiani, E.; Campello, S.; Borreca, A.; Puca, A.A.; et al. S-nitrosylation drives cell senescence and aging in mammals by controlling mitochondrial dynamics and mitophagy. *Proc. Natl. Acad. Sci. USA* **2018**, *115*, E3388–E3397. [CrossRef] [PubMed]
118. Rizza, S.; Di Leo, L.; Mandatori, S.; De Zio, D.; Filomeni, G. Mitophagy contributes to alpha-tocopheryl succinate toxicity in GSNOR-deficient hepatocellular carcinoma. *Biochem. Pharmacol.* **2020**, *176*, 113885. [CrossRef]
119. Benhar, M. Nitric oxide and the thioredoxin system: A complex interplay in redox regulation. *Biochim. Biophys. Acta* **2015**, *1850*, 2476–2484. [CrossRef]
120. Mannick, J.B.; Hausladen, A.; Liu, L.; Hess, D.T.; Zeng, M.; Miao, Q.X.; Kane, L.S.; Gow, A.J.; Stamler, J.S. Fas-induced caspase denitrosylation. *Science* **1999**, *284*, 651–654. [CrossRef]
121. Ito, T.; Yamakuchi, M.; Lowenstein, C.J. Thioredoxin increases exocytosis by denitrosylating N-ethylmaleimide-sensitive factor. *J. Biol. Chem.* **2011**, *286*, 11179–11184. [CrossRef]
122. Ovadia, H.; Haim, Y.; Nov, O.; Almog, O.; Kovsan, J.; Bashan, N.; Benhar, M.; Rudich, A. Increased adipocyte S-nitrosylation targets anti-lipolytic action of insulin: Relevance to adipose tissue dysfunction in obesity. *J. Biol. Chem.* **2011**, *286*, 30433–30443. [CrossRef]
123. Thom, S.R.; Bhopale, V.M.; Milovanova, T.N.; Yang, M.; Bogush, M. Thioredoxin reductase linked to cytoskeleton by focal adhesion kinase reverses actin S-nitrosylation and restores neutrophil beta (2) integrin function. *J. Biol. Chem.* **2012**, *287*, 30346–30357. [CrossRef] [PubMed]
124. Kelleher, Z.T.; Sha, Y.; Foster, M.W.; Foster, W.M.; Forrester, M.T.; Marshall, H.E. Thioredoxin-mediated denitrosylation regulates cytokine-induced nuclear factor κ B (NF- κ B) activation. *J. Biol. Chem.* **2014**, *289*, 3066–3072. [CrossRef] [PubMed]
125. Qu, Z.W.; Miao, W.Y.; Hu, S.Q.; Li, C.; Zhuo, X.L.; Zong, Y.Y.; Wu, Y.P.; Zhang, G.Y. N-Methyl-D-Aspartate Receptor-Dependent Denitrosylation of Neuronal Nitric Oxide Synthase Increase the Enzyme Activity. *PLoS ONE* **2012**, *7*, e52788. [CrossRef] [PubMed]
126. Ben-Lulu, S.; Ziv, T.; Admon, A.; Weisman-Shomer, P.; Benhar, M. A substrate trapping approach identifies proteins regulated by reversible S-nitrosylation. *Mol. Cell. Proteom.* **2014**, *13*, 2573–2583. [CrossRef] [PubMed]
127. González, R.; Rodríguez-Hernández, M.A.; Negrete, M.; Rangelova, K.; Rossin, A.; Choya-Foces, C.; Cruz-Ojeda, P.; Miranda-Vizuet, A.; Martínez-Ruiz, A.; Rius-Pérez, S.; et al. Downregulation of thioredoxin-1-dependent CD95 S-nitrosation by Sorafenib reduces liver cancer. *Redox Biol.* **2020**, *34*, 101528. [CrossRef]
128. Zai, A.; Rudd, M.A.; Scribner, A.W.; Loscalzo, J. Cell-surface protein disulfide isomerase catalyzes transnitrosation and regulates intracellular transfer of nitric oxide. *J. Clin. Investig.* **1999**, *103*, 393–399. [CrossRef]
129. Sliskovic, I.; Raturi, A.; Mutus, B. Characterization of the S-denitrosation activity of protein disulfide isomerase. *J. Biol. Chem.* **2005**, *280*, 8733–8741. [CrossRef]

130. Zhang, L.M.; St Croix, C.; Cao, R.; Wasserloos, K.; Watkins, S.C.; Stevens, T.; Li, S.; Tyurin, V.; Kagan, V.E.; Pitt, B.R. Cell-surface protein disulfide isomerase is required for transnitrosation of metallothionein by S-nitroso-albumin in intact rat pulmonary vascular endothelial cells. *Exp. Biol. Med.* **2006**, *231*, 1507–1515. [CrossRef]
131. Hou, Y.; Guo, Z.; Li, J.; Wang, P.G. Seleno compounds and glutathione peroxidase catalyzed decomposition of S-nitrosothiols. *Biochem. Biophys. Res. Commun.* **1996**, *228*, 88–93. [CrossRef]
132. Jahnová, J.; Luhová, L.; Petřivalský, M. S-Nitrosogluthathione Reductase-The Master Regulator of Protein S-Nitrosation in Plant NO Signaling. *Plants* **2019**, *8*, 48. [CrossRef]
133. Staab, C.A.; Ålander, J.; Brandt, M.; Lengqvist, J.; Morgenstern, R.; Grafström, R.C.; Höög, J.O. Reduction of S-nitrosogluthathione by alcohol dehydrogenase 3 is facilitated by substrate alcohols via direct cofactor recycling and leads to GSH-controlled formation of glutathione transferase inhibitors. *Biochem. J.* **2008**, *413*, 493–504. [CrossRef] [PubMed]
134. Benhar, M.; Thompson, J.W.; Moseley, M.A.; Stamler, J.S. Identification of S-nitrosylated targets of thioredoxin using a quantitative proteomic approach. *Biochemistry* **2010**, *49*, 6963–6969. [CrossRef] [PubMed]
135. Hao, L.; Dong, L.; Yu, Q.; Shen, W.; Wei, X. Edaravone inhibits procaspase-3 denitrosylation and activation through FasL-Trx2 pathway in KA-induced seizure. *Fundam. Clin. Pharm.* **2020**, *34*, 662–670. [CrossRef] [PubMed]
136. Pader, I.; Sengupta, R.; Cebula, M.; Xu, J.; Lundberg, J.O.; Holmgren, A.; Johansson, K.; Arnér, E.S. Thioredoxin-related protein of 14 kDa is an efficient L-cystine reductase and S-denitrosylase. *Proc. Natl. Acad. Sci. USA* **2014**, *111*, 6964–6969. [CrossRef] [PubMed]
137. Broniowska, K.A.; Diers, A.R.; Hogg, N. S-nitrosogluthathione. *Biochim. Biophys. Acta* **2013**, *1830*, 3173–3181. [CrossRef]
138. Kolesnik, B.; Palten, K.; Schrammel, A.; Stessel, H.; Schmidt, K.; Mayer, B.; Gorren, A.C. Efficient nitrosation of glutathione by nitric oxide. *Free Radic. Biol. Med.* **2013**, *63*, 51–64. [CrossRef]
139. Gow, A.J.; Buerk, D.G.; Ischiropoulos, H. A novel reaction mechanism for the formation of S-nitrosothiol in vivo. *J. Biol. Chem.* **1997**, *272*, 2841–2845. [CrossRef]
140. Furuhashi, S.; Sugita, H.; Takamori, H.; Horino, K.; Nakahara, O.; Okabe, H.; Miyake, K.; Tanaka, H.; Beppu, T.; Baba, H. NO donor and MEK inhibitor synergistically inhibit proliferation and invasion of cancer cells. *Int. J. Oncol.* **2012**, *40*, 807–815. [CrossRef]
141. Aranda-Caño, L.; Sánchez-Calvo, B.; Begara-Morales, J.C.; Chaki, M.; Mata-Pérez, C.; Padilla, M.N.; Valderrama, R.; Barroso, J.B. Post-translational modification of proteins mediated by nitro-fatty acids in plants: Nitroalkylation. *Plants* **2019**, *8*, 82. [CrossRef]
142. Mata-Pérez, C.; Sánchez-Calvo, B.; Begara-Morales, J.C.; Carreras, A.; Padilla, M.N.; Melguizo, M.; Valderrama, R.; Corpas, F.J.; Barroso, J.B. Nitro-linolenic acid is a nitric oxide donor. *Nitric Oxide* **2016**, *57*, 57–63. [CrossRef]
143. Buchan, G.J.; Bonacci, G.; Fazzari, M.; Salvatore, S.R.; Gelhaus Wendell, S. Nitro-fatty acid formation and metabolism. *Nitric Oxide* **2018**, *79*, 38–44. [CrossRef] [PubMed]
144. Mollenhauer, M.; Mehrkens, D.; Klinke, A.; Lange, M.; Remane, L.; Friedrichs, K.; Braumann, S.; Geißen, S.; Simsekylmaz, S.; Nettersheim, F.S.; et al. Nitro-fatty acids suppress ischemic ventricular arrhythmias by preserving calcium homeostasis. *Sci. Rep.* **2020**, *10*, 15319. [CrossRef] [PubMed]
145. Mata-Pérez, C.; Padilla, M.N.; Sánchez-Calvo, B.; Begara-Morales, J.C.; Valderrama, R.; Chaki, M.; Aranda-Caño, L.; Moreno-González, D.; Molina-Díaz, A.; Barroso, J.B. Endogenous Biosynthesis of S-Nitrosogluthathione From Nitro-Fatty Acids in Plants. *Front. Plant Sci.* **2020**, *11*, 962. [CrossRef] [PubMed]
146. Romero, J.M.; Bizzozero, O.A. Intracellular glutathione mediates the denitrosylation of protein nitrosothiols in the rat spinal cord. *J. Neurosci. Res.* **2009**, *87*, 701–709. [CrossRef] [PubMed]
147. Giustarini, D.; Milzani, A.; Aldini, G.; Carini, M.; Rossi, R.; Dalle-Donne, I. S-nitrosation versus S-glutathionylation of protein sulfhydryl groups by S-nitrosogluthathione. *Antioxid. Redox Signal.* **2005**, *7*, 930–939. [CrossRef]
148. Konorev, E.A.; Kalyansman, B.; Hogg, N. Modification of creatine kinase by S-nitrosothiols: S-nitrosylation vs S-thiolation. *Free Rad. Biol. Med.* **2000**, *28*, 1671–1678. [CrossRef]
149. Kaliyaperumal, K.; Sharma, A.K.; McDonald, D.G.; Dhindsa, J.S.; Yount, C.; Singh, A.K.; Won, J.S.; Singh, I. S-nitrosogluthathione-mediated STAT3 regulation in efficacy of radiotherapy and cisplatin therapy in head and neck squamous cell carcinoma. *Redox Biol.* **2015**, *6*, 41–50. [CrossRef]
150. Zhang, Y.; Sun, C.; Xiao, G.; Shan, H.; Tang, L.; Yi, Y.; Yu, W.; Gu, Y. S-nitrosylation of the Peroxiredoxin-2 promotes S-nitrosogluthathione-mediated lung cancer cells apoptosis via AMPK-SIRT1 pathway. *Cell Death Dis.* **2019**, *10*, 329. [CrossRef]
151. Townsend, D.M.; Findlay, V.J.; Fazilev, F.; Ogle, M.; Fraser, J.; Saavedra, J.E.; Ji, X.; Keefer, L.K.; Tew, K.D. A glutathione S-transferase pi-activated prodrug causes kinase activation concurrent with S-glutathionylation of proteins. *Mol. Pharmacol.* **2006**, *69*, 501–508. [CrossRef]
152. Townsend, D.M.; Manevich, Y.; He, L.; Xiong, Y.; Bowers, R.R., Jr.; Hutchens, S.; Tew, K.D. Nitrosative stress-induced S-glutathionylation of protein disulfide isomerase leads to activation of the unfolded protein response. *Cancer Res.* **2009**, *69*, 7626–7634. [CrossRef]
153. Wolhuter, K.; Whitwell, H.J.; Switzer, C.H.; Burgoyne, J.R.; Timms, J.F.; Eaton, P. Evidence against Stable Protein S-Nitrosylation as a Widespread Mechanism of Post-translational Regulation. *Mol. Cell* **2018**, *69*, 438–450. [CrossRef] [PubMed]

Review

Role of GSH and Iron-Sulfur Glutaredoxins in Iron Metabolism—Review

Trnka Daniel ^{1,†}, Hossain Md Faruq ^{1,†}, Jordt Laura Magdalena ¹, Gellert Manuela ¹ and Lillig Christopher Horst ^{2,*}

¹ Institute for Medical Biochemistry and Molecular Biology, University Medicine, University of Greifswald, 17475 Greifswald, Germany; danieltrnka@gmx.de (T.D.); mohammed.hossain@uni-greifswald.de (H.M.F.); L.Jordt@gmx.de (J.L.M.); manuela@gellert.org (G.M.)

² Christopher Horst Lillig, Institute for Medical Biochemistry and Molecular Biology, University Medicine Greifswald, Ferdinand-Sauerbruch-Straße, 17475 Greifswald, Germany

* Correspondence: horst@lillig.de; Tel.: +49-3834-865407; Fax: +49-3834-865402

† These authors contributed equally to this work.

Academic Editor: Pál Perjési

Received: 29 July 2020; Accepted: 22 August 2020; Published: 25 August 2020

Abstract: Glutathione (GSH) was initially identified and characterized for its redox properties and later for its contributions to detoxification reactions. Over the past decade, however, the essential contributions of glutathione to cellular iron metabolism have come more and more into focus. GSH is indispensable in mitochondrial iron-sulfur (FeS) cluster biosynthesis, primarily by co-ligating FeS clusters as a cofactor of the CGFS-type (class II) glutaredoxins (Grxs). GSH is required for the export of the yet to be defined FeS precursor from the mitochondria to the cytosol. In the cytosol, it is an essential cofactor, again of the multi-domain CGFS-type Grxs, master players in cellular iron and FeS trafficking. In this review, we summarize the recent advances and progress in this field. The most urgent open questions are discussed, such as the role of GSH in the export of FeS precursors from mitochondria, the physiological roles of the CGFS-type Grx interactions with Bola-like proteins and the cluster transfer between Grxs and recipient proteins.

Keywords: glutathione; glutaredoxin; iron-sulfur cluster; iron

1. Introduction

Glutathione, the γ -L-glutamyl-L-cysteinyl-glycine tri-peptide, is a ubiquitous nucleophile required in redox homeostasis, detoxification, and iron homeostasis [1]. Since the reactivity of glutathione (GSH) itself with proteins, small molecules, and xenobiotics is too low to be significant *in vivo*, see for instance, [2], GSH-dependent reactions need to be catalyzed by enzymes. These enzymes include glutaredoxins (Grxs), glutathione peroxidases (GPxs), glutathione reductase (GR), glutathione S-transferases (GSTs), and protein disulfide isomerases (PDIs) [1]. Nevertheless, the functions of GSH depend on the reactivity of its cysteinyl thiol group. Thiols can complex metals, be alkylated to thioethers, but they can also be oxidized to disulfides. In the case of glutathione, two molecules of reduced GSH can be oxidized to form glutathione disulfide (GSSG). Re-reduction is catalyzed by GR at the expense of NADPH. Being present in millimolar concentrations in most organisms, GSH was characterized as the “redox buffer” of the cell. In fact, the loss of GSH-utilizing enzymes may result in disrupted redox homeostasis, as in the case for GPxs [3,4], with effects as dramatic as cell death by a process named ferroptosis induced by the lack of GPx4 activity [5–7]. The loss of glutathione itself, however, firstly results in defects in cellular iron homeostasis [8,9]. The enzymes that catalyze or mediate most glutathione functions in iron metabolism are the iron-sulfur cluster (FeS)-containing Grxs.

In this review, we will address the functions of both GSH and FeS-Grxs in iron metabolism. This topic has been addressed before, see for instance [9–12]. The focus of this review is on mammalian cells, however, we take into account other taxa when discussing ground-breaking and major findings, both to illustrate the high degree of conservation in the systems as well as some unique aspects.

2. Glutathione, Glutaredoxins, and Iron-Metabolism

As early as 1972, Tanaka and coworkers reported that, in vitro, GSH may be able to complex iron, resulting in absorption spectra resembling those of FeS clusters [13]. It took nearly two decades before the essential function of GSH in the synthesis and maturation of FeS cluster proteins in vivo was discovered in yeast. Defects in the biosynthesis of FeS proteins in *Saccharomyces cerevisiae* are associated with a more than two-fold increase of GSH [14]. However, this increase was apparently not caused by concomitant disturbances in redox metabolism. In fact, the depletion of GSH impaired the maturation of FeS proteins substantially, most of all affecting the non-mitochondrial FeS proteins [15].

2.1. Iron-Sulfur Cluster Biogenesis

FeS clusters are essential for life. They participate in the transfer of electrons, are cofactors in enzymatic catalysis, control the stability of biomolecules, and act as regulatory elements [16–18]. Mitochondria are essential for FeS cluster biogenesis. Not only are all the FeS clusters required for energy conversion synthesized here, the maturation of cytosolic FeS clusters also depends on a yet to be defined mitochondrial precursor [19,20]. Mitochondrial FeS cluster biogenesis and the cluster transfer to target apo-proteins have been studied to great detail and reviewed comprehensively before, e.g., in [21–23]. In brief, Fe₂S₂ centers are synthesized from iron and cysteine-derived sulfur by the early iron-sulfur cluster (ISC) synthesis machinery. From there, the Fe₂S₂ centers are likely transferred to the monothiol Grx5 with the aid of a heat shock protein of 70 kDa (Hsp70) chaperone system, the details of which will be discussed below. In the present models, Grx5 acts as a hub, from which the FeS centers are (1) either directly, or with the help of additional “targeting factors”, transferred to Fe₂S₂ target proteins or (2) transferred to a protein complex composed of the assembly factors ISCA1, ISCA2, and IBA57, where they are combined to Fe₄S₄ centers [24]. Only recently, Lill and co-workers succeeded in biochemically reconstituting the assembly of Fe₄S₄ clusters [25]. The process requires the ISC machinery, holo-Grx5, and reduced Fdx2 for the reductive fusion of two Fe₂S₂ clusters into one Fe₄S₄ cluster. These clusters are trafficked by ISC-targeting factors, such as proteins from the BolA family and iron-sulfur cluster scaffold homolog 1 (NFU1) to apo-target proteins such as the mitochondrial aconitase (ACO2). The maturation of the Fe₄S₄ centers in the complex I (NADH-ubiquinone oxidoreductase, NDUF) subunits NDUFS1, NDUFV1, and NDUFS2, 7, and 8 seems to require the P-loop NTPase Ind1 (iron-sulfur protein required for NADH-dehydrogenase) [26]. The molecular mechanisms of cluster insertion and the recipient protein pre-requisites are still unclear.

The insertion of FeS proteins into apo-target proteins requires their cysteinyl sulfur ligands to be in the reduced thiol state. Under normal conditions in yeast mitochondria, this seems to be independent of the major thiol reducing systems, i.e., the GSH/Grx and thioredoxin (Trx) systems [27]. However, for mammalian cells and proteins, a number of conditions have been characterized that lead to the oxidation of such cysteinyl residues, for instance, in complex I subunits NDUFS1 and NDUFV1 in a murine Parkinson’s disease model as a consequence of GSH depletion [28]. In general, GSH appears to be a crucial factor for complex I activity, especially in neurons [29–31].

From groundbreaking work in yeast cells, it was established that cytosolic FeS biogenesis depends on a sulfur compound generated inside mitochondria [32]. This not yet specified sulfur compound (X-S) must be exported as source for cytosolic FeS cluster synthesis. This compound must be transported into the cytosol in an ATP-dependent manner. The ATP-binding cassette (ABC) transporter Atm1 (in human ABCB7), located in the inner mitochondrial membrane, soon came into focus as the prime candidate for this function [32]. Atm1/ABCB7 may also be the link for the necessity of GSH for the maturation of cytosolic FeS proteins. Structural analyses revealed a large cavity in the dimeric Atm1 close to the inner membrane surface that can accommodate GSH [33–35]. In fact, the size of the cavity also allows for the binding of GSH as part of a larger not yet defined substrate transported by Atm1 [34]. Mutations in the binding site of ABCB7 that inhibit binding of a GSH moiety result in decreased functions of cytosolic FeS proteins and mitochondrial iron overload [33,36,37]. The same phenotype is caused by GSH or Atm1 depletion in yeast [15]. Atm1 and the *Arabidopsis thaliana* homolog ATM3 transport GSSG with increased ATPase activity but neither Fe^{2+} nor reduced GSH stimulate the ATPase activity of the transporter [38]. Atm1 also transports GS-S-SG (glutathione trisulfide) [38]. Since substantial data suggest that only a sulfur compound is required as the mitochondrial contribution to cytosolic FeS biogenesis (for a summary, see [34]), such per- or poly-sulfides are compelling candidates as endogenous substrates. More recently, however, intact Fe_2S_2 clusters ligated by four GSH molecules have also been suggested as Atm1 substrate [39]. This is supported by recent kinetic studies that reported the transport of $(\text{GSH})_4\text{Fe}_2\text{S}_2$ by Atm1 with a ~100-fold increased activity in the presence of the cluster [40]. The open questions, in addition to the nature of the transported compound, are the generation of this GSH derivative(s) from the Grx5/GSH-ligated Fe_2S_2 cluster in mitochondria (see below) as well as the link to the cytosolic iron sulfur cluster assembly machinery (CIA). In vitro, the GSH-ligated Fe_2S_2 cluster itself can be used to reconstitute apo-proteins [41].

The biogenesis of cytosolic and nuclear FeS-proteins requires numerous proteins and is facilitated by the CIA, summarized in [42]. Overall, the process can be divided into two steps. First, a Fe_4S_4 cluster is assembled on a scaffold complex. Second, this cluster is transferred and inserted into recipient apo-proteins. Apart from the yet to be determined component X-S that has to be supplied by the mitochondrial FeS synthesis machinery, the cytosolic FeS protein biogenesis requires an iron source and the supply of electrons. The latter are supplied by the NADPH-dependent diflavin oxidoreductase 1 (NDOR1) and the FeS protein anamorsin/CIAPIN1 (see Figure 1) [43–46]. The first step is the assembly of the Fe_4S_4 cluster on the cytosolic FeS scaffold complex (see Figure 1) [47–49]. The heterotetrameric complex consists of two P-loop NTPases, CFD1 (cytosolic FeS cluster-deficient protein 1) and NBP35 (nucleotide-binding protein 35). The complex binds two Fe_4S_4 clusters, one at the N-terminus of NBP35 and the second one is transiently ligated between CFD1 and NBP35 [50]. The nature and source of the iron for the formation of this first cytosolic FeS cluster is still unclear. Multi-domain Grxs like yeast or mammalian Grx3 may be potential candidates. They do play a general role in iron trafficking through the cytoplasm in a GSH-dependent manner [51,52] (details below). Potentially, they function in concert with a BOLA family protein [10,53–56]. In the second step, the primarily assembled cluster is transferred and inserted into target proteins. This is facilitated by IOP1 (iron-only hydrogenase-like protein) and the CIA-targeting complex [57]. IOP1 may act as a CIA adapter protein, mediating the contact between early and late parts of the CIA machinery, although the exact mechanism is still under discussion (see Figure 1) [47,58,59]. Probably, cytosolic iron-sulfur protein assembly protein 1 (CIA1), CIA2b, and MMS19 (MMS19 nucleotide excision repair protein homolog) build variable hetero-complexes, called the CIA-targeting complexes, that directly interact with specific cytosolic and nuclear apo-FeS proteins (see Figure 1) [58,60].

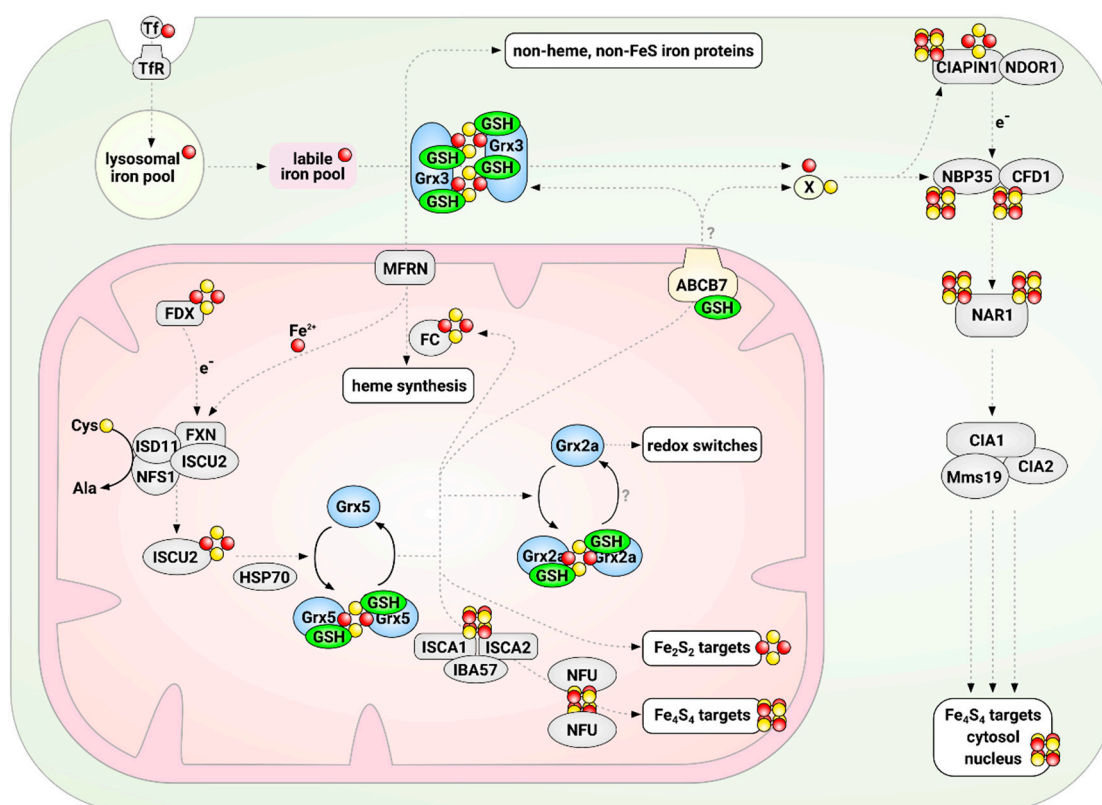


Figure 1. Glutathione and glutaredoxins in iron-sulfur cluster synthesis and maturation in mammalian cells. The initial synthesis of Fe_2S_2 clusters is catalyzed by the mitochondrial iron-sulfur cluster synthesis machinery on the scaffold protein ISCU2. From there, clusters are distributed in a process that depends on the CGFS-type Grx5 to Fe_2S_2 and Fe_4S_4 target proteins, e.g., in the mitochondrial electron chain. In addition, a yet to be uncovered compound “X” is exported in a glutathione (GSH)-dependent manner to the cytosol, where it serves as substrate for the cytosolic iron-sulfur cluster assembly machinery. The multi-domain CGFS-type Grx3 is in some way required for the distribution of iron from the so-called labile iron pool to most, if not all, cellular iron-dependent processes. Glutaredoxins are depicted in light blue, GSH in green, iron in red, and sulfur in yellow.

2.2. Glutaredoxins

Grxs form a branch of the Trx family, for an overview see [61]. Bacterial Grxs represent the most basic representation of the Trx-fold, consisting of a four-stranded central β -sheet surrounded by three α -helices, and Grxs of higher organisms frequently display additional N- and C-terminal helices (Figure 2). In 1976, the first Grx was defined as a GSH-dependent electron donor for ribonucleotide reductase (RNR) and thus DNA synthesis [62]. In the following years, Grxs were comprehensively characterized as oxidoreductases that catalyze the formation and reduction of disulfides, i.e., inter- and intra-molecular protein disulfides, and with high specificity disulfides between protein thiols and GSH, i.e., reversible (de-)glutathionylation. For comprehensive reviews on this topic, see for instance [61,63–67], and for a summary of the characteristics of the human Grxs, see Table 1. In brief, these redox-active Grxs (CPYC-type or class I Grxs) contain a consensus Cys-Pro-Tyr-Cys active site motif and catalyze thiol-disulfide exchange reactions in two connected reaction mechanisms. The formation and reduction of protein disulfides require both active site cysteinyl residues and (de-)glutathionylation of only the more N-terminal. The mechanisms were thus termed dithiol and monothiol reaction mechanisms. Both reactions are initiated by a nucleophilic attack of the more N-terminal cysteinyl residue, which is characterized by a particularly low pK_a value ≤ 5 [66,68–70], on the target disulfide. In the case of the dithiol reaction mechanism, the intermediate disulfide between the Grx and the target protein is reduced by the more C-terminal cysteinyl residue. The monothiol

mechanism results in a reduced protein and a disulfide between the Grx and GSH (see Figure 2). Reduction of the Grx with a disulfide in the active site by GSH results in the same Grx-GSH mixed disulfide, which can be reduced by another molecule of GSH, completing both reaction cycles. Both reactions are fully reversible, as Grxs catalyze both the oxidation and reduction of target proteins. A second class of Grxs came into focus much later. These proteins share the consensus active site motif Cys-Gly-Phe-Ser, hence CGFS-type or class II Grxs. With few exceptions [71,72], CGFS-type Grxs are inactive as oxidoreductases. Instead, these proteins function in cellular iron metabolism [10,51,52,73,74], see below.

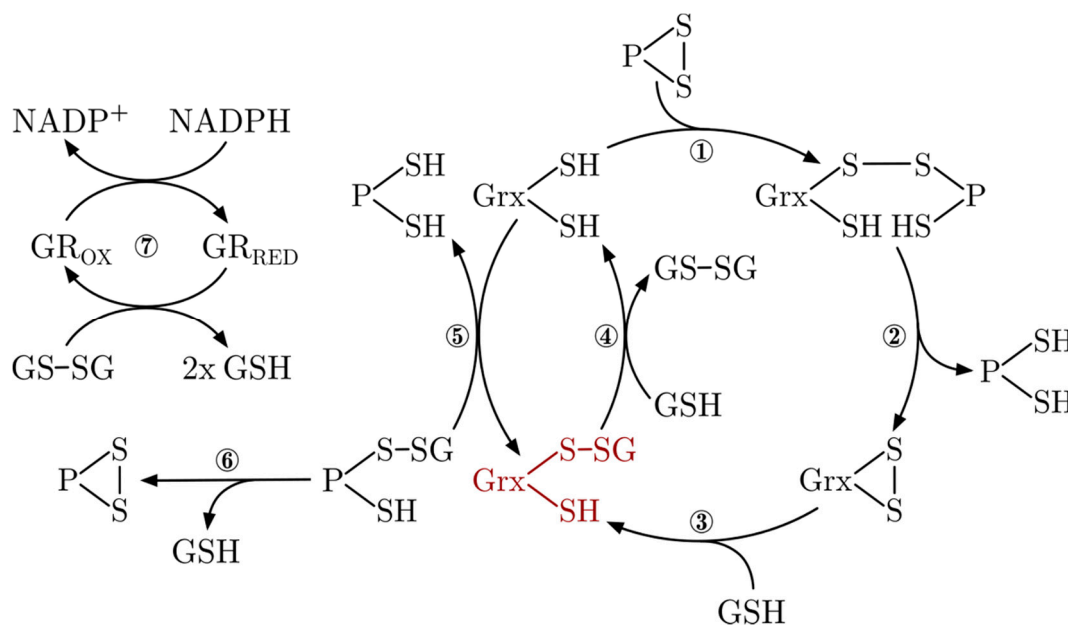


Figure 2. Glutaredoxin reaction mechanisms. Protein disulfides are reduced via a mechanism that involves both active site cysteinyl residues of the CxxC-type Grxs. A reduced Grx forms a mixed disulfide with the thiol of a target protein and its N-terminal active site Cys (1). This intermediate is reduced by the C-terminal active site Cys, releasing the reduced substrate target protein (2). The oxidized Grx can be sequentially reduced by two molecules of GSH (3+4). A Grx-S-S-GS mixed disulfide (red) can easily be formed from reduced Grx and glutathione disulfide (GSSG) in the reverse reaction (4). Reduced Grx can also catalyze the reversible (de-)glutathionylation of a target protein in a mechanism that only requires the N-terminal active site Cys (5). Some glutathionylated proteins containing two adjacent Cys can also oxidize and form an intra-molecular disulfide by releasing GSH (6). GSSG is reduced to two molecules of GSH by glutathione reductase (GR) at the expense of NADPH.

Table 1. Human glutaredoxins. Abbreviations: c: cytosol, m: mitochondria, n.a.: not available, n: nucleus.

Protein Name	Accession	Gene	Active Site	Functions and Reactions	FeS	Locali-Zation
Grx1	P35754	Glx	CPYC	Oxidoreductase, (de-)glutathionylation [75,76]	no	c/n
Grx2a	Q9NS18	Glx2	CSYC	Oxidoreductase, FeS as redox sensor [16,77,78]	Fe ₂ S ₂	m
Grx2b	Q9NS18-2	Glx2	CSYC	Not analyzed [77,79]	Fe ₂ S ₂	c/n
Grx2c	n.a.	Glx2	CSYC	Oxidoreductase, FeS as redox sensor [16,77,78]	Fe ₂ S ₂	c/n
Grx3	O76003	Glx3	2-CGFS	Fe/S biogenesis, iron trafficking [52,80]	2-Fe ₂ S ₂	c
Grx5	Q86SX6	Glx5	CGFS	Fe/S biogenesis [81,82]	Fe ₂ S ₂	m

For decades, Grxs were characterized as co-factorless oxidoreductases [67]. It therefore came as a big surprise when the first two FeS-Grxs were described, *Arabidopsis thaliana* GrxC1 [83,84] and human Grx2 [16,85]. In both cases, it turned out that the exchange of the prolyl residue in the CPYC consensus

active site for a glycyl and seryl residue, respectively, was sufficient to allow cluster ligation [84,85]. The second big surprise was the mode of cluster ligation itself in these proteins. The clusters are ligated in a dimeric holo-complex at the interface of two hardly interacting Grx monomers [84,86]. The $[\text{Fe}_2\text{S}_2]^{2+}$ clusters are ligated by the two more N-terminal cysteinyl residues of the active site and the thiol groups of two non-covalently bound GSH molecules [84–86]. These were the first examples of FeS clusters co-ligated by GSH. Following these two C(non-P)YC-type Grxs, all CGFS-type Grxs have been characterized as Fe_2S_2 -proteins, see for instance [10,74,80,81,87]. Both Grx sub-families bind the FeS cluster in a very similar way at the interface of the dimeric holo-complex, including co-ligation by GSH. However, one particular feature separates the two groups: the relative orientation of the Grx monomers in the holo-complex towards each other (Figure 3). Compared to the CGFS-type Grxs, the position of one monomer in the C(non-P)YC-type Grxs is tilted by approximately 90° toward the site relative to the other monomer. The sequestration of the N-terminal active site cysteinyl residue in the holo-complex of the redox-active, yet FeS-binding, Grxs suggests that the cluster serves as a regulatory mechanism controlling the activity of the proteins, for instance, by increased levels of GSSG or nitrogen oxide (NO) [16,88], or that it may serve other redox-independent functions [16,89].

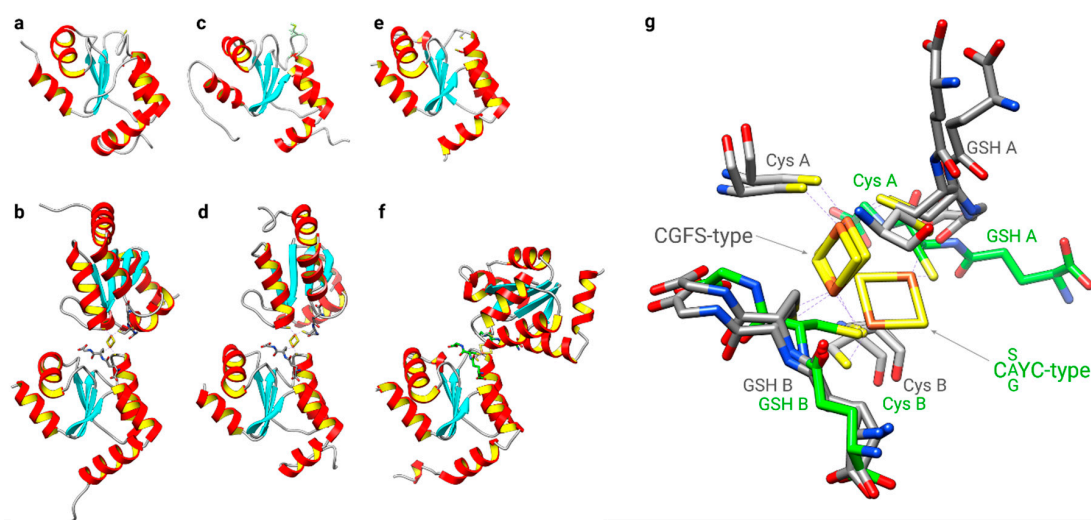


Figure 3. Structural comparison of both classes of FeS glutaredoxins. Structures of (a) apo- [PDB:1YKA] and (b) dimeric CGFS-type holo-Grx4 [PDB:2WCL] from *Escherichia coli*, CGFS-type human (c) apo- [PDB:2MMZ] and (d) holo-Grx5 [PDB:2WUL], and CSYC-type human Grx2 in (e) apo- [PDB:2FLS] and (f) holo-form [PDB:2HT9]. (g) Details of the alternative cluster coordination conformations of the holo-complexes, CGFS-type Grxs with GSH and active site cysteinyl residue carbon traces in gray, CSYC-type with carbon traces in green. “A” and “B” refer to the two subunits in the dimeric holo-complexes composed of the two subunits A and B, two non-covalently bound GSHs and the bridging Fe_2S_2 cluster.

Although both types of Grxs discussed here share highly similar 3-D structures (see Figure 3), as well as all elements and residues required to bind GSH [9], they exhibit completely different activities—oxidoreductase versus transferase. The mechanistic basis for this profound difference was the subject of many investigations and speculations [81,87,90,91], until two studies recently characterized the molecular basis of their distinct activity profiles [92,93]. In brief, the key determinants of their function are unique loop structures just before the active site. The engineering of a CxxC-type Grx with a CGFS-type loop switched its function from oxidoreductase to FeS transferase in a zebrafish model and the introduction of a CxxC-type loop into a CGFS-type Grx abolished its FeS transferase activity and activated the oxidative half-reaction (Figure 2, reaction 5 reverse) of the oxidoreductase [92]. The reductive half-reaction, requiring the interaction with the second GSH molecule (Figure 2, reaction 4), is dependent on further elements, characterized in detail in [93]. Together, these studies explain how

subtle structural differences determine the diverse Grx functions. An overview of the different classes of Grxs in different species is depicted in Figure 4.

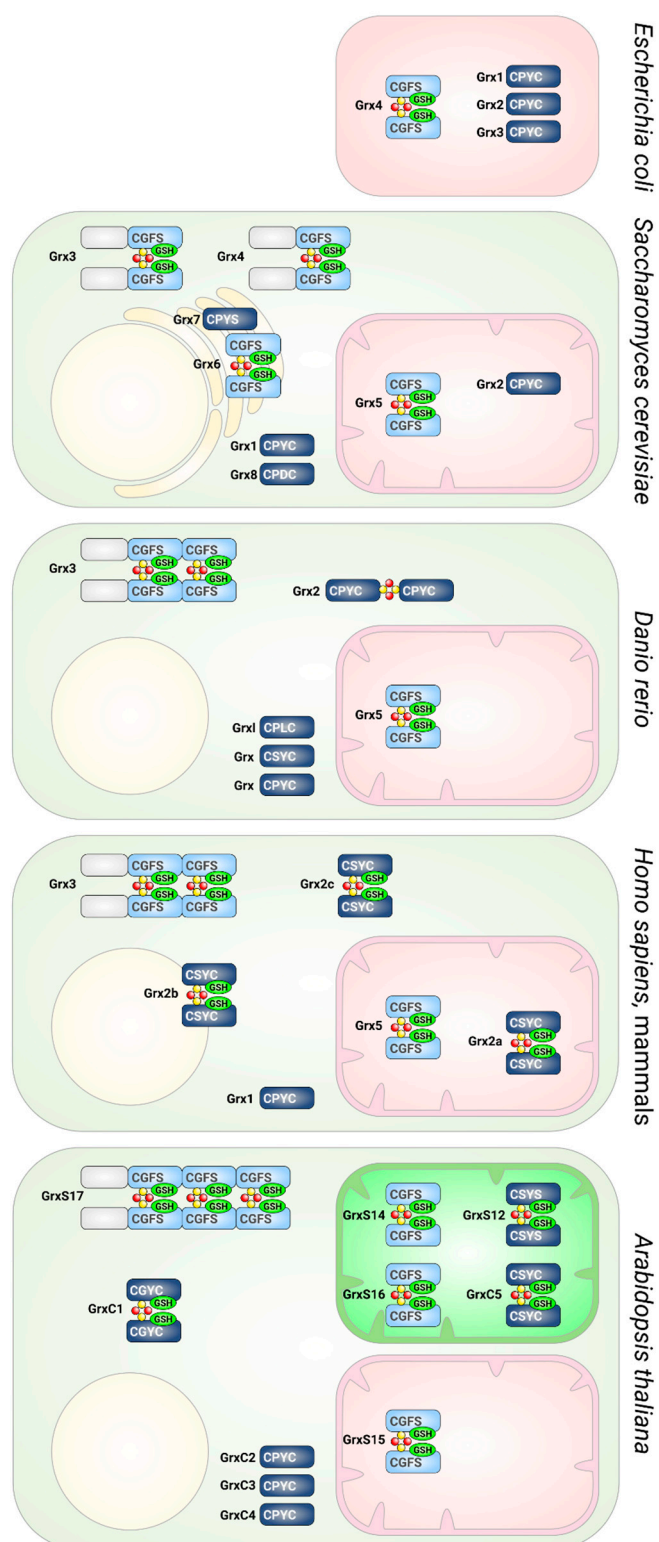


Figure 4. Glutaredoxins in different species. Presence and subcellular localization of Grxs in *Escherichia coli*, *Saccharomyces cerevisiae*, *Danio rerio*, humans, and *Arabidopsis thaliana*. CGFS-type Grxs are depicted in light blue, CxC-type in dark blue. The domain structures, active site sequences, and the ability to form FeS cluster-bridged holo-complexes are indicated.

2.2.1. Vertebrate- and Mammalian-Specific Glutaredoxin 2

Before it was described as an FeS protein, human Grx2 was characterized as a redox-active Grx with the ability to reduce mixed disulfides and effectively (de-)glutathionylate target proteins [79,94,95]. The human GLRX2 gene consists of five exons, including two alternative first exons (Ia and Ib) leading to three transcript variants. The core domain of Grx2, including the active site, is encoded by exon II-IV. GLRX2_v1 (exon Ia-II-III-IV) encodes the ubiquitously expressed Grx2a, including a mitochondrial targeting sequence. GLRX2_v2 and v3 are products of the alternative splice donor sites of exon Ib, encoding the nuclear and cytosolic isoforms Grx2b and Grx2c. The expression of Grx2b and Grx2c is restricted to the testis in adult human tissues, but has also been demonstrated in various cancer cell lines [77]. In contrast, the mouse GLRX2 gene consists of six exons, three constitutive exons (II, III, IV), two alternative first exons (Ia, Ib), and one single cassette exon. Five transcript variants encode three protein isoforms. The mitochondrial Grx2a and the nuclear/cytosolic Grx2c are conserved from mouse to human. Testis-specific Grx2d is unique to mouse [96]. Grx2 shares 34% sequence homology with Grx1 and a CSYC active site motif, with the exchange of the prolyl for a seryl residue [79,94]. This altered active site sequence results in an increased affinity for glutathionylated proteins and it can be reduced by either GSH or thioredoxin reductase, combining characteristics of Trxs and Grxs. Dimeric inactive holo-Grx2 bridges an FeS cluster. Degradation of the cluster in oxidative conditions, e.g., a more oxidized glutathione pool, results in monomeric active Grx2, indicating a function as a redox sensor *in vivo* [16]. Monomerization and cluster disassembly can cause lipid peroxidation, a drop in mitochondrial membrane potential, and eventually cell death [97]. The mitochondrial Grx2a was shown to participate in the maintenance of the redox equilibrium under conditions that promote oxidative damage to mitochondrial proteins. Especially for cells over-expressing Grx2a, protective functions have been described [88,98,99]. Grx2a over-expression decreased susceptibility towards apoptosis induced by doxorubicin (DOX) [100]. Grx2 is essential for mitochondrial morphology and dynamics in cardiomyocytes in humans and mice [101]. The loss of mitochondrial Grx2 is connected to increased mitochondrial proton leaks and respiration in muscle cells [102]. Genomes of other vertebrate species, e.g., zebrafish, contain genes encoding homologs to the cytosolic Grx2 isoform. This cytosolic zfGrx2 is essential for brain development. Zebrafish with silenced expression of cytosolic Grx2 lose essentially all types of neurons by apoptotic cell death and fail to develop an axonal scaffold. Only the re-introduction of wildtype Grx2c could rescue the defects, but not in either of the redox-inactive active site mutants [103]. The over-expression of Grx2c in SH-SY5Y neuroblastoma cells during retinoic acid-induced differentiation increases axon length and the number of branching points by up to two-fold [103]. Cytosolic Grx2 also has an essential function for the vascular development and maintenance of cardiovascular function [104,105]. Zebrafish lacking cytosolic Grx2 have an impaired heart looping and defects in heart functionality due to a failed migration of cardiac neural crest cells [106]. This heart looping defect could be rescued by introduction of the active site mutant of zfGrx2 that is still able to catalyze monothiol mechanism reactions [106]. Grx2c also has an essential function in spermatogenesis, a process that includes the migration of spermatogenic cells through the close Sertoli cell formation [77]. Recent results indicate a correlation between Grx2c expression and cancer-specific survival in clear cell renal cell carcinoma patients [107]. In a proteomic approach, Schütte et al. were able to identify target proteins, e.g., collapsin response mediator protein (CRMP) 2, that undergoes thiol-disulfide exchange reactions catalyzed by Grx2 [108]. In models of Parkinson's disease, the depletion of glutathione resulted in a dose-dependent Grx2 inhibition and, similar to gene silencing of Grx2, decreased iron incorporation into complex I and ACO2. The loss of Grx2 function also led to the activation of iron regulatory protein (IRP1), resulting in the increase in the iron uptake protein transferrin receptor, decreased levels of the iron storage protein ferritin, and mitochondrial iron accumulation. In the cytosol, the loss of Grx2 resembled iron starvation conditions.

2.2.2. Glutaredoxin 5

Human Grx5 is one of the central proteins in the mitochondrial ISC machinery, as well as in cluster trafficking and, therefore, iron homeostasis [109,110]. In humans, the maturation of mitochondrial FeS cluster-containing proteins can be divided into different steps. First, the initial Fe₂S₂ cluster is assembled on the iron-sulfur cluster enzyme ISCU (ISCU2) and involves at least 17 characterized proteins [111]. The human ISCU2-M140I variant can overcome the loss of frataxin. However, this is not by restoring its function in cluster assembly, but rather by the acceleration of cluster transfer from ISCU2 to Grx5 [112]. The release and transfer of the Fe₂S₂ cluster is facilitated by Hsp70 chaperones [22]. Chaperone binding enhanced the ATP-dependent cluster transfer from *E. coli* IscU in vitro [113]. In *S. cerevisiae*, the ATPase activity of the chaperone increased by Isu1 binding but not by interaction with Grx5. The association of Isu1, Grx5, and the chaperone is required for cluster transfer from Isu1 to Grx5 [114]. A study published in 2018, however, contradicted these findings by showing a cluster transfer from ISCU to Grx5 only in the absence of the human mitochondrial Hsp70 chaperones HSPA9 and HSC20 [115]. However, this study completely relied on in vitro data with assay times up to two hours, and therefore the results were mainly subjected to thermodynamic restrictions rather than physiological constraints.

Together with Grx5, ISCA1 and ISCA2 are proteins involved in the assembly of Fe₄S₄ clusters [22]. Until recently, only very slow rates of cluster transfer from Grx5 to ISCA1 and ISCA2 were demonstrated in vitro. Although new insights were provided by the structure of the ISCA2-IBA57 complex [10,11], the reductive fusion of the two Fe₂S₂ clusters to one Fe₄S₄ cluster has only recently been reported [25]. BolA-like proteins, more precisely BolA1 and BolA3, were also suggested to interact with Grx5 in the assembly of Fe₄S₄ and possibly Fe₂S₂ clusters, as summarized, e.g., in [22]. Both human BolA1 and BolA3, interact with apo- and holo-Grx5 to form hetero-clusters with different affinities as shown in in vivo and in vitro studies [116,117]. NMR, EPR, CD, and UV/vis spectroscopy were utilized to characterize and identify differences in the nature of the clusters bound in the BolA1-Grx5 and BolA3-Grx5 hetero-complexes [118].

The loss of Grx5 disrupts FeS assembly on target proteins and leads to mitochondrial iron overload [19,114]. In *Schizosaccharomyces pombe*, Grx5 depletion also led to a decrease in mitochondrial DNA [119]. Additionally, in *S. cerevisiae*, an iron-dependent increased rRNA degradation was observed upon Grx5 depletion due to iron overload [120]. In zebrafish, a lack of Grx5 led to the activation of IRP1 and blocked heme biosynthesis [121]. The first step in this pathway is catalyzed by aminolaevulinate synthase 2 (ALAS2). The over-expression of ALAS2 RNA without the iron response element regulated by IRP1 rescued the zebrafish embryos, while the expression of ALAS2, including the iron response element, did not [121]. Human patients with decreased levels of Grx5 develop iron overload and sideroblastic-like microcytic anemia [82,109].

The mechanisms of cluster transfer in the mitochondrial FeS cluster machinery, as well as to target proteins, remain to be revealed. Over the years, many studies have been published proposing cluster transfer between proteins that are clearly involved in the mitochondrial FeS cluster synthesis pathway, but they have relied solely on in vitro data (e.g., [115]). As mentioned above, these sorts of in vitro studies are restricted by thermodynamics and do not take physiological conditions nor enzymatic catalysis into account. An example of how this leads in an unavailing direction can be found for CSYC-type Grx2. Also located in the mitochondria, Grx2 complexes an FeS cluster [16]. In contrast to Grx5 depletion, the loss of Grx2 does not impair ISC biogenesis or transfer but leads to defects, e.g., in brain and heart development [103,106]. In vivo Grx2 and Grx5 display completely different functions in redox regulation and iron homeostasis, respectively. However, it was published that in vitro human Grx2 transferred its FeS cluster to human ferredoxin (Fdx1) (see Table 2 and Figure 5) with an apparent second-order rate constant of $1160 \pm 200 \text{ M}^{-1} \text{ min}^{-1}$ [122]. An essential reaction that takes more than 60 min is far away from being physiological and would be inconsonant with the human lifespan.

Table 2. FeS cluster transfer reactions analyzed in vitro. Abbreviations: A.v.: *Azotobacter vinelandii*, H.s.: *Homo sapiens*, P.: *Populus tremulus*, S.c.: *Saccharomyces cerevisiae*, S.p.: *Schizosaccharomyces pombe*, Syn.: *Synechocystis* sp.

Donor	Acceptor	Additional Factors	Transfer Rate (M ⁻¹ min ⁻¹)	Method	Assay Time (min)	Ref.
[Fe ₂ S ₂](GS) ₄	S.c. Grx3		1360 ± 110 1600 ± 450 2153 ± 281	CD	30	[41]
[Fe ₂ S ₂](GS) ₄	H.s. BolA1	DTT	60,000 ± 1200	CD	30	[123]
[Fe ₂ S ₂](GS) ₄	H.s. BolA3	DTT	28,000 ± 2800	CD	30	[124]
[Fe ₂ S ₂](GS) ₄	H.s. BolA3	DTT	29,000 ± 3000	CD	30	[124]
H.s. Grx2	H.s. Fdx1	GSH	1160 ± 200	CD	60	[122]
H.s. Grx3	H.s. Ciapin1			UV-Vis		[125]
H.s. Grx3	H.s. Ciapin1			CD, UV-Vis		[56]
H.s. Grx5	H.s. IscU		7500 ± 2300	CD	60	[115]
H.s. Grx5	H.s. IscU D37A		3500 ± 500	CD	58	[115]
H.s. Grx5	H.s. Nfu1		950 ± 450	CD	118	[115]
H.s. Grx5	H.s. Nfu1			CD, UV-Vis, NMR		[126]
H.s. Grx5	H.s. Fdx1	DTT, GSH, BolA3	2000 ± 700	CD	120	[115]
H.s. Grx5	H.s. Fdx2	DTT, GSH	650 ± 250	CD	120	[115]
H.s. Grx5	H.s. ISCA1/ISCA2	DTT, GSH		NMR	9–48 h	[127]
H.s. Grx5	H.s. ISCA2	DTT, GSH		NMR	9–48 h	[127]
H.s. Grx5	H.s. ISCA2 C79S	DTT, GSH		NMR	9–48 h	[127]
H.s. ISCA1	H.s. BolA1, H.s. Grx5	DTT, GSH		CD	60	[123]
H.s. ISCA2	H.s. BolA1, H.s. Grx5	DTT, GSH		CD	60	[123]
H.s. ISCU	H.s. BolA1, H.s. Grx5	DTT, GSH	3600 ± 400	CD	60	[123]
H.s. ISCU	H.s. BolA3, S.c. Grx3	DTT, GSH	4600 ± 870	CD	60	[124]
H.s. ISCU	H.s. BolA3, H.s. Grx5	DTT, GSH	14,000 ± 1000	CD	60	[124]
H.s. ISCU	H.s. Grx5	DTT, GSH	10,300 ± 1800	CD	10	[115]
H.s. ISCU	S.c. Grx3	GSH	3370 ± 200	CD	60	[128]
H.s. Nfu	H.s. Grx5	DTT, GSH	35,100 ± 2000	CD	60	[129]
H.s. Nfu	H.s. Grx2	GSH	2000 ± 150	CD	60	[122]
H.s. Nfu	S.c. Grx3	GSH	36,200 ± 7700	CD	60	[128]
H.s. Nfu	S.c. Grx3	DTT, GSH, H.s. HSPA9, HSC20, ATP, MgCl ₂	34,400 ± 4500	CD	60	[129]
H.s. Nfu1	H.s. BolA3, S.c. Grx3	DTT, GSH		CD	60	[124]
H.s. Nfu1	H.s. BolA3, H.s. Grx5	DTT, GSH		CD	60	[124]

Table 2. Cont.

Donor	Acceptor	Additional Factors	Transfer Rate ($M^{-1} \text{ min}^{-1}$)	Method	Assay Time (min)	Ref.
H.s. BolA1 H.s. Grx5	H.s. Fdx1	DTT, GSH		CD	60	[123]
H.s. BolA1 H.s. Grx5	H.s. Fdx2	DTT, GSH		CD	60	[123]
H.s. BolA1 H.s. Grx5	H.s. ISCA1	DTT, GSH		CD	60	[123]
H.s. BolA1 H.s. Grx5	H.s. ISCA2	DTT, GSH		CD	60	[123]
H.s. BolA3 S.c. Grx3	H.s. Fdx1	DTT, GSH	1800 ± 170	CD	60	[124]
H.s. BolA3 S.c. Grx3	H.s. Fdx2	DTT, GSH	2600 ± 540	CD	60	[124]
H.s. BolA3 S.c. Grx3	H.s. Nfu1	DTT, GSH		CD	60	[124]
H.s. BolA3 H.s. Grx5	H.s. Fdx1	DTT, GSH	1400 ± 140	CD	60	[124]
H.s. BolA3 H.s. Grx5	H.s. Fdx2	DTT, GSH	2800 ± 380	CD	60	[124]
H.s. BolA3 H.s. Grx5	H.s. Nfu1	DTT, GSH		CD	60	[124]
S.c. Grx3	H.s. Fdx1	GSH	2100 ± 500	CD	60	[122]
S.c. Grx3	H.s. Fdx2	GSH	695 ± 138	CD	240	[122]
S.c. Grx3	A.v. IscA		≥50,000	CD	10	[130]
S.p. Isal1	S.c. Grx3	GSH	6200 ± 1900	CD	60	[122]
A.v. Grx5	A.v. Fdx	DTT	2100	CD	160	[131]
A.v. Grx5	A.v. IscA		22,000	CD	10	[130]
A.v. IscA	S.c. Fra2-Grx3		15,000	CD	120	[130]
A.v. IscU	A.v. Grx5	GSH	30	CD	180	[131]
A.v. IscU	A.v. Grx5	A.v. HscA, A.v. HcsB, MgCl ₂ , ATP, KCl	20,000	CD	60	[131]
A.t. GrxS14	A.v. IscA		≥50,000	CD	10	[130]
A.t. GrxS14	A.t. SufA1		≥50,000	CD	10	[130]
A.t. GrxS15	A.t. (mito)Fdx1			Native PAGE		[132]
P. GrxS14	Syn. Fdx		20,000	CD	~60	[74]

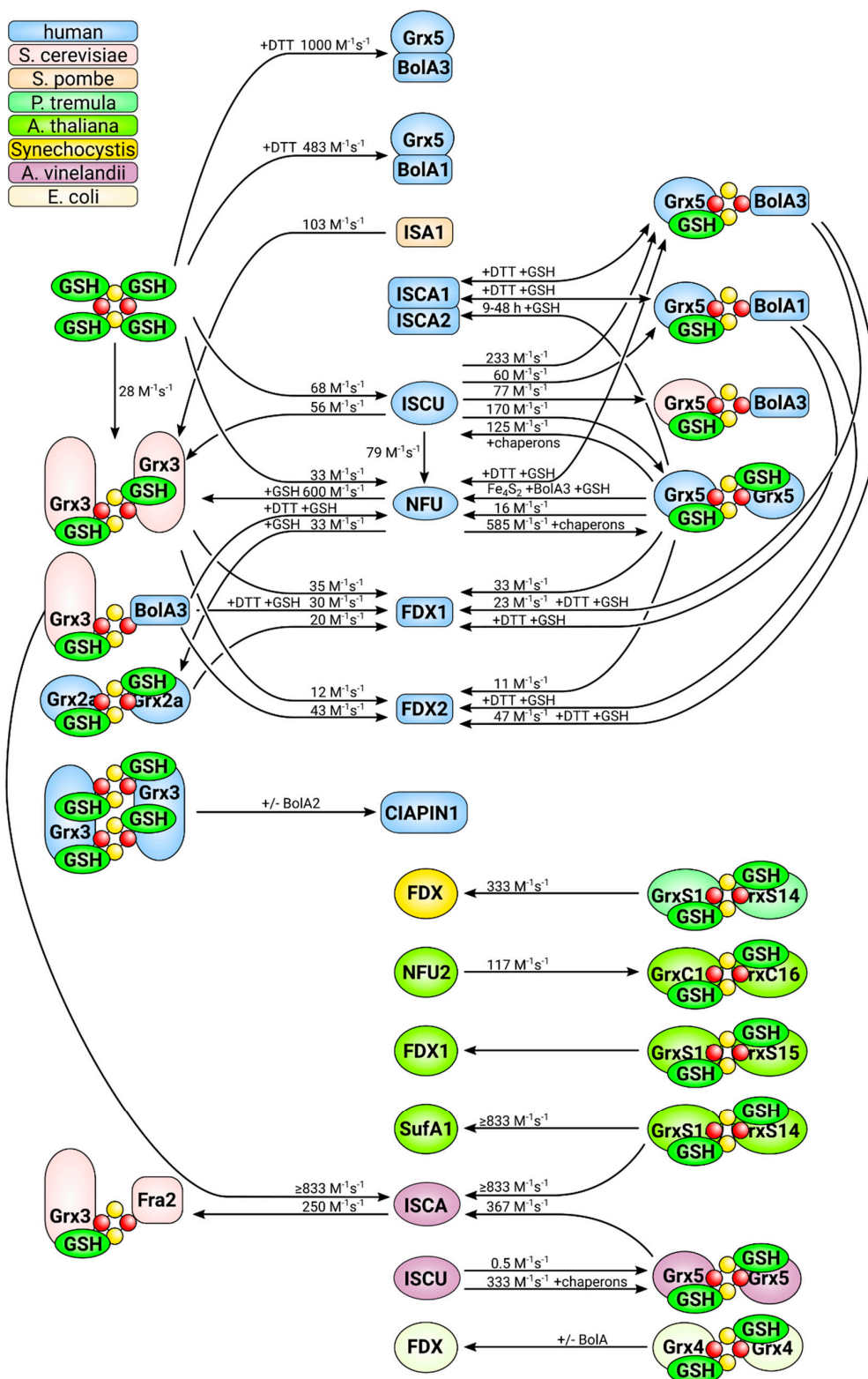


Figure 5. FeS cluster transfer reactions analyzed in vitro to date. This figure summarizes all in vitro cluster transfer reactions analyzed and described in the literature. The directions of the reactions are indicated by arrows. The origin of the different proteins used in the analyses, i.e., the species that encodes the respective protein, is color coded, as displayed in the top left corner. For details and references, see Table 2.

2.2.3. Multi-Domain Glutaredoxins, Glutaredoxin 3

Multi-domain Grxs are unique to eukaryotic cells. They consist of an N-terminal, normally redox inactive, and a Trx domain followed by one to three CGFS-type Grx domains, each of which can complex the GSH co-ligated Fe_2S_2 cluster in dimeric complexes. The yeast *Saccharomyces cerevisiae* expresses two closely related multi-domain Grxs containing a single CGFS-type Grx domain each, Grx3 and Grx4. Two major functions, both central for iron metabolism, were characterized for these proteins: (1) Grx3 and Grx4 have a central role in intra-cellular iron trafficking and sensing. The depletion of Grx3/4 specifically impaired all iron-requiring reactions in the cytosol, mitochondria, and nucleus, including the synthesis of FeS clusters, heme, and di-iron centers, such as in RNR (see Figure 1). The cells failed to insert iron into target proteins, as well as to deliver iron to mitochondria. Iron was simply not bio-available in the absence of the proteins [51] and (2) the availability of iron to form the FeS-bridged holo-complexes of Grx3 and 4 is used as sensor for the iron state of fungal cells. Extensive analyses of *S. cerevisiae* and *S. pombe* have uncovered unique mechanisms that control iron metabolism in different fungi, summarized recently in [11]. The common thread in these regulatory mechanisms are the multi-domain CGFS-type Grxs that interact, often together with BolA-type proteins (see below), with transcription factors dependent on the iron state of the cell, thus controlling the transcription of proteins and enzymes that take part in, or control, iron metabolism. For detailed discussion on this topic, see for instance [10,11,133,134].

Vertebrate-specific Grx3, also known as protein kinase C-interacting cousin of thioredoxin (PICOT), TXNL-2, and HUSSY-22, contains two C-terminal CGFS-type Grx domains [66,135,136]. Grx3 is ubiquitously expressed [80,137], the protein can complex two Fe_2S_2 clusters at the interfaces between the two CGFS-type Grx domains in a homo-dimeric holo-complex, and it binds iron in vivo [80]. The depletion of Grx3 in zebrafish embryos primarily affected hemoglobin maturation. The loss of Grx3 function did not affect globin biosynthesis, and instead heme did not mature [52]. This was likely caused by the loss of an essential FeS cluster in the enzyme ferrochelatase that catalyzes the final step in heme maturation, iron insertion [138]. Gene silencing of Grx3 in cells of human origin (HeLa cells) induced a phenotype resembling an iron starvation phenotype despite the sufficient bio-available iron. The protein levels of several cytosolic FeS proteins were altered, for instance, IRP1 and glutamine phosphoribosylpyrophosphate amidotransferase (GPAT). The protein levels of ferritin were decreased and the levels of the transferrin receptor increased, indicating the activation of IRP1. Apparently, the Grx3-depleted cells were unable to use iron efficiently, indicating a central role for Grx3 in iron metabolism [52] similar to the one described in yeast [51], i.e., a function in cellular iron trafficking. The molecular base of this function and how it relates to the observed defects in FeS protein maturation in the cytosol of eukaryotic cells is still unknown.

Human Grx3 was initially identified as an interaction partner of protein kinase C θ and is associated with various signaling pathways that lead to the activation of cells [136]. Grx3 is essential during development, the loss of Grx3 in mice resulted in embryonic death between E12.5 and E14.5, without apparent defects in organogenesis [139]. Grx3^{-/-} embryos did not exhibit obvious histological abnormalities, however, the embryos were reported to be of smaller body size and developed hemorrhages in the head [139,140]. It is noteworthy that the time point of embryonic death, E12.5, also marks the onset of definitive erythropoiesis in the fetal liver [141,142] and, from this point on, erythropoiesis is the major iron-consuming process. Grx3 can protect from cardiac hypertrophy in animal models. Grx3 protein levels were increased in these models and heterozygous Grx3^{+/-} mice were more vulnerable to developing cardiac hypertrophy, in contrast to wildtype mice [139,140]. Disturbances in iron metabolism have also been linked to cardiac pathologies. For instance, in Friedreich's ataxia patients, the (partial) loss of the FeS cluster biogenesis protein frataxin (Figure 1) causes mitochondrial iron overload and defects in mitochondrial FeS maturation, summarized in [23,143]. These defects frequently cause cardiomyopathy and cardiac hypertrophy [144]. To date, however, it is unclear whether the role of Grx3 in cardiac hypertrophy is connected to its role in iron metabolism.

2.3. Grxs and BolA-Like Proteins

Both genetic and biochemical evidence link BolA-like proteins to iron metabolism and to CGFS-type Grxs in particular [10,145]. It was hypothesized that both proteins interact in the transfer of FeS clusters to targeting complexes or recipient proteins. This is supported by a number of in vitro and structural studies [118]. Unlike the CGFS-type Grxs, BolA-like proteins from different species show a high degree of heterogeneity and a low degree of conservation, including some of the residues that were suggested to take part in the ligation of FeS clusters in both homo- and hetero-dimeric holo-complexes.

In *S. cerevisiae*, the regulation of iron metabolism by the transcription factors activator of iron transcription protein (Aft) 1 and Aft2 depends on the Grx3/Grx4 siblings and the proteins Fe repressor of activation (Fra) 1 and Fra2, for summaries, see [10,11]. Fra2 is BolA-like protein also known as BolA2. The Fe₂S₂ cluster in the hetero-dimeric complex between Grx3/4 and Fra2 is complexed by the Grx3/4 active site CGFS cysteinyl residue, a Fra2 histidyl residue, one GSH, and another ligand that is not a histidyl residue and remains elusive [146,147]. The conserved His103 residue is not required for hetero-dimer formation and cluster binding in vitro, but influences cluster stability [146]. In vitro studies described a cluster transfer between Grx3-Bol2 and Aft2, involving a ligand exchange mechanism and a specific protein–protein interaction that requires Aft2 Cys187 [148,149]. Cluster binding appeared to be more stable in the hetero-dimeric complex compared to Grx3/4 homo-dimers, although removal of this cluster did not disrupt the Grx3-Fra2 hetero-dimer, raising the question of whether it functions as an FeS scaffold or iron sensing protein [147]. In the proposed iron sensing mechanism in *S. pombe*, an FeS cluster is transferred from the transcription factor iron-sensing transcription factor 1 (Fep1) to Grx4-Fra2 in response to iron starvation, thereby activating gene expression to increase the intra-cellular iron pool [150].

The holo-complex of the human multi-domain CGFS-type Grx3 bridges two Fe₂S₂ clusters with four GSHs and its two conserved CGFS motifs [80]. In 2012, Li et al. demonstrated that human Grx3 forms a heterotrimeric complex with human BolA2 in vitro, and this was confirmed by Banci et al. [53,56]. As in yeast, cysteinyl and histidyl residues of Grx3 and BolA2, respectively, were proposed to be involved in cluster coordination [53,56]. In contrast to yeast, however, in vivo data supporting this interaction and a physiological role of this hetero-trimeric complex remain to be presented. In vitro data suggested more stable Fe₂S₂ clusters in the hetero-trimeric compared to the Grx3 homo-dimeric complexes, as observed in yeast. Nevertheless, a role of the BolA2-Grx3 complex in Fe₂S₂ cluster transfer in the cytosolic FeS protein maturation pathway was proposed [56]. Cluster transfer from homo-dimeric Grx3 to CIAPIN1 (also named anamorsin, see Figures 1 and 5) was demonstrated, the specific interactions between the two were proposed as key mechanisms in anamorsin maturation [125]. However, the hetero-complex with BolA2 was also reported to be able to transfer both bridging Fe₂S₂ clusters to CIAPIN1/anamorsin in vitro, and thus a function as an FeS cluster transfer component in the cytosolic FeS protein biogenesis was suggested [56]. The siRNA-mediated silencing of Grx3 induces an iron starvation phenotype in HeLa cells [52]. However, the silencing of BolA2 expression not only failed to induce a similar phenotype, but the co-silencing of Grx3 and BolA2 rescued the iron starvation phenotype to some degree (unpublished own data). These results imply an antagonistic rather than joint function of cytosolic Grx3 and BolA2. This fragmentary puzzle of information and results remains to be solved.

Mitochondria of eukaryotic cells usually harbor the CGFS-type Grx5 and two BolA-like proteins, BolA1 and BolA3, both of which can form hetero FeS-bridged complexes with Grx5. Uzarska et al. demonstrated that human apo-Grx5 and BolA1 or BolA3 also specifically interact in chemical shift assays [114]. This interaction involves the location surrounding the invariant histidyl residue in the BolAs and the GSH-binding site in Grx5 [117]. Complex holo-models suggest that Grx5-BolA3 undergo significant structural rearrangement upon dimer formation and FeS cluster binding (Figure 6) [118]. In the loop connecting β -strand 1 and 2 of BolA3, the Cys 59 residue moves towards the invariant C-terminal His 96 and coordinates the Fe₂S₂ together with the active site and GSH thiols of Grx5.

The complex with BolA1, on the other hand, seems to not involve structural re-arrangements and has a different orientation [118] (Figure 6).

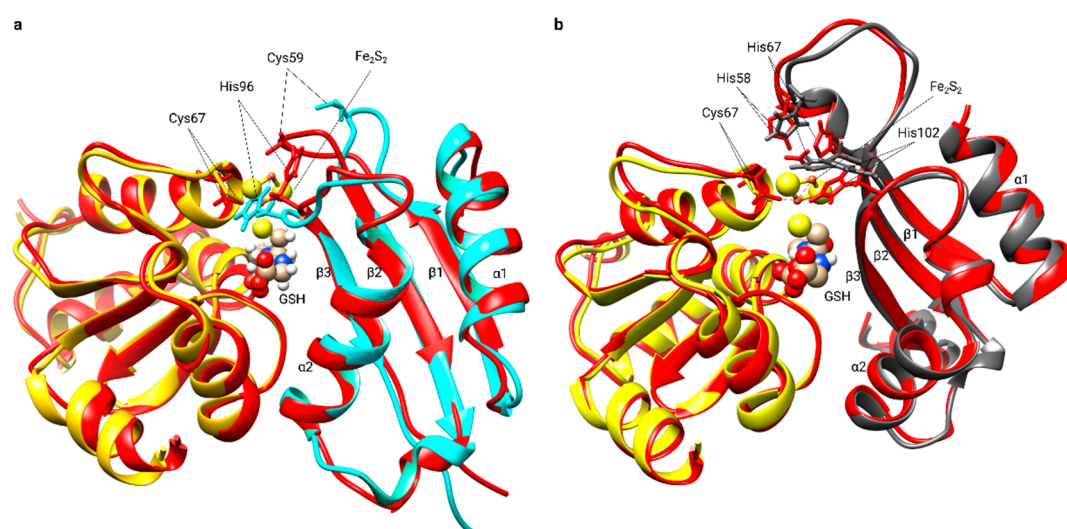


Figure 6. Structural rearrangements in Grx5 and BolA upon dimer formation. (a) Superimposition of the backbone structure of human apo-Grx5 [PDB:2WUL] (yellow) and human BolA3 [PDB: 2NCL] (cyan) with the Fe_2S_2 BolA3-Grx5 complex backbone structure (red). (b) Superimposition of the backbone structure of human apo-Grx5 [PDB:2WUL] (yellow) and human BolA1 [PDB:5LCI] (dark gray) with the Fe_2S_2 BolA1-Grx5 complex backbone structure (red). The GSH molecule and the Fe_2S_2 cluster are represented as balls and sticks. The invariant C-terminal His (His 96 in BolA3 and His 102 in BolA1), His 67 in BolA1, Cys 59 in BolA3, and Cys 67 in human Grx5 residues are shown.

In vivo and in vitro studies suggest specialized functions of yeast mitochondrial Bol1 and Bol3 in the same pathway, i.e., FeS protein maturation in mitochondria. The over-expression of Grx5 increases the BolA1 level but there is no effect on BolA3 [116]. BolA1 interacts with Grx5 via the Fe_2S_2 cluster, whereas BolA3 interacts with Nfu1 in the Fe_4S_4 cluster assembly, although the detailed mechanisms remain unsolved [116,117]. Yeast cells lacking BolA1 and BolA3 show defects in Fe_4S_4 enzymes, e.g., aconitase and lipoic acid synthase [116,151]. The interaction of the two human mitochondrial BolA-like proteins, BolA1 and BolA3, and Grx5 was characterized by a number of in vitro techniques [117]. Conserved histidyl residues (His102 in BolA1 and His96 in BolA3) and other potential cluster ligands, e.g., histidyl and cysteinyl residues in BolA1 and BolA3, respectively, are involved in hetero-dimeric cluster formation [10,117]. A reduced Rieske-type Fe_2S_2 cluster is coordinated by Grx5 and BolA1 with high affinity, whereas the oxidized, Fdx-like cluster of Grx5 and BolA3 is labile and BolA3 preferably interacts with Nfu1 [117,118]. Based solely on in vitro studies, Sen et al. concluded the contrary—a significant BolA3-Grx5 interaction and a weak BolA3-Nfu1 interaction [124]. Two BolA3-Grx5 hetero-complexes can transfer their Fe_2S_2 clusters to Nfu1 to form a Fe_4S_4 cluster in FeS protein maturation [126]. A role in cluster trafficking was ruled out for BolA1-Grx5 because of its structurally buried cluster and the lack of transfer efficiency to common Fe_2S_2 cluster acceptors, such as ferredoxins [123]. Patients with mutations in the Grx5 or the BolA3 gene suffer from variations of nonketotic hyperglycinemia with decreased lipoylation, likely caused by interruption of the cluster transfer pathway to the FeS protein lipoate synthase [110]. The physiological role of BolA1 and BolA3 in complex with Grx5 remains elusive. For more comprehensive summaries of the topic, we refer to [10,54,111].

2.4. FeS Cluster Transfer Reactions

CGFS-type Grxs and BolA-like proteins have been suggested to cooperate in the transfer of FeS clusters to target proteins and targeting protein complexes [53]. A number of studies, summarized in

Table 2 and Figure 5, have addressed such transfer reactions in vitro, mostly utilizing differences in the absorption or circular dichroism of the holo-complexes of target and recipient proteins. In brief, the combined in vitro data on these cluster transfer reactions can be summarized as follows: it appears that Fe₂S₂ clusters can be transferred between most proteins that have the ability to ligate them, independent of the physiological significance of these interactions and phylogenetics. The reactions are reversible and seem to primarily follow thermodynamic constraints. So far, evidence for the requirement of any form of catalysis has only been demonstrated for the transfer of the Fe₂S₂ cluster built in the initial scaffold ISCU to the Grx5 homolog of *Azotobacter vinelandii* in the form of the HscA/HscB chaperone system [131]. The rate constants, especially of the reactions regarded as physiologically significant, are generally low, in the range of 0.1–1.7·10¹ M⁻¹ s⁻¹. Astonishingly, some of the highest rate constants have been reported for cluster transfer reactions between proteins that cannot be considered physiologically meaningful, e.g., from human Nfu (mitochondrial) to *S. cerevisiae* Grx3 (cytosolic) with 6·10² M⁻¹ s⁻¹ [122], or from *S. cerevisiae* Grx3 to *Azotobacter vinelandii* ISCA at ≥8.3·10² M⁻¹ s⁻¹ [130]. In vitro, human Grx2, a CSYC-type Grx, can transfer its cluster to Fdx1 with similar (low) rates as CGFS-type Grx5, i.e., 1.9·10¹ M⁻¹ s⁻¹ and 3.3·10¹ M⁻¹ s⁻¹, respectively, summarized in Table 2 and Figure 5. In vivo, however, due to its different quaternary structure, the ubiquitously expressed [77] mitochondrial Fe₂S₂-Grx2a cannot compensate for the iron deficiency phenotype caused by Fe₂S₂-Grx5 depletion or loss, in neither zebrafish [82] nor in humans [82,109]. With respect to the role of the BolA-like proteins, no in vitro study so far has demonstrated that these proteins are strictly required for the transfer of FeS clusters from Grxs to any other protein or vice versa, nor that their presence would enhance the rate constants of the transfer reaction. To date, in vitro studies have not provided conclusive evidence on the nature of the efficiency, nor the specificity in cluster transfer reactions observed in vivo.

3. Other Glutathione-Iron Complexes

Dinitrosyl-iron complexes (DINICs) are the derivative of nitric oxide (NO), iron, and other ligands. They play a crucial role in stabilization, storage, and NO bio-activity [152]. The electron paramagnetic resonance (EPR) signal at $g = 2.03$ is a characteristic feature of DINICs and was identified in vivo in animal tissues and other organisms [153]. In general, DINICs are formed by the attachment of anionic ligands to an Fe(NO)₂ nucleus. One common ligand of these centers is the thiolate of glutathione (GS⁻). Depending on the number of iron-nitrosyl nuclei attached to the ligand(s), both mono- and bi-nuclear DINICs are formed [154]. Under physiological conditions, mononuclear thiol-ligated DINICs appear to be in equilibrium with binuclear DINICs of the Roussin's red salt thioether type [155]. FeS proteins may be the major source of protein-bound DINICs as demonstrated in *E. coli* when ·NO directly reacts with the FeS clusters [156]. ·NO may also react with superoxide (O₂⁻), yielding peroxynitrite (ONOO⁻) that can react with proteins, inducing carbonylation and nitration [61]. In a recent study, we provided evidence that FeS-Grx2 can inhibit ONOO⁻ formation in cells by the reaction of its GSH co-ligated FeS cluster with ·NO, yielding glutathionyl-DINICs [88]. Such glutathionyl-DINICs may biologically be the most significant form. For instance, they may play an important role in protein S-nitrosylation (S-NO).

Various studies and reviews have reported the formation of S-NOs in vivo, see for instance [157–160]. It is often described as the product of the reaction of the ·NO radical with thiol groups. However, this reaction as such cannot take place unless one electron is removed, e.g., by a metal/enzyme catalyst [161].



Glutathionyl-DINICs can release nitrosonium ions (NO⁺) that can react with GSH to form GS-NO [162]. This NO⁺ moiety can be transferred to other thiols by a nucleophilic attack on the electrophilic nitrogen atom of GS-NO—a process known as protein trans-nitrosylation [163].



The thiol peroxidases peroxiredoxin 1 (Prx1) is S-nitrosylated in mammalian cells [164]. This reaction is mediated by glutathionyl-DINICs and involves the reactive peroxidatic cysteinyl residue in the active site of Prx1. The reaction affects the reactivity of the protein and thus its enzymatic and signaling functions [165].

DINICs complexed with glutathione may also be of interest for therapeutic applications [153]. They might serve also as ·NO donors to regulate the muscle tonus around the vasculature [152] and have already been successfully tested as hypotensive drugs in clinical trials [166]. The stability of DINICs can be increased through their interaction with proteins [153]. For example, cysteinyl residues in serum albumin can modulate and prolong the vasodilating activity of glutathionyl-DINICs [152]. It is noteworthy that these DINICs do not seem to affect the cellular glutathione levels, nor cellular proliferation [167]. They are not toxic to HeLa cells [168] and they increase the viability of fibroblasts and rat cardiomyocytes [167,169]. Glutathionyl-DINICs were also reported to accelerate skin wound healing, to inhibit apoptosis, and to suppress endometriosis [9,170]. In heart infarction models, treatment reduced the size of the infarction zone and inhibited platelet aggregation [171,172]. In summary, treatment with glutathionyl-DINICs may develop into new therapeutic strategies.

4. Conclusions and Outlook

The past decade has seen some remarkable progress in our understanding of the role of GSH and Grxs in iron metabolism, particularly with respect to the synthesis and maturation of FeS proteins. Promising steps have been made towards re-building functional FeS transfer and targeting complexes in vitro. We have reached a molecular understanding of the factors that determine the GSH-dependent oxidoreductase and FeS scaffold functions of Grxs. With the unraveling of the yeast Grx3/4-Fra2-mediated regulation of iron homeostasis in yeast, we have been presented with the first well-characterized physiological function of a Grx-BolA hetero-complex. However, a number of urgent open questions remain to be answered. They include, without claiming completeness:

What is the role of GSH in the export of FeS precursors from mitochondria to the cytosolic FeS assembly machinery? What compound is exported and what is the source of iron for cytosolic FeS maturation?

Outside the well-established yeast Aft regulon, what are the physiological roles of the CGFS-type Grx interactions with BolA-like proteins? Are these interactions essential for mitochondrial and/or cytosolic FeS maturation and transfer reactions? Do (more) of these complexes function in iron sensing?

What is the mechanism of cluster transfer between Grxs and recipient proteins? What are the factors that ensure both the specificity and efficiency of the reactions in vivo that we are apparently missing in vitro to date?

Author Contributions: T.D., H.M.F., J.L.M., G.M., and L.C.H. wrote and revised the text. All authors have read and agreed to the published version of the manuscript.

Funding: This work was supported by grants from the Deutsche Forschungsgemeinschaft (LI 984/3-2, LI 984/4-1, and GRK1947-A1). We acknowledge support for the Article Processing Charge from the DFG (German Research Foundation, 393148499) and the Open Access Publication Fund of the University of Greifswald.

Conflicts of Interest: The authors declare no conflict of interest.

References

1. Deponte, M. The Incomplete Glutathione Puzzle: Just Guessing at Numbers and Figures? *Antioxid. Redox Signal.* **2017**, *27*, 1130–1161. [CrossRef] [PubMed]
2. Berndt, C.; Lillig, C.H.; Flohé, L. Redox regulation by glutathione needs enzymes. *Front. Pharmacol.* **2014**, *5*, 168. [CrossRef] [PubMed]
3. Handy, D.E.; Lubos, E.; Yang, Y.; Galbraith, J.D.; Kelly, N.; Zhang, Y.Y.; Leopold, J.A.; Loscalzo, J. Glutathione peroxidase-1 regulates mitochondrial function to modulate redox-dependent cellular responses. *J. Biol. Chem.* **2009**, *284*, 11913–11921. [CrossRef]

4. Sakai, O.; Uchida, T.; Imai, H.; Ueta, T. Glutathione peroxidase 4 plays an important role in oxidative homeostasis and wound repair in corneal epithelial cells. *FEBS Open Bio* **2016**, *6*, 1238–1247. [CrossRef] [PubMed]
5. Yang, W.S.; Stockwell, B.R. Ferroptosis: Death by Lipid Peroxidation. *Trends Cell Biol.* **2016**, *26*, 165–176. [CrossRef]
6. Cao, J.Y.; Dixon, S.J. Mechanisms of ferroptosis. *Cell. Mol. Life Sci.* **2016**, *73*, 2195–2209. [CrossRef]
7. Ingold, I.; Berndt, C.; Schmitt, S.; Doll, S.; Poschmann, G.; Buday, K.; Roveri, A.; Peng, X.; Freitas, F.P.; Seibt, T.; et al. Selenium Utilization by GPX4 Is Required to Prevent Hydroperoxide-Induced Ferroptosis. *Cell* **2018**, *172*, 409–422. [CrossRef]
8. Kumar, C.; Igarria, A.; D'autreaux, B.; Planson, A.G.; Junot, C.; Godat, E.; Bachhawat, A.K.; Delaunay-Moisan, A.; Toledano, M.B. Glutathione revisited: A vital function in iron metabolism and ancillary role in thiol-redox control. *EMBO J.* **2011**, *30*, 2044–2056. [CrossRef]
9. Berndt, C.; Lillig, C.H. Glutathione, Glutaredoxins, and Iron. *Antioxid. Redox Signal.* **2017**, *27*, 1235–1251. [CrossRef]
10. Li, H.; Outten, C.E. Monothiol CGFS glutaredoxins and BolA-like proteins: [2Fe-2S] binding partners in iron homeostasis. *Biochemistry* **2012**, *51*, 4377–4389. [CrossRef]
11. Gupta, M.; Outten, C.E. Iron-sulfur cluster signaling: The common thread in fungal iron regulation. *Curr. Opin. Chem. Biol.* **2020**, *55*, 189–201. [CrossRef] [PubMed]
12. Rouhier, N.; Couturier, J.; Johnson, M.K.; Jacquot, J.-P. Glutaredoxins: Roles in iron homeostasis. *Trends Biochem. Sci.* **2010**, *35*, 43–52. [CrossRef] [PubMed]
13. Sugiura, Y.; Tanaka, H. Iron-sulfide chelates of some sulfur-containing peptides as model complex of non-heme iron proteins. *Biochem. Biophys. Res. Commun.* **1972**, *46*, 335–340. [CrossRef]
14. Kispal, G.; Csere, P.; Guiard, B.; Lill, R. The ABC transporter Atm1p is required for mitochondrial iron homeostasis. *FEBS Lett.* **1997**, *418*, 346–350. [CrossRef]
15. Sipos, K.; Lange, H.; Fekete, Z.; Ullmann, P.; Lill, R.; Kispal, G. Maturation of cytosolic iron-sulfur proteins requires glutathione. *J. Biol. Chem.* **2002**, *277*, 26944–26949. [CrossRef] [PubMed]
16. Lillig, C.H.; Berndt, C.; Vergnolle, O.; Lönn, M.E.; Hudemann, C.; Bill, E.; Holmgren, A. Characterization of human glutaredoxin 2 as iron-sulfur protein: A possible role as redox sensor. *Proc. Natl. Acad. Sci. USA* **2005**, *102*, 8168–8173. [CrossRef]
17. Beinert, H.; Holm, R.H.; Münck, E. Iron-sulfur clusters: Nature's modular, multipurpose structures. *Science* **1997**, *277*, 653–659. [CrossRef]
18. Johnson, D.C.; Dean, D.R.; Smith, A.D.; Johnson, M.K. Structure, function, and formation of biological iron-sulfur clusters. *Annu. Rev. Biochem.* **2005**, *74*, 247–281. [CrossRef]
19. Lill, R.; Hoffmann, B.; Molik, S.; Pierik, A.J.; Rietzschel, N.; Stehling, O.; Uzarska, M.A.; Webert, H.; Wilbrecht, C.; Mühlhoff, U. The role of mitochondria in cellular iron-sulfur protein biogenesis and iron metabolism. *Biochim. Biophys. Acta BBA-Mol. Cell Res.* **2012**, *1823*, 1491–1508. [CrossRef]
20. Gerber, J.; Neumann, K.; Prohl, C.; Mühlhoff, U.; Lill, R. The Yeast Scaffold Proteins Isu1p and Isu2p Are Required inside Mitochondria for Maturation of Cytosolic Fe/S Proteins. *Mol. Cell. Biol.* **2004**, *24*, 4848–4857. [CrossRef]
21. Balk, J.; Schaedler, T.A. Iron cofactor assembly in plants. *Annu. Rev. Plant Biol.* **2014**, *65*, 125–153. [CrossRef] [PubMed]
22. Braymer, J.J.; Lill, R. Iron-sulfur cluster biogenesis and trafficking in mitochondria. *J. Biol. Chem.* **2017**, *292*, 12754–12763. [CrossRef] [PubMed]
23. Sheftel, A.; Stehling, O.; Lill, R. Iron-sulfur proteins in health and disease. *Trends Endocrinol. Metab.* **2010**, *21*, 302–314. [CrossRef] [PubMed]
24. Sheftel, A.D.; Wilbrecht, C.; Stehling, O.; Niggemeyer, B.; Elsässer, H.P.; Mühlhoff, U.; Lill, R. The human mitochondrial ISCA1, ISCA2, and IBA57 proteins are required for [4Fe-4S] protein maturation. *Mol. Biol. Cell* **2012**, *23*, 1157–1166. [CrossRef] [PubMed]
25. Weiler, B.D.; Brück, M.-C.; Kothe, I.; Bill, E.; Lill, R.; Mühlhoff, U. Mitochondrial [4Fe-4S] protein assembly involves reductive [2Fe-2S] cluster fusion on ISCA1–ISCA2 by electron flow from ferredoxin FDX2. *Proc. Natl. Acad. Sci. USA* **2020**. [CrossRef] [PubMed]

26. Sheftel, A.D.; Stehling, O.; Pierik, A.J.; Netz, D.J.; Kerscher, S.; Elsässer, H.P.; Wittig, I.; Balk, J.; Brandt, U.; Lill, R. Human ind1, an iron-sulfur cluster assembly factor for respiratory complex I. *Mol. Cell. Biol.* **2009**, *29*, 6059–6073. [CrossRef]
27. Braymer, J.J.; Stümpfig, M.; Thelen, S.; Mühlhoff, U.; Lill, R. Depletion of thiol reducing capacity impairs cytosolic but not mitochondrial iron-sulfur protein assembly machineries. *Biochim. Biophys. Acta Mol.-Cell Res.* **2019**, *1866*, 240–251. [CrossRef]
28. Danielson, S.R.; Held, J.M.; Oo, M.; Riley, R.; Gibson, B.W.; Andersen, J.K. Quantitative mapping of reversible mitochondrial Complex I cysteine oxidation in a Parkinson disease mouse model. *J. Biol. Chem.* **2011**, *286*, 7601–7608. [CrossRef]
29. Balijepalli, S.; Boyd, M.R.; Ravindranath, V. Inhibition of mitochondrial complex I by haloperidol: The role of thiol oxidation. *Neuropharmacology* **1999**, *38*, 567–577. [CrossRef]
30. Chinta, S.J.; Andersen, J.K. Redox imbalance in Parkinson's disease. *Biochim. Biophys. Acta BBA-Gen. Subj.* **2008**, *1780*, 1362–1367. [CrossRef]
31. Mailloux, R.J.; Willmore, W.G. S-glutathionylation reactions in mitochondrial function and disease. *Front. Cell Dev. Biol.* **2014**, *2*, 68. [CrossRef] [PubMed]
32. Kispal, G.; Csere, P.; Prohl, C.; Lill, R. The mitochondrial proteins Atm1p and Nfs1p are essential for biogenesis of cytosolic Fe/S proteins. *EMBO J.* **1999**, *18*, 3981–3989. [CrossRef] [PubMed]
33. Srinivasan, V.; Pierik, A.J.; Lill, R. Crystal structures of nucleotide-free and glutathione-bound mitochondrial ABC transporter Atm1. *Science* **2014**, *343*, 1137–1140. [CrossRef] [PubMed]
34. Lill, R.; Srinivasan, V.; Mühlhoff, U. The role of mitochondria in cytosolic-nuclear iron-sulfur protein biogenesis and in cellular iron regulation. *Curr. Opin. Microbiol.* **2014**, *22*, 111–119. [CrossRef]
35. Schaedler, T.A.; Faust, B.; Shintre, C.A.; Carpenter, E.P.; Srinivasan, V.; van Veen, H.W.; Balk, J. Structures and functions of mitochondrial ABC transporters. *Biochem. Soc. Trans.* **2015**, *43*, 943–951. [CrossRef]
36. Bekri, S.; Kispal, G.; Lange, H.; Fitzsimons, E.; Tolmie, J.; Lill, R.; Bishop, D.F. Human ABC7 transporter: Gene structure and mutation causing X-linked sideroblastic anemia with ataxia with disruption of cytosolic iron-sulfur protein maturation. *Blood* **2000**, *96*, 3256–3264. [CrossRef]
37. D'Hooghe, M.; Selleslag, D.; Mortier, G.; Van Coster, R.; Vermeersch, P.; Billiet, J.; Bekri, S. X-linked sideroblastic anemia and ataxia: A new family with identification of a fourth ABCB7 gene mutation. *Eur. J. Paediatr. Neurol.* **2012**, *16*, 730–735. [CrossRef]
38. Schaedler, T.A.; Thornton, J.D.; Kruse, I.; Schwarzländer, M.; Meyer, A.J.; van Veen, H.W.; Balk, J. A conserved mitochondrial ATP-binding cassette transporter exports glutathione polysulfide for cytosolic metal cofactor assembly. *J. Biol. Chem.* **2014**, *289*, 23264–23274. [CrossRef]
39. Li, J.; Cowan, J.A. Glutathione-coordinated [2Fe-2S] cluster: A viable physiological substrate for mitochondrial ABCB7 transport. *Chem. Commun. Camb. Engl.* **2015**, *51*, 2253–2255. [CrossRef]
40. Pearson, S.A.; Wachnowsky, C.; Cowan, J.A. Defining the mechanism of the mitochondrial Atm1p [2Fe-2S] cluster exporter. *Metallomics* **2020**, *12*, 902–915. [CrossRef]
41. Fidai, I.; Wachnowsky, C.; Cowan, J.A. Glutathione-complexed [2Fe-2S] clusters function in Fe-S cluster storage and trafficking. *J. Biol. Inorg. Chem. JBIC Publ. Soc. Biol. Inorg. Chem.* **2016**, *21*, 887–901. [CrossRef] [PubMed]
42. Lill, R. Function and biogenesis of iron-sulphur proteins. *Nature* **2009**, *460*, 831–838. [CrossRef] [PubMed]
43. Webert, H.; Freibert, S.A.; Gallo, A.; Heidenreich, T.; Linne, U.; Amlacher, S.; Hurt, E.; Mühlhoff, U.; Banci, L.; Lill, R. Functional reconstitution of mitochondrial Fe/S cluster synthesis on Isu1 reveals the involvement of ferredoxin. *Nat. Commun.* **2014**, *5*, 1–12. [CrossRef] [PubMed]
44. Vernis, L.; Facca, C.; Delagoutte, E.; Soler, N.; Chanet, R.; Guiard, B.; Faye, G.; Baldacci, G. A newly identified essential complex, Dre2-Tah18, controls mitochondria integrity and cell death after oxidative stress in yeast. *PLoS ONE* **2009**, *4*, e4376. [CrossRef] [PubMed]
45. Netz, D.J.; Stümpfig, M.; Doré, C.; Mühlhoff, U.; Pierik, A.J.; Lill, R. Tah18 transfers electrons to Dre2 in cytosolic iron-sulfur protein biogenesis. *Nat. Chem. Biol.* **2010**, *6*, 758–765. [CrossRef]
46. Banci, L.; Bertini, I.; Calderone, V.; Ciofi-Baffoni, S.; Giachetti, A.; Jaiswal, D.; Mikolajczyk, M.; Piccioli, M.; Winkelmann, J. Molecular view of an electron transfer process essential for iron-sulfur protein biogenesis. *Proc. Natl. Acad. Sci. USA* **2013**, *110*, 7136–7141. [CrossRef]
47. Balk, J.; Pierik, A.J.; Netz, D.J.; Mühlhoff, U.; Lill, R. The hydrogenase-like Nar1p is essential for maturation of cytosolic and nuclear iron-sulphur proteins. *EMBO J.* **2004**, *23*, 2105–2115. [CrossRef]

48. Balk, J.; Aguilar Netz, D.J.; Tepper, K.; Pierik, A.J.; Lill, R. The essential WD40 protein Cia1 is involved in a late step of cytosolic and nuclear iron-sulfur protein assembly. *Mol. Cell. Biol.* **2005**, *25*, 10833–10841. [CrossRef]
49. Song, D.; Lee, F.S. A role for IOP1 in mammalian cytosolic iron-sulfur protein biogenesis. *J. Biol. Chem.* **2008**, *283*, 9231–9238. [CrossRef]
50. Netz, D.J.; Pierik, A.J.; Stümpfig, M.; Bill, E.; Sharma, A.K.; Pallesen, L.J.; Walden, W.E.; Lill, R. A bridging [4Fe-4S] cluster and nucleotide binding are essential for function of the Cfd1-Nbp35 complex as a scaffold in iron-sulfur protein maturation. *J. Biol. Chem.* **2012**, *287*, 12365–12378. [CrossRef]
51. Mühlhoff, U.; Molik, S.; Godoy, J.R.; Uzarska, M.A.; Richter, N.; Seubert, A.; Zhang, Y.; Stubbe, J.; Pierrel, F.; Herrero, E.; et al. Cytosolic monothiol glutaredoxins function in intracellular iron sensing and trafficking via their bound iron-sulfur cluster. *Cell Metab.* **2010**, *12*, 373–385. [CrossRef] [PubMed]
52. Haunhorst, P.; Hanschmann, E.M.; Bräutigam, L.; Stehling, O.; Hoffmann, B.; Mühlhoff, U.; Lill, R.; Berndt, C.; Lillig, C.H. Crucial function of vertebrate glutaredoxin 3 (PICOT) in iron homeostasis and hemoglobin maturation. *Mol. Biol. Cell* **2013**, *24*, 1895–1903. [CrossRef] [PubMed]
53. Li, H.; Mapolelo, D.T.; Randeniya, S.; Johnson, M.K.; Outten, C.E. Human Glutaredoxin 3 Forms [2Fe-2S]-Bridged Complexes with Human BOLA2. *Biochemistry* **2012**, *51*, 1687–1696. [CrossRef] [PubMed]
54. Dhalleine, T.; Rouhier, N.; Couturier, J. Putative roles of glutaredoxin-BOLA holo-heterodimers in plants. *Plant Signal. Behav.* **2014**, *9*, e28564. [CrossRef]
55. Roret, T.; Tsan, P.; Couturier, J.; Zhang, B.; Johnson, M.K.; Rouhier, N.; Didierjean, C. Structural and spectroscopic insights into BOLA-glutaredoxin complexes. *J. Biol. Chem.* **2014**, *289*, 24588–24598. [CrossRef]
56. Banci, L.; Camponeschi, F.; Ciofi-Baffoni, S.; Muzzioli, R. Elucidating the Molecular Function of Human BOLA2 in GRX3-Dependent Anamorsin Maturation Pathway. *J. Am. Chem. Soc.* **2015**, *137*, 16133–16143. [CrossRef]
57. Seki, M.; Takeda, Y.; Iwai, K.; Tanaka, K. IOP1 protein is an external component of the human cytosolic iron-sulfur cluster assembly (CIA) machinery and functions in the MMS19 protein-dependent CIA pathway. *J. Biol. Chem.* **2013**, *288*, 16680–16689. [CrossRef]
58. Stehling, O.; Vashisht, A.A.; Mascarenhas, J.; Jonsson, Z.O.; Sharma, T.; Netz, D.J.; Pierik, A.J.; Wohlschlegel, J.A.; Lill, R. MMS19 assembles iron-sulfur proteins required for DNA metabolism and genomic integrity. *Science* **2012**, *337*, 195–199. [CrossRef]
59. Urzica, E.; Pierik, A.J.; Mühlhoff, U.; Lill, R. Crucial role of conserved cysteine residues in the assembly of two iron-sulfur clusters on the CIA protein Nar1. *Biochemistry* **2009**, *48*, 4946–4958. [CrossRef]
60. Gari, K.; León Ortiz, A.M.; Borel, V.; Flynn, H.; Skehel, J.M.; Boulton, S.J. MMS19 links cytoplasmic iron-sulfur cluster assembly to DNA metabolism. *Science* **2012**, *337*, 243–245. [CrossRef]
61. Hanschmann, E.-M.; Godoy, J.R.; Berndt, C.; Hudemann, C.; Lillig, C.H. Thioredoxins, glutaredoxins, and peroxiredoxins—Molecular mechanisms and health significance: From cofactors to antioxidants to redox signaling. *Antioxid. Redox Signal.* **2013**, *19*, 1539–1605. [CrossRef] [PubMed]
62. Holmgren, A. Glutathione-dependent synthesis of deoxyribonucleotides. Characterization of the enzymatic mechanism of *Escherichia coli* glutaredoxin. *J. Biol. Chem.* **1979**, *254*, 3672–3678. [PubMed]
63. Mieyal, J.J.; Gallogly, M.M.; Qanungo, S.; Sabens, E.A.; Shelton, M.D. Molecular mechanisms and clinical implications of reversible protein S-glutathionylation. *Antioxid. Redox Signal.* **2008**, *10*, 1941–1988. [CrossRef] [PubMed]
64. Gallogly, M.M.; Mieyal, J.J. Mechanisms of reversible protein glutathionylation in redox signaling and oxidative stress. *Curr. Opin. Pharmacol.* **2007**, *7*, 381–391. [CrossRef]
65. Sabens Liedhegner, E.A.; Gao, X.-H.; Mieyal, J.J. Mechanisms of altered redox regulation in neurodegenerative diseases—focus on s-glutathionylation. *Antioxid. Redox Signal.* **2012**, *16*, 543–566. [CrossRef]
66. Lillig, C.H.; Berndt, C.; Holmgren, A. Glutaredoxin systems. *Biochim. Biophys. Acta* **2008**, *1780*, 1304–1317. [CrossRef]
67. Holmgren, A.; Johansson, C.; Berndt, C.; Lönn, M.E.; Hudemann, C.; Lillig, C.H. Thiol redox control via thioredoxin and glutaredoxin systems. *Biochem. Soc. Trans.* **2005**, *33*, 1375–1377. [CrossRef]
68. Tamarit, J.; Belli, G.; Cabisco, E.; Herrero, E.; Ros, J. Biochemical characterization of yeast mitochondrial Grx5 monothiol glutaredoxin. *J. Biol. Chem.* **2003**, *278*, 25745–25751. [CrossRef]
69. Sagemark, J.; Elgán, T.H.; Bürglin, T.R.; Johansson, C.; Holmgren, A.; Berndt, K.D. Redox properties and evolution of human glutaredoxins. *Proteins* **2007**, *68*, 879–892. [CrossRef]

70. Gallogly, M.M.; Starke, D.W.; Leonberg, A.K.; Ospina, S.M.E.; Mieyal, J.J. Kinetic and mechanistic characterization and versatile catalytic properties of mammalian glutaredoxin 2: Implications for intracellular roles. *Biochemistry* **2008**, *47*, 11144–11157. [CrossRef]
71. Mesecke, N.; Spang, A.; Deponte, M.; Herrmann, J.M. A novel group of glutaredoxins in the cis-Golgi critical for oxidative stress resistance. *Mol. Biol. Cell* **2008**, *19*, 2673–2680. [CrossRef] [PubMed]
72. Ströher, E.; Millar, A.H. The biological roles of glutaredoxins. *Biochem. J.* **2012**, *446*, 333–348. [CrossRef] [PubMed]
73. Rodríguez-Manzanque, M.T.; Tamarit, J.; Bellí, G.; Ros, J.; Herrero, E. Grx5 is a mitochondrial glutaredoxin required for the activity of iron/sulfur enzymes. *Mol. Biol. Cell* **2002**, *13*, 1109–1121. [CrossRef] [PubMed]
74. Bandyopadhyay, S.; Gama, F.; Molina-Navarro, M.M.; Gualberto, J.M.; Claxton, R.; Naik, S.G.; Huynh, B.H.; Herrero, E.; Jacquot, J.P.; Johnson, M.K.; et al. Chloroplast monothiol glutaredoxins as scaffold proteins for the assembly and delivery of [2Fe–2S] clusters. *EMBO J.* **2008**, *27*, 1122–1133. [CrossRef]
75. Gravina, S.A.; Mieyal, J.J. Thioltransferase is a specific glutathionyl mixed disulfide oxidoreductase. *Biochemistry* **1993**, *32*, 3368–3376. [CrossRef]
76. Zahedi Avval, F.; Holmgren, A. Molecular mechanisms of thioredoxin and glutaredoxin as hydrogen donors for Mammalian S phase ribonucleotide reductase. *J. Biol. Chem.* **2009**, *284*, 8233–8240. [CrossRef]
77. Lönn, M.E.; Hudemann, C.; Berndt, C.; Cherkasov, V.; Capani, F.; Holmgren, A.; Lillig, C.H. Expression Pattern of Human Glutaredoxin 2 Isoforms: Identification and Characterization of Two Testis/Cancer Cell-Specific Isoforms. *Antioxid. Redox Signal.* **2008**, *10*, 547–558. [CrossRef]
78. Johansson, C.; Lillig, C.H.; Holmgren, A. Human Mitochondrial Glutaredoxin Reduces S-Glutathionylated Proteins with High Affinity Accepting Electrons from Either Glutathione or Thioredoxin Reductase. *J. Biol. Chem.* **2004**, *279*, 7537–7543. [CrossRef]
79. Lundberg, M.; Johansson, C.; Chandra, J.; Enoksson, M.; Jacobsson, G.; Ljung, J.; Johansson, M.; Holmgren, A. Cloning and expression of a novel human glutaredoxin (Grx2) with mitochondrial and nuclear isoforms. *J. Biol. Chem.* **2001**, *276*, 26269–26275. [CrossRef]
80. Haunhorst, P.; Berndt, C.; Eitner, S.; Godoy, J.R.; Lillig, C.H. Characterization of the human monothiol glutaredoxin 3 (PICOT) as iron-sulfur protein. *Biochem. Biophys. Res. Commun.* **2010**, *394*, 372–376. [CrossRef]
81. Johansson, C.; Roos, A.K.; Montano, S.J.; Sengupta, R.; Filippakopoulos, P.; Guo, K.; Von Delft, F.; Holmgren, A.; Oppermann, U.; Kavanagh, K.L. The crystal structure of human GLRX5: Iron-sulfur cluster co-ordination, tetrameric assembly and monomer activity. *Biochem. J.* **2011**, *433*, 303–311. [CrossRef] [PubMed]
82. Camaschella, C.; Campanella, A.; De Falco, L.; Boschetto, L.; Merlini, R.; Silvestri, L.; Levi, S.; Iolascon, A. The human counterpart of zebrafish shiraz shows sideroblastic-like microcytic anemia and iron overload. *Blood* **2007**, *110*, 1353–1358. [CrossRef] [PubMed]
83. Feng, Y.; Zhong, N.; Rouhier, N.; Hase, T.; Kusunoki, M.; Jacquot, J.P.; Jin, C.; Xia, B. Structural insight into poplar glutaredoxin C1 with a bridging iron-sulfur cluster at the active site. *Biochemistry* **2006**, *45*, 7998–8008. [CrossRef] [PubMed]
84. Rouhier, N.; Unno, H.; Bandyopadhyay, S.; Masip, L.; Kim, S.K.; Hirasawa, M.; Gualberto, J.M.; Lattard, V.; Kusunoki, M.; Knaff, D.B.; et al. Functional, structural, and spectroscopic characterization of a glutathione-ligated [2Fe-2S] cluster in poplar glutaredoxin C1. *Proc. Natl. Acad. Sci. USA* **2007**, *104*, 7379–7384. [CrossRef]
85. Berndt, C.; Hudemann, C.; Hanschmann, E.-M.; Axelsson, R.; Holmgren, A.; Lillig, C.H. How does iron-sulfur cluster coordination regulate the activity of human glutaredoxin 2? *Antioxid. Redox Signal.* **2007**, *9*, 151–157. [CrossRef]
86. Johansson, C.; Kavanagh, K.L.; Gileadi, O.; Oppermann, U. Reversible sequestration of active site cysteines in a 2Fe-2S-bridged dimer provides a mechanism for glutaredoxin 2 regulation in human mitochondria. *J. Biol. Chem.* **2007**, *282*, 3077–3082. [CrossRef]
87. Iwema, T.; Picciocchi, A.; Traore, D.A.K.; Ferrer, J.-L.; Chauvat, F.; Jacquamet, L. Structural Basis for Delivery of the Intact [Fe₂S₂] Cluster by Monothiol Glutaredoxin. *Biochemistry* **2009**, *48*, 6041–6043. [CrossRef]
88. Lepka, K.; Volbracht, K.; Bill, E.; Schneider, R.; Rios, N.; Hildebrandt, T.; Ingwersen, J.; Prozorovski, T.; Lillig, C.H.; van Horssen, J.; et al. Iron-sulfur glutaredoxin 2 protects oligodendrocytes against damage induced by nitric oxide release from activated microglia. *Glia* **2017**, *65*, 1521–1534. [CrossRef]

89. Couturier, J.; Przybyla-Toscano, J.; Roret, T.; Didierjean, C.; Rouhier, N. The roles of glutaredoxins ligating Fe–S clusters: Sensing, transfer or repair functions? *Biochim. Biophys. Acta BBA-Mol. Cell Res.* **2015**, *1853*, 1513–1527. [CrossRef]
90. Li, L.; Cheng, N.; Hirschi, K.D.; Wang, X. Structure of Arabidopsis chloroplastic monothiol glutaredoxin AtGRXcp. *Acta Crystallogr. D Biol. Crystallogr.* **2010**, *66*, 725–732. [CrossRef]
91. Wang, L.; Li, Y.; Jacquot, J.-P.; Rouhier, N.; Xia, B. Characterization of poplar GrxS14 in different structural forms. *Protein Cell* **2014**, *5*, 329–333. [CrossRef]
92. Trnka, D.; Engelke, A.D.; Gellert, M.; Moseler, A.; Hossain, M.F.; Lindenberg, T.T.; Pedroletti, L.; Odermatt, B.; de Souza, J.V.; Bronowska, A.K.; et al. Molecular basis for the distinct functions of redox-active and FeS-transferring glutaredoxins. *Nat. Commun.* **2020**, *11*, 3445. [CrossRef] [PubMed]
93. Liedgens, L.; Zimmermann, J.; Wäschenbach, L.; Geissel, F.; Laporte, H.; Gohlke, H.; Morgan, B.; Deponte, M. Quantitative assessment of the determinant structural differences between redox-active and inactive glutaredoxins. *Nat. Commun.* **2020**, *11*, 1725. [CrossRef] [PubMed]
94. Gladyshev, V.N.; Liu, A.; Novoselov, S.V.; Krysan, K.; Sun, Q.A.; Kryukov, V.M.; Kryukov, G.V.; Lou, M.F. Identification and characterization of a new mammalian glutaredoxin (thioltransferase), Grx2. *J. Biol. Chem.* **2001**, *276*, 30374–30380. [CrossRef] [PubMed]
95. Beer, S.M.; Taylor, E.R.; Brown, S.E.; Dahm, C.C.; Costa, N.J.; Runswick, M.J.; Murphy, M.P. Glutaredoxin 2 catalyzes the reversible oxidation and glutathionylation of mitochondrial membrane thiol proteins: Implications for mitochondrial redox regulation and antioxidant DEFENSE. *J. Biol. Chem.* **2004**, *279*, 47939–47951. [CrossRef]
96. Hudemann, C.; Lönn, M.E.; Godoy, J.R.; Avval, F.Z.; Capani, F.; Holmgren, A.; Lillig, C.H. Identification, expression pattern, and characterization of mouse glutaredoxin 2 isoforms. *Antioxid. Redox Signal.* **2009**, *11*, 1–14. [CrossRef] [PubMed]
97. Scalcon, V.; Tonolo, F.; Folda, A.; Bindoli, A.; Rigobello, M.P. Dimers of glutaredoxin 2 as mitochondrial redox sensors in selenite-induced oxidative stress. *Metallomics* **2019**, *11*, 1241–1251. [CrossRef]
98. Wu, H.; Xing, K.; Lou, M.F. Glutaredoxin 2 prevents H₂O₂-induced cell apoptosis by protecting complex I activity in the mitochondria. *Biochim. Biophys. Acta* **2010**, *1797*, 1705–1715. [CrossRef]
99. Diotte, N.M.; Xiong, Y.; Gao, J.; Chua, B.H.L.; Ho, Y.-S. Attenuation of doxorubicin-induced cardiac injury by mitochondrial glutaredoxin 2. *Biochim. Biophys. Acta* **2009**, *1793*, 427–438. [CrossRef]
100. Enoksson, M.; Fernandes, A.P.; Prast, S.; Lillig, C.H.; Holmgren, A.; Orrenius, S. Overexpression of glutaredoxin 2 attenuates apoptosis by preventing cytochrome c release. *Biochem. Biophys. Res. Commun.* **2005**, *327*, 774–779. [CrossRef]
101. Kanaan, G.N.; Ichim, B.; Gharibeh, L.; Maharsy, W.; Patten, D.A.; Xuan, J.Y.; Reunov, A.; Marshall, P.; Veinot, J.; Menzies, K.; et al. Glutaredoxin-2 controls cardiac mitochondrial dynamics and energetics in mice, and protects against human cardiac pathologies. *Redox Biol.* **2018**, *14*, 509–521. [CrossRef] [PubMed]
102. Young, A.; Gardiner, D.; Kuksal, N.; Gill, R.; O'Brien, M.; Mailloux, R.J. Deletion of the Glutaredoxin-2 Gene Protects Mice from Diet-Induced Weight Gain, Which Correlates with Increased Mitochondrial Respiration and Proton Leaks in Skeletal Muscle. *Antioxid. Redox Signal.* **2019**, *31*, 1272–1288. [CrossRef] [PubMed]
103. Bräutigam, L.; Schütte, L.D.; Godoy, J.R.; Prozorovski, T.; Gellert, M.; Hauptmann, G.; Holmgren, A.; Lillig, C.H.; Berndt, C. Vertebrate-specific glutaredoxin is essential for brain development. *Proc. Natl. Acad. Sci. USA* **2011**, *108*, 20532–20537. [CrossRef] [PubMed]
104. Bräutigam, L.; Jensen, L.D.E.; Poschmann, G.; Nyström, S.; Bannenberg, S.; Dreij, K.; Lepka, K.; Prozorovski, T.; Montano, S.J.; Aktas, O.; et al. Glutaredoxin regulates vascular development by reversible glutathionylation of sirtuin 1. *Proc. Natl. Acad. Sci. USA* **2013**, *110*, 20057–20062. [CrossRef] [PubMed]
105. Berndt, C.; Lillig, C.H.; Holmgren, A. Thiol-based mechanisms of the thioredoxin and glutaredoxin systems: Implications for diseases in the cardiovascular system. *Am. J. Physiol. Heart Circ. Physiol.* **2007**, *292*, H1227–H1236. [CrossRef]
106. Berndt, C.; Poschmann, G.; Stühler, K.; Holmgren, A.; Bräutigam, L. Zebrafish heart development is regulated via glutaredoxin 2 dependent migration and survival of neural crest cells. *Redox Biol.* **2014**, *2*, 673–678. [CrossRef]
107. Gellert, M.; Richter, E.; Mostertz, J.; Kantz, L.; Masur, K.; Hanschmann, E.M.; Ribback, S.; Kroeger, N.; Schaeffeler, E.; Winter, S.; et al. The cytosolic isoform of glutaredoxin 2 promotes cell migration and invasion. *Biochim. Biophys. Acta BBA-Gen. Subj.* **2020**, *1864*, 129599. [CrossRef]

108. Schütte, L.D.; Baumeister, S.; Weis, B.; Hudemann, C.; Hanschmann, E.-M.; Lillig, C.H. Identification of potential protein dithiol-disulfide substrates of mammalian Grx2. *Biochim. Biophys. Acta* **2013**, *1830*, 4999–5005. [CrossRef]
109. Ye, H.; Jeong, S.Y.; Ghosh, M.C.; Kovtunovych, G.; Silvestri, L.; Ortillo, D.; Uchida, N.; Tisdale, J.; Camaschella, C.; Rouault, T.A. Glutaredoxin 5 deficiency causes sideroblastic anemia by specifically impairing heme biosynthesis and depleting cytosolic iron in human erythroblasts. *J. Clin. Investig.* **2010**, *120*, 1749–1761. [CrossRef]
110. Baker, P.R.; Friederich, M.W.; Swanson, M.A.; Shaikh, T.; Bhattacharya, K.; Scharer, G.H.; Aicher, J.; Creadon-Swindell, G.; Geiger, E.; MacLean, K.N.; et al. Variant non ketotic hyperglycinemia is caused by mutations in LIAS, BOLA3 and the novel gene GLRX5. *Brain J. Neurol.* **2014**, *137*, 366–379. [CrossRef]
111. Ciofi-Baffoni, S.; Nasta, V.; Banci, L. Protein networks in the maturation of human iron-sulfur proteins. *Metallomics* **2018**, *10*, 49–72. [CrossRef] [PubMed]
112. Das, D.; Patra, S.; Bridwell-Rabb, J.; Barondeau, D.P. Mechanism of frataxin “bypass” in human iron-sulfur cluster biosynthesis with implications for Friedreich’s ataxia. *J. Biol. Chem.* **2019**, *294*, 9276–9284. [CrossRef] [PubMed]
113. Bonomi, F.; Iametti, S.; Morleo, A.; Ta, D.; Vickery, L.E. Facilitated transfer of IscU-[2Fe2S] clusters by chaperone-mediated ligand exchange. *Biochemistry* **2011**, *50*, 9641–9650. [CrossRef] [PubMed]
114. Uzarska, M.A.; Dutkiewicz, R.; Freibert, S.-A.; Lill, R.; Mühlenhoff, U. The mitochondrial Hsp70 chaperone Ssq1 facilitates Fe/S cluster transfer from Isu1 to Grx5 by complex formation. *Mol. Biol. Cell* **2013**, *24*, 1830–1841. [CrossRef]
115. Olive, J.A.; Cowan, J.A. Role of the HSPA9/HSC20 chaperone pair in promoting directional human iron-sulfur cluster exchange involving monothiol glutaredoxin 5. *J. Inorg. Biochem.* **2018**, *184*, 100–107. [CrossRef]
116. Melber, A.; Na, U.; Vashisht, A.; Weiler, B.D.; Lill, R.; Wohlschlegel, J.A.; Winge, D.R. Role of Nfu1 and Bol3 in iron-sulfur cluster transfer to mitochondrial clients. *Elife* **2016**, *5*, e15991. [CrossRef]
117. Uzarska, M.A.; Nasta, V.; Weiler, B.D.; Spantgar, F.; Ciofi-Baffoni, S.; Saviello, M.R.; Gonnelli, L.; Mühlenhoff, U.; Banci, L.; Lill, R. Mitochondrial Bol1 and Bol3 function as assembly factors for specific iron-sulfur proteins. *Elife* **2016**, *5*, e16673. [CrossRef]
118. Nasta, V.; Giachetti, A.; Ciofi-Baffoni, S.; Banci, L. Structural insights into the molecular function of human [2Fe-2S] BOLA1-GRX5 and [2Fe-2S] BOLA3-GRX5 complexes. *Biochim. Biophys. Acta Gen. Subj.* **2017**, *1861*, 2119–2131. [CrossRef]
119. Kim, K.-D.; Chung, W.-H.; Kim, H.-J.; Lee, K.-C.; Roe, J.-H. Monothiol glutaredoxin Grx5 interacts with Fe-S scaffold proteins Isa1 and Isa2 and supports Fe-S assembly and DNA integrity in mitochondria of fission yeast. *Biochem. Biophys. Res. Commun.* **2010**, *392*, 467–472. [CrossRef]
120. Zinskie, J.A.; Ghosh, A.; Trainor, B.M.; Shedlovskiy, D.; Pestov, D.G.; Shcherbik, N. Iron-dependent cleavage of ribosomal RNA during oxidative stress in the yeast *Saccharomyces cerevisiae*. *J. Biol. Chem.* **2018**, *293*, 14237–14248. [CrossRef]
121. Wingert, R.A.; Galloway, J.L.; Barut, B.; Foott, H.; Fraenkel, P.; Axe, J.L.; Weber, G.J.; Dooley, K.; Davidson, A.J.; Schmidt, B.; et al. Deficiency of glutaredoxin 5 reveals Fe-S clusters are required for vertebrate haem synthesis. *Nature* **2005**, *436*, 1035–1039. [CrossRef] [PubMed]
122. Fidai, I.; Wachnowsky, C.; Cowan, J.A. Mapping cellular Fe-S cluster uptake and exchange reactions-divergent pathways for iron-sulfur cluster delivery to human ferredoxins. *Met. Integr. Biometal. Sci.* **2016**, *8*, 1283–1293. [CrossRef] [PubMed]
123. Sen, S.; Hendricks, A.L.; Cowan, J.A. Cluster exchange reactivity of [2Fe-2S]-bridged heterodimeric BOLA1-GLRX5. *FEBS J.* **2020**. [CrossRef] [PubMed]
124. Sen, S.; Rao, B.; Wachnowsky, C.; Cowan, J.A. Cluster exchange reactivity of [2Fe-2S] cluster-bridged complexes of BOLA3 with monothiol glutaredoxins. *Met. Integr. Biometal. Sci.* **2018**, *10*, 1282–1290. [CrossRef]
125. Banci, L.; Ciofi-Baffoni, S.; Gajda, K.; Muzzioli, R.; Peruzzini, R.; Winkelmann, J. N-terminal domains mediate [2Fe-2S] cluster transfer from glutaredoxin-3 to anamorsin. *Nat. Chem. Biol.* **2015**, *11*, 772–778. [CrossRef]
126. Nasta, V.; Suraci, D.; Gourdoups, S.; Ciofi-Baffoni, S.; Banci, L. A pathway for assembling [4Fe-4S]²⁺ clusters in mitochondrial iron-sulfur protein biogenesis. *FEBS J.* **2020**, *287*, 2312–2327. [CrossRef]
127. Brancaccio, D.; Gallo, A.; Piccioli, M.; Novellino, E.; Ciofi-Baffoni, S.; Banci, L. [4Fe-4S] Cluster Assembly in Mitochondria and Its Impairment by Copper. *J. Am. Chem. Soc.* **2017**, *139*, 719–730. [CrossRef]

128. Wachnowsky, C.; Fidai, I.; Cowan, J.A. Cytosolic iron-sulfur cluster transfer—a proposed kinetic pathway for reconstitution of glutaredoxin 3. *FEBS Lett.* **2016**, *590*, 4531–4540. [CrossRef]
129. Wachnowsky, C.; Liu, Y.; Yoon, T.; Cowan, J.A. Regulation of human Nfu activity in Fe-S cluster delivery—characterization of the interaction between Nfu and the HSPA9/Hsc20 chaperone complex. *FEBS J.* **2018**, *285*, 391–410. [CrossRef]
130. Mapolelo, D.T.; Zhang, B.; Randeniya, S.; Albetel, A.N.; Li, H.; Couturier, J.; Outten, C.E.; Rouhier, N.; Johnson, M.K. Monothiol glutaredoxins and A-type proteins: Partners in Fe-S cluster trafficking. *Dalton Trans. Camb. Engl. 2003* **2013**, *42*, 3107–3115. [CrossRef]
131. Shakamuri, P.; Zhang, B.; Johnson, M.K. Monothiol glutaredoxins function in storing and transporting [Fe₂S₂] clusters assembled on IscU scaffold proteins. *J. Am. Chem. Soc.* **2012**, *134*, 15213–15216. [CrossRef] [PubMed]
132. Moseler, A.; Aller, I.; Wagner, S.; Nietzel, T.; Przybyla-Toscano, J.; Mühlenhoff, U.; Lill, R.; Berndt, C.; Rouhier, N.; Schwarzländer, M.; et al. The mitochondrial monothiol glutaredoxin S15 is essential for iron-sulfur protein maturation in *Arabidopsis thaliana*. *Proc. Natl. Acad. Sci. USA* **2015**, *112*, 13735–13740. [CrossRef] [PubMed]
133. Outten, C.E.; Albetel, A.-N. Iron sensing and regulation in *Saccharomyces cerevisiae*: Ironing out the mechanistic details. *Curr. Opin. Microbiol.* **2013**, *16*, 662–668. [CrossRef] [PubMed]
134. Mühlenhoff, U.; Hoffmann, B.; Richter, N.; Rietzschel, N.; Spantgar, F.; Stehling, O.; Uzarska, M.A.; Lill, R. Compartmentalization of iron between mitochondria and the cytosol and its regulation. *Eur. J. Cell Biol.* **2015**, *94*, 292–308. [CrossRef] [PubMed]
135. Stanchi, F.; Bertocco, E.; Toppo, S.; Dioguardi, R.; Simionati, B.; Cannata, N.; Zimbello, R.; Lanfranchi, G.; Valle, G. Characterization of 16 novel human genes showing high similarity to yeast sequences. *Yeast Chichester Engl.* **2001**, *18*, 69–80. [CrossRef]
136. Witte, S.; Villalba, M.; Bi, K.; Liu, Y.; Isakov, N.; Altman, A. Inhibition of the c-Jun N-terminal kinase/AP-1 and NF-kappaB pathways by PICOT, a novel protein kinase C-interacting protein with a thioredoxin homology domain. *J. Biol. Chem.* **2000**, *275*, 1902–1909. [CrossRef]
137. Godoy, J.R.; Funke, M.; Ackermann, W.; Haunhorst, P.; Oesteritz, S.; Capani, F.; Elsässer, H.P.; Lillig, C.H. Redox atlas of the mouse. Immunohistochemical detection of glutaredoxin-, peroxiredoxin-, and thioredoxin-family proteins in various tissues of the laboratory mouse. *Biochim. Biophys. Acta* **2011**, *1810*, 2–92. [CrossRef]
138. Lange, H.; Mühlenhoff, U.; Denzel, M.; Kispal, G.; Lill, R. The heme synthesis defect of mutants impaired in mitochondrial iron-sulfur protein biogenesis is caused by reversible inhibition of ferrochelatase. *J. Biol. Chem.* **2004**, *279*, 29101–29108. [CrossRef]
139. Cha, H.; Kim, J.M.; Oh, J.G.; Jeong, M.H.; Park, C.S.; Park, J.; Jeong, H.J.; Park, B.K.; Lee, Y.H.; Jeong, D.; et al. PICOT is a critical regulator of cardiac hypertrophy and cardiomyocyte contractility. *J. Mol. Cell. Cardiol.* **2008**, *45*, 796–803. [CrossRef]
140. Jeong, D.; Cha, H.; Kim, E.; Kang, M.; Yang, D.K.; Kim, J.M.; Yoon, P.O.; Oh, J.G.; Bernecker, O.Y.; Sakata, S. PICOT inhibits cardiac hypertrophy and enhances ventricular function and cardiomyocyte contractility. *Circ. Res.* **2006**, *99*, 307–314. [CrossRef]
141. Steiner, R.; Vogel, H. On the kinetics of erythroid cell differentiation in fetal mice. I. Microspectrophotometric determination of the hemoglobin content in erythroid cells during gestation. *J. Cell. Physiol.* **1973**, *81*, 323–338. [CrossRef] [PubMed]
142. Brotherton, T.W.; Chui, D.H.; Gaudie, J.; Patterson, M. Hemoglobin ontogeny during normal mouse fetal development. *Proc. Natl. Acad. Sci. USA* **1979**, *76*, 2853–2857. [CrossRef] [PubMed]
143. Ye, H.; Rouault, T.A. Human iron-sulfur cluster assembly, cellular iron homeostasis, and disease. *Biochemistry* **2010**, *49*, 4945–4956. [CrossRef] [PubMed]
144. Rajagopalan, B.; Francis, J.M.; Cooke, F.; Korlipara, L.P.; Blamire, A.M.; Schapira, A.H.; Madan, J.; Neubauer, S.; Cooper, J.M. Analysis of the factors influencing the cardiac phenotype in Friedreich’s ataxia. *Mov. Disord.* **2010**, *25*, 846–852. [CrossRef]
145. Huynen, M.A.; Spronk, C.A.E.M.; Gabaldón, T.; Snel, B. Combining data from genomes, Y2H and 3D structure indicates that BolA is a reductase interacting with a glutaredoxin. *FEBS Lett.* **2005**, *579*, 591–596. [CrossRef]

146. Li, H.; Mapolelo, D.T.; Dingra, N.N.; Keller, G.; Riggs-Gelasco, P.J.; Winge, D.R.; Johnson, M.K.; Outten, C.E. Histidine 103 in Fra2 is an iron-sulfur cluster ligand in the [2Fe-2S] Fra2-Grx3 complex and is required for in vivo iron signaling in yeast. *J. Biol. Chem.* **2011**, *286*, 867–876. [CrossRef]
147. Li, H.; Mapolelo, D.T.; Dingra, N.N.; Naik, S.G.; Lees, N.S.; Hoffman, B.M.; Riggs-Gelasco, P.J.; Huynh, B.H.; Johnson, M.K.; Outten, C.E. The Yeast Iron Regulatory Proteins Grx3/4 and Fra2 Form Heterodimeric Complexes Containing a [2Fe-2S] Cluster with Cysteinylyl and Histidyl Ligation. *Biochemistry* **2009**, *48*, 9569–9581. [CrossRef]
148. Poor, C.B.; Wegner, S.V.; Li, H.; Dlouhy, A.C.; Schuermann, J.P.; Sanishvili, R.; Hinshaw, J.R.; Riggs-Gelasco, P.J.; Outten, C.E.; He, C. Molecular mechanism and structure of the *Saccharomyces cerevisiae* iron regulator Aft2. *Proc. Natl. Acad. Sci. USA* **2014**, *111*, 4043–4048. [CrossRef]
149. Li, H.; Outten, C.E. The conserved CDC motif in the yeast iron regulator Aft2 mediates iron–sulfur cluster exchange and protein–protein interactions with Grx3 and Bol2. *JBIC J. Biol. Inorg. Chem.* **2019**, *24*, 809–815. [CrossRef]
150. Encinar del Dedo, J.; Gabrielli, N.; Carmona, M.; Ayté, J.; Hidalgo, E. A Cascade of Iron-Containing Proteins Governs the Genetic Iron Starvation Response to Promote Iron Uptake and Inhibit Iron Storage in Fission Yeast. *PLoS Genet.* **2015**, *11*, e1005106. [CrossRef]
151. Lill, R.; Freibert, S.-A. Mechanisms of Mitochondrial Iron-Sulfur Protein Biogenesis. *Annu. Rev. Biochem.* **2020**, *89*, 471–499. [CrossRef]
152. Liu, T.; Zhang, M.; Terry, M.H.; Schroeder, H.; Wilson, S.M.; Power, G.G.; Li, Q.; Tipple, T.E.; Borchardt, D.; Blood, A.B. Hemodynamic Effects of Glutathione-Liganded Binuclear Dinitrosyl Iron Complex: Evidence for Nitroxyl Generation and Modulation by Plasma Albumin. *Mol. Pharmacol.* **2018**, *93*, 427–437. [CrossRef] [PubMed]
153. Vanin, A.F. Dinitrosyl iron complexes with thiolate ligands: Physico-chemistry, biochemistry and physiology. *Nitric Oxide Biol. Chem.* **2009**, *21*, 1–13. [CrossRef] [PubMed]
154. Borodulin, R.R.; Dereven'kov, I.A.; Burbaev, D.S.; Makarov, S.V.; Mikoyan, V.D.; Serezhenkov, V.A.; Kubrina, L.N.; Ivanovic-Burmazovic, I.; Vanin, A.F. Redox activities of mono- and binuclear forms of low-molecular and protein-bound dinitrosyl iron complexes with thiol-containing ligands. *Nitric Oxide Biol. Chem.* **2014**, *40*, 100–109. [CrossRef] [PubMed]
155. Vanin, A.F. Dinitrosyl iron complexes with thiol-containing ligands as a “working form” of endogenous nitric oxide. *Nitric Oxide* **2016**, *54*, 15–29. [CrossRef] [PubMed]
156. Landry, A.P.; Duan, X.; Huang, H.; Ding, H. Iron-sulfur proteins are the major source of protein-bound dinitrosyl iron complexes formed in *Escherichia coli* cells under nitric oxide stress. *Free Radic. Biol. Med.* **2011**, *50*, 1582–1590. [CrossRef]
157. Foster, M.W.; Hess, D.T.; Stamler, J.S. Protein S-nitrosylation in health and disease: A current perspective. *Trends Mol. Med.* **2009**, *15*, 391–404. [CrossRef]
158. Chen, S.C.; Huang, B.; Liu, Y.C.; Shyu, K.G.; Lin, P.Y.; Wang, D.L. Acute hypoxia enhances proteins' S-nitrosylation in endothelial cells. *Biochem. Biophys. Res. Commun.* **2008**, *377*, 1274–1278. [CrossRef]
159. Murray, C.I.; Uhrigshardt, H.; O'Meally, R.N.; Cole, R.N.; Van Eyk, J.E. Identification and quantification of S-nitrosylation by cysteine reactive tandem mass tag switch assay. *Mol. Cell. Proteom. MCP* **2012**, *11*, M111.013441. [CrossRef]
160. Qu, Z.; Greenlief, C.M.; Gu, Z. Quantitative Proteomic Approaches for Analysis of Protein S-Nitrosylation. *J. Proteome Res.* **2016**, *15*, 1–14. [CrossRef]
161. Anand, P.; Stamler, J.S. Enzymatic mechanisms regulating protein S-nitrosylation: Implications in health and disease. *J. Mol. Med. Berl. Ger.* **2012**, *90*, 233–244. [CrossRef] [PubMed]
162. Borodulin, R.R.; Kubrina, L.N.; Mikoyan, V.D.; Poltorakov, A.P.; Shvydkiy, V.O.; Burbaev, D.S.; Serezhenkov, V.A.; Yakhontova, E.R.; Vanin, A.F. Dinitrosyl iron complexes with glutathione as NO and NO⁺ donors. *Nitric Oxide* **2013**, *29*, 4–16. [CrossRef] [PubMed]
163. Heinrich, T.A.; da Silva, R.S.; Miranda, K.M.; Switzer, C.H.; Wink, D.A.; Fukuto, J.M. Biological nitric oxide signalling: Chemistry and terminology. *Br. J. Pharmacol.* **2013**, *169*, 1417–1429. [CrossRef] [PubMed]
164. Martínez-Ruiz, A.; Lamas, S. Detection and proteomic identification of S-nitrosylated proteins in endothelial cells. *Arch. Biochem. Biophys.* **2004**, *423*, 192–199. [CrossRef] [PubMed]

165. Truzzi, D.R.; Alves, S.V.; Netto, L.E.S.; Augusto, O. The Peroxidatic Thiol of Peroxiredoxin 1 is Nitrosated by Nitrosoglutathione but Coordinates to the Dinitrosyl Iron Complex of Glutathione. *Antioxidants* **2020**, *9*, 276. [CrossRef]
166. Chazov, E.I.; Rodnenkov, O.V.; Zorin, A.V.; Lakomkin, V.L.; Gramovich, V.V.; Vyborov, O.N.; Dragnev, A.G.; Timoshin, A.A.; Buryachkovskaya, L.I.; Abramov, A.A.; et al. Hypotensive effect of Oxacom[®] containing a dinitrosyl iron complex with glutathione: Animal studies and clinical trials on healthy volunteers. *Nitric Oxide* **2012**, *26*, 148–156. [CrossRef]
167. Akentieva, N.P.; Sanina, N.A.; Gizatullin, A.R.; Shkondina, N.I.; Prikhodchenko, T.R.; Shram, S.I.; Zhelev, N.; Aldoshin, S.M. Cytoprotective Effects of Dinitrosyl Iron Complexes on Viability of Human Fibroblasts and Cardiomyocytes. *Front. Pharmacol.* **2019**, *10*, 1277. [CrossRef]
168. Giliano, N.Y.; Konevega, L.V.; Noskin, L.A.; Serezhenkov, V.A.; Poltorakov, A.P.; Vanin, A.F. Dinitrosyl iron complexes with thiol-containing ligands and apoptosis: Studies with HeLa cell cultures. *Nitric Oxide Biol. Chem.* **2011**, *24*, 151–159. [CrossRef]
169. Hou, J.; He, H.; Huang, S.; Qian, M.; Wang, J.; Tan, X.; Han, G.; Song, Y.; Xu, Z.; Liu, Y. A mitochondria-targeted nitric oxide donor triggered by superoxide radical to alleviate myocardial ischemia/reperfusion injury. *Chem. Commun.* **2019**, *55*, 1205–1208. [CrossRef]
170. Burgova, E.N.; Tkachev, N.A.; Adamyan, L.V.; Mikoyan, V.D.; Paklina, O.V.; Stepanyan, A.A.; Vanin, A.F. Dinitrosyl iron complexes with glutathione suppress experimental endometriosis in rats. *Eur. J. Pharmacol.* **2014**, *727*, 140–147. [CrossRef]
171. Pisarenko, O.I.; Serebryakova, L.I.; Tskitishvili, O.V.; Studneva, I.M.; Vanin, A.F.; Chazov, E.I. Cardioprotective efficacy of dinitrosyl iron complex with L-cysteine in rats in vivo. *Biol. Bull.* **2008**, *35*, 95–98. [CrossRef]
172. Mordvintsev, P.I.; Rudneva, V.G.; Vanin, A.F.; Shimkevich, L.L.; Khodorov, B.I. Inhibition of platelet aggregation by dinitrosyl iron complexes with low molecular weight ligands. *Biokhimiia Mosc. Russ.* **1986**, *51*, 1851–1857.



© 2020 by the authors. Licensee MDPI, Basel, Switzerland. This article is an open access article distributed under the terms and conditions of the Creative Commons Attribution (CC BY) license (<http://creativecommons.org/licenses/by/4.0/>).

Article

Profiling the Concentration of Reduced and Oxidized Glutathione in Rat Brain Using HPLC/DAD Chromatographic System

George Jitcă ^{1,2}, Erzsébet Fogarasi ^{3,*}, Bianca-Eugenia Ósz ¹, Camil Eugen Vari ¹, Ibolya Fülöp ³, Mircea Dumitru Croitoru ³, Carmen Maria Rusz ² and Maria Titica Dogaru ¹

¹ Department of Pharmacology and Clinical Pharmacy, Faculty of Pharmacy, George Emil Palade University of Medicine, Pharmacy, Science and Technology of Târgu Mureş, 540139 Târgu Mureş, Romania; george.jitca@umfst.ro (G.J.); bianca.osz@umfst.ro (B.-E.Ó.); camil.vari@umfst.ro (C.E.V.); maria_dogaru2004@yahoo.com (M.T.D.)

² Doctoral School of Medicine and Pharmacy, I.O.S.U.D., George Emil Palade University of Medicine, Pharmacy, Science and Technology of Târgu Mureş, 540139 Târgu Mureş, Romania; carmenrusz20@gmail.com

³ Department of Toxicology and Biopharmacy, Faculty of Pharmacy, George Emil Palade University of Medicine, Pharmacy, Science and Technology of Târgu Mureş, 540139 Târgu Mureş, Romania; ibolya.fulop@umfst.ro (I.F.); mircea.croitoru@umfst.ro (M.D.C.)

* Correspondence: erzsebet.fogarasi@umfst.ro

Abstract: This study aimed to develop a HPLC/DAD method in order to determine and quantify the reduced glutathione (GSH) and oxidized glutathione (GSSG) levels in rat brain. Due to the presence of the thiol group (-SH), GSH can interact with the Ellman's reagent (DTNB), with which it forms a reaction product through which the level of GSH can be quantified, using the DAD detection system. Chromatographic separation was achieved after a derivatization process by using a mobile phase acetonitrile (A) and phosphate buffer (20 mM, pH = 2.5) (B). The compounds of interest were detected at 330 nm using a chromatographic C8 column. The method of determination met the validation criteria, specified by the regulatory bodies. The applicability of the method was demonstrated in a chronic toxicology study of central nervous system (CNS), following different treatment regimens with haloperidol.

Keywords: oxidative stress; glutathione; brain; liquid chromatography; diode array detector

Citation: Jitcă, G.; Fogarasi, E.; Ósz, B.-E.; Vari, C.E.; Fülöp, I.; Croitoru, M.D.; Rusz, C.M.; Dogaru, M.T. Profiling the Concentration of Reduced and Oxidized Glutathione in Rat Brain Using HPLC/DAD Chromatographic System. *Molecules* **2021**, *26*, 6590. <https://doi.org/10.3390/molecules26216590>

Academic Editor: Marcello Locatelli

Received: 30 September 2021

Accepted: 29 October 2021

Published: 30 October 2021

Publisher's Note: MDPI stays neutral with regard to jurisdictional claims in published maps and institutional affiliations.



Copyright: © 2021 by the authors. Licensee MDPI, Basel, Switzerland. This article is an open access article distributed under the terms and conditions of the Creative Commons Attribution (CC BY) license (<https://creativecommons.org/licenses/by/4.0/>).

1. Introduction

Glutathione (GSH) is a tripeptide (L- γ -glutamyl-L-cysteinyl-glycine) that exhibits many biological roles, including the protection against reactive oxygen and nitrogen species (ROS and RNS). Thus, the GSH antioxidant pathway is one of the most important and well-represented components of the endogenous antioxidant system [1]. At the same time, the cysteine residue, reactive thiol (-SH) group, present in its chemical structure, is responsible for the antioxidant effect by neutralizing the ROS and RNS [2,3].

GSH is involved in many processes, such as defense and preservation of the organism, prevention or delay of age-related diseases onset, given the proportional increase of free radicals with aging [4]. It is found mainly in its reduced form (GSH) because the enzyme responsible for converting the oxidized form (GSSG) is induced by oxidative stress. Therefore, GSH/ GSSG ratio is considered an indicator of oxidative status [5,6]. It has been observed that the inherited enzyme defects related to GSH are very rare; in contrast, the imbalances in GSH homeostasis associated with the increase of the oxidative stress levels in central nervous system (CNS) are common in neurodegenerative diseases [7].

Low levels of GSH/ GSSG ratio are incriminated in the onset of diseases such as cancers [8,9], diabetes [10], CNS disorders: Parkinson's, Alzheimer's disease [11–13], or disorders that appear following psychotropic drug abuse [14]. GSH also accomplishes

a variety of functions at cellular level, which could explain the correlation between the depletion of this antioxidant molecule and the pathogenesis of neurodegenerative diseases.

In order to determine the concentrations of GSH, different analytical methods were applied: spectrophotometry [15], liquid chromatography tandem mass spectrometry (LC-MS) [16], or gas chromatography-mass spectrometry (GC-MS) [17]. Despite their advantages in terms of preparation time or analysis speed, there are important disadvantages that cannot be disregarded: lack of specificity (spectrophotometry) or high costs.

Along with malondialdehyde, which is another important marker of oxidative stress [18], the quantification of GSH/GSSG ratio can be used in estimating the oxidative status in multiple genetic or drug-induced diseases. To avoid the bias generated by the interaction between Ellman's reagent (5,5'-dithio-bis(2-nitrobenzoic) acid, DTNB) and another molecule (cysteine), and with the attempt to obtain as close GSH and GSSG values as the real ones, this study aims to validate a simple method of determination of GSH and GSSG levels in brain, with applicability in preclinical studies.

The chromatographic analysis of the analytes resulting from GSH with DTNB reaction (Figure 1) was performed with a high-performance liquid chromatographic (HPLC) system coupled with a diode array detector (HPLC/DAD). The main disadvantage of the photometric technique, frequently employed for the GSH measurement in biological samples, is the lack of specificity, because other thiol containing molecules, such as cysteine for example, could lead to false readings [19]. Furthermore, in photometric techniques it is difficult to obtain a high-quality blank, since both the reagent used and the sample can have a certain interfering color. Another disadvantage of the photometry used for GSH measurements is the low detectability, along with a narrow limit of concentrations that can precisely and accurately be measured. Due to these reasons, a chromatographic technique, such as the HPLC, could solve these problems by improving the detectability and the concentration range that can be used without further sample preparation process (dilution for example). Furthermore, with the possibility of separating interfering substances and the use of DAD "peak purity" test, the specificity could also be increased. From Figure 1 it can be seen that thiol interference could not be also avoided by HPLC, if the 2-Nitro-5-mercapto-benzoic acid (NMB) is measured as in the photometric technique. However, by following the GSH-DTNB peak, which lacks visible light absorption but has UV light absorption properties, a very good specificity could be attained, since even thiol interference could be avoided by chromatographic separation.

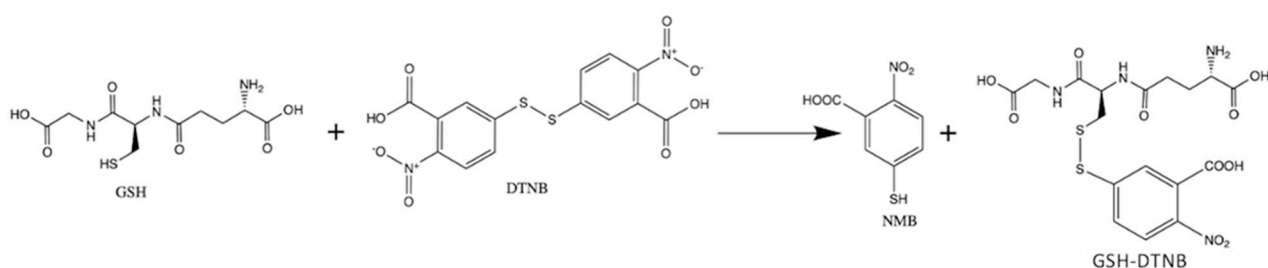


Figure 1. Reaction of Glutathione (GSH) with Ellman's reagent/ DTNB (5,5'-dithio-bis-(2-nitrobenzoic acid)); 2-Nitro-5-mercapto-benzoic acid (NMB).

Indeed, more time and higher costs could be needed for the chromatographic technique, but the significant improvement in the detectability, concentration, and the possibility to detect a GSH specific compound rather than a -SH specific compound justifies the importance of this research.

2. Results

In this analytical method, validation parameters are represented by: linearity, selectivity, accuracy, precision, lower limit of quantification (LLOQ), stability, and robustness.

All of these parameters were verified in accordance with the guidelines presented by the regulatory bodies (FDA 2018) [20].

2.1. Chromatographic Conditions

The chromatographic separation of GSH, after GSH derivatization, was evaluated by using a mobile phase consisted of acetonitrile (A) and phosphate buffer (20 mM, pH = 2.5) (B). The elution gradient is presented in Table 1. The injection volume was 50 μ L and a retention time of 6.22 ± 0.06 was obtained. The flow rate was set at 1 mL/min and the analytes were detected at 330 nm by a DAD (range: 200–700 nm) detector using a chromatographic column Zorbax Eclipse XDB-C8, 5 μ m, 4.6×150 mm. The GSH-DTNB reaction occurs at room temperature in 10 min. The reduction of GSSG occurs at 80 °C after 60 min of incubation in the presence of DTNB.

Table 1. Brief presentation of the mobile phase elution gradient program.

Time (min)	Phosphate Buffer, 20 mM, pH = 2.5 (%)	Acetonitrile (%)	Flow (mL/min)
0	98	2	1
19	50	50	1
19.1	98	2	1
21	98	2	1

2.2. Linearity and LLOQ

The linearity of the method was verified using an analytical curve on seven concentration levels, evaluated in triplicates. The derivatization reaction was performed for each level of concentration used for the analytical curve. The analytical curve for the GSH is described by the linear equation: $y = 1562x - 350.11$ with a determination coefficient $r^2 = 0.997$ (Figure 2A), while analytical curve for GSSG is described by the linear equation: $y = 2124.4x - 1493.4$, and $r^2 = 0.996$ (Figure 2B). y represents the analyte peak area and x is the concentration, as shown in Table 2.

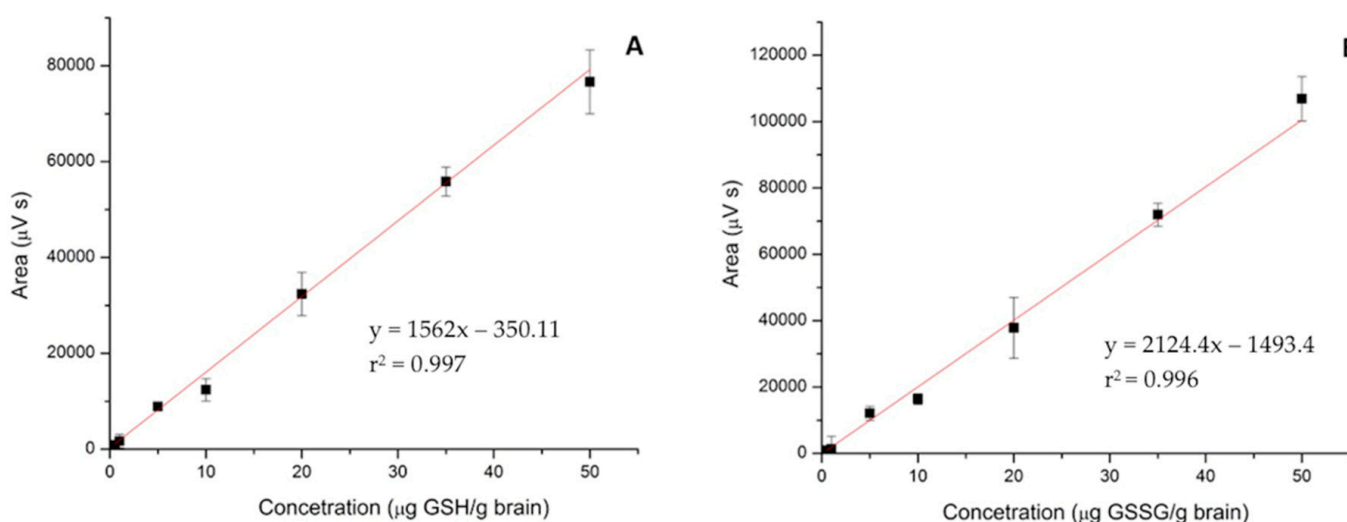


Figure 2. Analytical curves for reduced (GSH) (A) and oxidized glutathione (GSSG) (B) in the range 0.5–50 μ g/g brain.

Table 2. Validation results of the analytical factors of HPLC method.

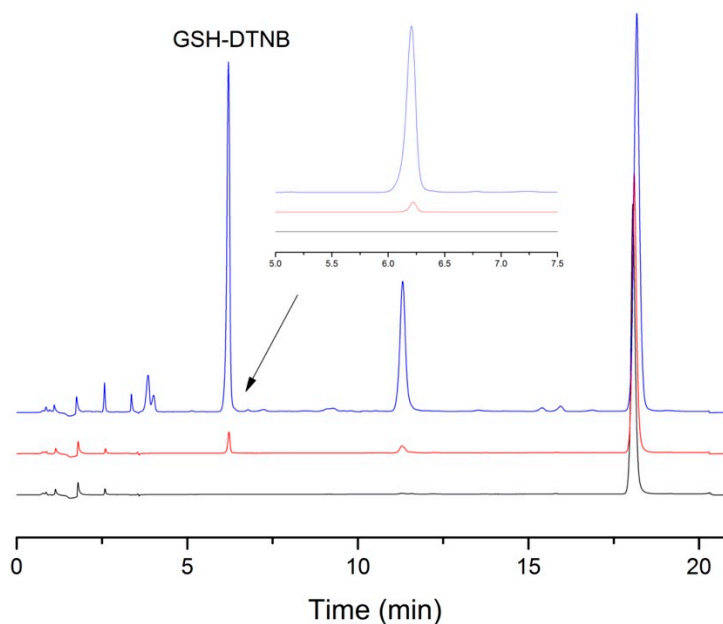
Analytical Factor	GSH	GSSG
LLOQ ($\mu\text{g/g}$ brain)	0.50	
rLLOQ (%)	97.11	98.86
LLOQrec ($\mu\text{g/g}$ brain)	0.50	0.50
rLLOQrec (%)	85.47	108.78
Slope	1562	2124.4
Y-intercept	−350.11	−1493.4
Determination coefficient (r^2)	0.997	0.996
Analytical range ($\mu\text{g/g}$ brain)	0.50–50	
Retention time	6.22 ± 0.06	

rLLOQ, relative lower limit of quantification; LLOQrec, recovery corrected LLOQ; rLLOQrec (%), relative recovery-corrected LLOQ;

2.3. Selectivity

In order to verify the selectivity, three samples were injected, prepared in triplicates according to the procedure described in Section 4.3. Sample preparation with the following modification: DTNB without GSH, DTNB with GSH, and brain sample with GSH and DTNB. At the retention time of the GSH-DTNB complex there are no overlapping peaks; the peak of interest has a corresponding purity, as can be seen in Figure 3.

- Ellman's reagent - reagent blank
- Ellman's reagent + GSH dissolved in water (corresponding to a final concentration of $5 \mu\text{g/g}$ brain)
- Ellman's reagent + brain spiked with GSH to form a final concentration of $5 \mu\text{g/g}$

**Figure 3.** Representative chromatograms of a spiked rat brain sample.

2.4. Accuracy

Quality control (QC) samples at LLOQ concentration were spiked in order to determine accuracy and precision. For each QC level, five replicates were analyzed in one run for the intra-day procedure.

Accuracy was evaluated based on GSH percentage and GSSG percentage recovered from the matrix. Results of accuracy for the intra- and inter-day precision for GSH and GSSG at LLOQ and QC levels are presented in Table 3.

Table 3. Accuracy and precision of reduced glutathione (GSH) and oxidized glutathione (GSSG) in lower limits of quantification and quality control samples.

Conc. ($\mu\text{g/g Brain}$)	Intra-Day			Inter-Day			
	Mean	RSD %	Accuracy %	Mean	RSD %	Accuracy %	
GSH	0.5	0.57	1.47	113.62	0.57	1.62	113.85
	15	14.27	6.73	95.15	13.28	6.56	88.54
	40	45.12	7.69	112.79	45.33	7.04	113.32
GSSG	0.5	0.45	0.15	90.88	0.49	9.74	97.45
	15	16.73	3.33	111.55	15.72	14.52	104.81
	40	44.03	5.79	110.08	42.48	13.38	106.20

2.5. Precision

Concerning the evaluation of inter-day precision, it has been evaluated in two different days, using five replicates for each QC level and at LLOQ concentration, respectively. The intra- and inter-day precision results were expressed as RSD%. The results for GSH and GSSG at LLOQ and three QC levels are presented in Table 3.

Both for intra- and inter-day analysis, the precision (RSD%) of QC samples was $\leq 15\%$ and the accuracy ranged $\pm 15\%$. These results demonstrated the fact that the method is reproducible for the determination of GSH and GSSG in rodent's brain, considering that accuracy and precision were found to be within acceptable limits.

2.6. Stability

The stability of the QC samples was stored at room temperature for 12 h and 24 h, respectively, both in five replicates was assessed; brain samples were stored at $-80\text{ }^{\circ}\text{C}$ prior to the analysis. For GSH samples, the analytical recovery varied between 87.18–114.78% after 12 h and between 94.86–118.29% after 24 h at room temperature ($25\text{ }^{\circ}\text{C}$). For GSSG samples, the analytical recovery varied between 87.88–111.45% after 12 h. The results are illustrated in Table 4.

Table 4. Stability assessment for samples stored at room temperature for 12 and 24 h, respectively.

Parameters	Stability for Samples Stored at Room Temperature						
	Conc. ($\mu\text{g/g Brain}$)						
	0.5		15		40		
		12 h	24 h	12 h	24 h	12 h	24 h
GSH	Mean	0.63	0.54	16.39	16.89	39.34	43.97
	Rec *, %	110.04	94.86	114.78	118.29	87.18	97.44
	RSD%	4.92	10.17	5.41	0.34	12.23	2.26
GSSG	Mean	0.51	-	14.71	-	87.88	-
	Rec *, %	111.45	-	87.88	-	92.93	-
	RSD%	0.52	-	4.27	-	8.33	-

* Recovery, average of three concentrations.

2.7. Robustness

The robustness of the method was evaluated with the performance of variations in two important chromatographic parameters: mobile phase pH and flow rate, which were modified throughout the analysis. All of the tests were performed at three levels of concentration of 0.5, 15, and 40 $\mu\text{g/g}$ for GSH in five replicates. Results are listed in Table 5.

Table 5. Robustness of the method by variation of two chromatographic parameters (mobile phase ratio and mobile phase pH value).

	Conc. ($\mu\text{g/g Brain}$)	Retention Time (min) \pm RSD, %	Peak Purity (%) \pm RSD, %
Mobile phase pH value			
2.3	0.5	6.95 \pm 0.06	99.25 \pm 1.12
	15	6.95 \pm 0.05	98.03 \pm 2.12
	40	6.95 \pm 0.04	98.16 \pm 0.99
2.5	0.5	6.24 \pm 0.03	96.42 \pm 1.22
	15	6.21 \pm 0.08	99.81 \pm 0.78
	40	6.21 \pm 0.06	99.68 \pm 0.73
2.7	0.5	6.96 \pm 0.04	98.16 \pm 1.36
	15	6.95 \pm 0.03	98.98 \pm 1.43
	40	6.95 \pm 0.09	98.64 \pm 2.43
Flow (mL/min)			
0.9	0.5	7.80 \pm 0.02	98.37 \pm 1.27
	15	7.78 \pm 0.10	99.17 \pm 2.54
	40	7.77 \pm 0.09	98.98 \pm 2.77
1.0	0.5	6.24 \pm 0.05	99.36 \pm 2.44
	15	6.21 \pm 0.05	98.13 \pm 1.87
	40	6.21 \pm 0.08	99.07 \pm 2.89
1.1	0.5	6.72 \pm 0.06	99.15 \pm 1.72
	15	6.68 \pm 0.03	99.67 \pm 1.99
	40	6.64 \pm 0.03	98.17 \pm 2.48

3. Discussion

Measurement of GSH in biological samples is of high importance in the study of oxidative stress and exogenous substances or pathological conditions associated with oxidative state [21,22].

It is well known that GSH has a low stability in the biological samples, because after the blood or the tissue is devoided by the normal oxygen supply, reactive species are formed, and those species could quickly oxidize the available reduced glutathione (GSH). This process makes the measurement of GSH in biological samples a challenge. Frequently, GSH is photometrically measured following a derivatization with the Ellman's reagent that forms a non-specific colored compound with the thiol groups [23]. Due to this fact, one can be certain on measuring thiol groups, not only GSH. In our paper, we developed an HPLC-UV method that was able to detect not the generally formed colored compound by the thiol groups with the Ellman's reagent, but the non-colored but UV absorbing compound formed after this reaction.

Our method has significant advantages over the most commonly used photometric method in the following parameters:

- specificity: using photometry we can be sure about the thiol molecule content of the sample, not GSH in a specific way. Furthermore, photometry does not easily allow a double blank: native color of the sample + native color of the reagents. This problem can be achieved by column separation;
- detectability: lower limits of GSH can be detected by the use of the HPLC method;

The increased temperature leads to the reduction of oxidized glutathione (GSSG), and reaction of the newly formed GSH with the Ellman's reagent is possible by reacting the brain sample with the Ellman's reagent at room temperature and high temperature (about 80 °C) to measure the GSSG content of the sample. This is an important step in evaluating the oxidative stress level, not because the absolute value of the GSH and GSSG is important but because of the ratio of the two components [24]. After the method development, on a number of 40 rats we measured the native GSH and GSSG content and the GSH/GSSG ratio.

The performance of the analytical method (validation) was measured according to international requirements [20]; therefore, one can consider valid any brain GSH/GSSG evaluation made with our method.

Indeed, sample preparation in the HPLC technique is not less time consuming than the photometric method, but is certainly less “sample consuming”. This makes room for analysis of very low quantity samples. Furthermore, the more time needed for the chromatographic analysis compared with the very fast and easy reading on a photometer is well compensated by the increased specificity and detectability that we have shown during our method validation.

GSSG does not react with Elman’s reagent directly. However, at high temperature (80 °C), Elman’s reagent reduces GSSG to GSH, and then the same reaction as in the case of GSH–Ellman’s reagent occurs. The reduction ratio of GSSG to GSH has high importance when GSSG is desired to be measured in biological samples. Reduction ratio of GSSG to GSH was measured after heating the samples for 60 min at 80 °C.

The newly analytical method, developed by our team, was successfully applied in detection of GSH and GSSG from rat brain samples in a pharmacological experiment that can change the level of the oxidative stress in rodent’s brain. Average concentrations of GSH and GSSG in untreated (blank) animals was $24.82 \pm 1.68 \mu\text{g/g}$ brain and $6.54 \pm 3.09 \mu\text{g/g}$ brain, respectively. It can be seen that the newly developed method is able to easily and precisely quantify the concentration of the compound of interest in the desired biological matrix.

4. Materials and Methods

4.1. Chemicals and Reagents

All chemicals and reagents used in this study were of analytical purity, being purchased from different providers: acetonitrile was purchased from VWR International, SAS, Fontenay-sous-Bois, France, anhydrous disodium phosphate (Na_2HPO_4), and 85% phosphoric acid solution (H_3PO_4) were purchased from Merck KGaA (Darmstadt, Germany). The Ellman’s reagent, trichloroacetic acid (TCA), ethylenediaminetetraacetate (EDTA-Na_2) powder, sodium chloride (NaCl) powder, phosphate buffer solution (PBS), GSH and GSSG powders were all purchased from Sigma-Aldrich (Darmstadt, Germany). Ultra pure water was obtained using the Milli-Q purification system (Merck Millipore Corporation, Burlington, MA, USA).

4.2. Preparation of Solutions

For GSH stock solution (5 mg/mL) preparation, 5 mg of reduced glutathione were dissolved in 1 mL of ultra pure water. GSSG stock solution (5 mg/mL) was obtained by dissolving 5 mg of oxidized glutathione in 1 mL of ultra pure water.

Working solutions for GSH and GSSG at 9 levels of concentration (25, 50, 250, 500, 750, 1000, 1500, 2000, 2500 $\mu\text{g/mL}$) were obtained by successive dilution of the stock solutions with ultra pure water. Seven (GSH, GSSG) triplicate samples for linearity (0.5–50 $\mu\text{g/g}$) and three QC samples were prepared (LLOQ, 15 $\mu\text{g/g}$, 40 $\mu\text{g/g}$) in five replicates.

The derivatization reaction with the Ellman’s reagent was applied individually to each sample, after the preparation of the calibration curve solutions.

4.3. Sample Preparation

With the aim of obtaining as accurate results as possible, for optimization of sample preparation and avoiding unnecessary prolongation of sample preparation which could influence the final results, we applied an automated homogenization method using the IKA Ultra-Turrax Tube [18].

Twenty Wistar male rats, weighing 400–500 g, were placed in individual plastic cages. The animals were maintained on a 12:12 h light dark cycle and fed ad libitum. Afterwards, the animals were decapitated under anesthesia with ketamine and xylazine in a dose mixture of ketamine (100 mg/kg) and xylazine (10 mg/kg) in order to collect the brain

samples. After brain samples extraction, these were immediately immersed in liquid nitrogen and stored at $-80\text{ }^{\circ}\text{C}$ until analysis.

In order to analyze GSH and GSSG, brains were homogenized using IKA Ultra-Turrax Tube Drive and then divided in equal quantities. 1g of each GSH and GSSG brain sample was then spiked with 10 μL of working solution, and then 3 mL of PBS were added. Samples were vortexed for 1 min, and immediately after they were centrifuged ($10,000\times g$ for 10 min). Following centrifugation, 500 μL supernatant was collected and 500 μL Ellman's reagent was added to the supernatant. The GSSG samples were then heated for 60 min at $80\text{ }^{\circ}\text{C}$ in the TS-100S, Thermo-Shaker (BioSan, Riga, Latvia). The GSH samples were not subjected to the heat-treatment, but instead they were left at room temperature for 10 min.

To both GSH and GSSG series of samples, 300 μL TCA 20% was added and then the samples were centrifuged at $13,000\times g$ for 10 min. After centrifugation, the supernatant was collected and transferred into HPLC vials.

4.4. Determination of the Degree of Reduction of Oxidized Glutathione

Following the reaction between Ellman's reagent and GSH, a GSH-DTNB reaction product is obtained. Thus, the quantification of GSSG levels requires the calculation of the difference between the total glutathione (TG) and GSH. The determination of TG can be done by reducing GSSG to GSH.

This method presents an advantage of chemical nature from the sample preparation point of view, because the reduction of GSSG will occur in the presence of Ellman's reagent at $80\text{ }^{\circ}\text{C}$, without the necessity of additional reducing compounds and preparation steps. The validation of this reduction process required the preparation of the samples in three different conditions:

1. Condition 1: Biological samples spiked with GSSG heated at $80\text{ }^{\circ}\text{C}$ for 60 min;
2. Condition 2: Biological samples spiked with GSH heated at $80\text{ }^{\circ}\text{C}$ for 60 min;
3. Condition 3 (control condition): Biological samples spiked with GSH stored at room temperature for 10 min;

The calculated differences between the two conditions (Condition 1 and 2) reflect the degree of GSSG reduction. The reduction degree of GSSG to GSH is presented in Table 6.

Table 6. Determination of the degree of reduction of oxidized glutathione.

Conc. ($\mu\text{g/g}$ Brain)	Percentage of Reduction (%)	SD (+/− %)
0.5	108.79	7.80
1	90.19	6.33
5	111.10	9.72
10	113.91	10.49
15	114.60	4.64
20	112.35	9.38
35	113.35	11.29
40	103.40	7.74
50	91.66	10.31

4.5. Instrumentation

The validation of the present method was performed using a HPLC Merck system: quaternary pump Merck Hitachi L-7100, auto sampler Merck Hitachi L-7200, column thermostat Merck Hitachi L-7360, DAD Merck Hitachi L-7455, interface Merck Hitachi L-7000, solvent degaser Merck Hitachi L-7612, software D-7000 HSM-Manager (Hitachi Corporation, Westford, MA, USA)

4.6. Study Application

The method was successfully applied in a chronic CNS toxicity study, following different haloperidol treatment regimens, in order to demonstrate the applicability. The brains were rapidly removed, frozen in liquid nitrogen, and stored at $-80\text{ }^{\circ}\text{C}$. The preparation of

the samples was performed according to the steps presented in Section 4.2 Preparation of Solutions, and for the analysis, the discussed method was applied.

4.7. Ethical Considerations

All of the experimental procedures were in accordance with the European Directive 2010/63/UE and the study was granted the approval of the Ethics Committee of Scientific Research of the George Emil Palade University of Medicine, Pharmacy, Science and Technology of Târgu Mureş (approval no. 533/2019) and National Sanitary Veterinary and Food Safety Authority (approval no. 42/2020).

5. Conclusions

In this article, an analytical method for quantifying the level of GSH and GSSG in the neural matrix (brain) was validated. In this regard, the analysis was performed using a C8 type chromatographic column and an elution gradient. Regarding the validation parameters examined, they were found to be in accordance with the regulatory guidelines and regulations (FDA 2018).

The developed method in this study is applicable in research studies that focus on quantification of GSH and GSSG levels in rodent brains, as markers of oxidative stress, with different etiologies.

Author Contributions: Data collection—G.J.; conceptualization—G.J., E.F., I.F., M.D.C.; investigation—G.J., E.F.; writing—original draft preparation, G.J.; writing—review and editing, G.J., B.-E.Ő., C.E.V., C.M.R.; visualization, G.J., B.-E.Ő., C.E.V., C.M.R., M.T.D.; funding acquisition, G.J. All authors have read and agreed to the published version of the manuscript.

Funding: This work was supported by the George Emil Palade University of Medicine, Pharmacy, Science and Technology of Târgu Mureş, research grant number 293/4/14.01.2020.

Institutional Review Board Statement: The study was conducted according to the guidelines of the Declaration of Helsinki, and approved by the Ethics Committee of Scientific Research of the George Emil Palade University of Medicine, Pharmacy, Science and Technology of Târgu Mureş (approval no. 533/2019) and by the National Sanitary Veterinary and Food Safety Authority (approval no.42/2020).

Informed Consent Statement: Not applicable.

Data Availability Statement: The datasets that support the findings of this study are available from the corresponding authors upon reasonable request.

Acknowledgments: This work was supported by the George Emil Palade University of Medicine, Pharmacy, Science and Technology of Târgu Mureş, research grant number 293/4/14.01.2020.

Conflicts of Interest: The authors declare no financial or other conflict of interest.

Sample Availability: Samples of the compounds are not available from the authors.

References

1. Lushchak, V.I. Glutathione homeostasis and functions: Potential targets for medical interventions. *J. Amino. Acids.* **2012**, *2012*, 736837. [CrossRef] [PubMed]
2. Cooper, A.J.; Pinto, J.T.; Callery, P.S. Reversible and irreversible protein glutathionylation: Biological and clinical aspects. *Expert Opin. Drug Metab. Toxicol.* **2011**, *7*, 891–910. [CrossRef] [PubMed]
3. Čapek, J.; Roušar, T. Detection of Oxidative Stress Induced by Nanomaterials in Cells-The Roles of Reactive Oxygen Species and Glutathione. *Molecules* **2021**, *26*, 4710. [CrossRef]
4. Pompella, A.; Visvikis, A.; Paolicchi, A.; De Tata, V.; Casini, A.F. The changing faces of glutathione, a cellular protagonist. *Biochem. Pharmacol.* **2003**, *66*, 1499–1503. [CrossRef]
5. Zitka, O.; Skalickova, S.; Gumulec, J.; Masarik, M.; Adam, V.; Hubalek, J.; Trnkova, L.; Kruseova, J.; Eckschlager, T.; Kizek, R. Redox status expressed as GSH:GSSG ratio as a marker for oxidative stress in paediatric tumour patients. *Oncol. Lett.* **2012**, *4*, 1247–1253. [CrossRef]
6. Kalinina, E.; Novichkova, M. Glutathione in Protein Redox Modulation through S-Glutathionylation and S-Nitrosylation. *Molecules* **2021**, *26*, 435. [CrossRef] [PubMed]

7. Aoyama, K.; Nakaki, T. Impaired glutathione synthesis in neurodegeneration. *Int. J. Mol. Sci.* **2013**, *14*, 21021–21044. [CrossRef] [PubMed]
8. Kennedy, L.; Sandhu, J.K.; Harper, M.E.; Cuperlovic-Culf, M. Role of Glutathione in Cancer: From Mechanisms to Therapies. *Biomolecules* **2020**, *10*, 1429. [CrossRef]
9. Hajdinák, P.; Szabó, M.; Kiss, E.; Veress, L.; Wunderlich, L.; Szarka, A. Genetic Polymorphism of GSTP-1 Affects Cyclophosphamide Treatment of Autoimmune Diseases. *Molecules* **2020**, *25*, 1542. [CrossRef] [PubMed]
10. Sekhar, R.V.; McKay, S.V.; Patel, S.G.; Guthikonda, A.P.; Reddy, V.T.; Balasubramanyam, A.; Jahoor, F. Glutathione synthesis is diminished in patients with uncontrolled diabetes and restored by dietary supplementation with cysteine and glycine. *Diabetes Care* **2011**, *34*, 162–167. [CrossRef]
11. Mandal, P.K.; Tripathi, M.; Sugunan, S. Brain oxidative stress: Detection and mapping of anti-oxidant marker 'Glutathione' in different brain regions of healthy male/female, MCI and Alzheimer patients using non-invasive magnetic resonance spectroscopy. *Biochem. Biophys. Res. Commun.* **2012**, *417*, 43–48. [CrossRef]
12. Liu, H.; Harrell, L.E.; Shenvi, S.; Hagen, T.; Liu, R.M. Gender differences in glutathione metabolism in Alzheimer's disease. *J. Neurosci. Res.* **2005**, *79*, 861–867. [CrossRef] [PubMed]
13. Mischley, L.K.; Standish, L.J.; Weiss, N.S.; Padowski, J.M.; Kavanagh, T.J.; White, C.C.; Rosenfeld, M.E. Glutathione as a Biomarker in Parkinson's Disease: Associations with Aging and Disease Severity. *Oxid. Med. Cell. Longev.* **2016**, *2016*, 9409363. [CrossRef] [PubMed]
14. Jitcă, G.; Ősz, B.E.; Tero-Vescan, A.; Vari, C.E. Psychoactive Drugs-From Chemical Structure to Oxidative Stress Related to Dopaminergic Neurotransmission. A Review. *Antioxidants* **2021**, *10*, 381. [CrossRef] [PubMed]
15. Zheng, X.; Duan, C.; Shen, J. Determination of reduced glutathione by spectrophotometry coupled with anti-interference compensation. *Anal. Methods* **2015**, *7*, 5006–5011. [CrossRef]
16. Squellerio, I.; Caruso, D.; Porro, B.; Veglia, F.; Tremoli, E.; Cavalca, V. Direct glutathione quantification in human blood by LC-MS/MS: Comparison with HPLC with electrochemical detection. *J. Pharm. Biomed. Anal.* **2012**, *71*, 111–118. [CrossRef]
17. Bollenbach, A.; Tsikas, D. Measurement of the tripeptides glutathione and ophthalmic acid by gas chromatography-mass spectrometry. *Anal. Biochem.* **2020**, 113841. [CrossRef] [PubMed]
18. Jitcă, G.; Fogarasi, E.; Ősz, B.E.; Vari, C.E.; Tero-Vescan, A.; Miklos, A.; Bătrînu, M.G.; Rusz, C.M.; Croitoru, M.D.; Dogaru, M.T. A Simple HPLC/DAD Method Validation for the Quantification of Malondialdehyde in Rodent's Brain. *Molecules* **2021**, *26*, 5066. [CrossRef] [PubMed]
19. Begaye, A.; Sackett, D.L. Measurement of ligand binding to tubulin by sulfhydryl reactivity. *Methods Cell Biol.* **2010**, *95*, 391–403. [CrossRef] [PubMed]
20. FDA. Guidance for Industry: Bioanalytical Method Validation. 2018. Available online: <https://doi.org/https://www.fda.gov/downloads/drugs/guidances/ucm070107.Pdf> (accessed on 5 September 2021).
21. Fogarasi, E.; Croitoru, M.; Fülöp, I.; Muntean, D. Is the Oxidative Stress Really a Disease? *Acta Marisiensis-Ser. Medica.* **2016**, *62*, 112–120. [CrossRef]
22. Appala, R.N.; Chigurupati, S.; Appala, R.V.; Krishnan Selvarajan, K.; Islam Mohammad, J. A Simple HPLC-UV Method for the Determination of Glutathione in PC-12 Cells. *Scientifica* **2016**, *2016*, 6897890. [CrossRef] [PubMed]
23. Adedeji, H.A.; Ishola, I.O.; Adeyemi, O.O. Novel action of metformin in the prevention of haloperidol-induced catalepsy in mice: Potential in the treatment of Parkinson's disease? *Prog. Neuropsychopharmacol. Biol. Psychiatry* **2014**, *48*, 245–251. [CrossRef] [PubMed]
24. Owen, J.B.; Butterfield, D.A. Measurement of oxidized/reduced glutathione ratio. *Methods Mol. Biol.* **2010**, *648*, 269–277. [CrossRef] [PubMed]

Article

Polymerized Whey Protein Concentrate-Based Glutathione Delivery System: Physicochemical Characterization, Bioavailability and Sub-Chronic Toxicity Evaluation

Siyu Zhang ^{1,†}, Cuina Wang ^{2,†}, Weigang Zhong ², Alyssa H. Kemp ³ , Mingrui Guo ^{1,3} and Adam Killparick ^{3,*}

¹ Key Laboratory of Dairy Science of Ministry of Education, Northeast Agricultural University, Harbin 150030, China; Zhangsiyu@neau.edu.cn (S.Z.); Ming.R.Guo@uvm.edu (M.G.)

² Department of Food Science, Jilin University, Changchun 130000, China; wangcuina@jlu.edu.cn (C.W.); zhongwg19@mails.jlu.edu.cn (W.Z.)

³ Department of Nutrition and Food Sciences, University of Vermont, Burlington, VT 05403, USA; Alyssa.H.Kemp@uvm.edu

* Correspondence: adam.killparick@uvm.edu

† These authors contributed equally to this work and should be considered joint first author.

Abstract: Glutathione (GSH) is a powerful antioxidant, but its application is limited due to poor storage stability and low bioavailability. A novel nutrient encapsulation and delivery system, consisting of polymerized whey protein concentrate and GSH, was prepared and in vivo bioavailability, antioxidant capacity and toxicity were evaluated. Polymerized whey protein concentrate encapsulated GSH (PWPC-GSH) showed a diameter of roughly 1115 ± 7.07 nm (D_{50}) and zeta potential of 30.37 ± 0.75 mV. Differential scanning calorimetry (DSC) confirmed that GSH was successfully dispersed in PWPC particles. In vivo pharmacokinetics study suggested that PWPC-GSH displayed 2.5-times and 2.6-fold enhancement in maximum concentration (C_{max}) and area under the concentration–time curve (AUC) as compared to free GSH. Additionally, compared with plasma of mice gavage with free GSH, significantly increased antioxidant capacity of plasma in mice with PWPC-GSH was observed ($p < 0.05$). Sub-chronic toxicity evaluation indicated that no adverse toxicological reactions related to oral administration of PWPC-GSH were observed on male and female rats with a diet containing PWPC-GSH up to 4% (w/w). Data indicated that PWPC may be an effective carrier for GSH to improve bioavailability and antioxidant capacity.

Keywords: polymerized whey protein; glutathione; physicochemical properties; pharmacokinetics; toxicity

Citation: Zhang, S.; Wang, C.; Zhong, W.; Kemp, A.H.; Guo, M.; Killparick, A. Polymerized Whey Protein Concentrate-Based Glutathione Delivery System: Physicochemical Characterization, Bioavailability and Sub-Chronic Toxicity Evaluation. *Molecules* **2021**, *26*, 1824. <https://doi.org/10.3390/molecules26071824>

Academic Editor: Pál Perjési

Received: 21 February 2021

Accepted: 22 March 2021

Published: 24 March 2021

Publisher's Note: MDPI stays neutral with regard to jurisdictional claims in published maps and institutional affiliations.



Copyright: © 2021 by the authors. Licensee MDPI, Basel, Switzerland. This article is an open access article distributed under the terms and conditions of the Creative Commons Attribution (CC BY) license (<https://creativecommons.org/licenses/by/4.0/>).

1. Introduction

Glutathione (γ -glutamyl-cysteinyl-glycine, GSH) is an abundant endogenous antioxidant composed of glutamate, glycine and cysteine and mainly exists in baker's yeast, wheat germ and animal liver. GSH is known to possess strong antioxidant properties as a result of its thiol (-SH) group inherent to the cysteine residue. The thiol group is involved in scavenging free radicals, thus protecting the integrity of the cell [1,2] and improving the immune system [3,4]. GSH can be a substrate of glutathione peroxidase (GSH-Px) and glutathione S-transferase (GST) [5], which have the function of detoxification [6]. GSH deficiency may play a role in various diseases, such as immunodeficiency disease [7], cancer [8], diabetes [9,10], cardiovascular disease [11,12], rheumatoid arthritis [13], and neurological disorders [14]. GSH has been used in clinical practice and consumer goods including cosmetic and function foods [15,16]. However, the poor storage stability, low bioavailability and ongoing debate as to whether orally administered GSH is absorbed still poses challenges for its broad clinical application. GSH is sensitive to temperature, light and pH due to the presence of the reduced thiol group. When exposed to external

environment, the thiol group of GSH can be oxidized into a disulfide bond, forming oxidizing glutathione (GSSG), which reduces the antioxidant activity. In addition, GSH is easily degraded in intestinal tract and liver by γ -glutamyltransferase [17] and only a small amount is known to reach portal circulation.

Whey protein, a by-product from the cheese industry, has two products available on market, which are whey protein concentrate (WPC) and whey protein isolate (WPI). Whey protein has high nutritional value and a complete amino acid profile, and has functions such as anti-oxidation [18,19], regulating immunity and inhibiting pathogenic bacteria.

Whey protein can be used as carrier of delivery systems due to different mechanisms. Whey protein belongs to the lipocalin protein family and can be used to carry hydrophobic compounds such as polyphenols [20,21] mainly by hydrophobic forces. Whey protein has excellent emulsification properties and can be used to carry fat-soluble substances such as oil [22,23] and vitamins [24–26]. Polymerized whey protein has high viscosity and can be used to carry bioactive substances such as 3,3'-diindolylmethane [27] and probiotics [28].

Whey protein consists of a group of globular proteins including β -lactoglobulin, α -lactalbumin, and bovine serum albumin, which are sensitive to heat treatment. When heated, its spatial structure changes, resulting in the exposure of thiol and hydrophobic groups and the subsequent formation of polymerized whey protein via disulfide bond interconnections and hydrophobic interactions [29].

In this study, polymerized whey protein concentrate (PWPC), induced by thermal treatment of whey protein concentrate, was used to construct a new encapsulate and delivery system for GSH. To this end, physicochemical properties of the developed system were characterized followed by evaluation of bioavailability and sub-chronic toxicity.

2. Results and Discussion

2.1. Physicochemical and Structural Properties of the PWPC-GSH System

PWPC-GSH system was prepared with advantages of simplicity, mildness, and organic solvent-free in comparison with other carriers based on poly isobutylcyanoacrylate [30], Eudragit RS 100/cyclodextrin [31] and montmorillonite [32]. As shown in Figure 1A, PWPC exhibited bimodal pattern with two peaks at 594 nm and 4580 nm with a wide particle size distribution (span of 9.22), consistent with previous research [33]. Combination with GSH (287.83 ± 6.18 nm) slightly increased particle size (D_{50}) from 1085 ± 35.35 to 1115 ± 7.07 nm with decreased span from 9.22 ± 0.22 to 6.86 ± 0.19 . Zeta potential for PWPC-GSH was found to be 30.37 ± 0.75 mV (Figure 1B). The high surface charge endowed the PWPC-GSH system high stability since strong electrostatic repulsion between molecules prevents polymerization, precipitation, and flocculation [34]. In addition, the positive surface charge of PWPC-GSH would favor absorption *in vivo* since cell membranes carries negative charges [35]. PWPC-GSH system displayed shear-thinning behavior in range of $1\text{--}300$ s⁻¹ (Figure 1C), indicating that interaction between droplets was weakened at higher shear rate [36].

A DSC thermogram of GSH demonstrated an exothermic peak at 198 °C and disappearance of this melting peak in the PWPC-GSH system, implying that GSH was molecularly dispersed in PWPC particles (Figure 2A) [37]. FTIR spectra analysis (Figure 2B) showed that PWPC displayed an amide I (C=O vibration) spectrum peak at 1654.39 cm⁻¹ and red shift occurred after binding with GSH, indicating that PWPC was structurally changed and intermolecular hydrogen bonds formed. This PWPC-GSH system exhibited morphology of vermicular aggregates with its majority at a size of roughly 200 nm, with some larger aggregates measuring upwards of approximately 400 nm (Figure 2C).

2.2. *In Vivo* Pharmacokinetic and Antioxidant Activity of PWPC-GSH

Whey protein has been widely studied as an effective means of nutrient delivery due to its resistance to digestion by pepsin [38], its non-toxic nature, widely available sources and broad biocompatibility. Pharmacokinetic studies of the PWPC-GSH delivery system and free GSH were conducted and plasma GSH concentration–time profiles for all groups

are shown in Figure 3A. GSH concentration was observed to be the highest in the plasma of PWPC-GSH group, followed by free GSH, PWPC, and the control group. The higher value in the plasma of mice gavage with PWPC-GSH than that of free GSH group may be due to the protection effect of highly viscous PWPC [39,40] by embedding GSH inside and preventing damage to gastrointestinal enzymes and an acidic environment. These results were consistent with previous studies that the bioavailability of quercetin and vitamin D were improved through whey protein encapsulating [41,42].

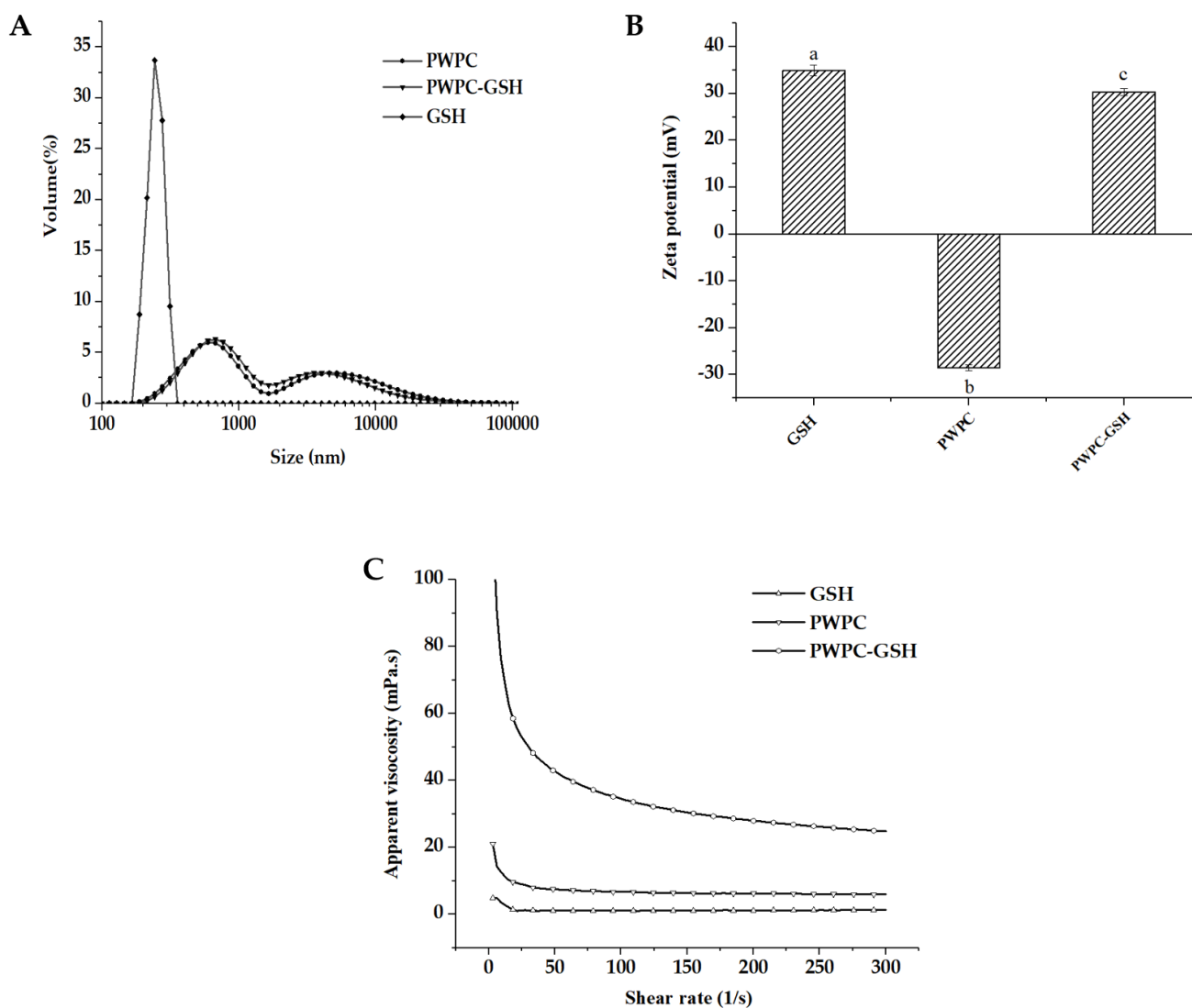


Figure 1. (A) Particle size distribution, (B) zeta potential, (C) apparent viscosity of glutathione (GSH), polymerized whey protein concentrate (PWPC) and polymerized whey protein concentrate encapsulated GSH (PWPC-GSH). In Figure 1B, completely different lower-case letters between samples mean significant difference ($p < 0.05$).

Pharmacokinetic parameters were calculated as shown in inset of Figure 3A. Compared with free GSH (maximum concentration (C_{max}) of 7.37 mg/L and area under the concentration–time curve (AUC) of 19.23 h \times mg/L), higher C_{max} (19.41 mg/L) and AUC (48.63 h \times mg/L) values were observed, indicating a higher rate and degree of GSH absorption into the blood circulation in mice after administration with PWP-GSH. The 2.5-fold and 2.6-fold higher C_{max} and AUC in the PWPC-GSH group suggested that the PWPC-GSH delivery system can improve the in vivo bioavailability of GSH effectively vs. GSH in its pure form on its own. Whey protein also appears to possess a protective effect on GSH as a carrier during absorption into intestinal tract which may due to the resistance to digestion

by pepsin. In addition to delivery of the GSH itself, the whey protein supplementation may have also contributed to the increase in GSH levels in vivo [43,44] by virtue of the abundance of cysteine residue inherent to whey protein, which has the capability to promote biosynthesis of GSH as a rate-limiting amino acid [45]. The lower time to maximum concentration (T_{max}) (1 h) occurred in the PWPC-GSH group in comparison with that in free GSH (2 h), indicating less time was required to reach the maximum concentration after administration. The plasma concentration of GSH in the GSH group reached its maximum levels after 1.5 to 2 h which echoed data reported in the early literature relative to orally administered free GSH [46].

Total antioxidative capacity of samples at different time points was measured using an assay kit and the results are shown in Figure 3B. Antioxidant capacity of plasma in mice gavage with PWPC-GSH was significantly higher than that of free GSH through the whole period ($p < 0.05$). The first reason for the increased antioxidant capacity of plasma after gavage of PWPC-GSH in mice was that GSH concentration in plasma was improved using PWPC as a delivery carrier. The second reason may be due to the antioxidant properties of whey protein [19,47] [48]. As shown in Figure 3B, the plasma antioxidant capacity of mice after gavage with PWPC was also slightly improved to a degree that may or may not be consistent with an additive effect.

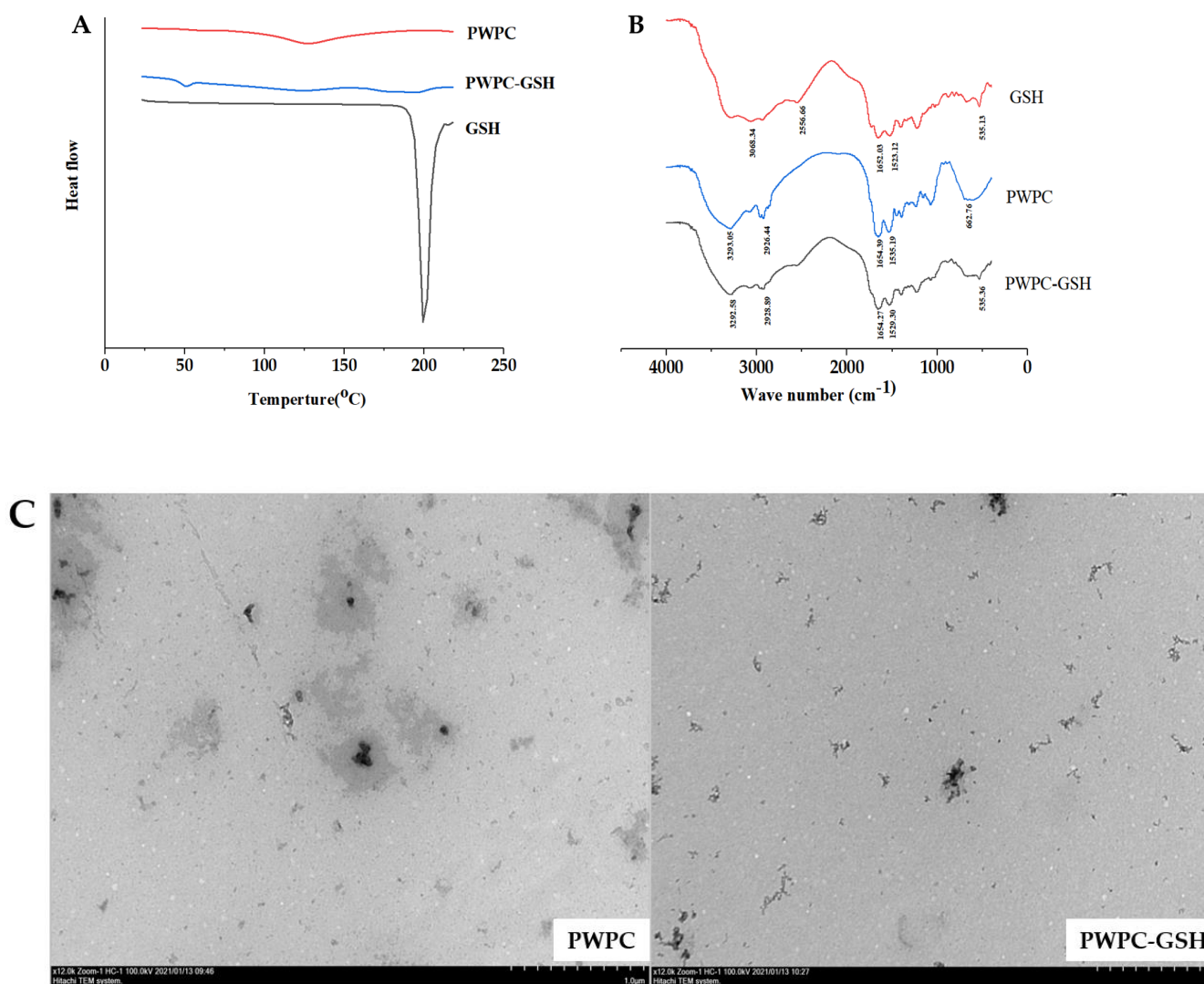


Figure 2. (A) Differential scanning calorimetry (DSC), (B) FT-IR spectrum, (C) TEM image of PWPC and PWPC-GSH.

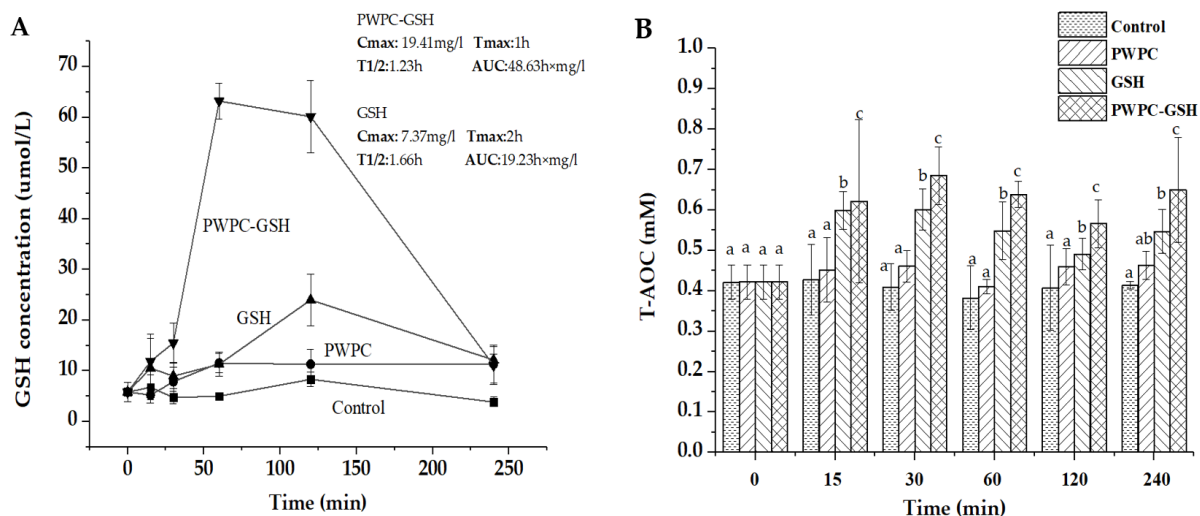


Figure 3. (A) GSH concentration (μM) in plasma of mice after oral administration of normal saline (control), PWPC, GSH, and PWPC-GSH. (B) In vivo antioxidant activity of plasma of mice after oral administration of normal saline (control), PWPC, GSH, and PWPC-GSH measured by an assay kit (ABTS method). In Figure 3B, completely different letter between samples at the same timepoint means significant difference ($p < 0.05$).

2.3. Toxicity Evaluation of PWPC-GSH System

2.3.1. Clinical Observations, Body Weight, and Food Consumption

During the experiment, there was no observed adverse effects in the experimental groups compared with the control groups. Body weight of all rats increased gradually as the treatment period progressed (Figure 4A). There was no statistically significant difference in body weight between female groups ($p < 0.05$). For male groups, from 16 days, the weight of rats in 1% male group was significantly different from that of the control ($p < 0.05$). However, the body weight changes were observed only in male groups and there was no dose-dependent effect, so it was interpreted as having no toxicological significance. During the study, the weight of rats in the experimental groups was comparable to that of rats in the control groups.

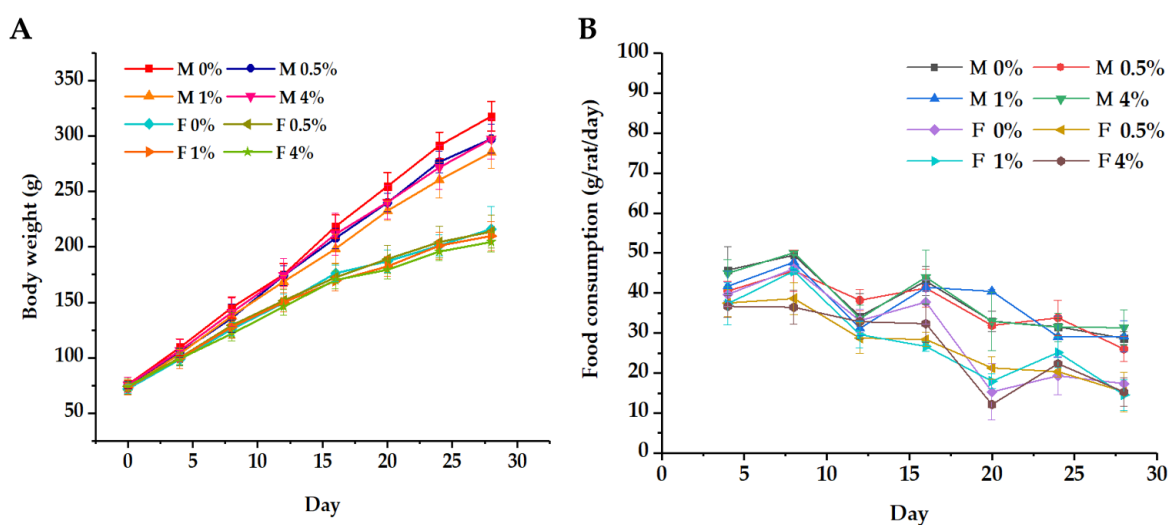


Figure 4. (A) Body weight and (B) food consumption curves of rats in a 28-day feeding test, 0%, 0.5%, 2% and 4% represent daily intake of 0% (w/w , control), 0.5% (w/w , low dose), 1% (w/w , medium dose) and 4% (w/w , high dose) of freeze-dried PWPC-GSH powder, respectively.

Results for food consumption of rats for 28 days are shown in Figure 4B. There was no PWPC-GSH-related toxicity effect observed in experimental groups although there was some significant difference between experimental groups and control groups at some time points. In female rats, there was a statistically significant difference in food consumption of the 0.5% and 4% groups and the control group on the 8th day ($p < 0.05$). However, this phenomenon was only observed in one time point and later returned to normal. Similar phenomenon was also observed in the experiment of Bauter et al. [49], and it was interpreted as having no toxicological relevance and no side effects. In contrast, no change in the food consumption was observed in the male groups.

2.3.2. Hematology

Results of the hematology in all groups were shown in Table S1 (supplementary materials). Some statistically significant differences occurred between control and treatment groups ($p < 0.05$).

In 0.5% and 4% groups, the values of mean platelet volume (WPV) were lower than that of the control group. In the 0.5% group, the lymphocyte (LYM) was significantly different from that of the control group ($p < 0.05$). However, all changes were observed only in male rats. In females, compared with the control, red blood cells (RBC) in the 1% group showed a significantly higher value ($p < 0.05$). This change may be caused by a lack of water and should not be considered as test-substance related. Hemoglobin (HGB) in 1% and 4% female groups was significantly higher than that in the control group ($p < 0.05$). On routine blood tests, there were no toxic reactions associated with taking PWPC-GSH. Although there were significant differences between some of the data and the control group, they were within the historical reference range [50]. These differences can only be observed in one sex, and there is no dose–effect relationship. Therefore, it is considered that this may be due to environmental temperature, placement time and other factors, which cause slight differences.

2.3.3. Serum Biochemistry

Results of serum biochemistry for rats in all groups are shown in Table S2 (supplementary materials). Compared to the control group, the 4% male group displayed significantly lower mean values of albumin (ALB) (33.01 ± 1.34 g/L, $p < 0.05$); the changes in ALB value correlate with liver function. The values of amylase (AMY), calcium (Ca) and glucose (GLU) were different from those of the control group. Amylase hydrolyzes starch and sugars are originally digested from polysaccharide compounds in foods. The decrease in amylase occurred in diabetes mellitus and severe liver disease. Further examination of rat liver tissue sections showed that there was no lesion in rat liver tissue. The slight decrease in the value of Glu was caused by fasting and starvation in the mice, while the low value of Ca was not clinically significant. These values were comparable to the control and within the bounds of historical data [51]. Compared with the control group, the alanine aminotransferase (ALT) and aminotransferase (AST) values were significantly lower in experimental groups ($p < 0.05$). Previous studies showed that the increased ALT and AST values had clinical significance, while the decreased values may be due to the benefits of PWPC-GSH in inhibiting liver injury [52,53], so it was regarded as not toxicologically relevant; in fact, this finding further illustrates the positive impact GSH has on liver function and protection.

Amylase (AMY) and GLU in the 1% and 4% female groups were significantly lower than those in the control group ($p < 0.05$) and the inorganic phosphorus (IP) level in the 0.5%, 1% and 4% female groups was significantly higher than that of the control group ($p < 0.05$). Amylase hydrolyzes starch and sugars were originally digested from polysaccharide compounds in foods. The decrease in amylase occurred in diabetes mellitus and severe liver disease. Further examination of rat liver tissue sections showed that there was no lesion in rat liver tissue. A slight decrease in Glu is usually caused by starvation. High IP values have no clinical significance. For males and females, the creatine kinase (CK) values in the control groups were not within the reference range; the difference was

due to instrumental error. The difference in CK was interpreted as having no toxicological significance if there was no associated microscopic change in the heart.

In blood biochemical tests, although there were significant differences in some data compared with the control group, there was no correlation between these changes in the organism and the dose of chemical exposure, so the effect was considered to be independent of the exposure [49].

2.3.4. Relative Organ Weights and Histopathology

Relative organ weight can reflect the nutritional status and damage of the animal internal organs. As shown in Table 1, male rats of experiment groups showed significantly lower final body weights than the control group ($p < 0.05$). In male rats, compared with the control group, there was no significant difference in the relative organ weight of rats in all groups except liver and kidney in the 4% group ($p < 0.05$). There was no evidence of liver and kidney lesions in the hematological analysis. Further observation of the liver and kidney by necropsy and histopathological tests confirmed that there was no damage or lesion in the liver and kidney. For female rats, the 4% group showed significantly lower final body weight ($p < 0.05$). There was no significant difference in relative organ weights between female rats in the experiment groups and the control group ($p < 0.05$).

Table 1. Relative organ weights for male rat.

		0%	0.5%	1%	4%
Body weight	M	296.8 ± 11.47	272.78 ± 10.28 **	261 ± 12.59 **	275 ± 18.70 *
	F	203.80 ± 10.14	205.20 ± 16.01	199.70 ± 11.93	192.10 ± 8.77 *
Brain	M	5.35 ± 0.85	5.90 ± 2.11	6.45 ± 0.63 *	6.67 ± 0.67 *
	F	7.14 ± 1.40	8.52 ± 0.86	8.22 ± 1.02	8.65 ± 0.84
Thymus	M	2.58 ± 0.60	3.01 ± 0.42	2.37 ± 0.38	2.66 ± 0.47
	F	3.36 ± 0.46	3.31 ± 0.38	3.40 ± 0.52	3.31 ± 0.44
Heart	M	3.80 ± 0.30	4.03 ± 0.50	3.92 ± 0.28	3.89 ± 0.28
	F	4.10 ± 0.01	3.99 ± 0.26	4.26 ± 0.37	4.08 ± 0.31
Lung	M	4.74 ± 0.38	5.31 ± 1.08	4.98 ± 0.52	4.78 ± 0.31
	F	5.44 ± 0.55	5.09 ± 0.39	5.19 ± 0.35	5.13 ± 0.33
Liver	M	39.00 ± 4.33	37.22 ± 4.83	36.62 ± 2.96	34.92 ± 2.83 *
	F	35.76 ± 2.74	38.28 ± 7.27	34.54 ± 2.14	36.08 ± 1.55
Spleen	M	2.79 ± 0.92	2.78 ± 0.72	2.47 ± 0.35	2.79 ± 0.39
	F	2.51 ± 0.32	2.56 ± 0.40	2.32 ± 0.34	2.57 ± 0.21
Kidney	M	9.16 ± 0.70	9.32 ± 0.39	9.38 ± 0.38	9.66 ± 0.51 *
	F	8.83 ± 0.46	8.54 ± 1.53	8.70 ± 0.31	9.47 ± 0.51
Bladder	M	0.28 ± 0.04	0.31 ± 0.07	0.32 ± 0.05	0.29 ± 0.07
	F	0.35 ± 0.03	0.36 ± 0.07	0.35 ± 0.04	0.35 ± 0.06
Testes	M	6.796 ± 1.79	8.62 ± 1.05	8.25 ± 0.23	8.67 ± 0.76
Epididymis	M	0.57 ± 0.11	0.48 ± 0.15	0.58 ± 0.09	0.59 ± 0.05
Seminal Vesicle	M	1.95 ± 0.58	1.47 ± 0.42	1.11 ± 0.68	1.59 ± 0.50
Ovary	F	0.71 ± 0.23	1.65 ± 0.28	0.54 ± 0.16	0.56 ± 0.14
Uterus	F	2.11 ± 0.62	1.98 ± 0.62	1.75 ± 0.65	1.99 ± 0.98

Note: * means the significant level is 0.05, ** means significant level is 0.01 compared with the control group. The values 0%, 0.5%, 2% and 4% represent daily intake of 0% (*w/w*, control), 0.5% (*w/w*, low dose), 1% (*w/w*, medium dose) and 4% (*w/w*, high dose) of freeze-dried PWPC-GSH powder; M and F represent male and female rats, respectively.

At autopsy, no treatment-related gross pathological changes were observed in any group of rats treated with PWPC-GSH, so histopathological examinations were performed on animals in the control and high-dose groups of both sexes. As shown in Figure 5, histopathological findings observed consisted of degeneration of some pyramidal cells in the brain and the c; local slight dilatation of myocardial fiber tract space; focal inflammatory cell infiltration in the liver; renal tubular epithelial cell edema; slight degeneration of the testicular tubules. These lesions are very mild and mostly spontaneous in animals used in the experiment [43,49]. Therefore, these results were independent of the use of PWPC-GSH which could be observed in the age and strain of the rats used in this study.

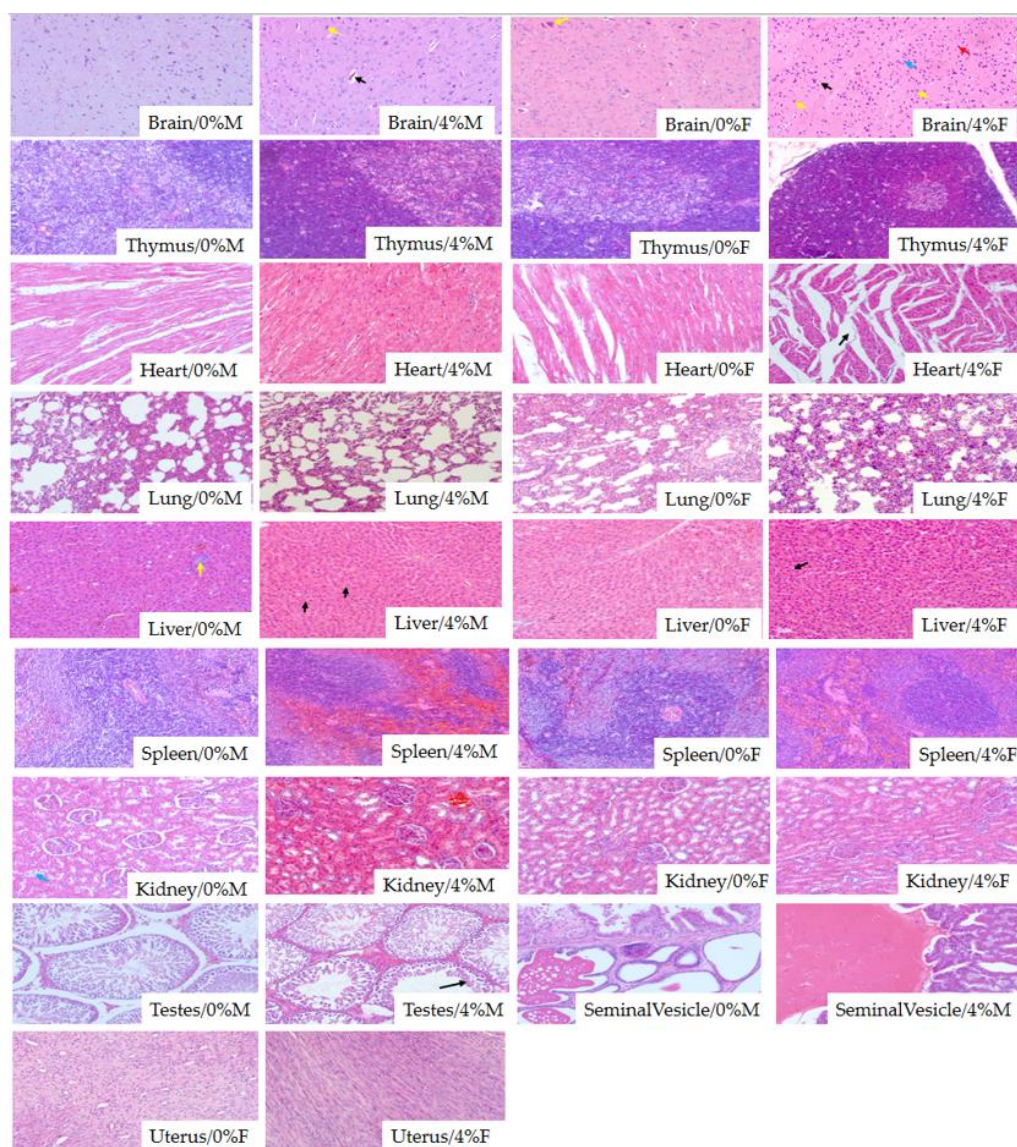


Figure 5. Microscopic examination results of organs for rats in the control and 4% groups. The values 0%, 4% represent daily intake of 0% (*w/w*, control), 4% (*w/w*, high dose) of freeze-dried PWPC-GSH powder. M and F represent male and female rats, respectively. For pictures of brain, black arrows represent vascular endothelium, yellow arrows represent the nucleus, red arrow are neurons and blue arrow are pyramidal cells. For picture of heart, black arrow represents the gap of cardiac muscle fiber bundle. For picture of liver, black arrows represent prototype vacuoles with regular shapes and yellow arrow represent red blood cells. For picture of testes, black arrows represent sperm cells.

3. Materials and Methods

3.1. Materials

Whey protein concentrate (WPC) was provided by Fonterra Co-operative Group (Auckland, New Zealand). GSH at purity of 98.7% was obtained from Kyowa Hakko Bio Co., Ltd (Tokyo, Japan). The GSH powder was stored in the dark to avoid oxidation. A reduced glutathione assay kit (A006-2-1), total antioxidative capacity measurement kit (ABTS method) (A015-2-1) were purchased from Nanjing Jiancheng bioengineering institute (Nanjing, China). Pentobarbital sodium, formalin and absolute ethanol were provided by Beijing chemical Works (Beijing, China).

3.2. Preparation of Polymerized Whey Protein Concentrate Based GSH Delivery System

The preparation of polymerized whey protein concentrate (PWPC) solution was performed according to Khan's method [54]. WPC solution (8%, *w/v*) was prepared by dissolving whey protein concentrate powder in deionized water. The stock solution was stored at 4 °C overnight for complete hydration. WPC solution was returned to ambient temperature and the pH was adjusted to 7 followed by thermal treatment at 80 °C for 15 min in a water bath. PWPC solution was obtained by cooling heated WPC solution in mixed water-ice quickly to room temperature (25 ± 1 °C). PWPC-GSH was obtained by mixing PWPC solution with GSH powder at a weight ratio of 1:1.25 and then stirring for 30 min for complete interaction.

3.3. Characterization of PWPC-GSH Delivery System

3.3.1. Particle Size and Zeta Potential Measurement

The PWPC and PWPC-GSH solutions were slowly added into sample pool until shading was 10–15% and the particle size was measured using Mastersizer 3000 (Malvern Instruments Ltd., Worcestershire, UK). Zeta potential was determined using a Malvern Nano Zetasizer (Malvern Instruments Ltd., Worcestershire, UK).

3.3.2. Flow Behavior Measurement

Flow behavior of suspensions was measured by a Haake Mars 40 Rheometer (Thermo Scientific, Waltham, MA, USA) equipped with a parallel plate which is 60 mm in diameter and 0.1 mm in thickness. The measurement gap width was set at 1000 μm and shear rates ranged from 0.1 to 300 s^{-1} .

3.3.3. Differential Scanning Calorimetry (DSC) Measurement

Thermal characteristics of samples were analyzed using Differential Scanning Calorimeter (DSC3, Mettler Toledo, Switzerland). Sample suspensions were pre-frozen overnight at -80 °C and then dried at 4 °C and 0.3 MPa for 24 h. A small amount of sample (3 mg) was placed and sealed in an aluminum plate with empty pan taken as the control. Calorimetric measurement was performed with the temperature increased from 20 to 220 °C at a heating rate of 10 °C/min.

3.3.4. Fourier Transform Infrared Spectrometry (FT-IR) Measurement

FT-IR spectra of freeze-dried samples were recorded using a Fourier Infrared Spectrometer (NICOLET IS10, Thermo Scientific, Waltham, MA, USA) in the wavelength range of 500–4500 cm^{-1} .

3.3.5. Transmission Electron Microscopy (TEM) Measurement

Appropriate amount of dispersion diluted to 0.02 mg/mL was dropped onto copper grid and the excess sample was removed with filter paper. Uranyl acetate solution (2%, *w/v*) was added and staining were kept for about 15 s. After drying at room temperature for 60 min, micromorphology photos were taken using a Transmission Electron Microscopy (H-7650, HITACHI, Tokyo, Japan) at 100 kV with magnification of 12,000.

3.4. Animal Care

Institute of Cancer Research (ICR) mice (male, 3 weeks, 18–22 g) and Sprague Dawley (SD) rats (male and female, 3 weeks) at Specific Pathogen Free (SPF) grade were provided by Beijing HFK Bioscience Co., Ltd. (Beijing, China). All animals were housed in plastic animal cages in a ventilated room. The room was maintained at 20–26 °C and 40–60% relative humidity with a 12-h light/dark cycle. Water and commercial laboratory complete food were available *ad libitum*. They were acclimated to the environment for 7 days before the experiment.

3.5. *In Vivo* Pharmacokinetic Study and Antioxidant Activity Analysis

Blood samples of mice were collected after oral administration of normal saline (control), PWPC, GSH, and PWPC-GSH solutions by gavage at several time points (0, 15 min, 30 min, 1 h, 2 h, and 4 h) in each group of 6 mice. According to the previous study [32], the dose of PWPC-GSH was adjusted to an equivalent amount of 100 mg/kg of GSH. Blood samples (about 0.5 mL) were collected in 1.5-mL centrifugal tubes with 30 μ L heparin solution by removing one eye of the mice. Plasma samples were obtained by centrifugation of blood at 6000 rpm for 2 min at room temperature and GSH concentration was determined by an assay kit. Pharmacokinetic parameters including maximum concentration (C_{max}), time to maximum concentration (T_{max}), area under the concentration–time curve (AUC), half-life ($T_{1/2}$), and mean residence time (MRT) were estimated by DAS 2.0 (BioGuider Co., Shanghai, China). Antioxidant activity of plasma was also determined using the total antioxidative capacity (T-AOC) measurement kit (ABTS method). The total antioxidant capacity of Trolox was determined by using Trolox as the standard, and the antioxidant Capacity of the sample can be expressed by Trolox-equivalent Antioxidant Capacity (TEAC).

3.6. *Sub-Chronic Toxicity Evaluation*

3.6.1. Experimental Design

In the 28-day subchronic toxicity test, 80 Sprague Dawley (SD) rats (40 males and 40 females) with a body weight of about 75g were divided into 4 groups (10 rats/sex/group). Animals were given a formulated diet containing freeze dried PWPC-GSH powder in daily dose of 0% (*w/w*, control), 0.5% (*w/w*, low dose), 1% (*w/w*, medium dose), and 4% (*w/w*, high dose) which corresponds to 0.25%, 0.5% and 2% percentage for GSH. The PWPC-GSH-containing diets were manufactured by Beijing HFK Bioscience Co., Ltd. (Beijing, China).

3.6.2. Clinical Examination, Body Weight, and Food Consumption

Coat condition, skin, mucous membranes, secretions, excretions, autonomic nervous system activity, changes in gait, and posture of each rat were observed each day throughout the study. Body weights at interval of 4 days were weighed and recorded. Food intake measured and expressed as mean food consumption (expressed as g/rat/day) was calculated for the corresponding intervals. Final weights (fasting) were recorded prior to the scheduled autopsy for calculating the relative weight of organs.

3.6.3. Clinical Pathology

At termination, all the animals were fasted for 12 h, but were free to drink water. Rats were anesthetized with 2% sodium pentobarbital solution of 0.2 mL/100 g weight [55]. Hematological and serum chemistry examination was performed by cardiac blood collection. In hematology analysis, ethylenediamine tetraacetic acid dipotassium salt (EDTA-2K) was used as an anticoagulant and was performed using the Exigo Animal Hematology Analyzer (Exigo-EOS, Sweden). In the serum chemistry examination, the blood samples were centrifuged at room temperature at 10,000 rpm for 3 min to obtain serum, and the serum chemical analysis was performed on an automatic biochemical analyzer (SMT-120V, Chengdu, China).

3.6.4. Organ Weights and Histopathology

At termination, all rats were anaesthetized by pentobarbital sodium. Then, a complete gross pathology examination was conducted by visual inspection. In the process of necropsy, the brain, heart, lung, liver, spleen, kidney and bladder of all animals were taken, and the reproductive organs including ovaries and uterus of female rats were taken, and the testis, epididymis and seminal vesicle of male rats were taken. All organs were removed and weighed. The organ coefficient was calculated by the ratio of organ weight to body weight, expressed as %. Tissue sections from these organs were fixed with 10% buffered formaldehyde except testes were fixed in Bouin solution, embedded in paraffin, sectioned

at 2–5 μm , mounted on glass microscope slides, stained with standard hematoxylin–eosin and examined using light microscopy. All histopathology procedures were carried out in the College of Animal Science and Veterinary Medicine, Jilin University.

3.7. Statistical Analysis

The significance differences of quantitative data between control and experimental groups were calculated using Version SPSS 20 (SPSS Inc., Chicago, IL, USA). The data were expressed as means \pm standard deviation. Levene’s test was used to conduct homogeneous analysis of the data. When the data were homogeneous, the LSD method was used for further analysis; when the data were heterogeneous, Dunnett’s test was used for analysis. All statistical tests were performed at the $p < 0.05$ and $p < 0.01$ levels of significance.

4. Conclusions

In this study, a novel polymerized whey protein concentrate-based glutathione oral delivery system with high stability was successfully developed resulting in greater delivery efficiency as evidenced by in vivo pharmacokinetic data and antioxidant activity analysis. Oral administration of PWPC-GSH in diet concentration up to 4% (w/w) for 28 days had no adverse effects on male and female rats. All results suggested that thermal treatment induced polymerized whey protein concentrate represents a viable, effective potential delivery system with the ability to enhance oral bioavailability of GSH.

Supplementary Materials: The following are available online: Table S1: Hematology of rats in 28-day toxicity study, Table S2: Serum biochemistry of rats in 28-day toxicity study

Author Contributions: S.Z.: Methodology, Formal analysis, Writing original draft. C.W.: Methodology, Formal analysis, Writing—review & editing. W.Z.: Methodology. A.H.K.: Data curation, Software. M.G.: Conceptualization, Supervision, Resource. A.K.: Project administration, Methodology. All authors have read and agreed to the published version of the manuscript.

Funding: Authors would like to thank FoodScience Cooperation, Williston, Vermont, USA for in part of funding this project.

Institutional Review Board Statement: All animal experiments were approved by the Animal Welfare and Research Ethics Committee at Jilin University (Approval ID: SY201905018).

Informed Consent Statement: Not applicable.

Data Availability Statement: Data available in a publicly accessible repository.

Conflicts of Interest: The authors declare no conflict of interest.

Sample Availability: Samples of the compounds are available from the authors.

References

- Lash, L.H.; Hagen, T.M.; Jones, D.P. Exogenous glutathione protects intestinal epithelial cells from oxidative injury. *Proc. Natl. Acad. Sci. USA* **1986**, *83*, 4641–4645. [CrossRef]
- Aw, T.Y. Intestinal glutathione: Determinant of mucosal peroxide transport, metabolism, and oxidative susceptibility. *Toxicol. Appl. Pharmacol.* **2005**, *204*, 320–328. [CrossRef]
- Li, P.; Yin, Y.L.; Li, D.; Kim, S.W.; Wu, G. Amino acids and immune function. *Br. J. Nutr.* **2007**, *98*, 237–252. [CrossRef]
- Fraternale, A.; Brundu, S.; Magnani, M. Glutathione and glutathione derivatives in immunotherapy. *Biol. Chem.* **2017**, *398*, 261–275. [CrossRef]
- Postić, S. Free radicals and antioxidants in normal physiological functions and human disease. *Int. J. Biochem. Cell Biol.* **2007**, *39*, 44–84.
- Pastore, S. Analysis of glutathione: Implication in redox and detoxification. *Clin. Chim. Acta* **2003**, *333*, 19–39. [CrossRef]
- Herzenberg, L.A. Glutathione Deficiency is associated with impaired survival in HIV disease. *Proc. Natl. Acad. Sci. USA* **1997**, *94*, 1967–1972. [CrossRef]
- Balendiran, G.K.; Dabur, R.; Fraser, D. The role of glutathione in cancer. *Cell Biochem. Funct.* **2004**, *22*, 343–352. [CrossRef] [PubMed]
- Wu, G.; Fang, Y.Z.; Yang, S.; Lupton, J.R.; Turner, N.D. Glutathione Metabolism and Its Implication for Health. *J. Nutr.* **2004**, *134*, 489–492. [CrossRef]

10. Grimble, R.F. The Effects of Sulfur Amino Acid Intake on Immune Function in Humans. *J. Nutr.* **2006**, *6*, 1660S–1665S. [CrossRef]
11. Kukreja, R.C.; Hess, M.L. The oxygen free radical system: From equations through membrane-protein interactions to cardiovascular injury and protection. *Cardiovasc. Res.* **1992**, *7*, 641–655. [CrossRef]
12. Dhalla, N.S.; Temsah, R.M.; Netticadan, T. Role of oxidative stress in cardiovascular diseases. *J. Hypertens.* **2000**, *18*, 655–673. [CrossRef] [PubMed]
13. Maurice, M.M. Evidence for the role of an altered redox state in hyporesponsiveness of synovial T cells in rheumatoid arthritis. *J. Immunol.* **1997**, *158*, 1458–1465. [PubMed]
14. Tretter, L.; Sipos, I.; Adamvizi, V. Initiation of neuronal damage by complex I deficiency and oxidative stress in Parkinson's disease. *Neurochem. Res.* **2004**, *29*, 569–577. [CrossRef] [PubMed]
15. Rahman, I.; Macnee, W. Oxidative stress and regulation of glutathione in lung inflammation. *Eur. Respir. J.* **2010**, *16*, 534–554. [CrossRef]
16. Estrela, J.M.; Ortega, A.; Obrador, E. Glutathione in Cancer Biology and Therapy. *Crit. Rev. Clin. Lab. Sci.* **2006**, *43*, 143–181. [CrossRef]
17. Witschi, A. The systemic availability of oral glutathione. *Eur. J. Clin. Pharmacol.* **1992**, *43*, 667–669. [CrossRef]
18. Peng, X.; Xiong, Y.L.; Kong, B. Antioxidant activity of peptide fractions from whey protein hydrolysates as measured by electron spin resonance. *Food Chem.* **2009**, *113*, 196–201. [CrossRef]
19. Tong, L.M.; Sasaki, S.; McClements, D.J.; Decker, E.A. Mechanisms of the antioxidant activity of a high molecular weight fraction of whey. *J. Agric. Food Chem.* **2000**, *48*, 1473–1478. [CrossRef]
20. Chung, C.; Rojanasasithara, T.; Mutilangi, W.; McClements, D.J. Enhanced stability of anthocyanin-based color in model beverage systems through whey protein isolate complexation. *Food Res. Int.* **2015**, *76*, 761–768. [CrossRef]
21. Chotiko, A.; Sathivel, S. Releasing characteristics of anthocyanins extract in pectin–whey protein complex microcapsules coated with zein. *J. Food Sci. Technol.* **2017**, *54*, 1–8. [CrossRef]
22. Weinbreck, F.; Minor, M.; De Kruif, C.G. Microencapsulation of oils using whey protein/gum Arabic coacervates. *J. Microencapsul.* **2004**, *21*, 667–679. [CrossRef]
23. Carneiro, H.C.F.; Tonon, R.V.; Grosso, C.R.F.; Hubinger, M.D. Encapsulation efficiency and oxidative stability of flaxseed oil microencapsulated by spray drying using different combinations of wall material. *J. Food Eng.* **2013**, *115*, 443–451. [CrossRef]
24. Abbasi, A.; Emam-D-Jomeh, Z.; Mousavi, M.A.; Davoodi, D. Stability of vitamin D₃ encapsulated in nanoparticles of whey protein isolate. *Food Chem.* **2014**, *143*, 379–383. [CrossRef] [PubMed]
25. Liang, L.; Leung Sok Line, V.; Remondetto Gabriele, E.; Subirade, M. In vitro release of α -tocopherol from emulsion-loaded β -lactoglobulin gels. *Int. Dairy J.* **2010**, *20*, 176–181. [CrossRef]
26. Somchue, W.; Sermsri, W.; Shiowatana, J.; Siripinyanond, A. Encapsulation of α -tocopherol in protein-based delivery particles. *Food Res. Int.* **2009**, *42*, 909–914. [CrossRef]
27. Wang, C.N.; Zhou, X.H.; Wang, H.; Sun, X.M.; Guo, M.R. Interactions between β -Lactoglobulin and 3,3'-Diindolylmethane in Model System. *Molecules* **2019**, *24*, 2151. [CrossRef]
28. Khem, S.; Small, D.M.; May, B.K. The behaviour of whey protein isolate in protecting *Lactobacillus plantarum*. *Food Chem.* **2016**, *190*, 717–723. [CrossRef] [PubMed]
29. Zhang, X.F.; Sun, X.M.; Gao, F.; Wang, J.Q.; Wang, C.N. Systematical characterization of physicochemical and rheological properties of thermal-induced polymerized whey protein. *J. Sci. Food Agric.* **2019**, *99*, 923–932. [CrossRef]
30. Gate, L.; Vauthier, C.; Couvreur, P.; Tew, K.D.; Tapiero, H. Glutathione-loaded poly(isobutylcyanoacrylate) nanoparticles and liposomes: Comparative effects in murine erythrocytes and macrophage-like cells. *STP Pharma Sci.* **2001**, *11*, 355–361.
31. Trapani, A.; Laquintana, V.; Denora, N.; Lopodota, A.; Cutrignelli, A.; Franco, M.; Trapani, G.; Liso, G. Eudragit RS 100 microparticles containing 2-hydroxypropyl- β -cyclodextrin and glutathione: Physicochemical characterization, drug release and transport studies. *Eur. J. Pharm. Sci.* **2007**, *30*, 64–74. [CrossRef] [PubMed]
32. Baek, M.; Choy, J.; Choi, S. Montmorillonite intercalated with glutathione for antioxidant delivery: Synthesis, characterization, and bioavailability evaluation. *Int. J. Pharm.* **2012**, *425*, 29–34. [CrossRef] [PubMed]
33. Liu, D.R.; Cheng, J.J.; Zhao, C.H.; Guo, M.R. Effect of sodium triphosphate on particle size of heat-induced whey protein concentrate aggregates. *Food Sci. Nutr.* **2018**, *6*, 1940–1949. [CrossRef] [PubMed]
34. Chen, L.; Chen, J.S.; Ren, J.Y.; Zhao, M.M. Effects of Ultrasound Pretreatment on the Enzymatic Hydrolysis of Soy Protein Isolates and on the Emulsifying Properties of Hydrolysates. *J. Agric. Food Chem.* **2011**, *59*, 2600–2609. [CrossRef] [PubMed]
35. Salatin, S.; Dizaj, S.M.; Khosroushahi, A.Y. Effect of the surface modification, size, and shape on cellular uptake of nanoparticles. *Cell Biol. Int.* **2015**, *39*, 881–890. [CrossRef]
36. Mantovani, R.A.; Fattori, J.; Michelon, M.; Cunha, R.L. Formation and pH-stability of whey protein fibrils in the presence of lecithin. *Food Hydrocoll.* **2016**, *60*, 288–298. [CrossRef]
37. Naji-Tabasi, S.; Razavi, S.M.; Mehditabar, H. Fabrication of basil seed gum nanoparticles as a novel oral delivery system of glutathione. *Carbohydr. Polym.* **2017**, *157*, 1703–1713. [CrossRef]
38. Guo, M.R.; Fox, P.F.; Flynn, A.; Kindstedt, P.S. Susceptibility of β -Lactoglobulin and Sodium Caseinate to Proteolysis by Pepsin and Trypsin. *J. Dairy Sci.* **1995**, *78*, 2336–2344. [CrossRef]
39. Fitzsimons, S.M.; Mulvihill, D.M.; Morris, E.R. Denaturation and aggregation processes in thermal gelation of whey proteins resolved by differential scanning calorimetry. *Food Hydrocoll.* **2007**, *21*, 638–644. [CrossRef]

40. Doherty, S.B.; Gee, V.L.; Ross, R.P.; Stanton, C.; Fitzgerald, G.F.; Brodkorb, A. Efficacy of whey protein gel networks as potential viability-enhancing scaffolds for cell immobilization of *Lactobacillus rhamnosus* GG. *J. Microbiol. Methods* **2010**, *80*, 231–241. [CrossRef]
41. Jain, A.; Sharma, G.; Ghoshal, G.; Kesharwani, P.; Singh, B.; Shivha, U.S.; Katare, O.P. Lycopene loaded whey protein isolate nanoparticles: An innovative endeavor for enhanced bioavailability of lycopene and anti-cancer activity. *Int. J. Pharm.* **2018**, *456*, 97–105. [CrossRef] [PubMed]
42. Liu, K.; Zha, X.Q.; Shen, W.D.; Li, Q.M.; Pan, L.H.; Luo, J.P. The hydrogel of whey protein isolate coated by lotus root amylopectin enhance the stability and bioavailability of quercetin. *Carbohydr. Polym.* **2020**, *236*, 116009. [CrossRef] [PubMed]
43. Bounous, G.; Gervais, F.; Amer, V.; Batist, G.; Gold, P. The influence of dietary whey protein on tissue glutathione and the diseases of aging. *Clin. Investig. Med.* **1990**, *12*, 343–349.
44. Micke, P.; Beeh, K.M.; Schlaak, J.F.; Buhl, R. Oral supplementation with whey proteins increases plasma glutathione levels of HIV-infected patients. *Eur. J. Clin. Investig.* **2001**, *31*, 171–178. [CrossRef] [PubMed]
45. Kent, K.D.; Harper, W.J.; Bomser, J.A. Effect of whey protein isolate on intracellular glutathione and oxidant-induced cell death in human prostate epithelial cells. *Toxicol. Int. J. Publ. Assoc. Bibra* **2003**, *17*, 27–33. [CrossRef]
46. Hagen, T.M.; Wierzbicka, G.T.; Sillau, A.H.; Bowman, B.B.; Jones, D.P. Bioavailability of dietary glutathione: Effect on plasma concentration. *Am. J. Physiol.* **1990**, *259*, G524–G529. [CrossRef]
47. Colbert, L.B.; Decker, E.A. Antioxidant Activity of an Ultrafiltration Permeate from Acid Whey. *J. Food Sci.* **1991**, *56*, 1248–1250. [CrossRef]
48. Taylor, M.J.; Richardson, T. Antioxidant Activity of Skim Milk: Effect of Heat and Resultant Sulfhydryl Groups. *J. Dairy Sci.* **1980**, *63*, 1783–1795. [CrossRef]
49. Bauter, M.R.; Mendes, O. Subchronic toxicity of lyophilized apoaequorin protein powder in Sprague-Dawley rats. *Toxicology Res. Appl.* **2018**, *2*, 1–15. [CrossRef]
50. Lee, J.M.; Lee, M.A.; Do, H.N.; Song, Y.I.; Bae, R.J.N.; Lee, H.Y.; Park, S.H.; Kang, J.S.; Kang, J.K. Historical control data from 13-week repeated toxicity studies in Crj:CD (SD) rats. *Lab. Anim. Res.* **2012**, *28*, 115–121. [CrossRef]
51. Petterino, C.; Argentino-Storino, A. Clinical chemistry and haematology historical data in control Sprague-Dawley rats from pre-clinical toxicity studies. *Exp. Toxicol. Pathol.* **2006**, *57*, 213–219. [CrossRef]
52. Saito, C.; Zwingmann, C.; Jaeschke, H. Novel Mechanisms protection against acetaminophen hepatotoxicity in mice by glutathione and N-acetylcysteine. *Hepatology* **2010**, *51*, 246–254. [CrossRef]
53. Gad, A.S.; Khadrawy, Y.A.; El-Nekeety, A.A.; Mohamed, S.R.; Hassan, N.S.; Abdel-Wahhab, M.A. Antioxidant activity and hepatoprotective effects of whey protein and Spirulina in rats. *Nutrition* **2011**, *27*, 582–589. [CrossRef] [PubMed]
54. Khan, A.; Wang, C.N.; Sun, X.M.; Adam, K.; Guo, M.R. Preparation and Characterization of Whey Protein Isolate–DIM Nanoparticles. *Int. J. Mol. Sci.* **2019**, *20*, 3917. [CrossRef] [PubMed]
55. Poon, R.; Lecavalier, P.; Mueller, R.; Valli, V.E.; Procter, B.G.; Chu, I. Subchronic oral toxicity of di-n-octyl phthalate and di(2-ethylhexyl) phthalate in the rat. *Food Chem. Toxicol.* **1997**, *35*, 225–239. [CrossRef]

Article

Sulodexide Increases Glutathione Synthesis and Causes Pro-Reducing Shift in Glutathione-Redox State in HUVECs Exposed to Oxygen–Glucose Deprivation: Implication for Protection of Endothelium against Ischemic Injury

Klaudia Bontor *  and Bożena Gabryel

Department of Pharmacology, School of Medicine in Katowice, Medical University of Silesia, 40-752 Katowice, Poland

* Correspondence: klaudia.bontor@sum.edu.pl; Tel./Fax: +48-32-252-38-35

Abstract: Sulodexide (SDX), a purified glycosaminoglycan mixture used to treat vascular diseases, has been reported to exert endothelial protective effects against ischemic injury. However, the mechanisms underlying these effects remain to be fully elucidated. The emerging evidence indicated that a relatively high intracellular concentration of reduced glutathione (GSH) and a maintenance of the redox environment participate in the endothelial cell survival during ischemia. Therefore, the aim of the present study was to examine the hypothesis that SDX alleviates oxygen–glucose deprivation (OGD)-induced human umbilical endothelial cells' (HUVECs) injury, which serves as the in vitro model of ischemia, by affecting the redox state of the GSH: glutathione disulfide (GSSG) pool. The cellular GSH, GSSG and total glutathione (tGSH) concentrations were measured by colorimetric method and the redox potential (ΔEh) of the GSSG/2GSH couple was calculated, using the Nernst equation. Furthermore, the levels of the glutamate–cysteine ligase catalytic subunit (GCLc) and the glutathione synthetase (GSS) proteins, a key enzyme for de novo GSH synthesis, were determined using enzyme-linked immunoassay (ELISA). We demonstrated that the SDX treatment in OGD conditions significantly elevated the intracellular GSH, enhanced the GSH:GSSG ratio, shifting the redox potential to a more pro-reducing status. Furthermore, SDX increased the levels of both GCLc and GSS. The results show that SDX protects the human endothelial cells against ischemic stress by affecting the GSH levels and cellular redox state. These changes suggest that the reduction in the ischemia-induced vascular endothelial cell injury through repressing apoptosis and oxidative stress associated with SDX treatment may be due to an increase in GSH synthesis and modulation of the GSH redox system.

Citation: Bontor, K.; Gabryel, B. Sulodexide Increases Glutathione Synthesis and Causes Pro-Reducing Shift in Glutathione-Redox State in HUVECs Exposed to Oxygen–Glucose Deprivation: Implication for Protection of Endothelium against Ischemic Injury. *Molecules* **2022**, *27*, 5465. <https://doi.org/10.3390/molecules27175465>

Academic Editor: Pál Perjési

Received: 13 July 2022

Accepted: 22 August 2022

Published: 25 August 2022

Publisher's Note: MDPI stays neutral with regard to jurisdictional claims in published maps and institutional affiliations.



Copyright: © 2022 by the authors. Licensee MDPI, Basel, Switzerland. This article is an open access article distributed under the terms and conditions of the Creative Commons Attribution (CC BY) license (<https://creativecommons.org/licenses/by/4.0/>).

Keywords: sulodexide; endothelial cells; ischemia; apoptosis; oxidative stress; GSH; GSSG; GCLc; GSS; redox potential

1. Introduction

Ischemia (oxygen and nutrient deficiency) plays a crucial role in the pathogenesis of cardiovascular diseases, including myocardial ischemia, ischemic stroke, and chronic or acute limb ischemia [1,2]. The vascular endothelium is the first site of ischemic injury. Multiple mechanisms can lead dysfunction already during ischemia to endothelial dysfunction and damage, e.g., the depletion of energy stores, disturbances in protein synthesis, increase in pro-inflammatory mediators, induction of adhesion molecules, and the modulation of ion channels and gap junction proteins [3].

One of the undesired consequences of ischemia is an increased potential for oxidative damage of cellular macromolecules, such as DNA, proteins, and lipids by reactive oxygen species (ROS). The major sources of intracellular ROS are mitochondrial electron transport, arachidonic acid pathway and activities of cellular oxidases [4]. The oxidative stress

generating from the excessive ROS production and decreased availability of antioxidants, such as glutathione, contributes to the loss of endothelial barrier function, glycocalyx degradation, apoptosis, and vascular injury [5,6]. Thus, a possible therapeutic target for endothelial protection is the enhancement of the endogenous antioxidant defense system.

Glutathione is a tripeptide (γ -L-glutamyl-L-cysteinyl-glycine) that serves as a major endogenous non-enzymatic antioxidant against the oxidative stress and endothelial dysfunction caused by ischemia [7]. Moreover, glutathione deficiency is known to contribute to the apoptosis of ischemic endothelial cells [8]. Glutathione exists in two forms, reduced (GSH) and oxidized (GSSG). GSH is involved in the neutralization of ROS, being reduced by oxidation to GSSG. The GSH:GSSG ratio is a critical determinant of the cellular redox status [9]. Meanwhile, the redox potential (ΔE_h) of the GSSG/2GSH couple, quantitatively calculated according to the Nernst equation, is considered as a major redox buffer in the cells. Furthermore, it is currently believed that the redox state of the GSSG/2GSH couple may be an indicator of the biological state of the cells, including apoptosis or necrosis [10].

GSH is synthesized *de novo* from precursor amino acids (glutamate, cysteine, and glycine) in a two-step ATP-dependent enzymatic process catalyzed by glutamate–cysteine ligase (GCL) and glutathione synthase (GSS). GCL catalyzes the rate-limiting reaction between glutamate and cysteine, whose product is γ -glutamylcysteine (γ GC). Then, GSS links γ GC to glycine to form GSH molecule [11]. GCL consists of catalytic (GCLc) and modifier (GCLm) subunits. GCLc exhibits all of the catalytic activity of the enzyme, whereas GCLm is enzymatically inactive but regulates the binding activity of GCLc to its substrates [12].

GSH is also synthesized via the salvage pathway, which either involves the reduction in GSSG by glutathione reductase or uses precursors formed from the hydrolysis of GSH or its conjugates by γ -glutamyltranspeptidase at the surface of the cell membrane transported back into cells as amino acids or dipeptides [13].

Decreased GSH levels and GSH:GSSG ratio were reported in many ischemic vascular diseases and may reflect a common pathophysiological mechanism [7]. Therefore, the search for suitable therapeutic agents to improve the GSH content and GSH–redox balance could be an effective means of treating ischemic injury.

SDX is a mixture of glycosaminoglycans (GAGs), purified from porcine mucosa consisting of 80% low-molecular weight heparin and 20% dermatan sulfate [14]. SDX possesses a wide range of pharmacological properties, such as antithrombotic, profibrinolytic, and lipid-lowering activity [15]. This drug is used in clinical practice for the treatment of chronic venous and arterial diseases [14,16]. Recently, SDX was associated with an improvement in the therapy for venous leg ulcers [17], deep vein thrombosis [18], cerebrovascular disorders [15], proteinuria, and cardiovascular disease in diabetes [17,19].

In vitro and *in vivo* studies have shown that SDX exerts anti-inflammatory [20], antioxidant [21], immunomodulatory [22], anti-proliferative [23], antiproteolytic [24], and vasculo-protective features [25].

The studies on the endothelial protective effect of SDX obtained the desired results. For example, SDX was reported to maintain or restore the integrity of the glycocalyx, a gel-like layer covering the luminal surface of vascular endothelium, possibly by providing precursors of endothelial GAGs [26]. SDX also alleviated the endothelial dysfunction in streptozotocin-induced diabetes in rats, by reducing the number of the circulating endothelial cells and improving the endothelium-dependent relaxation in the small arteries [27]. Furthermore, SDX has been shown to exert potent anti-senescent and anti-inflammatory effects in both venous [28], and arterial endothelial cells [29].

Several studies have shown that the antioxidant properties of SDX underlie many other bioactivities of this drug [30–33]. However, only a few studies have investigated the molecular mechanism of SDX against ischemic damage [34–39]. We previously described that SDX induces GSH-related genes in ischemic endothelial cells [37], but the direct contribution of GSH to the protective effects of SDX has yet to be established.

In this study, we investigated the ability of SDX to prevent apoptosis and oxidative stress in the human umbilical vein endothelial cells (HUVECs) induced by oxygen–glucose deprivation (OGD), a commonly used model of simulated ischemia *in vitro*, by affecting the intracellular tGSH, GSH, and GSSG concentrations, as well as the redox state of the GSH:GSSG pool. Furthermore, the levels of the GCLC and GSS proteins, the key enzymes for *de novo* GSH synthesis, were determined.

2. Results

2.1. Effect of SDX on Apoptosis

As shown in Figure 1A (upper panel), after 6 h of simulated ischemia, many of the endothelial cells detached from each other and exhibited cytoplasmic shrinkage. However, the SDX treatment in OGD suppressed the morphological changes of the HUVECs, and increased the number of surviving cells. These results were further confirmed by analysis of the apoptotic features, such as changes in nuclear morphology using Hoechst 33342. The Hoechst 33342 fluorochrome is used to detect the compacted state of chromatin. As shown in Figure 1A (middle panel), the control cells exhibited uniformly dispersed chromatin. However, the cells exposed to OGD for 6 h showed the typical features of apoptosis (chromatin condensation, nuclear shrinkage, and apoptotic bodies formation). Moreover, we found that the SDX treatment significantly inhibited the OGD-induced apoptotic nuclear damages.

As quantified in Figure 1B, AI was strongly increased after 6 h of OGD (median 29%, range 15–42) compared to the Control group (median 1.98%, range 1–7.6). A statistically significant decrease in AI was detected when the ischemic HUVECs were treated with SDX (median 13%, range 6–18).

2.2. Effect of SDX on Intracellular ROS Accumulation

To analyze whether the antiapoptotic action of SDX is associated with a decrease in ROS level, the HUVECs were incubated with the cell-permeable dye, CellROX Green Reagent, which exhibits green fluorescence and binds to nuclear DNA only upon oxidation. The fluorescence microscopy of the normoxic cells showed a weak punctate green fluorescence pattern, indicating basal mitochondrial ROS production (Figure 1A, lower panel). After 6 h of OGD, the staining pattern changed to bright nuclear fluorescence, showing the oxidation of CellROX Green Reagent and the binding of the oxidized dye to nuclear DNA. The co-incubation of the OGD-treated cells with SDX efficiently suppressed the bright nuclear fluorescence, indicating inhibition of the ROS accumulation.

As shown in Figure 1C, the intensity of the CellROX green fluorescence was dramatically increased in the OGD group (median 64.90, range 48.44–82.70) compared with the Control group (median 24.64, range 13.40–31.03). After treatment with SDX in OGD, the ROS-stimulated oxidation of the CellROX Green Reagent was significantly lower (median 38.44, range 33.45–44) compared to the OGD group.

Importantly, the decreased production of the ROS correlates with a reduction in the endothelial cell apoptosis, with the highest levels observed in the OGD + SDX group (Figure 1D, $R^2 = 0.63$ and $p < 0.001$).

2.3. Effect of SDX on Intracellular GSH Content, GSH:GSSG Ratio and Redox Potential

To confirm that SDX may exert antioxidant and endothelial protective effects by ameliorating the glutathione-dependent redox imbalance caused by ischemic injury, the concentrations of tGSH, GSH, and GSSG, the GSH:GSSG ratio, and the changes in the redox potential ΔE_h of the GSSG/2GSH couple were determined.

Our data indicate that the intracellular tGSH concentrations gradually decreased in response to 1, 3, and 6 h of OGD (median 17.01 nmol/mg protein, range 13.17–18.71; median 10.29 nmol/mg protein, range 8.9–11.61; median 2.6 nmol/mg protein, range 1.14–3.56, respectively) compared to the Control group (median 23.26 nmol/mg protein, range 17.78–25.4).

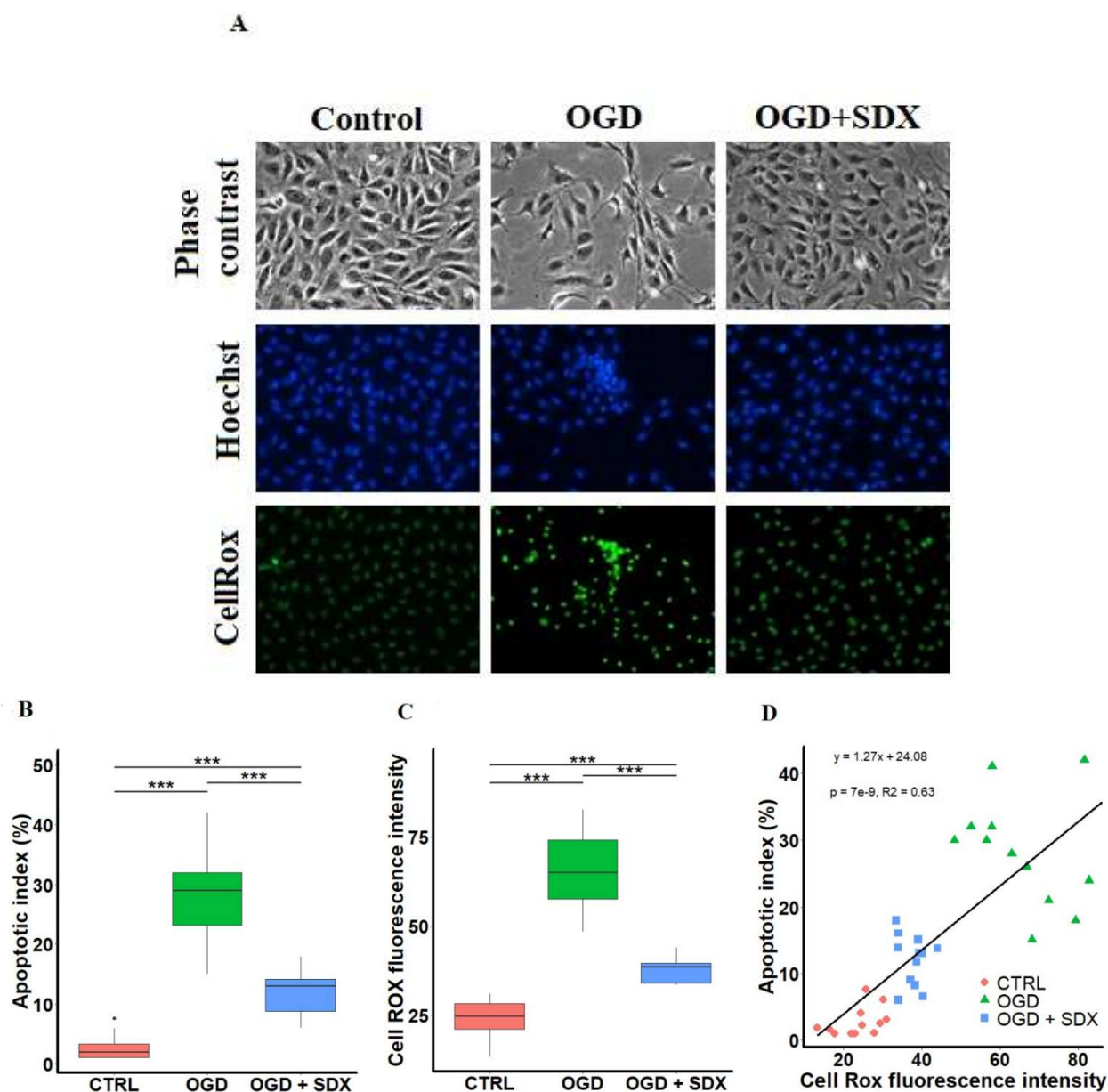


Figure 1. SDX cytoprotective effects against oxidative damage induced by OGD in human endothelial cells. HUVECs were treated for 6 h in OGD in the absence or presence of SDX (0.5 LRU/mL). (A) Microscopic observations. Morphology was visualized and photographed under an inverted phase contrast microscope (original magnification $\times 200$). Apoptotic cells were identified by Hoechst 33342 staining and intracellular ROS production was observed using CellROX Green Reagent. The images were examined under a fluorescence microscope (original magnification $\times 200$). Control: normal conditions; OGD: cells exposed to simulated ischemia in vitro only; OGD + SDX: cells exposed to simulated ischemia in vitro and treated with SDX. Apoptotic index (B) and quantification of CellROX green fluorescence intensity (C) in each corresponding group ($n = 12$). Data in panels (B,C) are box-plots representing the median and quartiles with the upper and lower limits. Significant results are marked with asterisks (***) $p < 0.001$); (D) Correlation between apoptotic index and ROS production. Apoptotic index and ROS generation were determined as described in panel (A). Pearson's correlation coefficient $R^2 = 0.63$ was calculated from the linear regression analysis between apoptotic index and CellROX green fluorescence intensity. Control group. [·] is the outlier.

As shown in Figure 2A, the SDX treatment for 1 and 3 h in OGD significantly elevated the intracellular tGSH (median 29.12 nmol/mg protein, range 26.96–33.64; median

30.26 nmol/mg protein, range 27.44–32.69, respectively). Compared with the Control group, the intracellular tGSH of the HUVECs treated with SDX in OGD for 6 h decreased significantly (median 9.3 nmol/mg protein, range 6.33–9.69). Compared with the 6 h OGD-treated cells, the intracellular tGSH was significantly increased after the SDX treatment.

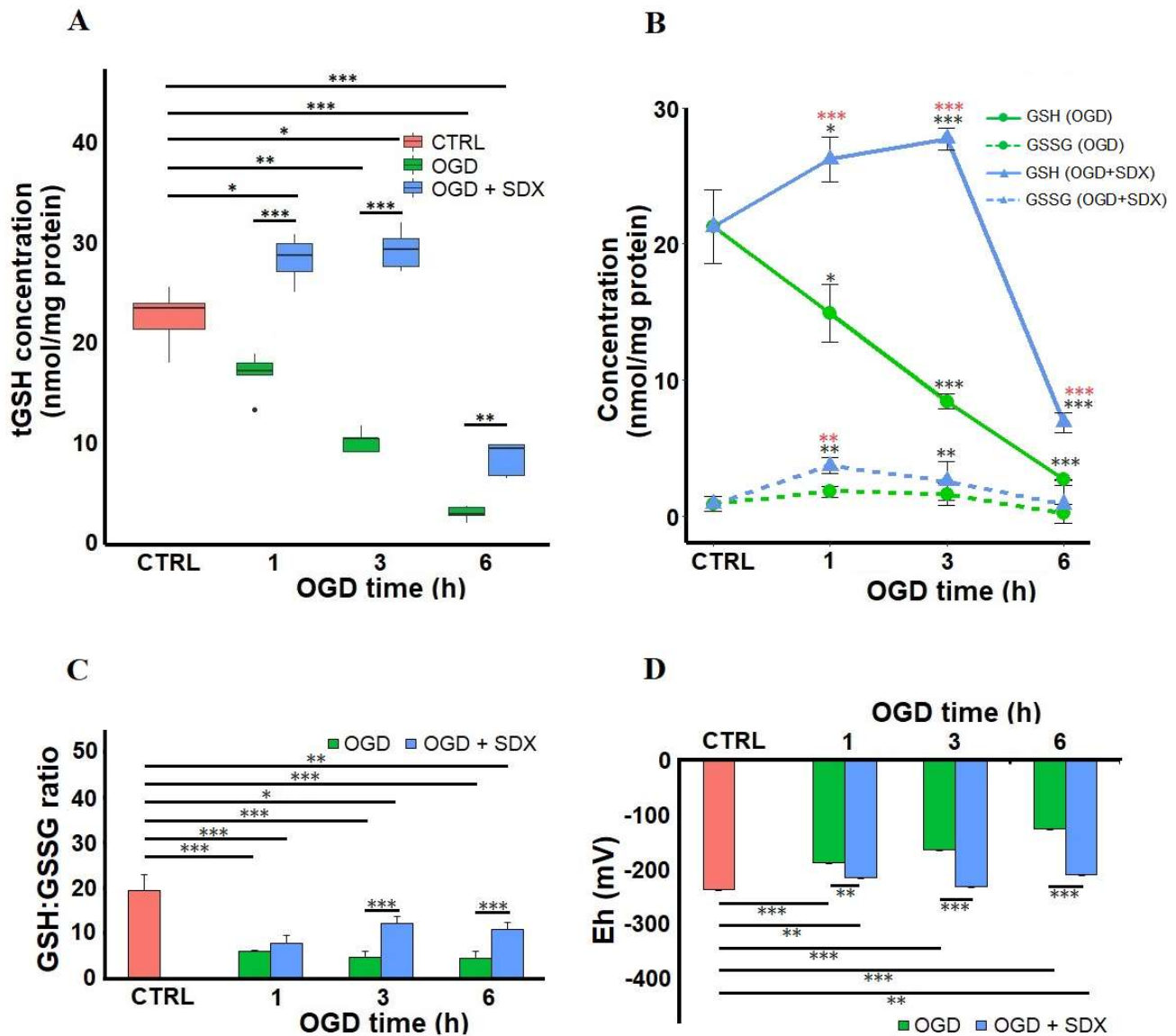


Figure 2. Time-dependent effects of SDX on the intracellular GSH level and redox state in human endothelial cells subjected to OGD. HUVECs were treated for 1, 3, or 6 h in OGD in the absence or presence of SDX (0.5 LRU/mL). The intracellular concentrations of total glutathione (tGSH) (A), reduced glutathione (GSH), and oxidized glutathione (GSSG) (B) were measured by colorimetric assay ($n = 4-6$). The tGSH, GSH, and GSSG levels were normalized to total protein concentrations and expressed as nmol/mg protein. The GSH:GSSG ratio (C) and the GSH redox potential (ΔEh) (D) for each incubation period were calculated. CTRL: normal conditions; OGD: cells exposed to simulated ischemia in vitro only; OGD + SDX: cells exposed to simulated ischemia in vitro and treated with SDX. Data in panel (A) are box-plots representing the median and quartiles with the upper and lower limits. Each point in panel (B) and bar graphs in panels (C,D) represent mean \pm standard deviation (SD). In panels (A–D), the asterisks indicate the statistically significant differences (* $p < 0.05$; ** $p < 0.01$; *** $p < 0.001$). In panel B, statistically significant differences between OGD groups and OGD + SDX groups are marked with red asterisks (*), while black asterisks (•) are used to mark the differences between the test groups and Control group. [•] is the outlier.

We further separately determined the effect of SDX on the GSH and GSSG concentrations. The results presented in Figure 2B show a significant gradual decrease in the GSH levels from 21.26 ± 2.69 nmol/mg protein in the control cells to 14.9 ± 2.13 , 8.42 ± 0.54 , and 2.67 ± 0.04 nmol/mg protein after 1, 3, and 6 h of OGD exposure, respectively. The GSSG levels, which were much lower than the GSH levels at baseline (0.87 ± 0.56 nmol/mg protein), increased to 1.77 ± 0.42 and 1.59 ± 0.8 nmol/mg protein after 1 and 3 h of OGD, respectively; and then decreased to 0.16 ± 0.7 nmol/mg protein after 6 h. It was observed that treatment with SDX for 1 and 3 h in OGD resulted in a significant increase in the intracellular GSH concentrations (26.22 ± 1.63 and 27.72 ± 0.83 nmol/mg protein, respectively). After 6 h treatment with SDX and OGD, the intracellular GSH level was significantly reduced (6.88 ± 0.73 nmol/mg protein) compared with the untreated HUVECs, but remained higher than in the corresponding OGD group. In addition, the treatment of the HUVECs with SDX for 1 and 3 h in OGD significantly increased the GSSG content (3.68 ± 0.56 and 2.54 ± 0.58 nmol/mg protein, respectively). The exposure of the cells to SDX for 6 h did not significantly affect the GSSG level, compared to the Control and corresponding OGD group (Figure 2B). The intracellular glutathione-redox balance was expressed as the GSH:GSSG ratio (Figure 2C). A higher GSH:GSSG ratio could make the endothelial cells more resistant to oxidative stress and compensate for the decrease in the GSH levels [10,40]. The intracellular GSH:GSSG ratio after 1, 3, and 6 h of OGD exposure was found to be significantly lower (5.98 ± 0.29 ; 4.69 ± 1.24 ; and 4.54 ± 1.42 , respectively) than in the control cells (19.48 ± 3.52). The redox balance shifts toward a more reducing state in the ischemic HUVECs treated with SDX for 3 or 6 h (12.27 ± 1.47 ; 10.74 ± 1.74 , respectively). However, there was no significant difference in the GSH:GSSG ratio between the SDX-treated and non-treated groups after 1 h of OGD (7.78 ± 1.78 vs. 5.98 ± 0.29) due to an increase in the intracellular GSSG level (Figure 2B,C).

Furthermore, the redox potential was determined according to the Nernst equation (Figure 2D) [41]. It was well known that an increase in the ΔE_h of the GSSG/2GSH couple can lead to apoptosis, and the antioxidants that decrease the ΔE_h have antiapoptotic properties [10,42]. It was shown that ΔE_h was increased in the cells exposed to OGD for 1, 3, or 6 h (-188 ± 12 ; -165 ± 5 ; and -127 ± 10 mV, respectively) compared to the control (-237 ± 5 mV). Moreover, the treatment of the cells with SDX for 1, 3, and 6 h resulted in a significant decrease in ΔE_h (-216 ± 10 ; -232 ± 5 ; and -211 ± 19 mV, respectively) compared with the corresponding OGD groups without SDX.

2.4. Effect of SDX on GCLc and GSS Protein Levels

We next measured the GCLc and GSS protein levels as a surrogate for their enzymatic activity in the ischemic HUVECs treated with SDX at different time points (Figure 3). Some of the studies have found a correlation between the protein contents and enzyme activity levels of GCL and GSS [43,44].

In this study, we revealed that the GCLc protein levels were significantly increased in the cells exposed to 1, 3, and 6 h of OGD alone (median 20.00 ng/mL, range 18.17–20.38; median 17.4 ng/mL, range 15.15–17.67; median 9.37 ng/mL, range 7.86–10.72, respectively) compared to the Control group (median 3.45 ng/mL, range 2.67–4.95). Moreover, the treatment of cells with SDX for 1 and 3 h in OGD resulted in a dramatic increase in the GCLc protein levels (median 35.76 ng/mL, range 30.24–40.84; median 40.37 ng/mL, range 36.9–42.7, respectively) (Figure 3A).

The treatment of the ischemic HUVECs with or without SDX resulted in similar GSS concentration profiles. The GSS concentrations were found to be increased in cells treated with OGD alone for 1, 3 or 6 h (median 17.32 ng/mL, range 14.98–18.48; median 15.06 ng/mL, range 11.13–16.32; median 8.08 ng/mL, range 6.05–10.48, respectively) compared to control (median 3.27 ng/mL, range 2.97–4.29). The protein levels of GSS were significantly increased after 1 and 3 h of incubation with SDX in OGD (median 33.26 ng/mL, range 24.7–38.12; median 37.34 ng/mL, range 36.37–40.25, respectively) (Figure 3B).

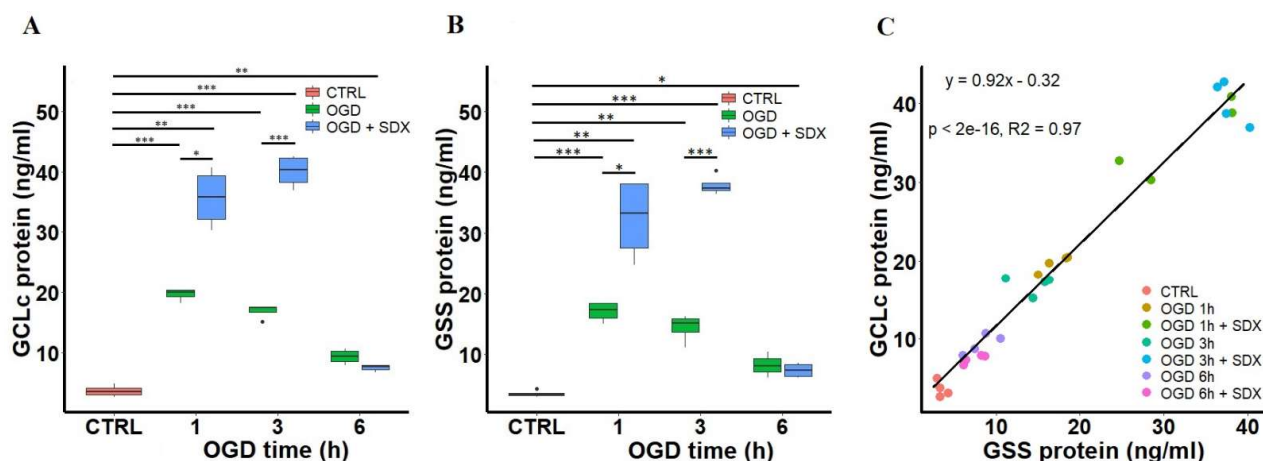


Figure 3. Time-dependent effects of SDX on the protein levels of GCLc and GSS in human endothelial cells subjected to OGD. HUVECs were treated with OGD for 1, 3, or 6 h in the absence or presence of SDX (0.5 LRU/mL). Quantitative analysis of GCLc (A) and GSS (B) levels in cell lysates was performed by ELISA ($n = 4$). The GCLc and GSS protein concentrations (ng/mL) were normalized to total lysate protein. CTRL: normal conditions; OGD: cells exposed only to simulated ischemia in vitro; OGD + SDX: cells exposed to simulated ischemia in vitro and treated with SDX. Data in panels (A,B) are box-plots representing the median and quartiles with the upper and lower limits. Significant results are marked with asterisks (* $p < 0.05$; ** $p < 0.01$; *** $p < 0.001$); (C) Correlation between GCLc and GSS protein levels. Pearson's correlation coefficient $R^2 = 0.97$ was calculated from the linear regression analysis between concentrations of GCLc and GSS in cell lysates obtained from ELISA. [-] is the outlier.

Moreover, GCLc and GSS proteins showed a very high correlation with each other (Figure 3C, $R^2 = 0.97$, and $p < 0.001$). This is likely due to the fact that both of the enzymes are coordinately regulated and the experimental conditions that induce the catalytic subunit of GCL also induce the GSS expression [45,46].

3. Discussion

The main findings of the present study were as follows: (i) the reduced ROS production in the SDX-treated HUVECs under OGD conditions was strongly correlated with attenuation of apoptosis; (ii) the GSH:GSSG ratios were increased by SDX primarily due to the increase in the GSH concentrations; (iii) the redox potentials (ΔE_h) of the GSSG/2GSH couple became more negative during SDX treatment, reflecting a pro-reducing shift; (iv) increases in the intracellular GCLc and GSS levels by SDX appear leading to a rapid de novo GSH synthesis, resulting in a prolonged and maintained antioxidant effect (Figure 4).

The oxidative stress and redox imbalance with low intracellular levels of GSH play a crucial role in the pathophysiology of ischemic vascular diseases [7].

Determining the time-dependent changes of the GSH concentrations and the GSH:GSSG ratios is very important, since GSH maintains the reduced redox state required for endothelial cell survival under ischemic conditions [47]. The decreased GSH levels, or the oxidation state of the GSSG/2GSH redox system measured as a decrease in the GSH:GSSG ratio, or an increase in the reduction potential calculated from the Nernst equation have been associated with apoptosis [10]. A parallel increase in the ROS production was also implicated in the apoptosis of vascular endothelium in response to ischemia [48]. In contrast, an increase in the GSH levels, GSH:GSSG ratio, and the resulting decrease in the redox potential of the GSSG/2GSH, coupled with a decrease in ROS production, were associated with the inhibition of apoptosis [10,40]. Therefore, the antioxidants regulating the glutathione redox status through the positive influence on the GSH amount and the GSH:GSSG ratio are thought to be effective in protecting the endothelium from ischemic damage.

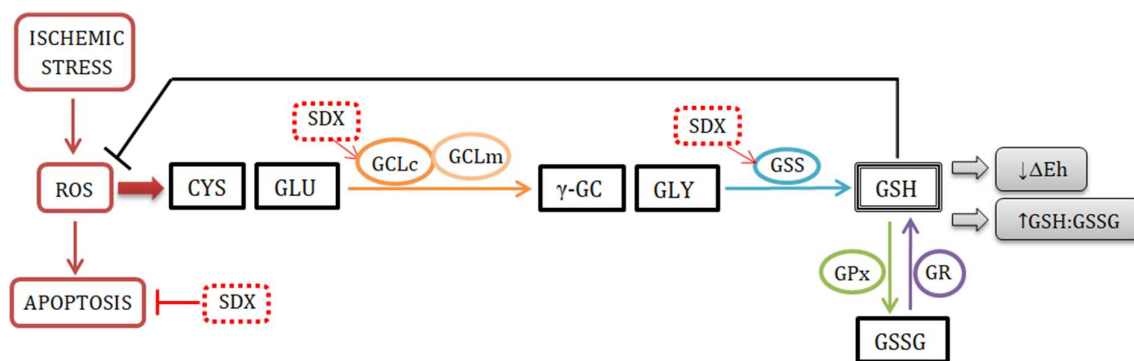


Figure 4. The mechanism of SDX antioxidant action. Abbreviations: ROS, reactive oxygen species; CYS, cysteine; GLU, glutamate; GCLc, catalytic subunit of glutamate–cysteine ligase; GCLm, modifier subunit of glutamate–cysteine ligase; γ -GC, γ -glutamyl cysteine; GLY, glycine; GSS, glutathione synthase; GSH, reduced form of glutathione; GPx, glutathione peroxidase; GSSG, oxidized form of glutathione; GR, glutathione reductase; ΔE_h , redox potential; SDX, sulodexide; \rightarrow , induction; \downarrow , inhibition.

SDX has been found to have distinct endothelial protective properties against ischemia due to its direct and indirect antioxidant actions, but it is not clear whether GSH plays a role in these effects [34,49]. We have previously described that SDX can protect the endothelial cells from ischemic injury via the nuclear factor-erythroid-2-related factor (Nrf2)/antioxidant response element (ARE) signaling pathway. Moreover, we have shown that SDX induces the rapid accumulation of Nrf2 in the nuclei of the OGD-stimulated HUVECs, leading to increased expression of the GSH-related genes [36,37].

In the present study, the SDX-associated decrease in endothelial apoptosis appears to be dependent on antioxidant activity, as suggested by the strong positive correlation between ROS and apoptotic cell death, indicating that a decrease in the ROS production led to a significant reduction in apoptosis (Figure 1). SDX was studied in the context of endothelial cell protection under oxidative stress, and the available data are consistent with our findings. A study by Połubińska et al. [50] showed that SDX was able to protect the HUVECs from oxidative stress induced by serum samples obtained from patients with peripheral vascular disease. In addition, another piece of research showed that SDX protected the human retinal endothelial cells (HRECs) from oxidative damage in an *in vitro* model of diabetic retinopathy [51]. It has been suggested that the underlying anti-oxidative mechanisms of SDX may involve the reduction in the pro-inflammatory cytokine expression and upregulation of superoxide dismutase activity [14]. Furthermore, SDX has been shown to inhibit apoptosis via a direct inhibition of caspase-3 [35].

This study demonstrated that the SDX treatment significantly increased the tGSH levels in the first 3 h of OGD, as also evidenced by an increase in the GSH and GSSG concentrations in the HUVECs (Figure 2A,B). The intracellular GSH level is maintained by *de novo* synthesis and the salvage pathways. In our experiment, the induction of GSH synthesis by SDX was not accompanied by a concomitant decrease in the GSSG concentrations (Figure 2B). This confirms that the increase in GSH levels after SDX treatment is mediated by *de novo* synthesis pathway.

The observed changes in the GSH:GSSG ratio indicate that the SDX treatment is associated with a pro-reducing shift in HUVEC exposed to OGD (Figure 2C), as well as an anti-apoptotic and antioxidant effect (Figure 1). The most proximate cause for these increases in the intracellular GSH:GSSG ratios appears to be the significant increase in GSH concentrations, as SDX also slightly increased the GSSG levels. It is worth highlighting that our results of a basal GSH:GSSG ratio (20:1 in the Control group) are in agreement with the study performed by Shrestha et al. [52] on vena cava endothelial cells (VCECs). Since the venous endothelial cells have a lower GSH:GSSG ratio than the arteries (30:1), they are more sensitive to oxidative stress [52,53].

A temporal relationship between a significant decrease in the cellular GSH and GSH:GSSG ratio and the onset of apoptotic cell death was demonstrated [54]. The evidence suggests that an early loss of the GSH:GSSG balance associated with a more oxidized GSH redox potential precedes the ROS-induced activation of the mitochondrial apoptotic pathway [8]. It was also shown that the disruption of de novo GSH synthesis with L-buthionine (S,R)-sulfoximine (BSO) activates the proapoptotic c-Jun N-terminal kinase (JNK), which plays a key role in the ischemia-induced apoptosis of the vascular endothelial cells [55]. Furthermore, a decreased GSH:GSSG associated with oxidizing conditions is responsible for formation of the S-glutathiolated proteins by a thiol/disulfide exchange mechanism between a SH group of protein and GSSG. The S-glutathiolation of proteins involved in both the receptor-mediated extrinsic and mitochondria-mediated intrinsic pathways of apoptosis is well known [8]. This process is observed under various pathological conditions within the cardiovascular system, including hypoxia/ischemia [56]. Thus, the anti-apoptotic effect of SDX appears to be mediated by significantly increased GSH levels and higher GSH:GSSG ratios.

Additionally, the shift in the GSH:GSSG ratios induced by SDX treatment in OGD appears to alter the redox state of the HUVECs toward a more negative potential (Figure 2D). This suggests that SDX induces a pro-reducing redox potential which may be due to an increased intracellular GSH concentration. Therefore, we next quantified the levels of GCLc and GSS, key enzymes for GSH biosynthesis. The ELISA results show that there are significant differences in the levels of GCLc and GSS between the groups treated without or with SDX after 1 and 3 h of OGD. This also supports our hypothesis that a strong SDX-induced increase in the levels of both the GCLc and GSS proteins may lead to the rapid production of GSH and a pro-reducing shift in the GSSG/2GSH couple, resulting in a prolonged and sustained antioxidant effect (Figures 1 and 3).

However, the increase in the endothelial GCLc and GSS protein levels was also observed in the HUVECs exposed to OGD alone compared to the control (Figure 3). At the same time, OGD alone significantly decreased the intracellular GSH (Figure 2). Both GCLc and GSS are inducible enzymes. The mechanisms underlying the ischemia-associated upregulation of GCLc and GSS proteins are unknown. Other researchers have also reported that oxidative stress or glutathione deficiency upregulates the expression of the proteins involved in GSH synthesis [57,58]. Moreover, the study by Krejsa et al. [59], performed on Jurkat cells, reported that the rapid activation of GCL after the H₂O₂ treatment was inversely proportional to the relative intracellular GSH content. Thus, our findings may support the idea that the upregulation of GCLc and GSS is likely an early adaptive response of the endothelial cells to the oxidative stress that occurs during an ischemic insult. Although the antioxidant system shows some compensatory adaptation to the ischemic conditions, the ability of the ischemic HUVECs non-treated with SDX to respond positively to ODG stress is impaired. In addition, the tissue GSH concentrations reflect not only intracellular accumulation, but also its efflux from the cells. The decreased GSH levels in response to ischemia may be associated with a cross-membrane export, mediated by multidrug resistance proteins (MRPs) [60]. Both GSH and GSSG are known to transport substrates for MRPs. The ability of MRPs to actively efflux the endogenous GSH has significant implications for ischemic vascular diseases [61]. It was shown that an increased expression of various MRP isoforms leads to decreased GSH concentrations in the endothelial cells, an alternation of redox status, and accelerated apoptosis [62,63]. Moreover, GSH depletion as such was recognized as a major contributor to the redox balance changes associated with apoptotic cell death [64]. Importantly, the MRPs' expression at the mRNA and protein levels and their transporter activities were observed in the HUVECs [65]. In view of the above, we cannot exclude the possibility that the endothelial protective mechanisms of SDX may involve some inhibitory effects on the efflux of cellular GSH. This will be the subject of our further research.

In summary, our study shows for the first time that SDX at a clinically relevant concentration (0.5 LRU/mL) and duration of action [20] significantly affects the glutathione

levels, increases the GSH:GSSG ratio, and increases the intracellular redox environment rate of reduction under cell-damaging ischemic conditions. Furthermore, the marked and potent induction of GCLc and GSS in response to SDX may confer an increased ability to rapidly synthesize GSH in the ischemic endothelial cells.

4. Materials and Methods

4.1. Cell Culture

The HUVECs were cultured as previously described [36]. In brief, the HUVEC cell line purchased from Clonetics (Lonza, Verviers, Belgium) was cultured in 75 cm² tissue culture flasks (CytoOne; USA Scientific, Ocala, FL, USA) at 1×10^4 cells/flask in endothelial basal medium (EGM-2; Clonetics) with EGM-2 BulletKit (Clonetics) at 37 °C in a humidified atmosphere of 5% CO₂ and 95% air. The medium was replaced every 3 days and the cells were subcultured after reaching around 90% confluence. The cells at passages three to five were used in the experiments.

4.2. In Vitro Model of Simulated Ischemia

In vitro ischemia was induced in the HUVECs by OGD as previously described [36]. Briefly, the culture medium (EGM-2 with EGM-BulletKit) was removed and the HUVECs were rinsed twice with glucose-free Dulbecco's Modified Eagle's Medium (DMEM, no glucose; Thermo Fisher Scientific, Waltham, MA, USA), previously equilibrated in a hypoxic chamber (Galaxy 48 R incubator; Eppendorf/Galaxy Corporation, Enfield, CT, USA), supplemented with 3% O₂, 5% CO₂, and 92% N₂ at 37 °C. For simulated ischemia in vitro, the confluent cells in DMEM without glucose were transferred to a hypoxic chamber flooded with 92% N₂, 5% CO, and 3% O₂ and incubated at 37 °C. The control cells in standard EGM-2 supplemented with EGM-2 BulletKit (normoxia) were not treated with OGD.

4.3. Drug Administration and Experimental Groups

The SDX (Vessel Due F, 300 LRU/mL) was purchased from Alfasigma S.p.A. (Bologna, Italy). The HUVECs were treated with 0.5 LRU/mL SDX during OGD. The concentration of SDX was based on the literature data [20]. The drug was added directly to the ischemic medium of the OGD, and the samples were harvested immediately after OGD. The cell cultures exposed only to simulated ischemia in vitro (OGD groups) were maintained in a hypoxic chamber for the same time as the cells treated with SDX during OGD.

Firstly, the HUVECs (5×10^4) were plated in 35-mm dishes and treated with or without SDX for 6 h in OGD to determine the effect of SDX on apoptosis and ROS accumulation. The cells were randomly divided into three groups: Control group; OGD group; and OGD + SDX group.

Then, the HUVECs were treated with SDX for 1, 3, or 6 h in OGD to determine the effect of SDX on total GSH (tGSH), GSH, GSSG, GCLc and GSS. For the GCLc and GSS protein assays, the cells were seeded at 1×10^4 /well on 24-well plates, and for GSH and GSSG measurement, the cells were cultured in 35-mm dishes at a density of 5×10^4 /dish. The cells were randomly assigned to the following experimental groups: Control group; and six groups of cells treated without/with SDX in accordance with OGD exposure time of 1, 3, and 6 h.

4.4. Apoptosis Assay

To detect the apoptotic cells, nuclear staining was performed with Hoechst 33342 (Sigma-Aldrich, St. Louis, MO, USA). The cells were rinsed with phosphate-buffered saline (PBS) and fixed with a 4% formaldehyde (in PBS) for 20 min at room temperature. After fixation, the cells were washed twice with PBS and stained with Hoechst 33342 (5 µg/mL) for 5 min in dark. The stained cells were washed three times with PBS and examined with a fluorescent microscope (Nikon TS-100 F, Nikon, Tokyo, Japan). The apoptotic cells were distinguished from the viable cells by condensed chromatin and shrunken nuclei, and by

the higher intensity of blue fluorescence of the nuclei. The data were presented as apoptotic index (AI) defined as the percentage of apoptotic cells, according to the equation:

$$\text{AI (\%)} = (\text{number of apoptotic cells} / \text{total number of cells}) \times 100 \quad (1)$$

The images were acquired from 12 randomly selected fields from three culture dishes in each group. The post-image acquisition analysis was performed using ImageJ software (1.48v, NIH, Bethesda, MD, USA, <http://imagej.nih.gov/ij/>).

4.5. Detection of Intracellular ROS

The intracellular ROS were analyzed by using the fluorogenic CellROX[®] Green Reagent (Life Technologies, Molecular Probes, Eugene, OR, USA), according to the manufacturer's instructions. After treatment, CellROX[®] Green Reagent (5 μM) was added to the cells and incubated at 37 °C for 30 min. The CellROX[®] then was removed and the cells were rinsed three times with PBS. The cells were fixed in 4% formaldehyde (in PBS) for 20 min in the dark before detection. The microscopic images of 12 randomly selected fields from three culture dishes in each group were acquired using the Nikon TS-100 F fluorescence microscope equipped with a Nikon DS Ri1-U2 camera and NIS-BR imaging software version 4.6.0 (Nikon, Tokyo, Japan). The intensities of the fluorescent signals were analyzed and quantified by using ImageJ software (1.48v, NIH, USA; <http://imagej.nih.gov/ij/>).

4.6. Measurement of GSH

The total, reduced, and oxidized GSH levels were determined using a Glutathione Colorimetric Detection Kit (Invitrogen[™], Life Technologies Co., Frederick, MD, USA), according to the manufacturer's instructions. Briefly, after treatment with/without SDX for 1, 3, or 6 h in OGD, the HUVECs were washed once with PBS and immediately precipitated in ice-cold 5% (*w/v*) 5-sulfo-salicylic acid (SSA, Sigma-Aldrich, St. Louis, MO, USA). The cells were then scraped and transferred to microcentrifuge tubes. The cell extracts were centrifuged at 14,000 rpm for 10 min at 4 °C. The supernatants were used for subsequent determination of total GSH and GSSG, and the remaining pellets were dissolved in RIPA lysis buffer (Sigma-Aldrich, St. Louis, MO, USA), plus 0.1 M NaOH for the determination of the total protein content.

To measure GSSG, the samples were treated with 2-vinylpyridine (2VP, Sigma-Aldrich, St. Louis, MO, USA). The analysis was performed according to the assay kit's instructions, and the absorbance was read at 405 nm in a microplate reader (Multiskan Ascent, Labsystems, Helsinki, Finland). The total GSH (tGSH) and GSSG concentrations were determined using the standard curve specific to each run. The amount of reduced GSH was obtained by subtracting GSSG from tGSH. The results were normalized to the total protein concentrations in the samples and expressed as nmol/mg protein. The ratio of GSH:GSSG was used to monitor the intracellular glutathione–redox balance [41].

4.7. Redox Potential Calculations

The redox potential (ΔE_h) of the GSSG/2GSH couple in the HUVECs was calculated from the GSH and GSSG concentrations, using the Nernst equation:

$$\Delta E_h = E_0 + RT/nF \ln [\text{GSSG}]/[\text{GSH}]^2 \quad (2)$$

where E_0 is the standard potential for the redox couple; R is the gas constant; T is the absolute temperature; n is the number of electron transferred ($n = 2$); and F is Faraday's constant. The E_0 value for the GSH/GSSG couple at pH = 7.4 is -264 mV [41].

4.8. Determination of Protein Content

The protein content was determined using Bradford Reagent (Sigma-Aldrich, St. Louis, MO, USA) with bovine serum albumin ($\geq 98\%$) (Sigma-Aldrich, St. Louis, MO, USA) as

standard. The absorbance was measured at 595 nm using a microplate reader (Multiskan Ascent, Labsystems, Helsinki, Finland).

4.9. Enzyme Linked Immunosorbent Assay (ELISA)

The quantitative determinations of the GCLc and GSS proteins were performed in cell culture lysates, using the Human GCLC (glutamate–cysteine ligase catalytic subunit) ELISA Kit and the Human GSS (Glutathione synthetase) ELISA Kit (Wuhan Fine Biological Technology Co., Ltd., Wuhan, China), according to the manufacturer’s instructions. The optical density (O.D.) values at 450 nm were read in a microplate reader (Multiskan Ascent; Labsystems, Helsinki, Finland). The GCLc and GSS protein concentrations in ng/mL were normalized to the total lysate protein to account for the differences in cell numbers.

4.10. Statistical Analysis

All of the statistical analyzes were performed using R version 4.2.1 software (<https://www.r-project.org/>). The normality and homogeneity of variance were tested with Shapiro–Wilk and Levene tests, respectively. The statistically significant differences ($p < 0.05$) were determined by analysis of variance (one-way ANOVA) followed by subsequent Tukey and Games–Howell multiple range tests as post-hoc analysis. The associations between the GCLc and GSS concentration, and between the apoptotic index and the CellRox fluorescence intensity were evaluated using Pearson’s r correlation coefficients.

Author Contributions: Conceptualization, K.B. and B.G.; methodology, K.B. and B.G.; formal analysis, B.G.; investigation, K.B. and B.G.; resources, B.G.; data curation, K.B.; writing—original draft preparation, K.B.; writing—review and editing, K.B. and B.G.; visualization, K.B.; supervision, B.G.; project administration, K.B.; funding acquisition, K.B. All authors have read and agreed to the published version of the manuscript.

Funding: This research was funded by National Science Centre, Poland, grant number 2019/35/N/NZ7/03071 (Preludium-18, K.B.).

Institutional Review Board Statement: Not applicable.

Informed Consent Statement: Not applicable.

Conflicts of Interest: The authors declare no conflict of interest. The funders had no role in the design of the study; in the collection, analyses, or interpretation of data; in the writing of the manuscript, or in the decision to publish the results.

References

- Hirase, T.; Node, K. Endothelial dysfunction as a cellular mechanism for vascular failure. *Am. J. Physiol. Heart Circ. Physiol.* **2012**, *302*, 499–505. [CrossRef] [PubMed]
- Vemulapalli, S.; Patel, M.R.; Jones, W.S. Limb Ischemia: Cardiovascular Diagnosis and Management from Head to Toe. *Curr. Cardiol. Rep.* **2015**, *17*, 57. [CrossRef] [PubMed]
- Yang, Q.; He, G.-W.; Underwood, M.J.; Yu, C.-M. Cellular and molecular mechanisms of endothelial ischemia/reperfusion injury: Perspectives and implications for postischemic myocardial protection. *Am. J. Transl. Res.* **2016**, *8*, 765–777. [PubMed]
- Shaito, A.; Aramouni, K.; Assaf, R.; Parenti, A.; Orekhov, A.; El Yazbi, A.; Pintus, G.; Eid, A.H. Oxidative Stress-Induced Endothelial Dysfunction in Cardiovascular Diseases. *Front. Biosci.* **2022**, *27*, 105. [CrossRef]
- Higashi, Y.; Maruhashi, T.; Noma, K.; Kihara, Y. Oxidative stress and endothelial dysfunction: Clinical evidence and therapeutic implications. *Trends Cardiovasc. Med.* **2014**, *24*, 165–169. [CrossRef] [PubMed]
- Dubois-Deruy, E.; Peugnet, V.; Turkieh, A.; Pinet, F. Oxidative Stress in Cardiovascular Diseases. *Antioxidants* **2020**, *9*, 864. [CrossRef] [PubMed]
- Matuz-Mares, D.; Riveros-Rosas, H.; Vilchis-Landeros, M.; Vázquez-Meza, H. Glutathione Participation in the Prevention of Cardiovascular Diseases. *Antioxidants* **2021**, *10*, 1220. [CrossRef]
- Circu, M.L.; Aw, T.Y. Glutathione and modulation of cell apoptosis. *Biochim. Biophys. Acta* **2012**, *1823*, 1767–1777. [CrossRef]
- Dhalla, N.S.; Elmoselhi, A.B.; Hata, T.; Makino, N. Status of myocardial antioxidants in ischemia–reperfusion injury. *Cardiovasc. Res.* **2000**, *47*, 446–456. [CrossRef]
- Schafer, F.Q.; Buettner, G.R. Redox environment of the cell as viewed through the redox state of the glutathione disulfide/glutathione couple. *Free Radic. Biol. Med.* **2001**, *30*, 1191–1212. [CrossRef]
- Lu, S.C. Glutathione synthesis. *Biochim. Biophys. Acta* **2013**, *1830*, 3143–3153. [CrossRef]



12. Akaboshi, T.; Yamanishi, R. Certain carotenoids enhance the intracellular glutathione level in a murine cultured macrophage cell line by inducing glutamate-cysteine-ligase. *Mol. Nutr. Food Res.* **2014**, *58*, 1291–1300. [CrossRef]
13. Lushchak, V.I. Glutathione Homeostasis and Functions: Potential Targets for Medical Interventions. *J. Amino Acids* **2012**, *2012*, 736837. [CrossRef]
14. Mannello, F.; Ligi, D.; Canale, M.; Raffetto, J.D. Sulodexide Down-Regulates the Release of Cytokines, Chemokines, and Leukocyte Colony Stimulating Factors from Human Macrophages: Role of Glycosaminoglycans in Inflammatory Pathways of Chronic Venous Disease. *Curr. Vasc. Pharmacol.* **2014**, *12*, 173–185. [CrossRef]
15. Coccheri, S.; Mannello, F. Development and use of sulodexide in vascular diseases: Implications for treatment. *Drug Des. Dev. Ther.* **2013**, *8*, 49–65. [CrossRef]
16. Coccheri, S. Biological and clinical effects of sulodexide in arterial disorders and diseases. *Int. Angiol.* **2014**, *33*, 263–274.
17. Carroll, B.J.; Piazza, G.; Goldhaber, S.Z. Sulodexide in venous disease. *J. Thromb. Haemost.* **2019**, *17*, 31–38. [CrossRef]
18. Chaitidis, N.; Kokkinidis, D.G.; Papadopoulou, Z.; Hasemaki, N.; Attaran, R.; Bakoyiannis, C. Management of Post-Thrombotic Syndrome: A Comprehensive Review. *Curr. Pharm. Des.* **2022**, *28*, 550–559. [CrossRef]
19. Yongwatana, K.; Supasynhd, O.; Satirapoj, B. Renal Effects of Sulodexide in Type 2 Diabetic Patients without Nephrotic Range Proteinuria. *J. Diabetes Res.* **2020**, *2020*, 2984680. [CrossRef]
20. Sosińska, P.; Baum, E.; Maćkowiak, B.; Maj, M.; Sumińska-Jasińska, K.; Staniszewski, R.; Bręborowicz, A. Sulodexide Reduces the Proinflammatory Effect of Serum from Patients with Peripheral Artery Disease in Human Arterial Endothelial Cells. *Cell. Physiol. Biochem.* **2016**, *40*, 1005–1012. [CrossRef]
21. Liu, Y.N.; Zhou, J.; Li, T.; Wu, J.; Xie, S.H.; Liu, H.-F.; Liu, Z.; Park, T.S.; Wang, Y.; Liu, W.J. Sulodexide Protects Renal Tubular Epithelial Cells from Oxidative Stress-Induced Injury via Upregulating Klotho Expression at an Early Stage of Diabetic Kidney Disease. *J. Diabetes Res.* **2017**, *2017*, 4989847. [CrossRef]
22. Pletinck, A.; Van Landschoot, M.; Steppan, S.; Laukens, D.; Passlick-Deetjen, J.; Vanholder, R.; Van Biesen, W. Oral supplementation with sulodexide inhibits neo-angiogenesis in a rat model of peritoneal perfusion. *Nephrol. Dial. Transplant.* **2012**, *27*, 548–556. [CrossRef]
23. Park, H.Y.; Kang, S.; Kim, G.Y.; Jang, Y.; Kwon, H.M.; Shim, W.H.; Cho, S.Y.; Cho, S.H. Inhibition of neointimal proliferation of rat carotid artery by sulodexide. *J. Korean Med. Sci.* **1997**, *12*, 210–214. [CrossRef]
24. Mannello, F.; Medda, V.; Ligi, D.; Raffetto, J.D. Glycosaminoglycan sulodexide inhibition of MMP-9 gelatinase secretion and activity: Possible pharmacological role against collagen degradation in vascular chronic diseases. *Curr. Vasc. Pharmacol.* **2013**, *11*, 354–365. [CrossRef]
25. Dobiaš, L.; Petrová, M.; Vojtko, R.; Uličná, O.; Vančová, O.; Kristová, V. Effect of Sulodexide on Vascular Responses and Liver Mitochondrial Function in Diabetic Rats. *Physiol. Res.* **2015**, *64*, S497–S505. [CrossRef]
26. Li, T.; Liu, X.; Zhao, Z.; Ni, L.; Liu, C. Sulodexide recovers endothelial function through reconstructing glycocalyx in the balloon-injury rat carotid artery model. *Oncotarget* **2017**, *8*, 91350–91361. [CrossRef]
27. Kristová, V.; Liskova, S.; Sotníková, R.; Vojtko, R.; Kurtanský, A. Sulodexide improves endothelial dysfunction in streptozotocin-induced diabetes in rats. *Physiol. Res.* **2008**, *57*, 491–494. [CrossRef]
28. Urbanek, T.; Krasinski, Z.; Suminska-Jasinska, K.; Baum, E.; Borej-Nowicka, G.; Begier-Krasinska, B.; Bręborowicz, A. Sulodexide Reduces the Inflammatory Reaction and Senescence of Endothelial Cells in Conditions Involving Chronic Venous Disease. *Int. Angiol.* **2016**, *35*, 140–147. [PubMed]
29. Sosińska-Zawierucha, P.; Mackowiak, B.; Staniszewski, R.; Sumińska-Jasińska, K.; Maj, M.; Krasinski, Z.; Bręborowicz, A. Sulodexide Slows Down the Senescence of Aortic Endothelial Cells Exposed to Serum from Patients with Peripheral Artery Diseases. *Cell. Physiol. Biochem.* **2018**, *45*, 2225–2232. [CrossRef] [PubMed]
30. Skrha, J.; Perusicová, J.; Kvasnička, J.; Hilgertová, J. The effect of glycosaminoglycan sulodexide on oxidative stress and fibrinolysis in diabetes mellitus. *Sb. Lek.* **1998**, *99*, 103–109. [PubMed]
31. Ciszewicz, M.; PoLubinska, A.; Antoniewicz, A.; Suminska-Jasinska, K.; Bręborowicz, A. Sulodexide suppresses inflammation in human endothelial cells and prevents glucose cytotoxicity. *Transl. Res.* **2009**, *153*, 118–123. [CrossRef]
32. Bilinska, M.; Wolszakiewicz, J.; Duda, M.; Janas, J.; Beręsewicz, A.; Piotrowicz, R. Antioxidative activity of sulodexide, a glycosaminoglycan, in patients with stable coronary artery disease: A pilot study. *Med. Sci. Monit.* **2009**, *15*, 618–623.
33. Jin, H.Y.; Lee, K.A.; Song, S.K.; Liu, W.J.; Choi, J.H.; Song, C.H.; Baek, H.S.; Park, T.S. Sulodexide prevents peripheral nerve damage in streptozotocin induced diabetic rats. *Eur. J. Pharmacol.* **2012**, *674*, 217–226. [CrossRef]
34. Gabryel, B.; Jarzabek, K.; Machnik, G.; Adamczyk, J.; Belowski, D.; Obuchowicz, E.; Urbanek, T. Superoxide dismutase 1 and glutathione peroxidase 1 are involved in the protective effect of sulodexide on vascular endothelial cells exposed to oxygen-glucose deprivation. *Microvasc. Res.* **2016**, *103*, 26–35. [CrossRef]
35. Yin, J.; Chen, W.; Ma, F.; Lu, Z.; Wu, R.; Zhang, G.; Wang, N.; Wang, F. Sulodexide pretreatment attenuates renal ischemia-reperfusion injury in rats. *Oncotarget* **2017**, *8*, 9986–9995. [CrossRef]
36. Gabryel, B.; Bontor, K.; Jarzabek, K.; Plato, M.; Pudelko, A.; Machnik, G.; Urbanek, T. Sulodexide up-regulates glutathione S-transferase P1 by enhancing Nrf2 expression and translocation in human umbilical vein endothelial cells injured by oxygen glucose deprivation. *Arch. Med. Sci.* **2019**, *16*, 957–963. [CrossRef]
37. Gabryel, B.; Bontor, K.; Urbanek, T. Sulodexide increases mRNA expression of glutathione-related genes in human umbilical endothelial cells exposed to oxygen-glucose deprivation. *Arch. Med. Sci.* **2019**, *16*, 1444–1447. [CrossRef]

38. Shen, D.; Chen, R.; Zhang, L.; Rao, Z.; Ruan, Y.; Li, L.; Chu, M.; Zhang, Y. Sulodexide attenuates endoplasmic reticulum stress induced by myocardial ischaemia/reperfusion by activating the PI3K/Akt pathway. *J. Cell. Mol. Med.* **2019**, *23*, 5063–5075. [CrossRef]
39. Yuan, T.; Yang, N.; Bi, W.; Zhang, J.; Li, X.; Shi, L.; Liu, Y.; Gao, X. Protective Role of Sulodexide on Renal Injury Induced by Limb Ischemia-Reperfusion. *Evid. Based Complement. Altern. Med.* **2021**, *2021*, 6629718. [CrossRef]
40. Li, C.; Zhang, W.-J.; Choi, J.; Frei, B. Quercetin affects glutathione levels and redox ratio in human aortic endothelial cells not through oxidation but formation and cellular export of quercetin-glutathione conjugates and upregulation of glutamate-cysteine ligase. *Redox Biol.* **2016**, *9*, 220–228. [CrossRef]
41. Jones, D.P. Redox potential of GSH/GSSG couple: Assay and biological significance. *Methods Enzymol.* **2002**, *348*, 93–112. [CrossRef]
42. Ha, K.-N.; Chen, Y.; Cai, J.; Sternberg, P. Increased Glutathione Synthesis through an ARE-Nrf2-Dependent Pathway by Zinc in the RPE: Implication for Protection against Oxidative Stress. *Investig. Ophthalmol. Vis. Sci.* **2006**, *47*, 2709–2715. [CrossRef]
43. Yuan, J.; Zhang, Z.; Li, L.; Song, W. Resveratrol affects the expression of glutamate cysteine ligase in the kidneys of aged rats. *Exp. Ther. Med.* **2014**, *7*, 1762–1766. [CrossRef]
44. Yang, Y.; Li, L.; Hang, Q.; Fang, Y.; Dong, X.; Cao, P.; Yin, Z.; Luo, L. γ -glutamylcysteine exhibits anti-inflammatory effects by increasing cellular glutathione level. *Redox Biol.* **2019**, *20*, 157–166. [CrossRef]
45. Yang, H.; Zeng, Y.; Lee, T.D.; Yang, Y.; Ou, X.; Chen, L.; Haque, M.; Rippe, R.; Lu, S.C. Role of AP-1 in the Coordinate Induction of Rat Glutamate-cysteine Ligase and Glutathione Synthetase by tert-Butylhydroquinone. *J. Biol. Chem.* **2002**, *277*, 35232–35239. [CrossRef]
46. Lee, T.D.; Yang, H.; Whang, J.; Lu, S.C. Cloning and characterization of the human glutathione synthetase 5'-flanking region. *Biochem. J.* **2005**, *390*, 521–528. [CrossRef]
47. Song, P.; Zou, M.-H. Redox regulation of endothelial cell fate. *Cell. Mol. Life Sci.* **2014**, *71*, 3219–3239. [CrossRef]
48. Daiber, A.; Chlopicki, S. Revisiting pharmacology of oxidative stress and endothelial dysfunction in cardiovascular disease: Evidence for redox-based therapies. *Free Radic. Biol. Med.* **2020**, *157*, 15–37. [CrossRef]
49. Masola, V.; Zaza, G.; Onisto, M.; Lupo, A.; Gambaro, G. Glycosaminoglycans, proteoglycans and sulodexide and the endothelium: Biological roles and pharmacological effects. *Int. Angiol.* **2014**, *33*, 243–254.
50. Połubińska, A.; Staniszewski, R.; Baum, E.; Sumińska-Jasińska, K.; Bręborowicz, A. Sulodexide modifies intravascular homeostasis what affects function of the endothelium. *Adv. Med. Sci.* **2013**, *58*, 304–310. [CrossRef]
51. Gericke, A.; Sumińska-Jasińska, K.; Bręborowicz, A. Sulodexide reduces glucose induced senescence in human retinal endothelial cells. *Sci. Rep.* **2021**, *11*, 11532. [CrossRef] [PubMed]
52. Shrestha, B.; Prasai, P.K.; Kaskas, A.M.; Khanna, A.; Letchuman, V.; Letchuman, S.; Alexander, J.S.; Orr, A.W.; Woolard, M.D.; Pattillo, C.B. Differential arterial and venous endothelial redox responses to oxidative stress. *Microcirculation* **2018**, *25*, e12486. [CrossRef] [PubMed]
53. Szasz, T.; Thakali, K.; Fink, G.D.; Watts, S.W. A comparison of arteries and veins in oxidative stress: Producers, destroyers, function, and disease. *Exp. Biol. Med.* **2007**, *232*, 27–37.
54. Wang, T.; Gotoh, Y.; Jennings, M.H.; Rhoads, C.A.; Aw, T.Y. Lipid hydroperoxide-induced apoptosis in human colonic CaCo-2 cells is associated with an early loss of cellular redox balance. *FASEB J.* **2000**, *14*, 1567–1576. [CrossRef] [PubMed]
55. Anathy, V.; Roberson, E.C.; Guala, A.S.; Godburn, K.E.; Budd, R.C.; Janssen-Heininger, Y.M. Redox-Based Regulation of Apoptosis: S-Glutathionylation As a Regulatory Mechanism to Control Cell Death. *Antioxid. Redox Signal.* **2012**, *16*, 496–505. [CrossRef] [PubMed]
56. Rashdan, N.A.; Shrestha, B.; Pattillo, C.B. S-glutathionylation, friend or foe in cardiovascular health and disease. *Redox Biol.* **2020**, *37*, 101693. [CrossRef] [PubMed]
57. Nakamura, Y.K.; Dubick, M.A.; Omaye, S.T. γ -Glutamylcysteine inhibits oxidative stress in human endothelial cells. *Life Sci.* **2012**, *90*, 116–121. [CrossRef]
58. Tian, L.; Shi, M.M.; Forman, H.J. Increased Transcription of the Regulatory Subunit of γ -Glutamylcysteine Synthetase in Rat Lung Epithelial L2 Cells Exposed to Oxidative Stress or Glutathione Depletion. *Arch. Biochem. Biophys.* **1997**, *342*, 126–133. [CrossRef]
59. Krejsa, C.M.; Franklin, C.C.; White, C.C.; Ledbetter, J.A.; Schieven, G.L.; Kavanagh, T.J. Rapid Activation of Glutamate Cysteine Ligase following Oxidative Stress. *J. Biol. Chem.* **2010**, *285*, 16116–16124. [CrossRef]
60. Ibbotson, K.; Yell, J.; Ronaldson, P.T. Nrf2 signaling increases expression of ATP-binding cassette subfamily C mRNA transcripts at the blood-brain barrier following hypoxia-reoxygenation stress. *Fluids Barriers CNS* **2017**, *14*, 51. [CrossRef]
61. Brzica, H.; Abdullahi, W.; Ibbotson, K.; Ronaldson, P.T. Role of Transporters in Central Nervous System Drug Delivery and Blood-Brain Barrier Protection: Relevance to Treatment of Stroke. *J. Cent. Nerv. Syst. Dis.* **2017**, *9*, 9380. [CrossRef] [PubMed]
62. Franco, R.; Cidlowski, J.A. Apoptosis and glutathione: Beyond an antioxidant. *Cell Death Differ.* **2009**, *16*, 1303–1314. [CrossRef] [PubMed]
63. Mueller, C.F.H.; Widder, J.D.; McNally, J.S.; McCann, L.; Jones, D.P.; Harrison, D.G. The Role of the Multidrug Resistance Protein-1 in Modulation of Endothelial Cell Oxidative Stress. *Circ. Res.* **2005**, *97*, 637–644. [CrossRef] [PubMed]

64. Franco, R.; Cidlowski, J.A. Glutathione Efflux and Cell Death. *Antioxid. Redox Signal.* **2012**, *17*, 1694–1713. [CrossRef]
65. Krawczenko, A.; Bielawska-Pohl, A.; Wojtowicz, K.; Jura, R.; Paprocka, M.; Wojdat, E.; Kozłowska, U.; Klimczak, A.; Grillon, C.; Kieda, C.; et al. Expression and activity of multidrug resistance proteins in mature endothelial cells and their precursors: A challenging correlation. *PLoS ONE* **2017**, *12*, e0172371. [CrossRef]

Review

Detection of Oxidative Stress Induced by Nanomaterials in Cells—The Roles of Reactive Oxygen Species and Glutathione

Jan Čapek *  and Tomáš Roušar 

Department of Biological and Biochemical Sciences, Faculty of Chemical Technology, University of Pardubice, Studentska 573, 532 10 Pardubice, Czech Republic; Tomas.Rousar@upce.cz

* Correspondence: jan.capek7@upce.cz; Tel.: +420-466-037-717

Abstract: The potential of nanomaterials use is huge, especially in fields such as medicine or industry. Due to widespread use of nanomaterials, their cytotoxicity and involvement in cellular pathways ought to be evaluated in detail. Nanomaterials can induce the production of a number of substances in cells, including reactive oxygen species (ROS), participating in physiological and pathological cellular processes. These highly reactive substances include: superoxide, singlet oxygen, hydroxyl radical, and hydrogen peroxide. For overall assessment, there are a number of fluorescent probes in particular that are very specific and selective for given ROS. In addition, due to the involvement of ROS in a number of cellular signaling pathways, understanding the principle of ROS production induced by nanomaterials is very important. For defense, the cells have a number of reparative and especially antioxidant mechanisms. One of the most potent antioxidants is a tripeptide glutathione. Thus, the glutathione depletion can be a characteristic manifestation of harmful effects caused by the prooxidative-acting of nanomaterials in cells. For these reasons, here we would like to provide a review on the current knowledge of ROS-mediated cellular nanotoxicity manifesting as glutathione depletion, including an overview of approaches for the detection of ROS levels in cells.

Citation: Čapek, J.; Roušar, T.

Detection of Oxidative Stress Induced by Nanomaterials in Cells—The Roles of Reactive Oxygen Species and

Glutathione. *Molecules* **2021**, *26*, 4710.

[https://doi.org/10.3390/](https://doi.org/10.3390/molecules26164710)

[molecules26164710](https://doi.org/10.3390/molecules26164710)

Academic Editor: Pál Perjési

Received: 1 July 2021

Accepted: 2 August 2021

Published: 4 August 2021

Publisher's Note: MDPI stays neutral with regard to jurisdictional claims in published maps and institutional affiliations.



Copyright: © 2021 by the authors. Licensee MDPI, Basel, Switzerland. This article is an open access article distributed under the terms and conditions of the Creative Commons Attribution (CC BY) license (<https://creativecommons.org/licenses/by/4.0/>).

Keywords: reactive oxygen species; oxidative stress; glutathione; nanotoxicity; cell injury; fluorescence probes

1. Introduction

Molecular oxygen (O₂) has a significant effect on numerous chemical reactions and biological processes. O₂ reductions are one of the most critical electrocatalytic reactions that function in electrochemical energy conversion [1]. Free radicals contain an unpaired electron mostly bound to oxygen atoms. Conversely, the group of compounds named reactive oxygen species (ROS) also contains molecules without an unpaired electron, e.g., hydrogen peroxide [2,3]. Thus, the group of ROS also contains oxygen free radicals such as superoxide or hydroxyl, alkoxyl, peroxy, and nitroxyl radicals [4,5]. The production of ROS is commonly linked with mitochondria, where the electrons are transferred through the respiratory chain to O₂ forming water [6,7]. Mitochondrial ROS production depends on many factors such as the membrane potential of mitochondria [8], concentration of mitochondrial respiratory substrates, or a type of cells [9]. Mitochondria are the most important sources of superoxide and hydrogen peroxide in mammalian cells. The production of these ROS occurs mainly on the mitochondrial respiratory complex I and III [7,10]. In addition to mitochondrial complexes, ROS is also produced in mammalian cells by the participation of other enzymes such as flavoproteins [11] and other enzymes involved in nutrient metabolism [12]. As ROS plays important roles in the regulation of cell death processes, i.e., apoptosis [13] or necrosis [14–16], their pathological roles have been identified in a number of diseases including cancer and other age-related degenerative processes [17,18]. Given their deleterious effects, ROS production is usually finely tuned by ROS-scavenging systems [9].

Nanomaterials (NMs) exhibit great potential for use in the biomedical, optical, and electronic fields [19–23]. However, nanomaterials have been considered as potentially toxic due to their unique properties. They have extremely high surface-to-volume ratios, making them very reactive and catalytically active [24]. Their toxic potential in cells is also supported by their small size, enabling them to easily penetrate cell membranes [25]. TiO₂ is one of the most commonly used nanomaterials in the chemical industry (e.g., cosmetics and pigments) [26]. In addition to white lead properties, TiO₂ can be very active in photocatalytic reactions with organic compounds, providing the formation of ROS including •OH, O₂•⁻, H₂O₂ [27]. In addition to TiO₂, other nanomaterials of different chemical compositions can produce ROS. The overview of NMs capable of ROS production is summarized in Table 1 including the lifetime.

Table 1. Overview of nanomaterials capable of ROS production [28].

Nanomaterial	Produced ROS	ROS	Half-Life
ZnO [29], SiO ₂ [29], TiO ₂ [30], CuO [31], Ag NPs [32]	Superoxide	O ₂ • ⁻	10 ⁻⁶ s
ZnO [33], TiO ₂ [34], CuO [35]	Hydroxyl radical	•OH	10 ⁻¹⁰ s
Polystyrene NPs [36], Au NPs [37], TiO ₂ [38], ZnO [39], Ag NPs [40]	Hydrogen peroxide	H ₂ O ₂	Stable (x.s, min)
TiO ₂ [41], Ag NPs [42], FeO [43]	Singlet oxygen	¹ O ₂	10 ⁻⁶ s

Nanomaterials or nanoparticles (NPs) can expose transition metals on their surface, which can generate ROS through Fenton or Haber-Weiss reactions [44]. During these reactions, hydrogen peroxide is reduced in the presence of transition metals (Fe²⁺, Cu⁺) to form a highly active and toxic hydroxyl radical. Thus, the role of nanomaterials in ROS-mediated cell damage is significant and ROS production induced by NMs can lead to the modulation of various intracellular pathways, e.g., NF-κB, caspases, MAPK, etc., involving the activation of cell death processes [45,46].

In this study, we aimed to provide a recent and detailed view on ROS production induced by nanomaterials. The importance of our review can be also supported by the role of increased ROS levels that can lead to glutathione depletion and to the activation of cellular signaling pathways, resulting in changes in cellular metabolism, cell damage, or even in cell death.

2. Reactive Oxygen Species

2.1. Superoxide

Superoxide radical is formed during enzymatic and non-enzymatic reactions in biological systems [1,47]. In atoms and molecules, paired electrons occur usually as antiparallel, which strongly limits the oxidation properties of O₂. After one-electron reduction of molecular oxygen, the superoxide radical (O₂•⁻) forms. This reaction is thermodynamically very unfavorable and the interaction of O₂ with another paramagnetic center is important for overcoming spin restriction [48]. Although the reactivity of O₂•⁻ is mild, the crucial role of superoxide is that it enables the formation of other ROS (Figure 1), playing important roles in the pathology of various diseases.

Superoxide radical (O₂•⁻) is formed mainly in mitochondria and its reactivity with biomolecules is relatively low. Superoxide can be produced after the reaction of molecular oxygen with divalent metals catalyzing a single-electron reduction under their simultaneous oxidation (equation 1).



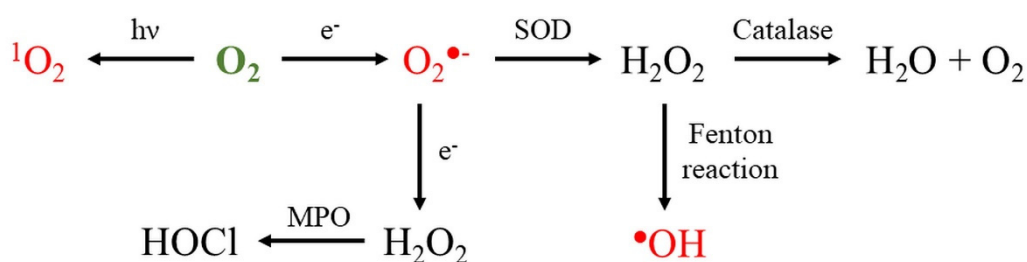
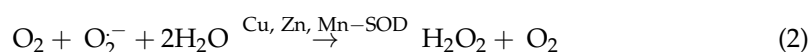


Figure 1. Formation of reactive oxygen species. Abbreviations: SOD = superoxide dismutase; MPO = myeloperoxidase; O_2 = oxygen; 1O_2 = singlet oxygen; $O_2^{\bullet-}$ = superoxide; H_2O_2 = hydrogen peroxide; $\bullet OH$ = hydroxyl radical; HOCl = hypochlorous acid; and $h\nu$ = radiation. ROS colored in red are free oxygen radicals.

Another formation can be catalyzed by enzymes including xanthine oxidase, lipoxygenase, or cyclooxygenase [49]. The superoxide radical may exist in two possible forms: either in the form of $O_2^{\bullet-}$ at physiological pH or as a hydroperoxyl radical (HO_2^{\bullet}) at low pH levels [50]. Hydroperoxyl radical penetrates better through phospholipid bilayers compared to the charged form $O_2^{\bullet-}$ [28,51]. The superoxide radical may react with another superoxide radical to form hydrogen peroxide and O_2 (equation 2). The reaction is catalyzed by the enzyme superoxide dismutase (SOD) [52,53]. A product of the dismutation reaction is H_2O_2 which becomes an important factor in the formation of the most reactive ROS, i.e., hydroxyl radical ($\bullet OH$) [54].



The mitochondrial electron transport chain (ETC) has been attributed to the role as the main ROS generator in cells. When transporting electrons, some of the electrons from the ETC can reduce molecular oxygen to $O_2^{\bullet-}$ [55]. The resulting $O_2^{\bullet-}$ is rapidly dismissed by mitochondrial superoxide dismutase (Mn-SOD) forming H_2O_2 [56]. Mitochondrial ETC consists of several electron transporters (flavoproteins, proteins containing iron and sulfur, ubiquinone, and cytochromes) with redox potentials ranging from -0.200 to $+0.600$ V [57,58]. According to the respective redox potentials, the individual electron carriers are arranged in individual complexes of the respiratory chain I–IV. Electrons that are transported into the respiratory chain as reducing equivalents of NADH or $FADH_2$ enter the ETC through mitochondrial Complexes I and II. Then, the electrons are transferred through ETC to Complex IV which reduces O_2 to H_2O . From the thermodynamical perspective, all these electron transport systems could transfer the electrons directly to O_2 to form $O_2^{\bullet-}$. However, there are only two major sites of the respiratory chain where ROS can be generated, i.e., at Complexes I and III [59,60].

In Complex I, a reaction occurs between O_2 and the reduced form of the flavinmononucleotide (FMN), leading to production of $O_2^{\bullet-}$. The amount of reduced FMN depends on the NADH/NAD⁺ ratio [61]. In Complex III, two specific binding sites for coenzyme Q10 are known, i.e., Q_i and Q_o . Superoxide production is located in Q_o . When antimycin A is added as an inhibitor of the Q_i site, $O_2^{\bullet-}$ production increases [62], while the addition of a myxothiazole inhibitor for the Q_o site decreases ROS production [63]. Under physiological conditions, the production of ROS in Complex III depends on the $\Delta\Psi$. The rate of $O_2^{\bullet-}$ formation may increase exponentially with increasing $\Delta\Psi$. This directly correlates with the fact that due to $\Delta\Psi$ fluctuations, the transport of electrons from heme bL to heme bH slows down, which then increases superoxide generation [64].

2.1.1. Role of Superoxide in Nanomaterial Toxicity

Damage to mitochondria and subsequent ROS leakage is a commonly accepted mechanism of nanoparticles toxicity. Damaged mitochondria release $O_2^{\bullet-}$ into the intermembrane space which can ultimately damage the cell [65]. Across different types of nanomaterials, their involvement in the ROS generation can be found. Far more often

than in size, their possible cytotoxic effects are chemically dependent. Despite the similar size and crystal shape of ZnO NPs and SiO₂ NPs, higher toxicity of ZnO NPs is observed, where cell viability is reduced and O₂^{•−} generation is reduced, due to which glutathione (GSH) depletion occurs [29]. TiO₂ nanoparticles generate O₂^{•−} [30] both in solution and in cells, and intracellular O₂^{•−} reduces the expression of histone deacetylase 9 (HDAC9), an epigenetic modifier [66]. Cellular internalization of TiO₂ NPs has been shown to activate macrophages and neutrophils contributing to the production of O₂^{•−} by the NADPH oxidase [67]. Oxidative stress induced by excessive O₂^{•−} production is an important mechanism of the CuO NPs toxicity [31]. CuO NPs can enter HepG2 cells, where they are capable of inducing cellular toxicity by generating O₂^{•−} leading to GSH depletion [68]. Activation of mitogen-activated protein kinases (MAPKs) and redox-sensitive transcription factors was demonstrated, suggesting that MAPK pathways and redox-sensitive transcription factors could be major factors of CuO NPs toxicity [69].

Analysis of mouse fibroblasts and human hepatocytes revealed that an increase in ROS levels induced by Ag NPs is accompanied by a reduction of mitochondrial membrane potential, release of cytochrome c into the cytosol, JNK activation, and translocation of Bax to mitochondria [32]. After exposure to Ag nanoparticles, GSH depletion occurs in liver cells, which is directly related to ROS production [70]. Ag NPs appear to induce DNA damage through a mechanism involving ROS production.

2.1.2. Methods for the Detection of Superoxide

MitoSox

Hydroethidium (HE) is a selective O₂^{•−} detection probe (Figure 2) that reacts very rapidly to changes in O₂^{•−} concentration, forming a red fluorescent product with 2-hydroxyethidium cation (2-OH-E⁺). Hydroethidine is a reduced form of ethidium that can be oxidized to ethidium in cells. The resulting ethidium intercalates nucleic acids and significantly increases its fluorescence, emitted at 610 nm (excitation = 535 nm) [23,71].

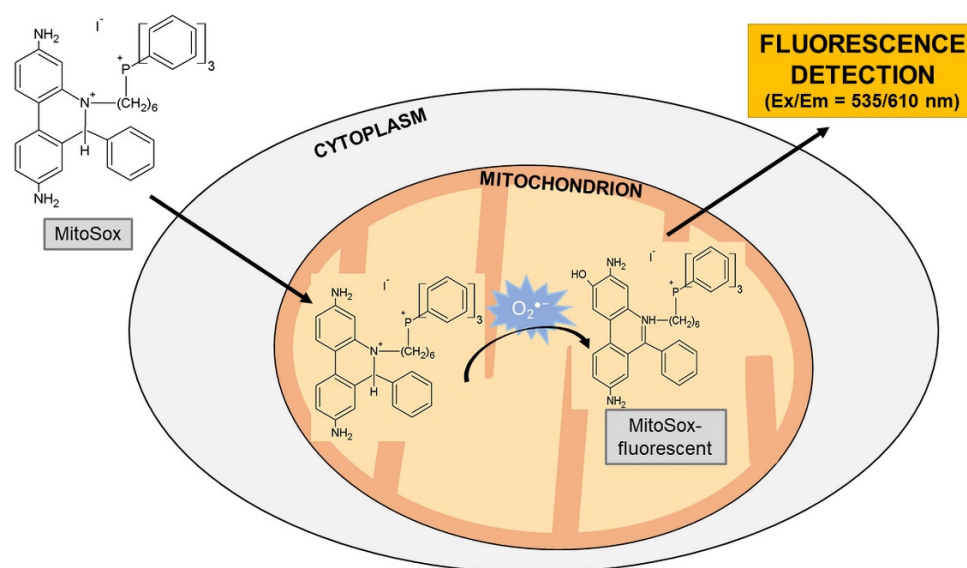


Figure 2. Detection of superoxide using MitoSox fluorescent probe. Abbreviation: O₂^{•−} = superoxide.

A new hydroethidine analog was synthesized for the purposes of O₂^{•−} detection, which is produced in mitochondria. This analog carries a charged triphenylphosphonium residue (Mito-HE; Mito-Sox Red). As the phosphonium residue is positively charged and surrounded by three lipophilic phenyl groups, it penetrates very easily through cell membranes, mainly through the inner mitochondrial membrane [72]. After they cross the cell membranes, they accumulate in mitochondria depending on the negative $\Delta\Psi$ [73]. Importantly, redistribution of MitoSox from mitochondria is dependent on decreasing

$\Delta\Psi$ based on various stimuli, which may not be ROS. For this reason, the use of MitoSox is a semi-quantitative test. Very important is the fact that MitoSox is transferred from mitochondria to the cytoplasm. Here, the supply of nucleic acids is higher and the increasing fluorescence is independent to mitochondrial ROS production, which may distort the results of individual measurements. The formation of MitoSox oxidation products in mitochondria may result in changes of values, which may reduce the passage of other MitoSox molecules into the mitochondria and generally affect measurements due to decreased MitoSox and ROS concentrations that are not produced by breathing chain breakage. The fluorescent product emits radiation at 580 nm with excitation at 540 nm [74–76].

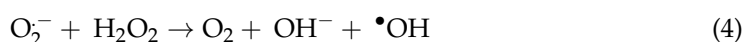
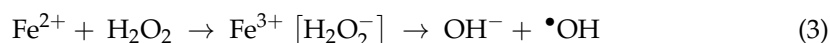
1,3-Diphenylisobenzofuran

The 1,3-diphenylisobenzofuran (DPBF) probe is a molecule that, when incorporated into liposome phospholipids, acquires fluorescent properties. It is used for the detection of $O_2^{\bullet-}$ and 1O_2 . After reaction with oxygen radicals, it produces a decrease of fluorescence, thus the fluorescence rates correlate inversely with increasing concentrations of $O_2^{\bullet-}$ and 1O_2 [77,78]. The reaction of DPBF with ROS such as singlet oxygen, hydroxyl, alkoxy and alkyl peroxy radicals gives 1,2-dibenzoylbenzene. In contrast, only reaction with H_2O_2 produces 9-hydroxyanthracen-10-(9H)-one. This product can be detected using fluorescence spectroscopy, NMR spectroscopy, or HPLC [79].

2.2. Hydroxyl Radical

The hydroxyl radical is a neutral form of the hydroxide ion. It belongs among the most reactive ROS because it can react with a variety of organic and inorganic compounds including DNA, proteins, and lipids, resulting in serious cell damage. The hydroxyl radical may be formed as a product of the Fenton or Haber–Weiss reaction [80–83].

The Fenton reaction is based on the reaction between H_2O_2 and Fe^{2+} . Iron is an essential component of many proteins involved in the transport or metabolism of oxygen due to its ability to undergo cyclic oxidation and reduction. Iron has to be present for the ongoing synthesis of iron-containing proteins. As such, it can directly lead to the formation of free radicals, which can cause cellular damage of large extent. The reaction of Fe^{2+} with H_2O_2 produces an oxidized form of iron (Fe^{3+}), as well as $\bullet OH$ and OH^- (Equation (3)).



Another possible reaction to form $\bullet OH$ is the Haber–Weiss reaction. In this reaction, less reactive $O_2^{\bullet-}$ and H_2O_2 react with each other (Equation (4)). As in the case of the Fenton reaction, very toxic $\bullet OH$ is formed. Very unfavorable thermodynamic conditions are applied to this reaction, in which the rate constant in the aqueous solution is close to zero. The presence of a transition metal catalyst is required to ensure the reaction. The iron atom serves as the catalyst. Both reactions produce highly reactive $\bullet OH$, which ultimately severely damages cells [84–87]. The Fenton reaction can be used to induce apoptosis in cancer cells, where $\bullet OH$ is formed on a copper ion [88,89].

2.2.1. Role of Hydroxyl Radical in Nanomaterial Toxicity

TiO_2 and ZnO NPs are widely used in cosmetics and industry [22]. Under the influence of UV radiation, ZnO NPs generate reactive oxygen species such as $\bullet OH$ or H_2O_2 , causing GSH depletion [33,90]. The rate of $\bullet OH$ generation and the total photocatalytic activity depends on the physical properties of the nanomaterial used, e.g., TiO_2 NPs [34]. Cu NPs play an important role as a cofactor in a number of enzymes such as cytochrome c oxidase [91]. However, they exhibit significant toxicity and can induce ROS production, including largely reactive $\bullet OH$. Copper can catalyze electron transfer (Cu^{2+} and Cu^+). This can give rise to $O_2^{\bullet-}$ reduction to H_2O_2 in cells, leading to GSH depletion [35]. Other

particles that induce $\bullet\text{OH}$ production include Fe_3O_4 [92], silica nanoparticle [93], and silver nanoparticles [94].

2.2.2. Methods for the Detection of Hydroxyl Radical

Terephthalic acid (TA) can be hydroxylated in presence of $\bullet\text{OH}$ to give the highly fluorescent product 2-hydroxy-TA [95]. TA has a configuration of two carboxylate anion (COO^-) side groups attached to a six-carbon ring at positions 1 and 4 to form a structurally symmetrical compound. Reaction of $\bullet\text{OH}$ with any of the four unsubstituted carbons will form only one hydroxylated product, 2-hydroxy-TA (2-OH-TA). TA is non-fluorescent, whereas 2-OH-TA is highly fluorescent. Neither TA nor 2-OH-TA is present in tissues physiologically. In addition, none of them is known to be involved in cellular functions, thus they exhibit no cellular toxicity [96].

Fluorogenic spin probes can be used to detect $\bullet\text{OH}$. Their signal can be detected both fluorometrically and using EPR spectroscopy. The rhodamine nitroxide probe is a non-fluorescent substance reacting quantitatively with $\bullet\text{OH}$ ($E_x/E_m = 560/588 \text{ nm}$) [97].

The HKOH-1 probe was designed for better uptake and longer retention in cells. The HKOH-1 probe has excellent sensitivity, selectivity, and extremely rapid turn-on response toward $\bullet\text{OH}$ in live cells in both confocal imaging and flow cytometry experiments [98].

2.3. Singlet Oxygen

Singlet oxygen ($^1\text{O}_2$), the highest energy state of molecular oxygen, has been extensively studied to oxidize toxic persistent organic contaminants [99]. Singlet oxygen is a highly reactive form of oxygen. It is produced during photochemical reactions or even physiologically in the respiratory chain of mitochondria. In excitation, molecular oxygen is excited to the first state ($1\Delta_g$) and then to the higher excited state ($1\Sigma_g$). In the first excited state, O_2 has two counter-spin electrons in a π orbital, while in the second excited state, O_2 has one counter-spin electron in two π orbitals [100,101]. The first excited state is highly reactive. $1\Delta_g$ $^1\text{O}_2$ is also produced physiologically, e.g., in the activation of neutrophils and macrophages [102,103]. It is a highly potent oxidizing agent that can cause fatal damage of DNA [104] or cell death [105,106].

Singlet oxygen reacts with several biological molecules including DNA, RNA, lipids, sterols, and especially proteins [107]. Amino acid residues of proteins can react with $^1\text{O}_2$ by direct chemical reaction or physical quenching. Physical quenching causes de-excitation of the singlet state of oxygen proved in proteins through the interaction with tryptophan residues [108].

2.3.1. Role of Singlet Oxygen in Nanomaterial Toxicity

Reactive oxygen species are formed by the reaction of photoinduced binding electrons with oxygen molecules. After the release of photoinduced electrons, valence band holes are formed on the surface of TiO_2 NPs that cannot oxidize water [109]. Another type of ROS that occurs during photocatalytic reactions on the surface of TiO_2 NPs is $^1\text{O}_2$ (Figure 3) [41]. Nanomaterials that can induce singlet oxygen production also include Ag NPs [42]. Nanomaterials-bound generation of $^1\text{O}_2$ can be also used in the treatment of tumors [43]. An activatable system has been developed that enables tumor-specific $^1\text{O}_2$ generation, based on a Fenton-like reaction between linoleic acid hydroperoxide (LAHP), tethered on FeO NPs and Fe^{2+} ions released from FeO NPs under acidic pH conditions [43]. After increased production of $^1\text{O}_2$ in cells, the intracellular concentration of GSH decreases [110–112].

2.3.2. Methods for the Detection of Singlet Oxygen

The DPAX-1 fluorescent probe (9-[2-(3-carboxy-9,10-diphenyl)-anthryl]-6-hydroxy-3H-xanthen-3-one) has been used to detect $^1\text{O}_2$ forming endoperoxide as a reaction product. The probe is based on 9,10-diphenylanthracene (DPA), conjugated to fluorescein. The high quantum yield and wavelength of the excitation radiation are suitable for biological applications [113]. The DMAX 9-[2-(3-carboxy-9,10-dimethyl)anthryl]-6-hydroxy-3H-xanthen-3-

one has been also used to detect $^1\text{O}_2$. The DMAX probe reacts much more specifically and faster with $^1\text{O}_2$ compared to the DPAX-1 probe [114].

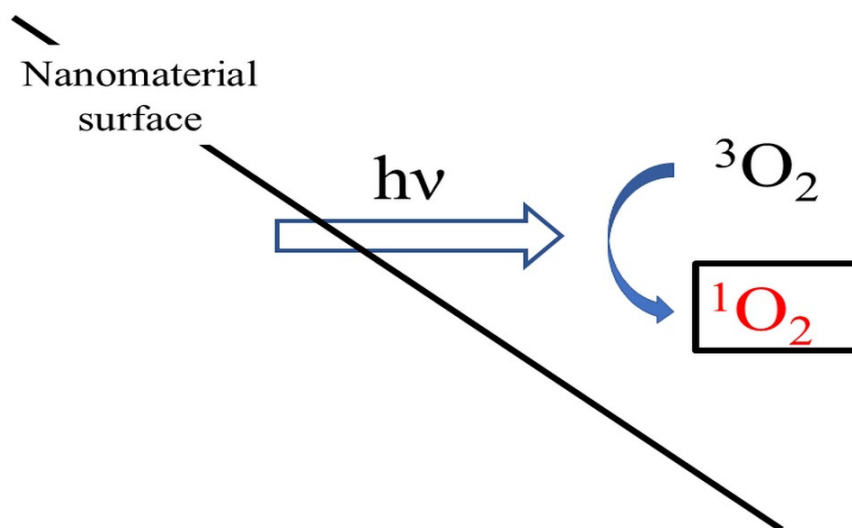


Figure 3. Generation of $^1\text{O}_2$ in a photocatalytic reaction on the TiO_2 surface. Abbreviations: $^3\text{O}_2$ = molecular oxygen; $^1\text{O}_2$ = singlet oxygen; and $h\nu$ = radiation.

Other approach for singlet oxygen detection are amino-functionalized nanoparticles covalently linked to Singlet Oxygen Sensor Green[®] (SOSG) which is an anthracene-fluorescein dye. The fluorescence of the SOSG molecule is inhibited by photoinduced intramolecular electron transfer. When anthracene is endoperoxidized in the presence of $^1\text{O}_2$, the electron transfer is blocked and fluorescein self-fluorescence is restored [115].

2.4. Hydrogen Peroxide

Hydrogen peroxide is formed directly through SOD-catalyzed dismutation from superoxide [116]. It belongs among ROS but it is not a free radical. The relatively long lifespan and size of H_2O_2 allows it to pass through cell membranes to different parts of the cell, which facilitates signaling reactions [117]. It causes cell damage at concentrations higher than 100 nM. Concentration of H_2O_2 in the range of 1–10 nM acts physiologically in the process of redox signaling [116]. It does not cause direct DNA damage but DNA damage is ensured due to $\bullet\text{OH}$ presence, which arises from H_2O_2 in the presence of transition metal ions [118]. Enzymes eliminating H_2O_2 include catalase, glutathione peroxidase, and peroxiredoxins [119].

In peroxisomes, the main metabolic process producing H_2O_2 is the β -oxidation of fatty acids through acyl-CoA-oxidase. Other enzymes involved in the formation of ROS include urate oxidase [120], D-aspartate oxidase [121], or xanthine oxidase [28].

2.4.1. Role of Hydrogen Peroxide in Nanomaterial Toxicity

Most nanomaterials that induce the production of $\text{O}_2^{\bullet-}$ also induce the production of H_2O_2 . In a study [36], colorectal cancer cells were exposed to polystyrene NPs (20 and 40 nm) with two surfactants (amino and carboxylic acid). After the exposure of cells to polystyrene NPs, a decrease in cell viability was observed and the induction of the apoptosis process was reduced by decreased H_2O_2 production by catalase. In another study [37], the authors observed a decrease in intracellular GSH concentration after the exposure of cells to 8 nm Au NPs. Subsequently, it was found that there was a decrease in mitochondrial membrane potential ($\Delta\Psi$) and cell apoptosis deepened after 48 h of incubation of cells with Au NPs. Then, a decreased mitochondrial GSH concentration and increased H_2O_2 production were observed. Other nanomaterials capable of induction of H_2O_2 formation are e.g., TiO_2 NPs [38], ZnO NPs [39], and Ag NPs [40].

2.4.2. Methods for the Detection of Hydrogen Peroxide

2',7'-Dichlorodihydrofluorescein

The 2',7'-dichlorodihydrofluorescein (DCFH) probe is a specific indicator of the presence of H_2O_2 . The diacetate form of DCFH (DCFH-DA) has been used to detect ROS in cells due to its ability to penetrate cell membranes. Two acetate groups are hydrolyzed by intracellular esterases after DCFH-DA transfer into cells. Then, the presence of peroxidases is important for the oxidation of DCFH by H_2O_2 . Other agents capable of oxidizing DCFH include hematin or cytochrome c [122,123] which may increase the fluorescence of the probe without any H_2O_2 production [124]. DCFH can be also oxidized with H_2O_2 in the presence of Fe^{2+} but this is most likely due to the formation of $\bullet OH$. In contrast, $O_2^{\bullet -}$ is unable to oxidize the DCFH probe [125]. In the presence of visible light or ultraviolet radiation, a DCF photoreduction can occur (Figure 4). The fluorescent product exhibits fluorescence at 522 nm (excitation at 498 nm).

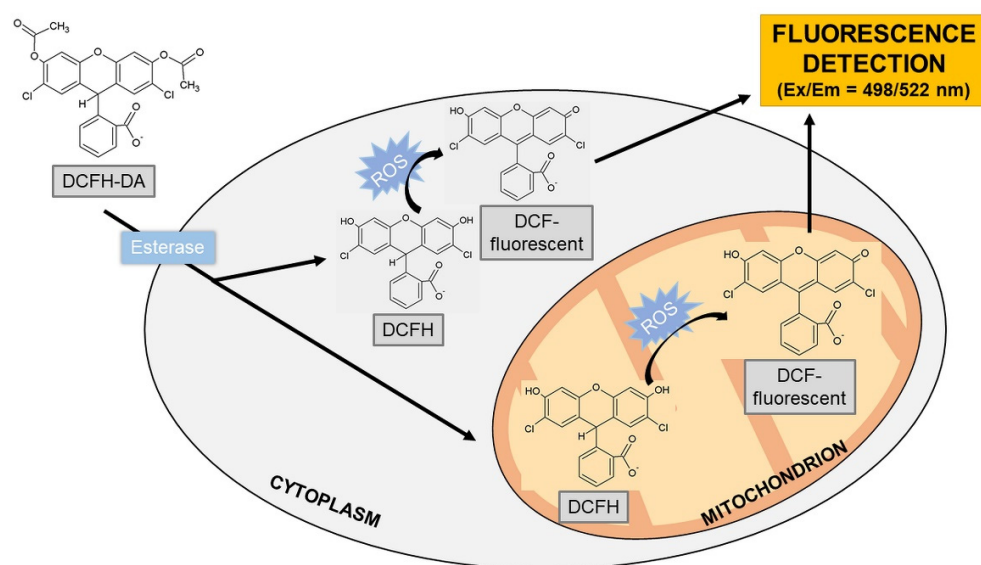


Figure 4. Detection of hydrogen peroxide using a probe DCFH-DA. Abbreviations: DCFH-DA = 2',7'-dichlorodihydrofluorescein diacetate; DCFH = 2',7'-dichlorodihydrofluorescein; DCF = 2',7'-dichlorofluorescein; and ROS = reactive oxygen species.

The oxidation of the probe produces a semichinone radical ($DCF^{\bullet -}$) that, when reacted with O_2 , gives rise to $O_2^{\bullet -}$. Dismutation of $O_2^{\bullet -}$ produces H_2O_2 that then artificially increases the oxidation of DCFH. The oxidation of DCFH results in the formation of a fluorescent product DCF exhibiting strong fluorescence. However, this reaction can increase the fluorescence intensity of the DCF product and give false-positive results [126–128]. In the case of the measurement of ROS production in tested nanomaterials, the form of DCFH-DA has been mostly used in ZnO_2 NMs [33,129–132] and TiO_2 NMs [133–136].

Amplex Red

Amplex Red (N-acetyl-3,7-dihydroxyphenoxazine) is a non-fluorescent molecule that can be specifically oxidized by H_2O_2 in the presence of horseradish peroxidase (HRP) to the highly fluorescent resorufin product (Figure 5), EX/EM 563/587 nm [137]. At excessive H_2O_2 concentrations, the fluorescent product resorufin can be further oxidized to non-fluorescent resazurin [138]. Amplex Red reacts with H_2O_2 stoichiometrically. It can also be used for the detection of $O_2^{\bullet -}$ in a mixture with SOD converting $O_2^{\bullet -}$ to H_2O_2 . The background fluorescence during the measurement is very low and the fluorescent product is very stable. These features increase the sensitivity of the measurement. Significant loss of fluorescence may be due to the oxidation of resorufin to the non-fluorescent resazurin product that can be catalyzed by HRP [139,140].

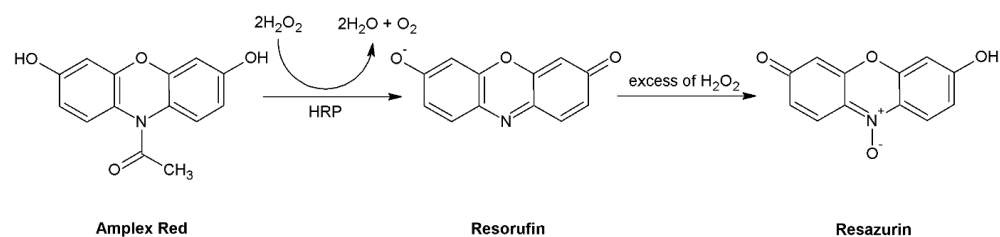


Figure 5. Oxidation of Amplex Red to a fluorescent (resorufin) and non-fluorescent (resazurin) product. Abbreviation: HRP = horseradish peroxidase.

HyPer Ratiometric Sensor

The H_2O_2 concentration can be measured using the expression of a HyPer genetically encoded ratio sensor. HyPer consists of the bacterial H_2O_2 -sensitive transcription factor OxyR, fused to the circular fluorescent protein YFP. Cysteine oxidation of the OxyR moiety induces a conformational change that results in an increase in YFP fluorescence intensity excited at 500 nm and a decrease in YFP emission excited at 420 nm. This reversible change can monitor the intracellular concentration of H_2O_2 [141].

Pentafluorobenzenesulfonyl Fluoresceins

Perhydrolysis of acyl resorufins is a reaction that acts as a fluorescent indicator for the determination of H_2O_2 . This method is based on deprotection rather than oxidation, which enables the fluorescence of resorufin and fluorescein. The selectivity of this method for H_2O_2 detection is higher compared to DCFH. For the above reasons, pentafluorobenzenesulfonyl fluoresceins have been proposed as selective fluorescent probes for H_2O_2 detection. Importantly, sulfonates are more stable to hydrolysis than esters. Fluoresceins have high fluorescence yields and the pentafluorobenzene ring increases the reactivity of sulfonates with H_2O_2 [142].

Europium Ion

The method is based on the binding of Eu^{3+} -tetracycline [Eu (tc)] linked to propane-sulfonic acid (MOPS) in an aqueous solution to H_2O_2 . After binding, a strongly fluorescent complex ([Eu (hp) (tc)]) is formed ($\lambda_{\text{EX/EM}} = 390\text{-}405 / 616 \text{ nm}$). The increase in fluorescence is up to 15x after H_2O_2 binding and it is strongly dependent on the pH value. The increase in fluorescence is most pronounced at the physiological pH environment. The fluorescence of the probe [Eu (tc)] is not affected by ammonium, chloride, sulphate, or nitrate ions. However, citrate and phosphate can interfere with the assay [143].

Homovanillic Acid

Recently, homovanillic acid (3-methoxy-4-hydroxyphenylacetic acid) has been increasingly used instead of scopoletin for H_2O_2 detection in mitochondria. In contrast to the fluorescent scopoletin indicating the presence of H_2O_2 by a fluorescence decrease, homovanillic acid becomes a fluorescent through H_2O_2 -induced oxidation in the presence of HRP [144]. The product of this reaction is a highly fluorescent dimer 2,2'-dihydroxy-3,3'-dimethoxydiphenyl-5,5'-diacetic acid [145]. In the following Table 2, an overview of all described fluorescent probes for ROS detection are summarized.

Table 2. Overview of fluorescent probes for the detection of ROS [79,95,97,98,114,115,137,141–143,145].

Type of ROS	Fluorescent Probe	Excitation/Emission Wavelengths
Superoxide	MitoSox	535/610 nm
	1,3-diphenylisobenzofuran	410/455 nm
Hydroxyl radical	Terephthalic acid	310/420 nm
	Rhodamine nitroxide	560/588 nm
	HKOH-1	500/520 nm
Singlet oxygen	DPAX-1	495/515 nm
	DMAX	495/515 nm
	Singlet Oxygen Sensor Green®	504/525 nm
Hydrogen peroxide	2',7'-dichlorodihydrofluorescein	498/522 nm
	Amplex Red	563/587 nm
	HyPer ratiometric sensor	485/516 nm
	Pentafluorobenzenesulfonyl fluoresceins	485/530 nm
	Europium ion	400/616 nm
	Homovanilic acid	312/420 nm

3. Role of Reactive Oxygen Species Induced by Nanoparticles in Cell Signaling

Nanomaterials are capable of interfering with cell signaling pathways. Recently, three main pathways participating in the apoptosis process have been identified (Figure 6). The first pathway is the direct NMs occupation of the FADD receptor. The second pathway is the modulation of the function of mitochondria in the presence of NMs and the third is the localization of NMs pacting in the endoplasmic reticulum. All of these pathways converge upon caspase activation, thereby the mitochondria produce higher levels of ROS, increase production of Bid protein, and activate Bax or Bak1 proteins, which can ultimately lead to organelle damage, DNA cleavage, and cell death [146].

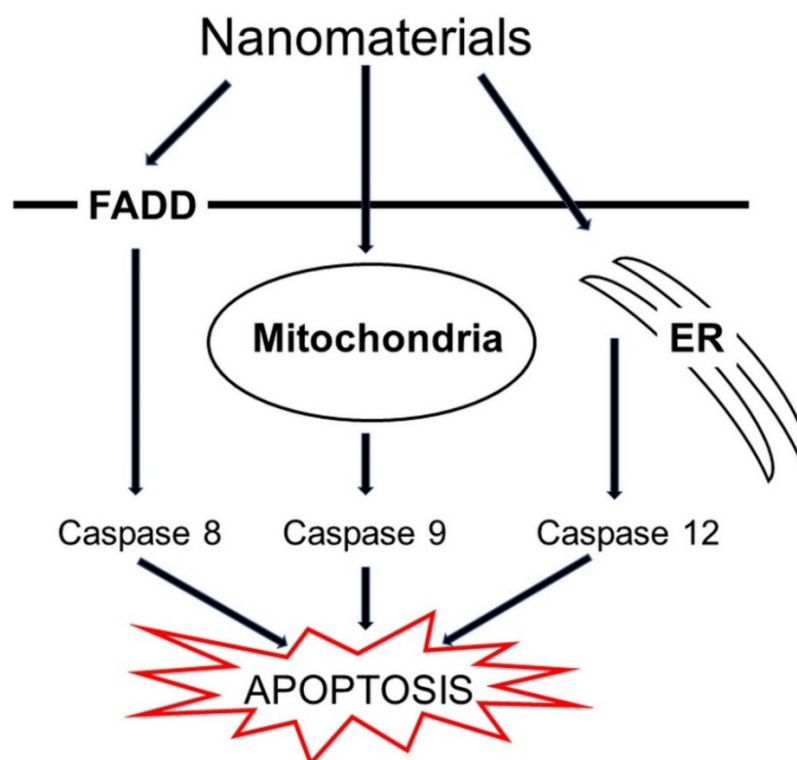


Figure 6. Possible pathways of induction of apoptosis by nanomaterials in cells. Abbreviations: ER = endoplasmic reticulum and FADD = FAS-associated death domain protein.

The dynamic and rapid nature of ROS signaling is the result of ROS production and removal. The balance between the production and removal of ROS is balanced due to their interaction. This causes rapid changes in ROS levels [147]. ROS play an important role in activating many cellular proteins and factors, e.g., NF- κ B, MAPK, Keap1-Nrf2-ARE, or PI3K-Akt [148,149].

The NF- κ B family is a family of transcriptional proteins consisting of five members, i.e., NF- κ B1, NF- κ B2, RelA, RelB, and c-Rel [150]. The activation of the transcription factor NF- κ B involves signal-dependent degradation of phosphorylated inhibitors such as I κ B α . The mechanism of NF- κ B activation by H₂O₂ [151] or O₂^{•-} [152] is different from the activation in the presence of cytokines or mitogens. Serines 32 and 36 play a key role in the activation of NF- κ B by cytokines, while tyrosine residues 42 and serine/threonine in the PEST domain of the I κ B α protein play a key role in the activation by H₂O₂ [153]. H₂O₂ activates I κ B α kinase without subsequent serine phosphorylation of I κ B α . In contrast, H₂O₂, similar to TNF, induces serine phosphorylation of the p65 subunit of NF- κ B, leading to its nuclear translocation [154]. Nanoparticles participate directly in the activation of the factor NF- κ B through increased ROS production which was confirmed by the translocation of the high-mobility group box 1 (HMGB1) protein from the nucleus to the cytoplasm observed in cells after exposure to silica nanoparticles [155]. Subsequently, HMGB1 binds to the TLR4 receptor; this complex regulates the expression of the myeloid differentiation factor and activates the NF- κ B-signaling pathway.

In eukaryotic cells, signaling by MAPK kinases is very important. Various MAPK pathways can be activated by different stimuli. Ultimately, activated MAPK pathways coordinate gene transcription activation, acting in the regulation of protein synthesis, cell cycle, cell death, and cell differentiation [156]. The MAPK cascade is composed of three distinct signaling modules, i.e., the c-Jun N-terminal kinase cascade, the p38 MAPK cascade, and the extracellular signal-regulated kinase ERK [157]. Several cellular stimuli activating ROS production can also activate MAPK activation itself [158]. For instance, MAPK kinases can be activated by H₂O₂ [159]. MAPK activation occurs by activating growth factor receptors in several cell types [160]. Another mechanism of MAPK activation by ROS is the inactivation of the MKP protein by its oxidation [161]. The physiological FEM protein keeps the MAPK signaling pathway inactive. In addition to the activation of MAPK, the JNK pathway is also activated during the oxidation of the FEM protein [162]. A number of studies have demonstrated the activation of a variety of kinases by ROS, including ASK1 [163], MEKK1 [164], c-Src [165], and EGFR [166]. These activated kinases ultimately can activate the MAPK cascade [167]. Cerium oxide particles have been shown to activate ROS production and to reduce SOD and glutathione peroxidase activities. This results in increased phosphorylation levels of p38 MAPK as well as ERK1/2 and JNK [168]. The nanoparticles that can damage cells through p38 MAPK activation are silica NPs [169,170], polystyrene NPs [171], and TiO₂ NPs [172]. Conversely, the exposure to Au [173] and iron oxide [174] NPs causes the osteogenic differentiation through the activation of relevant genes by p38 MAPK.

The tumor suppressor protein p53 induces apoptotic cell death in response to oncogenic stress. Malignant progression is dependent on the loss of p53 function by mutations in the TP53 gene itself or defects in signaling pathways. Phosphorylation of p53 regulates the ability to activate the expression of apoptotic target genes [175]. Overexpression of p53 transactivates a number of p53 genes. Many of these genes encode redox active proteins including enzymes (quinone oxidoreductase and proline oxidase) generating ROS. Ultimately, this regulation of ROS production leads to oxidative stress that can induce apoptosis [176]. Increasing the intracellular concentration of ROS leads to the activation of the p38 protein, which increases the expression and transcriptional activity of p53 [177]. The p53 protein transcriptionally activates the PUMA gene encoding two proteins, PUMA- α and PUMA- β , of similar activity. These proteins bind to Bcl-2 and integrate into the mitochondria, where they induce the release of cytochrome c [178–180].

Last but not least, ROS activate the JNK kinase pathway, which plays an important role in the apoptosis process [4,181]. During intracellular ROS production, there is a permanent activation of JNK [182]. This is due to the inactivation of MAPK phosphatases (FEM) by oxidation of their catalytic cysteine in the presence of intracellularly accumulated H_2O_2 . Expression of catalytically inactive FEMs prolongs JNK activation [183].

4. Current Trends in the Evaluation of Nanotoxicity In Vitro

The number of studies focusing on nanotoxicity testing has been growing very rapidly in the last two decades. The cause of that can be also found in the perpetual production of new nanomaterials for its following use in industry or medicine. Conversely, especially in medicine, nanomaterials raise some concerns regarding their cytotoxicity or biocompatibility. Thus, a number of scientific projects have been assessing the toxicity of the selected nanomaterials and creating the risk management framework for the use of nanomaterials in medical applications [184].

Recent studies on nanotoxicity have been using basic assays for the evaluation of cell function changes, e.g., cell viability, membrane integrity, and enzyme activities measurements. To estimate the oxidative status in cells, the levels of antioxidants can be measured using a number of methods. In addition to the most frequently used methods, other approaches have been used to characterize the cellular nanotoxicity recently. These methods include scanning electron microscopy [185], liquid cell transmission electron microscopy [186], atomic force microscopy [187], and hyperspectral and laser confocal microscopy applied to cell-nanoparticles interactions [185]. All these microscopic methods are very sensitive and specific, which allows for a very detailed description of the function state of the cells after nanomaterials treatment. To understand the toxicity of nanomaterials, we need to develop new and innovative methods that will provide us with information about the changes in the intracellular environment after exposure to nanomaterials. In addition, there is a need to develop methods that are fast, robust, and combine several biological tests. In contrast to conventional assays using lipophilic fluorescent probes detecting ROS levels, a nanoelectrode has been developed to study the toxicity of magnetic nanoparticles. The nanoelectrode is composed of individual platinum nanoelectrodes with a cavity at the tip. It is part of an upright microscope and is used to measure intracellular ROS [188].

A further topic of interest in nanotoxicity testing is the use of newly developed relevant biological models. In comparison to two-dimensional (2D) cultured cell lines, those new biological models ought to provide accurate predictions of nanomaterials effects in vivo. Thus, some new scientific studies described the use of pulmonary fibrosis models [189], organ on-chip technology bridging the differences between 2D in vitro and three-dimensional (3D) in vivo models from skin, the lung, and the liver [190,191], or on-chip placenta models [192]. Despite advanced organ on-chip models, a number of concerns have to be solved to ensure the comparability to living systems in obtained outcomes [193].

5. Conclusions

Currently, nanotechnology is considered to be one of the most attractive research topics due to its huge application potential and commercial impact. Due to the large number of newly manufactured nanomaterials, it is necessary to evaluate their possible cytotoxic effects in men. At present, there is a large request to investigate the potential acute and chronic effects of nanomaterials especially in vitro in cells. Those studies can provide a mechanistic view on nanomaterial cellular acting. However, the use of proper and relevant bioanalytical methods for evaluating the nanomaterials effects in cells is necessary.

In this study, we aimed to provide a recent and detailed view on ROS production induced by nanomaterials, especially considering the metallic nanoparticles. In cells, the nanotoxicity can be mediated by a number of substances including ROS. Depending on the composition and shape of a nanomaterial, a variety of ROS can be formed in cells, i.e., $O_2^{\bullet-}$, 1O_2 , $\bullet OH$, and H_2O_2 . Thus, the importance of the present review can

be recognized in the mechanistic description of a relation of nanomaterials of different chemical compositions and ROS production. We provided the current knowledge of ROS-mediated cellular nanotoxicity together with the possibilities of ROS detection in cells using specific fluorescent probes. In addition, we summarized the detailed description of the relationship between nanomaterials-mediated ROS production and glutathione depletion. Altogether, the prooxidative action of nanomaterials can ultimately lead to the activation of cellular signaling pathways, causing a change in cellular metabolism, cell damage, or even cell death.

Funding: Financial support was received from the Ministry of Education, Youth, and Sports of the Czech Republic via project NANOBIO (Reg. No. CZ.02.1.01/0.0/0.0/17_048/0007421).

Institutional Review Board Statement: Not applicable.

Informed Consent Statement: Not applicable.

Data Availability Statement: Not applicable.

Conflicts of Interest: The authors declare no conflict of interest.

References

- Hayyan, M.; Hashim, M.A.; AlNashef, I.M. Superoxide Ion: Generation and Chemical Implications. *Chem. Rev.* **2016**, *116*, 3029–3085. [CrossRef] [PubMed]
- Lushchak, V.I. Free radicals, reactive oxygen species, oxidative stress and its classification. *Chem. Biol. Interact.* **2014**, *224*, 164–175. [CrossRef] [PubMed]
- Juan, C.A.; Perez de la Lastra, J.M.; Plou, F.J.; Perez-Lebena, E. The Chemistry of Reactive Oxygen Species (ROS) Revisited: Outlining Their Role in Biological Macromolecules (DNA, Lipids and Proteins) and Induced Pathologies. *Int. J. Mol. Sci.* **2021**, *22*, 4642. [CrossRef] [PubMed]
- Simon, H.U.; Haj-Yehia, A.; Levi-Schaffer, F. Role of reactive oxygen species (ROS) in apoptosis induction. *Apoptosis* **2000**, *5*, 415–418. [CrossRef] [PubMed]
- Wagner, H.; Cheng, J.W.; Ko, E.Y. Role of reactive oxygen species in male infertility: An updated review of literature. *Arab. J. Urol.* **2018**, *16*, 35–43. [CrossRef] [PubMed]
- Ott, M.; Gogvadze, V.; Orrenius, S.; Zhivotovsky, B. Mitochondria, oxidative stress and cell death. *Apoptosis* **2007**, *12*, 913–922. [CrossRef] [PubMed]
- Zhao, R.Z.; Jiang, S.; Zhang, L.; Yu, Z.B. Mitochondrial electron transport chain, ROS generation and uncoupling (Review). *Int. J. Mol. Med.* **2019**, *44*, 3–15. [CrossRef] [PubMed]
- Suski, J.; Lebiezinska, M.; Bonora, M.; Pinton, P.; Duszynski, J.; Wieckowski, M.R. Relation Between Mitochondrial Membrane Potential and ROS Formation. *Methods Mol. Biol.* **2018**, *1782*, 357–381. [PubMed]
- Mazat, J.P.; Devin, A.; Ransac, S. Modelling mitochondrial ROS production by the respiratory chain. *Cell Mol. Life Sci.* **2020**, *77*, 455–465. [CrossRef] [PubMed]
- Parey, K.; Wirth, C.; Vonck, J.; Zickermann, V. Respiratory complex I—structure, mechanism and evolution. *Curr. Opin. Struct. Biol.* **2020**, *63*, 1–9. [CrossRef]
- Husen, P.; Nielsen, C.; Martino, C.F.; Solov'yov, I.A. Molecular Oxygen Binding in the Mitochondrial Electron Transfer Flavoprotein. *J. Chem. Inf. Model.* **2019**, *59*, 4868–4879. [CrossRef] [PubMed]
- Mailloux, R.J. An Update on Mitochondrial Reactive Oxygen Species Production. *Antioxidants* **2020**, *9*, 472. [CrossRef] [PubMed]
- Papa, S.; Skulachev, V.P. Reactive oxygen species, mitochondria, apoptosis and aging. *Mol. Cell Biochem.* **1997**, *174*, 305–319. [CrossRef] [PubMed]
- Ventura, J.J.; Cogswell, P.; Flavell, R.A.; Baldwin, A.S., Jr.; Davis, R.J. JNK potentiates TNF-stimulated necrosis by increasing the production of cytotoxic reactive oxygen species. *Genes Dev.* **2004**, *18*, 2905–2915. [CrossRef] [PubMed]
- Zhang, M.; Harashima, N.; Moritani, T.; Huang, W.; Harada, M. The Roles of ROS and Caspases in TRAIL-Induced Apoptosis and Necroptosis in Human Pancreatic Cancer Cells. *PLoS ONE* **2015**, *10*, e0127386. [CrossRef] [PubMed]
- Yang, J.; Zhao, X.; Tang, M.; Li, L.; Lei, Y.; Cheng, P.; Guo, W.; Zheng, Y.; Wang, W.; Luo, N.; et al. The role of ROS and subsequent DNA-damage response in PUMA-induced apoptosis of ovarian cancer cells. *Oncotarget* **2017**, *8*, 23492–23506. [CrossRef] [PubMed]
- Liou, G.Y.; Storz, P. Reactive oxygen species in cancer. *Free Radic. Res.* **2010**, *44*, 479–496. [CrossRef]
- Storz, P. Reactive oxygen species in tumor progression. *Front. BioSci.* **2005**, *10*, 1881–1896. [CrossRef]
- Zhou, B.; Guo, X.; Yang, N.; Huang, Z.; Huang, L.; Fang, Z.; Zhang, C.; Li, L.; Yu, C. Surface engineering strategies of gold nanomaterials and their applications in biomedicine and detection. *J. Mater. Chem. B* **2021**, *9*, 5583–5598. [CrossRef]
- Sakr, T.M.; Korany, M.; Katti, K.V. Selenium nanomaterials in biomedicine—An overview of new opportunities in nanomedicine of selenium. *J. Drug Deliv. Sci. Technol.* **2018**, *46*, 223–233. [CrossRef]

21. Mehlenbacher, R.D.; Kolbl, R.; Lay, A.; Dionne, J.A. Nanomaterials for in vivo imaging of mechanical forces and electrical fields. *Nat. Rev. Mater.* **2017**, *3*, 1–17. [CrossRef]
22. Musial, J.; Krakowiak, R.; Mlynarczyk, D.T.; Goslinski, T.; Stanisz, B.J. Titanium Dioxide Nanoparticles in Food and Personal Care Products—What Do We Know about Their Safety? *Nanomaterials* **2020**, *10*, 1110. [CrossRef]
23. Holmila, R.J.; Vance, S.A.; King, S.B.; Tsang, A.W.; Singh, R.; Furdui, C.M. Silver Nanoparticles Induce Mitochondrial Protein Oxidation in Lung Cells Impacting Cell Cycle and Proliferation. *Antioxidants* **2019**, *8*, 552. [CrossRef] [PubMed]
24. Drasler, B.; Sayre, P.; Steinhäuser, K.G.; Petri-Fink, A.; Rothen-Rutishauser, B. In vitro approaches to assess the hazard of nanomaterials. *NanoImpact* **2017**, *8*, 99–116. [CrossRef]
25. Yin, J.J.; Liu, J.; Ehrenshaft, M.; Roberts, J.E.; Fu, P.P.; Mason, R.P.; Zhao, B. Phototoxicity of nano titanium dioxides in HaCaT keratinocytes—generation of reactive oxygen species and cell damage. *Toxicol. Appl. Pharmacol.* **2012**, *263*, 81–88. [CrossRef]
26. Ray, P.C.; Yu, H.T.; Fu, P.P. Toxicity and Environmental Risks of Nanomaterials: Challenges and Future Needs. *J. Environ. Sci. Health C* **2009**, *27*, 1–35. [CrossRef]
27. Daimon, T.; Nosaka, Y. Formation and behavior of singlet molecular oxygen in TiO₂ photocatalysis studied by detection of near-infrared phosphorescence. *J. Phys. Chem. C* **2007**, *111*, 4420–4424. [CrossRef]
28. Phaniendra, A.; Jestadi, D.B.; Periyasamy, L. Free Radicals: Properties, Sources, Targets, and Their Implication in Various Diseases. *Indian J. Clin. Biochem.* **2015**, *30*, 11–26. [CrossRef] [PubMed]
29. Yang, H.; Liu, C.; Yang, D.; Zhang, H.; Xi, Z. Comparative study of cytotoxicity, oxidative stress and genotoxicity induced by four typical nanomaterials: The role of particle size, shape and composition. *J. Appl. Toxicol.* **2009**, *29*, 69–78. [CrossRef]
30. He, X.; Sanders, S.; Aker, W.G.; Lin, Y.; Douglas, J.; Hwang, H.M. Assessing the effects of surface-bound humic acid on the phototoxicity of anatase and rutile TiO₂ nanoparticles in vitro. *J. Environ. Sci.* **2016**, *42*, 50–60. [CrossRef] [PubMed]
31. Zhang, J.; Wang, B.; Wang, H.; He, H.; Wu, Q.; Qin, X.; Yang, X.; Chen, L.; Xu, G.; Yuan, Z.; et al. Disruption of the superoxide anions-mitophagy regulation axis mediates copper oxide nanoparticles-induced vascular endothelial cell death. *Free Radic. Biol. Med.* **2018**, *129*, 268–278. [CrossRef] [PubMed]
32. Onodera, A.; Nishiumi, F.; Kakiguchi, K.; Tanaka, A.; Tanabe, N.; Honma, A.; Yayama, K.; Yoshioka, Y.; Nakahira, K.; Yonemura, S.; et al. Short-term changes in intracellular ROS localisation after the silver nanoparticles exposure depending on particle size. *Toxicol. Rep.* **2015**, *2*, 574–579. [CrossRef]
33. Ahamed, M.; Akhtar, M.J.; Raja, M.; Ahmad, I.; Siddiqui, M.K.; AlSalhi, M.S.; Alrokayan, S.A. ZnO nanorod-induced apoptosis in human alveolar adenocarcinoma cells via p53, survivin and bax/bcl-2 pathways: Role of oxidative stress. *Nanomedicine* **2011**, *7*, 904–913. [CrossRef] [PubMed]
34. Jimenez-Relinque, E.; Castellote, M. Hydroxyl radical and free and shallowly trapped electron generation and electron/hole recombination rates in TiO₂ photocatalysis using different combinations of anatase and rutile. *Appl. Catal. A Gen.* **2018**, *565*, 20–25. [CrossRef]
35. Thit, A.; Selck, H.; Bjerregaard, H.F. Toxic mechanisms of copper oxide nanoparticles in epithelial kidney cells. *Toxicol. In Vitro* **2015**, *29*, 1053–1059. [CrossRef]
36. Thubagere, A.; Reinhard, B.M. Nanoparticle-induced apoptosis propagates through hydrogen-peroxide-mediated bystander killing: Insights from a human intestinal epithelium in vitro model. *ACS Nano* **2010**, *4*, 3611–3622. [CrossRef]
37. Gao, W.; Xu, K.; Ji, L.; Tang, B. Effect of gold nanoparticles on glutathione depletion-induced hydrogen peroxide generation and apoptosis in HL7702 cells. *Toxicol. Lett.* **2011**, *205*, 86–95. [CrossRef] [PubMed]
38. Wang, J.X.; Fan, Y.B.; Gao, Y.; Hu, Q.H.; Wang, T.C. TiO₂ nanoparticles translocation and potential toxicological effect in rats after intraarticular injection. *Biomaterials* **2009**, *30*, 4590–4600. [CrossRef] [PubMed]
39. Guo, D.; Bi, H.; Liu, B.; Wu, Q.; Wang, D.; Cui, Y. Reactive oxygen species-induced cytotoxic effects of zinc oxide nanoparticles in rat retinal ganglion cells. *Toxicol. In Vitro* **2013**, *27*, 731–738. [CrossRef]
40. Yang, E.J.; Kim, S.; Kim, J.S.; Choi, I.H. Inflammasome formation and IL-1β release by human blood monocytes in response to silver nanoparticles. *Biomaterials* **2012**, *33*, 6858–6867. [CrossRef] [PubMed]
41. Hirakawa, K.; Hirano, T. Singlet oxygen generation photocatalyzed by TiO₂ particles and its contribution to biomolecule damage. *Chem. Lett.* **2006**, *35*, 832–833. [CrossRef]
42. Lee, S.H.; Jun, B.H. Silver Nanoparticles: Synthesis and Application for Nanomedicine. *Int. J. Mol. Sci.* **2019**, *20*, 865. [CrossRef] [PubMed]
43. Zhou, Z.; Song, J.; Tian, R.; Yang, Z.; Yu, G.; Lin, L.; Zhang, G.; Fan, W.; Zhang, F.; Niu, G.; et al. Activatable Singlet Oxygen Generation from Lipid Hydroperoxide Nanoparticles for Cancer Therapy. *Angew. Chem. Int. Ed. Engl.* **2017**, *56*, 6492–6496. [CrossRef]
44. Abdal Dayem, A.; Hossain, M.K.; Lee, S.B.; Kim, K.; Saha, S.K.; Yang, G.M.; Choi, H.Y.; Cho, S.G. The Role of Reactive Oxygen Species (ROS) in the Biological Activities of Metallic Nanoparticles. *Int. J. Mol. Sci.* **2017**, *18*, 120. [CrossRef]
45. Kermanizadeh, A.; Jantzen, K.; Ward, M.B.; Durhuus, J.A.; Juel Rasmussen, L.; Loft, S.; Moller, P. Nanomaterial-induced cell death in pulmonary and hepatic cells following exposure to three different metallic materials: The role of autophagy and apoptosis. *Nanotoxicology* **2017**, *11*, 184–200. [CrossRef] [PubMed]
46. Ge, D.; Du, Q.; Ran, B.; Liu, X.; Wang, X.; Ma, X.; Cheng, F.; Sun, B. The neurotoxicity induced by engineered nanomaterials. *Int. J. Nanomed.* **2019**, *14*, 4167–4186. [CrossRef] [PubMed]
47. Fridovich, I. Biological effects of the superoxide radical. *Arch. Biochem. Biophys.* **1986**, *247*, 1–11. [CrossRef]

48. Apel, K.; Hirt, H. Reactive oxygen species: Metabolism, oxidative stress, and signal transduction. *Annu. Rev. Plant. Biol.* **2004**, *55*, 373–399. [CrossRef]
49. McIntyre, M.; Bohr, D.F.; Dominiczak, A.F. Endothelial function in hypertension: The role of superoxide anion. *Hypertension* **1999**, *34*, 539–545. [CrossRef]
50. Bielski, B.H.J.; Cabelli, D.E. Superoxide and Hydroxyl Radical Chemistry in Aqueous Solution. *Act. Oxyg. Chem.* **1995**, *2*, 66–104.
51. Ahsan, H.; Ali, A.; Ali, R. Oxygen free radicals and systemic autoimmunity. *Clin. Exp. Immunol.* **2003**, *131*, 398–404. [CrossRef]
52. Perry, J.J.P.; Shin, D.S.; Getzoff, E.D.; Tainer, J.A. The structural biochemistry of the superoxide dismutases. *Bba-Proteins Proteom.* **2010**, *1804*, 245–262. [CrossRef]
53. Borgstahl, G.E.O.; Oberley-Deegan, R.E. Superoxide Dismutases (SODs) and SOD Mimetics. *Antioxidants* **2018**, *7*, 156. [CrossRef]
54. Landis, G.N.; Tower, J. Superoxide dismutase evolution and life span regulation. *Mech. Ageing Dev.* **2005**, *126*, 365–379. [CrossRef] [PubMed]
55. Loschen, G.; Flohe, L.; Chance, B. Respiratory Chain Linked H₂O₂ Production in Pigeon Heart Mitochondria. *FEBS Lett.* **1971**, *18*, 261–264. [CrossRef]
56. Loschen, G.; Azzi, A.; Richter, C.; Flohe, L. Superoxide Radicals as Precursors of Mitochondrial Hydrogen-Peroxide. *FEBS Lett.* **1974**, *42*, 68–72. [CrossRef]
57. Wilson, D.F.; Erecinska, M.; Dutton, P.L. Thermodynamic Relationships in Mitochondrial Oxidative-Phosphorylation. *Annu. Rev. Biophys. Bio* **1974**, *3*, 203–230. [CrossRef] [PubMed]
58. Ballard, J.W.; Youngson, N.A. Review: Can diet influence the selective advantage of mitochondrial DNA haplotypes? *Biosci. Rep.* **2015**, *35*. [CrossRef] [PubMed]
59. Liu, Y.B.; Fiskum, G.; Schubert, D. Generation of reactive oxygen species by the mitochondrial electron transport chain. *J. NeuroChem.* **2002**, *80*, 780–787. [CrossRef] [PubMed]
60. Kushnareva, Y.; Murphy, A.N.; Andreyev, A. Complex I-mediated reactive oxygen species generation: Modulation by cytochrome c and NAD(P)⁺ oxidation-reduction state. *Biochem. J.* **2002**, *368*, 545–553. [CrossRef]
61. Murphy, M.P. How mitochondria produce reactive oxygen species. *Biochem. J.* **2009**, *417*, 1–13. [CrossRef] [PubMed]
62. Wikstrom, M.K.; Berden, J.A. Oxidoreduction of cytochrome b in the presence of antimycin. *Biochim. Biophys. Acta* **1972**, *283*, 403–420. [CrossRef]
63. Muller, F.; Crofts, A.R.; Kramer, D.M. Multiple Q-cycle bypass reactions at the Q_o site of the cytochrome *bc*₁ complex. *Biochemistry* **2002**, *41*, 7866–7874. [CrossRef] [PubMed]
64. Bleier, L.; Drose, S. Superoxide generation by complex III: From mechanistic rationales to functional consequences. *Biochim. Biophys. Acta* **2013**, *1827*, 1320–1331. [CrossRef] [PubMed]
65. Grzelak, A.; Wojewodzka, M.; Meczynska-Wielgosz, S.; Zuberek, M.; Wojciechowska, D.; Kruszewski, M. Crucial role of chelatable iron in silver nanoparticles induced DNA damage and cytotoxicity. *Redox Biol.* **2018**, *15*, 435–440. [CrossRef] [PubMed]
66. Jayaram, D.T.; Payne, C.K. Intracellular Generation of Superoxide by TiO₂ Nanoparticles Decreases Histone Deacetylase 9 (HDAC9), an Epigenetic Modifier. *Bioconjug. Chem.* **2020**, *31*, 1354–1361. [CrossRef]
67. Masoud, R.; Bizouarn, T.; Trepout, S.; Wien, F.; Baciou, L.; Marco, S.; Houee Levin, C. Titanium Dioxide Nanoparticles Increase Superoxide Anion Production by Acting on NADPH Oxidase. *PLoS ONE* **2015**, *10*, e0144829. [CrossRef]
68. Akhtar, M.J.; Kumar, S.; Alhadlaq, H.A.; Alrokayan, S.A.; Abu-Salah, K.M.; Ahamed, M. Dose-dependent genotoxicity of copper oxide nanoparticles stimulated by reactive oxygen species in human lung epithelial cells. *Toxicol. Ind. Health* **2016**, *32*, 809–821. [CrossRef] [PubMed]
69. Piret, J.P.; Jacques, D.; Audinot, J.N.; Mejia, J.; Boilan, E.; Noel, F.; Fransolet, M.; Demazy, C.; Lucas, S.; Saout, C.; et al. Copper (II) oxide nanoparticles penetrate into HepG2 cells, exert cytotoxicity via oxidative stress and induce pro-inflammatory response. *Nanoscale* **2012**, *4*, 7168–7184. [CrossRef]
70. Piao, M.J.; Kang, K.A.; Lee, I.K.; Kim, H.S.; Kim, S.; Choi, J.Y.; Choi, J.; Hyun, J.W. Silver nanoparticles induce oxidative cell damage in human liver cells through inhibition of reduced glutathione and induction of mitochondria-involved apoptosis. *Toxicol. Lett.* **2011**, *201*, 92–100. [CrossRef] [PubMed]
71. Zielonka, J.; Srinivasan, S.; Hardy, M.; Ouari, O.; Lopez, M.; Vasquez-Vivar, J.; Avadhani, N.G.; Kalyanaraman, B. Cytochrome c-mediated oxidation of hydroethidine and mito-hydroethidine in mitochondria: Identification of homo- and heterodimers. *Free Radic. Biol. Med.* **2008**, *44*, 835–846. [CrossRef] [PubMed]
72. Ross, M.F.; Kelso, G.F.; Blaikie, F.H.; James, A.M.; Cocheme, H.M.; Filipovska, A.; Da Ros, T.; Hurd, T.R.; Smith, R.A.J.; Murphy, M.P. Lipophilic triphenylphosphonium cations as tools in mitochondrial bioenergetics and free radical biology. *Biochemistry* **2005**, *70*, 222–230. [CrossRef] [PubMed]
73. Robinson, K.M.; Janes, M.S.; Pehar, M.; Monette, J.S.; Ross, M.F.; Hagen, T.M.; Murphy, M.P.; Beckman, J.S. Selective fluorescent imaging of superoxide in vivo using ethidium-based probes. *Proc. Natl. Acad. Sci. USA* **2006**, *103*, 15038–15043. [CrossRef] [PubMed]
74. Kauffman, M.E.; Kauffman, M.K.; Traore, K.; Zhu, H.; Trush, M.A.; Jia, Z.; Li, Y.R. MitoSOX-Based Flow Cytometry for Detecting Mitochondrial ROS. *React. Oxyg. Species* **2016**, *2*, 361–370. [CrossRef]
75. Mukhopadhyay, P.; Rajesh, M.; Yoshihiro, K.; Hasko, G.; Pacher, P. Simple quantitative detection of mitochondrial superoxide production in live cells. *BioChem. Biophys. Res. Commun.* **2007**, *358*, 203–208. [CrossRef] [PubMed]

76. Roelofs, B.A.; Ge, S.X.; Studlack, P.E.; Polster, B.M. Low micromolar concentrations of the superoxide probe MitoSOX uncouple neural mitochondria and inhibit complex IV. *Free Radic. Biol. Med.* **2015**, *86*, 250–258. [CrossRef]
77. Ohyashiki, T.; Nunomura, M.; Katoh, T. Detection of superoxide anion radical in phospholipid liposomal membrane by fluorescence quenching method using 1,3-diphenylisobenzofuran. *Bba-Biomembranes* **1999**, *1421*, 131–139. [CrossRef]
78. Krieg, M. Determination of singlet oxygen quantum yields with 1,3-diphenylisobenzofuran in model membrane systems. *J. BioChem. Biophys. Methods* **1993**, *27*, 143–149. [CrossRef]
79. Zamojc, K.; Zdrowowicz, M.; Rudnicki-Velasquez, P.B.; Krzyminski, K.; Zaborowski, B.; Niedzialkowski, P.; Jacewicz, D.; Chmurzynski, L. The development of 1,3-diphenylisobenzofuran as a highly selective probe for the detection and quantitative determination of hydrogen peroxide. *Free Radic. Res.* **2017**, *51*, 38–46. [CrossRef]
80. Andresen, M.; Regueira, T.; Bruhn, A.; Perez, D.; Strobel, P.; Dougnac, A.; Marshall, G.; Leighton, F. Lipoperoxidation and protein oxidative damage exhibit different kinetics during septic shock. *Mediat. Inflamm.* **2008**. [CrossRef] [PubMed]
81. Wu, D.F.; Cederbaum, A.I. Alcohol, oxidative stress, and free radical damage. *Alcohol. Res. Health* **2003**, *27*, 277–284. [PubMed]
82. Halliwell, B.; Chirico, S. Lipid-Peroxidation — Its Mechanism, Measurement, and Significance. *Am. J. Clin. Nutr.* **1993**, *57*, 715–725. [CrossRef] [PubMed]
83. Wang, X.; Zhang, L. Kinetic study of hydroxyl radical formation in a continuous hydroxyl generation system. *RSC Adv.* **2018**, *8*, 40632–40638. [CrossRef]
84. Kehler, J.P. The Haber-Weiss reaction and mechanisms of toxicity. *Toxicology* **2000**, *149*, 43–50. [CrossRef]
85. Weinstein, J.; Bielski, B.H.J. Kinetics of the Interaction of HO₂ and O₂-Radicals with Hydrogen-Peroxide—Haber-Weiss Reaction. *J. Am. Chem. Soc.* **1979**, *101*, 58–62. [CrossRef]
86. Koppenol, W.H. The Haber-Weiss cycle—70 years later. *Redox Rep.* **2001**, *6*, 229–234. [CrossRef]
87. Fischbacher, A.; von Sonntag, C.; Schmidt, T.C. Hydroxyl radical yields in the Fenton process under various pH, ligand concentrations and hydrogen peroxide/Fe (II) ratios. *Chemosphere* **2017**, *182*, 738–744. [CrossRef]
88. Wang, T.; Zhang, H.; Liu, H.; Yuan, Q.; Ren, F.; Han, Y.; Sun, Q.; Li, Z.; Gao, M. Boosting H₂O₂-Guided Chemodynamic Therapy of Cancer by Enhancing Reaction Kinetics through Versatile Biomimetic Fenton Nanocatalysts and the Second Near-Infrared Light Irradiation. *Adv. Funct. Mater.* **2019**, *30*. [CrossRef]
89. Li, X.; Hao, S.J.; Han, A.L.; Yang, Y.Y.; Fang, G.Z.; Liu, J.F.; Wang, S. Intracellular Fenton reaction based on mitochondria-targeted copper (II)-peptide complex for induced apoptosis. *J. Mater. Chem. B* **2019**, *7*, 4008–4016. [CrossRef]
90. Hackenberg, S.; Scherzed, A.; Technau, A.; Kessler, M.; Froelich, K.; Ginzkey, C.; Koehler, C.; Burghartz, M.; Hagen, R.; Kleinsasser, N. Cytotoxic, genotoxic and pro-inflammatory effects of zinc oxide nanoparticles in human nasal mucosa cells in vitro. *Toxicol. In Vitro* **2011**, *25*, 657–663. [CrossRef]
91. Ekici, S.; Turkarlan, S.; Pawlik, G.; Dancis, A.; Baliga, N.S.; Koch, H.G.; Daldal, F. Intracytoplasmic copper homeostasis controls cytochrome c oxidase production. *mBio* **2014**, *5*. [CrossRef]
92. Huang, G.; Chen, H.; Dong, Y.; Luo, X.; Yu, H.; Moore, Z.; Bey, E.A.; Boothman, D.A.; Gao, J. Superparamagnetic iron oxide nanoparticles: Amplifying ROS stress to improve anticancer drug efficacy. *Theranostics* **2013**, *3*, 116–126. [CrossRef] [PubMed]
93. Lehman, S.E.; Morris, A.S.; Mueller, P.S.; Salem, A.K.; Grassian, V.H.; Larsen, S.C. Silica nanoparticle-generated ROS as a predictor of cellular toxicity: Mechanistic insights and safety by design. *Environ. Sci-Nano* **2016**, *3*, 56–66. [CrossRef]
94. Chairuangkitti, P.; Lawanprasert, S.; Roytrakul, S.; Aueviriyavit, S.; Phummiratch, D.; Kulthong, K.; Chanvorachote, P.; Maniratanachote, R. Silver nanoparticles induce toxicity in A549 cells via ROS-dependent and ROS-independent pathways. *Toxicol. In Vitro* **2013**, *27*, 330–338. [CrossRef] [PubMed]
95. Fang, X.W.; Mark, G.; von Sonntag, C. OH radical formation by ultrasound in aqueous solutions Part : The chemistry underlying the terephthalate dosimeter. *Ultrason. SonoChem.* **1996**, *3*, 57–63. [CrossRef]
96. Yan, E.B.; Unthank, J.K.; Castillo-Melendez, M.; Miller, S.L.; Langford, S.J.; Walker, D.W. Novel method for in vivo hydroxyl radical measurement by microdialysis in fetal sheep brain in utero. *J. Appl. Physiol.* **2005**, *98*, 2304–2310. [CrossRef] [PubMed]
97. Yapici, N.B.; Jockusch, S.; Moscatelli, A.; Mandalapu, S.R.; Itagaki, Y.; Bates, D.K.; Wiseman, S.; Gibson, K.M.; Turro, N.J.; Bi, L.R. New Rhodamine Nitroxide Based Fluorescent Probes for Intracellular Hydroxyl Radical Identification in Living Cells. *Org. Lett.* **2012**, *14*, 50–53. [CrossRef]
98. Bai, X.Y.; Huang, Y.Y.; Lu, M.Y.; Yang, D. HKOH-1: A Highly Sensitive and Selective Fluorescent Probe for Detecting Endogenous Hydroxyl Radicals in Living Cells. *Angew. Chem. Int. Ed.* **2017**, *56*, 12873–12877. [CrossRef]
99. Cheng, X.; Guo, H.; Zhang, Y.; Wu, X.; Liu, Y. Non-photochemical production of singlet oxygen via activation of persulfate by carbon nanotubes. *Water Res.* **2017**, *113*, 80–88. [CrossRef] [PubMed]
100. Cadenas, E. Biochemistry of Oxygen-Toxicity. *Annu. Rev. BioChem.* **1989**, *58*, 79–110. [CrossRef] [PubMed]
101. Agnez-Lima, L.F.; Melo, J.T.A.; Silva, A.E.; Oliveira, A.H.S.; Timoteo, A.R.S.; Lima-Bessa, K.M.; Martinez, G.R.; Medeiros, M.H.G.; Di Mascio, P.; Galhardo, R.S.; et al. DNA damage by singlet oxygen and cellular protective mechanisms. *Mutat. Res. Rev. Mutat.* **2012**, *751*, 15–28. [CrossRef] [PubMed]
102. Hampton, M.B.; Kettle, A.J.; Winterbourn, C.C. Inside the neutrophil phagosome: Oxidants, myeloperoxidase, and bacterial killing. *Blood* **1998**, *92*, 3007–3017. [CrossRef] [PubMed]
103. Bigot, E.; Bataille, R.; Patrice, T. Increased singlet oxygen-induced secondary ROS production in the serum of cancer patients. *J. PhotoChem. PhotoBiol. B* **2012**, *107*, 14–19. [CrossRef]
104. Sies, H.; Menck, C.F.M. Singlet Oxygen Induced DNA Damage. *Mutat Res.* **1992**, *275*, 367–375. [CrossRef]

105. Kanofsky, J.R. Singlet Oxygen Production by Biological-Systems. *Chem. Biol. Interact.* **1989**, *70*, 1–28. [CrossRef]
106. Dumont, E.; Gruber, R.; Bignon, E.; Morell, C.; Moreau, Y.; Monari, A.; Ravanat, J.L. Probing the reactivity of singlet oxygen with purines. *Nucleic Acids Res.* **2016**, *44*, 56–62. [CrossRef] [PubMed]
107. Davies, M.J. Singlet oxygen-mediated damage to proteins and its consequences. *BioChem. Biophys. Res. Commun.* **2003**, *305*, 761–770. [CrossRef]
108. Gracanin, M.; Hawkins, C.L.; Pattison, D.I.; Davies, M.J. Singlet-oxygen-mediated amino acid and protein oxidation: Formation of tryptophan peroxides and decomposition products. *Free Radic. Bio Med.* **2009**, *47*, 92–102. [CrossRef]
109. Hirakawa, T.; Nosaka, Y. Properties of $O_2^{\cdot -}$ and OH center dot formed in TiO₂ aqueous suspensions by photocatalytic reaction and the influence of H₂O₂ and some ions. *Langmuir* **2002**, *18*, 3247–3254. [CrossRef]
110. Kim, S.Y.; Lee, S.M.; Park, J.W. Antioxidant enzyme inhibitors enhance singlet oxygen-induced cell death in HL-60 cells. *Free Radic. Res.* **2006**, *40*, 1190–1197. [CrossRef] [PubMed]
111. Deng, J.; Liu, F.; Wang, L.; An, Y.; Gao, M.; Wang, Z.; Zhao, Y. Hypoxia- and singlet oxygen-responsive chemo-photodynamic Micelles featured with glutathione depletion and aldehyde production. *Biomater. Sci.* **2018**, *7*, 429–441. [CrossRef]
112. Kim, S.Y.; Lee, S.M.; Tak, J.K.; Choi, K.S.; Kwon, T.K.; Park, J.W. Regulation of singlet oxygen-induced apoptosis by cytosolic NADP⁺-dependent isocitrate dehydrogenase. *Mol. Cell Biochem.* **2007**, *302*, 27–34. [CrossRef]
113. Umezawa, N.; Tanaka, K.; Urano, Y.; Kikuchi, K.; Higuchi, T.; Nagano, T. Novel Fluorescent Probes for Singlet Oxygen. *Angew. Chem. Int. Ed. Engl.* **1999**, *38*, 2899–2901. [CrossRef]
114. Brega, V.; Yan, Y.; Thomas, S.W., 3rd. Acenes beyond organic electronics: Sensing of singlet oxygen and stimuli-responsive materials. *Org. Biomol. Chem.* **2020**, *18*, 9191–9209. [CrossRef] [PubMed]
115. Ruiz-Gonzalez, R.; Bresoli-Obach, R.; Gulias, O.; Agut, M.; Savoie, H.; Boyle, R.W.; Nonell, S.; Giuntini, F. NanoSOSG: A Nanostructured Fluorescent Probe for the Detection of Intracellular Singlet Oxygen. *Angew. Chem. Int. Ed. Engl.* **2017**, *56*, 2885–2888. [CrossRef]
116. Lennicke, C.; Rahn, J.; Lichtenfels, R.; Wessjohann, L.A.; Seliger, B. Hydrogen peroxide—Production, fate and role in redox signaling of tumor cells. *Cell Commun. Signal.* **2015**, *13*, 39. [CrossRef] [PubMed]
117. Hossain, M.A.; Bhattacharjee, S.; Armin, S.M.; Qian, P.; Xin, W.; Li, H.Y.; Burritt, D.J.; Fujita, M.; Tran, L.S. Hydrogen peroxide priming modulates abiotic oxidative stress tolerance: Insights from ROS detoxification and scavenging. *Front. Plant. Sci.* **2015**, *6*, 420. [CrossRef] [PubMed]
118. Halliwell, B.; Clement, M.V.; Long, L.H. Hydrogen peroxide in the human body. *FEBS Lett.* **2000**, *486*, 10–13. [CrossRef]
119. Mates, J.M.; Perez-Gomez, C.; De Castro, I.N. Antioxidant enzymes and human diseases. *Clin. Biochem.* **1999**, *32*, 595–603. [CrossRef]
120. Angermuller, S.; Islinger, M.; Volkl, A. Peroxisomes and reactive oxygen species, a lasting challenge. *HistoChem. Cell Biol.* **2009**, *131*, 459–463. [CrossRef]
121. Topo, E.; Fisher, G.; Sorricelli, A.; Errico, F.; Usiello, A.; D’Aniello, A. Thyroid hormones and D-aspartic acid, D-aspartate oxidase, D-aspartate racemase, H₂O₂, and ROS in rats and mice. *Chem. Biodivers.* **2010**, *7*, 1467–1478. [CrossRef] [PubMed]
122. Royall, J.A.; Ischiropoulos, H. Evaluation of 2',7'-Dichlorofluorescein and Dihydrorhodamine 123 as Fluorescent-Probes for Intracellular H₂O₂ in Cultured Endothelial-Cells. *Arch. Biochem. Biophys.* **1993**, *302*, 348–355. [CrossRef] [PubMed]
123. Rastogi, R.P.; Singh, S.P.; Hader, D.P.; Sinha, R.P. Detection of reactive oxygen species (ROS) by the oxidant-sensing probe 2',7'-dichlorodihydrofluorescein diacetate in the cyanobacterium *Anabaena variabilis* PCC 7937. *Biochem. Biophys. Res. Commun.* **2010**, *397*, 603–607. [CrossRef] [PubMed]
124. Gomes, A.; Fernandes, E.; Lima, J.L.F.C. Fluorescence probes used for detection of reactive oxygen species. *J. Biochem. Biophys Meth.* **2005**, *65*, 45–80. [CrossRef]
125. Crow, J.P. Dichlorodihydrofluorescein and dihydrorhodamine 123 are sensitive indicators of peroxynitrite in vitro: Implications for intracellular measurement of reactive nitrogen and oxygen species. *Nitric Oxide* **1997**, *1*, 145–157. [CrossRef]
126. Chignell, C.F.; Sik, R.H. A photochemical study of cells loaded with 2',7'-dichlorofluorescein: Implications for the detection of reactive oxygen species generated during UVA irradiation. *Free Radic. Biol. Med.* **2003**, *34*, 1029–1034. [PubMed]
127. Zhu, H.; Bannenberg, G.L.; Moldeus, P.; Shertzer, H.G. Oxidation pathways for the intracellular probe 2',7'-dichlorofluorescein. *Arch. Toxicol.* **1994**, *68*, 582–587. [CrossRef]
128. Lebel, C.P.; Ischiropoulos, H.; Bondy, S.C. Evaluation of the Probe 2',7'-Dichlorofluorescein as an Indicator of Reactive Oxygen Species Formation and Oxidative Stress. *Chem. Res. Toxicol.* **1992**, *5*, 227–231. [CrossRef]
129. Hsiao, I.L.; Huang, Y.J. Titanium Oxide Shell Coatings Decrease the Cytotoxicity of ZnO Nanoparticles. *Chem. Res. Toxicol.* **2011**, *24*, 303–313. [CrossRef] [PubMed]
130. Akhtar, M.J.; Ahamed, M.; Kumar, S.; Khan, M.M.; Ahmad, J.; Alrokayan, S.A. Zinc oxide nanoparticles selectively induce apoptosis in human cancer cells through reactive oxygen species. *Int. J. Nanomed.* **2012**, *7*, 845–857.
131. Sharma, V.; Anderson, D.; Dhawan, A. Zinc oxide nanoparticles induce oxidative DNA damage and ROS-triggered mitochondria mediated apoptosis in human liver cells (HepG2). *Apoptosis* **2012**, *17*, 852–870. [CrossRef] [PubMed]
132. Setyawati, M.I.; Tay, C.Y.; Leong, D.T. Effect of zinc oxide nanomaterials-induced oxidative stress on the p53 pathway. *Biomaterials* **2013**, *34*, 10133–10142. [CrossRef]

133. Aliakbari, F.; Haji Hosseinali, S.; Khalili Sarokhalil, Z.; Shahpasand, K.; Akbar Saboury, A.; Akhtari, K.; Falahati, M. Reactive oxygen species generated by titanium oxide nanoparticles stimulate the hemoglobin denaturation and cytotoxicity against human lymphocyte cell. *J. Biomol. Struct. Dyn.* **2019**, *37*, 4875–4881. [CrossRef] [PubMed]
134. Bhattacharya, K.; Davoren, M.; Boertz, J.; Schins, R.P.; Hoffmann, E.; Dopp, E. Titanium dioxide nanoparticles induce oxidative stress and DNA-adduct formation but not DNA-breakage in human lung cells. *Part. Fibre Toxicol.* **2009**, *6*, 17. [CrossRef]
135. Liu, S.; Xu, L.; Zhang, T.; Ren, G.; Yang, Z. Oxidative stress and apoptosis induced by nanosized titanium dioxide in PC12 cells. *Toxicology* **2010**, *267*, 172–177. [CrossRef] [PubMed]
136. Park, E.J.; Yi, J.; Chung, K.H.; Ryu, D.Y.; Choi, J.; Park, K. Oxidative stress and apoptosis induced by titanium dioxide nanoparticles in cultured BEAS-2B cells. *Toxicol. Lett.* **2008**, *180*, 222–229. [CrossRef] [PubMed]
137. Miwa, S.; Treumann, A.; Bell, A.; Vistoli, G.; Nelson, G.; Hay, S.; von Zglinicki, T. Carboxylesterase converts Amplex red to resorufin: Implications for mitochondrial H₂O₂ release assays. *Free Radic. Biol. Med.* **2016**, *90*, 173–183. [CrossRef] [PubMed]
138. Zhu, A.; Romero, R.; Petty, H.R. A sensitive fluorimetric assay for pyruvate. *Anal. Biochem.* **2010**, *396*, 146–151. [CrossRef] [PubMed]
139. Towne, V.; Will, M.; Oswald, B.; Zhao, Q.J. Complexities in horseradish peroxidase-catalyzed oxidation of dihydroxyphenoxazine derivatives: Appropriate ranges for pH values and hydrogen peroxide concentrations in quantitative analysis. *Anal. Biochem.* **2004**, *334*, 290–296. [CrossRef] [PubMed]
140. Debski, D.; Smulik, R.; Zielonka, J.; Michalowski, B.; Jakubowska, M.; Debowska, K.; Adamus, J.; Marcinek, A.; Kalyanaraman, B.; Sikora, A. Mechanism of oxidative conversion of Amplex (R) Red to resorufin: Pulse radiolysis and enzymatic studies. *Free Radic. Bio Med.* **2016**, *95*, 323–332. [CrossRef]
141. Niethammer, P.; Grabher, C.; Look, A.T.; Mitchison, T.J. A tissue-scale gradient of hydrogen peroxide mediates rapid wound detection in zebrafish. *Nature* **2009**, *459*, 996–999. [CrossRef] [PubMed]
142. Maeda, H.; Fukuyasu, Y.; Yoshida, S.; Fukuda, M.; Saeki, K.; Matsuno, H.; Yamauchi, Y.; Yoshida, K.; Hirata, K.; Miyamoto, K. Fluorescent probes for hydrogen peroxide based on a non-oxidative mechanism. *Angew. Chem. Int. Ed. Engl.* **2004**, *43*, 2389–2391. [CrossRef] [PubMed]
143. Wolfbeis, O.S.; Durkop, A.; Wu, M.; Lin, Z.H. A europium-ion-based luminescent sensing probe for hydrogen peroxide. *Angew. Chem. Int. Ed.* **2002**, *41*, 4495–4498. [CrossRef]
144. Staniek, K.; Nohl, H. H₂O₂ detection from intact mitochondria as a measure for one-electron reduction of dioxygen requires a non-invasive assay system. *Bba-Bioenergetics* **1999**, *1413*, 70–80. [CrossRef]
145. Bartosz, G. Use of spectroscopic probes for detection of reactive oxygen species. *Clin. Chim. Acta* **2006**, *368*, 53–76. [CrossRef] [PubMed]
146. Mohammadinejad, R.; Moosavi, M.A.; Tavakol, S.; Vardar, D.O.; Hosseini, A.; Rahmati, M.; Dini, L.; Hussain, S.; Mandegary, A.; Klionsky, D.J. Necrotic, apoptotic and autophagic cell fates triggered by nanoparticles. *Autophagy* **2019**, *15*, 4–33. [CrossRef] [PubMed]
147. Mittler, R.; Vanderauwera, S.; Suzuki, N.; Miller, G.; Tognetti, V.B.; Vandepoele, K.; Gollery, M.; Shulaev, V.; Van Breusegem, F. ROS signaling: The new wave? *Trends Plant. Sci.* **2011**, *16*, 300–309. [CrossRef] [PubMed]
148. Zhang, J.; Wang, X.; Vikash, V.; Ye, Q.; Wu, D.; Liu, Y.; Dong, W. ROS and ROS-Mediated Cellular Signaling. *Oxid Med. Cell Longev.* **2016**. [CrossRef] [PubMed]
149. Bae, Y.S.; Oh, H.; Rhee, S.G.; Yoo, Y.D. Regulation of reactive oxygen species generation in cell signaling. *Mol. Cells* **2011**, *32*, 491–509. [CrossRef]
150. Bonizzi, G.; Karin, M. The two NF-kappaB activation pathways and their role in innate and adaptive immunity. *Trends Immunol.* **2004**, *25*, 280–288. [CrossRef]
151. Kaul, N.; Gopalakrishna, R.; Gundimeda, U.; Choi, J.; Forman, H.J. Role of protein kinase C in basal and hydrogen peroxide-stimulated NF-kappa B activation in the murine macrophage J774A.1 cell line. *Arch. Biochem. Biophys.* **1998**, *350*, 79–86. [CrossRef] [PubMed]
152. Schmidt, K.N.; Amstad, P.; Cerutti, P.; Baeuerle, P.A. The roles of hydrogen peroxide and superoxide as messengers in the activation of transcription factor NF-kappa B. *Chem. Biol.* **1995**, *2*, 13–22. [CrossRef]
153. Schoonbroodt, S.; Ferreira, V.; Best-Belpomme, M.; Boelaert, J.R.; Legrand-Poels, S.; Korner, M.; Piette, J. Crucial role of the amino-terminal tyrosine residue 42 and the carboxyl-terminal PEST domain of I kappa B alpha in NF-kappa B activation by an oxidative stress. *J. Immunol.* **2000**, *164*, 4292–4300. [CrossRef] [PubMed]
154. Takada, Y.; Mukhopadhyay, A.; Kundu, G.C.; Mahabeleshwar, G.H.; Singh, S.; Aggarwal, B.B. Hydrogen peroxide activates NF-kappa B through tyrosine phosphorylation of I kappa B alpha and serine phosphorylation of p65: Evidence for the involvement of I kappa B alpha kinase and Syk protein-tyrosine kinase. *J. Biol. Chem.* **2003**, *278*, 24233–24241. [CrossRef]
155. Liu, X.; Lu, B.; Fu, J.; Zhu, X.; Song, E.; Song, Y. Amorphous silica nanoparticles induce inflammation via activation of NLRP3 inflammasome and HMGB1/TLR4/MYD88/NF-kb signaling pathway in HUVEC cells. *J. Hazard. Mater.* **2021**, *404*, 124050. [CrossRef] [PubMed]
156. Kyriakis, J.M.; Avruch, J. Sounding the alarm: Protein kinase cascades activated by stress and inflammation. *J. Biol. Chem.* **1996**, *271*, 24313–24316. [CrossRef]
157. Nakano, H.; Nakajima, A.; Sakon-Komazawa, S.; Piao, J.H.; Xue, X.; Okumura, K. Reactive oxygen species mediate crosstalk between NF-kappaB and JNK. *Cell Death Differ.* **2006**, *13*, 730–737. [CrossRef]

158. Torres, M.; Forman, H.J. Redox signaling and the MAP kinase pathways. *Biofactors* **2003**, *17*, 287–296. [CrossRef] [PubMed]
159. Dabrowski, A.; Boguslowicz, C.; Dabrowska, M.; Tribillo, I.; Gabryelewicz, A. Reactive oxygen species activate mitogen-activated protein kinases in pancreatic acinar cells. *Pancreas* **2000**, *21*, 376–384. [CrossRef]
160. Guyton, K.Z.; Liu, Y.; Gorospe, M.; Xu, Q.; Holbrook, N.J. Activation of mitogen-activated protein kinase by H₂O₂. Role in cell survival following oxidant injury. *J. Biol. Chem.* **1996**, *271*, 4138–4142. [CrossRef] [PubMed]
161. Hou, N.; Torii, S.; Saito, N.; Hosaka, M.; Takeuchi, T. Reactive oxygen species-mediated pancreatic beta-cell death is regulated by interactions between stress-activated protein kinases, p38 and c-Jun N-terminal kinase, and mitogen-activated protein kinase phosphatases. *Endocrinology* **2008**, *149*, 1654–1665. [CrossRef] [PubMed]
162. Choi, B.H.; Hur, E.M.; Lee, J.H.; Jun, D.J.; Kim, K.T. Protein kinase Cdelta-mediated proteasomal degradation of MAP kinase phosphatase-1 contributes to glutamate-induced neuronal cell death. *J. Cell Sci.* **2006**, *119*, 1329–1340. [CrossRef] [PubMed]
163. Matsuzawa, A.; Saegusa, K.; Noguchi, T.; Sadamitsu, C.; Nishitoh, H.; Nagai, S.; Koyasu, S.; Matsumoto, K.; Takeda, K.; Ichijo, H. ROS-dependent activation of the TRAF6-ASK1-p38 pathway is selectively required for TLR4-mediated innate immunity. *Nat. Immunol.* **2005**, *6*, 587–592. [CrossRef] [PubMed]
164. Pitzschke, A.; Djamei, A.; Bitton, F.; Hirt, H. A Major Role of the MEKK1-MKK1/2-MPK4 Pathway in ROS Signalling. *Mol. Plant.* **2009**, *2*, 120–137. [CrossRef] [PubMed]
165. Lluís, J.M.; Buricchi, F.; Chiarugi, P.; Morales, A.; Fernandez-Checa, J.C. Dual role of mitochondrial reactive oxygen species in hypoxia signaling: Activation of nuclear factor- κ B via c-SRC and oxidant-dependent cell death. *Cancer Res.* **2007**, *67*, 7368–7377. [CrossRef] [PubMed]
166. Dong, J.; Ramachandiran, S.; Tikoo, K.; Jia, Z.; Lau, S.S.; Monks, T.J. EGFR-independent activation of p38 MAPK and EGFR-dependent activation of ERK1/2 are required for ROS-induced renal cell death. *Am. J. Physiol. Renal Physiol.* **2004**, *287*, 1049–1058. [CrossRef] [PubMed]
167. Forman, H.J.; Torres, M. Reactive oxygen species and cell signaling: Respiratory burst in macrophage signaling. *Am. J. Respir. Crit. Care Med.* **2002**, *166*. [CrossRef]
168. Cheng, G.; Guo, W.; Han, L.; Chen, E.; Kong, L.; Wang, L.; Ai, W.; Song, N.; Li, H.; Chen, H. Cerium oxide nanoparticles induce cytotoxicity in human hepatoma SMMC-7721 cells via oxidative stress and the activation of MAPK signaling pathways. *Toxicol. In Vitro* **2013**, *27*, 1082–1088. [CrossRef] [PubMed]
169. Guo, C.; Xia, Y.; Niu, P.; Jiang, L.; Duan, J.; Yu, Y.; Zhou, X.; Li, Y.; Sun, Z. Silica nanoparticles induce oxidative stress, inflammation, and endothelial dysfunction in vitro via activation of the MAPK/Nrf2 pathway and nuclear factor-kappaB signaling. *Int. J. Nanomed.* **2015**, *10*, 1463–1477. [CrossRef]
170. You, R.; Ho, Y.S.; Hung, C.H.; Liu, Y.; Huang, C.X.; Chan, H.N.; Ho, S.L.; Lui, S.Y.; Li, H.W.; Chang, R.C. Silica nanoparticles induce neurodegeneration-like changes in behavior, neuropathology, and affect synapse through MAPK activation. *Part. Fibre Toxicol.* **2018**, *15*, 28. [CrossRef]
171. Hu, Q.; Wang, H.; He, C.; Jin, Y.; Fu, Z. Polystyrene nanoparticles trigger the activation of p38 MAPK and apoptosis via inducing oxidative stress in zebrafish and macrophage cells. *Environ. Pollut.* **2021**, *269*, 116075. [CrossRef] [PubMed]
172. Zhou, Y.; Ji, J.; Ji, L.; Wang, L.; Hong, F. Respiratory exposure to nano-TiO₂ induces pulmonary toxicity in mice involving reactive free radical-activated TGF-beta/Smad/p38MAPK/Wnt pathways. *J. Biomed. Mater. Res. A* **2019**, *107*, 2567–2575. [CrossRef] [PubMed]
173. Yi, C.; Liu, D.; Fong, C.C.; Zhang, J.; Yang, M. Gold nanoparticles promote osteogenic differentiation of mesenchymal stem cells through p38 MAPK pathway. *ACS Nano* **2010**, *4*, 6439–6448. [CrossRef] [PubMed]
174. Wang, Q.; Chen, B.; Cao, M.; Sun, J.; Wu, H.; Zhao, P.; Xing, J.; Yang, Y.; Zhang, X.; Ji, M.; et al. Response of MAPK pathway to iron oxide nanoparticles in vitro treatment promotes osteogenic differentiation of hBMSCs. *Biomaterials* **2016**, *86*, 11–20. [CrossRef] [PubMed]
175. Vousden, K.H.; Lu, X. Live or let die: The cell's response to p53. *Nat. Rev. Cancer* **2002**, *2*, 594–604. [CrossRef]
176. Liu, B.; Chen, Y.; St Clair, D.K. ROS and p53: A versatile partnership. *Free Radic. Biol. Med.* **2008**, *44*, 1529–1535. [CrossRef]
177. Song, Y.X.; Li, X.W.; Li, Y.; Li, N.; Shi, X.X.; Ding, H.Y.; Zhang, Y.H.; Li, X.B.; Liu, G.W.; Wang, Z. Non-esterified fatty acids activate the ROS-p38-p53/Nrf2 signaling pathway to induce bovine hepatocyte apoptosis in vitro. *Apoptosis* **2014**, *19*, 984–997. [CrossRef] [PubMed]
178. Nakano, K.; Vousden, K.H. PUMA, a novel proapoptotic gene, is induced by p53. *Mol. Cell* **2001**, *7*, 683–694. [CrossRef]
179. Liu, B.R.; Yuan, B.; Zhang, L.; Mu, W.M.; Wang, C.M. ROS/p38/p53/Puma signaling pathway is involved in emodin-induced apoptosis of human colorectal cancer cells. *Int. J. Clin. Exp. Med.* **2015**, *8*, 15413–15422. [PubMed]
180. Yu, J.; Zhang, L. PUMA, a potent killer with or without p53. *Oncogene* **2008**, *27*, 71–83. [CrossRef] [PubMed]
181. Samuelson, J.T.; Dahl, J.E.; Karlsson, S.; Morisbak, E.; Becher, R. Apoptosis induced by the monomers HEMA and TEGDMA involves formation of ROS and differential activation of the MAP-kinases p38, JNK and ERK. *Dent. Mater.* **2007**, *23*, 34–39. [CrossRef]
182. Sakon, S.; Xue, X.; Takekawa, M.; Sasazuki, T.; Okazaki, T.; Kojima, Y.; Piao, J.H.; Yagita, H.; Okumura, K.; Doi, T.; et al. NF-kappaB inhibits TNF-induced accumulation of ROS that mediate prolonged MAPK activation and necrotic cell death. *Embo J.* **2003**, *22*, 3898–3909. [CrossRef] [PubMed]
183. Kamata, H.; Honda, S.; Maeda, S.; Chang, L.; Hirata, H.; Karin, M. Reactive oxygen species promote TNFalpha-induced death and sustained JNK activation by inhibiting MAP kinase phosphatases. *Cell* **2005**, *120*, 649–661. [CrossRef] [PubMed]

184. Akcan, R.; Aydogan, H.C.; Yildirim, M.S.; Tastekin, B.; Saglam, N. Nanotoxicity: A challenge for future medicine. *Turk. J. Med. Sci.* **2020**, *50*, 1180–1196. [CrossRef] [PubMed]
185. Graham, U.M.; Dozier, A.K.; Oberdorster, G.; Yokel, R.A.; Molina, R.; Brain, J.D.; Pinto, J.M.; Weuve, J.; Bennett, D.A. Tissue Specific Fate of Nanomaterials by Advanced Analytical Imaging Techniques—A Review. *Chem. Res. Toxicol.* **2020**, *33*, 1145–1162. [CrossRef] [PubMed]
186. Pu, S.; Gong, C.; Robertson, A.W. Liquid cell transmission electron microscopy and its applications. *R. Soc. Open Sci.* **2020**, *7*, 191204. [CrossRef]
187. Kiio, T.M.; Park, S. Nano-scientific Application of Atomic Force Microscopy in Pathology: From Molecules to Tissues. *Int. J. Med. Sci.* **2020**, *17*, 844–858. [CrossRef] [PubMed]
188. Erofeev, A.; Gorelkin, P.; Garanina, A.; Alova, A.; Efremova, M.; Vorobyeva, N.; Edwards, C.; Korchev, Y.; Majouga, A. Novel method for rapid toxicity screening of magnetic nanoparticles. *Sci. Rep.* **2018**, *8*, 7462. [CrossRef]
189. Rahman, L.; Williams, A.; Gelda, K.; Nikota, J.; Wu, D.; Vogel, U.; Halappanavar, S. 21st Century Tools for Nanotoxicology: Transcriptomic Biomarker Panel and Precision-Cut Lung Slice Organ Mimic System for the Assessment of Nanomaterial-Induced Lung Fibrosis. *Small* **2020**, *16*. [CrossRef]
190. Kohl, Y.; Runden-Pran, E.; Mariussen, E.; Hesler, M.; El Yamani, N.; Longhin, E.M.; Dusinska, M. Genotoxicity of Nanomaterials: Advanced In Vitro Models and High Throughput Methods for Human Hazard Assessment-A Review. *Nanomaterials (Basel)* **2020**, *10*, 1911. [CrossRef] [PubMed]
191. Zhang, M.; Xu, C.; Jiang, L.; Qin, J. A 3D human lung-on-a-chip model for nanotoxicity testing. *Toxicol. Res.* **2018**, *7*, 1048–1060. [CrossRef] [PubMed]
192. Yin, F.; Zhu, Y.; Zhang, M.; Yu, H.; Chen, W.; Qin, J. A 3D human placenta-on-a-chip model to probe nanoparticle exposure at the placental barrier. *Toxicol. In Vitro* **2019**, *54*, 105–113. [CrossRef] [PubMed]
193. van Duinen, V.; Trietsch, S.J.; Joore, J.; Vulto, P.; Hankemeier, T. Microfluidic 3D cell culture: From tools to tissue models. *Curr. Opin. Biotechnol.* **2015**, *35*, 118–126. [CrossRef] [PubMed]

Review

Glutathione-Mediated Conjugation of Anticancer Drugs: An Overview of Reaction Mechanisms and Biological Significance for Drug Detoxification and Bioactivation

Agnieszka Potęga 

Department of Pharmaceutical Technology and Biochemistry, Faculty of Chemistry, Gdańsk University of Technology, Gabriela Narutowicza Str. 11/12, 80-233 Gdańsk, Poland; agnieszka.potega@pg.edu.pl; Tel.: +48-58-347-15-16

Abstract: The effectiveness of many anticancer drugs depends on the creation of specific metabolites that may alter their therapeutic or toxic properties. One significant route of biotransformation is a conjugation of electrophilic compounds with reduced glutathione, which can be non-enzymatic and/or catalyzed by glutathione-dependent enzymes. Glutathione usually combines with anticancer drugs and/or their metabolites to form more polar and water-soluble glutathione S-conjugates, readily excreted outside the body. In this regard, glutathione plays a role in detoxification, decreasing the likelihood that a xenobiotic will react with cellular targets. However, some drugs once transformed into thioethers are more active or toxic than the parent compound. Thus, glutathione conjugation may also lead to pharmacological or toxicological effects through bioactivation reactions. My purpose here is to provide a broad overview of the mechanisms of glutathione-mediated conjugation of anticancer drugs. Additionally, I discuss the biological importance of glutathione conjugation to anticancer drug detoxification and bioactivation pathways. I also consider the potential role of glutathione in the metabolism of unsymmetrical bisacridines, a novel prosperous class of anticancer compounds developed in our laboratory. The knowledge on glutathione-mediated conjugation of anticancer drugs presented in this review may be noteworthy for improving cancer therapy and preventing drug resistance in cancers.

Keywords: anticancer drugs; glutathione; mechanisms of glutathione conjugation reaction; detoxification; bioactivation

Citation: Potęga, A. Glutathione-Mediated Conjugation of Anticancer Drugs: An Overview of Reaction Mechanisms and Biological Significance for Drug Detoxification and Bioactivation. *Molecules* **2022**, *27*, 5252. <https://doi.org/10.3390/molecules27165252>

Academic Editor: Pál Perjési

Received: 29 July 2022

Accepted: 15 August 2022

Published: 17 August 2022

Publisher's Note: MDPI stays neutral with regard to jurisdictional claims in published maps and institutional affiliations.



Copyright: © 2022 by the author. Licensee MDPI, Basel, Switzerland. This article is an open access article distributed under the terms and conditions of the Creative Commons Attribution (CC BY) license (<https://creativecommons.org/licenses/by/4.0/>).

1. Introduction: The Place of Glutathione in Drug Metabolism

Living organisms are continuously and unavoidably exposed to xenobiotics, including anticancer drugs. Many of these compounds are lipophilic in nature, and the body can only expel them through chemical modifications, known as biotransformations. Generally, these occur by mechanisms conveniently categorized as phase I and phase II metabolic transformations, which act in a tightly integrated manner [1,2]. Phase I metabolism alters the chemical structure of the drug by 'functionalization reactions' which introduce a polar functional group onto the molecule. Thus, phase I reactions are usually oxidation, reduction, dealkylation, epoxidation, oxidative deamination reactions, etc., which are primarily catalyzed by enzymes of the cytochrome P450 (P450; E.C. 1.14.-.-) superfamily [1,3]. These reactions typically result in metabolites that are more water-soluble than the parent compounds and still retain some of their pharmacological activity [4]. Phase II metabolism generally serves as a detoxifying step in the metabolism of drugs and other xenobiotics and involves 'conjugation reactions' that couple the drug and/or its phase I metabolite molecule with an activated conjugating molecule. Conjugation usually renders the compound pharmacologically inert, more polar, and water soluble, so it can easily be excreted out of the body. The most prevalent phase II metabolic pathways include glucuronidation, sulfation,

and glutathione conjugation [1,5]. The concept of two phases can also be extended to phase III, which is the excretion of the resulting phase II metabolites (conjugates) [6].

Although metabolic transformations aim to inactivate drugs, some chemical modifications, both in phase I and II metabolism, may also lead to the formation of highly reactive species, i.e., reactive drug metabolites, which are more pharmacologically active and/or toxic in comparison to the original compound [4,7]. Therefore, early knowledge about pharmacological and/or toxicological effects of metabolites of drug candidates is extremely desired for assessing their bioavailability, activity, and safety profiles in humans. In this regard, much attention is also paid to understanding the mechanisms of reactive metabolite generation.

This work is focused on the conjugation reaction of xenobiotics with the reduced tripeptide glutathione (GSH = L- γ -glutamyl-L-cysteinyl-glycine), which is a significant route of drug elimination in phase II metabolism in many species [8]. GSH conjugation reaction may be non-enzymatic (i.e., chemical), but it is significantly accelerated by various GSH-dependent enzymes [9,10], mainly a family of GSH S-transferase (GST; E.C. 2.5.1.18) enzymes [11]. A number of anticancer therapeutics are known to undergo GSH conjugation reaction [12–17]. GSH can combine with electrophilic anticancer drugs and/or their phase I metabolites to form less toxic compounds than parent compounds and more polar, water-soluble GSH S-conjugates (thioethers). Further, GSH S-conjugates are substrates for transporters (phase III) involved in the biliary and renal excretion, which facilitates their clearance from the body [18]. Thus, GSH plays a role in detoxification, decreasing the likelihood that a xenobiotic will react with molecular and cellular targets. This may affect the efficacy and interactions of a variety of anticancer interventions. Moreover, numerous studies support the view that, in some cases, GSH conjugation may also play an important role in bioactivation reactions as it is able to generate GSH S-conjugates that are more active than the original parent xenobiotic [18–20]. If these reactive metabolites interact with critical cellular macromolecules (i.e., proteins, nucleic acids), toxicity can be ensued. By participating in the formation of toxic metabolites of some anticancer drugs, GSH may also affect the cellular uptake of other agents. For this reason, knowledge of these interactions may be useful in designing combination therapy for neoplastic diseases.

Given this background, the study on GSH conjugation is a crucial factor for the determination of drug therapeutic efficacy and potential toxicity. Depending on the structure and physico-chemical properties of the substrate, the conjugation reaction may proceed according to various mechanisms. In this review, I discuss some of them in the context of anticancer drugs. In addition, I also indicate the potential significance of GSH conjugation in the detoxification and bioactivation of clinically important anticancer drugs.

To continue the search for potential anticancer drugs, a completely novel class of acridine derivatives of extraordinary structures, unsymmetrical bisacridines (UAs), has been synthesized and developed by our research group [21,22]. They were characterized with respect to their physico-chemical properties [23] and the role of phase I and phase II metabolic transformations in their action [24,25]. UAs exhibited high cytotoxic activity against a lot of cancer cell lines and high anticancer efficacy against several types of human cancer xenografts in nude mice [26]. These are mainly cancers that are extremely resistant to chemotherapy and are usually characterized by increased activity of various GST isoenzymes relative to normal tissues. Preliminary studies with rat liver microsomal and cytosolic subfractions showed the ability of C-2028 (9-[N-[(imidazo [4,5,1-de]-acridin-6-on-5-yl)aminopropyl]-N-methylaminopropylamino]-1'-nitroacridine, a representative UA) to GST-mediated and/or direct GSH conjugation [25]. This finding may suggest an important role of detoxifying transformations in UA metabolism, the consequences of which for the anticancer and/or toxic activities of the compounds are not yet well understood. Herein, I would like to present some considerations on this issue and indicate the likely mechanism of UA-GSH S-conjugate formation.

2. Glutathione

2.1. Glutathione Structure as a Determinant of Its Biological Functions

Glutathione is the predominant intracellular thiol-containing tripeptide found in all animal tissues, plants, fungi, and some microorganisms [27,28]. Under physiological conditions, it is mainly present in the cytoplasm in the reduced form (GSH), which is also the biologically active form. GSH is less easily oxidized than its precursors, cysteine and γ -glutamylcysteine; the fully oxidized form with a disulfide between two identical GSH molecules (GSSG) represents less than 1% of the total GSH pool in the cell [29]. GSH concentration in human cells typically ranges from 0.1 to 10 mmol/L, being most focused in the liver (up to 10 mmol/L), spleen, kidney, lens, erythrocytes, and leukocytes [30,31], wherein its depletion and/or altered level are associated with various diseases, including cancer, cardiovascular, inflammatory, immune, metabolic, and neurodegenerative diseases [32]. Maintaining optimal GSH:GSSG ratios in the cell is critical to survival; hence, tight regulation of this system is imperative [33].

The characteristic structural features of the GSH molecule (Figure 1) determine its many diverse biological functions. In contrast to an α -peptide linkage usually found in a number of endogenous peptides, the L-glutamic acid (Glu) and L-cysteine (Cys) of GSH are joined by an unusual γ -peptide linkage [28]. Such a bond promotes GSH resistance to hydrolysis by most intracellular aminopeptidases as well as provides for specificity in other GSH-enzyme interactions [34]. In turn, the activity of the high electron-donating sulfhydryl (thiol, -SH) group of Cys residue supports the reducing properties of GSH by way of a thiol-exchange system (-SH to -S-S-), enabling the participation of GSH in intracellular antioxidative and detoxifying reactions [35]. The reactivity of -SH is due to the thiolate anion (S^-), the relative concentration of which is regulated by the acidity of thiol ($pK_a = 9.2$). At physiological pH, for every 100 GSH molecules in the -SH state, approximately 3.7 are in a thiolate form [36]. Due to the polarizability of the sulfur atom, GSH is a strong 'soft' nucleophile, and unlike other phase II enzyme cofactors such as uridine 5'-diphosphoglucuronic acid (UDPGA) and 3'-phosphoadenosine-5'-phosphosulfate (PAPS), it easily reacts with various 'soft' electrophiles [10], which may also be anticancer drugs. Net-negative charge of cysteinyl residue and overall GSH hydrophilicity greatly increase the aqueous solubility of the lipophilic moieties with which it becomes conjugated. GSH S-conjugates usually achieve a molecular weight higher than 300–500 g/mol (average molecular weight of GSH = 307.3235 g/mol) and are thus preferentially secreted via the biliary system. Then, the final cysteinyl conjugates are reabsorbed into the liver, from where they travel to the kidney for acetylation and excretion as a mercapturic acid [37].

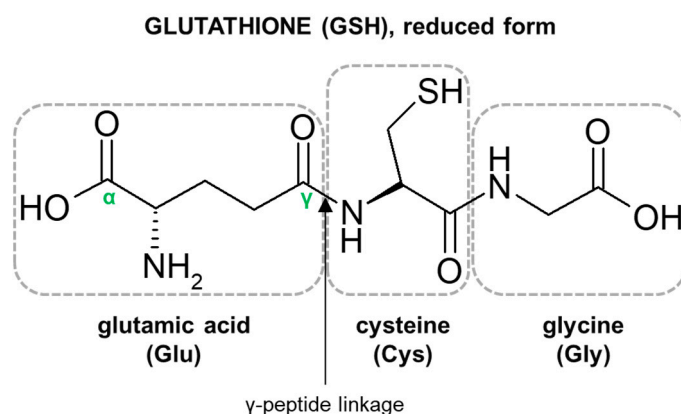


Figure 1. Structure of the tripeptide glutathione (GSH). Glutamic acid (Glu) is linked in a γ -peptide linkage (via its γ -carboxyl group) to cysteine (Cys), which in turn forms an α -peptide linkage with glycine (Gly).

2.2. Biological Functions of Glutathione

Reduced GSH has been adopted through evolution to perform multiple significant cellular functions in living organisms. It is responsible for the correct thiol–disulfide balance and the associated oxidation-reduction potential of cells [38]. The biologically important role of GSH is related to the possibility of regeneration of the -SH moieties of proteins, which counteracts the effects of oxidative reactions, inactivating cell proteins [39]. This compound is also involved in the reduction of ribonucleotides to deoxyribonucleotides, i.e., it has a direct impact on DNA biosynthesis and the related proliferation process [8]. Moreover, it mediates in the synthesis of proteins and in amino acid transport [40]. Further, GSH serves as a reservoir and transporter of cysteine [41], a regulator of calcium ion homeostasis [42], a versatile cofactor for many cytoplasmic enzymes [8], and it is a link in the mitochondrial mechanism to cell death [43].

In addition to the functions mentioned, GSH is an important component of the system that detoxifies both electrophilic xenobiotics and metabolically produced free radicals, i.e., reactive oxygen species (ROS), by the formation of GSH S-conjugates. Thus, it plays a central role in the protection of cells against a variety of exogenous and endogenous potentially harmful compounds [28,44]. The reactions to form GSH S-conjugates may be non-enzymatic, although they are greatly accelerated by GSH-dependent enzymes such as GSTs [11]. Hence, the effectiveness of the detoxification pathway depends upon the intracellular concentration of GSH, the presence of GSTs of appropriate specificity, and/or the capacity of the cell for rapid resynthesis of GSH [45]. Conjugation reactions of GSH with electrophilic compounds to GSH S-conjugates occur mainly in the liver, which exports GSH and has the highest GST activity [28]. Although by conjugation with GSH many compounds are rendered less toxic than the original parent xenobiotic, it has also been reported that some drugs, including those with anticancer activity, become more reactive following this reaction. Thus, GSH conjugation may also play an important role in drug bioactivation processes [18–20].

Overall, GSH acts in catalysis, metabolism, and transport. As knowledge about this tripeptide grows, it becomes more obvious that the GSH status is a highly sensitive indicator of cell functionality and viability. Moreover, although all GSH activities are important in the maintenance of normal cell homeostasis in living organisms, these can also constitute an advantage for cancer cells, allowing disease progression and resistance to therapy.

2.3. Outline of the Regulation of Glutathione Levels in the Cell

Adequate intracellular GSH levels (and therefore the GSH:GSSG ratio) need to be carefully maintained in the cell. These are altered in biosynthesis, biodegradation, and consumption processes [44,46], which are presented schematically in Figure 2.

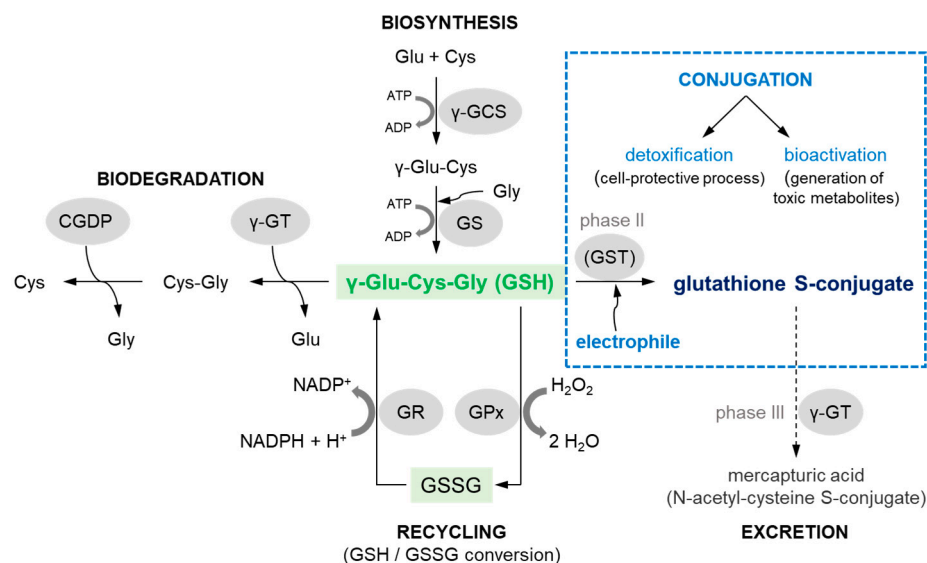


Figure 2. Comprehensive scheme of biosynthesis, biodegradation, and the most important reactions that reduced glutathione (GSH) may undergo in mammalian cells (scheme based on [47]). ADP = adenosine 5'-(trihydrogen diphosphate); ATP = adenosine 5'-(tetrahydrogen triphosphate); CGDP = cysteinylglycine dipeptidase; Cys = cysteine; Cys-Gly = cysteinylglycine; Glu = glutamic acid; Gly = glycine; GPx = GSH peroxidase; GR = GSH reductase; GS = GSH synthetase; GSSG = glutathione (oxidized form); GST = GSH S-transferase; H⁺ = positively charged hydrogen ion; H₂O = water; H₂O₂ = hydrogen peroxide; NADPH/NADP⁺ = β-nicotinamide adenine dinucleotide 2'-phosphate, reduced/oxidized form, respectively; γ-GCS = γ-glutamylcysteine synthetase; γ-Glu-Cys = γ-glutamylcysteine; γ-GT = γ-glutamyl transferase.

GSH biosynthesis, GSH biodegradation, and the recycling of component amino acids occur in the γ-glutamyl cycle, also known as the Meister cycle [48]. Briefly, GSH is synthesized intracellularly de novo from three precursor amino acids: L-glutamic acid (Glu), L-cysteine (Cys), and glycine (Gly). This requires the consecutive action of two enzymes, γ-glutamylcysteine synthetase (γ-GCS) and GSH synthetase (GS) (biosynthesis pathway in Figure 2). The bioavailability of Cys is rate-limiting for the synthesis of GSH [49]. GSH breakdown is initiated by the action of γ-glutamyl transferase (γ-GT), an enzyme attached to the external surface of certain cell membranes [30]. γ-GT transfers a Glu to other amino acids releasing cysteinylglycine (Cys-Gly), which in turn can be broken down by a cysteinylglycine dipeptidase (CGDP) to produce Cys and Gly [44] (biodegradation pathway in Figure 2). Reactions leading to a decrease in GSH levels in cells are also reactions with ROS and electrophilic compounds formed from xenobiotics that are considered to be toxic to the cell. In a recycling pathway GSH peroxidase (GPx), in concert with catalase and superoxide dismutase, detoxifies ROS such as hydrogen peroxide (H₂O₂) with GSH acting as an electron donor in the reduction reaction, producing GSSG as an end product. Within cells, GSH is regenerated from GSSG by GSH reductase (GR) in a process that requires reduced β-nicotinamide adenine dinucleotide 2'-phosphate (NADPH) [8].

The nucleophilic conjugation of GSH with a wide spectrum of electrophiles (conjugation pathway in Figure 2) and transport of the corresponding GSH S-conjugates out of the cells have been shown to work as a system in the detoxification of xenobiotics, including anticancer drugs. The major components of this system include GSH, GSH-related enzymes (mainly GSTs), and GSH S-conjugate export pumps (GS-X pumps) [50]. Some researchers assume the further metabolism and/or excretion of GSH-labeled substances as phase III metabolic reactions (Figure 3). At the cell surface, the catabolism of GSH S-conjugate is initiated by the membrane-bound γ-GT, which removes (extracellularly) the GSH γ-glutamyl moiety and transfers it to appropriate acceptors. The resulting cysteinylglycine S-conjugate is further converted by cysteinylglycine dipeptidase (CGDP) to remove the

glycyl group and produce the cysteine S-conjugate. Then, this compound re-enters the cell via various transport proteins where cytosolic N-acetyltransferases (NATs) create a mercapturic acid derivative of the xenobiotic (S-substituted N-acetyl-L-cysteine conjugate) [51,52]. The final product of the above reactions is generally non-toxic, more polar, and more water-soluble than the parent compound, and can be readily excreted outside the body through bile or urine [52]. Although, the presented mercapturic acid pathway and trafficking of mercapturic acid derivatives may vary with different compounds and species [18], GSH conjugation represents a cell-protective process through detoxification mechanism.

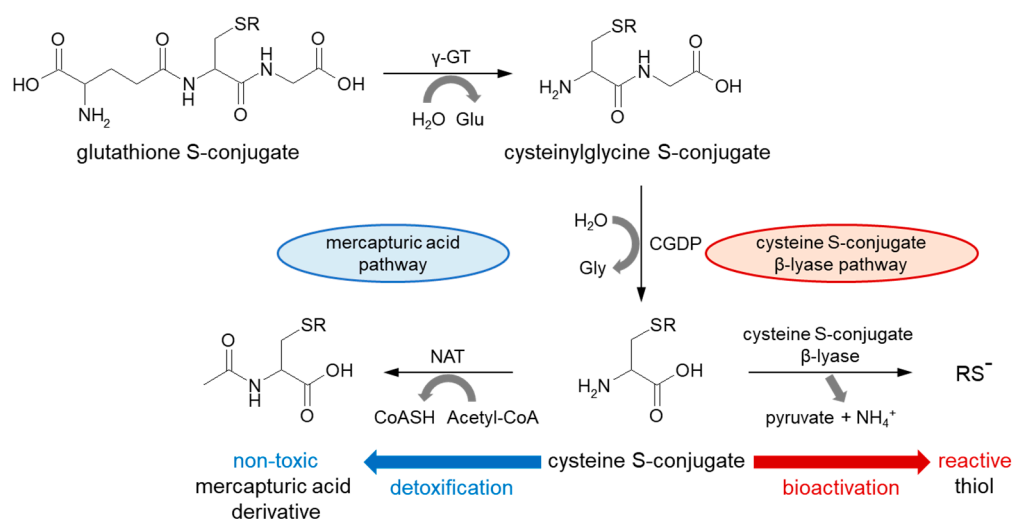


Figure 3. Metabolism of GSH conjugated product to mercapturic acid conjugated product in the mercapturic acid pathway and cysteine S-conjugate β -lyase-dependent bioactivation of cysteine S-conjugate. Acetyl-CoA = acetyl coenzyme A; CGDP = cysteinylglycine dipeptidase; CoASH = coenzyme A; Glu = glutamic acid; Gly = glycine; H_2O = water; NAT = N-acetyltransferase; NH_4^+ = ammonium ion; γ -GT = γ -glutamyl transferase.

Alternatively, in recent years, it has been documented that the formation of glutathione S- and cysteine S-conjugates may be bioactivation events as the intermediate metabolites are toxic (i.e., cytotoxic, genotoxic, or mutagenic) [53,54]. For example, instead of intracellular acetylation, some cysteine S-conjugates (which usually contain a strong electron-withdrawing group attached to the sulfur atom) may be converted through β -elimination by cysteine S-conjugate β -lyases (present in the cytosol and mitochondria) to pyruvate, ammonium ion (NH_4^+), and an unstable and highly reactive thiol (RS^-) [52,55]. This constitutes a bioactivation pathway. The sulfur-containing fragment further released in this process is presumably a sulfenic acid ($RS-OH$). Recent studies suggest that the coupling of enzymes of the mercapturic acid pathway to cysteine S-conjugate β -lyases may be more common in nature and more widespread in the metabolism of electrophilic xenobiotics than previously realized [18]. However, before addressing these aspects in the context of anticancer drugs, it is important to know the major mechanisms of their conjugation with GSH.

3. Overview of Mechanisms of Glutathione Conjugation of Anticancer Drugs

As previously stated, the important part of the GSH molecule in terms of its chemical activity is the nucleophilic sulfhydryl (thiol, $-SH$) group of the cysteine residue. Generally, as illustrated in Figure 4, conjugation with GSH involves attachment of the xenobiotic molecule or its phase I metabolite (assigned as R-X) with this group to form the GSH S-conjugate (assigned as R-SG). In fact, the reactive nucleophilic species is the thiolate anion of GSH (GS^-), whose concentrations at physiological pH are approximately 1% of GSH concentration (pK_a of GSH = 9.2) [38]. Due to the low electronegativity and high polarizability of the sulfur atom, GSH acts as a 'soft' nucleophile and, as such, can be

used to sense the reactivity of ‘soft’ electrophiles (i.e., compounds that contain an acceptor atom with high polarizability, low electronegativity, and often unshared *p* or *d* valence electrons) [51]. Xenobiotics that are conjugated with GSH are either very electrophilic right away or are metabolized to electrophilic compounds. Some reactions of the tripeptide GSH with cellular electrophiles have spontaneous rates which vary considerably depending on the reactivity of the electrophile, and frequently, but not always, are catalyzed by various GST isoenzymes [34]. However, non-enzymatic reactions are usually much slower than those catalyzed by GSTs.

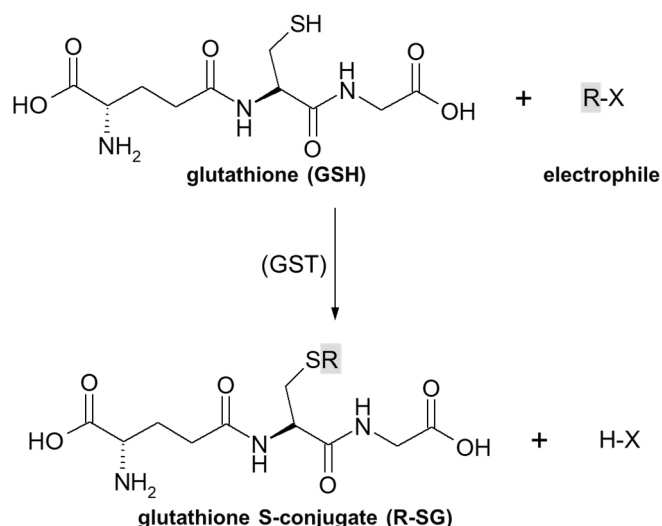


Figure 4. General scheme of glutathione (GSH) conjugation to a generic electrophile (R-X) to form the glutathione S-conjugate (R-SG). The reaction may be catalyzed by the enzyme glutathione S-transferase (GST).

There are several main mechanisms of GSH conjugation involved in detoxification and the potential bioactivation of anticancer drugs. Common GSH conjugation reactions are nucleophilic substitutions (including replacement of halogen atom or group of atoms with GSH molecule, the opening of the strained oxirane ring), nucleophilic displacement from saturated and aromatic carbon atoms, or nucleophilic addition to a polarized double or triple bond (Michael addition). The term ‘GSH S-conjugate’ usually refers to the product of the attack of GSH on an electrophilic carbon atom; however, GSH may also react with electrophilic oxygen, nitrogen, and sulfur atoms [56]. Below, I discuss certain mechanisms of these reactions for the selected known anticancer drugs.

3.1. Nucleophilic Substitution

Substitution reactions, which involve the reaction of a nucleophile with an electrophile, are prevalent in physiological and metabolic processes, in the action of some drugs, and in the chemical synthesis of nearly all drugs [57]. Thus, nucleophilic substitution is also the basic and the most widespread mechanism of GSH conjugation of electrophilic compounds. It is observed in several families of anticancer drugs, including alkyl, allylic, benzylic, and aryl halides, nitrogen mustard derivatives, or platinum complexes [33]. Electrophiles are positively charged or have a polarized bond with a partial positive character. Electrophiles capable of undergoing substitution reactions have a leaving group—a species that can accept and stabilize the pair of electrons that make up the bond being broken [57].

A common type of nucleophilic substitution reaction is the bimolecular nucleophilic substitution reaction, or S_N2 reaction for short, where one atom or functional group is replaced with an electronegative GSH molecule (the frame in Figure 5). In this case, bond formation and bond breaking occur simultaneously and the leaving group tends to be a weaker base than the nucleophile. Halide ions, such as I^- , Br^- , and Cl^- , are very good leaving groups and thus give fast reactions [58].

3.1.1. Halogen Atom as a Leaving Group

The S_N2 reaction mechanism of alkyl halide with GSH can be illustrated by the conjugation of 3-bromopyruvic acid (3-BrPA) with GSH (Figure 5A). 3-BrPA is the brominated derivative of pyruvic acid with proven anticancer activity against many different cancers in children and adults [59,60]. Like other α -bromoketones, it is widely known as a strong alkylating agent with a high affinity for protein binding as well as an antimetabolite [17]. Moreover, being an inhibitor of key glycolysis enzymes, including hexokinase II [61] and glyceraldehyde 3-phosphate dehydrogenase [62], 3-BrPA inhibits the growth of neoplastic cells that perform aerobic glycolysis known as the 'Warburg effect' [63]. Additionally, it also selectively blocks mitochondrial oxidative phosphorylation, angiogenesis, and energy production in cancer cells [63,64].

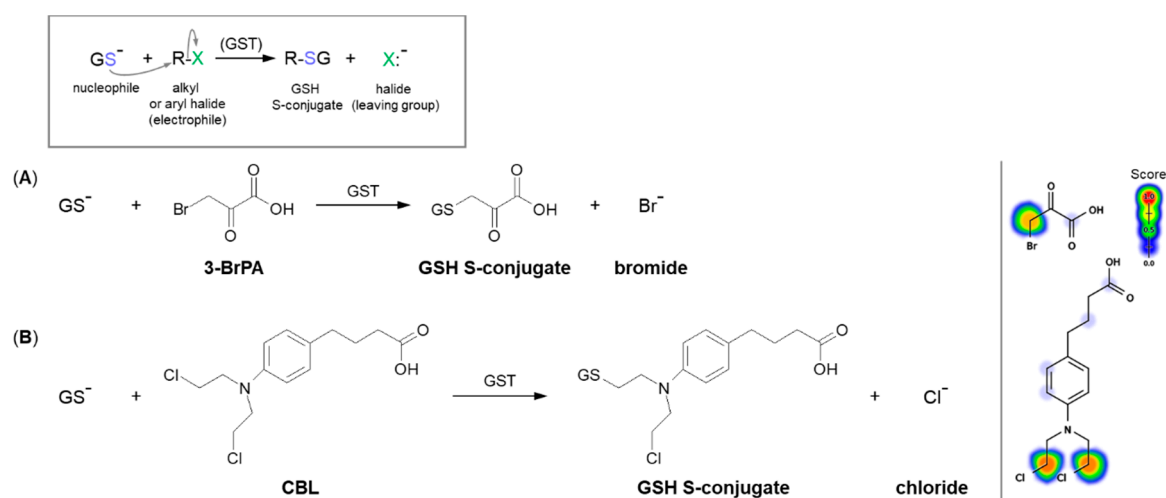


Figure 5. Reaction schemes of nucleophilic substitution of the thiolate anion of GSH (GS^-) to the halogen atom (leaving group) in (A) 3-bromopyruvic acid (3-BrPA) [17] and (B) chlorambucil (CBL) [65]. The frame shows the general scheme of the GSH conjugation reaction. Predicted bioactive sites of GSH conjugation for anticancer drugs were obtained by XenoSite Reactivity Predictor available at <https://swami.wustl.edu/xenosite/p/reactivity> (accessed on 18 May 2022).

Based on a chemical view, the thiolate anion of GSH (GS^-) easily attacks the carbon atom to which the bromine atom is attached. This reaction occurs because of the imbalance of the electron density between the carbon and halogen since it is a polar covalent bond. The more electronegative bromine atom pulls the electron density, thus making the carbon partially positively charged (an electrophilic center) and susceptible to a nucleophilic GS^- attack [66]. A bromine atom built into the structure of the 3-BrPA molecule is a good leaving group because the negatively charged bromine atom (bromide) is stable enough to exist on its own when it leaves the molecule. Hence, the conjugation to GSH does not require any prior metabolic activation of the parent compound. 3-BrPA was reported to form GSH S-conjugate both under GST catalysis and also in an enzyme-free system. Further, it is eliminated through the mercapturic acid synthesis pathway where it is excreted from the cell by ATP-binding cassette transporter proteins [17,67].

Another example of a similar S_N2 reaction is the GSH conjugation of chlorambucil (CBL; the brand name: Leukeran) (Figure 5B). CBL is an alkylating agent approved for use in various malignant and non-malignant neoplasms, such as chronic lymphocytic leukemia [68], lymphosarcoma [69], and giant follicular lymphoma [70]. In the presence of GSH, CBL behaves as an efficient substrate for GSTA1-1 and GSTP1-1 isoenzymes [65,71]. As with the 3-BrPA, the formation of the corresponding GSH S-conjugate undergoes without prior CBL activation as the negatively charged chlorine atom (chloride) is a good enough leaving group. Moreover, kinetic data suggest that the rate-limiting of the catalytic reaction between CBL and GSH is the reaction product release [65].

3.1.2. Tensioned Ring-Opening Reaction

The next type of GSH conjugation mechanism is the attachment of the thiolate anion (GS^-) to the epoxide, four-membered lactone, or three-membered aziridine resulting in ring-opening (Figure 6). Such reactions take place quite easily because the rings are composed of three or four carbon atoms which are highly tensed and their energy is quite high. Additionally, such a process will be easier, if the tensed system includes a heteroatom, because it will inductively decrease the electron density on adjacent carbon atoms [72,73]. Under basic conditions, ring-opening occurs by an $\text{S}_{\text{N}}2$ mechanism, and the less substituted carbon is the site of GS^- nucleophilic attack. The described transformation can take place stereoselectively, depending on the GST isoenzyme that catalyzes a reaction.

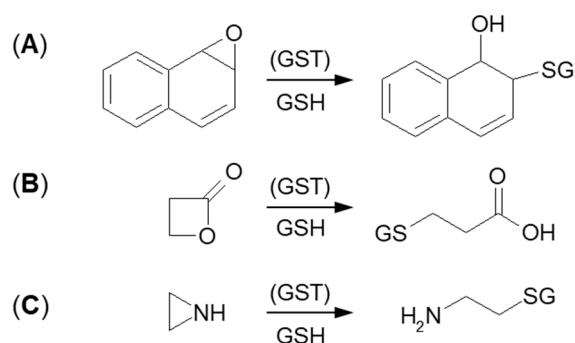


Figure 6. GSH conjugation via opening the tensioned ring of (A) epoxy, (B) lactone, and (C) aziridine.

Formation of GSH S-conjugate, accompanied by the aziridine ring-opening, takes place, e.g., in the case of cyclophosphamide and thiotepa. Cyclophosphamide (CP; the brand name: Cytoxan) belongs to the alkylating agent and nitrogen mustard family of medications [74,75]. Its mechanism of action, quite similar to that of chlorambucil, relies on interfering with the duplication of DNA and RNA synthesis [76]. It is a chemotherapeutic approved to treat malignant lymphomas, neuroblastoma, multiple myeloma, leukemias, ovarian, breast, and many other cancers [77]. Such a wide spectrum of clinical uses makes it an essential component of numerous combination chemotherapeutic regimens. Moreover, CP is also used to suppress the immune system [78].

A prerequisite for conjugation with GSH is the presence of a reactive electrophilic metabolite(s). Unlike 3-BrPA and CBL, CP must undergo previous metabolic activation by hepatic microsomal mixed-function oxidases (i.e., P450s, mainly 2B6, 2C8, and 2C9) (Figure 7) [79,80]. The generally accepted mechanism for the generation of active metabolites of CP involves oxidation to the primary 4-hydroxycyclophosphamide (4-OH-CP) metabolite, which stays in tautomeric equilibrium with the ring-opened aldophosphamide (APA). Then, non-enzymatic cleavage of APA results in the formation of two toxic species—phosphoramidate mustard (PAM) and acrolein. PAM is believed to unfold cell toxicity by DNA alkylation [81] while acrolein is held to be responsible for some aspects of host toxicity, such as hemorrhagic cystitis [82]. Therefore, GSH conjugation can result in the formation of three types of GSH S-conjugates, i.e., 4-monogluthionyl CP (4-GSCP) (1), mono- (2) and digluthionyl PAMs (3) [13,83]. The formation of 4-GSCP was found to be reversible, and by APA hydrolysis, PAM was formed. Thus, 4-GSCP can be considered a stable reservoir for the generation of PAM that subsequently undergoes two consecutive GSH conjugations. The reaction with nucleophilic GSH was established to proceed through the positively charged and highly polarized aziridinium ion (aziridinium intermediate) that can be opened in both the enzyme-catalyzed and the chemical reactions. On the other hand, the second GSH conjugation reaction was shown to occur through the direct displacement of chloride [13]. The 4-GSCP formation reaction can be catalyzed by various GSTs isoenzymes, whereas GST1A-1 has the greatest effect on the rate of monogluthionyl PAM formation. Melphalan, mechlorethamine, ifosfamide, carmustine, lomustine, and

nimustine are examples of other anticancer-active nitrogen mustard derivatives that react with GSH in a manner similar to that described for CP [13,80].

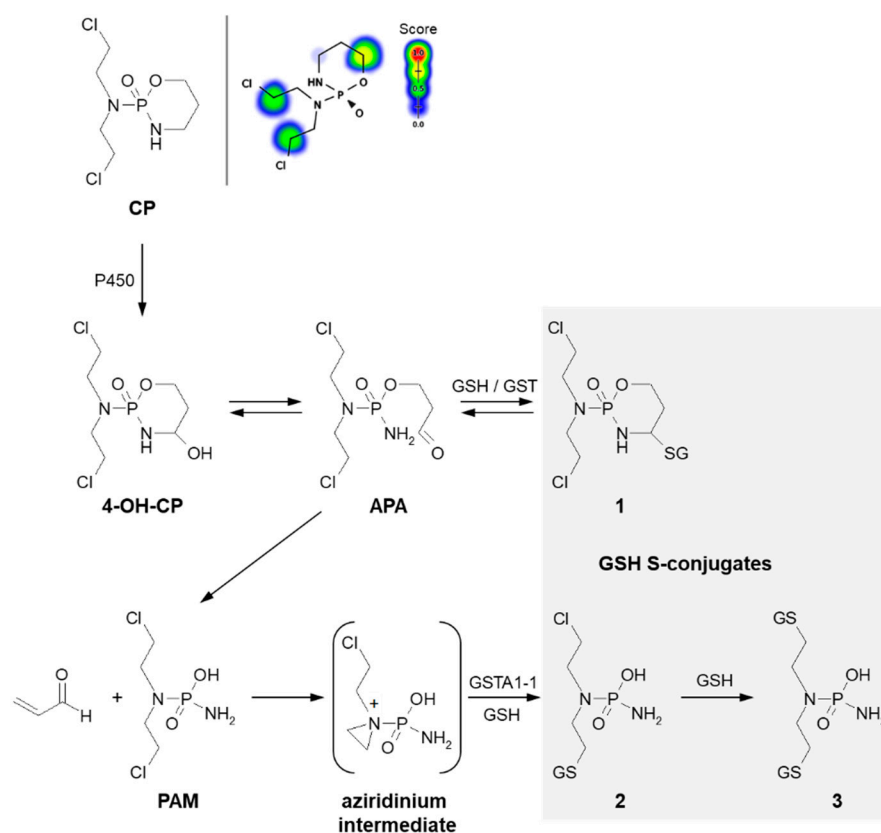


Figure 7. Scheme of cyclophosphamide (CP) activation and drug reaction with GSH [74]. Possible GSH S-conjugates: 1: 4-monogluthionyl cyclophosphamide, 2: monogluthionyl phosphoramidate mustard, 3: digluthionyl phosphoramidate mustard. 4-OH-CP = 4-hydroxycyclophosphamide; APA = aldophosphamide; PAM = phosphoramidate mustard; P450 = cytochrome P450. Predicted bioactive sites of GSH conjugation for anticancer drug were obtained by XenoSite Reactivity Predictor available at <https://swami.wustl.edu/xenosite/p/reactivity> (accessed on 18 May 2022).

Thiotepa (N,N',N'' -triethylenethiophosphoramidate; the brand name: Tepadina) also acts as an alkylating agent [84]. Being active against a wide variety of cancers, it is commonly used in combination with other chemotherapeutic agents to treat ovarian cancer, bladder cancer, and breast cancer [85,86]. Chemically, it is an organophosphorus compound containing a four-coordinated phosphorus atom and three aziridine moieties (Figure 8) through which the drug probably induces crosslinks with DNA, interfering with DNA replication and cell division [87]. The major metabolite formed from thiotepa during P450-catalyzed transformation (i.e., desulfuration reaction) is N,N',N'' -triethylenephosphoramidate (tepa) [88]. In turn, when reacting with GSH, the tensioned ring of thiotepa containing a nitrogen atom as a heteroatom is opened, leading to the formation of mono- (1) and digluthionyl thiotepa (2). In the metabolic pathway of thiotepa, 2-aminoethyl GSH (3), which is the product of the direct GSH conjugation of aziridine, was also characterized. The results confirmed that only thiotepa but not its monogluthionyl S-conjugate is a substrate for GSTs (mainly A1-1 and P1-1 isoenzymes). Moreover, the non-enzymatic reaction of the aziridinium moieties of thiotepa with GSH is strongly dependent on the pH, and the yield of the reaction is greatest at low pH [89].

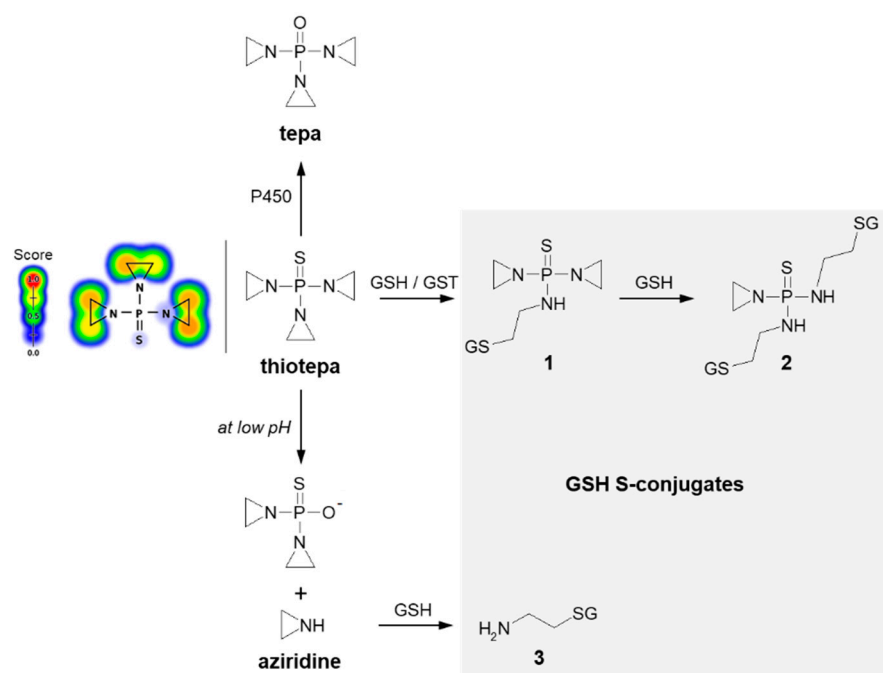


Figure 8. Scheme of thiotepa activation and drug reaction with GSH [89]. Possible GSH S-conjugates: **1**: monogluthionyl thiotepa, **2**: digluthionyl thiotepa, **3**: 2-aminoethyl glutathione. P450 = cytochrome P450. Predicted bioactive sites of GSH conjugation for anticancer drug were obtained by XenoSite Reactivity Predictor available at <https://swami.wustl.edu/xenosite/p/reactivity> (accessed on 18 May 2022).

3.1.3. Glutathione Conjugation with an Atom Different from a Carbon Atom

GSH conjugation can also take place at an atom different from a carbon atom. Such a mechanism was described, e.g., for cisplatin (*cis*-diamminedichloroplatinum (II), *cis*-DDP). It is the most successful drug in the family of platinum-based anticancer compounds [90] and is extremely effective against a wide range of human solid neoplasms, including breast, testicular, and ovarian cancers [91–93]. The generally recognized mode of action of this non-organic drug is by binding to DNA (via cross-linking) and inhibiting its replication, which ultimately results in the death of the fastest proliferating cancer cells [94]. After *cis*-DDP enters the cell, there is a rapid replacement of one or both chloride ligands by water molecules (Figure 9) [52,95,96]. The resulting new platinum (II) aqua species are potent electrophiles and are thus predicted to readily react with a number of nucleophilic biological targets with the loss of the bound water molecules. Indeed, besides DNA, cisplatin is known to efficiently bind sulfur-containing proteins, which also perform a transport role for the drug, or various nucleophilic compounds, including thiols (e.g., GSH, N-acetylcysteine) [97,98]. Protein binding is related to the occurrence of drug resistance and toxic effects [99], which will be discussed further in this work. Ishikawa and Ali-Osman [100] first reported the formation of a digluthionyl platinum conjugate in L1210 leukemia cells. Nagar et al. [101] found cisplatin-GSH S-conjugate in *Rattus norvegicus* and proposed the structure of the GSH-conjugated metabolite based on mass spectrometry.

There are several other platinum-based anticancer compounds such as carboplatin, picoplatin, and oxaliplatin, heavily applied in chemotherapy regimens [90], that conjugate to GSH in a similar manner to cisplatin [102,103]. No significant differences in their mechanism of action but several differences in effectiveness are observed. Some platinum derivatives are more tolerated by the human body than cisplatin [104].

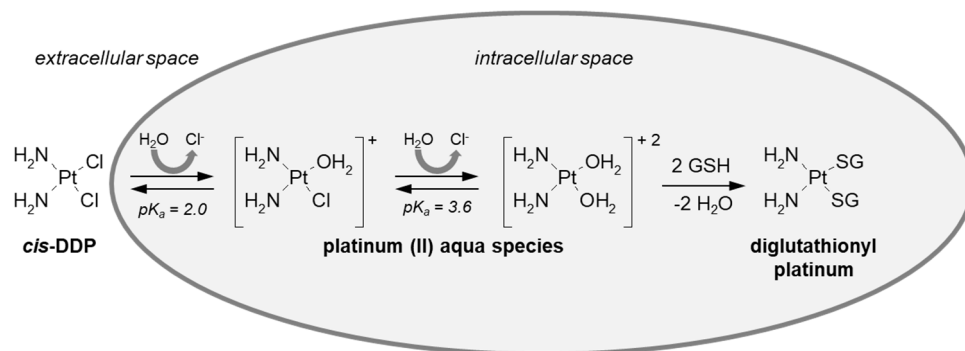


Figure 9. Reaction scheme of cisplatin (*cis*-DDP) conjugation with GSH.

3.1.4. Aromatic Nucleophilic Substitution

Although aromatic rings are usually nucleophilic, some aromatic GST substrates can undergo nucleophilic aromatic substitution (S_NAr). In short, the aromatic ring is then not the attacking species but must be electron-poor (electrophilic). This is due to the negative inductive and mesomeric effects of its substituents. The rate-determining step of the reaction is an attack of the aromatic ring by the nucleophile, which disrupts aromaticity. The position in which the nucleophile attacks is defined by where the leaving group is, not by electronic and steric factors (i.e., no mix of *ortho*- and *para*- products as with electrophilic aromatic substitution) [57,58]. A typical illustration of the S_NAr reaction may be the substitution of GSH to 1-chloro-2,4-dinitrobenzene (CDNB), a model substrate for a GST conjugation activity [105]. The generally accepted mechanism of GS-DNB conjugate formation involves an addition-elimination sequence with a short-lived non-aromatic complex intermediate, the so-called Meisenheimer complex [106,107]. Among anticancer drugs, the S_NAr reaction is characteristic of GSH conjugation of PABA/NO. It was shown that this O^2 -aryl diazeniumdiolate produces anticancer effects comparable with cisplatin in a human ovarian cancer model grown in SCID mice and is also potent against the proliferation of the OVCAR-3 cell line [107–109]. GSH addition, selectively catalyzed by GST, proceeds with the formation of a Meisenheimer intermediate (Figure 10). PABA/NO was designed as a prodrug as the diazeniumdiolate ion leaving group subsequently spontaneously releases two moles of nitric oxide (NO) at physiological pH [108–111]. Therefore, within the GST-overexpressing cancer cells, the intracellular GSH is irreversibly consumed, and the NO generated this way could contribute to cancer therapy by inhibiting DNA synthesis, forming toxic reactive nitrogen/oxygen intermediates and inhibiting enzymes capable of preventing or repairing cellular damage [107].

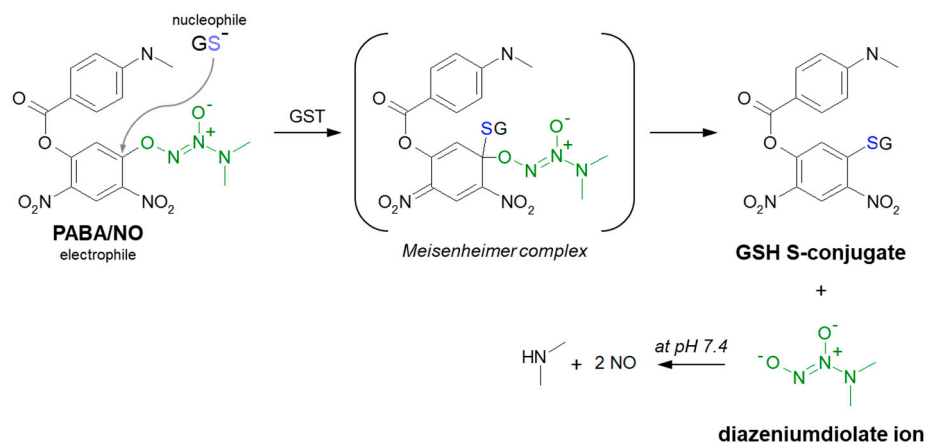


Figure 10. Scheme of the GST-catalyzed reaction of GSH with PABA/NO showing the formation of the Meisenheimer complex as the reaction intermediate [107]. A leaving group in PABA/NO molecule is marked in green.

Referring to the unsymmetrical bisacridines (UAs) studied in our group, the S-conjugate formation between GSH and UA derivative most likely occurs also according to the classical S_NAr mechanism. The general proposed mechanism of enzymatic GSH conjugation for a representative UA, compound C-2028, is shown in Figure 11. In the first step, GST-mediated deprotonation of the GSH molecule to the thiolate anion (GS^-) should take place. We assume that the electronegative nitrogen atom of the amino (-NH-) functional group (electron-withdrawing group) decreases the electron density in the entire acridine ring and thus helps to stabilize a negatively charged intermediate, i.e., Meisenheimer complex [58], formed after the nucleophile attack. As a result, the nitro group may be easily removed from this transition state in the form of nitrite anion (NO_2^-) [112,113]. We provided evidence that the reaction did not require prior reduction of the nitro group, which would explain the observed lack of P450 involvement in the process [25]. Moreover, the results of our studies also indicated that 1-nitroacridine did not give any enzymatic GSH S-conjugate, while in the case of 1-nitro-9-aminoacridine and 1-nitro-9-methylaminoacridine, such products were detected (unpublished data). Thus, the presence of nitrogen atom from the amino group may be crucial in the GSH conjugation mechanism. Neither the structures of the proposed intermediate nor the GSH S-conjugate have been finally confirmed yet.

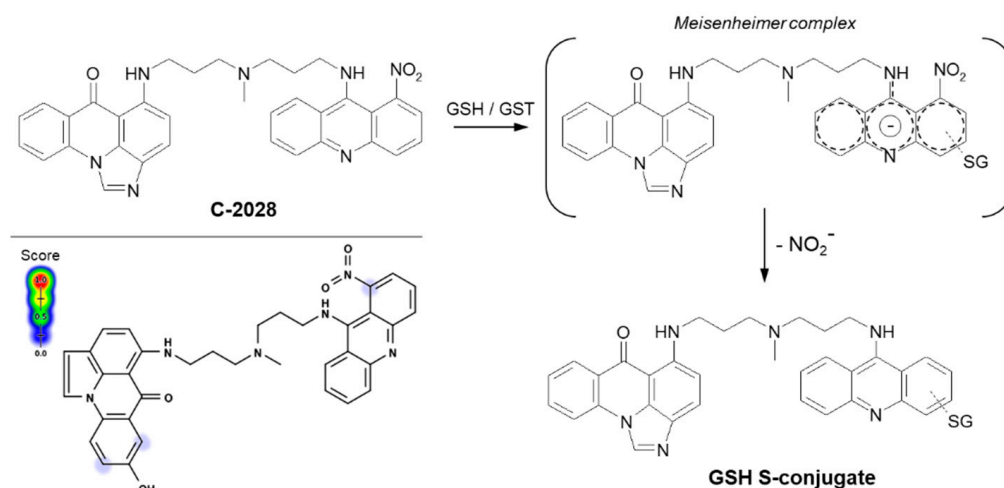


Figure 11. The proposed GSH-mediated metabolic pathway of C-2028, the representing anticancer unsymmetrical bisacridine derivative [25]. Predicted bioactive sites of GSH conjugation for anticancer agent were obtained by XenoSite Reactivity Predictor available at <https://swami.wustl.edu/xenosite/p/reactivity> (accessed on 18 May 2022).

3.2. Nucleophilic Addition (Michael Addition)

Some reactions leading to the formation of GSH S-conjugates occur through Michael addition (or conjugate addition). Such a mechanism applies to α,β -unsaturated compounds (the so-called Michael acceptors) characterized by having carbon–carbon double ($C=C$) or carbon–carbon triple ($C\equiv C$) bonds with a strongly electron-withdrawing substituent(s) (e.g., a carbonyl, carboxyl, or nitro group) (Figure 12) [114]. This results in a polarizable electron density at the π bond, where the β -carbon atom (β -C) is positively polarized and becomes the preferred site of an attack of a soft nucleophile (Michael donor), e.g., the thiol group of cysteine in GSH. Although many of them can form thioethers non-enzymatically, GST-catalyzed Michael addition is much faster [10,115]. Compounds possessing Michael acceptor units feature a broad spectrum of bioactivity. They are considered to be particularly reactive and are thus capable of bonding with biological macromolecules [116].

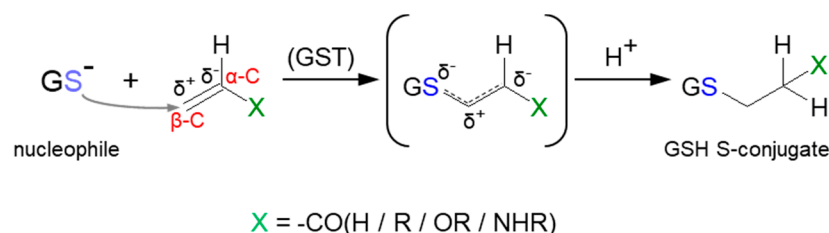


Figure 12. General scheme of Michael addition (or conjugate addition) to α,β -unsaturated compound with carbon–carbon double (C=C) bond.

Mitoxantrone (MTX; the brand name: Novantrone), a synthetic anthraquinone anti-neoplastic agent, is an example of a compound that undergoes GSH conjugation by Michael addition. MTX is a potent type II topoisomerase inhibitor that disrupts DNA synthesis and DNA repair in both healthy cells and cancer cells by intercalation between DNA bases [117]. It is commonly applied in the treatment of breast [118] and prostate [119] cancers, lymphomas [120], and leukemias, primarily acute myeloid leukemia [121], with excellent efficacy.

In the case of MTX, at least two GSH conjugation pathways were identified (Figure 13). MTX is known to resist reductive enzymatic activation but is subject to facile oxidative enzymatic action [122]. The development of GSH-dependent resistance provides further evidence that the oxidative activation may be a relevant mode of drug action. The *in vivo* and *in vitro* studies of Mewes et al. [122] performed using minipigs, cultured rat hepatocytes, and human HepG2 hepatoma cells, respectively, revealed the formation of a major monogluthathionyl MTX (1) and its various degradation products. The ability of MTX to react with GSH enables the formation of an MTX quinone derivative by two-electron oxidation of the parent drug, which is in the form of a hydroquinone. Additionally, there are also data confirming the possibility of the formation of another MTX-GSH S-conjugate (2) [117]. Following the MTX enzymatic oxidation process within the aromatic ring containing polyamine side chains, the intramolecular Michael addition occurs. Presumably, the mechanism of this GSH conjugation reaction takes place via a labile iminium ion intermediate which activates the aromatic ring towards the attack of the external cellular nucleophile (e.g., GSH, DNA).

Another example of a Michael addition-type reaction is infigratinib (INF, NVP-BGJ398). It is a novel small-molecule chemotherapeutic drug used for first-line treatment of advanced or metastatic cholangiocarcinoma (bile duct cancer). It was discovered that INF inhibits human fibroblast growth factor receptors (FGFRs), which are a family of receptor tyrosine kinases that may be upregulated in different cancer cell types [123]. For this reason, it is an investigational drug under development for the treatment of patients with various FGFR-driven diseases [124,125]. Al-Shakliah et al. [126] detected at least three GSH S-conjugate metabolites of INF using liquid chromatography ion trap mass spectrometry (LC-ITMS). As shown in Figure 14, the halogenated benzene ring of the INF structure undergoes metabolic bioactivation sequentially by dechlorination, O-demethylation, and oxidation to form the reactive 1,4-benzoquinone intermediate that is attacked by GSH [126,127].

The next example is helenalin, a natural sesquiterpene lactone present in a large number of species mostly from the *Asteraceae* family, which has a variety of observed effects *in vitro*, including anti-inflammatory and anticancer activities [128–130]. As the compound structure contains reactive Michael acceptor systems (i.e., α,β -unsaturated ketone moiety and α,β -unsaturated lactone moiety), it is able to easily react with GSH [131]. The 2 β -mono- (1) and 2,13 β -diglutathionyl (2) conjugates of helenalin were shown to be formed by spontaneous Michael addition at physiological pH (Figure 15A). Interestingly, these were found to inhibit GST from horse liver, while free helenalin showed no inhibitory activity [132].

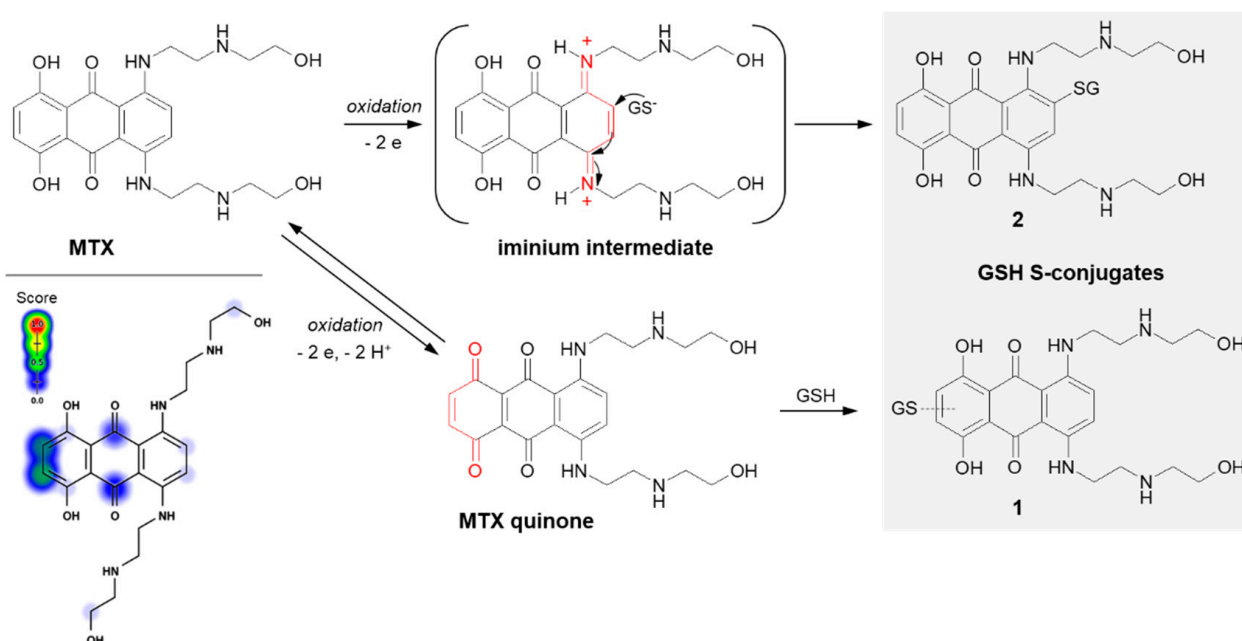


Figure 13. Scheme of mitoxantrone (MTX) activation and drug reaction with GSH [16,117]. The Michael acceptor moieties are marked in red. Predicted bioactive sites of GSH conjugation for anticancer drug were obtained by XenoSite Reactivity Predictor available at <https://swami.wustl.edu/xenosite/p/reactivity> (accessed on 18 May 2022).

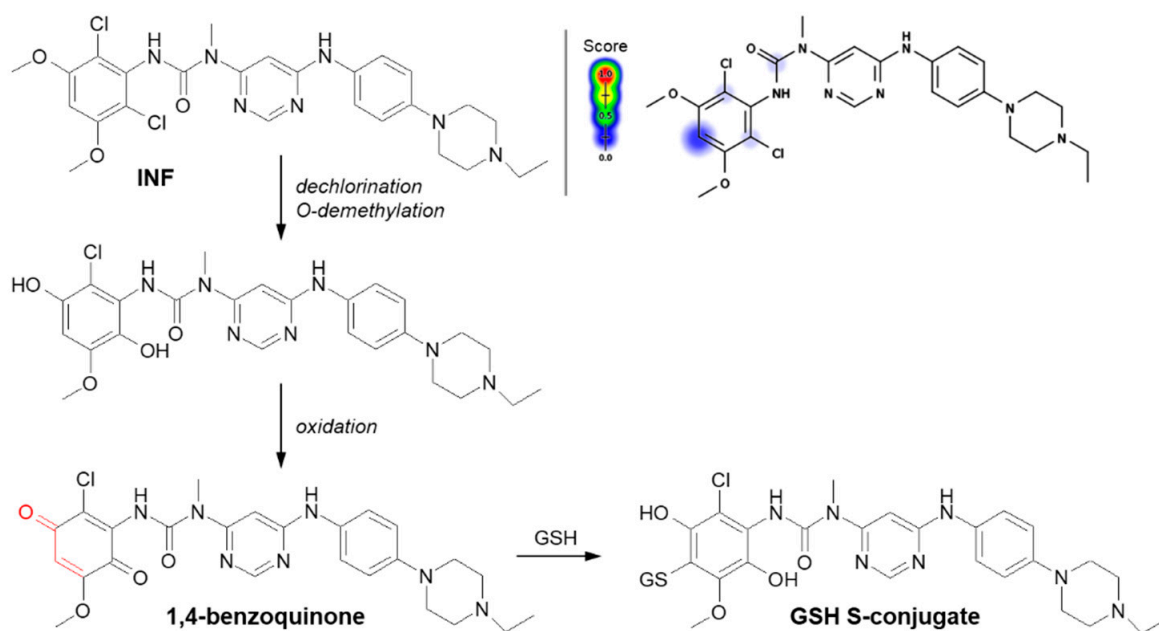


Figure 14. Reaction scheme of ingfigratinib (INF) conjugation with GSH [126]. A Michael acceptor moiety is marked in red. Predicted bioactive sites of GSH conjugation for anticancer drug were obtained by XenoSite Reactivity Predictor available at <https://swami.wustl.edu/xenosite/p/reactivity> (accessed on 18 May 2022).

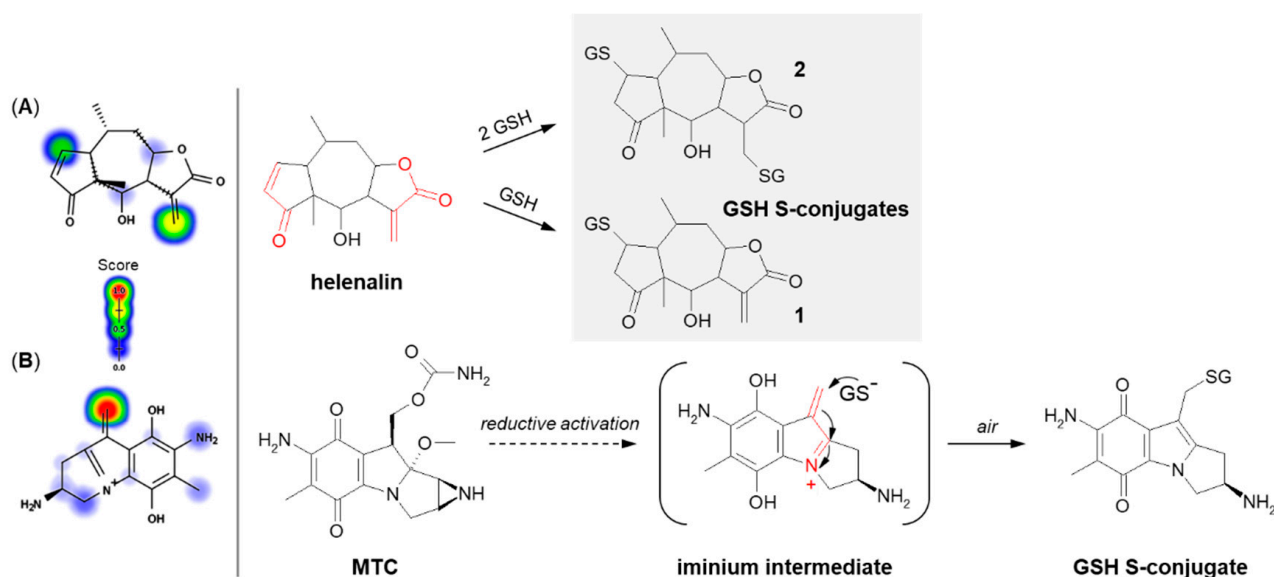


Figure 15. Reaction schemes of (A) helenalin [131] and (B) mitomycin C (MTC) [133] conjugation with GSH. The Michael acceptor moieties are marked in red. Predicted bioactive sites of GSH conjugation for anticancer drugs were obtained by XenoSite Reactivity Predictor available at <https://swami.wustl.edu/xenosite/p/reactivity> (accessed on 18 May 2022).

Mitomycin C (MTC) is a natural cytostatic antibiotic used as a chemotherapeutic agent by virtue of its anticancer activity. The mechanism of drug action is typical for that based on DNA alkylation [134,135]. Importantly, MTC requires previous activation via enzymatic reduction (bioreductive activation) to exert its biological effects. One-electron reduction steps to the corresponding semiquinone and then to hydroquinone initiates a cascade of consecutive reactions (i.e., spontaneous elimination of methanol from hydroquinone, elimination of the carbamate group, opening of the aziridine ring) that gives an unstable iminium intermediate which reacts with GSH through a Michael-type reaction [133,136] (Figure 15B). MTC was shown to form both mono- and diglutathionyl conjugates. It was also found that GSH itself did not reduce MTC, and unreduced drug did not form conjugates with GSH [137].

A few more examples of Michael acceptor-containing anticancer therapeutics metabolizing through GSH conjugation are afatinib, ibrutinib, and neratinib (Figure 16) [138,139]. They are all inhibitors of various tyrosine kinases and use their own Michael acceptor moiety for irreversible binding to a free cysteine residue of the targeted protein. In recent years, such a targeted covalent modification of regulatory proteins by Michael acceptors became recognized as a promising approach to drug discovery [140]. It can be expected that GSH plays an integral role in the clearance of these electrophilic drugs. Shibata and Chiba [138] showed that both afatinib and neratinib undergo extensive conjugation with GSH in buffer and cytosolic subfraction deriving from liver and kidney tissues, whereas ibrutinib has exhibited much lower degree of GSH/GST-dependent conjugation [138]. These findings may be helpful in optimizing pharmacokinetics in humans during the development stage of other targeted covalent inhibitors.

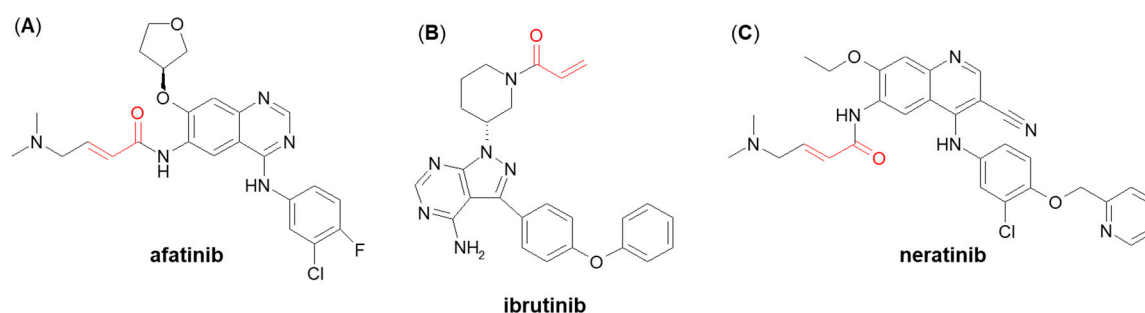


Figure 16. Chemical structures of (A) afatinib, (B) ibrutinib, and (C) neratinib. The Michael acceptor moieties are marked in red.

4. Possible Biological Consequences of Glutathione Conjugation of Anticancer Drugs

It is widely recognized that GSH conjugation of xenobiotics and conversion of thioethers to mercapturic acids is a biochemical defense of organisms against potentially harmful compounds [18]. In general, as a result of the detoxification process, many substances lose their toxic properties—completely or partially. However, in special cases, a diversion of this pathway (e.g., by the action of cysteine S-conjugate β -lyase) may lead to the bioactivation of some anticancer drugs rather than to detoxification [19,52], which means increasing their toxicity. Therefore, we can talk about the two directions of GSH conjugation of anticancer drugs, the possible consequences of which may be cancer treatment, resistance, or development. In this chapter, I would like to address this topic.

4.1. Glutathione Conjugation as a Detoxification Reaction

The importance of GSH conjugation in the detoxification of a drug depends on the extent to which it is metabolized to reactive intermediates [34]. The reaction can be non-enzymatic (i.e., chemical) or enzyme-catalyzed, with GSTs playing the greatest role. The first is assumed to be particularly effective when soft and strong electrophiles are generated. In turn, the conjugation of soft but weak electrophiles (or hard electrophiles) requires enzymatic intervention to bring about effective GSH conjugation [10]. In order to deal with the wide variety of potential substrates, a multiplicity of GSTs exists—each tissue has its own collection, and each isoenzyme has a different substrate specificity. In humans, the highest cytosolic GST activity level is present in the liver, followed by the kidneys, lungs, and intestines [52,141]. There are many reports demonstrating that structurally different anticancer drugs form GSH S-conjugates through a GST-catalyzed process which are then degraded and removed from the body [18,51]. On the one hand, the GSH-related detoxification pathway reduces the drug reactivity and prevents further damage to the cellular macromolecules that could be caused by electrophilic metabolites and/or ROS. In some cases, conjugation with GSH can lead to the formation of up to 60% of the biliary metabolites [34]. The effectiveness of the detoxification pathway may depend on the intracellular concentration of GSH, the presence of GST of appropriate specificity, and/or the capacity of the cell for rapid resynthesis of GSH [45]. However, it should be remembered that the enhanced non-enzymatic GSH conjugation or overexpression of genes encoding particular GSTs in many cancers, relative to surrounding healthy tissues, were found to contribute to increased detoxification of anticancer drugs and, hence, to the development of drug resistance [50,142–145]. This frequently leads to a drop in the therapeutic effect of the chemotherapeutic and consequently to the decrease in its effectiveness during cancer therapy [141].

Cancer drug resistance is one of the problems usually associated with treatment with alkylating drugs [146–148]. For example, the detoxification of 3-bromopyruvic acid appears to be confirmed by a reduction in cancer cell viability due to a depletion in GSH levels in cells [67,149]. For chlorambucil, an inverse relationship was found between the GSH concentration and/or the GST activity and the number of DNA cross-links formed [150,151].

There are studies showing that both GSH levels and the presence of GSTs, and especially GSTA1-1, can influence the concentration of aziridinium intermediate formed from the cyclophosphamide and the toxicity of the compound [152]. GST-catalyzed GSH conjugation of thiotepa might be an important factor in the development of drug resistance since the overexpression of GSTP1-1, and to a lesser extent, GSTA1-1, is observed in cancer cells [89,153]. To overcome drug resistance, it is suggested that the moderate decline in the GSH level and/or GST activity would be a very effective approach for increasing the sensitivity of cancer cells to chemotherapy [147,154].

At this point, the phenomenon of ferroptosis should be mentioned. It is described as an intracellular iron-dependent and lipid peroxidation-driven regulated cell death pathway, which is different from other cell necrosis, apoptosis, and autophagy in morphology, biochemistry, and genetics [155]. Extensive studies suggest that ferroptosis correlates with cancer therapy resistance, and inducing ferroptosis has been demonstrated to reverse drug resistance [156]. Ferroptosis can be induced by agents causing the depletion of GSH (a cofactor of selenium-dependent GSH peroxidase 4 (GPx4)) or direct inhibition of GPx4 [155–158]. Thus, marked GSH consumption by electrophilic compounds may result in a reduction of GPx4 in drug-resistant cells, which provides new opportunities for cancer therapy. On the other hand, ferroptosis can be also involved in hepatotoxicity due to GSH depletion caused by drug overdose. For example, at nontoxic doses, the metabolite of acetaminophen (a drug used to treat pain and fever) is efficiently detoxified by GSH, forming an acetaminophen-GSH S-conjugate via Michael addition. However, when overdosed, it can cause potentially fatal hepatic centrilobular necrosis [159].

4.2. Glutathione Conjugation as a Bioactivation Reaction

In addition to its 'classic' function in anticancer drug detoxification, GSH together with enzymes of the GST family may be also involved in bioactivation reactions. In this case, the product of the initial conjugation is still reactive or even more reactive than the parent compound, and cellular macromolecules, within either cancer or normal cells of the host, become the main targets for their attack [19]. Different authors have reported some interesting findings on this topic [52,54,115,160,161]. Among the anticancer drugs, it is worth mentioning the examples of conjugates that are activated through (i) cysteine S-conjugate β -lyase, (ii) direct-acting GSH S-conjugates, (iii) conjugates that are activated through redox cycling, and (iv) conjugates that release the original reactive parent compound, i.e., GSH S-conjugates as targeted anticancer prodrugs [18,19]. These may be either toxic or pharmacologically active for the cells in which they were produced [52].

The effectiveness of high-dose *cis*-DDP therapy is limited due to its side effects in the form of nephrotoxicity, ototoxicity, and neurotoxicity [162,163]. Damage of renal cells has been proven to be the result of cysteine S-conjugate β -lyase activity, which undergoes overexpression in this organ [164]. Figure 17 shows the activation pathway of *cis*-DDP to nephrotoxic species, which follows the mercapturic acid synthesis pathway, i.e., the conversion of *cis*-DDP to its GSH S-conjugate (Pt-GSH), and then to cysteine S-conjugate (Pt-Cys), the highly reactive and cytotoxic thiol version of cisplatin [18,52]. Cysteine S-conjugate β -lyase converts a drug intermediate into a thiol-reactive metabolite containing a Pt-SH (or Pt-S⁻) moiety that binds at thiophilic centers of mitochondrial proteins present in renal proximal tubule cells [164].

Further, there is strong evidence that GSH participates in the formation of a toxic metabolite of busulfan (the brand name: Busulfex) [18,19]. It is a cell-cycle non-specific bifunctional alkylating anticancer agent in the class of alkyl sulfonates. The drug is used in pediatrics and adults in combination with cyclophosphamide or fludarabine/clofarabine as a conditioning agent prior to bone marrow transplantation, especially in chronic myelogenous leukemia and other leukemias, lymphomas, and myeloproliferative disorders [165–167]. Toxicity related to busulfan treatment may include interstitial pulmonary fibrosis (the so-called 'busulfan lung'), hyperpigmentation, seizures, hepatic (veno-occlusive disease) or sinusoidal obstruction syndrome [168]. It is believed that the above toxic effects

are due to busulfan irreversible GSH conjugation catalyzed mainly by GSTA1-1 isoenzyme [169,170]. As a result of this reaction, presented in Figure 18, a positively charged product, glutathionyl-tetrahydrothiophene (GS-THT⁺), is formed. This ion is not sufficiently electrophilic to alkylate macromolecules, so it is then converted to γ -glutamyl-dehydroalanyl-glycine (EdAG) and the oxidation product of tetrahydrothiophene (THT) during β -elimination reaction. EdAG, which is an α,β -unsaturated dehydroalanyl analog of GSH, is considered to be a source of toxicity due to its chemical reactivity. Subsequently, it condenses with another GSH molecule via a Michael addition reaction to produce an oxidized lanthionine thioether (GSG). Unlike GSSG, GSG does not undergo reduction and reacts with protein thiol groups, resulting in the formation of irreversibly glutathionylated proteins. Irreversible glutathionylation has important implications for the mechanism of busulfan toxicity as it can lead to the loss of function of many proteins that are normally regulated by the reversible GSH conjugation reaction [171].

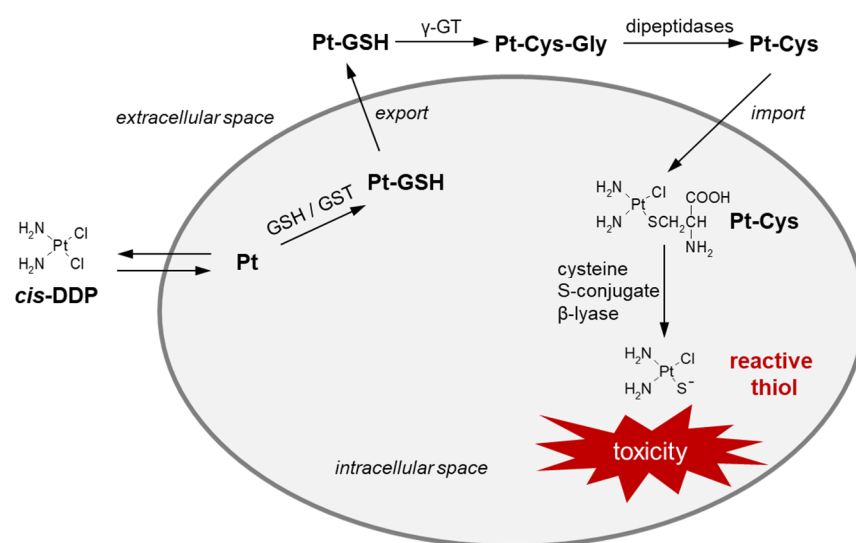


Figure 17. Cisplatin (*cis*-DDP) bioactivation through GSH S-conjugate (Pt-GSH) and cysteine S-conjugate (Pt-Cys) formation [18,52]. *cis*-DDP = cisplatin; GSH = glutathione; GST = glutathione S-transferase; γ -GT = γ -glutamyl transferase; Pt = platinum (II) aqua species.

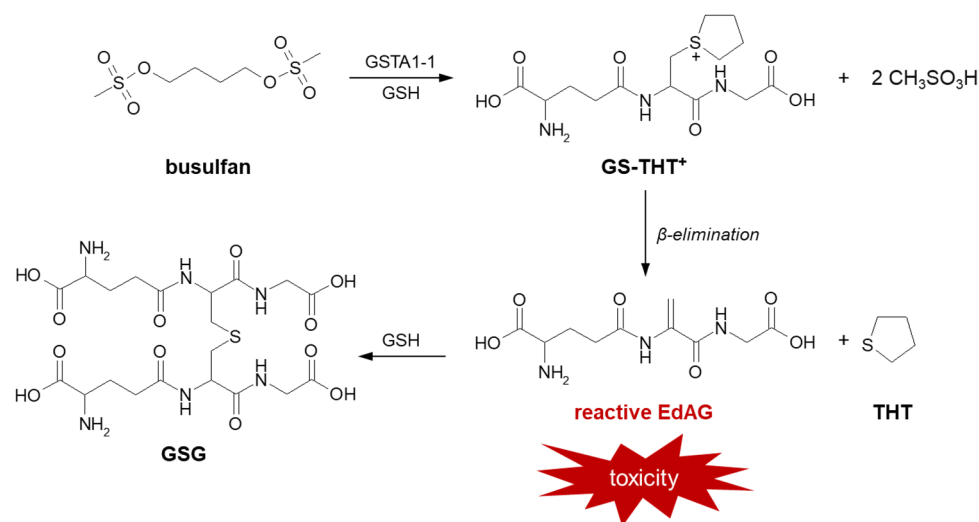


Figure 18. Formation of reactive busulfan metabolites in a GSH-dependent pathway [170]. EdAG = γ -glutamyl-dehydroalanyl-glycine; GSG = EdAG-GSH S-conjugate; GSH = glutathione; GST = glutathione S-transferase; GS-THT⁺ = glutathionyl-tetrahydrothiophene; THT = tetrahydrothiophene.

Drug precursors are pharmacologically inactive molecules *in vitro* that are converted into their active parent drugs *in vivo* after chemical modifications and/or enzymatic reactions [172]. They are often designed to improve the bioavailability of active drugs by increasing their amount in targeted cells and reducing off-target effects. A well-known example of a prodrug activated by GSH conjugation is azathioprine (brand name: Imuran). It is a methyl-nitroimidazole derivative of 6-mercaptapurine (6-MP) whose action of disrupting the formation of RNA and DNA in the cells assigns it to the purine analog and antimetabolite family of anticancer chemotherapeutics [173]. Enzymatic GSH conjugation of azathioprine, with the highest reaction efficiency observed for GSTA2-2, converts it into 6-MP and various methyl-nitroimidazole derivatives (Figure 19A) [174]. Released 6-MP incorporates into replicating nucleic acids, leading to an arrest of the *de novo* purine biosynthetic pathway [160,175]. In turn, GS-imidazole conjugate is believed to be the major route of azathioprine toxicity, especially hepatotoxicity, due to the high consumption of GSH, which is normally present in abundance in hepatocytes [176]. To sum up, the involvement of GSH in the metabolism of azathioprine is important for the toxification of the drug as well as the modulation of the therapeutic and toxic effects of the resulting 6-MP.

The category of targeted anticancer prodrugs also includes diarylsulfonylureas. A representative compound of this class, sulofenur (LY-186641) shows therapeutic efficacy against a wide variety of cancers [177,178]; however, it causes hemolytic anemia and methemoglobinemia at dose-limiting toxicities [179,180]. The anticancer and toxicological mechanism(s) of action of the drug is not well understood, but unlike other antineoplastic agents, sulofenur does not interfere with DNA, RNA, or protein synthesis, or with polynucleotide function. It undergoes metabolic transformation to form *p*-chlorophenyl isocyanate (CPIC), which could carbamoylate biological macromolecules directly or interact with GSH to give GSH S-conjugate (S-(N-*p*-chlorophenylcarbamoyl) GSH, SCPG) (Figure 19B) [181]. The resulting intermediate metabolite is further biotransformed via the mercapturic acid synthesis pathway to the corresponding N-acetylcysteine conjugate [N-acetyl-S-(*p*-chlorophenylcarbamoyl) cysteine, NACC], which expresses selective anticancer activity comparable to that observed for parent compound and has low toxicity [182]. The produced S-conjugates of GSH and cysteine are susceptible to thiol group exchange reactions and can therefore act as carbamoylating compounds for cellular macromolecules. Structural analogs of sulofenur have been studied and undergo similar metabolic pathways, which makes them promising anticancer drugs.

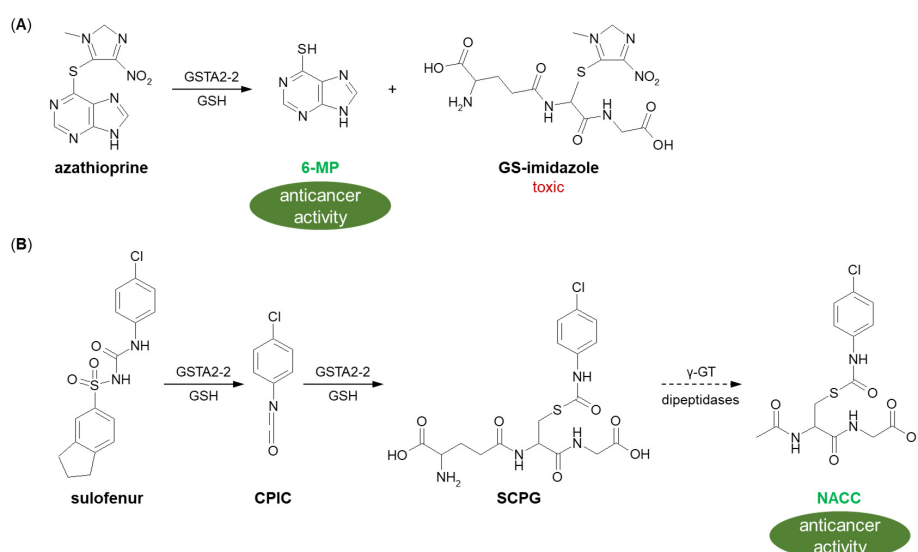


Figure 19. (A) Azathioprine [174] and (B) sulofenur [181] bioactivation to anticancer-active metabolites by GST-mediated GSH conjugation. 6-MP = 6-mercaptopurine; CPIC = *p*-chlorophenyl isocyanate; GSH = glutathione; GST = glutathione S-transferase; NACC = N-acetyl-S-(*p*-chlorophenylcarbamoyl) cysteine; SCPG = S-(N-*p*-chlorophenylcarbamoyl) GSH.

4.3. Anticancer Unsymmetrical Bisacridine Derivatives—Possible Biological Consequences of Glutathione Conjugation

The formation of GSH S-conjugate indicates the generation of reactive electrophilic metabolite(s) from a drug candidate that can bind to macromolecules of biological importance. When conjugation reaction is catalyzed by GST, the enzyme is a prime target for the attack. We predict that in vivo-formed GSH-conjugated metabolites of anticancer-active UAs (i.a., C-2028) would (i) lower the concentration of the nitroaromatic compound and its nitro group reduction derivatives, decreasing the overall toxicity of the chemotherapeutic agent (detoxification pathway) or (ii) serve as UA latent species (bioactivation pathway). This has not been fully recognized yet. Therefore, future works should focus on determining whether GSH S-conjugates of UAs exhibit any specific biological activity related to the toxicity and/or anticancer effects of these agents. Our preliminary studies revealed that the depletion of cellular GSH by buthionine sulfoximine (a specific inhibitor of γ -GCS) [183] or inhibition of GST activity by ethacrynic acid [184] decreased the sensitivity of Du-145 human prostate and H460 human lung cancer cell lines to C-2028, albeit to an extent dependent on the cell line (unpublished data). In line with these results, we can speculate on the GSH conjugation of UA as a bioactivation reaction.

One group of prodrugs may be molecules whose enzymatic activation occurs through a GSH-conjugate intermediate [185]. Compounds as NO donors, such as PABA/NO, are an important example. The presence of an easily reducible nitro group in the UA molecule suggests such an opportunity also among these potential anticancer drugs. Thus, the reduction of the nitro group may be a potential route of UA toxicity. In fact, UAs as NO-releasing agents would be able to induce differentiation and cell death in a variety of cancer cells through GSH consumption, DNA synthesis inhibition, and the inhibition of enzymes involved in the defense against cell damage. In this respect, the combination of UA molecules with the conventional anticancer treatment could be particularly effective.

5. Concluding Remarks

In this work, the main mechanisms and the role of GSH conjugation in the biological action of several diverse anticancer chemotherapeutics have been discussed. The knowledge in these fields collected above was summarized in Table 1. The reactivity towards the thiol group of GSH (nucleophile) was predicted for most compounds (electrophiles) using the GSH model in the Xenosite Reactivity Predictor available at <https://swami.wustl.edu/xenosite/p/reactivity> (accessed on 18 May 2022), and these results matched the practical results found in the literature. The structure and physico-chemical properties of the substrate specify the type of GSH conjugation reaction and its subsequent consequences. Examples presented here clearly show that GSH/GST-mediated conjugation of anticancer drugs may represent a pathway for drug detoxification, cancer drug resistance, treatment, or therapy development. Thus, the GSH status of cancer or normal cells, the substrate selectivity of the GST, and the chemical properties of the GSH S-conjugate formed are among the strong determinants of the effectiveness and/or toxicity of the therapy. In conclusion, the knowledge about GSH conjugation of any anticancer drug may be exploited for the design and development of new anticancer drugs with better pharmacokinetic properties and lower overall toxicity, targeting specific cancers and avoiding the mechanisms of cancer cell resistance.

Table 1. Overview of the mechanisms and the role of GSH conjugation of anticancer drugs discussed in this work.

Anticancer Drug	Type of GSH Conjugation Mechanism	The Crucial Role of GSH Conjugation in Drug Response
azathioprine	S _N 2/substitution of imidazole	bioactivation
3-bromopyruvic acid	S _N 2/substitution of halide	detoxification
busulfan	Michael addition	bioactivation (toxification)
chlorambucil	S _N 2/substitution of halide	detoxification
cisplatin	S _N 2/conjugation with an atom different from a carbon atom	bioactivation (toxification)
cyclophosphamide	S _N 2/tensioned ring-opening and substitution of halide	detoxification
helenalin	Michael addition	detoxification
infigratinib	Michael addition	detoxification
mitomycin C	Michael addition	detoxification
mitoxantrone	Michael addition	detoxification
PABA/NO	S _N Ar	bioactivation
sulofenur	Michael addition	bioactivation
thiotepa	S _N 2/tensioned ring-opening	detoxification
unsymmetrical bisacridine	S _N Ar (supposed)	ND

ND = not detected; S_N2 = bimolecular nucleophilic substitution reaction; S_NAr = aromatic nucleophilic substitution.

Funding: This research received no external funding.

Institutional Review Board Statement: Not applicable.

Informed Consent Statement: Not applicable.

Data Availability Statement: Not applicable.

Acknowledgments: The author wishes to thank Zofia Mazerska (Department of Pharmaceutical Technology and Biochemistry, Faculty of Chemistry, Gdańsk University of Technology, Gdańsk, Poland) for her valuable comments on the manuscript.

Conflicts of Interest: The author declares no conflict of interest.

Abbreviations

3-BrPA, 3-bromopyruvic acid; 6-MP, 6-mercaptopurine; C-2028, 9-[N-[(imidazo [4,5,1-de]acridin-6-on-5-yl)aminopropyl]-N-methylaminopropylamino]-1'-nitroacridine; CBL, chlorambucil; *cis*-DDP, cisplatin; CP, cyclophosphamide; Cys, L-cysteine; Glu, L-glutamic acid; Gly, glycine; GSH, L-γ-glutamyl-L-cysteinyl-glycine, glutathione (reduced form); GSSG, glutathione disulfide (oxidized form); GST, glutathione S-transferase; INF, infigratinib; MTC, mitomycin C; MTX, mitoxantrone; NO, nitric oxide; P450, cytochrome P450; ROS, reactive oxygen species; S_N2, bimolecular nucleophilic substitution reaction; S_NAr, aromatic nucleophilic substitution; UA, unsymmetrical bisacridine.

References

- Kumar, G.N.; Surapaneni, S. Role of drug metabolism in drug discovery and development. *Med. Res. Rev.* **2001**, *21*, 397–411. [CrossRef] [PubMed]
- Bachmann, K. Chapter 8—Drug Metabolism. In *Pharmacology: Principles and Practise*, 1st ed.; Hacker, M., Messer, W., Bachmann, K., Eds.; Academic Press: San Diego, CA, USA, 2009; pp. 131–173. [CrossRef]
- Penner, N.; Woodward, C.; Prakash, C. Drug Metabolizing Enzymes and Biotransformation Reactions. In *ADME-Enabling Technologies in Drug Design and Development*, 1st ed.; Zhang, D., Surapaneni, S., Eds.; John Wiley & Sons, Inc.: Hoboken, NJ, USA, 2012; pp. 545–565.
- Baillie, T.A. Cytochrome P450 and Other Enzymes in Drug Discovery and Development. In *Drug Metabolizing Enzymes*, 1st ed.; Lee, J., Obach, R.S., Fisher, M.B., Eds.; CRC Press, LLC: Boca Raton, FL, USA, 2003; pp. 147–154. [CrossRef]

5. Jančová, P.; Šiller, M. Phase II Drug Metabolism. In *Topics on Drug Metabolism*; Paxton, J., Ed.; IntechOpen: London, UK, 2012; pp. 35–60. [CrossRef]
6. Döring, B.; Petzinger, E. Phase 0 and phase III transport in various organs: Combined concept of phases in xenobiotic transport and metabolism. *Drug Metab. Rev.* **2014**, *46*, 261–282. [CrossRef] [PubMed]
7. Attia, S.M. Deleterious effects of reactive metabolites. *Oxidative Med. Cell. Longev.* **2010**, *3*, 238–253. [CrossRef] [PubMed]
8. Lushchak, V.I. Glutathione homeostasis and functions: Potential targets for medical interventions. *J. Amino Acids* **2012**, *2012*, 736837. [CrossRef]
9. Satoh, K. The high non-enzymatic conjugation rates of some glutathione S-transferase (GST) substrates at high glutathione concentrations. *Carcinogenesis* **1995**, *16*, 869–874. [CrossRef]
10. Deponte, M. Glutathione catalysis and the reaction mechanisms of glutathione-dependent enzymes. *Biochim. Biophys. Acta Gen. Sub.* **2013**, *1830*, 3217–3266. [CrossRef]
11. Armstrong, R.N. Structure, catalytic mechanism, and evolution of the glutathione transferases. *Chem. Res. Toxicol.* **1997**, *10*, 2–18. [CrossRef]
12. Dirven, H.A.A.M.; Megens, L.; Oudshoorn, M.J.; Dingemans, M.A.; Van Ommen, B.; Van Bladeren, P.J. Glutathione conjugation of the cytostatic drug ifosfamide and the role of human glutathione S-transferases. *Chem. Res. Toxicol.* **1995**, *8*, 979–986. [CrossRef]
13. Dirven, H.A.A.M.; Van Ommen, B.; Van Bladeren, P.J. Glutathione conjugation of alkylating cytostatic drugs with a nitrogen mustard group and the role of glutathione S-transferases. *Chem. Res. Toxicol.* **1996**, *9*, 351–360. [CrossRef]
14. Cnubben, N.H.; Rommens, A.J.; Oudshoorn, M.J.; Van Bladeren, P.J. Glutathione-dependent biotransformation of the alkylating drug thiotepa and transport of its metabolite monogluthionylthiotepa in human MCF-7 breast cancer cells. *Cancer Res.* **1998**, *58*, 4616–4623.
15. Zhang, K.; Wong, K.P.; Chow, P. Conjugation of chlorambucil with GSH by GST purified from human colon adenocarcinoma cells and its inhibition by plant polyphenols. *Life Sci.* **2003**, *72*, 2629–2640. [CrossRef]
16. Rossato, L.G.; Costa, V.M.; De Pinho, P.G.; Arbo, M.D.; De Freitas, V.; Vilain, L.; De Lourdes Bastos, M.; Palmeira, C.; Remião, F. The metabolic profile of mitoxantrone and its relation with mitoxantrone-induced cardiotoxicity. *Arch. Toxicol.* **2013**, *87*, 1809–1820. [CrossRef] [PubMed]
17. El Sayed, S.M.; Baghdadi, H.; Zolaly, M.; Almaramhy, H.H.; Ayat, M.; Donki, J.G. The promising anticancer drug 3-bromopyruvate is metabolized through glutathione conjugation which affects chemoresistance and clinical practice: An evidence-based view. *Med. Hypotheses* **2017**, *100*, 67–77. [CrossRef]
18. Cooper, A.J.L.; Hanigan, M.H. 10.17—Metabolism of Glutathione S-Conjugates: Multiple Pathways. In *Comprehensive Toxicology*, 3rd ed.; McQueen, C.A., Ed.; Elsevier Ltd.: Oxford, UK, 2018; pp. 363–406. [CrossRef]
19. Van Bladeren, P.J. Glutathione conjugation as a bioactivation reaction. *Chem. Biol. Interact.* **2000**, *129*, 61–76. [CrossRef]
20. Dekant, W. The Role of Biotransformation and Bioactivation in Toxicity. In *Molecular, Clinical and Environmental Toxicology*; Luch, A., Ed.; Experientia Supplementum: Basel, Switzerland, 2009; pp. 57–86.
21. Konopa, J.K.; Horowska, B.; Paluszkiwicz, E.M.; Borowa-Mazgaj, B.; Augustin, E.A.; Skwarska, A.; Mazerska, Z. Asymmetric Bis-Acridines with Antitumour Activity and Use Thereof. European Patent EP3070078A1, 4 October 2017.
22. Konopa, J.K.; Horowska, B.; Paluszkiwicz, E.M.; Borowa-Mazgaj, B.; Augustin, E.A.; Skwarska, A.; Mazerska, Z. Asymmetric Bis-Acridines with Antitumour Activity and Their Uses. United States Patent US10202349B2, 12 February 2019.
23. Kosno, M.; Laskowski, T.; Frackowiak, J.E.; Potęga, A.; Kurdyn, A.; Andrałojć, W.; Borzyszkowska-Bukowska, J.; Szwarc-Karabyka, K.; Mazerska, Z. Acid–base equilibrium and self-association in relation to high antitumor activity of selected unsymmetrical bisacridines established by extensive chemometric analysis. *Molecules* **2022**, *27*, 3995. [CrossRef]
24. Mieszkowska, A.; Nowicka, A.M.; Kowalczyk, A.; Potęga, A.; Pawłowska, M.; Kosno, M.; Augustin, E.; Mazerska, Z. Metabolic Profiles of new unsymmetrical bisacridine antitumor agents in electrochemical and enzymatic noncellular systems and in tumor cells. *Pharmaceuticals* **2021**, *14*, 317. [CrossRef] [PubMed]
25. Potęga, A.; Kosno, M.; Mazerska, Z. Novel insights into conjugation of antitumor-active unsymmetrical bisacridine C-2028 with glutathione: Characteristics of non-enzymatic and glutathione S-transferase-mediated reactions. *J. Pharm. Anal.* **2021**, *11*, 791–798. [CrossRef]
26. Paluszkiwicz, E.; Horowska, B.; Borowa-Mazgaj, B.; Peszyńska-Sularz, G.; Paradziej-Łukowicz, J.; Augustin, E.; Konopa, J.; Mazerska, Z. Design, synthesis and high antitumor potential of new unsymmetrical bisacridine derivatives towards human solid tumors, specifically pancreatic cancers and their unique ability to stabilize DNA G-quadruplexes. *Eur. J. Med. Chem.* **2020**, *204*, 11259. [CrossRef]
27. Chasseaud, L.F. The Role of Glutathione and Glutathione S-Transferases in the Metabolism of Chemical Carcinogens and Other Electrophilic Agents. In *Advances in Cancer Research*; Klein, G., Weinhouse, S., Eds.; Academic Press: San Diego, CA, USA, 1979; pp. 175–274. [CrossRef]
28. Anderson, M.E. Glutathione: An overview of biosynthesis and modulation. *Chem. Biol. Interact.* **1998**, *111–112*, 1–14. [CrossRef]
29. Lenton, K.J.; Therriault, H.; Wagner, J.R. Analysis of glutathione and glutathione disulfide in whole cells and mitochondria by postcolumn derivatization high-performance liquid chromatography with *ortho*-phthalaldehyde. *Anal. Biochem.* **1999**, *274*, 125–130. [CrossRef]
30. Meister, A. Glutathione metabolism and its selective modification. *J. Biol. Chem.* **1988**, *263*, 17205–17208. [CrossRef]

31. Josephy, P.D.; Mannervik, B. Biochemistry of Glutathione. In *Molecular Toxicology*, 2nd ed.; Oxford University Press, Inc.: New York, NY, USA, 2006; pp. 333–364.
32. Ballatori, N.; Krance, S.M.; Notenboom, S.; Shi, S.; Tieu, K.; Hammond, C.L. Glutathione dysregulation and the etiology and progression of human diseases. *Biol. Chem.* **2009**, *390*, 191–214. [CrossRef] [PubMed]
33. Townsend, D.M.; Tew, K.D.; Tapiero, H. The importance of glutathione in human disease. *Biomed. Pharmacother.* **2003**, *57*, 145–155. [CrossRef]
34. Ketterer, B.; Coles, B.; Meyer, D.J. The role of glutathione in detoxication. *Environ. Health Perspect.* **1983**, *49*, 59–69. [CrossRef] [PubMed]
35. Park, H.-A.; Khanna, S.; Rink, C.; Gnyawali, S.; Roy, S.; Sen, C.K. Glutathione disulfide induces neural cell death via a 12-lipoxygenase pathway. *Cell Death Differ.* **2009**, *16*, 1167–1179. [CrossRef] [PubMed]
36. Aldini, G.; Altomare, A.; Baron, G.; Vistoli, G.; Carini, M.; Borsani, L.; Sergio, F. N-Acetylcysteine as an antioxidant and disulphide breaking agent: The reasons why. *Free Radic. Res.* **2018**, *52*, 751–762. [CrossRef]
37. Jeffery, E.H. 2—Biochemical Basis of Toxicity. In *Handbook of Toxicologic Pathology*, 2nd ed.; Haschek, W.M., Rousseaux, C.G., Wallig, M.A., Eds.; Academic Press: San Diego, CA, USA, 2002; pp. 15–37. [CrossRef]
38. Ulrich, K.; Jakob, U. The role of thiols in antioxidant systems. *Free Radic. Biol. Med.* **2019**, *140*, 14–27. [CrossRef]
39. Xiong, Y.; Uys, J.D.; Tew, K.D.; Townsend, D.M. S-Glutathionylation: From molecular mechanisms to health outcomes. *Antioxid. Redox Signal.* **2011**, *15*, 233–270. [CrossRef]
40. Sies, H. Glutathione and its role in cellular functions. *Free Radic. Biol. Med.* **1999**, *27*, 916–921. [CrossRef]
41. Lu, S.C. Regulation of glutathione synthesis. *Mol. Aspects. Med.* **2009**, *30*, 42–59. [CrossRef]
42. Gomez, L.D.; Noctor, G.; Knight, M.R.; Foyer, C.H. Regulation of calcium signalling and gene expression by glutathione. *J. Exp. Bot.* **2004**, *55*, 1851–1859. [CrossRef] [PubMed]
43. Circu, M.L.; Aw, T.J. Glutathione and apoptosis. *Free Radic. Res.* **2009**, *42*, 689–706. [CrossRef] [PubMed]
44. Forman, H.J.; Zhang, H.; Rinna, A. Glutathione: Overview of its protective roles, measurement, and biosynthesis. *Mol. Asp. Med.* **2009**, *30*, 1–12. [CrossRef] [PubMed]
45. Arrick, B.A.; Nathan, C.F. Glutathione metabolism as a determinant of therapeutic efficacy: A review. *Cancer Res.* **1984**, *44*, 4224–4232.
46. Perrone, G.G.; Grant, C.M.; Dawes, I.W. Genetic and environmental factors influencing glutathione homeostasis in *Saccharomyces cerevisiae*. *Mol. Biol. Cell* **2005**, *16*, 218–230. [CrossRef]
47. Liu, X.; Zhang, S.; Whitworth, R.J.; Stuart, J.J.; Chen, M.-S. Unbalanced activation of glutathione metabolic pathways suggests potential involvement in plant defense against the gall midge *Mayetiola destructor* in wheat. *Sci. Rep.* **2015**, *5*, 8092. [CrossRef]
48. Meister, A. Glutathione; Metabolism and function via the γ -glutamyl cycle. *Life Sci.* **1974**, *15*, 177–190. [CrossRef]
49. Griffith, O.W. Biologic and pharmacologic regulation of mammalian glutathione synthesis. *Free Radic. Biol. Med.* **1999**, *27*, 922–935. [CrossRef]
50. Zhang, K.; Mack, P.; Wong, K.P. Glutathione-related mechanisms in cellular resistance to anticancer drugs. *Int. J. Oncol.* **1998**, *12*, 871–953. [CrossRef]
51. Cooper, A.J.L.; Hanigan, M.H. 4.17—Enzymes Involved in Processing Glutathione Conjugates. In *Comprehensive Toxicology*, 2nd ed.; McQueen, C.A., Ed.; Elsevier Ltd.: Oxford, UK, 2010; pp. 323–366. [CrossRef]
52. Ramsay, E.E.; Dilda, P.J. Glutathione S-conjugates as prodrugs to target drug-resistant tumors. *Front. Pharmacol.* **2014**, *5*, 181. [CrossRef]
53. Monks, T.J.; Anders, M.W.; Dekant, W.; Stevens, J.L.; Lau, S.S.; Van Bladeren, P.J. Glutathione conjugate mediated toxicities. *Toxicol. Appl. Pharmacol.* **1990**, *106*, 1–19. [CrossRef]
54. Toyoda, Y.; Takada, T.; Suzuki, H. Spontaneous production of glutathione-conjugated forms of 1,2-dichloropropane: Comparative study on metabolic activation processes of dihaloalkanes associated with occupational cholangiocarcinoma. *Oxidative Med. Cell. Longev.* **2017**, *2017*, 9736836. [CrossRef] [PubMed]
55. Cooper, A.J.L.; Pinto, J.T. Cysteine S-conjugate β -lyases. *Amino Acids* **2006**, *30*, 1–15. [CrossRef]
56. Ketterer, B.; Mulder, G.J. Glutathione Conjugation. In *Conjugation Reactions in Drug Metabolism*, 1st ed.; Mulder, G.J., Ed.; Taylor & Francis Ltd.: London, UK, 1990; pp. 307–364.
57. Li, J.C.; Renslo, A. Chapter 6: Nucleophilic Substitution, Addition, and Elimination Reactions. In *The Organic Chemistry of Medicinal Agents*; Renslo, A., Ed.; McGraw Hill: New York, NY, USA, 2016.
58. Ouellette, R.J.; Rawn, J.D. Nucleophilic Substitutions and Elimination Reactions. In *Organic Chemistry: Structure, Mechanism, Synthesis*, 2nd ed.; Ouellette, R.J., Rawn, J.D., Eds.; Academic Press: San Diego, CA, USA, 2018; pp. 299–319. [CrossRef]
59. Azevedo-Silva, J.; Queiros, O.; Baltazar, F.; Ułaszewski, S.; Goffeau, A.; Ko, Y.H.; Pedersen, P.L.; Preto, A.; Casal, M. The anticancer agent 3-bromopyruvate: A simple but powerful molecule taken from the lab to the bedside. *J. Bioenerg. Biomembr.* **2016**, *48*, 349–362. [CrossRef]
60. El Sayed, S.M.; Mohamed, W.G.; Seddik, M.-A.H.; Ahmed, A.-S.A.; Mahmoud, A.G.; Amer, W.H.; Helmy Nabo, M.M.; Hamed, A.R.; Ahmed, N.S.; Abd-Allah, A.A.-R. Safety and outcome of treatment of metastatic melanoma using 3-bromopyruvate: A concise literature review and case study. *Chin. J. Cancer.* **2014**, *33*, 356–364. [CrossRef]
61. Rai, Y.; Yadav, P.; Kumari, N.; Kalra, N.; Bhatt, A.N. Hexokinase II inhibition by 3-bromopyruvate sensitizes myeloid leukemic cells K-562 to anti-leukemic drug, daunorubicin. *Biosci. Rep.* **2019**, *39*, 1–18. [CrossRef] [PubMed]

62. Ganapathy-Kanniappan, S.; Geschwind, J.-F.H.; Kunjithapatham, R.; Buijs, M.; Vossen, J.A.; Tchernyshyov, I.; Cole, R.N.; Syed, L.H.; Rao, P.P.; Ota, S.; et al. Glyceraldehyde-3-phosphate dehydrogenase (GAPDH) is pyruvylated during 3-bromopyruvate mediated cancer cell death. *Anticancer Res.* **2009**, *29*, 4909–4918. [PubMed]
63. Fan, T.; Sun, G.; Sun, X.; Zhao, L.; Zhong, R.; Peng, Y. Tumor energy metabolism and potential of 3-bromopyruvate as an inhibitor of aerobic glycolysis: Implications in tumor treatment. *Cancers* **2019**, *11*, 317. [CrossRef]
64. Attia, Y.M.; El-Abhar, H.S.; Al Marzabani, M.M.; Shouman, S.A. Targeting glycolysis by 3-bromopyruvate improves tamoxifen cytotoxicity of breast cancer cell lines. *BMC Cancer* **2015**, *15*, 838. [CrossRef]
65. Karpusas, M.; Axarli, I.; Chiniadis, L.; Papakyriakou, A.; Bethanis, K.; Scopelidou, K.; Clonis, Y.D.; Labrou, N.E. The interaction of the chemotherapeutic drug chlorambucil with human glutathione transferase A1-1: Kinetic and structural analysis. *PLoS ONE* **2013**, *8*, e56337. [CrossRef]
66. Fischer, G.; Sieber, M.; Schellenberger, A. The carbonyl reactivity of 3-bromopyruvate and related compounds. *Bioorg. Chem.* **1982**, *11*, 478–484. [CrossRef]
67. Sadowska-Bartosz, I.; Szewczyk, R.; Jaremko, L.; Jaremko, M.; Bartosz, G. Anticancer agent 3-bromopyruvic acid forms a conjugate with glutathione. *Pharmacol. Rep.* **2016**, *68*, 502–505. [CrossRef] [PubMed]
68. Goede, V.; Eichhorst, B.; Fischer, K.; Wendtner, C.-M.; Hallek, M. Past, present and future role of chlorambucil in the treatment of chronic lymphocytic leukemia. *Leuk. Lymphoma* **2015**, *56*, 1585–1592. [CrossRef]
69. Leblond, V.; Johnson, S.; Chevret, S.; Coppelstone, A.; Rule, S.; Tournilhac, O.; Seymour, J.F.; Patmore, R.D.; Wright, D.; Morel, P.; et al. Results of a randomized trial of chlorambucil versus fludarabine for patients with untreated Waldenström macroglobulinemia, marginal zone lymphoma, or lymphoplasmacytic lymphoma. *J. Clin. Oncol.* **2013**, *31*, 301–307. [CrossRef] [PubMed]
70. Ardesna, K.M.; Smith, P.; Norton, A.; Hancock, B.W.; Hoskin, P.J.; MacLennan, K.A.; Marcus, R.E.; Jelliffe, A.; Vaughan Hudson, G.; Linch, D.C. Long-term effect of a watch and wait policy versus immediate systemic treatment for asymptomatic advanced-stage non-Hodgkin lymphoma: a randomised controlled trial. *Lancet* **2003**, *362*, 516–522. [CrossRef]
71. Parker, L.J.; Ciccone, S.; Italiano, L.C.; Primavera, A.; Oakley, A.J.; Morton, C.J.; Hancock, N.C.; Lo Bello, M.; Parker, M.W. The anti-cancer drug chlorambucil as a substrate for the human polymorphic enzyme glutathione transferase P1-1: Kinetic properties and crystallographic characterisation of allelic variants. *J. Mol. Biol.* **2008**, *380*, 131–144. [CrossRef]
72. Cobb, D.; Boehlert, C.; Lewis, D.; Armstrong, R.N. Stereoselectivity of isozyme C of glutathione S-transferase toward arene and azaarene oxides. *Biochemistry* **1983**, *22*, 805–812. [CrossRef]
73. Andrew, A.W.; Hayes, W.; Kruger, C.L. *Hayes' Principles and Methods of Toxicology*; CRC Press, LLC: Boca Raton, FL, USA, 2014; p. 71.
74. Hassan, F.; Preiss, R. Cyclophosphamide and related anticancer drugs. *J. Chromatogr. B Biomed. Appl.* **2001**, *764*, 173–192. [CrossRef]
75. Singh, R.K.; Kumar, S.; Prasad, D.N.; Bhardwaj, T.R. Therapeutic journey of nitrogen mustard as alkylating anticancer agents: Historic to future perspectives. *Eur. J. Med. Chem.* **2018**, *151*, 401–433. [CrossRef]
76. Colvin, O.M. An overview of cyclophosphamide development and clinical applications. *Curr. Pharm. Des.* **1999**, *5*, 555–560.
77. Hubbard, R.D.; Fidanze, S. 7.06—Alkylating and Platinum Antitumor Compounds. In *Comprehensive Medicinal Chemistry II*; Taylor, J.B., Triggle, D.J., Eds.; Elsevier Ltd.: Oxford, UK, 2007; pp. 129–148. [CrossRef]
78. Ahlmann, M.; Hempel, G. The effect of cyclophosphamide on the immune system: Implications for clinical cancer therapy. *Cancer Chemother. Pharmacol.* **2016**, *78*, 661–671. [CrossRef] [PubMed]
79. Bagley, C.M.; Bostick, F.W.; DeVita, V.T. Clinical pharmacology of cyclophosphamide. *Cancer Res.* **1973**, *33*, 226–233. [PubMed]
80. Li, F.; Patterson, A.D.; Höfer, C.C.; Krausz, K.W.; Gonzalez, F.J.; Idle, J.R. Comparative metabolism of cyclophosphamide and ifosfamide in the mouse using UPLC-ESI-QTOFMS-based metabolomics. *Biochem. Pharmacol.* **2010**, *80*, 1063–1074. [CrossRef]
81. Groehler, A.; Villalta, P.W.; Campbell, C.; Tretyakova, N. Covalent DNA-protein cross-linking by phosphoramidate mustard and nornitrogen mustard in human cells. *Chem. Res. Toxicol.* **2016**, *29*, 190–202. [CrossRef] [PubMed]
82. Mills, K.A.; Chess-Williams, R.; McDermott, C. Novel insights into the mechanism of cyclophosphamide-induced bladder toxicity: Chloroacetaldehyde's contribution to urothelial dysfunction in vitro. *Arch. Toxicol.* **2019**, *93*, 3291–3303. [CrossRef] [PubMed]
83. Yuan, Z.M.; Smith, P.B.; Brundrett, R.B.; Colvin, M.; Fenselau, C. Glutathione conjugation with phosphoramidate mustard and cyclophosphamide. A mechanistic study using tandem mass spectrometry. *Drug Metab. Dispos.* **1991**, *19*, 625–629. [PubMed]
84. Cohen, N.A.; Egorin, M.J.; Snyder, S.W.; Ashar, B.; Wietharn, B.E.; Pan, S.S.; Ross, D.D.; Hilton, J. Interaction of N,N',N''-triethylenethiophosphoramidate and N,N',N''-triethylenephosphoramidate with cellular DNA. *Cancer Res.* **1991**, *51*, 4360–4366.
85. Van der Wall, E.; Beijnen, J.H.; Rodenhuis, S. High-dose chemotherapy regimens for solid tumors. *Cancer Treat. Rev.* **1995**, *21*, 105–132. [CrossRef]
86. Van Maanen, M.J.; Smeets, C.J.M.; Beijnen, J.H. Chemistry, pharmacology and pharmacokinetics of N,N',N''-triethylenethiophosphoramidate (ThioTEPA). *Cancer Treat. Rev.* **2000**, *26*, 257–268. [CrossRef]
87. Torabifard, H.; Fattahi, A. DFT study on Thiotepa and Tepa interactions with their DNA receptor. *Struct. Chem.* **2013**, *24*, 1–11. [CrossRef]
88. Jacobson, P.A.; Green, K.; Birnbaum, A.; Rimmel, R.P. Cytochrome P450 isozymes 3A4 and 2B6 are involved in the in vitro human metabolism of thiotepa to TEPA. *Cancer Chemother. Pharmacol.* **2002**, *49*, 461–467. [CrossRef] [PubMed]

89. Dirven, H.A.A.M.; Dictus, E.L.J.T.; Broeders, N.L.H.L.; Van Ommen, B.; Van Bladeren, P.J. The role of human glutathione S-transferase isoenzymes in the formation of glutathione conjugates of the alkylating cytostatic drug thiotepa. *Cancer Res.* **1995**, *55*, 1701–1706. [PubMed]
90. Galanski, M.; Jakupec, M.A.; Keppler, B.K. Update of the preclinical situation of anticancer platinum complexes: Novel design strategies and innovative analytical approaches. *Curr. Med. Chem.* **2005**, *12*, 2075–2094. [CrossRef] [PubMed]
91. Florea, A.-M.; Büsselberg, D. Cisplatin as an anti-tumor drug: Cellular mechanisms of activity, drug resistance and induced side effects. *Cancers* **2011**, *3*, 1351–1371. [CrossRef]
92. Dasari, S.; Tchounwou, P.B. Cisplatin in cancer therapy: Molecular mechanisms of action. *Eur. J. Pharmacol.* **2014**, *740*, 364–378. [CrossRef]
93. Makowiec, T. Cisplatin and beyond: Molecular mechanisms of action and drug resistance development in cancer chemotherapy. *Radiol. Oncol.* **2019**, *53*, 148–158. [CrossRef]
94. Todd, R.C.; Lippard, S.J. Inhibition of transcription by platinum antitumor compounds. *Metallomics* **2009**, *1*, 280–291. [CrossRef]
95. Segal, E.; Le Pecq, J.B. Role of ligand exchange processes in the reaction kinetics of the antitumor drug cis-diamminedichloroplatinum(II) with its targets. *Cancer Res.* **1985**, *45*, 492–498.
96. Klein, A.V.; Hambley, T.W. Platinum drug distribution in cancer cells and tumors. *Chem. Rev.* **2009**, *109*, 4911–4920. [CrossRef]
97. Casini, A.; Reedijk, J. Interactions of anticancer Pt compounds with proteins: An overlooked topic in medicinal inorganic chemistry? *Chem. Sci.* **2012**, *3*, 3135–3144. [CrossRef]
98. Corinti, D.; Paciotti, R.; Re, N.; Coletti, C.; Chiavarino, B.; Crestoni, M.E.; Fornarini, S. Binding motifs of cisplatin interaction with simple biomolecules and aminoacid targets probed by IR ion spectroscopy. *Pure Appl. Chem.* **2020**, *92*, 3–13. [CrossRef]
99. Aldossary, S.A. Review on pharmacology of cisplatin: Clinical use, toxicity and mechanism of resistance of cisplatin. *Biomed. Pharmacol. J.* **2019**, *12*, 7–15. [CrossRef]
100. Ishikawa, T.; Ali-Osman, F. Glutathione-associated cis-diamminedichloroplatinum(II) metabolism and ATP-dependent efflux from leukemia cells. Molecular characterization of glutathione-platinum complex and its biological significance. *J. Biol. Chem.* **1993**, *268*, 20116–20125. [CrossRef]
101. Nagar, R.; Khan, A.R.; Poonia, A.; Mishra, P.K.; Singh, S. Metabolism of cisplatin in the organs of Rattus norvegicus: Role of glutathione S-transferase P1. *Eur. J. Drug Metab. Pharmacokinet.* **2015**, *40*, 45–51. [CrossRef] [PubMed]
102. Rabik, C.A.; Dolan, M.E. Molecular mechanisms of resistance and toxicity associated with platinating agents. *Cancer Treat. Rev.* **2007**, *33*, 9–23. [CrossRef] [PubMed]
103. Moyer, A.M.; Sun, Z.; Batzler, A.J.; Li, L.; Schaid, D.J.; Yang, P.; Weinshilboum, R.M. Glutathione pathway genetic polymorphisms and lung cancer survival after platinum-based chemotherapy. *Cancer Epidemiol. Biomarkers Prev.* **2010**, *19*, 811–821. [CrossRef]
104. Zhou, J.; Kang, Y.; Chen, L.; Wang, H.; Liu, J.; Zeng, S.; Yu, L. The drug-resistance mechanisms of five platinum-based antitumor agents. *Front. Pharmacol.* **2020**, *11*, 343. [CrossRef]
105. Temellini, A.; Castiglioni, M.; Giuliani, L.; Mussi, A.; Giulianotti, P.C.; Pietrabissa, A.; Angeletti, C.A.; Mosca, F.; Pacifici, G.M. Glutathione conjugation with 1-chloro-2,4-dinitrobenzene (CDNB): Interindividual variability in human liver, lung, kidney and intestine. *Int. J. Clin. Pharmacol. Ther.* **1995**, *33*, 498–503.
106. Kwan, E.E.; Zeng, Y.; Besser, H.A.; Jacobsen, E.N. Concerted nucleophilic aromatic substitutions. *Nat. Chem.* **2018**, *10*, 917–923. [CrossRef]
107. Ji, X.; Pal, A.; Kalathur, R.; Hu, X.; Gu, Y.; Saavedra, J.E.; Buzard, G.S.; Srinivasan, A.; Keefer, L.K.; Singh, S.V. Structure-based design of anticancer prodrug PABA/NO. *Drug Des. Dev. Ther.* **2008**, *2*, 123–130. [CrossRef]
108. Findlay, V.J.; Townsend, D.M.; Saavedra, J.E.; Buzard, G.S.; Citro, M.L.; Keefer, L.K.; Ji, X.; Tew, K.D. Tumor cell responses to a novel glutathione S-transferase-activated nitric oxide-releasing prodrug. *Mol. Pharmacol.* **2004**, *65*, 1070–1079. [CrossRef] [PubMed]
109. Saavedra, J.E.; Srinivasan, A.; Buzard, G.S.; Davies, K.M.; Waterhouse, D.J.; Inami, K.; Wilde, T.C.; Citro, M.L.; Cuellar, M.; Deschamps, J.R.; et al. PABA/NO as an anticancer lead: Analogue synthesis, structure revision, solution chemistry, reactivity toward glutathione, and in vitro activity. *J. Med. Chem.* **2006**, *49*, 1157–1164. [CrossRef] [PubMed]
110. Hutchens, S.; Manevich, Y.; He, L.; Tew, K.D.; Townsend, D.M. Cellular resistance to a nitric oxide releasing glutathione S-transferase P-activated prodrug, PABA/NO. *Investig. New Drugs* **2011**, *29*, 719–729. [CrossRef] [PubMed]
111. Saavedra, J.E.; Srinivasan, A.; Bonifant, C.L.; Chu, J.; Shanklin, A.P.; Flippen-Anderson, J.L.; Rice, W.G.; Turpin, J.A.; Davies, K.M.; Keefer, L.K. The secondary amine/as nucleophile and leaving nitric oxide complex ion $R_2N[N(O)NO]^-$ group in S_NAr reactions. *J. Org. Chem.* **2001**, *66*, 3090–3098. [CrossRef] [PubMed]
112. Rickert, D.E. Metabolism of nitroaromatic compounds. *Drug Metab. Rev.* **1987**, *18*, 23–53. [CrossRef]
113. Rusinov, V.L.; Sapozhnikova, I.M.; Ulomskii, E.N.; Medvedeva, N.R.; Egorov, V.V.; Kiselev, O.I.; Deeva, E.G.; Vasin, A.V.; Chupakhin, O.N. Nucleophilic substitution of nitro group in nitrotriazolotriazines as a model of potential interaction with cysteine-containing proteins. *Chem. Heterocycl. Compd.* **2015**, *51*, 275–280. [CrossRef]
114. Schwöbel, J.A.H.; Wondrousch, D.; Koleva, Y.K.; Madden, J.C.; Cronin, M.T.D.; Schüürmann, G. Prediction of Michael-type acceptor reactivity toward glutathione. *Chem. Res. Toxicol.* **2010**, *23*, 1576–1585. [CrossRef]
115. Ruzza, P.; Calderan, A. Glutathione transferase (GST)-activated prodrugs. *Pharmaceutics* **2013**, *5*, 220–231. [CrossRef]
116. Schultz, T.W.; Yarbrough, J.W.; Hunter, R.S.; Aptula, A.O. Verification of the structural alerts for Michael acceptors. *Chem. Res. Toxicol.* **2007**, *20*, 1359–1363. [CrossRef]

117. Evison, B.J.; Sleebs, B.E.; Watson, K.G.; Phillips, D.R.; Cutts, S.M. Mitoxantrone, more than just another topoisomerase II poison. *Med. Res. Rev.* **2016**, *36*, 248–299. [CrossRef]
118. Hainswort, J.D.; Andrews, M.B.; Johnson, D.H.; Greco, F.A. Mitoxantrone, fluorouracil, and high-dose leucovorin: An effective, well-tolerated regimen for metastatic breast cancer. *J. Clin. Oncol.* **1991**, *9*, 1731–1735. [CrossRef] [PubMed]
119. Basch, E.M.; Scholz, M.; De Bono, J.S.; Vogelzang, N.; De Souza, P.; Marx, G.; Vaishampayan, U.; George, S.; Schwarz, J.K.; Antonarakis, E.S.; et al. Cabozantinib versus mitoxantrone-prednisone in symptomatic metastatic castration-resistant prostate cancer: A randomized Phase 3 trial with a primary pain endpoint. *Eur. Urol.* **2019**, *75*, 929–937. [CrossRef] [PubMed]
120. Nastoupil, L.J.; McLaughlin, P.; Feng, L.; Neelapu, S.S.; Samaniego, F.; Hagemester, F.B.; Ayala, A.; Romaguera, J.E.; Goy, A.H.; Neal, E.; et al. High ten-year remission rates following rituximab, fludarabine, mitoxantrone and dexamethasone (R-FND) with interferon maintenance in indolent lymphoma: Results of a randomized study. *Br. J. Haematol.* **2017**, *177*, 263–270. [CrossRef] [PubMed]
121. Advani, A.S.; Cooper, B.; Visconte, V.; Elson, P.; Chan, R.; Carew, J.; Wei, W.; Mukherjee, S.; Gerds, A.; Carraway, H.; et al. A Phase I/II trial of MEC (Mitoxantrone, Etoposide, Cytarabine) in combination with ixazomib for relapsed refractory acute myeloid leukemia. *Clin. Cancer Res.* **2019**, *25*, 4231–4237. [CrossRef]
122. Mewes, K.; Blanz, J.; Ehninger, G.; Gebhardt, R.; Zeller, K.-P. Cytochrome P-450-induced cytotoxicity of mitoxantrone by formation of electrophilic intermediates. *Cancer Res.* **1993**, *53*, 5135–5142.
123. Guagnano, V.; Furet, P.; Spanka, C.; Bordas, V.; Le Douget, M.; Stamm, C.; Brueggen, J.; Jensen, M.R.; Schnell, C.; Schmid, H.; et al. Discovery of 3-(2,6-dichloro-3,5-dimethoxy-phenyl)-1-{6-[4-(4-ethyl-piperazin-1-yl)-phenylamino]-pyrimidin-4-yl}-1-methyl-urea (NVP-BGJ398), a potent and selective inhibitor of the fibroblast growth factor receptor family of receptor tyrosine kinase. *J. Med. Chem.* **2011**, *27*, 7066–7083. [CrossRef]
124. Komla-Ebri, D.; Dambrose, E.; Kramer, I.; Benoist-Lassel, C.; Kaci, N.; Le Gall, C.; Martin, L.; Busca, P.; Barbault, F.; Graus-Porta, D.; et al. Tyrosine kinase inhibitor NVP-BGJ398 functionally improves FGFR3-related dwarfism in mouse model. *J. Clin. Investig.* **2016**, *126*, 1871–1884. [CrossRef]
125. Javle, M.; Lowery, M.; Shroff, R.T.; Weiss, K.H.; Springfield, C.; Borad, M.J.; Ramanathan, R.K.; Goyal, L.; Sadeghi, S.; Macarulla, T.; et al. Phase II Study of BGJ398 in patients with FGFR-altered advanced cholangiocarcinoma. *J. Clin. Oncol.* **2018**, *36*, 276–282. [CrossRef]
126. Al-Shakliah, N.S.; Attwa, M.W.; Kadi, A.A.; AlRabiah, H. Identification and characterization of in silico, in vivo, in vitro, and reactive metabolites of infigratinib using LC-ITMS: Bioactivation pathway elucidation and in silico toxicity studies of its metabolites. *RSC Adv.* **2020**, *10*, 16231–16244. [CrossRef]
127. Zhao, Z.; Koeplinger, K.A.; Padbury, G.E.; Hauer, M.J.; Bundy, G.L.; Banitt, L.S.; Schwartz, T.M.; Zimmermann, D.C.; Harbach, P.R.; Mayo, J.K. Bioactivation of 6,7-dimethyl-2,4-di-1-pyrrolidinyl-7h-pyrrolo[2,3-d]pyrimidine (U-89843) to reactive intermediates that bind covalently to macromolecules and produce genotoxicity. *Chem. Res. Toxicol.* **1996**, *9*, 1230–1239. [CrossRef]
128. Lyss, G.; Schmidt, T.J.; Merfort, I.; Pahl, H.L. Helenalin, an anti-inflammatory sesquiterpene lactone from Arnica, selectively inhibits transcription factor NF- κ B. *Biol. Chem.* **1997**, *378*, 951–962. [CrossRef] [PubMed]
129. Lim, C.B.; Fu, P.Y.; Ky, N.; Zhu, H.S.; Feng, X.L.; Li, J.; Srinivasan, K.G.; Hamza, M.S.; Zhao, Y. NF- κ B p65 repression by the sesquiterpene lactone, helenalin, contributes to the induction of autophagy cell death. *BMC Complement. Altern. Med.* **2012**, *12*, 93. [CrossRef] [PubMed]
130. Jakobs, A.; Steinmann, S.; Henrich, S.M.; Schmidt, T.J.; Klempnaue, K.H. Helenalin acetate, a natural sesquiterpene lactone with anti-inflammatory and anti-cancer activity, disrupts the cooperation of CCAAT box/enhancer-binding protein β (C/EBP β) and co-activator p300. *J. Biol. Chem.* **2016**, *9*, 26098–26108. [CrossRef] [PubMed]
131. Jürgens, F.M.; Behrens, M.; Humpf, H.-U.; Robledo, S.M.; Schmidt, T.J. In vitro metabolism of helenalin acetate and 11 α ,13-dihydrohelenalin acetate: Natural sesquiterpene lactones from Arnica. *Metabolites* **2022**, *12*, 88. [CrossRef]
132. Schmidt, T.J. Glutathione adducts of helenalin and 11 α ,13-dihydrohelenalin acetate inhibit glutathione S-transferase from horse liver. *Planta Med.* **2000**, *66*, 106–109. [CrossRef] [PubMed]
133. Lang, W.; Caldwell, G.W.; Masucci, J.A. Evaluation of the effect of oxygen exposure on human liver microsomal metabolism of mitomycin C in the presence of glutathione using liquid chromatography–quadrupole time of flight mass spectrometry. *Anal. Biochem.* **2005**, *343*, 268–276. [CrossRef]
134. Verweij, J.; Pinedo, H.M. Mitomycin C: Mechanism of action, usefulness and limitations. *Anticancer Drugs* **1990**, *1*, 5–13. [CrossRef]
135. Tomasz, M. Mitomycin C: Small, fast and deadly (but very selective). *Chem. Biol.* **1995**, *2*, 575–579. [CrossRef]
136. Avendaño, C.; Menéndez, J.C. Chapter 6 Anticancer Drugs That Interact with the DNA Minor Groove. In *Medicinal Chemistry of Anticancer Drugs*, 2nd ed.; Avendaño, C., Menéndez, J.C., Eds.; Elsevier Ltd.: Oxford, UK, 2015; pp. 243–271. [CrossRef]
137. Sharma, M.; Tomasz, M. Conjugation of glutathione and other thiols with bioreductively activated mitomycin C. Effect of thiols on the reductive activation. *Chem. Res. Toxicol.* **1994**, *7*, 390–400. [CrossRef]
138. Shibata, Y.; Chiba, M. The role of extrahepatic metabolism in the pharmacokinetics of the targeted covalent inhibitors afatinib, ibrutinib, and neratinib. *Drug Metab. Dispos.* **2015**, *43*, 375–384. [CrossRef]
139. Rood, J.J.M.; Dormans, P.J.A.; Van Haren, M.J.; Schellens, J.H.M.; Beijnen, J.H.; Sparidans, R.W. Bioanalysis of ibrutinib, and its dihydrodiol- and glutathione cycle metabolites by liquid chromatography–tandem mass spectrometry. *J. Chromatogr. B* **2018**, *1090*, 14–21. [CrossRef] [PubMed]

140. Piesche, M.; Roos, J.; Kühn, B.; Fettel, J.; Hellmuth, N.; Brat, C.; Maucher, I.V.; Awad, O.; Matrone, C.; Comerma Steffensen, S.G.; et al. The emerging therapeutic potential of nitro fatty acids and other Michael acceptor-containing drugs for the treatment of inflammation and cancer. *Front. Pharmacol.* **2020**, *11*, 1297. [CrossRef] [PubMed]
141. Hayes, J.D.; Flanagan, J.U.; Jowsey, I.R. Glutathione transferases. *Annu. Rev. Pharmacol. Toxicol.* **2005**, *45*, 51–88. [CrossRef]
142. Bansal, A.; Simon, M. Glutathione metabolism in cancer progression and treatment resistance. *J. Cell Biol.* **2018**, *217*, 2291. [CrossRef] [PubMed]
143. Desideri, E.; Ciccarone, F.; Ciriolo, M.R. Targeting glutathione metabolism: Partner in crime in anticancer therapy. *Nutrients* **2019**, *11*, 1926. [CrossRef]
144. Cazenave, L.A.; Moscow, J.A.; Myers, C.E.; Cowan, K.H. Glutathione S-transferase and drug resistance. *Cancer Treat. Res.* **1989**, *48*, 171–187. [CrossRef]
145. Townsend, D.M.; Tew, K.D. The role of glutathione-S-transferase in anti-cancer drug resistance. *Oncogene* **2003**, *22*, 7369–7375. [CrossRef]
146. Damia, G.; D’Incalci, M. Mechanisms of resistance to alkylating agents. *Cytotechnology* **1998**, *27*, 165–173. [CrossRef]
147. Bukowski, K.; Kciuk, M.; Kontek, R. Mechanisms of multidrug resistance in cancer chemotherapy. *Int. J. Mol. Sci.* **2020**, *21*, 3233. [CrossRef]
148. Highley, M.S.; Landuyt, B.; Prenen, H.; Harper, P.C.; De Bruijn, E.A. The Nitrogen Mustards. *Pharmacol. Rev.* **2022**, *74*, 552–599. [CrossRef]
149. Pieńkowska, N.; Bartosz, G.; Furdak, P.; Sadowska-Bartosz, I. Delphinidin increases the sensitivity of ovarian cancer cell lines to 3-bromopyruvate. *Int. J. Mol. Sci.* **2021**, *22*, 709. [CrossRef] [PubMed]
150. Johnston, J.B.; Israels, L.G.; Goldenberg, G.J.; Anhalt, C.D.; Verburg, L.; Mowat, M.R.; Begleiter, A. Glutathione S-transferase activity, sulfhydryl group and glutathione levels, and DNA cross-linking activity with chlorambucil in chronic lymphocytic leukemia. *J. Natl. Cancer Inst.* **1990**, *82*, 776–779. [CrossRef]
151. Niedźwiecka, K.; Dyląg, M.; Augustyniak, D.; Majkowska-Skrobek, G.; Cal-Bąkowska, M.; Ko, Y.H.; Pedersen, P.L.; Goffeau, A.; Ułaszewski, S. Glutathione may have implications in the design of 3-bromopyruvate treatment protocols for both fungal and algal infections as well as multiple myeloma. *Oncotarget* **2016**, *7*, 65614–65626. [CrossRef] [PubMed]
152. Dirven, H.A.; Van Ommen, B.; Van Bladeren, P.J. Involvement of human glutathione S-transferase isoenzymes in the conjugation of cyclophosphamide metabolites with glutathione. *Cancer Res.* **1994**, *54*, 6215–6220. [PubMed]
153. Ekhardt, C.; Rodenhuis, S.; Smits, P.H.M.; Beijnen, J.H.; Huitema, A.D.R. Relations between polymorphisms in drug-metabolising enzymes and toxicity of chemotherapy with cyclophosphamide, thiotepa and carboplatin. *Pharmacogenet. Genom.* **2008**, *18*, 1009–1015. [CrossRef]
154. Kennedy, L.; Sandhu, J.K.; Harper, M.E.; Cuperlovic-Culf, M. Role of glutathione in cancer: From mechanisms to therapies. *Biomolecules* **2020**, *10*, 1429. [CrossRef]
155. Dixon, S.J.; Lemberg, K.M.; Lamprecht, M.R.; Skouta, R.; Zaitsev, E.M.; Gleason, C.E.; Patel, D.N.; Bauer, A.J.; Cantley, A.M.; Yang, W.S.; et al. Ferroptosis: An iron-dependent form of nonapoptotic cell death. *Cell* **2012**, *149*, 1060–1072. [CrossRef]
156. Zhang, C.; Liu, X.; Jin, S.; Chen, Y.; Guo, R. Ferroptosis in cancer therapy: A novel approach to reversing drug resistance. *Mol. Cancer* **2022**, *21*, 47. [CrossRef]
157. Shimada, K.; Skouta, R.; Viswanathan, V.S.; Cheah, J.H.; Clemons, P.A.; Shamji, A.F.; Clish, C.B.; Brown, L.M.; Girotti, A.W.; Cornish, V.W.; et al. Regulation of ferroptotic cancer cell death by GPX4. *Cell* **2014**, *156*, 317–331. [CrossRef]
158. Cao, J.Y.; Poddar, A.; Magtanong, L.; Lumb, J.H.; Mileur, T.R.; Reid, M.A.; Dovey, C.M.; Wang, J.; Locasale, J.W.; Stone, E.; et al. A genome-wide haploid genetic screen identifies regulators of glutathione abundance and ferroptosis sensitivity. *Cell Rep.* **2019**, *26*, 1544–1556. [CrossRef]
159. James, L.P.; Mayeux, P.R.; Hinson, J.A. Acetaminophen-induced hepatotoxicity. *Drug Metab. Dispos.* **2003**, *31*, 1499–1506. [CrossRef] [PubMed]
160. Modén, O.; Mannervik, B. Glutathione transferases in the bioactivation of azathioprine. *Adv. Cancer Res.* **2014**, *122*, 199–244. [CrossRef] [PubMed]
161. Liu, R.; Zhou, F.; He, H.; Wei, J.; Tian, X.; Ding, L. Metabolism and bioactivation of corynoline with characterization of the glutathione/cysteine conjugate and evaluation of its hepatotoxicity in mice. *Front. Pharmacol.* **2018**, *9*, 1264. [CrossRef]
162. Townsend, D.M.; Deng, M.; Zhang, L.; Lopus, M.G.; Hanigan, M.H. Metabolism of cisplatin to a nephrotoxin in proximal tubule cells. *J. Am. Soc. Nephrol.* **2003**, *14*, 1–10. [CrossRef] [PubMed]
163. Manohar, S.; Leung, N. Cisplatin nephrotoxicity: A review of the literature. *J. Nephrol.* **2018**, *31*, 15–25. [CrossRef] [PubMed]
164. Zhang, L.; Hanigan, M.H. Role of cysteine S-conjugate β -lyase in the metabolism of cisplatin. *J. Pharmacol. Exp. Ther.* **2003**, *306*, 988–994. [CrossRef] [PubMed]
165. Hassan, M.; Ljungman, P.; Ringdén, O.; Öberg, G.; Nilsson, C.; Békassy, A.; Bielenstein, M.; Abdel-Rehim, M.; Georén, S.; Astner, L. The effect of busulphan on the pharmacokinetics of cyclophosphamide and its 4-hydroxy metabolite: Time interval influence on therapeutic efficacy and therapy-related toxicity. *Bone Marrow Transplant.* **2000**, *25*, 915–924. [CrossRef]
166. Hassan, M.; Andersson, B.S. Role of pharmacogenetics in busulfan/cyclophosphamide conditioning therapy prior to hematopoietic stem cell transplantation. *Pharmacogenomics* **2013**, *14*, 75–87. [CrossRef]

167. Pidala, J.; Kim, J.; Anasetti, C.; Kharfan-Dabaja, M.A.; Nishihori, T.; Field, T.; Perkins, J.; Perez, L.; Fernandez, H.F. Pharmacokinetic targeting of intravenous busulfan reduces conditioning regimen related toxicity following allogeneic hematopoietic cell transplantation for acute myelogenous leukemia. *J. Hematol. Oncol.* **2010**, *3*, 36. [CrossRef]
168. Busulfan. In *Meyler's Side Effects of Drugs*, 16th ed.; Aronson, J.K. (Ed.) Elsevier Ltd.: Oxford, UK, 2016; pp. 1100–1103. [CrossRef]
169. Czerwinski, M.; Gibbs, J.P.; Slattery, J.T. Busulfan conjugation by glutathione S-transferases alpha, mu, and pi. *Drug Metab. Dispos.* **1996**, *24*, 1015–1019.
170. Scian, M.; Atkins, W.M. The busulfan metabolite EdAG irreversibly glutathionylates glutaredoxins. *Arch. Biochem. Biophys.* **2015**, *583*, 96–104. [CrossRef] [PubMed]
171. Younis, I.R.; Elliott, M.; Peer, C.J.; Cooper, A.J.; Pinto, J.T.; Konat, G.W.; Kraszpulski, M.; Petros, W.P.; Callery, P.S. Dehydroalanine analog of glutathione: An electrophilic busulfan metabolite that binds to human glutathione S-transferase A1-1. *J. Pharmacol. Exp. Ther.* **2008**, *327*, 770–776. [CrossRef]
172. Rautio, J.; Kumpulainen, H.; Heimbach, T.; Oliyai, R.; Oh, D.; Järvinen Jo, T.; Savolainen, J. Prodrugs: Design and clinical applications. *Nat. Rev. Drug Discov.* **2008**, *7*, 255–270. [CrossRef] [PubMed]
173. Geary, R.B.; Barclay, M.L. Azathioprine and 6-mercaptopurine pharmacogenetics and metabolite monitoring in inflammatory bowel disease. *J. Gastroenterol. Hepatol.* **2005**, *20*, 1149–1157. [CrossRef]
174. Kurtovic, S.; Modén, O.; Shokeer, A.; Mannervik, B. Structural determinants of glutathione transferases with azathioprine activity identified by DNA shuffling of alpha class members. *J. Mol. Biol.* **2008**, *375*, 1365–1379. [CrossRef] [PubMed]
175. Eklund, B.I.; Moberg, M.; Bergquist, J.; Mannervik, B. Divergent activities of human glutathione transferases in the bioactivation of azathioprine. *Mol. Pharmacol.* **2006**, *70*, 747–754. [CrossRef]
176. Lee, A.U.; Farrell, G.C. Mechanism of azathioprine-induced injury to hepatocytes: Roles of glutathione depletion and mitochondrial injury. *J. Hepatol.* **2001**, *35*, 756–764. [CrossRef]
177. Munshi, N.C.; Seitz, D.E.; Fossella, F.; Lippman, S.M.; Einhorn, L.H. Phase II study of sulofenur (LY 186641). A novel antineoplastic agent in advanced non-small cell lung cancer. *Investig. New Drugs* **1993**, *11*, 87–90. [CrossRef]
178. Houghton, P.J.; Houghton, J.A. Antitumor diarylsulfonylureas: Novel agents with unfulfilled promise. *Investig. New Drugs* **1996**, *14*, 271–280. [CrossRef]
179. Ehlhardt, W.J.; Woodland, J.M.; Worzalla, J.F.; Bewley, J.R.; Grindey, G.B.; Todd, G.C.; Toth, J.E.; Howbert, J.J. Comparison of metabolism and toxicity to the structure of the anticancer agent sulofenur and related sulfonylureas. *Chem. Res. Toxicol.* **1992**, *5*, 667–673. [CrossRef]
180. Phelps, P.C.; Best, C.J.M.; Berezsky, I.K.; Merriman, R.L.; Tanzer, L.R.; Boder, G.B.; Trump, B.F. Studies on the mechanism of sulofenur and LY295501 toxicity: Effect on the regulation of cytosolic calcium in relation to cytotoxicity in normal and tumorigenic rat kidney cell lines. *Cancer Lett.* **1995**, *97*, 7–15. [CrossRef]
181. Jochheim, C.M.; Davis, M.R.; Baillie, K.M.; Ehlhardt, W.J.; Baillie, T.A. Glutathione-dependent metabolism of the antitumor agent sulofenur. Evidence for the formation of p-chlorophenyl isocyanate as a reactive intermediate. *Chem. Res. Toxicol.* **2002**, *15*, 240–248. [CrossRef] [PubMed]
182. Chen, W.; Jiang, Z.; Zhang, X.; Feng, J.; Ling, Y. N-acetyl-S-(p-chlorophenylcarbamoyl)cysteine induces mitochondrial-mediated apoptosis and suppresses migration in melanoma cells. *Oncol. Rep.* **2015**, *34*, 2547–2556. [CrossRef] [PubMed]
183. Drew, R.; Miners, J.O. The effects of buthionine sulphoximine (BSO) on glutathione depletion and xenobiotic biotransformation. *Biochem. Pharmacol.* **1984**, *33*, 2989–2994. [CrossRef]
184. Ploemen, J.H.; Van Ommen, B.; Van Bladeren, P.J. Inhibition of rat and human glutathione S-transferase isoenzymes by ethacrynic acid and its glutathione conjugate. *Biochem. Pharmacol.* **1990**, *40*, 1631–1635. [CrossRef]
185. Allocati, N.; Masulli, M.; Di Ilio, C.; Federici, L. Glutathione transferases: Substrates, inhibitors and pro-drugs in cancer and neurodegenerative diseases. *Oncogenesis* **2018**, *7*, 8. [CrossRef]

Article

Genetic Polymorphism of GSTP-1 Affects Cyclophosphamide Treatment of Autoimmune Diseases

Péter Hajdinák ^{1,*} , Melinda Szabó ², Emese Kiss ², Lili Veress ², Lívius Wunderlich ¹ and András Szarka ^{1,3,*} 

¹ Department of Applied Biotechnology and Food Science, Laboratory of Biochemistry and Molecular Biology, Budapest University of Technology and Economics, Szent Gellért tér 4., Budapest 1111, Hungary; livius@mail.bme.hu

² National Institute of Rheumatology and Physiotherapy, Clinical Immunology Adult and Pediatric Rheumatology, Frankel Leó u. 25-29., Budapest 1023, Hungary; szabo.melinda@gmail.com (M.Sz.); drkiss.emese@gmail.com (E.K.); liliveress@gmail.com (L.V.)

³ Pathobiochemistry Research Group of Hungarian Academy of Sciences and Semmelweis University, P.O. Box 260, Budapest 1444, Hungary

* Correspondence: hajdinak@mail.bme.hu (P.H.); szarka@mail.bme.hu (A.Sz.); Tel.: +36-1-4633858 (A.Sz.); Fax: +36-1-4633855 (P.H. and A.Sz.)

Academic Editor: Pál Perjési

Received: 15 February 2020; Accepted: 25 March 2020; Published: 28 March 2020

Abstract: Cyclophosphamide is one of the most potent and reliable anti-cancer and immunosuppressive drugs. In our study, 33 individuals with different autoimmune diseases were treated with cyclophosphamide according to standard protocols. The responses to the treatments were determined by measuring the alteration of several typical parameters characterizing the given autoimmune diseases over time. We concluded that about 45% of the patients responded to the treatment. Patients were genotyped for polymorphisms of the CYP3A4, CYP2B6, GSTM1, GSTT1, and GSTP1 genes and disease remission cases were compared to the individual polymorphic genotypes. It was found that the GSTP1 I105V allelic variation significantly associated with the cyclophosphamide treatment-dependent disease-remissions. At the same time the GSH content of the erythrocytes in the patients with I105V allelic variation did not change. It appears that the individuals carrying the Ile105Val SNP in at least one copy had a significantly higher response rate to the treatment. Since this variant of GSTP1 can be characterized by lower conjugation capacity that results in an elongated and higher therapeutic dose of cyclophosphamide, our data suggest that the decreased activity of this variant of GSTP1 can be in the background of the more effective disease treatment.

Keywords: cyclophosphamide; autoimmune diseases; glutathione; glutathione-S-transferase; polymorphism

1. Introduction

Cyclophosphamide (CYC) is a highly efficient anti-cancer drug and immunosuppressive agent. It was first synthesized in the late 1950s and became one of the best characterized and most widely administered drugs [1]. Cyclophosphamide and its derivatives are strong alkylating agents inducing the formation of monofunctional guanine-N7 adducts and interstrand guanine–guanine crosslinks inside the DNA [2]. The extensive alkylation may lead to DNA damage and consequently to the death of frequently proliferating cells.

CYC is a prodrug, which is activated by biotransformation phase I enzymes. Seventy to eighty percent of the administered CYC is transformed to 4-hydroxycyclophosphamide by hepatic cytochrome P450 (CYP) enzymes (Figure 1). Several CYP isoenzymes are involved in the 4-hydroxylation of CYC in humans, including CYP3A4 and CYP2B6. The latter displays the highest 4-hydroxylase activity [3–5]. 4-hydroxycyclophosphamide is not cytotoxic and readily diffuses into cells [5]. Under physiological conditions, 4-hydroxycyclophosphamide exists in equilibrium with its aldehyde tautomer, aldophosphamide (Figure 1). Aldophosphamide either breaks up spontaneously into two bioactive toxic compounds such as phosphoramidate mustard and acrolein or gets oxidized enzymatically by aldehyde dehydrogenases resulting in inactive, non-toxic carboxyphosphamide (Figure 1). Phosphoramidate mustard, which is a bi-functional DNA alkylating agent, is the therapeutically active metabolite, while acrolein is a highly reactive aldehyde and enhances the cytotoxic effect of cyclophosphamide by depleting the cellular glutathione pool [5–7].

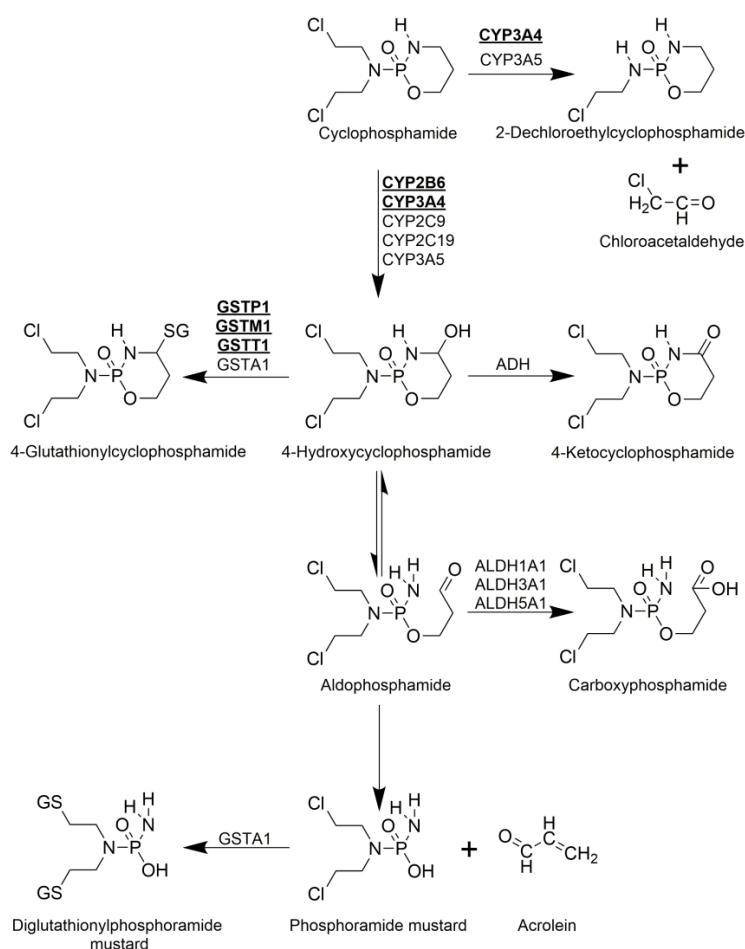


Figure 1. Metabolism of cyclophosphamide. Activation is shown vertically, while inactivation pathways are depicted horizontally. Cyclophosphamide (CYC) is administered as a prodrug and is hydroxylated by hepatic CYPs to form 4-hydroxycyclophosphamide (4-OH-CYC). 4-OH-CYC exists in equilibrium with its tautomer, aldophosphamide, which can break up spontaneously to result in the therapeutically active, cytotoxic phosphoramidate mustard and acrolein. 4-OH-CYC can be oxidized by alcohol dehydrogenase (ADH) resulting in nontoxic 4-keto-CYC or can be conjugated with glutathione by GSTs to form 4-glutathionyl-CYC. Aldophosphamide can be oxidized by aldehyde dehydrogenases (ALDH) resulting in inactive carboxyphosphamide, while phosphoramidate mustard can be detoxified by conjugating it with glutathione. Furthermore, as a minor pathway, direct detoxification of CYC is also possible by converting it to 2-Dechloroethylcyclophosphamide.

Biotransformation Phase II enzymes, such as glutathione-S-transferases (GST), catalyse the neutralization of active intermediaries of CYC by conjugation with glutathione, resulting in 4-glutathionylcyclophosphamide or diglutathionylphosphoramidate mustard. The isoforms GSTM1, GSTP1, and GSTT1 are only involved in the production of 4-glutathionylcyclophosphamide (Figure 1) [4,7,8].

Although direct detoxification of CYC is also possible, less than 5% of the administered CYC is eliminated this way. The direct detoxification is catalysed by CYP3A4 and CYP3A5 and results in the formation of 2-dechloroethylcyclophosphamide via side chain oxidation [5].

The level of the bioactive phosphoramidate mustard is determined by the rate of enzymatic activation and detoxification of CYC and its metabolites. The enzymes involved in CYC metabolism are known to be highly polymorphic and have alleles with decreased or missing activity [4,7]. Thus, genetic differences may be responsible for the earlier observed large interindividual variations in both efficacy and toxicity of CYC treatment [4,7,9]. For example, deletions in GSTM1, GSTT1 and some single nucleotide polymorphism of GSTP1 result in reduced detoxification rate of 4-hydroxycyclophosphamide, which may lead to a prolonged exposure to activated CYC and to the possibility of increased response. On the other hand, the prolonged exposure may increase the occurrence of adverse drug reactions [7,8]. Thus, in our study the connection between the genotype of the patients and the response to the CYC treatment in a series of chronic autoimmune diseases was investigated.

2. Results and Discussion

2.1. Patient Characteristics and Cyclophosphamide Treatment

Thirty-three patients diagnosed with various auto-immune diseases were involved in our study (Table 1). Twenty-nine of the 33 (87.9%) CYC treated patients were female and all the patients were Caucasian (Table 1). Since the vast majority of autoimmune patients are female, the female/male ratio of our study group is in concordance with the ratio in the scientific literature [10]. Their average age was 51 ± 15 years. The patients were treated one to eight times (mean \pm SD: 3.03 ± 2.44) with CYC, and they received various doses of CYC occasionally (0.50 to 1.60 g, mean \pm SD: 1.18 ± 0.31 g) in each pulse, 3.66 ± 3.42 g cumulative dose altogether. Upon CYC treatment, remission of the diseases was observed in 14 cases (42.42%).

2.2. Allele Frequencies

Allele-specific PCR discrimination method was used to genotype the study group. Homozygous wild type (WT), homozygous variant, and heterozygous allelic variations could be distinguished in the investigated (CYP2B6, CYP3A4 and GSTP1 genes) single nucleotide polymorphisms (SNPs). GSTM1 and GSTT1 deletion variants could only be detected in homozygous form. In concert with earlier studies [4,11], no variant alleles could be found in the investigated CYP3A4 SNPs (Table 2). In contrast, in the cases of CYP2B6, Q172H, and K262R wild type, heterozygous and homozygous variant patients could also be found in our study group (Table 2). The allelic frequencies of Q172H and K262R were 11% and 33% respectively. Earlier studies found similar frequencies both for K262R and Q172H [4,12–14]. Allelic frequencies of the investigated GST genes were quite diverse, both variant and wild type alleles were abundant in all three cases (Table 2). Their frequencies were similar to those found in Caucasians in earlier studies (Table A1) [4,7,15,16].

Table 1. Patient characteristics at baseline and outcome of the CYC treatment. Thirty-three patients diagnosed with various autoimmune diseases were included in the study. Data in square brackets represent the range of the given trait in the study population.

Clinical characteristics (n = 33)	
Sex, n	29 female/ 4 male
Ethnic origin, Caucasian, [%] (n)	100.00 (33)
Age at sample collection, mean ± SD	50.81 ± 15.24 [24–82]
Treatment	
Cumulative dose of CYC, mean ± SD [g]	3.66 ± 3.42 [0.5–12.6]
CYC pulses, mean ± SD	3.03 ± 2.44 [1–8]
Response to CYC treatment, [%] (n)	42.42% (14)
Biological characteristics	
Erythrocyte sedimentation rate, mean ± SD [mm/h]	26.84 ± 17.17 [4–67]
C-reactive protein, mean ± SD [mg/L]	8.43 ± 7.14 [1.15–34.12]
Diseases	
ANCA-associated vasculitis, [%] (n)	18.18 (6)
Large vessel vasculitis, [%] (n)	3.03 (1)
Systemic sclerosis, [%] (n)	27.27 (9)
Interstitial lung disease, [%] (n)	12.12 (4)
Systemic lupus erythematosus, [%] (n)	21.21 (7)
Retroperitoneal fibrosis, [%] (n)	6.06 (2)
Dermatomyositis, [%] (n)	6.06 (2)
Sarcoidosis, [%] (n)	6.06 (2)

Table 2. Association between response to CYC treatment and CYP3A4, CYP2B6, GSTM1, GSTP1, and GSTT1 polymorphisms. Significant association was only found between GSTP1 (I105V) variant and response to CYC treatment ($p < 0.05$).

	WT Responders/All Carriers [n, (%)	Heterozygous Variant Responders/All Carriers [n, (%)	Homozygous Variant Responders/All Carriers [n, (%)	<i>p</i>
CYP3A4*2 (S222P)	14/33 (42.42%)	—	—	N/A
CYP3A4*1B (-289A->G)	14/33 (42.42%)	—	—	N/A
CYP3A4*3 (M445T)	14/33 (42.42%)	—	—	N/A
CYP2B6 (Q172H)	12/27 (44.44%)	2/5 (40%)	0/1 (0%)	0.62
CYP2B6 (K262R)	4/14 (28.57%)	9/16 (56.25%)	1/3 (33%)	0.12
GSTM1 (deletion)	7/16 (43.75%)	N/A ¹	7/17 (41.17%)	0.88
GSTP1 (I105V)	3/14 (21.42%)	8/13 (61.53%)	3/6 (50%)	0.03 *
GSTT1 (deletion)	9/24 (37.5%)	N/A ¹	4/8 (50%)	0.41

¹ GSTM1 and GSTT1 deletion variants could only be detected in homozygous form. * The presented *p* value is from a post-hoc analysis assuming a dominant genetic model.

Alleles without genetic variability (CYP3A4 -289A->G, CYP3A4 S222P, CYP3A4 M445T) were not investigated further in our study. Regarding the polymorph alleles of the CYP2B6 (Q172H or K262R), GSTM1 and GSTT1 genes, the genetic polymorphisms could not be associated with the response to CYC treatment (Table 2). In the cases of CYP2B6, Q172H, and K262R SNPs, the heterozygous and wild type patients were compared, since there was a low number of homozygous variant patients.

The GSTP1 I105V allelic variation was associated with the CYC treatment dependent on disease remissions (Table 2). It appears that the individuals carrying the Ile105Val SNP in at least one copy had a significantly higher response rate. Since GSTP1 is active only in its homodimer form [17,18], in heterozygous patients only one fourth of the enzymes are expected to have full activity. On the basis of this consideration and the low number of patients homozygous for the variant GSTP1 allele, the

groups of homozygote variant and heterozygous patients were combined and compared to the wild type, as it was also done in earlier works [7,19–22].

GSTP1 plays a major role in 4-hydroxycyclophosphamide conjugation with about 1.9 mM of K_M and 35.1 nmol/min/mg protein of V_{max} values [8]. The latter high value underlines the importance of GSTP1 in CYC detoxification. Since the variant isoform of GSTP1 can be characterized by lower conjugation capacity [23–25] that results in an elongated and higher therapeutic dose of CYC, our data suggest that the decreased activity of the variant GSTP1 can be in the background of the higher response rate. Necessarily, the limited number of patients we could involve in the study and the facts that they were all diagnosed with autoimmune diseases and most of them were women might distort the allele frequencies and our results. However, our findings are in concert with earlier works. Several studies reported association between GSTP1 I105V polymorphism and increased response to cyclophosphamide-based therapies in breast and other cancer patients [24,26]. The effects of the variant allele included improved overall survival and decreased rate of relapse for both heterozygous and homozygous variant patients [24,26–30]. Due to its lower detoxification capacity, the I105V polymorphism may also have negative effects. Zhong et al. [31] reported increased risk of myelotoxicity and gastrointestinal toxicity in patients with systemic lupus erythematosus carrying at least one copy of the variant allele when they are treated with CYC. Another study reported that, carrying at least one allele of I105V results in a significantly increased risk of developing therapy-related acute myeloid leukemia after cytotoxic chemotherapy [32]. At the same time, there are studies that did not find any effect of I105V polymorphism on the CYC therapy, or the polymorphism showed a nonsignificant trend toward a lower probability of achieving global remission [4,7]. It seems that ethnicity differences and study group sizes also influence the results regarding the effect of GSTP1 I105V [26].

2.3. Blood Glutathione Levels

Blood samples were taken from each patient right before and 8 h after the first CYC treatment then before and after the CYC treatment when its dose was adjusted to determine the possible glutathione (GSH) level fluctuations. The latter is presented in the manuscript, but significant differences could not be observed between the GSH levels of the two samples (data not shown). The GSH level of both the plasma and the erythrocytes was measured. As it was expected on the base of the earlier observations [33–35], the GSH concentration in the erythrocytes was much higher than in the plasma (Table 3). No significant changes in GSH levels from both sources was found due to CYC treatment by using Wilcoxon matched pairs test (Table 3).

Table 3. Plasma and erythrocyte glutathione content of 33 patients before and 8 h after cyclophosphamide treatment. No significant changes in glutathione levels have been observed.

		All Patients	p^*	WT for GSTP1	GSTP1 I105V Carriers	p^{**}
Plasma GSH content before treatment, mean \pm SD	[μ M]	0.47 \pm 0.56	0.68	—	—	—
Plasma GSH content 8 h after treatment, mean \pm SD	[μ M]	0.64 \pm 0.82		—	—	—
Erythrocyte GSH content before treatment, mean \pm SD	[μ mol/L red blood cells]	2285.50 \pm 1822.34	0.73	2172.56 \pm 1519.79	2271.03 \pm 2069.04	0.90
Erythrocyte GSH content 8 h after treatment, mean \pm SD	[μ mol/L red blood cells]	2472.80 \pm 2235.55		2334.50 \pm 2076.64	2853.45 \pm 2421.49	1.00

* The p -value presented is from comparing the plasma and erythrocyte GSH contents of all patients before and 8 h after CYC treatment. ** The p -value presented is from comparing the erythrocyte GSH content of WT and GSTP1 I105V carrier patients before and 8 h after CYC treatment.

It has been found earlier, that almost exclusively the P1 isoform of GST can be found in the erythrocytes [36]. Since GSH levels were high enough in most of the erythrocyte samples, it is expected

that GSH was not a limiting factor for the conjugation. In general, 2200 $\mu\text{mol}/(\text{L red blood cells})$ of GSH concentration could be measured in the erythrocytes, and the K_M for GSH of the human erythrocyte GST was around 110 μM [37]. It should be noted that there is no measurable GST activity in the plasma, and the erythrocytes are considered to be the main carriers of 4-hydroxycyclophosphamide [5,37–40]. On the basis of these considerations, we have compared the erythrocyte GSH levels of patients carrying the variant GSTP1 I105V allele in at least one copy to the wild type patients (Table 3). We found no significant differences between these groups, which suggests that this polymorphism does not affect the erythrocyte GSH levels. Thus, our results for erythrocyte glutathione content further support our hypothesis, that the decreased catalytic activity of the variant GSTP1 enzyme (both heterozygous and homozygous variant) can be responsible for the increased response rate to therapeutic CYC.

2.4. Other Parameters

Further characteristic parameters of the patients responding and not responding to CYC treatment were compared (Table 4). Blood samples taken a couple days before CYC treatment were investigated. While there were no significant differences, some tendencies could be found. The samples from responding individuals could be characterized by lower erythrocyte sedimentation rates and lower C-reactive protein levels than those from non-responding patients. Interestingly, we also found some non-significant trends ($p = 0.10$) indicating that lower dosage cyclophosphamide treatment might have resulted in slightly higher disease remission rates. These phenomena should be investigated in a larger population. We have also compared the ages of the successfully and unsuccessfully treated groups, but no significant difference has been found.

Table 4. Comparison of variables of patients responding and not responding to CYC treatment. The data of 33 patients were analyzed. No significant differences between the responding and non-responding populations were observed.

	Responder, Mean \pm SD	Non-responder, Mean \pm SD	<i>p</i>
Age	49.21 \pm 19.06	52.05 \pm 11.93	0.54
Erythrocyte sedimentation rate, [mm/h]	21.28 \pm 13.28	31.16 \pm 18.90	0.15
C-reactive protein, [mg/L]	5.05 \pm 3.34	10.70 \pm 8.48	0.08
Cumulative dose of CYC [g]	2.87 \pm 3.12	4.47 \pm 3.57	0.10

3. Patients and Methods

3.1. Cyclophosphamide Treatment

Patients diagnosed with large vessel vasculitis (LVV), antineutrophil cytoplasmic antibody associated vasculitis (AAV), dermatomyositis (DM), systemic sclerosis (SSc), systemic lupus erythematosus (SLE), retroperitoneal fibrosis (RF), interstitial lung disease (ILD) or sarcoidosis and treated with CYC were chosen to take part in our study. The ethnicity of all patients was Caucasian.

CYC treatments were carried out according to the standard medical protocols of the given diseases. A patient was defined as a responder if remission of the symptoms was clearly observed and further biological therapies were not necessary to apply. In the case of the response, the treatment was continued by *per os* administration of synthetic disease-modifying antirheumatic drugs (DMARDs).

This survey was conducted in compliance with the protocol of Good Clinical Practices and Declaration of Helsinki principles and was carried out with the approval of the Ethics Committee of the Medical Research Council, Research and Ethics Committee (TUKEB; GLUTCYC-1-2016). All participants gave a written informed consent.

3.2. DNA Sample Preparation

Buccal cells were collected by rubbing the inner surface of the cheek's epithelium with sterile cotton swab sticks for about 30 s. The buns were separated by cutting the stick with scissors and placed in sterile microcentrifuge tubes containing 0.5 mL lysis buffer (0.1 M NaCl, 0.01M Tris-HCl, 0.5% SDS,

0.2 mg/mL proteinase K, pH 8). The collected samples were incubated for 12 h at 56 °C, and the cotton swabs were removed after the incubation period. One-hundred-and-sixty-seven microliters of 6 M NaCl solution was added to the lysates, followed by centrifugation at 17,000× *g*, for 10 min (room temperature). The supernatants were transferred into new tubes and supplemented with 690 µL of chilled (−20 °C) isopropyl alcohol. After an incubation at −20 °C for 2 h, the samples were centrifuged at 20,000× *g*, 4 °C for 20 min and the supernatants were carefully removed. The DNA pellets were washed with −20 °C 70% (*v/v*) ethanol, and centrifuged (20,000× *g*, 4 °C, 20 min) again. After removal of the supernatants, the pellets were dried and dissolved in 50 µL TE buffer (5 mM Tris, 0.5 mM EDTA, pH 8). The DNA concentrations were measured with Nanodrop Spectrophotometer (Thermo Fisher Scientific, Waltham, MA, USA) and the samples were stored at −80 °C until use.

3.3. PCR

The analysis of CYP and GST polymorphisms was carried out by a standard, three-step polymerase chain reactions (PCR) followed by agarose gel electrophoresis. Allele variations of CYP3A4 (CYP3A4*1B (-289A->G), CYP3A4*2 (S222P), CYP3A4*3 (M445T)), CYP2B6 (Q172H & K262R), and GSTP1 (I105V) were investigated. GSTM1 and GSTT1 null mutations were also analysed. The nucleotide sequences of the primers and the used annealing temperatures are listed in Table A2.

3.4. Determination of Blood Glutathione Content

Venous blood samples were collected into EDTA-VACUETTE tubes (Greiner, Kremsmünster, Austria) right before and 8 h after CYC treatment. Blood samples were immediately centrifuged for separating the erythrocyte and plasma fractions (at 3000× *g* for 5 min, at room temperature). 0.5 mL 10% (*w/v*) 5-sulphosalicylic acid (SSA, Sigma-Aldrich, St. Louis, MO, USA) solutions were mixed to the same volume of both fractions. The samples were stored at −80 °C for no more than 2 days.

Before the derivatization of the glutathione (GSH) content of the samples with the fluorescent dye monochlorobimane, the frozen samples were thawed, centrifuged (17,000× *g*, 5 min, room temperature) and 100 µL of the supernatants were transferred into new tubes. Triethanolamine was added to the samples at a final concentration of 400 mM to adjust the pH to being slightly alkaline. The GSH content of the samples was conjugated immediately by monochlorobimane (1 mM) in the presence of glutathione-S-transferase enzyme (100 mU/mL). The reaction was carried out in the dark at room temperature for 15 min and stopped with the addition of trichloroacetic acid at a final concentration of 10% (*w/v*) [41,42]. The samples were centrifuged at 16,000× *g*, at 4 °C for 10 min to pellet the precipitated proteins. Fifty microliters of the supernatant was loaded into a Waters 2690 HPLC for separation equipped with a Waters 2475 fluorescent detector set to 395 nm excitation and 477 nm emission wavelengths. Samples and standards were separated on a Teknokroma Nucleosil 100C-18 (Teknokroma Analítica, Barcelona, Spain), 5 µm, 250 × 4.6 mm column. The separation was carried out with a 32.5 min protocol employing the linear gradient of 0.25% (*v/v*) aqueous acetic acid/sodium acetate buffer pH 3.5 as Solvent A and methanol as Solvent B: 0–17.5 min 18% Solvent B/ 82% Solvent A; 17.5–20 min linear gradient to 100% Solvent B; 20–27.5 min Solvent B; 27.5–28 min linear gradient to 18% Solvent B/ 82% Solvent A; 28 to 32.5 min 18% Solvent B/ 82% Solvent A with 1 mL/min permanent flow rate. Standards were prepared from reduced glutathione dissolved in 5% SSA [0–20 µM], and their glutathione content (similarly to the samples) was conjugated with monochlorobimane. Based on our standards, the retention time of glutathione conjugated by monochlorobimane was 8.5 min [42].

3.5. Statistical Analysis

For the primary data analysis, Chi-square test was used to compare response rates between genotype groups (categorical variables). If the observed frequency in a cell of the contingency table was <5, then Fisher's exact test was used. On reviewing our results, we conducted a post-hoc analysis assuming a dominant genetic effect in the case of GSTP1 I105V [7,19–22]. Therefore, heterozygous and

homozygous variant patients were combined and compared to wild type patients using Fisher's exact test. The *p*-value presented for GSTP1 I105V in Table 2 came from this post-hoc analysis.

The non-parametric Mann-Whitney and Wilcoxon matched pairs tests were used to compare continuous variables. Mann-Whitney test was used to analyse the erythrocyte GSH with GSTP1 genotype as grouping variable; age; erythrocyte sedimentation rate; C-reactive protein and cumulative dose of CYC. For comparing blood glutathione levels before and 8 h after CYC treatment, Wilcoxon matched pairs test was used. Statistical analyses were performed by StatSoft STATISTICA™ 10 (StatSoft, Tulsa, OK, USA, 2010).

4. Conclusions

CYC treatment is one of the most common and reliable possibilities for suppressing the symptoms of autoimmune diseases. Unfortunately, high interindividual variations in treatment efficacy and response have been observed. One of the factors influencing the response to the treatment can be the genetic background of the patients. In our study, we focused on the bioactivation and elimination of CYC. The relations of the CYC treatment response and various biotransformation-dependent factors such as CYP and GST enzyme polymorphisms and GSH levels of the blood were investigated.

On one hand, a clear association between GSTP1 genetic polymorphism and CYC treatment response was found. Significantly higher response rate to CYC treatment could be observed in individuals carrying one or two copies of the gene of the less active variant GSTP1 (I105V) isoenzyme. Since GSTP1 is the main GST isotype in the erythrocytes, it is not surprising that the weakened first detoxification reaction may result in a higher amount of 4-hydroxycyclophosphamide transported into the proliferating cells, that can enhance its cytostatic effect.

On the other hand, no significant blood GSH depletion could be observed upon CYC treatment. This observation suggests that GSH level was not a limiting factor for the biotransformation. According to these findings, it seems that CYC treatment has little effect on the glutathione pool in the erythrocytes.

Author Contributions: Conceptualization, M.Sz. and A.Sz.; methodology, P.H., M.Sz., L.W.; validation, E.K.; investigation, P.H., M.Sz., L.V.; resources, A.Sz.; data curation, P.H.; writing—original draft preparation, P.H. and L.W.; writing—review and editing, A.Sz.; visualization, P.H.; supervision, A.Sz.; project administration, P.H.; funding acquisition, A.Sz. All authors have read and agreed to the published version of the manuscript.

Funding: This research was funded by the National Research, Development and Innovation Fund of Hungary under Grant K 123752, 129593, 2018-1.2.1-NKP-2018-00005 and by the BME-Biotechnology FIKP grant of ITM.

Conflicts of Interest: The authors declare no conflict of interest. The funders had no role in the design of the study; in the collection, analyses, or interpretation of data; in the writing of the manuscript, or in the decision to publish the results.

Appendix A

Table A1. Allele frequency of GSTP1 I105V in various populations.

Study Population Ancestry	GSTP1 I105V Frequency [%]	Ref.
Tanzanian	16	
South African Venda	12	[43]
Zimbabwean	21	
Gambian	53	[44]
Dutch	53	[4]
French	46	[7]
Serbian	61 *	[45]
Turkish	29 **	[46]
Han Chinese	20.5	[31]
Bangladeshi	29	[26]
Delhi	32	[47]

* % of the study group carrying at least on copy of the variant allele; ** % of the studied haplotypes has I105V.

Table A2. Primers, annealing temperatures and polymerization length used for genotyping.

Genetic Variations	Reverse and Forward Primers (5'-3')	Ann. Temp. (°C)	Polymerization Length (sec)	Product Length
CYP3A4*1B (-289A->G)	GGAAACAGGCGTGGAAACAC and CCTTTGAGTTCATATTCTATGAGGTATGAT	59	30	416 bp
	or CCTTTGAGTTCATATTCTATGAGGTATGAC			
CYP3A4*2 (S222P)	TTTGATTTTTTGGATCCATTCTTTCACT or TTTGATTTTTTGGATCCATTCTTTCCACC	58	60	867 bp
	and CAATGCCCTAATCTCTTTGCCT			
CYP3A4*3 (M445T)	ACCCAGAAACTGCATTGGTAT or ACCCAGAAACTGCATTGGTAC	60	20	237 bp
	and TGGGCCTAATTGATTCTTTGGC			
CYP2B6 (Q172H)	CAGTGCTGAGCCTGGTGTAT and ATGATGTTGGCGGTAATGCAC	54	60	931 bp
	or ATGATGTTGGCGGTAATGCAA			
CYP2B6 (K262R)	GGCGGTCTGATCTGGAAAGT and GGTAGGTGTCGATGAGGTTCT	60	60	859 bp
	or GGTAGGTGTCGATGAGGTTCC			
GSTP1 (I105V)	GGACCTCCGCTGCAAATCCA or GGACCTCCGCTGCAAATCCG	60	60	928 bp
	and ACATAGTCATCCTTGCCCGC			
GSTM1 del	GAACCTCCCTGAAAAGCTAAAGC and GTTGGGCTCAAATATACGGTGG	57	20	219 bp [48]
	TTCCTTACTGGTCTCACATCTC and TCACCGGATCATGGCCAGCA			
GSTT1 del	TTCCTTACTGGTCTCACATCTC and TCACCGGATCATGGCCAGCA	60.8	30	480 bp [49]

References

- Emadi, A.; Jones, R.J.; Brodsky, R.A. Cyclophosphamide and cancer: Golden anniversary. *Nat. Rev. Clin. Oncol.* **2009**, *6*, 638–647. [CrossRef] [PubMed]
- Povirk, L.F.; Shuker, D.E. DNA damage and mutagenesis induced by nitrogen mustards. *Mutat. Res. Genet. Toxicol.* **1994**, *318*, 205–226. [CrossRef]
- Roy, P.; Yu, L.J.; Crespi, C.L.; Waxman, D.J. Development of a substrate-activity based approach to identify the major human liver P-450 catalysts of cyclophosphamide and ifosfamide activation based on cDNA-expressed activities and liver microsomal P-450 profiles. *Drug Metab. Dispos.* **1999**, *27*, 655–666. [PubMed]
- Ekhart, C.; Doodeman, V.D.; Rodenhuis, S.; Smits, P.H.M.; Beijnen, J.H.; Huitema, A.D.R. Influence of polymorphisms of drug metabolizing enzymes (CYP2B6, CYP2C9, CYP2C19, CYP3A4, CYP3A5, GSTA1, GSTP1, ALDH1A1 and ALDH3A1) on the pharmacokinetics of cyclophosphamide and 4-hydroxycyclophosphamide. *Pharmacogenet. Genomics* **2008**, *18*, 515–523. [CrossRef] [PubMed]
- de Jonge, M.E.; Huitema, A.D.R.; Rodenhuis, S.; Beijnen, J.H. Clinical Pharmacokinetics of Cyclophosphamide. *Clin. Pharmacokinet.* **2005**, *44*, 1135–1164. [CrossRef]
- Raccor, B.S.; Claessens, A.J.; Dinh, J.C.; Park, J.R.; Hawkins, D.S.; Thomas, S.S.; Makar, K.W.; McCune, J.S.; Totah, R.A. Potential contribution of cytochrome P450 2B6 to hepatic 4-hydroxycyclophosphamide formation in vitro and in vivo. *Drug Metab. Dispos.* **2012**, *40*, 54–63. [CrossRef]
- Audemard-Verger, A.; Martin Silva, N.; Verstuyft, C.; Costedoat-Chalumeau, N.; Hummel, A.; Le Guern, V.; Sacré, K.; Meyer, O.; Daugas, E.; Goujard, C.; et al. Glutathione S Transferases Polymorphisms Are Independent Prognostic Factors in Lupus Nephritis Treated with Cyclophosphamide. *PLoS ONE* **2016**, *11*, e0151696. [CrossRef]

8. Dirven, H.A.A.M.; van Ommen, B.; van Bladeren, P.J. Involvement of human glutathione S-transferase isoenzymes in the conjugation of cyclophosphamide metabolites with glutathione. *Cancer Res.* **1994**, *54*, 6215–6220.
9. Huitema, A.D.R.; Spaander, M.; Mathôt, R.A.A.; Tibben, M.M.; Holtkamp, M.J.; Beijnen, J.H.; Rodenhuis, S. Relationship between exposure and toxicity in high-dose chemotherapy with cyclophosphamide, thiopeta and carboplatin. *Ann. Oncol.* **2002**, *13*, 374–384. [CrossRef]
10. Fairweather, D.; Frisancho-Kiss, S.; Rose, N.R. Sex differences in autoimmune disease from a pathological perspective. *Am. J. Pathol.* **2008**, *173*, 600–609. [CrossRef]
11. Ekins, S.; Bravi, G.; Wikel, J.H.; Wrighton, S.A. Three-dimensional-quantitative structure activity relationship analysis of cytochrome P-450 3A4 substrates. *J. Pharmacol. Exp. Ther.* **1999**, *291*, 424–433. [PubMed]
12. Labib, R.M.; Abdelrahim, M.E.A.; Elnadi, E.; Hesham, R.M.; Yassin, D. CYP2B6rs2279343 is associated with improved survival of pediatric Rhabdomyosarcoma treated with cyclophosphamide. *PLoS ONE* **2016**, *11*, e0158890. [CrossRef] [PubMed]
13. Yang, H.C.; Chu, S.K.; Huang, C.L.; Kuo, H.W.; Wang, S.C.; Liu, S.W.; Ho, I.K.; Liu, Y.L. Genome-Wide Pharmacogenomic Study on Methadone Maintenance Treatment Identifies SNP rs17180299 and Multiple Haplotypes on CYP2B6, SPON1, and GSG1L Associated with Plasma Concentrations of Methadone R- and S-enantiomers in Heroin-Dependent Patients. *PLoS Genet.* **2016**, *12*, e1005910. [CrossRef] [PubMed]
14. Tomaz, P.R.X.; Santos, J.R.; Issa, J.S.; Abe, T.O.; Gaya, P.V.; Krieger, J.E.; Pereira, A.C.; Santos, P.C.J.L. CYP2B6 rs2279343 polymorphism is associated with smoking cessation success in bupropion therapy. *Eur. J. Clin. Pharmacol.* **2015**, *71*, 1067–1073. [CrossRef] [PubMed]
15. Harrison, D.J.; Cantlay, A.M.; Rae, F.; Lamb, D.; Smith, C.A.D. Frequency of glutathione S-transferase M1 deletion in smokers with emphysema and lung cancer. *Hum. Exp. Toxicol.* **1997**, *16*, 356–360. [CrossRef]
16. Arruda, V.R.; Grignolli, C.E.; Gonçalves, M.S.; Soares, M.C.; Menezes, R.; Saad, S.T.; Costa, F.F. Prevalence of homozygosity for the deleted alleles of glutathione S-transferase mu (GSTM1) and theta (GSTT1) among distinct ethnic groups from Brazil: Relevance to environmental carcinogenesis? *Clin. Genet.* **1998**, *54*, 210–214.
17. Gildenhuis, S.; Wallace, L.A.; Burke, J.P.; Balchin, D.; Sayed, Y.; Dirr, H.W. Class Pi glutathione transferase unfolds via a dimeric and not monomeric intermediate: Functional implications for an unstable monomer. *Biochemistry* **2010**, *49*, 5074–5081. [CrossRef]
18. Fabrini, R.; De Luca, A.; Stella, L.; Mei, G.; Orioni, B.; Ciccone, S.; Federici, G.; Lo Bello, M.; Ricci, G. Monomer–Dimer Equilibrium in Glutathione Transferases: A Critical Re-Examination. *Biochemistry* **2009**, *48*, 10473–10482. [CrossRef]
19. Debes, J.D.; Yokomizo, A.; McDonnell, S.K.; Hebring, S.J.; Christensen, G.B.; Cunningham, J.M.; Jacobsen, S.J.; Tindall, D.J.; Liu, W.; Schaid, D.J.; et al. Glutathione-S-transferase P1 polymorphism I105V in familial and sporadic prostate cancer. *Cancer Genet. Cytogenet.* **2004**, *155*, 82–86. [CrossRef]
20. Helzlsouer, K.J.; Selmin, O.; Huang, H.Y.; Strickland, P.T.; Hoffman, S.; Alberg, A.J.; Watson, M.; Comstock, G.W.; Bell, D. Association between glutathione S-transferase M1, P1, and T1 genetic polymorphisms and development of breast cancer. *J. Natl. Cancer Inst.* **1998**, *90*, 512–518. [CrossRef]
21. Lecomte, T.; Landi, B.; Beaune, P.; Laurent-Puig, P.; Loriot, M.A. Glutathione S-transferase P1 polymorphism (Ile105Val) predicts cumulative neuropathy in patients receiving oxaliplatin-based chemotherapy. *Clin. Cancer Res.* **2006**, *12*, 3050–3056. [CrossRef]
22. Lavigne, J.A.; Helzlsouer, K.J.; Huang, H.Y.; Strickland, P.T.; Bell, D.A.; Selmin, O.; Watson, M.A.; Hoffman, S.; Comstock, G.W.; Yager, J.D. An association between the allele coding for a low activity variant of catechol-O-methyltransferase and the risk for breast cancer. *Cancer Res.* **1997**, *57*, 5493–5497. [PubMed]
23. Sailaja, K.; Surekha, D.; Rao, D.N.; Rao, D.R.; Vishnupriya, S. Association of the GSTP1 gene (Ile105Val) polymorphism with chronic myeloid leukemia. *Asian Pac. J. Cancer Prev.* **2010**, *11*, 461–464.
24. Pinto, N.; Ludeman, S.M.; Dolan, M.E. Drug focus: Pharmacogenetic studies related to cyclophosphamide-based therapy. *Pharmacogenomics* **2009**, *10*, 1897–1903. [CrossRef] [PubMed]
25. Marsh, S.; McLeod, H.L. Cancer pharmacogenetics. *Br. J. Cancer* **2004**, *90*, 8–11. [CrossRef]
26. Islam, M.S.; Islam, M.S.; Parvin, S.; Ahmed, M.U.; Sayeed, M.S.B.; Uddin, M.M.N.; Hussain, S.M.A.; Hasnat, A. Effect of GSTP1 and ABCC4 gene polymorphisms on response and toxicity of

- cyclophosphamide-epirubicin-5-fluorouracil-based chemotherapy in Bangladeshi breast cancer patients. *Tumor Biol.* **2015**, *36*, 5451–5457. [CrossRef] [PubMed]
27. Sweeney, C.; McClure, G.Y.; Fares, M.Y.; Stone, A.; Coles, B.F.; Thompson, P.A.; Korourian, S.; Hutchins, L.F.; Kadlubar, F.F.; Ambrosone, C.B. Association between survival after treatment for breast cancer and glutathione S-transferase P1 Ile105Val polymorphism. *Cancer Res.* **2000**, *60*, 5621–5624.
 28. Hohaus, S.; Di Ruscio, A.; Di Febo, A.; Massini, G.; D’Alo’, F.; Guidi, F.; Mansueto, G.; Voso, M.T.; Leone, G. Glutathione S-transferase P1 genotype and prognosis in Hodgkin’s lymphoma. *Clin. Cancer Res.* **2005**, *11*, 2175–2179. [CrossRef]
 29. Stanulla, M.; Schrappe, M.; Brechlin, A.M.; Zimmermann, M.; Welte, K. Polymorphisms within glutathione S-transferase genes (GSTM1, GSTT1, GSTP1) and risk of relapse in childhood B-cell precursor acute lymphoblastic leukemia: A case-control study. *Blood* **2000**, *95*, 1222–1228. [CrossRef]
 30. Dasgupta, R.K.; Adamson, P.J.; Davies, F.E.; Rollinson, S.; Roddam, P.L.; Ashcroft, A.J.; Dring, A.M.; Fenton, J.A.L.; Child, J.A.; Allan, J.M.; et al. Polymorphic variation in GSTP1 modulates outcome following therapy for multiple myeloma. *Blood* **2003**, *102*, 2345–2350. [CrossRef]
 31. Zhong, S.; Huang, M.; Yang, X.; Liang, L.; Wang, Y.; Romkes, M.; Duan, W.; Chan, E.; Zhou, S.F. Relationship of glutathione S-transferase genotypes with side-effects of pulsed cyclophosphamide therapy in patients with systemic lupus erythematosus. *Br. J. Clin. Pharmacol.* **2006**, *62*, 457–472. [CrossRef] [PubMed]
 32. Allan, J.M.; Wild, C.P.; Rollinson, S.; Willett, E.V.; Moorman, A.V.; Dovey, G.J.; Roddam, P.L.; Roman, E.; Cartwright, R.A.; Morgan, G.J. Polymorphism in glutathione S-transferase P1 is associated with susceptibility to chemotherapy-induced leukemia. *Proc. Natl. Acad. Sci. USA* **2001**, *98*, 11592–11597. [CrossRef] [PubMed]
 33. van ’t Erve, T.J.; Wagner, B.A.; Ryckman, K.K.; Raife, T.J.; Buettner, G.R. The concentration of glutathione in human erythrocytes is a heritable trait. *Free Radic. Biol. Med.* **2013**, *65*, 742–749. [CrossRef] [PubMed]
 34. Michelet, F.; Gueguen, R.; Leroy, P.; Wellman, M.; Nicolas, A.; Siest, G. Blood and plasma glutathione measured in healthy subjects by HPLC: Relation to sex, aging, biological variables, and life habits. *Clin. Chem.* **1995**, *41*, 1509–1517. [CrossRef] [PubMed]
 35. Yang, C.-S.; Chou, S.-T.; Liu, L.; Tsai, P.-J.; Kuo, J.-S. Effect of ageing on human plasma glutathione concentrations as determined by high-performance liquid chromatography with fluorimetric detection. *J. Chromatogr. B Biomed. Sci. Appl.* **1995**, *674*, 23–30. [CrossRef]
 36. Dessi, M.; Noce, A.; Dawood, K.F.; Galli, F.; Taccone-Gallucci, M.; Fabrini, R.; Bocedi, A.; Massoud, R.; Fucci, G.; Pastore, A.; et al. Erythrocyte glutathione transferase: A potential new biomarker in chronic kidney diseases which correlates with plasma homocysteine. *Amino Acids* **2012**, *43*, 347–354. [CrossRef] [PubMed]
 37. Bocedi, A.; Fabrini, R.; Lai, O.; Alfieri, L.; Roncoroni, C.; Noce, A.; Pedersen, J.; Ricci, G. Erythrocyte glutathione transferase: A general probe for chemical contaminations in mammals. *Cell Death Discov.* **2016**, *2*, 16029. [CrossRef]
 38. Fabrini, R.; Bocedi, A.; Massoud, R.; Federici, G.; Ricci, G. Spectrophotometric assay for serum glutathione transferase: A re-examination. *Clin. Biochem.* **2012**, *45*, 668–671. [CrossRef]
 39. Highley, M.S.; Harper, P.G.; Slee, P.H.; DeBruijn, E. Preferential location of circulating activated cyclophosphamide within the erythrocyte. *Int. J. Cancer* **1996**, *65*, 711–712.
 40. Highley, M.S.; Schrijvers, D.; Van Oosterom, A.T.; Harper, P.G.; Momerency, G.; Van Cauwenberghe, K.; Maes, R.A.A.; De Bruijn, E.A.; Edelstein, M.B. Activated oxazaphosphorines are transported predominantly by erythrocytes. *Ann. Oncol.* **1997**, *8*, 1139–1144. [CrossRef]
 41. Lőrincz, T.; Szarka, A. The determination of hepatic glutathione at tissue and subcellular level. *J. Pharmacol. Toxicol. Methods* **2017**, *88*, 32–39. [CrossRef] [PubMed]
 42. Hajdinák, P.; Czobor, Á.; Lőrincz, T.; Szarka, A. The Problem of Glutathione Determination: A Comparative Study on the Measurement of Glutathione from Plant Cells. *Period. Polytech. Chem. Eng.* **2018**, *63*, 1–10. [CrossRef]
 43. Dandara, C.; Sayi, J.; Masimirembwa, C.M.; Magimba, A.; Kaaya, S.; De Sommers, K.; Snyman, J.R.; Hasler, J.A. Genetic polymorphism of cytochrome P450 1A1 (Cyp1A1) and glutathione transferases (M1, T1 and P1) among Africans. *Clin. Chem. Lab. Med.* **2002**, *40*, 952–957. [CrossRef] [PubMed]
 44. Wild, C.P.; Yin, F.; Turner, P.C.; Chemin, I.; Chapot, B.; Mendy, M.; Whittle, H.; Kirk, G.D.; Hall, A.J. Environmental and genetic determinants of aflatoxin–albumin adducts in The Gambia. *Int. J. Cancer* **2000**, *86*, 1–7. [CrossRef]

45. Simeunovic, D.; Odanovic, N.; Pljesa-Ercegovac, M.; Radic, T.; Radovanovic, S.; Coric, V.; Milinkovic, I.; Matic, M.; Djukic, T.; Ristic, A.; et al. Glutathione transferase P1 polymorphism might be a risk determinant in heart failure. *Dis. Markers* **2019**, *2019*, 1–11. [CrossRef] [PubMed]
46. Karaca, S.; Karaca, M.; Cesuroglu, T.; Erge, S.; Polimanti, R. GSTM1, GSTP1, and GSTT1 genetic variability in Turkish and worldwide populations. *Am. J. Hum. Biol.* **2015**, *27*, 310–316. [CrossRef] [PubMed]
47. Sharma, A.; Pandey, A.; Sharma, S.; Chatterjee, I.; Mehrotra, R.; Sehgal, A.; Sharma, J.K. Genetic polymorphism of glutathione S-transferase P1 (GSTP1) in Delhi population and comparison with other global populations. *Meta Gene* **2014**, *2*, 134–142. [CrossRef]
48. Kiran, B.; Karkucak, M.; Ozan, H.; Yakut, T.; Ozerkan, K.; Sag, S.; Ture, M. GST (GSTM1, GSTT1, and GSTP1) polymorphisms in the genetic susceptibility of Turkish patients to cervical cancer. *J. Gynecol. Oncol.* **2010**, *21*, 169–173. [CrossRef]
49. Pemble, S.; Schroeder, K.R.; Spencer, S.R.; Meyer, D.J.; Hallier, E.; Bolt, H.M.; Ketterer, B.; Taylor, J.B. Human glutathione S-transferase theta (GSTT1): cDNA cloning and the characterization of a genetic polymorphism. *Biochem. J.* **1994**, *300*, 271–276. [CrossRef]

Sample Availability: In accordance with the Act CXII of 2011 on the Right of Informational Self-Determination and on Freedom of Information, and with the Act XXI of 2008 on the Protection of Human Genetic Data, samples of the patients are not available from the authors.



© 2020 by the authors. Licensee MDPI, Basel, Switzerland. This article is an open access article distributed under the terms and conditions of the Creative Commons Attribution (CC BY) license (<http://creativecommons.org/licenses/by/4.0/>).

Article

Reaction of Chalcones with Cellular Thiols. The Effect of the 4-Substitution of Chalcones and Protonation State of the Thiols on the Addition Process. Diastereoselective Thiol Addition

Fatemeh Kenari ¹, Szilárd Molnár ^{1,2} and Pál Perjési ^{1,*}

¹ Institute of Pharmaceutical Chemistry, University of Pécs, H-7624 Pécs, Hungary; kenari.fatemeh@pte.hu (F.K.); molnar.szilard@pte.hu (S.M.)

² Research Institute for Viticulture and Oenology, University of Pécs, H-7624 Pécs, Hungary

* Correspondence: pal.perjesi@gytk.pte.hu; Tel.: +36-72-503-650

Abstract: Several biological effects of chalcones have been reported to be associated with their thiol reactivity. In vivo, the reactions can result in the formation of small-molecule or protein thiol adducts. Both types of reactions can play a role in the biological effects of this class of compounds. Progress of the reaction of 4-methyl- and 4-methoxychalcone with glutathione and *N*-acetylcysteine was studied by the HPLC-UV-VIS method. The reactions were conducted under three different pH conditions. HPLC-MS measurements confirmed the structure of the formed adducts. The chalcones reacted with both thiols under all incubation conditions. The initial rate and composition of the equilibrium mixtures depended on the ratio of the deprotonated form of the thiols. In the reaction of 4-methoxychalcone with *N*-acetylcysteine under strongly basic conditions, transformation of the kinetic adduct into the thermodynamically more stable one was observed. Addition of *S*-protonated *N*-acetylcysteine onto the polar double bonds of the chalcones showed different degrees of diastereoselectivity. Both chalcones showed a Michael-type addition reaction with the ionized and non-ionized forms of the investigated thiols. The initial reactivity of the chalcones and the equilibrium composition of the incubates showed a positive correlation with the degree of ionization of the thiols. Conversions showed systematic differences under each set of conditions. The observed differences can hint at the difference in reported biological actions of 4-methyl- and 4-methoxy-substituted chalcones.

Keywords: chalcone; glutathione; cysteine; thiols; Michael addition; diastereoselective addition

Citation: Kenari, F.; Molnár, S.; Perjési, P. Reaction of Chalcones with Cellular Thiols. The Effect of the 4-Substitution of Chalcones and Protonation State of the Thiols on the Addition Process. Diastereoselective Thiol Addition. *Molecules* **2021**, *26*, 4332. <https://doi.org/10.3390/molecules26144332>

Academic Editor: Federica Belluti

Received: 18 June 2021

Accepted: 14 July 2021

Published: 17 July 2021

Publisher's Note: MDPI stays neutral with regard to jurisdictional claims in published maps and institutional affiliations.



Copyright: © 2021 by the authors. Licensee MDPI, Basel, Switzerland. This article is an open access article distributed under the terms and conditions of the Creative Commons Attribution (CC BY) license (<https://creativecommons.org/licenses/by/4.0/>).

1. Introduction

Chalcones (Figure 1) are intermediary compounds of the biosynthetic pathway of a large and widespread group of plant constituents known collectively as flavonoids [1]. Several compounds display in vitro cytotoxic (cell growth inhibitor) activity toward cultured tumor cells among the naturally occurring chalcones and their synthetic analogues. Chalcones are also effective as cell proliferation inhibitors and as antitumor-promoting, anti-inflammatory, and chemopreventive agents [2–5]. Their activity is the result of either covalent or noncovalent interactions [2]. Covalent interactions are mainly based on the Michael acceptor activity of the α,β -unsaturated carbonyl system or the radical-scavenging or reductive potential of the compounds [6–8]. Several biological effects (e.g., NQO1 inducer [9], anti-inflammatory [10], GST P1-1 inhibitory [11]) of chalcones have been associated with their Michael-type reactivity toward protein thiols or reduced glutathione (GSH). It was suggested that the lower GSH depletion potential of chalcones with strong electron donor substituents (e.g., dimethylamino) on the B ring could be the consequence of the lower Michael-type reactivity of the derivatives toward GSH [12]. In contrast, higher reactivity toward GSH and other thiols was parallel with the higher NQO1-inducing potential of the investigated chalcones [13].

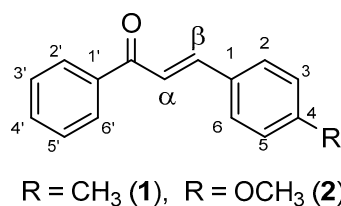


Figure 1. Structure and numbering of the investigated chalcones (**1** and **2**).

In our present study, reactions of two chalcones with different 4-substitutions (4-CH₃ (**1**) and 4-OCH₃ (**2**)) with two cellular thiols (GSH and NAC) were investigated to get information about (a) how the pH of the reaction medium affects the reactivity and stereochemical outcome of the reactions and (b) how the thiol reactivity of the compounds is related to their biological activities. Since thiol reactivity can be the molecular basis of modulation of the function of thiol switches [14] and the biological effects of covalent modifiers [15], the thiol reactivity of different chalcones is of interest in understanding their biological activities. Glutathione is an endogenous thiol, whose thiol reactivity plays an important role in maintaining redox homeostasis and protecting cellular nucleophilic sites of proteins from harmful electrophiles [16]. NAC is an exogenous thiol; however, it is one of the precursors of GSH biosynthesis, possesses mucolytic action, and is used as an antidote in paracetamol intoxication [17]. Considering their different pK_a values [18], the two compounds are also perfect models for reactivity screening of compounds with surface protein thiols with different molecular surroundings [19].

The selected substituents have different electron-donating capacities, which results in different reactivities and biological activities. For example, the tumor promotion inhibitory effect of 4-methyl-4'-hydroxychalcone is about twice as high as that of the 4-methoxy analogue [20]. Comparison of the *in vitro* cytotoxicity of **1** and **2** toward five different cancer cells showed that the 4-methyl derivative (**1**) is more effective toward most of the tested cell lines [21]. Furthermore, multiple regression analysis showed that cytotoxicity of a series of chalcones toward murine and human cancer cells increases as the Hammett sigma (σ) values of the substituent elevates [22]. In contrast, among the cyclic analogues ($n = 5, 6$, and 7) of the two chalcones, the methoxy-substituted (**2**) cyclic derivatives showed much higher *in vitro* cancer cell cytotoxicity than those of **1** [23]. Furthermore, the seven-membered analogues of **1** and **2** showed different *in vitro* effects on the cell cycle of Jurkat T cells [24].

The Michael reaction refers to the addition of a nucleophile (Michael donor) to an activated α,β -unsaturated carbonyl compound (Michael acceptor), and it is typically base-catalyzed. Among the most commonly studied nucleophiles, one finds hydroxide ions (OH⁻), water, and amines; a more limited number of investigations have been reported with thiolate ions (ArS⁻, RS⁻), oxide ions (ArO⁻, RO⁻), and cyanide ions (CN⁻). The reactions can also be categorized based on the charge of the nucleophilic reactants, which could be (a) negatively charged (e.g., OH⁻, RS⁻, CN⁻) or (b) neutral (e.g., amines, thiols). Both kinds of nucleophiles can be added onto protonated or non-protonated α,β -unsaturated enones. Since the experimental pK_b value of (*E*)-chalcone was reported to be -5.00 [25], only additions onto the non-protonated chalcones were taken into consideration. The general mechanisms of the addition of deprotonated (path A) and neutral (path B) nucleophiles onto non-protonated chalcones are shown in Figure 2.

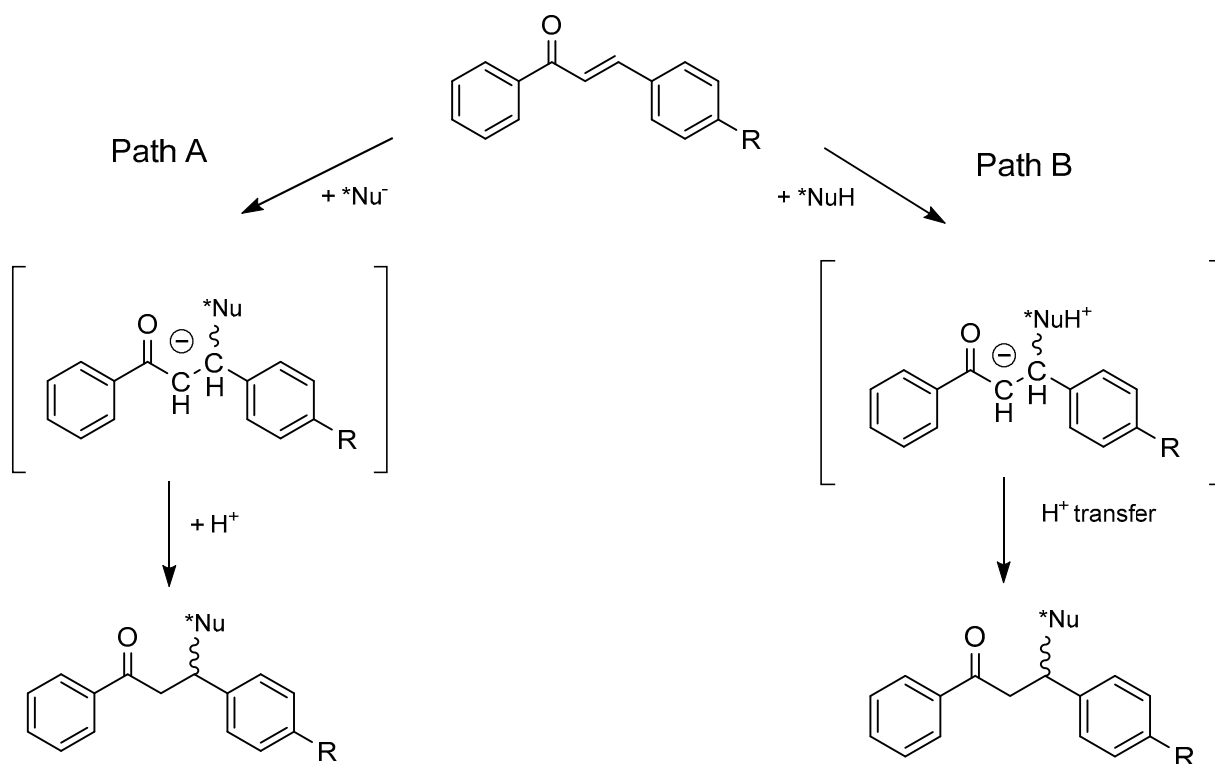


Figure 2. General mechanisms of the addition reaction of nucleophiles onto the activated double bonds of chalcones.

As shown in Figure 2, the primary adduct of the addition reactions either possesses a negative charge (path A) or has a zwitterion structure (path B). The second step of the reactions is an acid–base process, which can occur in an intermolecular or—in the case of the zwitterion intermediates—an intramolecular manner [26].

Previously, we reported the synthesis and reactions of two 4'-hydroxychalcones and their bis-methyleneamino (Mannich) derivatives. It was found that the Mannich derivatives showed significantly increased reactivity [27] and diastereoselectivity [28] in comparison to the respective non-Mannich derivatives when the reactions were conducted under acidic (about pH 3) conditions.

We investigated the reactions under three conditions with different pH: (a) pH 8.0/8.53, (b) pH 6.3/6.8, and (c) pH 3.2/3.7. The first pH values indicate the pH of the aqueous solution of the thiols before starting the incubations. The second pH values indicate the virtual pH of the incubation mixtures, which contained 75.5% *v/v* methanol (MeOH). The basic pH was selected because such conditions mimic the GST-catalyzed reactions; the ionization of the GSH thiol moiety increases due to its interaction with the basic imidazole N atom in the active site of the enzyme [29]. The slightly acidic conditions resemble the slightly acidic pH of the cancer cells [30]. The stronger acid conditions were selected to compare the reactivity of the protonated (neutral) and the ionized forms of the thiol functions of the two compounds. The pK_a of the thiol group of GSH and NAC was reported to be 8.83 and 9.52, respectively [18]. Accordingly, the thiol function of both compounds exists exclusively in the protonated (neutral) form under such acidic conditions. The stereoselectivity of the reactions was monitored by comparing the HPLC peak areas of the respective chalcone–GSH and chalcone–NAC adducts.

The reactions are reported to be reversible, accordingly resulting in the formation of an equilibrium mixture. To qualitatively characterize the progress of the addition processes, the composition of the incubation mixtures was analyzed at the 15, 45, 75, 105, 135, 165, 195, 225, 255, 285, and 315 min time points by HPLC-UV-VIS.

2. Results

2.1. Reactions under Basic (pH 8.0/8.5) Conditions

Initially, we investigated the reactions of the two chalcones under basic conditions. Considering the pK_a values of GSH (8.83) and NAC (9.52), about 31.9% of the GSH molecules and 8.7% of the NAC molecules existed under pH 8.5 conditions (the virtual pH of the incubates) in the more reactive thiolate form. By the end of the investigated period (315 min), the initial area of the HPLC peak corresponding to the parent compounds **1** and **2** reduced to 3.7% and 7.9%, respectively (Table 1). While the compounds were incubated with NAC, the respective figures were 5.2% and 9.8% (Table 2). Progress curve changes in the chromatographic peak areas of the starting chalcones (**1** and **2**) as a function of the incubation time of the reactions indicated that the compositions reflect those of the equilibrium in each case (Figures 3 and 4).

Change of chromatographic areas as a function of time, GSH, pH 8.0/8.5

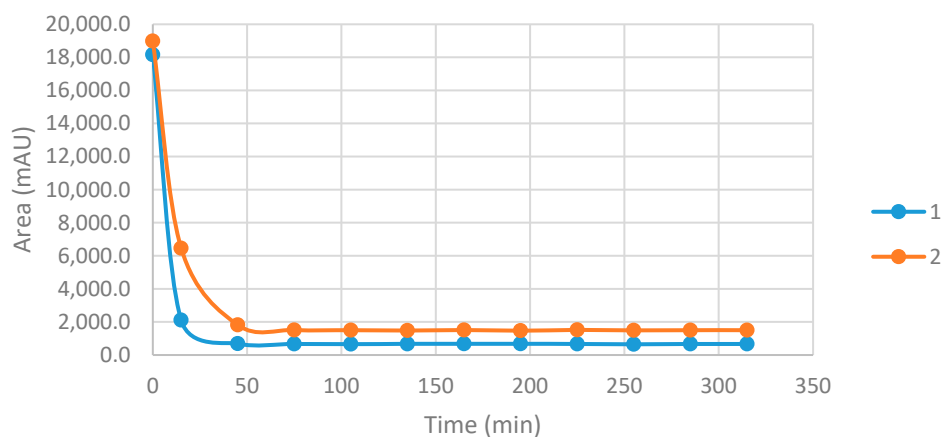


Figure 3. Change in the chromatographic peak area of chalcones **1** and **2** in the chalcone–GSH incubations at pH 8.0/8.5.

Change of chromatographic areas as a function of time, NAC, pH 8.0/8.5

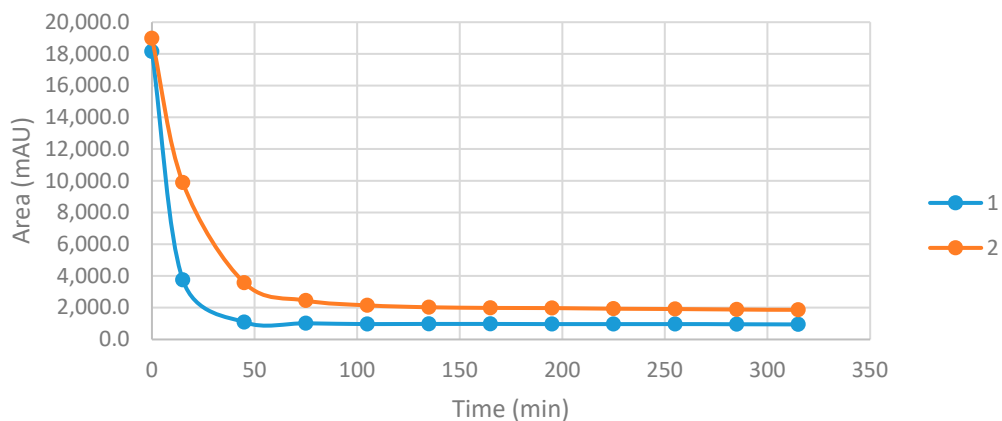


Figure 4. Change in the chromatographic peak area of chalcones **1** and **2** in the chalcone–NAC incubations at pH 8.0/8.5.

As a result of the addition reactions, a new chiral center was formed. Considering the inherent chirality of the two thiols, the formation of two diastereomeric adducts was

expected. However, using our HPLC conditions, the 1-GSH and 2-GSH conjugates were not separated (Table 1).

In the case of NAC incubations, the formed 1-NAC and 2-NAC adducts were only partially separated. Based on the integration of the two overlapping peaks, the ratio of the two diastereomeric adducts (NAC-1 and NAC-2) showed a different (1.7–1.2 times) excess of the less polar diastereomers (Table 2). The structure of the parent chalcones (1 and 2) as well as their GSH and NAC conjugates was verified by HPLC-MS (Table S1 and Figures S10–S15).

Table 1. Retention times (t_R)¹ and integrated peak areas (A) of the investigated chalcones (1 and 2) and their GSH adducts².

pH ³	Compound	t_R (E)-Chalcone	Area Ratio ⁴ A_{315}/A_0	t_R (Z)-Chalcone	Area (Z)-Chalcone	t_R GSH-1	Area GSH-1	t_R GSH-2	Area GSH-2
3.2	1	16.4	0.81	16.2	<100	13.8	4245	N/D ⁵	-
3.2	2	15.9	0.96	15.7	<100	11.9	3352	N/D ⁵	-
6.3	1	16.3	0.09	16.0	<100	13.2	16,571	N/D ⁵	-
6.3	2	15.8	0.21	15.5	<100	11.3	17,160	N/D ⁵	-
8	1	16.3	0.04	16.1 ⁶	<100	13.3	17,419	N/D ⁵	-
8	2	15.7	0.08	15.5	<100	11.0	20,387	N/D ⁵	-

¹ Retention times in minutes; ² data refer to the average of two independent measurements at the 315 min time point; ³ pH value of the aqueous thiol solution; ⁴ ratio of peak areas measured at 0 and 315 min; ⁵ not detectable; ⁶ only detectable at the 15, 45, 75, 135, and 165 min time points.

Table 2. Retention times (t_R)¹ and integrated peak areas (A) of the investigated chalcones (1 and 2) and their NAC adducts².

pH ³	Compound	t_R (E)-Chalcone	Area Ratio ⁴ A_{315}/A_0	t_R (Z)-Chalcone	Area (Z)-Chalcone	t_R NAC-1	Area NAC-1	t_R NAC-2	Area NAC-2
3.2	1	16.3	0.89	16.1	<100	15.2	1260	15.3	2173
3.2	2	15.8	0.98	15.5	<100	14.1	1156	14.2	1507
6.3	1	16.3	0.24	16.0	<100	15.1	4906	15.2	6457
6.3	2	15.8	0.47	15.5	<100	14.1	4712	14.2	5422
8	1	16.2	0.05	16.0	<100	15.1	6167	15.2	8875
8	2	15.7	0.10	15.5	<100	14.1	7167	14.2	8975

¹ Retention times in minutes; ² data refer to the average of two independent measurements at the 315 min time point; ³ pH value of the aqueous thiol solution; ⁴ ratio of peak areas measured at 0 and 315 min.

The progress curves of the formation of the diastereomeric NAC adducts—based on the integrated HPLC peak areas (AUCs)—are shown in Figures 5 and 6. As shown, the formation of the 1-NAC diastereomers is increased in the first 45 min and remained the same over the time of incubation. In the case of the 2-NAC diastereomers, rapid formation of the kinetic product (NAC-1) was observed in the first 15 min. After that, however, the NAC-1 isomer of 2 was transisomerized to the thermodynamic product (NAC-2), reaching the equilibrium composition by the 105 min time point (Figures 5 and 6).

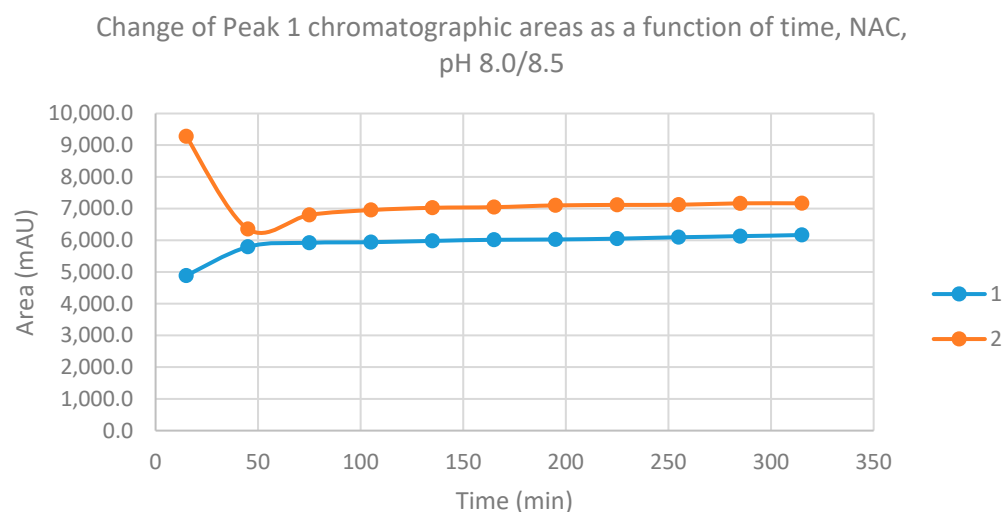


Figure 5. Change in the chromatographic peak area of adduct 1 of chalcones **1** and **2** in the chalcone–NAC incubations at pH 8.0/8.5.

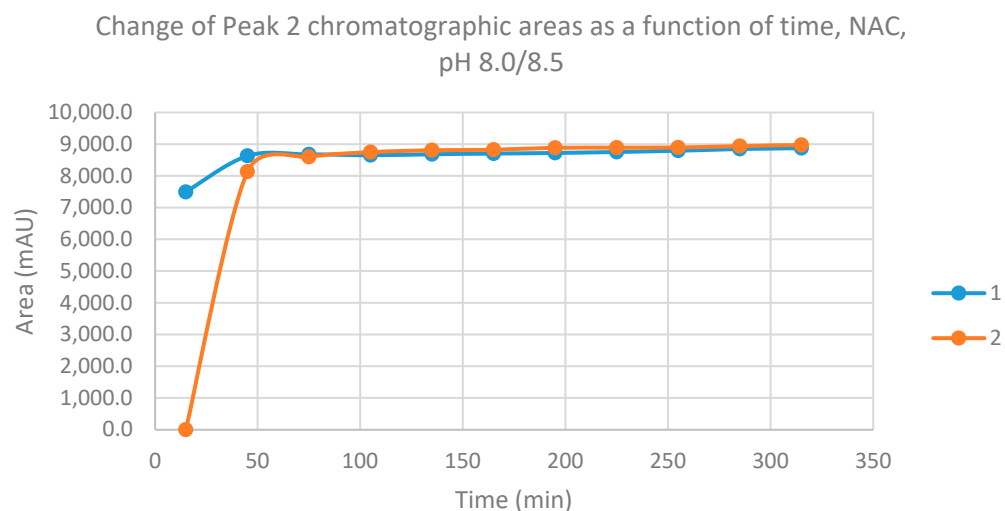


Figure 6. Change in the chromatographic peak area of adduct 2 of chalcones **1** and **2** in the chalcone–NAC incubations at pH 8.0/8.5.

Further to the above data, it is worth mentioning that during the incubations with GSH and NAC, small new peaks appeared in the chromatograms with a somewhat shorter retention time than that of unreacted **1** and **2** (Tables 1 and 2). Based on our previous results [31], the new peaks were supposed to be those of the respective (*Z*) diastereomers. Since such isomerization could not be observed in the incubations performed without the thiols, the formation of the (*Z*) isomer can be considered due to the retro-Michael reaction. To identify the structure of the expected (*Z*) diastereomers, light-initiated isomerization of **1** and **2** was performed. Based on the result of the light-initiated isomerization experiment, the formed compounds were identified as the respective (*Z*) isomers (Figures S16 and S17).

2.2. Reactions under Slightly Acidic (pH 6.3/6.8) Conditions

Reactions under slightly acidic conditions mimic the cellular milieu of cancer cells [30]. Under these experimental conditions (pH 6.8), about 0.9% of GSH and 0.2% of NAC molecules exist in the more reactive thiolate form. The progress of the reactions under such conditions was more restricted than that observed at pH 8.0/8.5. In the GSH incubations, the initial area of the parent compounds **1** and **2** was reduced to 9.4% and 21.4%, respec-

tively, by the end of the investigated period (Table 1). The respective figures for the NAC incubations were 24.4% and 46.8% (Table 2).

Progression curves of the reactions (Figures 7 and 8) indicated that the percentage figures represent compositions close to equilibrium. Similar to the results obtained under pH 8.0/8.5 conditions, the formation of a small amount of (Z) isomers was detected in the incubation mixtures.

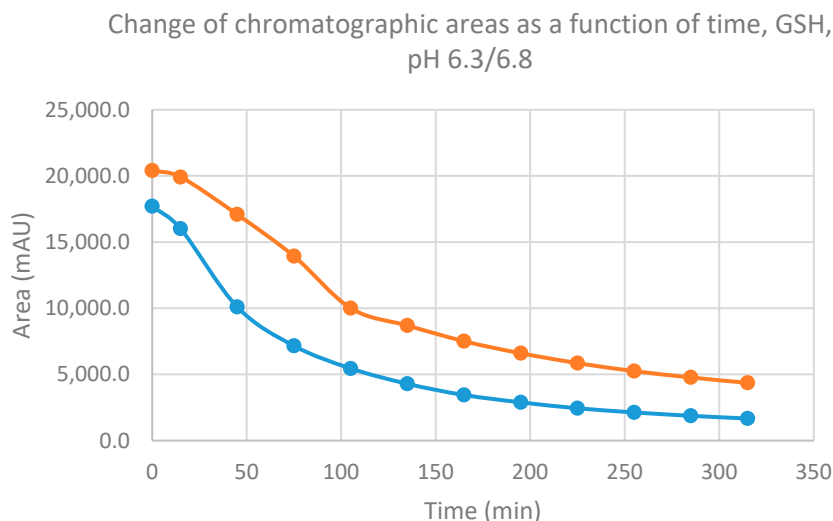


Figure 7. Change in the chromatographic peak area of chalcones 1 and 2 in the chalcone–GSH incubations at pH 6.3/6.8.

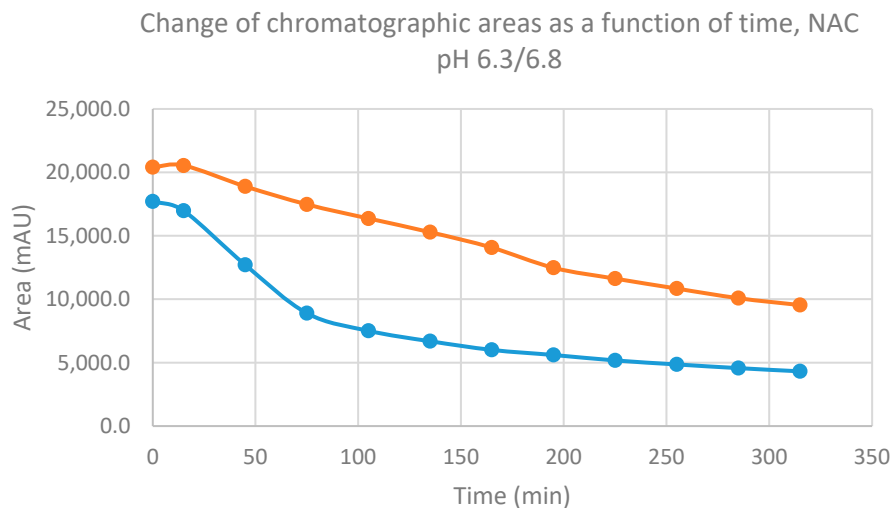


Figure 8. Change in the chromatographic peak area of chalcones 1 and 2 in the chalcone–NAC incubations at pH 6.3/6.8.

Progression curves of the formation of the chalcone–GSH and chalcone–NAC adducts showed two parallel concave curves with finite limits (Figures S1–S4).

2.3. Reactions under Acidic (pH 3.2/3.7) Conditions

Reactions under stronger acidic conditions proceeded to a much lower extent than those under the above two conditions. Under stronger acidic conditions, the thiol function of both GSH and NAC exists exclusively in protonated (neutral) form. Although protonated thiols can act as nucleophilic reagents, their reactivity is much lower than that of their deprotonated (negatively charged) counterparts [32].

Only a small amount of adducts were detected in each case in the chalcone–GSH/NAC incubates (Table 2). The chromatographic peak area values of the (*Z*) isomers were similar to those in the respective incubates at pH 8.0/8.5 and pH 6.3/6.8 (Tables 1 and 2).

Progression curves of the reaction of chalcones with GSH showed a linear downhill shape (Figure S5). A similar linear reduction in the chromatographic peak areas was observed in the NAC incubations (Figure S6).

Over the whole incubation period, the chromatographic peak areas of the chalcone–GSH (Figure S7) and chalcone–NAC diastereomers continuously increased (Figures S8 and S9).

3. Discussion

Our experiments demonstrated that both GSH and NAC react with the investigated chalcones under acidic (pH 3.2/3.7, pH 6.3/6.8) and basic (pH 8.0/8.5) conditions. However, the rate of the initial reactions and the composition of the equilibrium mixtures were affected by the nature of the reactants and the pH of the incubation mixtures.

Analysis of the effect of the 4-substituents under basic (pH 8.0/8.5) or slightly acidic (pH 6.3/6.8) conditions showed 4-methyl-substituted **1** to display higher initial reactivity. ^{13}C NMR shifts, indicating the electron density around the particular nucleus of the *beta*-C atom of **1** (144.9 ppm) and **2** (144.6 ppm), were reported to be similar [33]. The observed difference in the reactivity of chalcones **1** and **2** can be explained by the stability of the thiol adducts. An early work of Humphlett et al. demonstrated that the activity of the α -hydrogen atom of the adduct, the resonance stabilization of the enone formed by cleavage, and the anionic stability of the thiolate ion are the determining factors of the reverse process. The authors found the α -keto and β -phenyl substitutions as determining factors in the effective reverse reactions [34]. Since the 4-methoxy substitution can more effectively increase the electron density on the carbon–carbon double bond, and the formed chalcone is resonance stabilized, the elimination process is more effective in the case of **2** than **1**. Similar conclusions were made by d'Oliveira et al. while investigating a few chalcones and their rigid quinolone analogues [35].

The retro-thia-Michael reactions can result in the formation of the respective (*Z*) isomers as well. Therefore, to obtain authentic reference (*Z*) isomers, the stereochemically homogeneous (*E*) isomers (**1** and **2**) were submitted with light-initiated isomerization, as published before [30]. As a result, HPLC-MS data agreed with the respective (*Z*) isomers (Figures S16 and S17).

Comparison of the $\text{p}K_a$ values of GSH (8.83) and NAC (9.52) thiols, and the respective conversions of the starting chalcones (Tables 1 and 2), showed that the higher the $\text{p}K_a$ of the thiol, the lower the conversion of the chalcones in the case of both derivatives at each investigated pH. This observation reflects the importance of acidity (K_a) of the thiol group that regulates the relative amount of RS^- concerning RSH , hence the equilibrium.

HPLC analysis of the reactions of **1** and **2** with NAC showed a different (1.7–1.2 times) excess of the less polar diastereomer (Table 2). The observed diastereoselectivity was affected by both the nature of the 4-substituent and the pH. Thus, at each different pH value, it was the methyl-substituted **1** that showed higher diastereoselectivity. In contrast, in the case of both chalcones, diastereoselectivity decreased with the increase in the pH. HPLC-UV-Vis chromatograms of the chalcone **1**-NAC incubations at pH 8.0/8.3, pH 6.3/6.8, and pH 3.2/3.7 (315 min time point) are shown in Figures S18–S20, respectively. The corresponding HPLC-UV-Vis chromatograms of the chalcone **2**-NAC incubations are shown in Figures S21–S23.

These observations give additional indirect support to the formation of a six-membered, hydrogen-bond-stabilized cyclic intermediate in the reactions of chalcones with the protonated form of thiols. The formation of such a cyclic intermediate was suggested earlier in the reaction of GSH with the bis-Mannich derivatives of 4'-hydroxychalcones [27]. According to our previous explanation, the protonated thiol attacks the planar enone moiety from

the *Re*-side, resulting in a six-membered intermediate with a pseudoequatorial position of the bulky aryl ring (Figure 9).

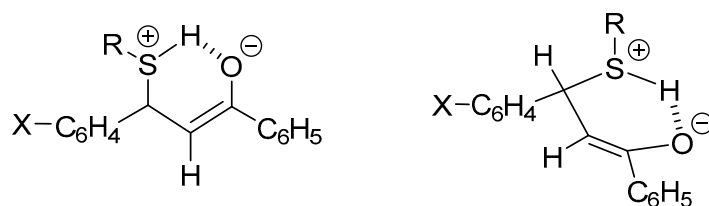


Figure 9. Possible enolate intermediate of the addition of protonated thiols onto chalcones.

Michael-type thiol reactivity of chalcones and related compounds is frequently associated with biological activities [6–11,36]. In contrast, several examples demonstrate that non-covalent interactions of chalcones with cellular macromolecules can play an important role in the biological effects of the compounds [37]. In a QSAR study, Katsori et al. found the clog *P* parameter to play an important part in the QSAR relationships. The authors found the electronic effects are comparatively unimportant in the anticancer effect of the investigated chalcones [38]. Comparison of the spontaneous thiol reactivities of the two chalcones under pH 8.0/8.5 and pH 6.3/6.8 conditions toward GSH and NAC showed some characteristic differences. Conversion of **1** with both GSH and NAC was higher than **2** under all investigated conditions (Tables 1 and 2). The experimental log *P* of **2** and **3** has been reported to be 4.12 and 3.67, respectively [39]. Thus, it is reasonable to suppose that both the thiol reactivity and the lipophilic properties contributed to the reported biological effects of the investigated compounds and their cyclic analogues.

4. Materials and Methods

4.1. Chemicals and Reagents

Chalcones **1** and **2** were synthesized, as reported before [40]. Their purity was tested by TLC and HPLC-UV-VIS. Reduced L-glutathione and *N*-acetyl L-cysteine were obtained from Sigma-Aldrich (Budapest, Hungary). The methanol CHROMASOLV gradient for HPLC was obtained from Honeywell (Hungary). Trifluoroacetic acid HiperSolve CHROMANORM was obtained from VWR (Budapest, Hungary) and formic acid from Fischer Chemicals. Deionized water for use in HPLC and HPLC-MS measurements was purified by Millipore Direct-Q™ at the Institute of Pharmaceutical Chemistry (University of Pécs). Mobile phases used for HPLC measurements were degassed by an ultrasonic water bath before use.

4.2. Preparation of Solutions

To evaluate the reactivity of the investigated chalcones and their analogues with thiols, reduced glutathione (GSH) and *N*-acetylcysteine (NAC) solutions were prepared as follows: Each solution was prepared at three different pH values (3.2, 6.3, and 8.0). The pH was set using 1M NaOH solution. (a) Solutions of GSH and NAC were prepared in water to a final volume of 1.5 cm³ with a concentration of 2.0 × 10⁻¹ mol·L⁻¹ (0.3 mmol thiol). (b) Chalcone solutions were freshly prepared before incubation to a 4.6 cm³ volume of HPLC-grade methanol with a concentration of 6.5 × 10⁻³ mol·L⁻¹ (0.03 mmol chalcone). (c) The GSH/NAC and chalcone solutions were pre-incubated in a 37 °C water bath for 15 min in the dark. Then, the solutions were mixed, resulting in a mixture of the thiol and the chalcone in a molar ratio of 10:1. The mixture was kept in the dark in a temperature-controlled (37 °C) water bath for a total duration of 315 min. To monitor the reaction by RP-HPLC, samples were taken at time points of 15, 45, 75, 105, 135, 165, 195, 225, 255, 285, and 315 min.

To evaluate the initial (0 min) peak area of chalcones **1** and **2**, 4.6 cm³ methanolic solution of each was prepared as above (method (b)), and the solutions were diluted with

1.5 mL of aqueous solution with the respective pH before analysis. Before mixing, the solutions were pre-incubated at 37 °C for 30 min.

To compare the products of the previously proven light-initiated *E/Z* isomerization of the parent compounds [26] with those of the non-light (retro-Michael addition)-initiated isomerization, solutions of chalcones **1** and **2** were prepared by method (b), and the solutions were subjected to unscattered laboratory light for 1 week. The solutions were analyzed by HPLC-UV-VIS and HPLC-MS.

4.3. RP-HPLC-UV-VIS Measurements

The measurements were performed on an Agilent 1100 HPLC system coupled with a UV-VIS detector. The wavelength was set at 260 nm. The separation of the components was carried out in a reversed-phase chromatographic system. A Zobrax Eclipse XBD-C8 column (150 mm × 4.6 mm, particle size 5 µm; Agilent Technologies, Waldbronn, Germany) was used. The injection volume was 10 µL. During the time of the measurement, the column oven was set at room temperature (25 °C). Data were recorded and evaluated by the use of Agilent Chem Station (B.03.01). Gradient elution was performed at a flow rate of 1.2 mL/min; the mobile phase consisted of (A) water and 0.1% trifluoroacetic acid and (B) methanol and 0.1% trifluoroacetic acid. The gradient profile was as follows: an isocratic period of 8 min of 40% mobile phase B, followed by a linear increase to 60% in 4 min, a second linear gradient to 90% in 3 min, and a 5 min isocratic period of 90%. The column was then equilibrated to the initial conditions with a 2 min linear gradient to 40%, followed by 3 min of the isocratic period.

4.4. HPLC-MS Measurements

HPLC ESI-MS analyses were performed on an Ultimate 3000 liquid chromatograph (Dionex, Sunnyvale, CA, USA) coupled with a Thermo Q Exactive Focus quadrupole-Orbitrap hybrid mass spectrometer (Thermo Fisher Scientific, Waltham, MA, USA). The scan monitored *m/z* values ranging from 100 to 1000 Da. Data acquisition was carried out using Q Exactive Focus 2.1 and Xcalibur 4.2 software (Thermo Fisher Scientific). Analysis of compounds and adducts was performed in HESI positive and negative ionization modes with the following parameters: spray voltage, 3500 V; vaporizer temperature, 300 °C; capillary temperature, 350 °C; spray and auxiliary gas flows, 30 and 10 arbitrary units, respectively; resolution, 35,000 at 200 *m/z*; and fragmentation, 20 eV.

HPLC separation was performed on an Accucore C18 column (150 mm × 2.1 mm, particle size 2.6 µm), and an Accucore C18 guard column (5 mm × 2.1 mm, particle size 2.6 µm) was also used. The injection volume was 5 µL; the flow rate was set to 0.4 mL/min. Data analysis and evaluations were performed using Xcalibur 4.2 and FreeStyle 1.7 software. A binary gradient of eluents was used, consisting of mobile phases A and B.

The parameters of the gradient in chalcones were (A) water and 0.1% formic acid and (B) methanol and 0.1% formic acid. The gradient elution was as follows: isocratic elution for 1 min to 20% eluent B, continued by a linear gradient to 100% in 9 min, followed by an isocratic plateau for 2 min. Then, the column was equilibrated back to 20% in 0.5 min and continued isocratically for 2.5 min. The sampler was at room temperature, and the column oven was kept at 40 °C.

The parameters of the gradient in the case of adducts were (A) water and 0.1% formic acid and (B) methanol and 0.1% formic acid. The gradient elution was as follows: isocratic elution for 1 min to 10% eluent B, continued by a linear gradient to 95% in 13 min, followed by an isocratic plateau for 3 min. Finally, the column was equilibrated back to 10% in 0.1 min and continued isocratically for 2.9 min. The sampler was at room temperature, and the column oven was kept at 40 °C. The diode array detector was also set at 260 nm wavelength alongside MS analysis.

5. Conclusions

The present work aimed to investigate the thiol reactivity of two 4-substituted chalcone derivatives (**1** and **2**) with different experimental log-*P*-values. HPLC-UV-VIS and HPLC-MS investigations of spontaneous reactions of the two chalcones at three different pH values revealed that the compounds have similar reactivities. Furthermore, comparison of the composition of the equilibrium mixtures revealed the importance of the electronic effect of the 4-substituent on the stability of the enolate intermediates.

HPLC analysis of the incubation mixtures of **1** and **2** with NAC demonstrated different stereochemistry of the addition of the protonated and non-protonated thiol nucleophile onto the enone moiety. The results provided further support for the dominant conformation-derived diastereoselective addition of the protonated thiols onto the chalcones' polar carbon-carbon double bond.

We could not find a direct correlation of the thiol reactivities and the previously published biological (cancer cell cytotoxic) effects of chalcones **1** and **2**. It is reasonable to suppose that both thiol reactivities and lipophilic properties contributed to the reported biological effects of the investigated compounds and their cyclic analogues.

Supplementary Materials: The following are available: Table S1. Mass spectrometry data; Figure S1. Change in the chromatographic peak area of adduct 1 of chalcones **1** and **2** in the chalcone-GSH incubations at pH 8.0/8.5. Figure S2. Change in the chromatographic peak area of adduct 1 of chalcones **1** and **2** in the chalcone-GSH incubations at pH 6.3/6.8. Figure S3. Change in the chromatographic peak area of adduct 1 of chalcones **1** and **2** in the chalcone-NAC incubations at pH 6.3/6.8. Figure S4. Change in the chromatographic peak area of adduct 2 of chalcones **1** and **2** in the chalcone-NAC incubations at pH 6.3/6.8. Figure S5. Change in the chromatographic peak area of chalcones **1** and **2** in the chalcone-GSH incubations at pH 3.2/3.7. Figure S6. Change in the chromatographic peak area of chalcones **1** and **2** in the chalcone-NAC incubations at pH 3.2/3.7. Figure S7. Change in the chromatographic peak area of adduct 1 of chalcones **1** and **2** in the chalcone-GSH incubations at pH 3.2/3.7. Figure S8. Change in the chromatographic peak area of adduct 1 of chalcones **1** and **2** in the chalcone-NAC incubations at pH 3.2/3.7. Figure S9. Change in the chromatographic peak area of adduct 2 of chalcones **1** and **2** in the chalcone-NAC incubations at pH 3.2/3.7. Figure S10. High-resolution, positive-mode HESI MS spectrum of chalcone **1**. Figure S11. High-resolution, positive-mode HESI MS spectrum of chalcone **2**. Figure S12. High-resolution, positive-mode HESI MS spectrum of chalcone **1**-GSH conjugate. Figure S13. High-resolution, negative-mode HESI MS spectrum of chalcone **1**-NAC conjugate. Figure S14. High-resolution, positive-mode HESI MS spectrum of chalcone **2**-GSH conjugate. Figure S15. High-resolution, negative-mode HESI MS spectrum of chalcone **2**-NAC conjugate. Figure S16. HPLC-UV-VIS spectrum of (*E*)(*t_R* 16.354 min)/(*Z*)(*t_R* 16.128 min) isomeric mixture of chalcone **1**. Figure S17. HPLC-UV-VIS spectrum of (*E*)(*t_R* 15.607 min)/(*Z*)(*t_R* 15.855 min) isomeric mixture of chalcone **2**. Figure S18. HPLC-UV-VIS chromatogram of pH 8.0/8.5 incubation (315 min time point) of chalcone **1** and NAC. Figure S19. HPLC-UV-VIS chromatogram of pH 6.3/6.8 incubation (315 min time point) of chalcone **1** and NAC. Figure S20. HPLC-UV-VIS chromatogram of pH 3.2/3.7 incubation (315 min time point) of chalcone **1** and NAC. Figure S21. HPLC-UV-VIS chromatogram of pH 8.0/8.5 incubation (315 min time point) of chalcone **2** and NAC. Figure S22. HPLC-UV-VIS chromatogram of pH 6.3/6.8 incubation (315 min time point) of chalcone **2** and NAC. Figure S23. HPLC-UV-VIS chromatogram of pH 3.2/3.7 incubation (315 min time point) of chalcone **2** and NAC.

Author Contributions: Conceptualization, P.P.; methodology, P.P., F.K. and S.M.; formal analysis, F.K. and S.M.; writing—original draft preparation, P.P., F.K. and S.M.; writing—review and editing, P.P. All authors have read and agreed to the published version of the manuscript.

Funding: This research was funded by the EFOP Operational Program "Comprehensive Development for Implementing Smart Specialization Strategies" at the University of Pécs (grant no. EFOP-3.6.1-16-2016-00004).

Institutional Review Board Statement: Not applicable.

Informed Consent Statement: Not applicable.

Data Availability Statement: Not applicable.

Conflicts of Interest: The authors declare no conflict of interest.

Sample Availability: Samples of the compounds 1 and 2 are available from the authors.

References

- Rozmer, Z.; Perjési, P. Naturally occurring chalcones and their biological activities. *Phytochem. Rev.* **2016**, *15*, 87–120. [CrossRef]
- Gomes, M.N.; Muratov, E.N.; Pereira, M.; Peixoto, J.C.; Rosseto, L.P.; Cravo, P.V.L.; Andrade, C.H.; Neves, B.J. Chalcone derivatives: Promising starting points for drug design. *Molecules* **2017**, *22*, 1210. [CrossRef]
- Zhou, B. Diverse molecular targets for chalcones with varied bioactivities. *Med. Chem.* **2015**, *5*, 388–404. [CrossRef]
- Mahapatra, D.K.; Bharti, S.K.; Asati, V. Chalcone derivatives: Anti-inflammatory potential and molecular targets perspectives. *Curr. Top. Med. Chem.* **2017**, *17*, 3146–3169. [CrossRef]
- Orlikova, B.; Tasdemir, D.; Golais, F.; Dicato, M.; Diederich, M. Dietary chalcones with chemopreventive and chemotherapeutic potential. *Genes Nutr.* **2011**, *6*, 125–147. [CrossRef]
- Amslinger, S.; Al-Rifai, N.; Winter, K.; Wörmann, K.; Scholz, R.; Baumeister, P.; Wild, M. Reactivity assessment of chalcones by a kinetic thiol assay. *Org. Biomol. Chem.* **2013**, *11*, 549–554. [CrossRef]
- Al-Rifai, N.; Rücker, H.; Amslinger, S. Opening or closing the lock? when reactivity is the key to biological activity. *Chem. Eur. J.* **2013**, *19*, 15384–15395. [CrossRef]
- Zhuang, C.; Zhang, W.; Sheng, C.; Zhang, W.; Xing, C.; Miao, Z. Chalcone: A privileged structure in medicinal chemistry. *Chem. Rev.* **2017**, *117*, 7762–7810. [CrossRef]
- Dinkova-Kostova, A.T.; Holtzclaw, W.D.; Cole, R.N.; Itoh, K.; Wakabayashi, N.; Katoh, Y.; Yamamoto, M.; Talalay, P. Direct Evidence That sulfhydryl groups of keap1 are the sensors regulating induction of phase 2 enzymes that protect against carcinogens and oxidants. *Proc. Natl. Acad. Sci. USA* **2002**, *99*, 11908–11913. [CrossRef]
- Nasir Abbas Bukhari, S.; Jantan, I.; Jasamai, M. Anti-inflammatory trends of 1, 3-diphenyl-2-propen-1-one derivatives. *Mini Rev. Med. Chem.* **2012**, *13*, 87–94. [CrossRef]
- Wang, J.; Wang, S.; Song, D.; Zhao, D.; Sha, Y.; Jiang, Y.; Jing, Y.; Cheng, M. Chalcone derivatives inhibit glutathione S-transferase P1-1 activity: Insights into the interaction mode of α , β -unsaturated carbonyl compounds. *Chem. Biol. Drug Des.* **2009**, *73*, 511–514. [CrossRef]
- Jin, Y.L.; Jin, X.Y.; Jin, F.; Sohn, D.H.; Kim, H.S. Structure activity relationship studies of anti-inflammatory TMMC derivatives: 4-dimethylamino group on the B ring responsible for lowering the potency. *Arch. Pharm. Res.* **2009**, *31*, 1145. [CrossRef]
- Dinkova-Kostova, A.T.; Massiah, M.A.; Bozak, R.E.; Hicks, R.J.; Talalay, P. Potency of michael reaction acceptors as inducers of enzymes that protect against carcinogenesis depends on their reactivity with sulfhydryl groups. *Proc. Natl. Acad. Sci. USA* **2001**, *98*, 3404–3409. [CrossRef] [PubMed]
- Groitel, B.; Jakob, U. Thiol-based redox switches. *Biochim. Biophys. Acta* **2014**, *1844*, 1335–1343. [CrossRef] [PubMed]
- Jackson, P.A.; Widen, J.C.; Harki, D.A.; Brummond, K.M. Covalent modifiers: A chemical perspective on the reactivity of α , β -unsaturated carbonyls with thiols via hetero-michael addition reactions. *J. Med. Chem.* **2017**, *60*, 839–885. [CrossRef] [PubMed]
- Poole, L.B. The basics of thiols and cysteines in redox biology and chemistry. *Free Radic. Biol. Med.* **2015**, *80*, 148–157. [CrossRef]
- Samuni, Y.; Goldstein, S.; Dean, O.M.; Berk, M. The chemistry and biological activities of N-acetylcysteine. *Biochim. Biophys. Acta* **2013**, *1830*, 4117–4129. [CrossRef] [PubMed]
- Aldini, G.; Altomare, A.; Baron, G.; Vistoli, G.; Carini, M.; Borsani, L.; Sergio, F. N-acetylcysteine as an antioxidant and disulphide breaking agent: The reasons why. *Free Radic. Res.* **2018**, *52*, 751–762. [CrossRef]
- Roos, G.; Foloppe, N.; Messens, J. Understanding the pK(a) of redox cysteines: The key role of hydrogen bonding. *Antioxid. Redox Signal.* **2013**, *18*, 94–127. [CrossRef]
- Shibata, S. Anti-tumorigenic chalcones. *Stem Cells* **1994**, *12*, 44–52. [CrossRef]
- Drutovic, D.; Chripkova, M.; Pilatova, M.; Kruzliak, P.; Pal Perjesi, P.; Sarissky, M.; Lupi, M.; Damia, G.; Brogginini, M.; Mojzis, J. Benzylidenetetralones, cyclic chalcone analogues, induce cell cycle arrest and apoptosis in HCT116 colorectal cancer cells. *Tumor Biol.* **2014**, *35*, 9967–9975. [CrossRef]
- Dimmock, J.R.; Elias, D.W.; Beazely, M.A.; Kandepu, N.M. Bioactivities of chalcones. *Curr. Med. Chem.* **1999**, *6*, 1125–1149.
- Dimmock, J.R.; Kandepu, N.M.; Nazarali, A.J.; Kowalchuk, T.P.; Motaganahalli, N.; Quail, J.W.; Mykytiuk, P.A.; Audette, G.F.; Prasad, L.; Perjési, P.; et al. Conformational and quantitative structure–activity relationship study of cytotoxic 2-arylidenebenzocycloalkanones. *J. Med. Chem.* **1999**, *42*, 1358–1366. [CrossRef]
- Rozmer, Z.; Berki, T.; Maász, G.; Perjési, P. Different effects of two cyclic chalcone analogues on redox status of jurkat T cells. *Toxicol. In Vitro* **2014**, *28*, 1359–1365. [CrossRef]
- Noyce, D.S.; Jorgenson, M. Jeffraim. Carbonyl reactions. XIX. The basicities of substituted chalcones. *J. Am. Chem. Soc.* **1962**, *84*, 4312–4319. [CrossRef]
- Bernasconi, C.R. Nucleophilic addition to olefins. Kinetics and mechanism. *Tetrahedron* **1989**, *45*, 4017–4090. [CrossRef]
- Bernardes, A.; Pérez, C.; Mayer, M.; da Silva, C.; Martins, F.; Perjési, P. Study of reactions of two mannich bases derived of 4'-hydroxychalcones with glutathione by RP-TLC, RP-HPLC and RP-HPLC-ESI-MS analysis. *J. Braz. Chem. Soc.* **2017**, *28*, 1048–1062. [CrossRef]

28. Bernardes, A.; D'Oliveira, G.D.C.; Silezin, A.; Kuzma, M.; Molnár, S.; Noda Pérez, C.; Perjési, P. Reagent-induced asymmetric induction in addition reaction of reduced glutathione onto bis-mannich chalcones. *Arch. Pharm.* **2018**, *351*, 1700386. [CrossRef]
29. Caccuri, A.M.; Antonini, G.; Board, P.G.; Parker, M.W.; Nicotra, M.; Bello, M.L.; Federici, G.; Ricci, G. Proton release on binding of glutathione to alpha, mu and delta class glutathione transferases. *Biochem. J.* **1999**, *344*, 419–425. [CrossRef] [PubMed]
30. Rohani, N.; Hao, L.; Alexis, M.; Joughin, B.; Krismer, K.; Moufarrej, M.; Soltis, A.; Lauffenburger, D.; Yaffe, M.; Burge, C.; et al. Acidification of tumor at stromal boundaries drives transcriptome alterations associated with aggressive phenotypes. *Cancer Res.* **2019**, *79*, 1952–1966. [CrossRef] [PubMed]
31. Perjési, P. (E)-2-benzylidenebenzocyclanones: Part XIII—(E)/(Z)-isomerization of some cyclic chalcone analogues. Effect of ring size on lipophilicity of geometric isomers. *Monatsh. Chem. Chem. Mon.* **2015**, *146*, 1275–1281. [CrossRef]
32. LoPachin, R.M.; Gavin, T. Reactions of electrophiles with nucleophilic thiolate sites: Relevance to pathophysiological mechanisms and remediation. *Free Radic. Res.* **2016**, *50*, 195–205. [CrossRef] [PubMed]
33. Perjési, P.; Linnanto, J.; Kolehmainen, E.; Ósz, E.; Virtanen, E. E-2-benzylidenebenzocycloalkanones. IV. Studies on transmission of substituent effects on ¹³C NMR chemical shifts of E-2-(X-benzylidene)-1-tetralones, and -benzosuberones. Comparison with the ¹³C NMR data of chalcones and E-2-(X-benzylidene)-1-indanones. *J. Mol. Struct.* **2005**, *740*, 81–89. [CrossRef]
34. Allen, C.F.H.; Humphlett, W.J. The thermal reversibility of the michael reaction V. The effect of the structure of certain thiol adducts on cleavage. *Can. J. Chem.* **1966**, *44*, 2315–2321. [CrossRef]
35. d'Oliveira, G.D.C.; Custodio, J.M.F.; Moura, A.F.; Napolitano, H.B.; Pérez, C.N.; Moraes, M.O.; Prókai, L.; Perjési, P. Different reactivity to glutathione but similar tumor cell toxicity of chalcones and their quinolinone analogues. *Med. Chem. Res.* **2019**, *28*, 1448–1460. [CrossRef]
36. De Freitas Silva, M.; Pruccoli, L.; Morroni, F.; Sita, G.; Seghetti, F.; Viegas Jr, C.; Tarozzi, A. The keap1/Nrf2-ARE pathway as a pharmacological target for chalcones. *Molecules* **2018**, *23*, 1803. [CrossRef] [PubMed]
37. Kozurkova, M.; Tomeckova, V. Interaction of chalcone derivatives with important biomacromolecules. In *Chalcones and Their Synthetic Analogs*; Perjési, P., Ed.; Nova Science Publisher: New York, NY, USA, 2020; pp. 95–133.
38. Katsori, A.-M.; Hadjipavlou-Litina, D. Chalcones in cancer: Understanding their role in terms of QSAR. *Curr. Med. Chem.* **2009**, *16*, 1062–1081. [CrossRef] [PubMed]
39. Rozmer, Z.; Perjési, P.; Takács-Novák, K. Use of RP-TLC for determination of log P of isomeric chalcones and cyclic chalcone analogues. *JPC Mod. TLC* **2006**, *19*, 124–128. [CrossRef]
40. Perjési, P.; Földesi, A.; Szabó, D. Synthesis of 4,6-diaryl-2,3-dihydro-6H-1,3-thiazine-2-thiones by the reaction of chalcones with dithiocarbamic acid. *Acta Chim. Hung.* **1986**, *122*, 119–125. [CrossRef]

Article

New Insights on Glutathione's Supramolecular Arrangement and Its In Silico Analysis as an Angiotensin-Converting Enzyme Inhibitor

Antônio S. N. Aguiar ^{1,*}, Igor D. Borges ^{1,2}, Leonardo L. Borges ^{1,3}, Lucas D. Dias ^{1,4}, Ademir J. Camargo ¹, Pál Perjesi ⁴ and Hamilton B. Napolitano ^{1,4,*}

¹ Grupo de Química Teórica e Estrutural de Anápolis, Universidade Estadual de Goiás, Anápolis 75132-903, GO, Brazil

² Centro de Pesquisa e Eficiência Energética, CAO A Montadora de Veículos LTDA, Anápolis 75184-000, GO, Brazil

³ Escola de Ciências Médicas e da Vida, Pontifícia Universidade Católica de Goiás, Goiânia 74605-010, GO, Brazil

⁴ Laboratório de Novos Materiais, Universidade Evangélica de Goiás, Anápolis 75083-515, GO, Brazil

* Correspondence: toninho.quimica@gmail.com (A.S.N.A.); hbnapolitano@gmail.com (H.B.N.)

Abstract: Angiotensin-converting enzyme (ACE) inhibitors are one of the most active classes for cardiovascular diseases and hypertension treatment. In this regard, developing active and non-toxic ACE inhibitors is still a continuous challenge. Furthermore, the literature survey shows that oxidative stress plays a significant role in the development of hypertension. Herein, glutathione's molecular structure and supramolecular arrangements are evaluated as a potential ACE inhibitor. The tripeptide molecular modeling by density functional theory, the electronic structure by the frontier molecular orbitals, and the molecular electrostatic potential map to understand the biochemical processes inside the cell were analyzed. The supramolecular arrangements were studied by Hirshfeld surfaces, quantum theory of atoms in molecules, and natural bond orbital analyses. They showed distinct patterns of intermolecular interactions in each polymorph, as well as distinct stabilizations of these. Additionally, the molecular docking study presented the interactions between the active site residues of the ACE and glutathione via seven hydrogen bonds. The pharmacophore design indicated that the hydrogen bond acceptors are necessary for the interaction of this ligand with the binding site. The results provide useful information for the development of GSH analogs with higher ACE inhibitor activity.

Keywords: glutathione; supramolecular arrangement; M06-2X/6-311++G(d,p); DFT; molecular docking; angiotensin-converting enzyme

Citation: Aguiar, A.S.N.; Borges, I.D.; Borges, L.L.; Dias, L.D.; Camargo, A.J.; Perjesi, P.; Napolitano, H.B. New Insights on Glutathione's Supramolecular Arrangement and Its In Silico Analysis as an Angiotensin-Converting Enzyme Inhibitor. *Molecules* **2022**, *27*, 7958. <https://doi.org/10.3390/molecules27227958>

Academic Editor: Hyun-Ock Pae

Received: 28 September 2022

Accepted: 10 November 2022

Published: 17 November 2022

Publisher's Note: MDPI stays neutral with regard to jurisdictional claims in published maps and institutional affiliations.



Copyright: © 2022 by the authors. Licensee MDPI, Basel, Switzerland. This article is an open access article distributed under the terms and conditions of the Creative Commons Attribution (CC BY) license (<https://creativecommons.org/licenses/by/4.0/>).

1. Introduction

Cardiovascular disease (CD) is still the leading cause of mortality worldwide [1]. It is one of the costliest diseases for governments and healthcare systems (up to USD 320 billion/year) [2]. In 2019, according to a report from the World Health Organization (WHO), 17.9 million people died from CD, including clinical disorders of the heart and blood vessels [3]. There are several risk factors for CD, such as high blood pressure, diabetes mellitus, smoking, dyslipidemia, and being overweight/obesity [4,5]. Regarding increased blood pressure, its physiopathology is multifactorial and based on salt intake, obesity/insulin resistance, the influence of the sympathetic nervous system, and the renin–angiotensin–aldosterone system [6]. Among these factors, the renin–angiotensin–aldosterone system exerts a controlling function on blood pressure and hypertension via the synthesis of angiotensin II (a potent vasoconstrictor) [7] catalyzed by the angiotensin-converting enzyme (ACE, EC 3.4.15.1) [8]. ACE inhibitors comprise the first line of medicines employed in hypertension therapy, heart failure, myocardial infarction, and diabetic nephropathy [9].

The history of the development of inhibitors of the enzyme started in the 1960s when Rocha e Silva recognized that the effect of bradykinin (an important vasodilator peptide in controlling blood pressure) could be boosted by some peptides (BFP) found in the venom of a Brazilian snake, *Bothrops jararaca* [10]. Later, it was recognized that these peptides could inhibit the enzyme (named kininase II at that time) that can reduce the vasodilation effect of bradykinin. Further research clarified that the molecular basis of the enzymatic inhibition of bradykinin inactivation is the same as that in the formation of angiotensin II from the inactive angiotensin I. Currently, the enzyme catalyzing these reactions is called ACE [11]. Based on these observations, a series of compounds have been synthesized [12] and isolated from natural sources [13,14] that showed an effective inhibitory action on the enzyme [9]. Today, ACE inhibitors are widely used to manage hypertension [15]. Captopril, enalapril, and lisinopril are commercially available antihypertensive drugs to treat hypertension. However, their use presents some adverse effects, for instance, first-dose hypotension, hyperkalemia, renal dysfunction, angioedema, and cough [16,17].

In this regard, there is a great interest in developing new ACE inhibitors that present lower adverse effects compared to these clinically used antihypertensive drugs. As selected examples, some candidates are evaluated and described in the literature, such as the analogs of lisinopril [18], thymosin alpha-1 (Th α 1) peptide [19], gonadotropin-releasing hormone (GnRH) [20], C-domain-specific phosphinic inhibitor, RXPA380 [21], and glucosides derived from eugenol [22]. Some of these studies also reported the characterization and modeling by molecular docking of the interaction between the candidates and the active site residues of the ACE.

Furthermore, the literature survey indicated that oxidative stress is frequently associated with high blood pressure [23]. Based on these clinical observations, several compounds with antioxidant capacity (among them GSH) were tested as potential ACE inhibitors. Such compounds (similar to captopril, a registered ACE inhibitor with thiol functionality) could act as dual-acting antihypertensive agents. In vitro inhibitory studies showed GSH to have ACE inhibitory activity falling into the μ M range [23,24]. For example, the K_i constants for GSH and lisinopril against an angiotensin-converting enzyme purified from human plasma were determined as 11.7 μ M and 0.662 nM, respectively [23].

Glutathione is a tripeptide composed of glutamine, cysteine, and glycine, which plays a pivotal role as a biological antioxidant [25,26]. Moreover, it is widely applied in the cosmetic, food, and pharmaceutical industries [27], as described in the European Pharmacopoeia [28]. In this regard, the supramolecular arrangements of GSH polymorphs (GSHA and GSHB) and molecular modeling by density functional theory (DFT) were compared to verify the conformations of the lowest energies in the system. The electronic structure by the frontier molecular orbitals and the molecular electrostatic potential (MEP) map were carried out to understand the molecular contact regions and predict the regions of electrophilic and radical attacks during the biochemical processes. In addition, the hydrogen bonds on supramolecular arrangements were studied by Hirshfeld surfaces (HS), quantum theory of atoms in molecules (QTAIM), and natural bonding orbital (NBO) analyses. Finally, in silico analysis validated the co-crystallized ligand (lisinopril, a commercial ACE inhibitor) with the angiotensin-converting enzyme via redocking analysis. To evaluate the GSH ACE inhibitor, the same model employed in the lisinopril redocking was also used for the GSH in the ACE.

2. Results and Discussion

2.1. Solid State Analysis

The crystal structure of the GSH is a ubiquitous thiol-containing tripeptide (*L*- γ -glutamyl-*L*-cysteinylglycine) that exists in its zwitterionic form. This structure is also reflected in the IR spectrum of the compounds recorded in KBr. Above the 3000 cm^{-1} regions, several associated OH, NH, NH_2 , and NH_3^+ (3346, 3249, and 3126) bands can be seen. A band at 2524 cm^{-1} can be associated with the cysteine thiol (SH) group. The 1713 cm^{-1} band corresponds to the $\nu\text{C}=\text{O}$ band of the protonated carboxyl groups, while

the strong bands at 1537 and 1385 cm^{-1} are related to the asymmetric and symmetric stretches, respectively, of the deprotonated CO_2^- group [29].

The low molecular weight sulfur (thiols) present in GSH are easily oxidized and can be regenerated rapidly; these characteristics allow them to play an essential role in cell biology, such as protecting cells via an antioxidant process [30]. The polymorphism has been observed only under ambient pressure conditions, revealing that their polymorphs crystallize in the orthorhombic space group $P2_12_12_1$. The differences in the geometry, crystal data, and structure refinement details for GSHA and GSHB are summarized in Table 1. The ORTEP diagrams of the GSHA and GSHB can be found in Figure 1, as well as the overlap of these polymorphs.

Table 1. Crystallographic data and structure refinement parameters for GSHA and GSHB.

Crystallographic Data	GSHA	GSHB
Empirical formula	$\text{C}_{10}\text{H}_{17}\text{N}_3\text{O}_6\text{S}$	$\text{C}_{10}\text{H}_{17}\text{N}_3\text{O}_6\text{S}$
Formula weight	307.33	307.33
Crystal system	orthorhombic	orthorhombic
Space group	$P2_12_12_1$	$P2_12_12_1$
a (Å)	5.2748(2)	5.6131(11)
b (Å)	8.3459(3)	8.720(2)
c (Å)	25.496(3)	27.940(5)
α (°)	90	90
β (°)	90	90
γ (°)	90	90
Volume (Å ³)	1122.39(14)	1367.6(5)
Z	4	4
ρ_{calc} (g/cm ³)	1.819	1.492
μ (mm ⁻¹)	0.077	0.146
F(000)	648.0	648.0
Crystal size/mm ³	$0.2 \times 0.2 \times 0.1$	$0.19 \times 0.14 \times 0.11$
Radiation	synchrotron ($\lambda = 0.47670$)	synchrotron ($\lambda = 0.5636$)
2 θ range for data collection/°	3.444 to 34.714	2.312 to 55.978
Index ranges	$-6 \leq h \leq 6$ $-10 \leq k \leq 10$ $-14 \leq l \leq 14$	$-9 \leq h \leq 9$ $-14 \leq k \leq 14$ $-46 \leq l \leq 44$
Reflections collected	5512	36,183
Goodness of fit on F ²	1.115	1.268
Final R indexes [all data]	$R_1 = 0.0483$, $wR_2 = 0.0449$	$R_1 = 0.0340$, $wR_2 = 0.0780$
Largest diff. peak/hole (eÅ ⁻³)	0.24/−0.29	0.50/−0.53
Flack parameter	−0.2(3)	−0.01(4)

The results obtained for the GSH conformer molecular geometries were compared to the crystallographic model through the mean absolute deviation percentage formula,

$$\text{MADP} = \frac{100}{n} \sum_{i=1}^n \left| \frac{\chi_{DFT} - \chi_{XRD}}{\chi_{XRD}} \right|, \quad (1)$$

where χ_{DFT} and χ_{XRD} indicate the theoretical and experimental bond length or angle, respectively. The exchange and correlation functional M06-2X captures medium-range electronic correlation and can satisfactorily describe scattering interactions such as non-covalent interactions [31,32]. Other functionals were tested, such as the hybrid functional B3LYP, the highly parameterized empirical functional M06-HF [31], and the double-hybrid functional B2-PLYP [33]. However, the MAPD values showed that the functional M06-2X can satisfactorily describe scattering interactions, such as non-covalent interactions [31]. The graph presented in Figure 2 shows the results of the MAPD values obtained for the different levels of theory for GSH.

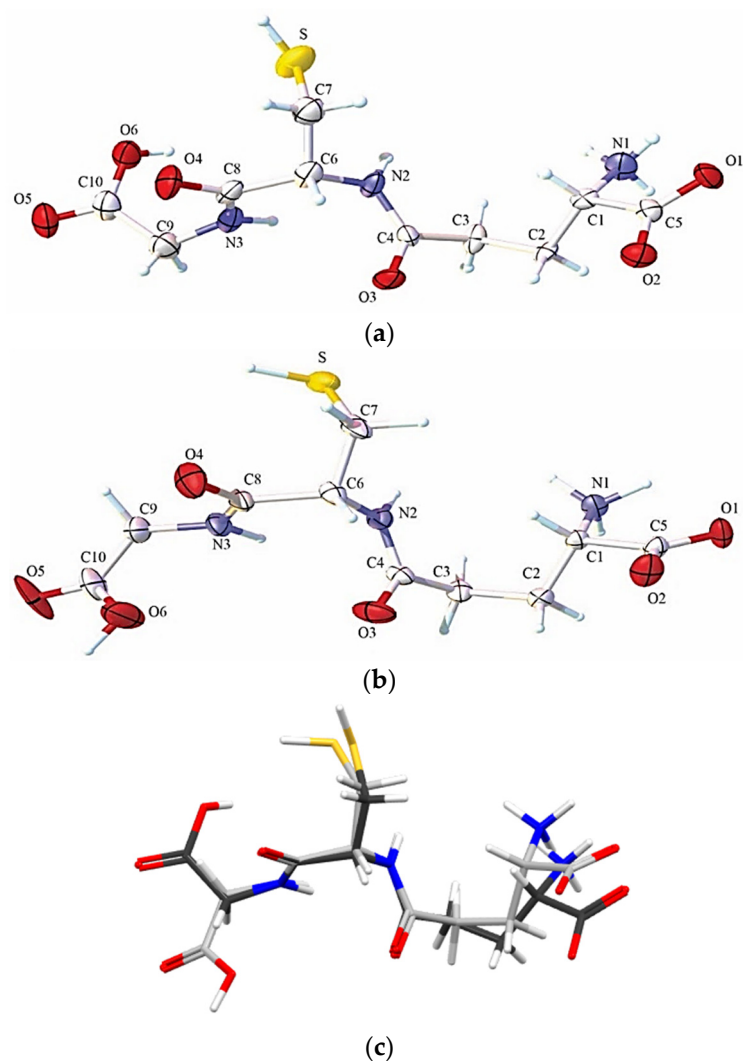


Figure 1. ORTEP diagram for (a) GSHA, (b) GS HB, and (c) the overlapping structure. The ellipsoids are represented at a 75% probability level with the atomic numbering scheme. The hydrogen atoms are represented by spheres with arbitrary radii. (c) The overlap of GSHA and GS HB polymorphs.

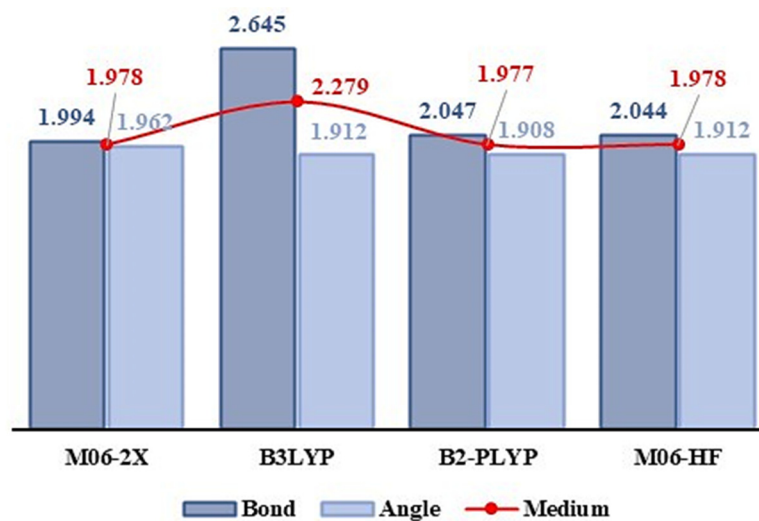


Figure 2. Graph of the mean absolute deviations for geometric parameters obtained by the exchange and correlation functionals M06-2X, B3LYP, B2-PLYP, and M06-HF (compared to experimental results).

The MAPD values obtained for bond lengths and angles, at the M06-2X/6-311++G(d,p) level of theory, were 1.994 and 1.530%, respectively, where the Pearson correlation coefficients were 0.9790 and 0.9816. Figure 3 presents the graphs comparing the geometric properties obtained experimentally and theoretically. Regarding the lengths, stretching of the N₂-C₄, N₃-C₈, O₁-C₅, O₆-C₁₀, and C₁₀-C₉ and the compression of the N₁-C₁ and O₂-C₅ bonds were observed. In the GSH crystal, the molecules are found in the zwitterionic form, observed in the glutamic acid portion. In this structure, the O₁-C₅ and O₂-C₅ bonds have similar lengths (1.24 and 1.25 Å, respectively), making clear the resonant effect stabilizing the zwitterion conjugate base. However, theoretical calculations show that the isolated proton remains connected to the O₁ atom, stretching the O₁-C₅ bond by 6.4% and compressing the O₂-C₅ bond by 4.9%.

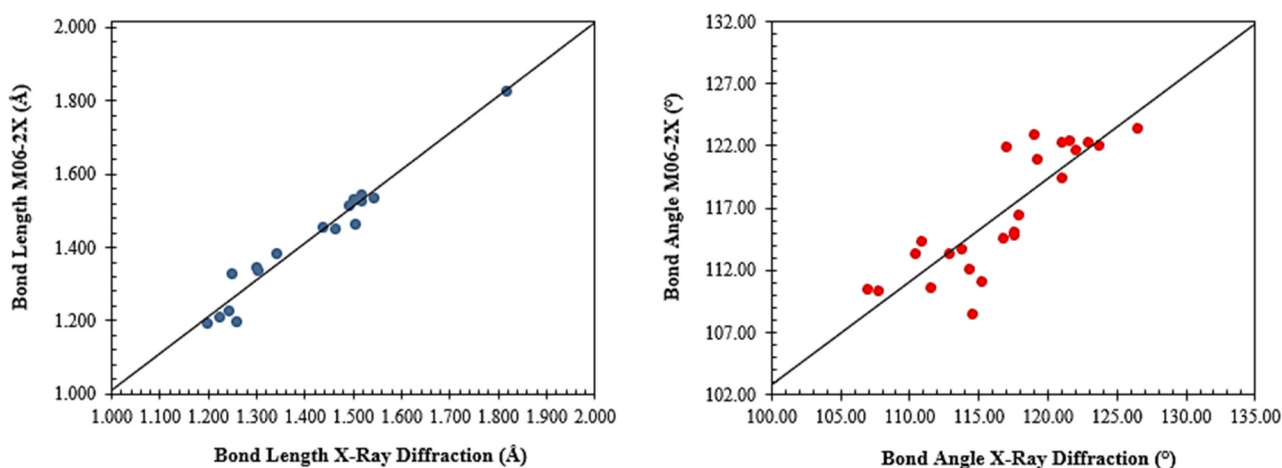


Figure 3. Comparison graphs of the geometric parameters' bond length and angle, obtained by XRD and the M06-2X/6-311++G(d,p) level of theory for the glutathione.

The transit of the proton from the primary amino group to the conjugate base also compresses the N₁-C₁ bond by 2.8%, leaving the electron pair of the N atom free to resonate along the bond. The calculations also showed that the N₂-C₄ and N₃-C₈ peptide bonds are stretched by 3.2 and 3.5% in the free form of the molecule. Finally, the O₆-C₁₀ bond of the glycine portion is stretched by 2.6% in the isolated form of the molecule. This effect is explained by the strong O₆-H \cdots O₃ interaction in the crystalline state, causing the proton to approach the O₆ atom, stretching O₆-C₁₀.

The zwitterionic form of GSH is predominant in the crystalline state. However, thermodynamic calculations (Table 2) showed that, when it is kept isolated, the lowest energy state for the molecule is the neutral form, and 134.03 kcal/mol is more stable than the ionized form. In addition, all thermodynamic parameters (internal energy, enthalpy, free energy, entropy, etc.) calculated for both forms resulted in values lower than their ionized state, except in the case of entropy, which is 18.47 cal/mol·K higher for the neutral form. A relaxed scan calculation was carried out to verify the change in the total energy of the molecular system in which the proton starts from the N₁ atom, bound at 1.0 Å, towards the O₁ atom. From the scan plot shown in Figure 4, it is possible to verify that the system's total energy decays as H⁺ approaches the conjugated carbonyl base.

Table 2. Glutathione thermochemical properties obtained at the M06-2X/6-311++G(d,p) level of theory.

Thermochemical Property	Neutral	Zwitterion	Diff*
Electronic Energy (kcal/mol)	−881,611.16	−881,477.12	−134.03
Zero-Point Energy (kcal/mol)	−881,430.11	−881,287.93	−142.18
Internal Energy (kcal/mol)	−881,419.18	−881,280.20	−138.98
Enthalpy (kcal/mol)	−881,418.59	−881,279.61	−138.98
Free Energy (kcal/mol)	−881,458.22	−881,313.73	−144.48
Entropy (cal/molK)	132.92	114.45	18.47
Heat Capacity (cal/molK)	69.59	50.57	-
Polarizability (a.u.)	174.96	162.49	-
Dipole Moment (Debye)	6.46	13.45	-

* $Diff = \varepsilon_n - \varepsilon_z$, where ε_n is the thermochemical property of the neutral form and ε_z is the ionized form.

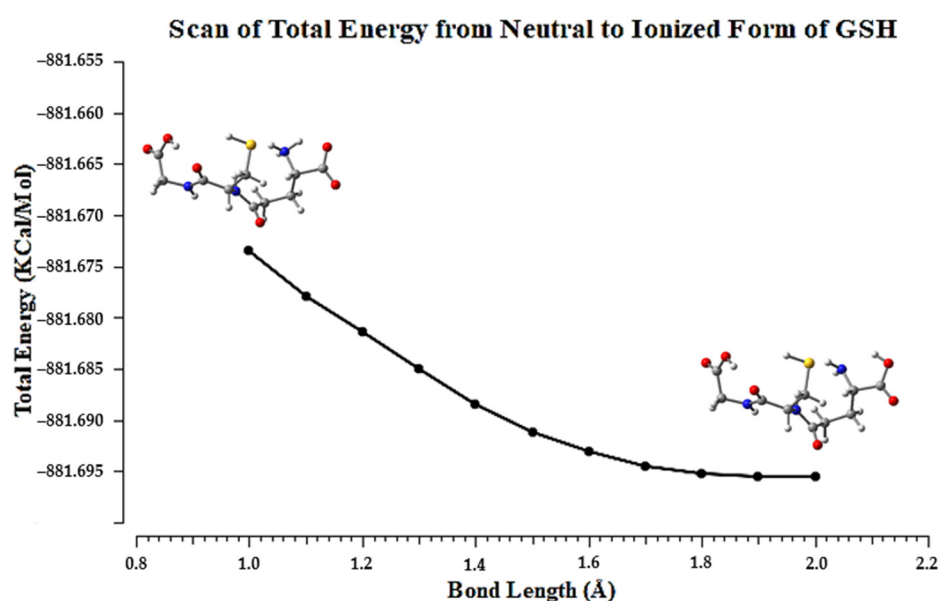


Figure 4. Plot showing the total energy derived from a relaxed potential energy surface sweep for the proton transition to the neutral and ionized forms of GSH, varying the distance $N_1 \cdots H$ by 1.0 Å in 0.1 Å increments.

Deviations greater than 2.0% also occurred in the bond angles. In the carboxyl group of the glutamic acid portion, a 4.3% increase in the $O_2-C_5-C_1$ angle and a 2.3% decrease in the $O_1-C_5-O_2$ angle were observed; the angles formed by C_1 were also increased by the proton transition in the molecular structure (3.2% in $N_1-C_1-C_2$ and 3.4% in $N_1-C_1-C_5$). On the other hand, the $C_5-C_1-C_2$ angle decreased by 5.2%. However, the distinction between the molecular structures of GSH in both polymorphs lies in the torsion of the tripeptide's carboxyl group of the glycine portion. The overlap of the peptide bond, $O_4=C_8-N_3-C_9$, showed that the dihedral angles are -6.93° and 1.23° , respectively, in GSHA and GSHB, and the $-COOH$ groups are at 73.63° and $77^\circ.51^\circ$ out of the plane of the peptide bond in the respective polymorphs. Figure 5 shows the overlapping of the molecular structures of GSHA and GSHB, starting from this dihedral, where the RMS was 0.0292 \AA . Torsions in the other portions of the molecule were also observed. Namely, the dihedral angle of $C_8-C_6-C_7-S$ (cysteine portion) is -66.29° and -58.05° , respectively, while the dihedral angle of the glutamic acid portion is 145.94° and 112.44° .

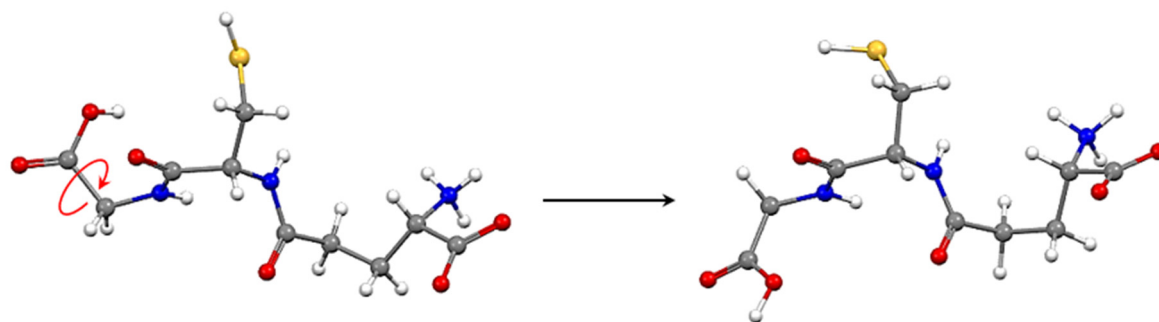


Figure 5. Torsion of the carboxyl group, -COOH, of the glycine portion in the glutathione molecule, and the overlapping of their molecular structures from the peptide bond that joins the glycine chain to the cysteine chain.

2.2. Molecular Modeling Analysis

The frontier molecular orbitals, HOMO and LUMO, are represented in Figure 6, and their values are shown in Table 3. These orbitals resulted in a very high energy gap (242.6 kcal/mol), calculated by $GAP = E_{LUMO} - E_{HOMO}$, and indicating the high kinetic stability of the GSH molecule. Its antioxidant power is related to protection against reactive oxygen species and electrophilic species produced in cellular oxidative processes; therefore, the values found for the energies of the frontier orbitals agree with this statement, indicating that the GSH molecule is a reductant ($E_{HOMO} < 0$), but not an oxidant ($E_{LUMO} > 0$). HOMO has a lone pair and pure p orbital characteristics, whose occupancy is $1.85558e$. LUMO, on the other hand, is an σ^* antibonding orbital located on the longitudinal axis of the $C_{10}-O_5$ bond, formed by the contribution of 65.02% of the C_{10} atom $sp^{1.86}$ and 34.98% of the O_5 atom $sp^{1.37}$; it has an occupancy of $0.01811e$.

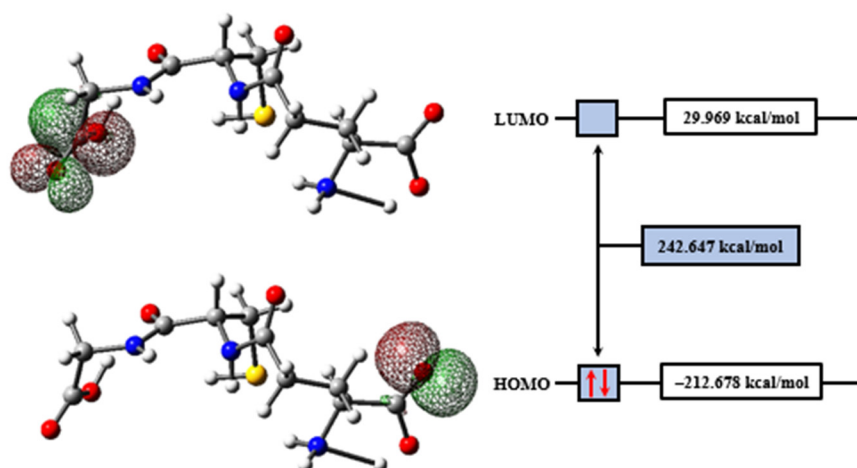
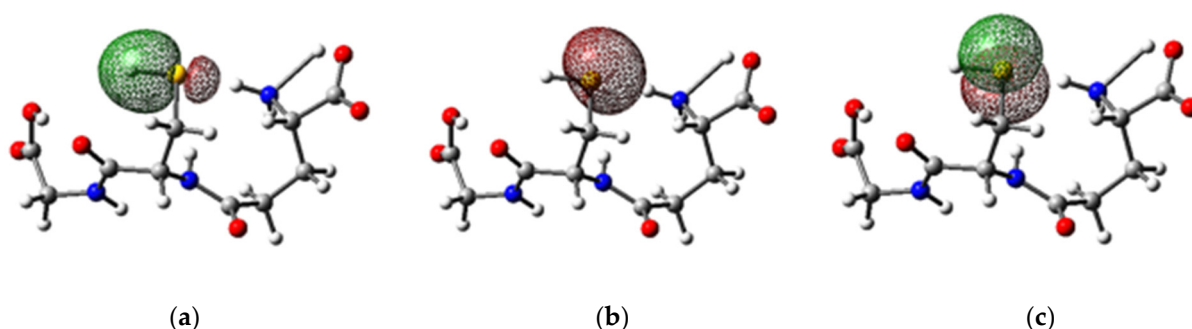


Figure 6. HOMO and LUMO plots for GSH calculated at the M06-2X/6-311++G(d,p) level of theory.

The sulfhydryl group (-SH) of the cysteine portion is highly polarizable, characterizing it as a good nucleophile [34,35]. The σ bonding orbital of the S-H bond has an occupancy of $1.99027e$ and is formed by the contribution of 57.66% of the $sp^{5.61}d^{0.04}$ orbital of S and 42.34% of the s orbital of H (Figure 7a). The lone pair form the η_1 bonding orbitals ($sp^{0.47}$), with an occupancy of $1.98974e$ (Figure 7b), and η_2 bonding orbital (p), with an occupancy of $1.95353e$ (Figure 7c). The calculated energies of these orbitals were -406.650 , -460.529 , and -213.606 kcal/mol, explaining the process of oxidation of GSH to glutathione disulfide through the activity of the glutathione oxidase enzyme, glutathione peroxidase, and glutathione reductase.

Table 3. Reactivity indices for the glutathione obtained at the M06-2X/6-311++G(d,p) level of theory.

Descriptors	(kcal/mol)
E_{HOMO}	−212.678
E_{LUMO}	29.969
GAP	242.647
Ionization Energy (I)	212.678
Electronic Affinity (A)	−29.969
Electronegativity (χ)	91.355
Chemical Potential (μ)	−91.355
Chemical Hardness (η)	242.647
Chemical Softness (σ)	0.004
Electrophilicity Index (ω)	17.197

**Figure 7.** Isosurface plots of the (a) s orbitals of the S-H bond, and of the lone pairs (b) $\eta_1(S)$ and (c) $\eta_2(S)$ of the S atom in glutathione, calculated at the M06-2X/6-311++G(d,p) level of theory.

From the energies of the HOMO and LUMO, the chemical reactivity descriptors of the GSH were determined as the potential chemical,

$$\mu = \left(\frac{\partial E}{\partial N} \right)_v = -\frac{I + A}{2} = -\chi, \quad (2)$$

chemical hardness

$$\eta = \frac{1}{2} \left(\frac{\partial^2 E}{\partial N^2} \right)_v = \frac{I - A}{2}, \quad (3)$$

and the global electrophilicity index,

$$\omega = \frac{\mu^2}{2\eta} \quad (4)$$

where E is the energy of the system, N is the number of electrons, v is the external potential generated by nuclei, $I \approx -E_{\text{HOMO}}$ is the ionization potential, and $A \approx -E_{\text{LUMO}}$ is the electron affinity. The high values found for the energy gap, as well as η , indicate that the GSH molecule is kinetically stable, having a low electron affinity and high electron transfer power during chemical processes.

Compared to other organic compounds, the results show that the GSH molecule has a nucleophilic character ($\omega < 0.93$ a.u.) [36]. Oxygen atoms of the carboxyl groups and the carbonyl groups of GSH have a high charge density, showing the behavior of a Lewis base. This can be seen by the red color on the electronic isodensity surface of the MEP map represented in Figure 8. On the other hand, regions of lower charge density appear in blue and show the behavior of a Lewis acid.

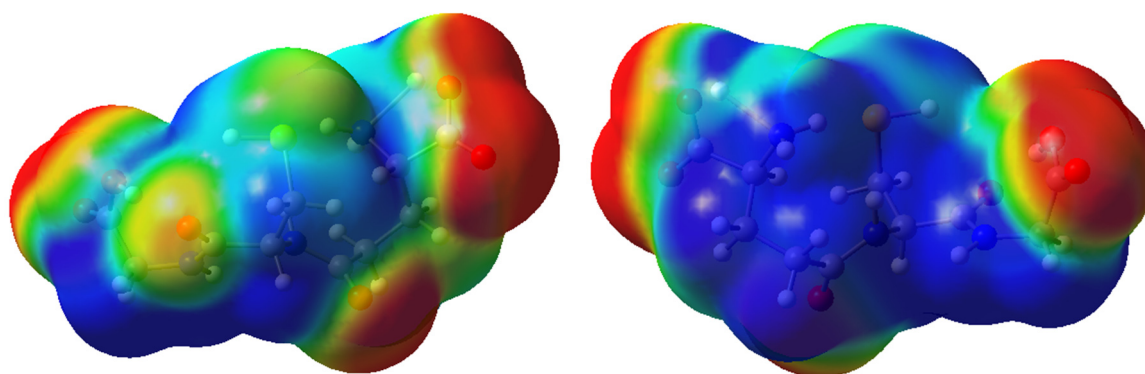


Figure 8. MEP surface at $\rho(r) = 4.0 \times 10^{-4}$ electrons/Bohr³ contour of the total SCF electronic density for glutathione molecule at the M06-2X/6-311++G(d,p) level of theory.

To determine the local electrophilicity, the Fukui function [37,38] was used to predict the regions of nucleophilic,

$$f^+ = \left[\frac{\partial \rho(r)}{\partial N} \right]_{v(r)}^+, \quad (5)$$

electrophilic,

$$f^- = \left[\frac{\partial \rho(r)}{\partial N} \right]_{v(r)}^-, \quad (6)$$

and radical attacks,

$$f^0 = \left[\frac{\partial \rho(r)}{\partial N} \right]_{v(r)}^0. \quad (7)$$

Radical reactions caused by pathological processes, by the administration of oxidizing drugs, or even by physical activities can cause oxidative transformations of phospholipids, proteins, and deoxyribonucleic acid (DNA) in cell membranes. According to Fukui index calculations, the O₁ and O₂ atoms of the carboxyl group and the N₁ atom of the amine group in the glutamic acid portion (Figure 9a) are favorable to the capture of free radicals produced in these processes, which explains the antioxidant character of GSH. Furthermore, the S atom in the cysteine portion can also undergo radical attacks resulting in the oxidized form of GSH, glutathione disulfide (GSSG), by the intervention of the enzymes glutathione oxidase or glutathione peroxidase. The calculations of the Fukui indices also indicated that GSH has active sites favorable to electrophilic attacks, identified by the isosurface regions in Figure 9b. All the oxygen and nitrogen atoms along the GSH molecule favor this type of attack. This can be explained by the mesomeric effect caused by the delocalized electrons of the carboxyl and amide groups in the tripeptide molecule. In addition, C atoms are favorable to electrophilic attacks, resulting from the inductive effect caused by the presence of O and N atoms, which reduces the charge density in the carbon chain skeleton.

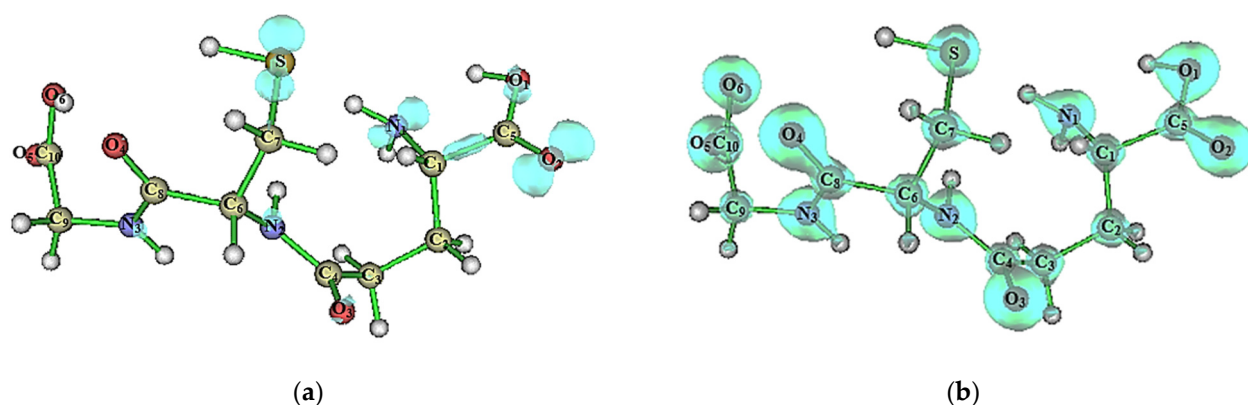


Figure 9. Isosurfaces of the (a) f^0 and (b) f^- functions, calculated at a proper value of 0.5 for the glutathione molecule.

2.3. Supramolecular Arrangement

The molecular topology of the crystals by HS mapped with d_{norm} helps us to understand better the crystallographic forces driving the molecular arrangement and the interactions reported in Table 4. The contacts that are shorter than the sum of the van der Waals radii are represented by the red spots on a predominantly blue surface [39]. The crystal packing of GSHA is stabilized by the bifurcated intermolecular interactions $S-H \cdots O_1$ and $S-H \cdots O_2$ observed in the cysteine portion, involving the thiol group forming a motif [40] $R_1^2(4)$, and, for GSHB, $S-H \cdots O_1$ was observed forming a motif $C_1^1(11)$ and the intermolecular interactions $N_1-H \cdots O_2$ [$C_1^1(5)$] and $N_2-H \cdots O_2$ [$C_1^1(8)$]; these contacts form bifurcates in each compound. The red convex area above the glutamic acid correlates with the hydrogen bond interactions $N_1-H \cdots O_4$ [$C_1^1(5)$] and $N_1-H \cdots O_1$ [$C_1^1(5)$]. Furthermore, the interactions $O_6-H \cdots O_3$ [$C_1^1(10)$] and $N_3-H \cdots O_5$ [$C_1^1(5)$] involve part of the glycine. The presence of weak non-classical H-bond interactions is also evident in the GSHA, which is $C_2-H \cdots O_4$ [$C_1^1(8)$] and, for GSHB, $C_3-H \cdots O_2$ [$C_1^1(6)$].

The fingerprint plots (Figure 10) allow us to analyze the differences in the intermolecular patterns of the contacts and quantitatively evaluate the contributions among atoms [41]. The contacts involving $H \cdots O$ accumulated a percentage of 50% and are viewed as a distinct pair of spikes, evidence that the H-bonds are dominant in the crystalline environment [42]. The $H \cdots H$ contacts, close to 34%, with a decrease of 0.8% for GSHB, contribute to the overall crystal packing. In contrast, the proportion of $S \cdots H$ increased from 6.3% for GSHA to 9.6% for GSHB. In addition, weak $C \cdots H$ contacts decreased from 3% in GSHA to 2% in GSHB, indicating that the GSHA forms more H-bonds than GSHB.

The topological parameters for the intermolecular interactions in the molecular arrangements of the GSH polymorphs are presented in Table 4, and the molecular graphs are represented in Figure 11. In QTAIM, the observable properties of the molecular system are contained in electron density $\rho(\mathbf{r})$, in which the Laplacian electron density, $\nabla^2\rho$, determines the depletions or peaks of the electron charge concentration between nuclear attractors, indicating the location of bond critical points (BCPs) [43–45]. In other words, $\nabla^2\rho$ corresponds to the concentration of the electronic charge in the intranuclear region of two attractors. If the electron density is accumulated in the intranuclear region, its value is negative in the BCP, and the interaction is shared so that the attractors are covalently attached. On the other hand, if $\nabla^2\rho > 0$, the electron density is concentrated in the attractors, a closed-shell interaction in which the attractors are linked by weak interactions. The low values of the electron density ($\rho < 0.1$) and the positive Laplacian found on the BCP indicate closed-shell interactions [43–46]. Furthermore, when the values for the ratio $|v|/G < 1.0$ and the total energies are very low, $h(\mathbf{r}) \approx 0$, this indicates the intermolecular interactions in the supramolecular arrangement of GSH are of low intensity, configuring hydrogen bonding. In the $O_6-H \cdots O_3$ and $N_1-H \cdots O_2$ interactions, the values found for

the ratio $|v|/G = 1.0$, with $h < 0$; however, these values do not indicate that the hydrogen bonds in these interactions have any covalent character, as the values of $h(\mathbf{r})$ are minimal.

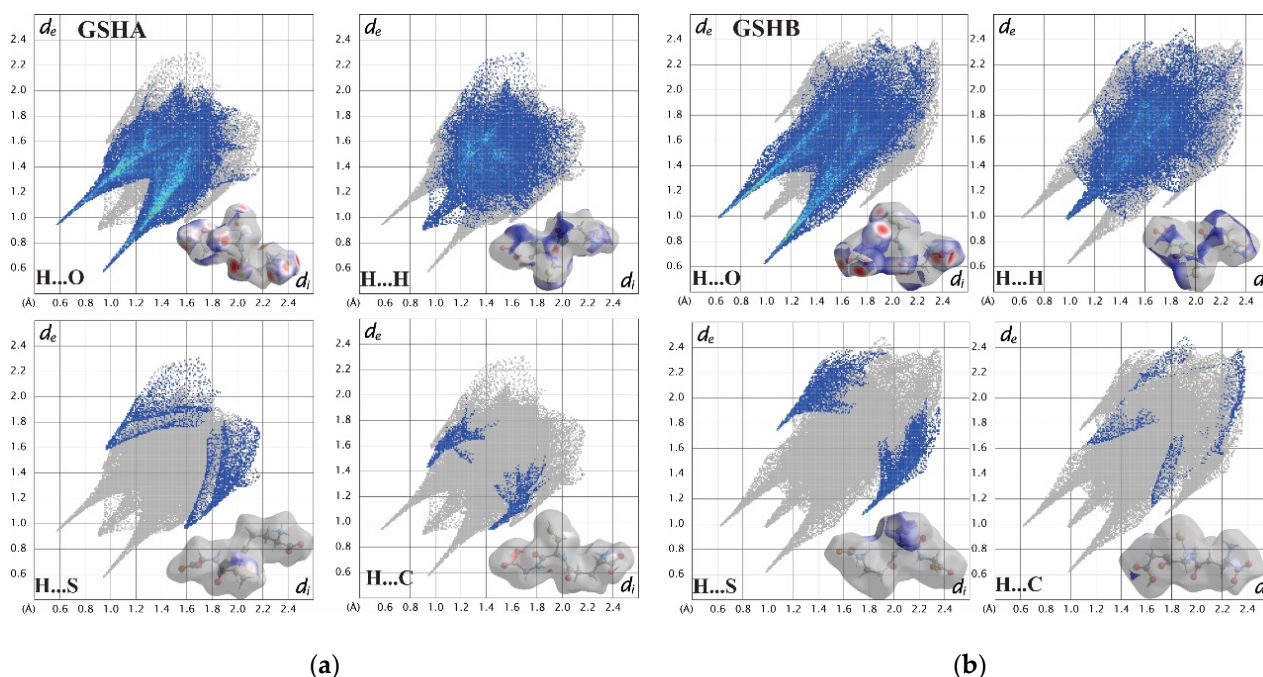


Figure 10. Fingerprint plots for (a) GSHA and (b) GSHB.

Table 4. Hydrogen bond geometry and topological parameters by QTAIM obtained for GSHA and GSHB glutathione molecular interactions.

D–H···A	D–H (Å)	H···A (Å)	D···A (Å)	D–H···A (°)	$\rho_{BCP}^{(a)}$ (a.u.)	$\nabla^2\rho_{BCP}^{(b)}$ (a.u.)	$G(\mathbf{r})^{(c)}$ (a.u.)	$v(\mathbf{r})^{(d)}$ (a.u.)	$h(\mathbf{r})^{(e)}$ (a.u.)	$\frac{ v(\mathbf{r}) }{G(\mathbf{r})}$
GSHA										
S–H···O ₁ ^I	1.2000	2.5900	3.691(5)	152	0.0175	0.0655	0.0140	−0.0116	0.0024	0.8
S–H···O ₂ ^I	1.2000	2.1500	3.261(8)	153′	0.0174	0.0660	0.0140	−0.0115	0.0025	0.8
O ₆ –H···O ₃ ^{II}	0.8300	1.6600	2.465(4)	164	0.0469	0.2126	0.0543	−0.0554	−0.0011	1.0
N ₁ –H···O ₁ ^{III}	0.8900	1.8200	2.669(10)	157′	0.0134	0.0512	0.0110	−0.0091	0.0018	0.8
N ₁ –H···O ₂ ^{II}	0.8900	2.2900	2.947(4)	130	0.0302	0.1483	0.0331	−0.0291	0.0040	0.9
N ₁ –H···O ₄ ^{IV}	0.8900	2.4800	3.122(6)	130	0.0085	0.0319	0.0067	−0.0055	0.0012	0.8
N ₂ –H···O ₂ ^{II}	0.8600	1.9900	2.675(7)	136′	0.0244	0.1175	0.0251	−0.0208	0.0043	0.8
N ₃ –H···O ₅ ^V	0.8600	2.0700	2.672(8)	127′	0.0214	0.1034	0.0216	−0.0173	0.0043	0.8
C ₂ –H···O ₄ ^{IV}	0.9700	2.4200	3.097(5)	127	0.0116	0.0416	0.0089	−0.0075	0.0015	0.8
GSHB										
S–H···O ₁ ^{VII}	1.3400	2.1800	3.4603(8)	158	0.0154	0.0538	0.0114	−0.0094	0.0020	0.8
N ₁ –H···O ₄ ^{VIII}	1.0200	1.8400	2.8034(6)	155	0.0310	0.1209	0.0285	−0.0267	0.0018	0.9
N ₁ –H···O ₁ ^{IX}	1.0200	1.9600	2.8383(7)	142′	0.0222	0.0956	0.0208	−0.0177	0.0031	0.9
N ₁ –H···O ₂ ^{II}	1.0200	1.7200	2.6959(6)	158′	0.0438	0.1527	0.0407	−0.0431	−0.0025	1.1
N ₂ –H···O ₂ ^{II}	1.0100	1.9600	2.8984(7)	154	0.0222	0.0993	0.0214	−0.0179	0.0035	0.8
N ₃ –H···O ₅ ^X	1.0100	2.0000	2.8712(7)	144′	0.0214	0.0924	0.0199	−0.0166	0.0032	0.8
O ₆ –H···O ₃ ^{XI}	0.9600	1.6400	2.5987(6)	172	0.0495	0.1628	0.0463	−0.0519	−0.0056	1.1
C ₃ –H···O ₂ ^{II}	1.0900	2.5200	3.3842(8)	135	0.0098	0.0297	0.0068	−0.0062	0.0006	0.9
Symmetry codes:	(I) $\frac{3}{2} + x, \frac{3}{2} - y, 1 - z$	(V) $2 - x, -\frac{1}{2} + y, \frac{1}{2} - z$	(IX) $\frac{1}{2} + x, \frac{3}{2} - y, -z$				(X) $2 - x, \frac{1}{2} + y, \frac{1}{2} - z$			
	(II) $1 + x, y, z$	(VI) $-1 + x, y, z$					(XI) $1 - x, -\frac{1}{2} + y, \frac{1}{2} - z$			
	(III) $\frac{1}{2} + x, \frac{1}{2} - y, 1 - z$	(VII) $1 + x, -1 + y, z$								
	(IV) $-1 + x, -1 + y, z$	(VIII) $x, 1 + y, z$								
Topological Properties:	(a) Total electronic density on BCP	(c) Lagrangian Kinetic energy					(e) Total energy density			
	(b) Laplacian of electron density on BCP	(d) Potential energy density								

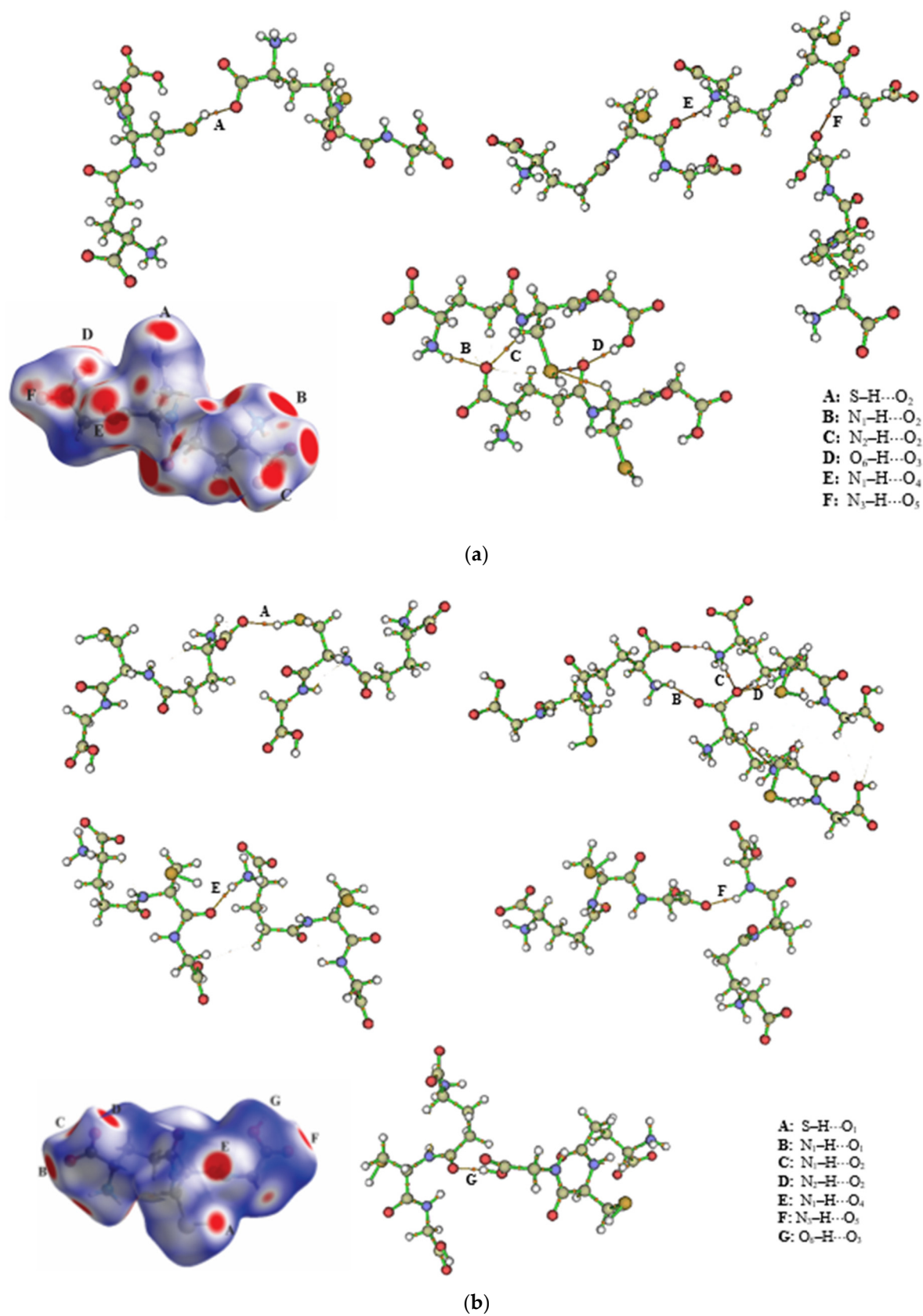


Figure 11. Molecular graphs of some bond paths of the intermolecular interactions in the supramolecular arrangements of the (a) GSHA and (b) GSHB polymorphs.

Closed-shell interactions are weak compared to shared interactions. The analysis of the NBO calculations showed that the hydrogen bonds in the supramolecular arrangements of GSH are stabilized by the hyperconjugation of lone pairs (Lewis type) with σ^* antibonding orbitals (non-Lewis type) of the interacting region of the neighboring molecule at higher energies. The most significant results of the NBO calculations are found in Tables S1 and S2 (Supplementary Materials). They show that the higher hyperconjugation energies stabilize the molecules in the GSHB polymorph more than in the GSHA polymorph. As an example, we cite the interactions that are commonly found in both polymorphs with high $E^{(2)}$ energies. The $O_6-H \cdots O_3$ interaction is stabilized by the hyperconjugation of the lone pairs of the O_3 atom with the σ^* antibonding orbitals of the O_6-H bond, $\eta_x(O_3) \rightarrow \sigma^*(O_6-H)$, $x = 1; 2$. The hyperconjugation of the $\eta_1(O_3)$ orbital (occupancy 1.98e, $sp^{0.7}$ hybrid) resulted in energy equal to 8.52 kcal/mol in GSHA and 7.80 kcal/mol in GSHB (ratio 1.1:1); on the other hand, the hyperconjugation of the $\eta_2(O_3)$ orbital (occupancy 1.88, pure p) resulted in energy equal to 9.45 kcal/mol in GSHA and 22.01 kcal/mol in GSHB (ratio 1:2.3). This means that the $O_6-H \cdots O_3$ interaction is more cohesive in the GSHB polymorph. Two other essential interactions in both polymorphs were $N_2-H \cdots O_2$ and $N_3-H \cdots O_5$. The first is stabilized by the hyperconjugation of the two lone pairs of O_2 , η_1 (occupancy 1.98e, $sp^{0.6}$ hybrid) and η_2 (occupancy 1.89e, pure p) with the σ^* antibonding orbital of the N_2-H bond in GSHA, with energies of 2.01 and 2.93 kcal/mol, but only by the lone pair η_2 (occupancy 1.96e, pure p) in GSHB, with an energy of 6.80 kcal/mol. In the $N_3-H \cdots O_5$ interaction, only the η_2 lone pair of O_5 (occupancy 1.86e, pure p) contributes to its stabilization in GSHA, while the two lone pairs of O_5 , η_1 (occupancy 1.97e, hybrid $sp^{0.7}$) and η_2 (occupancy 1.87e, pure p) hyperconjugate with the σ^* antibonding orbital of the N_3-H bond in GSHB; however, both energies in this polymorph further stabilize the interaction.

2.4. Molecular Docking Analysis

The ACE (EC 3.4.15.1), a Zn metalloproteinase, plays an essential role in cardiovascular function by converting the decapeptide angiotensin I to angiotensin II (vasopressor octapeptide). There are two isoforms of ACE (somatic and testis) that are transcribed from the same gene in a tissue-specific manner [47]. The somatic form consists of two homologous domains (N and C domain), each containing an active site with a conserved zinc-binding motif. Despite the high sequence similarity between the two domains, they differ in substrate and inhibitor specificity and their activation by chloride ions [48]. The C domain seems to be the dominant angiotensin-converting site [47]. Docking calculations indicate that lisinopril had the higher affinity for ACE_C. [48]. Recently, the binding activity of several peptides with ACE inhibitory activity was modeled by in silico approaches, such as the quantitative structure–activity relationship (QSAR) and molecular docking. The methods provide details illuminating the interaction mechanism between the receptor and the ligands [48–52].

In the present work, using redocking analysis, molecular docking was validated for a co-crystallized ligand (lisinopril, a commercial ACE inhibitor) with the ACE. The same model employed in redocking lisinopril was also used for GSH. Seven of the ten poses presented RMSD values less than 2.0 Å. As shown in Figure 12, the residues involved in the interaction and the types of non-bonding interactions involved between the studied complexes were Gln281, Ala353, Ala354, Ala 356, Tyr520, Tyr523, His387, and Phe512 (Conventional hydrogen bond, Unfavorable Acceptor–Acceptor, Pi-Sulfur, van der Waals). Some compounds of the herbal species *Cucurbita pepo* L. presented potential interaction in silico with the ACE, and the His353 also interacted by a hydrogen bond. Thus, it seems that His353 represents a critical interaction point. The number and the distances of hydrogen bonds play an essential role in the potential biological interaction between the ligand and the binding site. According to Figure 13, the hydrogen bond distances ranged from 1.91 to 2.60 Å [53,54].

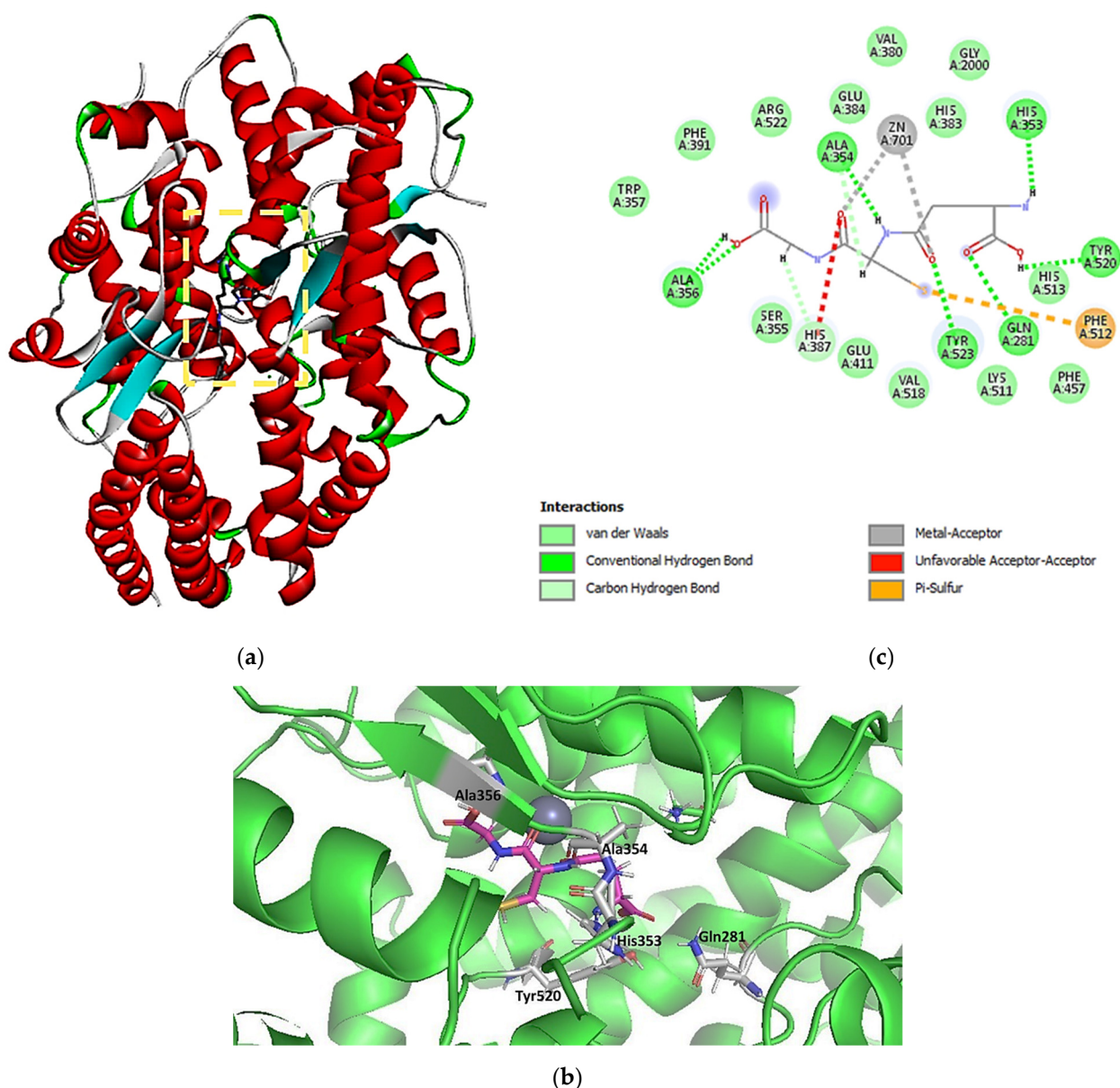


Figure 12. Crystal structure of lisinopril complexed with lisinopril (a); 2D (b) and 3D (c) forms of interaction between glutathione with the ACE binding site (pose 1; PDB ID: 1O86).

Furthermore, the same carboxyl group interacting with Gln281 also appears in the pharmacophore model (Figures 12c and 14). GSH is a well-known endogenous antioxidant [55,56]. This substance is synthesized in the liver and is involved in various organic processes such as antioxidant defense, metabolism, and regulation. Moreover, after drug treatment, GSH reduces oxidative stress in the heart of diabetic rabbits and also has a protective effect in mice from sepsis by inhibiting the inflammation process [57,58]. Thus, GSH may have protective cardiovascular effects associated with its antioxidant properties, which could provide vascular protection. Furthermore, GSH presents a potential impact on antihypertension, and its antioxidant properties can reduce vascular damage [59].

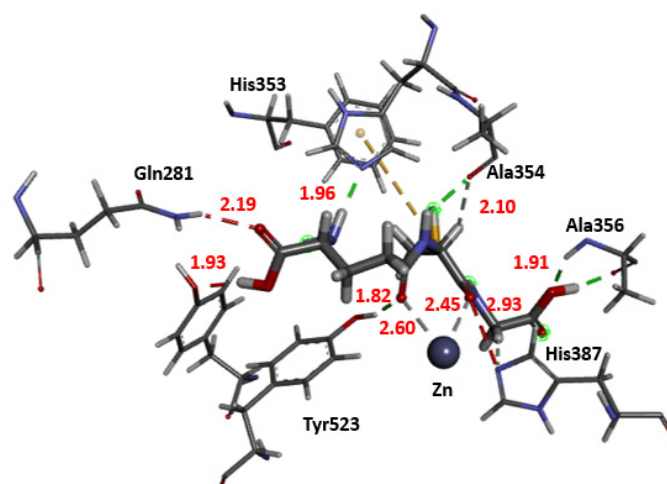


Figure 13. 3D representation of distance interactions of the glutathione and angiotensin-converting enzyme binding site.

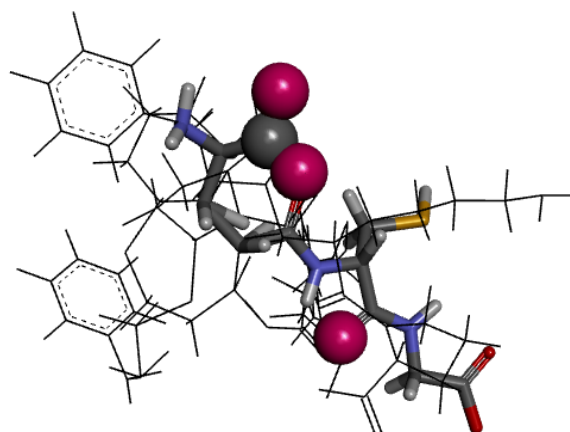


Figure 14. Spatial fitting of glutathione to the angiotensin-converting enzyme (ACE) antagonist pharmacophore. Hydrogen-bond acceptors and negative pharmacophore features are represented in red and gray, respectively.

In addition, when oxidative stress creates vascular damage by promoting cell growth, extracellular matrix protein deposition, endothelial dysfunction, and increased vascular tone, these features contribute to the vascular phenotype in hypertension [60]. In the study performed by Bessa, S. S. and colleagues (2009), it was observed that in hypertensives, both systolic and diastolic pressures were negatively correlated with glutathione S-transferase in Egyptian patients [61]. Beyond oxidative stress, our results suggest that glutathione might interact with some regulatory points in the cardiovascular system, such as the angiotensin-converting enzyme, playing an essential role in blood pressure regulation.

3. Computational Procedures

3.1. Computational Methods

The crystallographic information files of GSHA and GSHB were obtained from the Cambridge Crystallographic Data Centre (CCDC) [62] under codes 762195 and 1500579, respectively. Theoretical calculations were carried out for both conformations [63] using the highly parameterized empirical exchange–correlation functional M06-2X [31], combined with the triple- ζ basis set 6-311++G(d,p), in gas phase, implemented in the Gaussian16 [64] software package. Frontier molecular orbitals (FMOs) [63], the highest occupied molecular orbital (HOMO), and the lowest unoccupied molecular orbital (LUMO) were calculated and the chemical reactivity and kinetic stability of both molecules were obtained. To verify

the electronic charge distribution on the GSH molecular surface, the MEP [65] map was obtained through electrostatic potential $V(\mathbf{r})$ [66],

$$V(\mathbf{r}) = \sum_{\alpha} \frac{Z_{\alpha}}{|\mathbf{r}_{\alpha} - \mathbf{r}|} - \int \frac{\rho(\mathbf{r}')}{|\mathbf{r}' - \mathbf{r}|} d\mathbf{r}', \quad (8)$$

where Z_{α} is the charge of nuclei α at point \mathbf{r}_{α} and $\rho(\mathbf{r}')$ is the charge density at the point \mathbf{r}' . This function has been used for predicting nucleophilic and electrophilic regions and is valuable in studying intermolecular interactions. To predict the local electrophilicity, we used the Fukui function [67]

$$f(\mathbf{r}) = \left[\frac{\partial \rho(\mathbf{r})}{\partial N} \right]_v, \quad (9)$$

where N is the number of electrons present in the system and the constant term v in the partial derivative is external potential. Fukui indices have been widely used to predict the reactive sites of organic molecules, so the function values are higher in these regions than in regions with no reactivity. All calculations were carried out by DFT, implemented in the Gaussian 16 [64] software package at the M06-2X/6-311++G(d,p) level of theory in the gas phase, and the results were obtained by the GaussView 6 [68] software.

3.2. Supramolecular Arrangement

HS analysis using the CrystalExplorer program [69] was employed to study the intermolecular interactions [39]. The normalized distance (d_{norm}) is constructed by the distance from the surface to the nearest nucleus inside the surface (d_i) and outside the surface (d_e), the distance from the surface to the nearest inner atom, and the van der Waals radii of the internal and external atoms (r_i^{vdW} and r_e^{vdW}) [39],

$$d_{norm} = \frac{d_i - r_i^{vdW}}{r_i^{vdW}} + \frac{d_e - r_e^{vdW}}{r_e^{vdW}} \quad (10)$$

In addition, an analysis of intermolecular contacts and their contributions to the packaging of crystals, based on the combination of d_e vs. d_i plots, generate fingerprints, which summarize the percentage contribution to the nature and type of intermolecular interaction present in the molecule [41]. The topological parameters of GSH molecular systems were obtained by the QTAIM [43] by Multiwfn software [70], and the stabilities of the interaction were verified by NBO [71] calculations; a second-order perturbation theory formula provides the hyperconjugation energies:

$$E_{i \rightarrow j^*}^{(2)} = -n_{\sigma} \frac{\langle \sigma_i | \hat{F} | \sigma_j^* \rangle^2}{\epsilon_{j^*} - \epsilon_i} = -n_{\sigma} \frac{F_{ij}^2}{\epsilon_{j^*} - \epsilon_i}, \quad (11)$$

where $\langle \sigma | \hat{F} | \sigma \rangle^2$ or F_{ij}^2 is the Fock matrix element between the natural bond orbitals i and j ; ϵ_{σ^*} is the energy of the antibonding orbital σ^* and ϵ_{σ} is the energy of the bonding orbital σ ; and n_{σ} stands for the population occupation of the σ donor orbital. Theoretical calculations were carried out at the M06-2X/6-311G++(d,p) level of theory, in which the atom positions were fixed in their crystallographic positions.

3.3. Molecular Docking Analysis

ACE (PDB ID: 1O86) was downloaded from Protein Data Bank (<https://www.rcsb.org>; accessed on 12 September 2022) for molecular docking simulations. The enzyme was prepared by adding hydrogen atoms, and water molecules were removed. Next, the GSH molecule was saved in mol2 format. After that, the binding site of the macromolecule was selected, and the grid box was determined (X, Y, and Z coordinates). The downloaded file was saved in PDB format before being subjected to GOLD Suite 5.7.0 (Mark Thompson and Planaria Software LLC) [72,73] to locate the binding site and determine the binding

affinity. Biovia Discovery Studio 3.5 software was employed to obtain the 2D interaction figures, and PyMOL Molecular Graphics System 2.0 was used to obtain the 3D interaction images. Redocking with the co-crystallized ligand (lisinopril) was carried out to validate the models obtained. The CHEMPLP score function was used.

3.4. Pharmacophore Design

Binding DB (<https://www.bindingdb.org/bind/index.jsp>; accessed on 7 September 2022) was used to identify the compounds with antagonist activity against the ACE. The five molecules with the lowest half-maximal inhibitory concentration (IC_{50}) were selected to obtain pharmacophore models. PharmaGist web server [73,74] (<https://bioinfo3d.cs.tau.ac.il/PharmaGist/>; accessed on 10 September 2022) was employed to obtain the 3D pharmacophore model from the set of ACE antagonists and GSH. The algorithm determines potential pharmacophores and selects the highest-scoring ones. The suggested pharmacophore hits were determined after the spatial alignment of the GSH with the five EGFR antagonists. Pharmacophore analysis was used to search the possible critical features of ACE antagonists responsible for the interaction of the binding site. Hydrogen bond acceptors, donors, hydrophobic groups, and aromatic rings were selected to generate the pharmacophore models. A minimum of three to a maximum of six elements was considered. The following weights were used as default in the program (3.0 for aromatic rings, 1.0 for charges, 1.5 for hydrogen bond donors or acceptors, and 0.3 for hydrophobic groups). The images were generated in Biovia Discovery Studio 3.5

4. Conclusions

A comparison of the crystalline structures of GSH showed that the torsion of the carboxyl group in the glycine portion did not change the crystalline characteristics of the polymorphs, so they are in the same space group. Furthermore, the theoretical calculations showed that, when kept isolated, the molecule tends to remain in the neutral form, while in the crystalline environment, the zwitterionic form is predominant. The calculations also proved the antioxidant power of GSH by the frontier molecular orbitals and showed the regions where electrophilic and radical attacks occur in chemical processes. In supramolecular arrangements, some variations were observed in the contacts that form the intermolecular interactions, so they are more stabilized in GSHB compared to GSHA. In addition, the molecular docking analysis showed interactions between the active site residues of the ACE and glutathione through seven hydrogens. Moreover, these hydrogen bond acceptors are essential for binding the GSH with the ACE. The observed results suggest that glutathione analogs would be attractive dual-acting (antioxidant plus ACE inhibitor) antihypertensive agents and provide useful information for developing GSH analogs with higher ACE inhibitor activity.

Supplementary Materials: The following supporting information can be downloaded at: <https://www.mdpi.com/article/10.3390/molecules27227958/s1>, Table S1: Second-order perturbation theory analysis in NBO basis obtained at M06-2X/6-311++G(d,p) level of theory for the GSHA polymorph; Table S2: Second-order perturbation theory analysis in NBO basis obtained at M06-2X/6-311++G(d,p) level of theory for the GSHB polymorph.

Author Contributions: Conceptualization, A.S.N.A., L.L.B., P.P. and H.B.N.; methodology, A.S.N.A., I.D.B., L.L.B., L.D.D., A.J.C., P.P. and H.B.N.; software, H.B.N.; validation, A.J.C., P.P. and H.B.N.; formal analysis, A.S.N.A., I.D.B., L.L.B., L.D.D., A.J.C., P.P. and H.B.N.; investigation, A.S.N.A., I.D.B., L.L.B., L.D.D., A.J.C., P.P. and H.B.N.; resources, A.S.N.A., I.D.B., L.L.B., L.D.D., A.J.C. and P.P.; data curation, A.S.N.A., A.J.C., P.P. and H.B.N.; writing—original draft preparation, A.S.N.A., I.D.B., L.L.B., L.D.D., A.J.C., P.P. and H.B.N.; writing—review and editing, A.S.N.A., L.L.B., L.D.D., P.P. and H.B.N.; visualization, A.S.N.A., I.D.B., L.L.B., L.D.D., A.J.C., P.P. and H.B.N.; supervision, A.S.N.A., A.J.C., P.P. and H.B.N.; project administration, A.S.N.A., P.P. and H.B.N.; funding acquisition, P.P. and H.B.N. All authors have read and agreed to the published version of the manuscript.

Funding: This research received no external funding.

Institutional Review Board Statement: Not applicable.

Informed Consent Statement: Not applicable.

Data Availability Statement: The data presented in this study are available in supplementary material.

Acknowledgments: The authors are grateful to the Coordenação de Aperfeiçoamento de Pessoal de Nível Superior (CAPES), Conselho Nacional de Desenvolvimento Científico e Tecnológico (CNPq) and Fundação de Amparo à Pesquisa de Goiás (FAPEG). Theoretical calculations were carried out in the High-Performance Computing Center of the Universidade Estadual de Goiás. L. D. Dias thanks CNPq for post-doc grant 151188/2022-0.

Conflicts of Interest: The authors declare that they have no known competing financial interest or personal relationships that could have appeared to influence the work reported in this paper.

Sample Availability: Samples of the compounds are not available from the authors.

References

1. Mc Namara, K.; Alzubaidi, H.; Jackson, J.K. Cardiovascular Disease as a Leading Cause of Death: How Are Pharmacists Getting Involved. *Integr. Pharm. Res. Pract.* **2019**, *8*, 1–11. [CrossRef] [PubMed]
2. Birger, M.; Kaldjian, A.S.; Roth, G.A.; Moran, A.E.; Dieleman, J.L.; Bellows, B.K. Spending on Cardiovascular Disease and Cardiovascular Risk Factors in the United States: 1996 to 2016. *Circulation* **2021**, *144*, 271–282. [CrossRef] [PubMed]
3. Malinowski, B.; Zalewska, K.; Węsierska, A.; Sokołowska, M.M.; Socha, M.; Liczner, G.; Pawlak-Osińska, K.; Wiciński, M. Intermittent Fasting in Cardiovascular Disorders—An Overview. *Nutrients* **2019**, *11*, 673. [CrossRef] [PubMed]
4. Bays, H.E.; Taub, P.R.; Epstein, E.; Michos, E.D.; Ferraro, R.A.; Bailey, A.L.; Kelli, H.M.; Ferdinand, K.C.; Echols, M.R.; Weintraub, H.; et al. Ten Things to Know about Ten Cardiovascular Disease Risk Factors. *Am. J. Prev. Cardiol.* **2021**, *5*, 100149. [CrossRef] [PubMed]
5. Flora, G.D.; Nayak, M.K. A Brief Review of Cardiovascular Diseases, Associated Risk Factors and Current Treatment Regimes. *Curr. Pharm. Des.* **2019**, *25*, 4063–4084. [CrossRef]
6. Beevers, G. ABC of Hypertension: The Pathophysiology of Hypertension. *BMJ* **2001**, *322*, 912–916. [CrossRef]
7. Nguyen Dinh Cat, A.; Touyz, R.M. Cell Signaling of Angiotensin II on Vascular Tone: Novel Mechanisms. *Curr. Hypertens. Rep.* **2011**, *13*, 122–128. [CrossRef]
8. Wong, M.K.S. Angiotensin Converting Enzymes. In *Handbook of Hormones*; Elsevier: Amsterdam, The Netherlands, 2016; pp. 263–e29D-4.
9. Chen, J.; Wang, Y.; Ye, R.; Wu, Y.; Xia, W. Comparison of Analytical Methods to Assay Inhibitors of Angiotensin I-Converting Enzyme. *Food Chem.* **2013**, *141*, 3329–3334. [CrossRef]
10. Hawgood, B.J. Maurício Rocha E Silva MD: Snake Venom, Bradykinin and the Rise of Autopharmacology. *Toxicon* **1997**, *35*, 1569–1580. [CrossRef]
11. Ferreira, S.H. Angiotensin Converting Enzyme: History and Relevance. *Semin. Perinatol.* **2000**, *24*, 7–10. [CrossRef]
12. Acharya, K.R.; Sturrock, E.D.; Riordan, J.F.; Ehlers, M.R.W. Ace Revisited: A New Target for Structure-Based Drug Design. *Nat. Rev. Drug Discov.* **2003**, *2*, 891–902. [CrossRef] [PubMed]
13. Wijesekara, I.; Kim, S.-K. Angiotensin-I-Converting Enzyme (ACE) Inhibitors from Marine Resources: Prospects in the Pharmaceutical Industry. *Mar. Drugs* **2010**, *8*, 1080–1093. [CrossRef] [PubMed]
14. Chakraborty, R.; Roy, S. Angiotensin-Converting Enzyme Inhibitors from Plants: A Review of Their Diversity, Modes of Action, Prospects, and Concerns in the Management of Diabetes-Centric Complications. *J. Integr. Med.* **2021**, *19*, 478–492. [CrossRef]
15. Turner, J.M.; Kodali, R. Should Angiotensin-Converting Enzyme Inhibitors Ever Be Used for the Management of Hypertension? *Curr. Cardiol. Rep.* **2020**, *22*, 95. [CrossRef] [PubMed]
16. Khan, M.A.H.; Imig, J.D. Antihypertensive Drugs. In *Reference Module in Biomedical Sciences*; Elsevier: Amsterdam, The Netherlands, 2018.
17. Alderman, C.P. Adverse Effects of the Angiotensin-Converting Enzyme Inhibitors. *Ann. Pharmacother.* **1996**, *30*, 55–61. [CrossRef] [PubMed]
18. Nchinda, A.T.; Chibale, K.; Redelinghuys, P.; Sturrock, E.D. Synthesis and Molecular Modeling of a Lisinopril-Tryptophan Analogue Inhibitor of Angiotensin I-Converting Enzyme. *Bioorganic Med. Chem. Lett.* **2006**, *16*, 4616–4619. [CrossRef] [PubMed]
19. Kharazmi-Khorassani, J.; Asodeh, A.; Tanzadehpanah, H. Antioxidant and Angiotensin-Converting Enzyme (ACE) Inhibitory Activity of Thymosin Alpha-1 (Th α 1) Peptide. *Bioorg. Chem.* **2019**, *87*, 743–752. [CrossRef]
20. Papakyriakou, A.; Spyroulias, G.A.; Sturrock, E.D.; Manessi-Zoupa, E.; Cordopatis, P. Simulated Interactions between Angiotensin-Converting Enzyme and Substrate Gonadotropin-Releasing Hormone: Novel Insights into Domain Selectivity. *Biochemistry* **2007**, *46*, 8753–8765. [CrossRef]
21. Corradi, H.R.; Chitapi, I.; Sewell, B.T.; Georgiadis, D.; Dive, V.; Sturrock, E.D.; Acharya, K.R. The Structure of Testis Angiotensin-Converting Enzyme in Complex with the C Domain-Specific Inhibitor RXPA380. *Biochemistry* **2007**, *46*, 5473–5478. [CrossRef]

22. Alvarenga, D.J.; Matias, L.M.F.; Cordeiro, C.F.; de Souza, T.B.; Lavorato, S.N.; Pereira, M.G.A.G.; Dias, D.F.; Carvalho, D.T. Synthesis of Eugenol-Derived Glucosides and Evaluation of Their Ability in Inhibiting the Angiotensin Converting Enzyme. *Nat. Prod. Res.* **2022**, *36*, 2246–2253. [CrossRef]
23. Basi, Z.; Turkoglu, V. In Vitro Effect of Oxidized and Reduced Glutathione Peptides on Angiotensin Converting Enzyme Purified from Human Plasma. *J. Chromatogr. B* **2019**, *1104*, 190–195. [CrossRef] [PubMed]
24. Bas, Z. Inhibition Effect of Nicotinamide (Vitamin B3) and Reduced Glutathione (GSH) Peptide on Angiotensin-Converting Enzyme Activity Purified from Sheep Kidney. *Int. J. Biol. Macromol.* **2021**, *189*, 65–71. [CrossRef] [PubMed]
25. Yesiltepe, O.; Güler Çelik, E.; Geyik, C.; Gümüş, Z.P.; Odaci Demirkol, D.; Coşkunol, H.; Timur, S. Preparation of Glutathione Loaded Nanoemulsions and Testing of Hepatoprotective Activity on THLE-2 Cells. *Turk. J. Chem.* **2021**, *45*, 436–451. [CrossRef] [PubMed]
26. Aquilano, K.; Baldelli, S.; Ciriolo, M.R. Glutathione: New Roles in Redox Signaling for an Old Antioxidant. *Front. Pharmacol.* **2014**, *5*, 196. [CrossRef] [PubMed]
27. Li, Y.; Wei, G.; Chen, J. Glutathione: A Review on Biotechnological Production. *Appl. Microbiol. Biotechnol.* **2004**, *66*, 233–242. [CrossRef] [PubMed]
28. Glutathione. *Monograph*; European Pharmacopoeia: Strasbourg, France, 2018.
29. Pál, P.; Caridad, N.P.; Hamilton, B.N.; Hawsar, O.M. Physico-Chemical Characterization of Glutathione (GSH). In *Glutathione. Biosynthesis, Functions and Biological Implications*; Nova Science Publishers: Hauppauge, NY, USA, 2019; pp. 3–53.
30. Jefferies, H.; Coster, J.; Khalil, A.; Bot, J.; McCauley, R.D.; Hall, J.C. Glutathione. *ANZ J. Surg.* **2003**, *73*, 517–522. [CrossRef]
31. Zhao, Y.; Truhlar, D.G. The M06 Suite of Density Functionals for Main Group Thermochemistry, Thermochemical Kinetics, Noncovalent Interactions, Excited States, and Transition Elements: Two New Functionals and Systematic Testing of Four M06-Class Functionals and 12 Other Functionals. *Theor. Chem. Acc.* **2008**, *120*, 215–241. [CrossRef]
32. Zhao, Y.; Schultz, N.E.; Truhlar, D.G. Exchange-Correlation Functional with Broad Accuracy for Metallic and Nonmetallic Compounds, Kinetics, and Noncovalent Interactions. *J. Chem. Phys.* **2005**, *123*. [CrossRef]
33. Grimme, S. Semiempirical Hybrid Density Functional with Perturbative Second-Order Correlation. *J. Chem. Phys.* **2006**, *124*, 034108. [CrossRef]
34. Heitmann, P. A Model for Sulfhydryl Groups in Proteins. Hydrophobic Interactions of the Cysteine Side Chain in Micelles. *Eur. J. Biochem.* **1968**, *3*, 346–350. [CrossRef]
35. LoPachin, R.M.; Barber, D.S. Synaptic Cysteine Sulfhydryl Groups as Targets of Electrophilic Neurotoxicants. *Toxicol. Sci.* **2006**, *94*, 240–255. [CrossRef]
36. Pérez, P.; Domingo, L.R.; Aurell, M.J.; Contreras, R. Quantitative Characterization of the Global Electrophilicity Pattern of Some Reagents Involved in 1,3-Dipolar Cycloaddition Reactions. *Tetrahedron* **2003**, *59*, 3117–3125. [CrossRef]
37. Fukui, K. The Role of Frontier Orbitals in Chemical Reactions. *Angew. Chem.-Int. Ed.* **1982**, *21*, 801–876. [CrossRef]
38. Fukui, K. Role of Frontier Orbitals in Chemical Reactions. *Science* **1982**, *218*, 747–754. [CrossRef] [PubMed]
39. Spackman, M.A.; Jayatilaka, D. Hirshfeld Surface Analysis. *CrystEngComm* **2009**, *11*, 19–32. [CrossRef]
40. Bernstein, J.; Davis, R.E.; Shimon, L.; Chang, N.-L. Patterns in Hydrogen Bonding: Functionality and Graph Set Analysis in Crystals. *Angew. Chem. Int. Ed. Engl.* **1995**, *34*, 1555–1573. [CrossRef]
41. Spackman, M.A.; McKinnon, J.J. Fingerprinting Intermolecular Interactions in Molecular Crystals. *CrystEngComm* **2002**, *4*, 378–392. [CrossRef]
42. Çakmak, Ş.; Demircioğlu, Z.; Uzun, S.; Veyisoğlu, A.; Yakan, H.; Ersanli, C.C. Synthesis, X-Ray Structure, Antimicrobial Activity, DFT and Molecular Docking Studies of *N*-(Thiophen-2-Ylmethyl)Thiophene-2-Carboxamide. *Acta Crystallogr. C Struct. Chem.* **2022**, *78*, 390–397. [CrossRef]
43. Bader, R.F.W. Atoms in Molecules. *Acc. Chem. Res.* **1985**, *18*, 9–15. [CrossRef]
44. Matta, C.F.M.; Boyd, R.J. *The Quantum Theory of Atoms in Molecules*; Wiley-VCH: Weinheim, Germany, 2007; ISBN 9783527307487.
45. March, N.H. Electron Density Theory of Atoms and Molecules. *J. Phys. Chem.* **1982**, *86*, 2262–2267. [CrossRef]
46. Bader, R.F.W. *Atoms in Molecules—A Quantum Theory*; Clarendon Press Publication: Oxford, UK, 1994; ISBN 9780198558651.
47. Natesh, R.; Schwager, S.L.U.; Sturrock, E.D.; Acharya, K.R. Crystal Structure of the Human Angiotensin-Converting Enzyme–Lisinopril Complex. *Nature* **2003**, *421*, 551–554. [CrossRef] [PubMed]
48. Tzakos, A.G.; Gerothanassis, I.P. Domain-Selective Ligand-Binding Modes and Atomic Level Pharmacophore Refinement in Angiotensin I Converting Enzyme (ACE) Inhibitors. *ChemBioChem* **2005**, *6*, 1089–1103. [CrossRef] [PubMed]
49. Wang, F.; Zhou, B. Insight into Structural Requirements of ACE Inhibitory Dipeptides: QSAR and Molecular Docking Studies. *Mol. Divers.* **2020**, *24*, 957–969. [CrossRef] [PubMed]
50. Qi, C.; Lin, G.; Zhang, R.; Wu, W. Studies on the Bioactivities of ACE-Inhibitory Peptides with Phenylalanine C-Terminus Using 3D-QSAR, Molecular Docking and *in Vitro* Evaluation. *Mol. Inform.* **2017**, *36*, 1600157. [CrossRef] [PubMed]
51. Gonzalez Amaya, J.A.; Cabrera, D.Z.; Matallana, A.M.; Arevalo, K.G.; Guevara-Pulido, J. In-Silico Design of New Enalapril Analogs (ACE Inhibitors) Using QSAR and Molecular Docking Models. *Inform. Med. Unlocked* **2020**, *19*, 100336. [CrossRef]
52. Gu, Y.; Wu, J. LC–MS/MS Coupled with QSAR Modeling in Characterising of Angiotensin I-Converting Enzyme Inhibitory Peptides from Soybean Proteins. *Food Chem.* **2013**, *141*, 2682–2690. [CrossRef]

53. Fu, Y.; Liu, X.; Ma, Q.; Yi, J.; Cai, S. Phytochemical Bioaccessibility and *in Vitro* Antidiabetic Effects of Chinese Sumac (*Rhus Chinensis* Mill.) Fruits after a Simulated Digestion: Insights into the Mechanisms with Molecular Docking Analysis. *Int. J. Food Sci. Technol.* **2022**, *57*, 2656–2669. [CrossRef]
54. Oke, A.M.; Adelakun, A.O.; Akintelu, S.A.; Soetan, E.A.; Oyebamiji, A.K.; Ewemoje, T.A. Inhibition of Angiotensin Converting Enzyme by Phytochemicals in Cucurbita Pepo L.: In Silico Approach. *Pharmacol. Res.-Mod. Chin. Med.* **2022**, *4*, 100142. [CrossRef]
55. Juárez Olguín, H.; Calderón Guzmán, D.; Hernández García, E.; Barragán Mejía, G. The Role of Dopamine and Its Dysfunction as a Consequence of Oxidative Stress. *Oxidative Med. Cell. Longev.* **2016**, *2016*, 9730467. [CrossRef]
56. Kanazawa, K.; Sakakibara, H. High Content of Dopamine, a Strong Antioxidant, in Cavendish Banana. *J. Agric. Food Chem.* **2000**, *48*, 844–848. [CrossRef]
57. Gumieniczek, A. Modification of Oxidative Stress by Pioglitazone in the Heart of Alloxan-Induced Diabetic Rabbits. *J. Biomed. Sci.* **2005**, *12*, 531–537. [CrossRef] [PubMed]
58. Villa, P.; Saccani, A.; Sica, A.; Ghezzi, P. Glutathione Protects Mice from Lethal Sepsis by Limiting Inflammation and Potentiating Host Defense. *J. Infect. Dis.* **2002**, *185*, 1115–1120. [CrossRef] [PubMed]
59. Delles, C.; Miller, W.H.; Dominiczak, A.F. Targeting Reactive Oxygen Species in Hypertension. *Antioxid. Redox Signal.* **2008**, *10*, 1061–1078. [CrossRef]
60. Paravicini, T.M.; Touyz, R.M. NADPH Oxidases, Reactive Oxygen Species, and Hypertension: Clinical Implications and Therapeutic Possibilities. *Diabetes Care* **2008**, *31*, S170–S180. [CrossRef] [PubMed]
61. Bessa, S.S.; Ali, E.M.M.; Hamdy, S.M. The Role of Glutathione S- Transferase M1 and T1 Gene Polymorphisms and Oxidative Stress-Related Parameters in Egyptian Patients with Essential Hypertension. *Eur. J. Intern. Med.* **2009**, *20*, 625–630. [CrossRef]
62. Allen, F.H.; Bellard, S.; Brice, M.D.; Cartwright, B.A.; Doubleday, A.; Higgs, H.; Hummelink, T.; Hummelink-Peters, B.G.; Kennard, O.; Motherwell, W.D.S.; et al. The Cambridge Crystallographic Data Centre: Computer-Based Search, Retrieval, Analysis and Display of Information. *Acta Crystallogr. B* **1979**, *35*, 2331–2339. [CrossRef]
63. Zhang, G.; Musgrave, C.B. Comparison of DFT Methods for Molecular Orbital Eigenvalue Calculations. *J. Phys. Chem. A* **2007**, *111*, 1554–1561. [CrossRef]
64. Frisch, M.J.; Trucks, G.W.; Schlegel, H.B.; Scuseria, G.E.; Robb, M.A.; Cheeseman, J.R.; Scalmani, G.; Barone, V.; Petersson, G.A.; Nakatsuji, H.; et al. *Gaussian 16, Revision C.01 2016*; Gaussian Inc.: Wallingford, CT, USA, 2016.
65. Sjöberg, P.; Politzer, P. Use of the Electrostatic Potential at the Molecular Surface to Interpret and Predict Nucleophilic Processes. *J. Phys. Chem.* **1990**, *94*, 3959–3961. [CrossRef]
66. Politzer, P.; Murray, J.S. The Fundamental Nature and Role of the Electrostatic Potential in Atoms and Molecules. *Theor. Chem. Acc.* **2002**, *108*, 134–142. [CrossRef]
67. Parr, R.G.; Yang, W.; Hill, C.; Carolina, N. Density Functional Approach to the Frontier-Electron Theory of Chemical Reactivity. *J. Am. Chem. Soc.* **1984**, *106*, 4049–4050. [CrossRef]
68. Dennington, R.; Keith, T.A.; Millam, J.M. *GaussView 6 2016*; Semichem Inc.: Shawnee, KS, USA, 2016.
69. Spackman, P.R.; Turner, M.J.; McKinnon, J.J.; Wolff, S.K.; Grimwood, D.J.; Jayatilaka, D.; Spackman, M.A. *CrystalExplorer, Version 21.5*; University of Western Australia: Perth, Australia, 2021.
70. Lu, T. *Multiwfn. Software Manual, Version 2014*; Beijing Kein Research Center for Natural Sciences: Beijing, China, 2014; Volume 3.
71. Weinhold, F.; Landis, C.R. Natural Bond Orbitals and Extensions of Localized Bonding Concepts. *Chem. Educ. Res. Pract.* **2001**, *2*, 91–104. [CrossRef]
72. Jones, G.; Willett, P.; Glen, R.C.; Leach, A.R.; Taylor, R. Development and Validation of a Genetic Algorithm for Flexible Docking 1 Edited by F. E. Cohen. *J. Mol. Biol.* **1997**, *267*, 727–748. [CrossRef] [PubMed]
73. Schneidman-Duhovny, D.; Dror, O.; Inbar, Y.; Nussinov, R.; Wolfson, H.J. PharmaGist: A Webserver for Ligand-Based Pharmacophore Detection. *Nucleic Acids Res.* **2008**, *36*, W223–W228. [CrossRef] [PubMed]
74. Schneidman-Duhovny, D.; Dror, O.; Inbar, Y.; Nussinov, R.; Wolfson, H.J. Deterministic Pharmacophore Detection via Multiple Flexible Alignment of Drug-Like Molecules. *J. Comput. Biol.* **2008**, *15*, 737–754. [CrossRef] [PubMed]

MDPI
St. Alban-Anlage 66
4052 Basel
Switzerland
www.mdpi.com

Molecules Editorial Office
E-mail: molecules@mdpi.com
www.mdpi.com/journal/molecules



Disclaimer/Publisher's Note: The statements, opinions and data contained in all publications are solely those of the individual author(s) and contributor(s) and not of MDPI and/or the editor(s). MDPI and/or the editor(s) disclaim responsibility for any injury to people or property resulting from any ideas, methods, instructions or products referred to in the content.



Academic Open
Access Publishing

www.mdpi.com

ISBN 978-3-0365-8666-3